APPENDIX D

A STUDY TO DETERMINE THE FEASIBILITY OF
A SMALL MANEUVERING SUBSATELLITE (SMS)
IN SUPPORT OF A LARGE RADIO ASTRONOMY
OBSERVATORY

FINAL REPORT

7274-945001

September 1966

For

THE UNIVERSITY MICHIGAN
Radio Astronomy Observatory
Ann Arbor, Michigan

ABSTRACT

This report summarizes the result of a study conducted by Bell Aerosystems Company to establish the feasibility of utilizing small maneuverable subsatellites to maintain and process a large orbital telescope. This study was conducted under contract (5269-1) to the University of Michigan, Ann Arbor, Michigan.

The technical direction for this study was provided by Mr. Richard Stewart. The principal investigator was Mr. Nelson Paul. The following technical personnel contributed to this study and their contribution is hereby gratefully acknowledged.

Mr. A. Adler
Mr. R. Ames
Mr. J. Mark
Dr. G. Fejer
Mr. N. Paul
Mr. J. Piston
Mr. R. Stewart

The University of Michigan monitor was Mr. W. Lindsay, Engineering Manager, KWOT. Acknowledgement is also given to Prof. F. T. Haddock, Director, Radio Astronomy Observatory, University of Michigan, for the advice and direction he provided during the course of the study.

CONTENTS

CONTENTS (CONT)

ILLUSTRATIONS

TABLES

SYMBOLS

$\bar{r}_f$	Radius vector from the earth to the subsattelite (SMS)
$\bar{r}_s$	Radius vector from the earth to the Central Observatory
r_s	Magnitude of $\bar{r}_s$
$\ddot{\bar{r}}_s$	Acceleration of r_s
$\bar{R}$	Radius vector from the Central Observatory to the SMS
r_o, R_o	Unperturbed distance from Central Observatory to the SMS
r_e	Radius of the earth (3,440 n.mi.)
r	True distance from Central Observatory to the SMS
$\Delta r = r - r_o$	Deviation of SMS from its unperturbed position
X, Y, Z	Coordinate system centered at the Central Observatory
x, y, z,	Position coordinates in the X, Y, Z system
$\dot{x}, \dot{y}, \dot{z},$	Time rate of change of position coordinates
$\ddot{x}, \ddot{y}, \ddot{z}$	Acceleration of position coordinates
x_o, y_o, z_o	Components of position at initial time
F_x, F_y, F_z:	Non-conservative forces
F_{CF}	Magnitude of centrifugal force
$\frac{F_x}{m}, \frac{F_y}{m}, \frac{F_z}{m}$	Non-conservative accelerations
$\frac{F_x'}{m}, \frac{F_y'}{m}, \frac{F_z'}{m}$	Thrust Accelerations
$\bar{V}$	Velocity in absolute system
L	Lagrangian

T	Kinetic energy
U	Potential Energy
g	Acceleration caused by gravity at any point
g_e	Gravitational constant at r_e (32.146 ft/sec^2) 9.831 m/sec^2
m	Mass of individual SMS
K	Constant, function of orbital parameters
k	Spring constant
P	Period of motion
N	Frequency of oscillation
A,B,C,D_i,E_i,F_i:	Constants, solution coefficients
d_A, d_B, d_i:	Distance from SMU A, B, and C, resp.
υ	True anomoly
ω	Radion frequency of oscillation
ω_o	Antenna system rotation rate (2π rads/hr.)
$\alpha\beta$	Arbitrary radian frequency coefficients
i	Inclination angle between the system plane and an inertially fixed reference plane passing through the center of mass of the Central Observatory
Ω'	Angle to the line of nodes from an initially fixed reference
$i' \dot{\Omega}'$	Time derivatives of i' , and Ω'
δP	Precession angle
$\Theta A, \Theta B$	Angle from Central Observatory measured at A and B respectively

1.0 INTRODUCTION

The objective of this study was the determination of the feasibility of using active control, as exerted by subsatellites, on a large radio astronomy telescope. Specifically, it was to determine the feasibility of and the gross requirements for the SMS to perform stationkeeping and precession functions for the large array. Studies conducted on untethered subsatellites (Reference 1 , and 2) indicate that an SMS could be suitable for deployment, stationkeeping, precession, and calibration of the KWOT system. However, for this initial feasibility study, it was deemed that stationkeeping and precession were likely to be the most significant, hence efforts were concentrated on these items. Should the use of SMS's prove feasible, which will be shown later, then further study of the other items will be warranted. The large radio astronomy telescope antenna KWOT is shown in Figure 1-1. The KWOT antenna, as currently envisioned, consists of a combination rhombic interferometer antenna. The interferometer consists of a set of dipoles arrays-normal to the axis of the rhombic-which would act as a passive receiver of a radio source data and enable accurate position information. The rhombic would function as an ambiguity resolver through the cross correlation of its unidirectional beam with the axisymmetrical interferometer. Physically, this system as shown in Figure 1-1, consists of a 10 kilometer rhombic array and perpendicular to this rhombic array a 10 kilometer line upon which the dipole interferometer elements would be spaced, plus supporting structure.

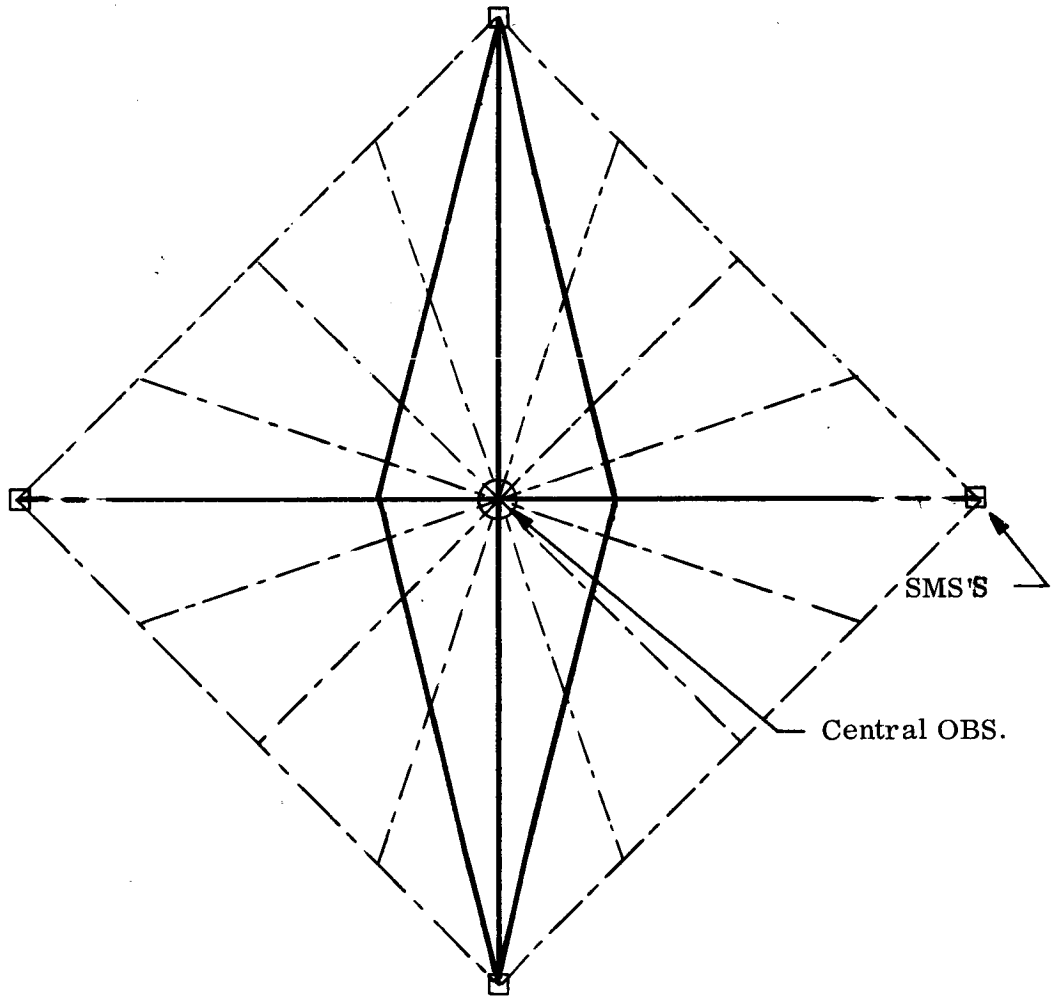

Figure 1-1. Schematic of KWOT System

Referring to the figure, it may be seen that two sets of supporting structure are depicted; the first set is the antenna as initially envisioned at the onset of this study, which contains a large number of nonconducting supporting elements, and the second is the currently envisioned array which is somewhat simpler. The latter array, as will be shown later, is also simple from the point of view of dynamic control.

The subsatellites, as initially viewed for the study consisted as principally a means of providing propulsion in any desired direction, with the appropriate position sensing and control logic. These would be located at the periphery of the antenna.

In order to find a suitable point of departure, it was necessary to make some initial assumptions regarding the KWOT system and the subsatellites. These assumptions appear in the following paragraphs.

1.1 CHARACTERISTICS

1.1.1 Initial Characteristics

The gross initial characteristics of the vehicle of concern to the SMS study was: that the KWOT was assumed to consist of .02" diameter Kapton tubing for the web structure; that any distributed masses along the antenna were sufficiently small to be neglected; and that the gross total weight of the SMS's would be on the order of 130 to 150 pounds.

1.1.2 Dynamic Characteristics

The gross dynamic characteristics of the antenna were assumed to consist of the system spinning about the central observatory at some constant angular velocity, initially assumed to be 1 rev/hr. Similarly, it was assumed that the entire array was precessing as a plane, to obtain complete coverage of the clestial sphere, at some constant rate initially assumed to be $1/2^{\circ}$ per hour.

1.1.3 Control Concept

The control concept initially assumed was that of a simple threshold system monitoring the SMS's, hence, the array is in a prespecified "control corridor." The magnitude of SMS motion within this corridor was assumed to be ±25 meters in all three axes. The path this volume sweeps out is the control corridor. Consequently it is not significant what the natural behavior of the antenna might be since as soon as any SMS would reach the limit of the volume, the thrusters would fire to bring it back within the boundary.

1.1.4 Orbital Characteristics

Two initial orbital characteristics were assumed, elliptical and circular. It is desirable to have the KWOT out of the magnetosphere for the longest time possible, hence, from this viewpoint an elliptical orbit is in order. However, elliptical orbits present the greatest problem in terms of gravity gradient effects. Hence for a worse case assumption, an elliptical orbit of 20,000 n.mi. perigee and 100,000 n.mi. apogee was studied as shown in Figure 1-2, the circular orbit of corresponding period, which would also have some time outside the magnetosphere, is one of 60,000 n.mi. These orbits therefore bracket the anticipated range of interests.

1.2 MOTION STUDY

Based upon the above assumptions, a study was conducted of the motion of the subsatellites, effects of perturbations, stabilization and control, and system ΔV requirements. The motion of the subsatellites was found to be regular and describable by a set of exact differential equations. The environmental perturbation forces and induced perturbation forces were both found to be negligible.

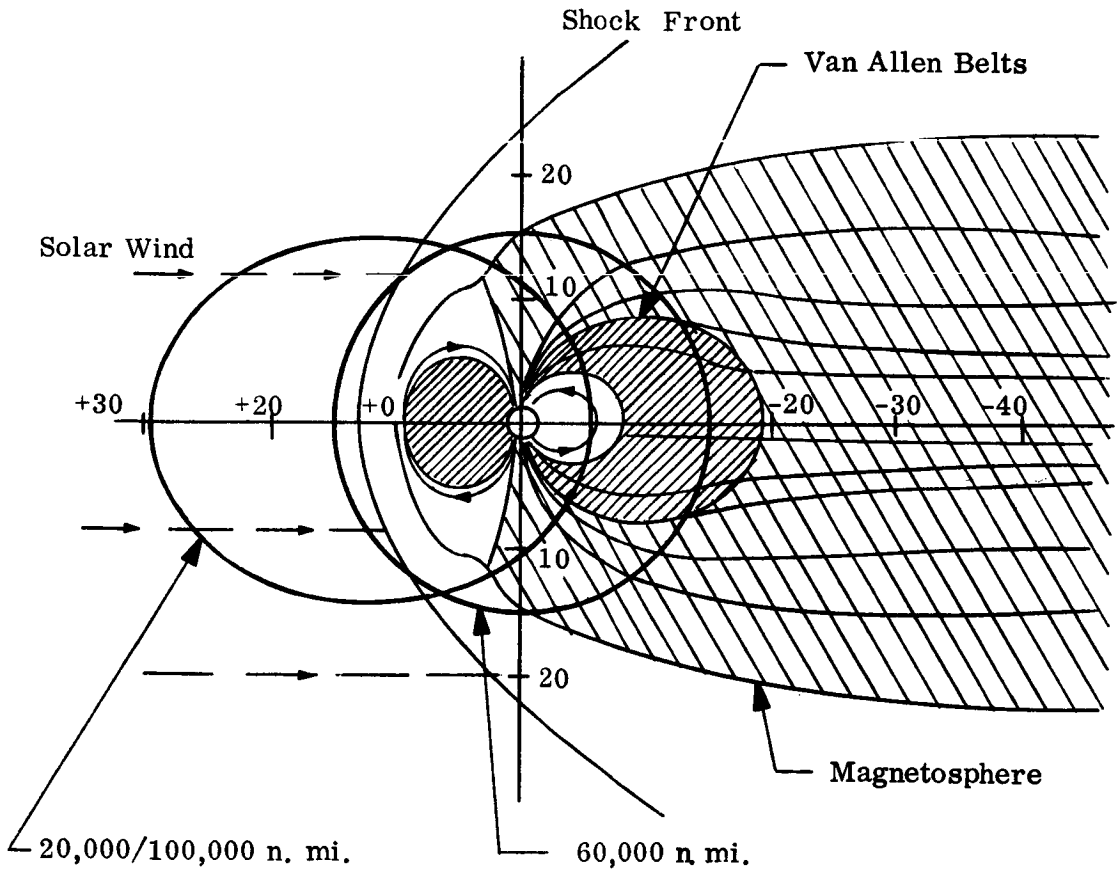

Figure 1-2. Schematic of KWOT Orbits

The environmental perturbances include the effects of solar radiation pressure, solar wind, solar flares, atmospheric drag and particulate drag from passage through the Van Allen Belts. The indirect perturbations forces are the, RF currents, indirect charges and currents caused by passage of the antenna through the magnetosphere. The significant disturbance is the gravity differential or gravity gradient. Active control was found to be required to overcome the gravity gradient effects for the elliptical orbit, however over the greater portion of the orbit, these control requirements are very small (a thruster firing - 12-14 hrs). In the case of a circular orbit, the pertubation caused by the gravity gradient, would be very small, if any.

The second significant disturbance force acting on the KWOT system is that induced to precess the antenna. The latter force predominates over the majority of the orbit for a precession rate of 1/2 deg/hr. This is shown in a schematic of Figure 1-3, wherein the firings of the SMS thrusters (that are required because the subsatellites have reached the limits of the control region) occur about once an hour for precession, or about once for every antenna revolution. For the great majority of the orbit the gravity differential forces do not cause sufficient disturbance to the spinning system to cause the subsatellites to reach the edge of the control region for several hours. However, it should be pointed out that at perigee where the gravity gradient is most severe, it requires thruster firings on the order of once every half a revolution of the antenna. A detailed description of the motion of the subsatellites as well as the investigation of the control problem is given in subsequent chapters.

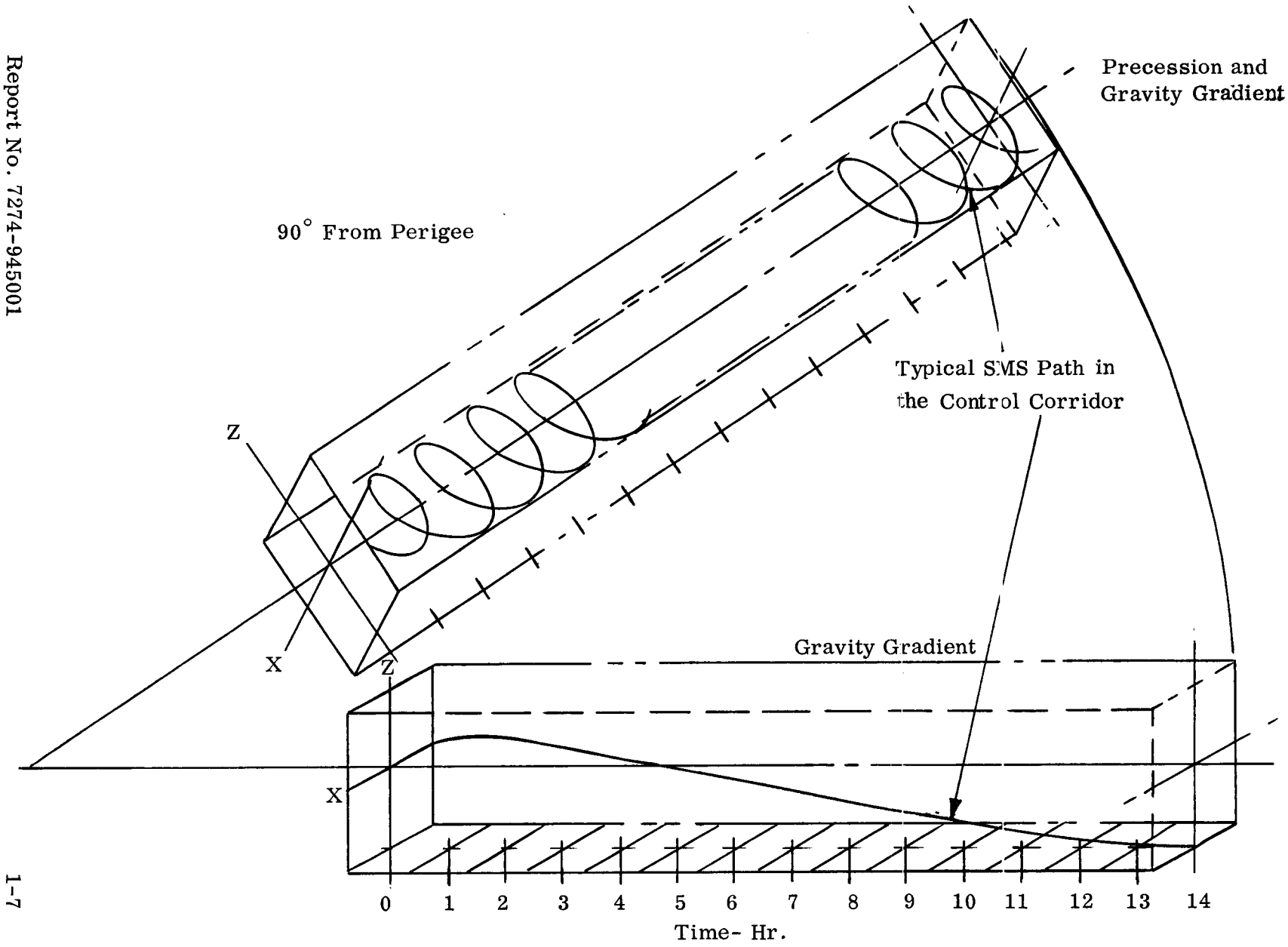

Figure 1-3. Schematic of Drift Due to Gravity Gradient and Gravity Gradient with Precession

Since, as will be seen in the ensuing sections, the control of the KWOT array, by SMS's is feasible, further detailed study is warranted. Feasibility does not imply that the SMS is the only means of achieving this control; rather that it is one means, which is simple and readily achievable. The future studies which are warranted as a result of this effort are delineated in section 8.

2.0 DERIVATION OF THE EQUATIONS OF MOTION

The basic function of the SMS in the KWOT system is to provide control actions which will maintain the shape, and spatial orientation of the antenna within predetermined tolerances. In order to design this control system, it is necessary to know the disturbing forces and the resulting motion of the SMS. In the case of the KWOT system, the disturbing forces, as will be shown, are extremely small, and the motion, as will be seen, consists of a slow drift away from the initial conditions. The significance of this motion is discussed in Section 4.0.

The equations of motion are developed in several steps. First, the general differential equations are obtained for the motion of a point mass in the gravity field of a spherical earth. Next, the gravity forces due to other heavenly bodies are shown to be negligible. The equations are then linearized by an expansion of the gravity terms. Inclusion of the tension forces as a function of the rotation rate completes the simplifying assumptions. Approximate solutions, which are valid for the rotating antenna system are then obtained, and some conclusions about the motion are made.

2.1 DERIVATION

The method of Lagrange is employed to derive the equations of motion of a single SMS with respect to the Central Observatory. It will be shown that this approach adequately represents the motion of each SMS whether or not there are interconnections between SMS or Central Observatory.

Figure 2-1 shows the coordinate system used in the derivation. The frame of reference is a set of non-rotating axes with the origin located in the Central Observtory. The Central Observatory is assumed to be moving along a Keplerian orbit. The X-axis, at perigee, is aligned with the radius vector from the center of the earth to the

Note:

X, Y Axes in Plane
of Orbit

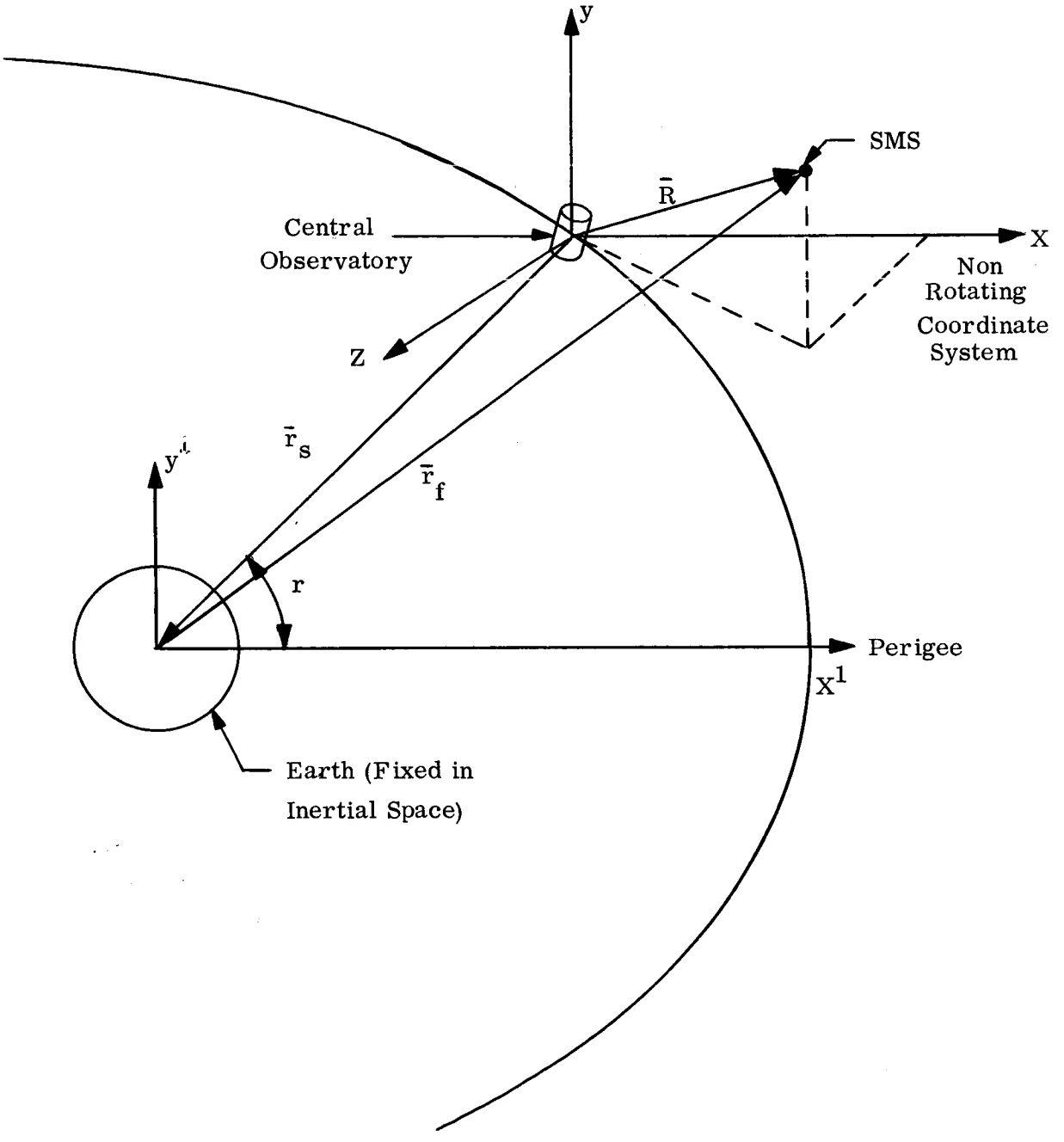

Figure 2-1. KWOT Coordinate System

Central Observatory. The Y-axis is in the orbital plane, and at perigee, is aligned with the velocity vector. The z-axis is perpendicular to the orbital plane and forms the third axis of a right-handed set. The earth is taken as the absolute system.

The position of a point mass representing the SMS is given by:

$$\bar{r}_f = \bar{r}_s + \bar{R} \qquad (1) \quad (2\text{-}1)$$

The velocity, with respect to the absolute system, is given by:

$$V = \frac{d\bar{r}_f}{dt} = \frac{d\bar{r}_s}{dt} + \frac{d\bar{R}}{dt} \qquad (2) \quad (2\text{-}2)$$

The vectors in equations (1) and (2) have the following components:

$$\bar{r}_s = (-r_s \cos \upsilon \ , \ -r_s \sin \upsilon \ , \ 0)$$

$$\bar{R} = (x, y, z)$$

$$\bar{r}_f = (x + r_s \cos \upsilon \ , y + r_s \sin \upsilon \ , z)$$

$$\bar{V} = (\dot{x} + \dot{r}_s \cos \upsilon - r_s \sin \upsilon \dot{\upsilon} \ , \ \dot{y} + \dot{r}_s \sin \upsilon + r_s \cos \upsilon \dot{\upsilon} \ , \ \dot{z})$$

Expressions for the kinetic and potential energy can now be obtained as follows:

Kinetic Energy:

$$T = 1/2 \ mV^2 = 1/2 \ m \ (\bar{V} \cdot \bar{V}) = \frac{m}{2} \left\{ \dot{x}^2 + \dot{y}^2 + \dot{z}^2 \dot{r}_s^2 + r_s^2 \upsilon^{\circ 2} + 2(\dot{x} \cos \upsilon + \dot{y} \sin \upsilon) \dot{r}_s + 2 r_s \upsilon (\dot{y} \cos \upsilon - \dot{x} \sin \upsilon) \right\} \qquad (2\text{-}3)$$

Potential Energy with respect to earth:

$$U = -mgr_f = -mg_e \frac{r_e^2}{r_f} \qquad (2\text{-}4)$$

With the kinetic and potential energy specified, the Lagrangian L = T - U can be formed and the Lagrangian differential equations formed.

$$\frac{d}{dt}\left\langle \frac{\partial L}{\partial \dot{x}} \right\rangle - \frac{\partial L}{\partial x} = F_x \quad (x \quad y, z)$$

where F_X, F_y and F_Z are non-conservative forces, such as the thrust components, etc.

The operations indicated in equation 2-5 are carried out in detail only for the x components; the y and z components are, obviously, similar in their derivation.

The Lagrangian is:

$$L = \frac{m}{2}\left\{ \dot{x}^2 + \dot{y}^2 + \dot{z}^2 + r_s^2 \upsilon + \underset{s}{} 2\, rs \quad \left(\dot{x} \cos \upsilon + y \sin \upsilon\right) \right.$$

$$\left. +2 r_s \upsilon \quad (\dot{y} \cos \upsilon - \dot{x} \sin \upsilon) \right\} + \frac{mg_e \quad r_e^2}{\sqrt{(x+r_s \cos \ddot{\upsilon})^2 + (y + r_s \sin \upsilon)^2 + z^2}}$$

From (2-5a) we obtain (2-5a)

$$\frac{\partial L}{\partial x} = m(x + r_s \cos \upsilon - r_s \dot{\upsilon} \sin \upsilon) \qquad (2\text{-}5b)$$

$$\frac{d}{dt}\left(\frac{\partial L}{\partial x}\right) = m \left\{ \ddot{x} + (\ddot{r}_s - r_s \dot{\upsilon}^2) \cos \upsilon - (2\dot{r}_s \dot{\upsilon} + \dot{r}_s \ddot{\upsilon} \sin \upsilon \right\}$$

$$L_x = \frac{-m\, g_e r_e^2 (x + r_s \cos \quad)}{(x+r_s \cos \quad)^2 + (y + r_s \sin \quad)^2 + Z^2 \quad 3/2} = \frac{-m\, g_e r_e^2 (x + r_s \cos \quad)}{r_f}$$

Therefore:

$$\frac{d}{dt}\frac{\partial L}{\partial \dot{x}} - \frac{\partial L}{\partial x} = m \ddot{x} + \left[\ddot{r}_s - r_s \dot{\upsilon}^2\right] \cos \upsilon - \left[2 \dot{r}_s \dot{\upsilon} + r_s \ddot{\upsilon}\right] \sin$$

$$+ \frac{g_e r_e^2}{r_f^3} (x + r_s \cos \upsilon) = F_x$$

From Kepler's equations we have

$$\ddot{r}_s - r_s \dot{\upsilon}^2 = - \frac{g_e r_e^2}{r_s^2} \qquad (2\text{-}5d)$$

and $$\frac{d}{dt}\left(r_s^2 \dot{\upsilon}\right) = 0 \qquad (2\text{-}5e)$$

which gives after differentiation

$$2\dot{r}_s\upsilon + r_s^2\ddot{\upsilon} = 0$$

$$2\dot{r}_s\upsilon + r_s\ddot{\upsilon} = 0 \qquad (2\text{-}5f)$$

Substituting (5d) and (5e) into (5c) gives:

$$m\left\{\ddot{x} - \frac{g_e r_e^2}{r_s^2}\cos\upsilon + \frac{g_e r_e^2}{r_f^3}(k + r_s\cos\upsilon)\right\} = F_x \qquad (2\text{-}5g)$$

Equation (5g), along with the y and z equations, are rearranged for convenience and shown as equation (6).

$$\ddot{x} + \frac{g_e r_e^2}{r_s^2}\left\{\frac{r_g^3}{r_f^3}\left\langle\frac{x}{r_s} + \cos\upsilon\right\rangle - \cos\upsilon\right\} = \frac{F_x}{m} \qquad (2\text{-}6)$$

$$\ddot{y} + \frac{g_e r_e^2}{r_s^2}\left\{\frac{r_s^3}{r_f^3}\left\langle\frac{y}{r_s} + \sin\upsilon\right\rangle - \sin\upsilon\right\} = \frac{F_y}{m}$$

$$\ddot{z} + \frac{g_e r_e^2}{r_s^2}\left\{\frac{r_s^2}{r_f^2}\left\langle\frac{z}{r_s}\right\rangle\right\} = \frac{F_z}{m}$$

where g_e = acceleration caused by gravity at the surface of the earth.

r_e = radius of the earth

υ = true anomaly

F_x, F_y, F_z = Non-gravitational forces.

Before continuing with this development, it is useful to have some discussion concerning the physical significance of the above equations. They represent the motion of a point mass under the influence of a time variant vector forcefield (assuming F_x, F_y, $F_z = 0$) formed by the difference between the gravity vector at the assumed SMS

point mass and the gravity vector at the origin of coordinates, the point mass equivalency for the Control Observatory. The equations have been developed assuming the gravity field for an homogeneous, spherical earth. Introduction of the additional terms to account for other gravitational fields, such as caused by the sun, moon, etc., complicates the equations unnecessarily. The magnitude of some of the gravitational force accelerations are shown in Table 2-1, where they are compared with those of a spherical earth.

It can be seen that, although the additional gravity terms are important in describing the total motion of the system, the relative motion, which is due to the gravity gradients is dominated by the earth's gravity.

Oblateness effects which decrease with increasing altitude are negligible at the minimum (20,000 n.mi.) altitude considered, giving an acceleration of less than 10^{-4} that of the spherical earth.

TABLE 2-1

COMPARISON OF ACCELERATION DUE TO GRAVITY FORCES

Source	Acceleration meters/sec2	Gradient Meters/sec^2/meter
Spherical Earth	$.214 \times 10^{-1}$	$-.639 \times 10^{-8}$
Sun	$.591 \times 10^{-2}$	$-.592 \times 10^{-11}$
Moon	$.123 \times 10^{-5}$	$-.616 \times 10^{-12}$
Jupiter	$.319 \times 10^{-6}$	$-.505 \times 10^{-16}$
Oblate Earth Effects	$.37 \times 10^{-5}$	-----

Therefore, keeping only the forces from the gravity field due to the spherical earth, the equations can be further simplified by expanding the expression, $\left\langle \frac{r_s}{r_f} \right\rangle^3$, into a Taylor series. The first two terms of this series are:

$$\left\langle \frac{r_s}{r_f} \right\rangle^3 = 1 - \frac{3x}{r_s} \cos \upsilon - \frac{3y}{r_s} \sin \upsilon$$

Higher order terms have been dropped since x, y, z are all much less than r_s ($x/r_s = 10^{-6}$). Substituting into the basic equations then yields:

$$\ddot{x} + \frac{g_e r_e^2}{r_s^3} (1 - 3 \cos^2 \upsilon) x - \frac{g_e r_e^2}{r_s^3} (3 \sin \upsilon \cos \upsilon) y = \frac{F_x}{m}$$

$$\ddot{y} + \frac{g_e r_e^2}{r_s^3} (1 - 3 \sin^2 \upsilon) y - \frac{g_e r_e^2}{r_s^3} (3 \sin \upsilon \cos \upsilon) x = \frac{F_y}{m}$$

$$\ddot{z} + \frac{g_e r_e^2}{r_s^3} z = \frac{F_z}{m}$$

The parameters r_s and υ are functions of the KWOT orbit and are defined by the basic Keplerian equations:

$$\ddot{r}_s - r_s \dot{\upsilon}^2 = - \frac{g_e r_e^2}{r_s^2}$$

$$\frac{d}{dt} (r_s^2 \dot{\upsilon}) = 0$$

The values r_s and υ are shown in Figure 2-2 for both the 20,000/100,000, and the 60,000 n.mi. circular orbits. Some of the other pertinent orbital parameters are listed below.

Orbit	60,000 n.mi. Circular	20,000/100,000 n.mi. Elliptical
Period	111.2 hours	111.2 hrs.
Apogee Altitude	---	100,000 n. mi.
Perigee Altitude	---	20,000 n. mi.
Semi-major Axis	63,340 n.mi.	63,340 n. mi.
Eccentricity	0	.6315

The terms F_x, F_y and F_z consist of the non-gravity forces which act on the system. It has been shown that the induced and environmental perturbation forces are negligible (Section 3). The remaining forces which are involved arise from the tension in the lines connecting the SMS to the Central Observatory and from thrust forces. In the remainder of the derivation the thrust forces will be carried in the equations as constants.

The forces due to the elastic lines from the Central Observatory to the SMS are considered next.

A spring constant, k, of 0.0296 lb/ft ($.0216 \frac{kg}{m}$) was used in this analysis.

For the case of a 130 lb. subsatellite, the period of the motion with the above springs constant is:

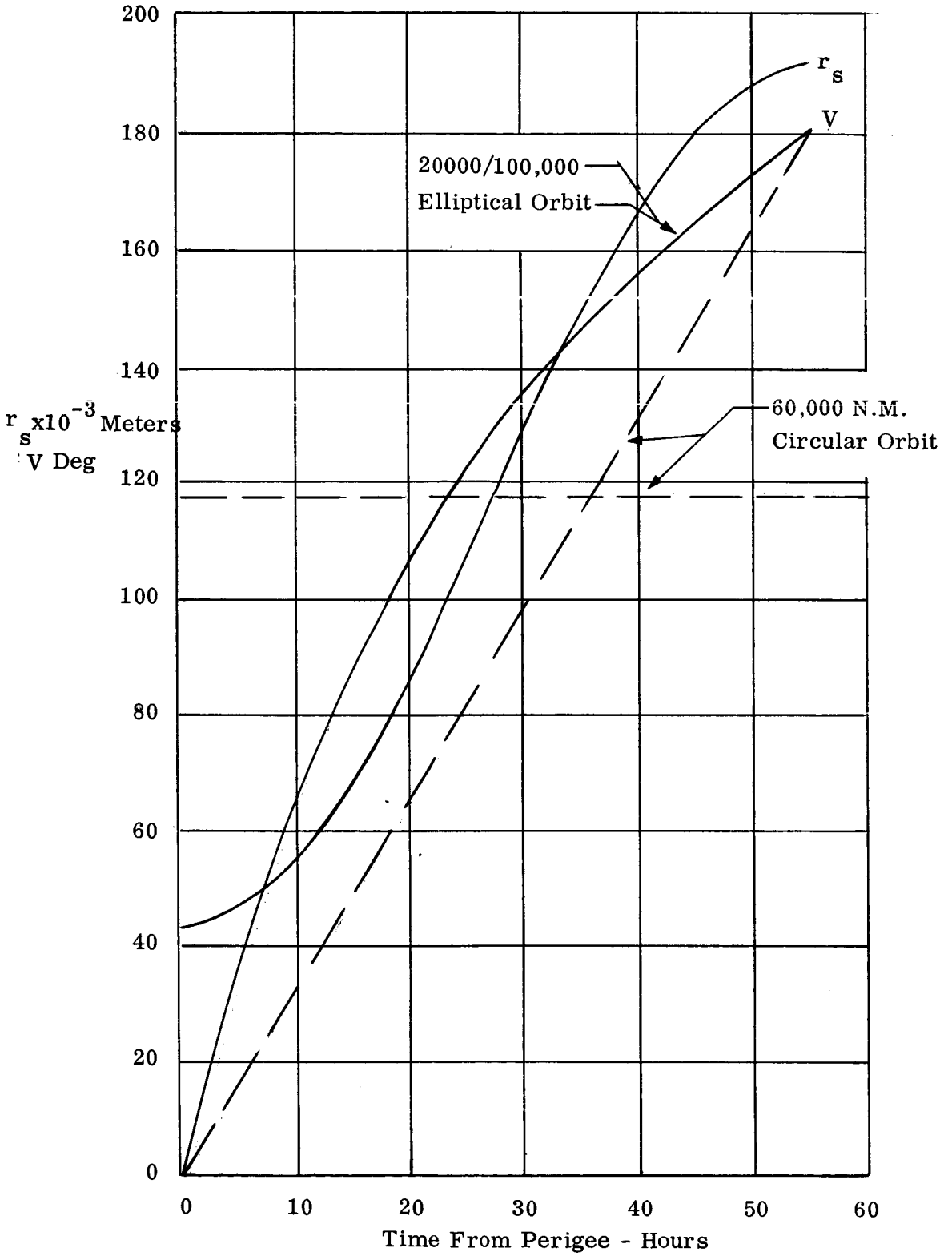

Figure 2-2. Orbital Parameters for the Typical KWOT Orbits

$$P = 2\pi \Big/ \sqrt{k/m} = \frac{2\pi}{\sqrt{\frac{.0296}{130/32.2}}} = \frac{2\pi}{.0862} = 72.8 \text{ sec.}$$

The frequency per hour is thus

$$N = \frac{3600}{P} = 49.5 \text{ cycles/hour.}$$

Since the antenna is assumed to be rotating at one revolution per hour, the line will stretch to an equilibrium point where the centrifugal and tension forces are in balance. Thus

$$m\, r\, \omega^2 = k(r-r_o)$$

$$r-r_o = \Delta r = \frac{m\, r\omega^2}{k}$$

which gives, for the assumed values

$$\Delta r = \left\langle \frac{130}{32.2} \right\rangle \frac{(16400)\ (1.75 \times 10^{-4})^2}{.0296} = 6.8 \text{ ft} = 2.1 \text{ meters}$$

It may be assumed, therefore, that because of the high frequency of oscillation, compared to the antenna rotation rates, there will be no coupling between the elastic and rotational motions. Furthermore, the net force acting on each SMS from the lines will be constant and directed radially inward toward the Central Observatory.

The magnitude of the centrifugal force can be obtained as:

$$F_{CF} = - m\, F_o \omega^2$$

and the x, y, z components are

$$\left\langle \frac{F_x}{m} \right\rangle = -x\omega_o^2$$

$$\left\langle \frac{F_y}{m} \right\rangle = -y\omega_o^2$$

$$\left\langle \frac{F_z}{m} \right\rangle = -z\omega_o^2$$

Components of centrifugal force can now be added to equation (2-8) to yield:

$$\ddot{x} + x\left[K^2 (1-3\cos^2 \upsilon) + \omega_o^2\right] - y(3K^2 \sin\upsilon \cos\upsilon) = \frac{F'_x}{m}$$

$$\ddot{y} + y\left[K^2 (1-3\sin^2 \upsilon) + \omega_o^2\right] - x(3K^2 \sin\upsilon \cos\upsilon) = \frac{F_y}{m}$$

$$\ddot{z} + (K^2 + \omega_o^2)\, z = \frac{F_z}{m}$$

where $K^2 = \dfrac{g_e r_e^2}{r_s^3}$

ω_o = antenna system rotation rate, nominally 1 rev/hr (1.754×10^{-3} rad/sec)

$\dfrac{F'_x}{m}, \dfrac{F'_y}{m}, \dfrac{F'_z}{m}$ = thrust accelerations

This is a set of coupled, second degree differential equations with time variant coefficients, an exact solution of which is, probably, not possible. It is, however, possible to obtain solutions when the coefficients are assumed constant.

Let:

$$A = \omega_o^2 + K^2 (1-3\cos^2 \upsilon)$$

$$B = \omega_o^2 + K^2 (1-3\sin^2 \upsilon)$$

$$C = 3K^2 \upsilon \sin \upsilon \cos$$

$$D + \omega_o^2 + K^2$$

Figure 2-3 is a graph showing the variation of the A, B and C coefficients as time from perigee. On the basis of this figure and some simple calculations, the following facts can be noted:

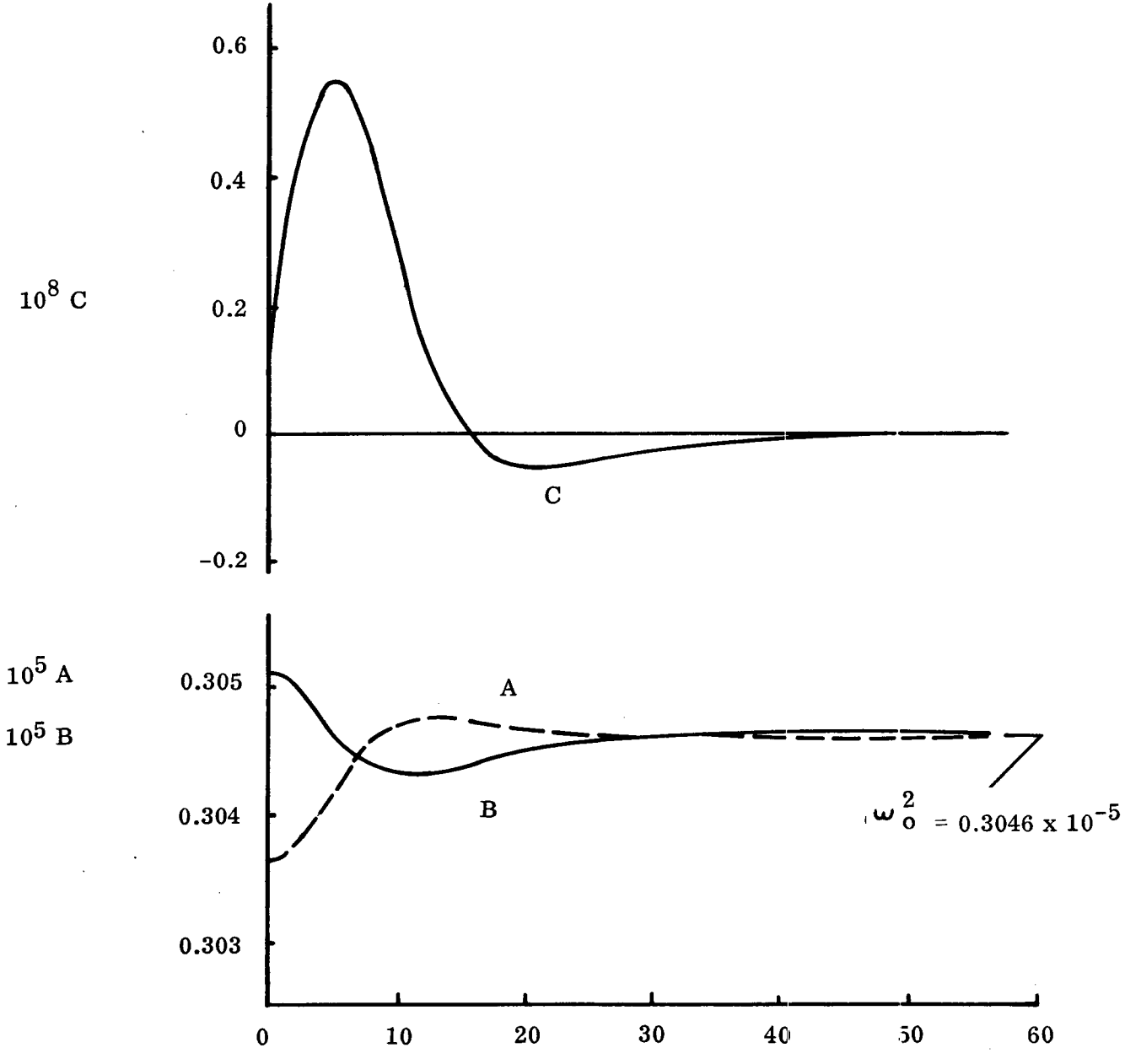

Figure 2-3. Variation of Differential Equation Coefficients

a) $K^2 << \omega_o^2$ $(K^2/\omega_o^2 < .0016)$

b) $C << A$ or B $(C/A = C/B < 2. \times 10^{-3})$

c) A and B vary less than 1% over the entire KWOT orbit.

The physical significance attached here is that the tension forces of the lines connecting the SMS to the Central Observatory are much larger (3 orders of magnitude) than the forces arising from the gradient of the earth's gravity field.

This information about the coefficients can be used to obtain approximate solutions to the equations of motion. There are, in fact, a number of different techniques which can be used, each having various advantages and disadvantages. For the purposes of this study, it was assumed that the coefficients were piecewise constant. This decision is based, in part, on the fact that each SMS is under active control, and the motion will be corrected and/or altered at intervals which are frequent compared to the orbital period. Thus, the accuracy of the solutions should be more than adequate for the "coasting" i.e., non-thrusting portions of the flight, which will be, at most, a few hours in duration, as shown in Section 6.

$$x = D_1 \sin\alpha t + D_2 \cos\alpha t + D_3 \sin\beta t + D_4 \cos\beta t + D_5$$

$$y = E_1 \sin\alpha t + E_2 \cos\alpha t + E_3 \sin\beta t + E_4 \cos\beta t + E_5$$

$$z = F_1 \sin\beta t + F_2 \cos\beta t + F_3$$

The following relationships hold when $\omega^2 > k^2$

$$\alpha^2 = \omega^2 - 2K^2$$

$$\alpha \cong \omega - \frac{K^2}{\omega}$$

$$\beta^2 = \omega^2 + K^2$$

$$\beta \cong \omega + \frac{K^2}{2\omega}$$

The relationships between the D_i, E_i, F_i constants and the initial conditions are given in Table 2-2.

TABLE 2-2

CONSTANTS IN THE SOLUTIONS OF THE EQUATIONS OF MOTION

$$D_1 = \frac{x_o}{\alpha} \cos^2 \omega + \frac{y_o}{\alpha} \cos \upsilon \sin \upsilon$$

$$D_2 = (x_o - D_5) \cos^2 \upsilon + (y_o - E_5) \sin \upsilon \cos \upsilon$$

$$D_3 = \frac{x_o}{\beta} \sin^2 \upsilon - \frac{y_o}{\beta} \sin \upsilon \cos \upsilon$$

$$D_4 = (x_o - D_5) \sin^2 \upsilon - (y_o - E_5) \sin \upsilon \cos \upsilon$$

$$D_5 = \frac{B_{f_x} + C_{f_y}}{\alpha 2 \quad \beta 2}$$

$$E_1 = \frac{\dot{x}_o}{\alpha} \sin \upsilon \cos \upsilon + \frac{\dot{y}_o}{\alpha} \sin^2 \upsilon$$

$$E_2 = (x_o - D_5) \sin \upsilon \cos \upsilon + (y_o - E_5) \sin^2 \upsilon$$

$$E_3 = \frac{-x_o}{\beta} \sin \upsilon \cos \upsilon + \frac{\dot{y}_o}{\beta} \cos^2 \upsilon$$

$$E_4 = -(x_o - D_5) \sin \upsilon \cos \upsilon + (y_o - E_5) \cos^2 \upsilon$$

$$E_5 = \frac{A_{f_y} + C_{f_x}}{\alpha 2 \quad \beta 2}$$

$$F_1 = \frac{z_o}{\beta}$$

$$F_2 = z_o - \frac{f_z}{\beta^2}$$

$$F_3 = \frac{f_z}{\beta^2}$$

These equations can be put into a somewhat more useful form by making the following small angle approximations:

$$\sin(\alpha t) = \sin\left[\left(\omega_o - \frac{K^2}{\omega}\right)t\right] = \sin\omega_o t \cos\left(\frac{K^2}{\omega}t\right) - \cos\omega_o t \sin\left(\frac{K^2 t}{\omega}\right)$$

$$\cong \sin\omega_o t - \frac{K^2 t}{\omega}\cos\omega_o t$$

$$\cos(\alpha t) \cong \cos\omega_o t + \frac{K^2 t}{\omega_o}\sin\omega_o t$$

$$\sin(\beta t) \cong \sin\omega_o t + \frac{K^2 t}{2\omega_o}\cos\omega_o t \qquad (14)$$

$$\cos(\beta t) \cong \cos\omega_o t - \frac{K^2 t}{2\omega_o}\sin\omega_o t$$

By substituting these approximations into the equation (13) and manipulating the results the following can be obtained:

$$x = x_R + \frac{t}{2}\frac{K^2}{\omega_o^2}\left[(1-3\cos^2\ )x_R - 3\sin\cos\ y_R\right]$$

$$y = y_R + \frac{t}{2}\frac{K^2}{\omega_o^2}\left[(1-3\sin^2\ )y_R - 3\sin\cos\ x_R\right] \qquad (15)$$

$$z = z_R + \frac{t}{2}\frac{K^2}{\omega_o^2}\left[\dot{z}_R\right]$$

Where, x_R, y_R and z_R are the solutions which would be obtained for unperturbed, circular motion of the SMS. That is:

$$x_R = \frac{\dot{x}_o}{\omega_o}\sin\omega_o t + (x_o - D_5)\cos\omega_o t + D_5$$

$$y_R = \frac{y_o}{\omega_o}\sin\omega_o t + (y_o - E_5)\cos\omega_o t + E_5$$

$$z_R = \frac{z_o}{\omega_o}\sin\omega_o t + (z_o - F_3)\cos\omega_o t + F_3$$

$\dot{x}_R$, $\dot{y}_R$ and $\dot{z}_R$ are the corresponding velocities.

$$x_R = x_o \cos \omega_o t - (x_o - D_5) \sin \omega_o t$$

$$y_R = y_o \cos \omega_o t - (y_o - E_5) \sin \omega_o t \qquad (17)$$

$$z_R = z_o \cos \omega_o t - (z_o - F_3) \sin \omega_o t$$

Equations (15) or (13) form a set of closed from solutions to the equations of motion. Simplifying assumptions have been made to the effect that (a) the motion takes place in the gravity field of a spherical homogeneous earth and (b) the tension in the lines connecting the SMS to the Central Observatory is constant and radial in direction. The validity of these assumptions has been justified but not limited on the basis of frequent control actions.

The motion described by Equation (15) is basically a simple harmonic motion which becomes perturbed with increasing time. The perturbation rates are small when compared to the basic precession motion required for the mapping mission (Section 5). It should be pointed out that the equations are not valid for a non-rotating antenna system. This, however, creates no problems since the perturbation forces involved in station-keeping are small compared to the control forces available.

3.0 PERTURBATION FORCES

3.1 ENVIRONMENTAL PERTURBATION FORCES

Environmental perturbation forces result, as the name implies, from the environment in which the KWOT exists. Sources producing EPF include solar radiation pressure, solar wind and atmospheric drag. An investigation was made to determine the significance of these forces. The magnitudes and directions were established. Acceleration effects on the SMS were determined and are listed in Table 3.1, along with the source and direction of the forces. The accelerations are based on a 130 lb SMS and are presented this way for ease of comparison with the gravity accelerations.

It became apparent early in the investigation that the environmental perturbation forces would be very small compared to the gravity gradient forces (Table 2-1, Section 2.0) across the antenna. Therefore this phase of the study was terminated once the gross effects had been determined.

3.2 INDUCED PERTURBATION FORCES

Induced perturbation forces result from the interaction of electrical currents associated with the antenna with the earth's magnetic field. There are three sources which may give rise to electro-magnetic perturbation forces. These sources are:

(a) currents caused by the impressed radio frequency voltages;
(b) currents induced by the motion of the antenna in the magnetic field;
(c) currents created by charges, which have accumulated on the antenna, moving in the magnetic field.

An analysis of the forces caused by the above mentioned currents is presented in Appendix A. The results, as previously suspected, show that the induced electrodynamic forces are all negligible. The magnitudes of a gross estimation of some of the forces are shown in Table 3.1.

TABLE 3-1

PERTURBATION FORCES

Source	Order of Magnitude		Direction or Effect	Reference	Comments
	Force, Newton Meter^2	Acceleration m/sec^2			
ENVIRONMENTAL					
a) Solar Radiation Pressure	9×10^{-6}	0.58×10^{-9}	Radial from sun	3	Largest EPF
b) Solar Wind	1.57×10^{-9}	0.101×10^{-12}	Radial from sun	3	
c) Atmospheric Drag	3×10^{-16}	Negligible	Opposite to velocity	3	
d) Van Allen Belt Particulate Drag	6.7×10^{-10}	Negligible	Opposite to velocity	4	
e) Solar Flares	Increase (a) and (b) 2 to 4 times		Radial from sun	3	Effects magnitude of (a) and (b)
INDUCED					
f) R.F. Currents	Negligible	Negligible	Change antenna shape	Appendix A	
g) Induced Currents	1.6×10^{-13}	Negligible	Change antenna shape	Appendix A	
h) Induced Charges	4×10^{-3} *	Negligible	Slow orbital and rotational motion	Appendix A	

*Newtons/Coul.

References:

3. Smith, R. E., "Space Environment Criteria Conditions for Use in Space Vehicle Development", NASA TM-X-53273, May 1965

4. USAF AFSC, "Space Planners Guide", July 1965.

4.0 MOTION STUDIES

4.1 MOTION CHARACTERISTICS

The primary mission of the KWOT is to provide a sky map of the radio noise emanating from galactic space. The fulfillment of this mission will require a regulated movement of the unidirectional antenna axis over the entire celestial sphere. A nominal motion, which is described subsequently, has been selected by the University of Michigan. The relation of the SMS motion to this desired mapping motion is covered in this section.

The nominal mapping motion, which is discussed more fully in section 5 and 6 consists of revolving the directional axis of the antenna about an axis perpendicular to its plane. This motion provides for mapping a great circle on the celestial sphere. Then, by precessing the spin axis, succeeding great circles can be mapped. The rotation rate will probably be about one revolution/hour, since this rate, or higher, provides a certain inherent stability for the system. Precession rates of 1/4 to 1/2 degree per hour will produce complete sky coverage approximately once per month.

Based on the nominal mapping motion and the associated antenna characteristics, certain boundaries or tolerances can be prescribed. In order to keep the antenna beam distortion below a given level, each end of the antenna system (and perhaps also the ends of the minor axis of the rhombic) must be maintained, within a certain tolerance, at fixed distances with respect to both the central observatory and each of the adjacent ends. Preliminary studies at the University of Michigan have indicated this tolerance will be about ±25 meters. The basic antenna dimension from the Central Observatory to the SMS is 5000 meters.

4.2 SMS MOTIONS

Based on the discussions of the previous paragraphs, the desired motion of each separate SMS can be described. It is, in fact, movement around a great circle situated on an imagimary sphere of 5000 meter radius whose center is located in the central observatory. Each SMS is separated from its neighbor by an angle of 90° and is moving with an angular rate of 360 deg/hr. The rotation plane will be precessing at a given rate, probably 1/4 to 1/2 deg/hr.

Furthermore, if the actual position of each SMS remains within ±25 meters of the desired position, then the actual motion will be satisfactorily close to the desired motion.

Let us first consider the SMS motion as defined by Eq. 15 of section 2, which is written here for convenience:

$$x = x_R + \frac{t}{2}\frac{K^2}{\omega_o^2}\left[(1-3\cos^2\nu)\,\dot{x}_R - 3\sin\nu\cos\nu\,\dot{y}_R\right] \qquad (4\text{-}1)$$

$$y = y_R + \frac{t}{2}\frac{K^2}{\omega_o^2}\left[(1-3\sin^2\nu)\,\dot{y}_R - 3\sin\nu\cos\nu\,\dot{x}_R\right]$$

$$z = z_R - \frac{t}{2}\frac{K^2}{\omega_o^2}\,\dot{z}_R$$

The terms x_R, y_R, and z_R represent the unperturbed motion of a point moving at constant speed on a circle around the origin of coordinates. This motion is confined to the plane in which it starts. The remaining terms on the right represent perturbations away from the circular motion. These perturbations are due to the gravity gradient across the antenna system and are functions of time, position in orbit and the circular velocity components of the unperturbed motion. The actual position of the SMS is given by the x,

y, and z coordinates, and is not confined to the original plane of motion. A plot representing the typical motion of an SMS is given in Figure 4-1, which shows the difference between the actual position and the unperturbed position as a function of time. It can be seen that the position oscillates about the unperturbed position with the frequency of the antenna rotation frequency.

The time variation of position shown in Figure 4-1 is typical of the motion in any of the three axes for any arbitrary orientation of the antenna system. The rate of increase of the amplitude of the motion is the maximum which would be experienced anywhere on either of the KWOT orbits considered. This is because the initial conditions selected for this case are those of perigee of the elliptical orbit, where the gradient (perturbation) forces are at a maximum.

Figure 4-2 depicts the same motion defined by figure 4-1, but in spatial a coordinate system to give insight into the position the SMS described as a function of time. Depicted is the uncontrolled drift at the point of perigee passage, as well as the corrected motion as it would most likely occur under active thruster control. It is interesting to note that the subsatellite would exit the control corridor under these conditions at 73 minutes from perigee, unless some correction is exercised.

The maximum rate of increase of amplitude for the motion can be estimated by dividing the maximum difference between perturbed and unperturbed motion by the time. Consider the x component from eq 4-1. The difference divided by the time is:

$$\frac{\Delta x}{t} = \frac{x-x_R}{t} = \frac{1/2\ K^2}{\omega_{2_o}} (1-3\cos^2 \nu)\ \dot{x}_R$$

$\Delta X = X - X_R$
$\Delta Z = Z - Z_R$
$\Delta Y \approx 0$
20,000/100,000 N.Mi. Elliptical Orbit
Epoch = 0

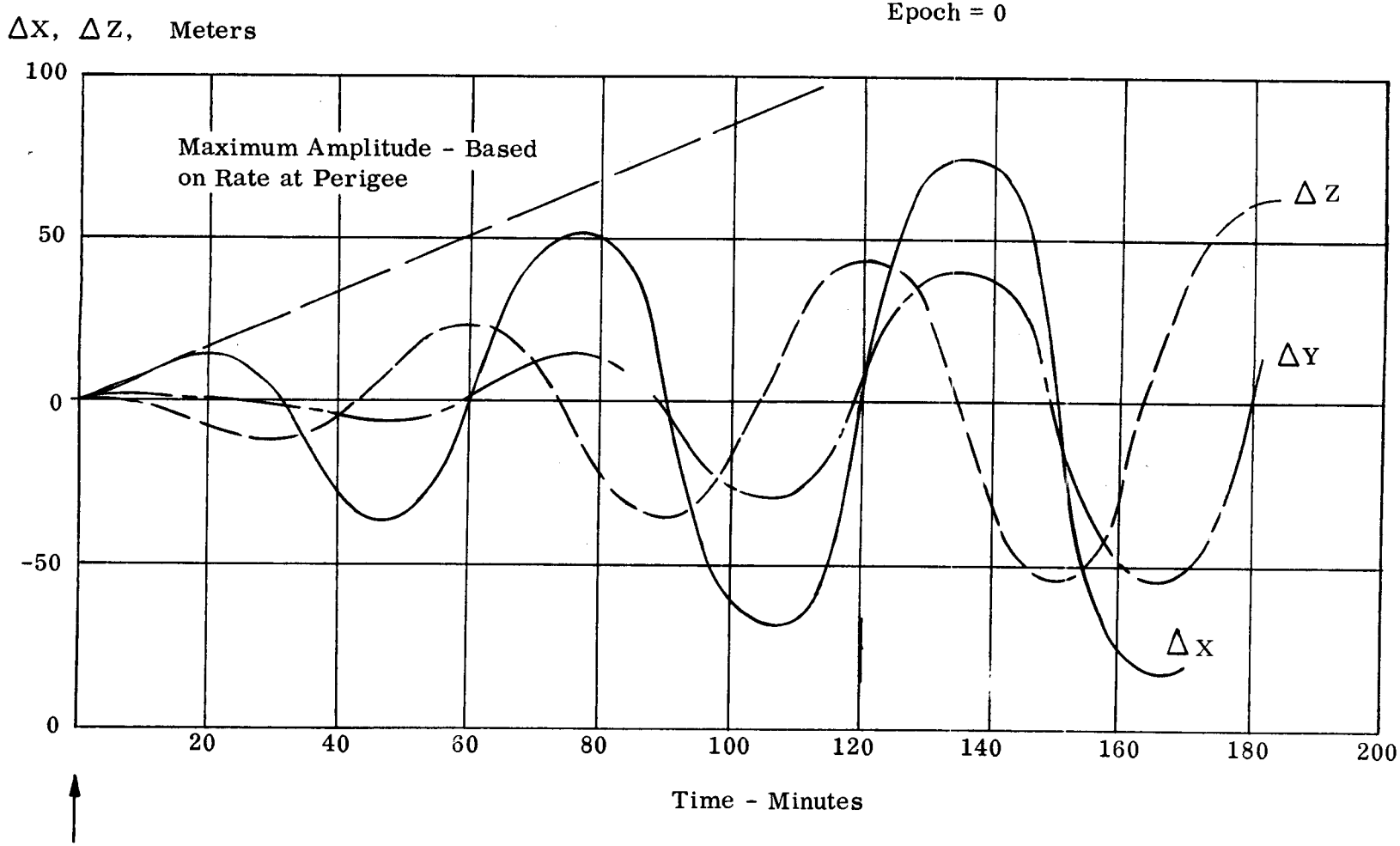

Figure 4-1. Typical Motion of a Single SMS.

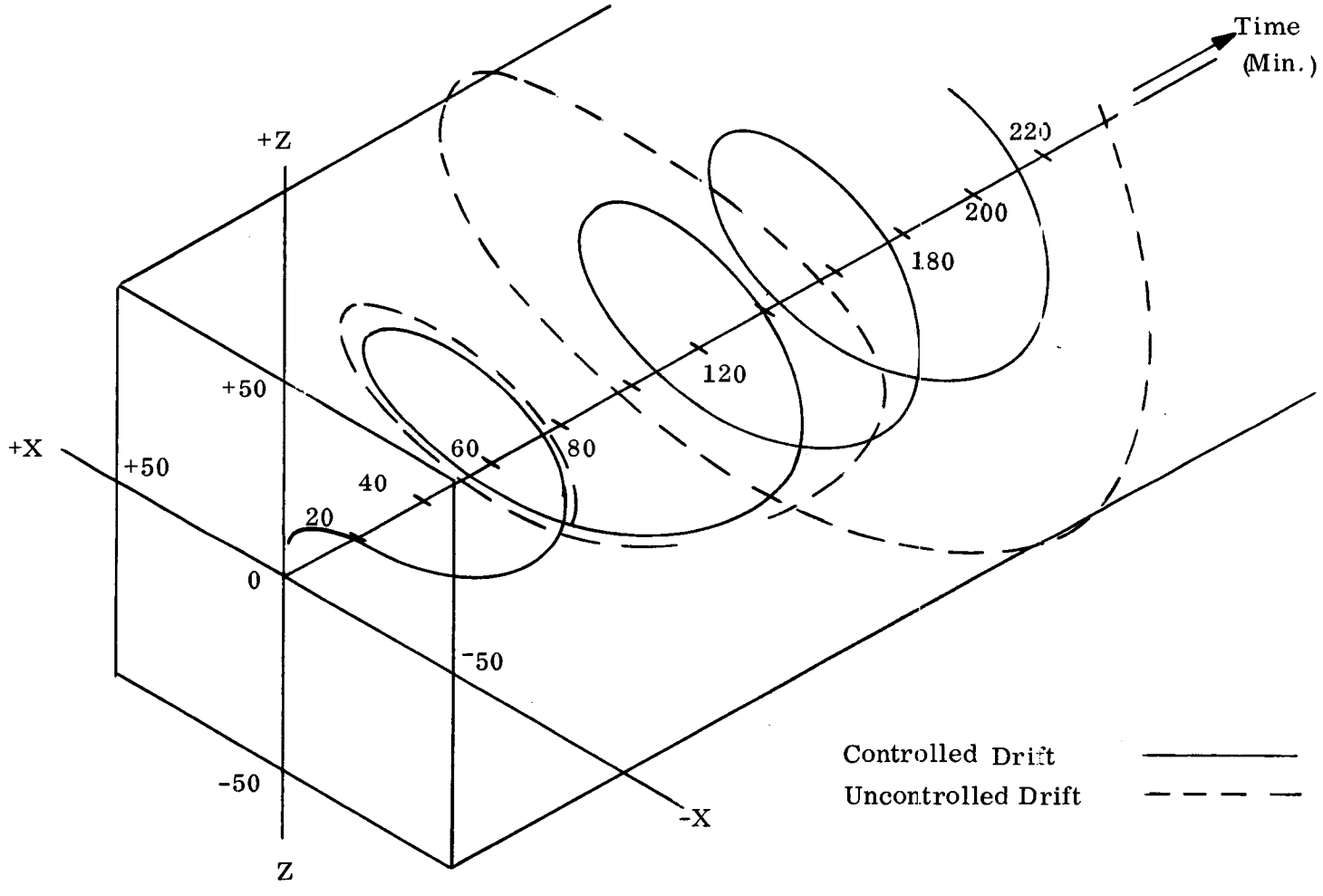

Figure 4-2. SMS Drift Due to Gravity Gradient at Perigee.

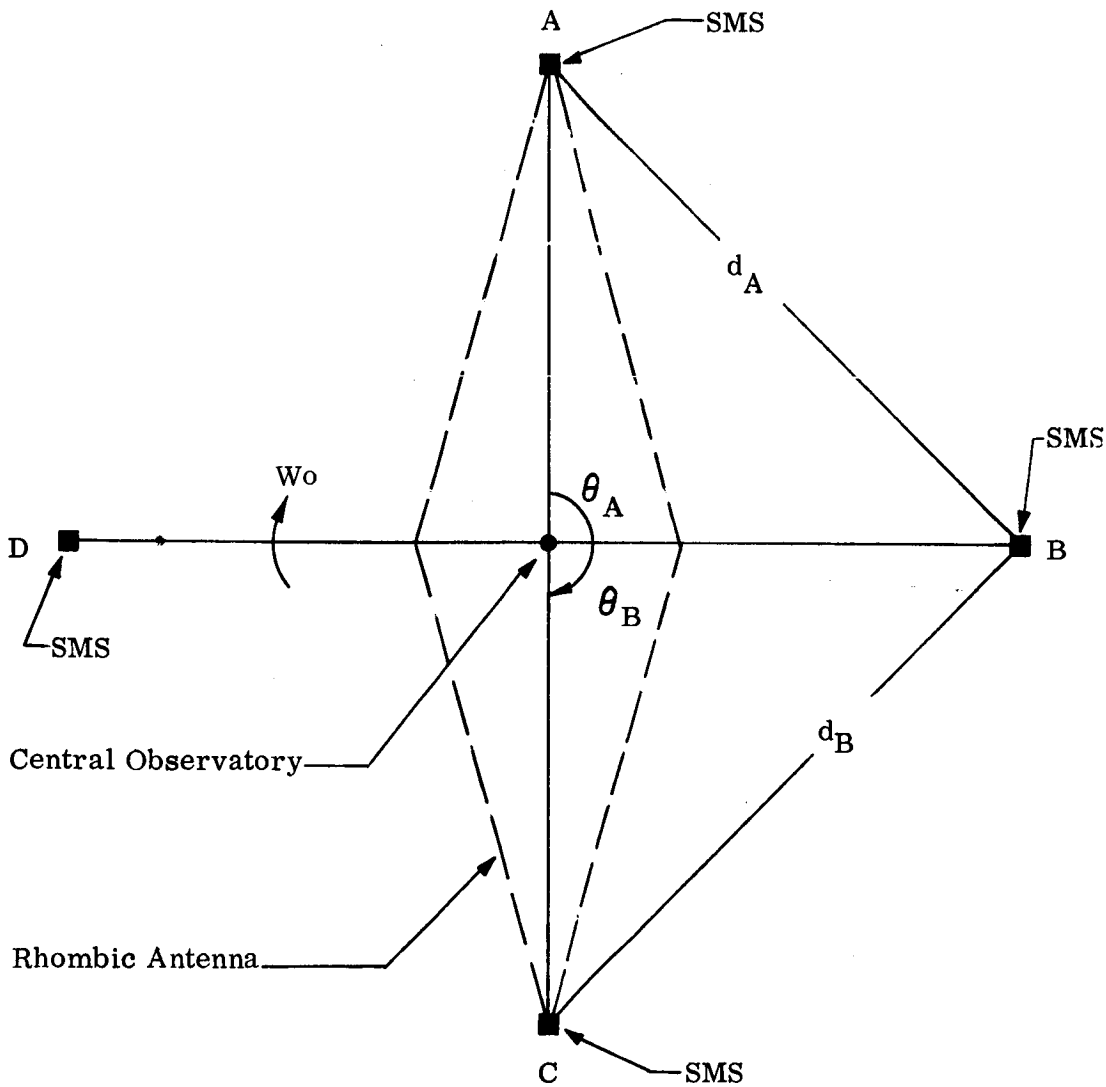

Figure 4-3. Basic KWOT Configuration

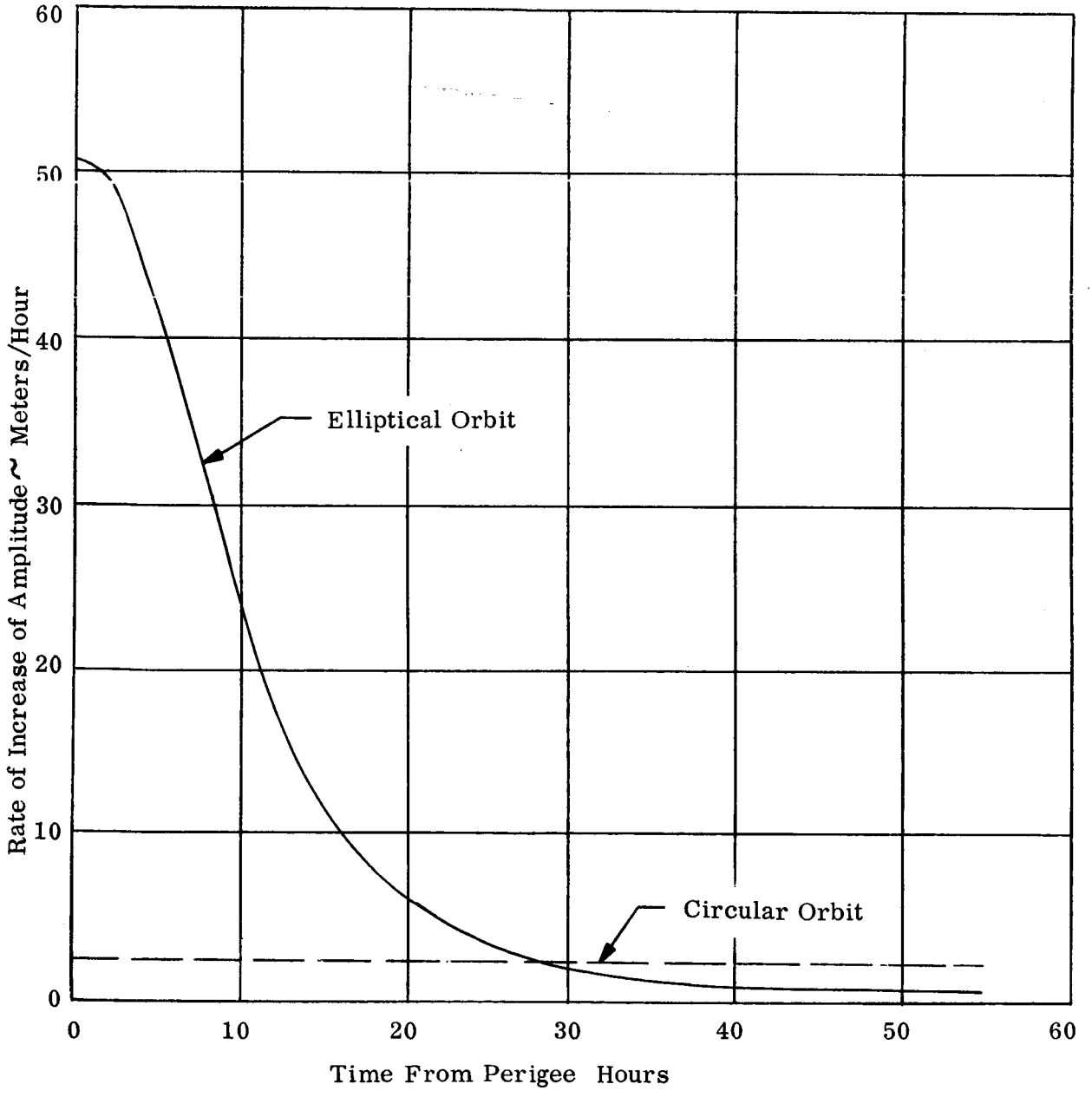

Figure 4-4. Maximum Rate of Increase of Amplitude versus Time

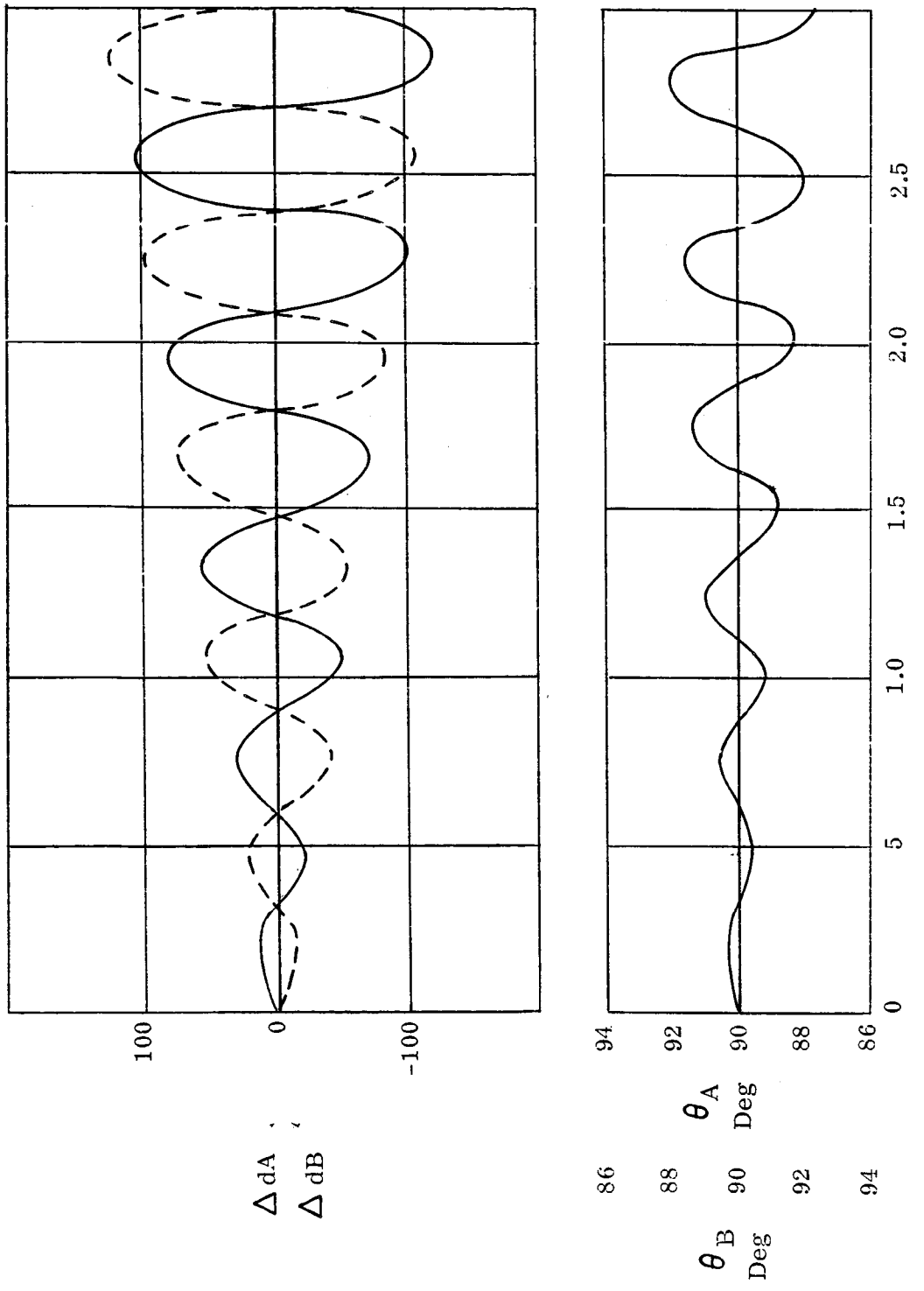

Figure 4-5. Variation of Distance and Angle Between Adjacent Ends of the KWOT Antenna.

where an initial condition of $y_R = 0$ is assumed, since

$$\left| 1-3\cos^2\nu \right| \leq 2 \text{ and } (\dot{x}_R)_{max} = \dot{x}_o = 8.76 \text{ m/sec, then} \qquad (4\text{-}3)$$

$$\frac{\Delta x}{t} \leq 4.38 \frac{K^2}{\omega_o^2}$$

Equation (3) is plotted inFigure 4-4 for both the elliptical and circular orbits. Note that this is the maximum possible rate; the actual rate of increase for any particular coordinate will vary with orbital position and antenna orientation.

Of somewhat more significance is the motion of the antenna system itself. The antenna configuration is defined by the relative positions of the four SMS's and the C.O. This is shown in Figure 4-3.

where:

A, B, C, D - Positions of the 4 SMS's

O - position of C. O.

θ_A -)<AOB

θ_B -)<BOC

d_A (d_B) = Distance between A and B (B and C)
= 7071 meters nominally.

The relative motion of four SMS's can be described by the quantities θ_A, θ_B, d_A and d_B. In addition, the planarity of the antenna can be determined by considering the respective inclinations of planes AOB and BOC.

Several cases were examined with variations in both epoch and antenna orientation. Equations 4-1 were used to described the motion of pts A, B, and C, separately. The variables d, θ , and i (inclination) can then be determined from geometrical considerations.

In general, the variation of the parameters considered was regular and well behaved. Typical variations of d_A, d_B, θ_A, and θ_B are shown in Figure 4-5. The antenna plane is initially in the x-z plane and the epoch was zero (i.e. perigee passage occurred at t = 0).

The quantities Δd_A and Δd_B which are plotted in the figure 4-3 are defined as:

$$\Delta d_A = d_A - 7071 \text{ meters}$$

$$\Delta d_B = d_B - 7071 \text{ meters} \qquad (4\text{-}4)$$

and are the differences between the perturbed and unperturbed distances between the respective subsatellites.

A number of cases were examined in addition to the one presented here, for various antenna orientation angles and epochs. From these runs four particulary significant conclusions about the antenna motion were reached. These are listed below.

1. A straight line can be placed through the central observatory and any two opposite ends (such as A and C) of the antenna. This relationship held exactly during all cases considered, up to approximately 50 hours from the initial point. This can be seen from Figure 4-4 where it is obvious that $\theta_A + \theta_B = 180°$.
2. The angular separation, θ_A (or θ_B) varies sinusoidally with an increasing amplitude and a period of 30 minutes. (See Fig. 4-4.) This indicates that the points A and B oscillate rather than having a constant motion with respect to each other.
3. The inclination angles of both planes (AOB and BOC) with respect to the original plane of motion are identical. This implies that the entire antenna remains in planar motion.

There was no significant variation in the inclination of the antenna plane with respect to the orbital plane for the cases studied, although some small angle "wobble" was present in all cases.

4. The displacement of any two SMS's from each other is of the same order of magnitude as the displacement of either SMS from its unperturbed position. This is due to the "out-of-phase" motion of any two adjacent SMS's. Thus, when Point A (for example) is at its maximum displacement from its unperturbed position, Point B is at its minimum. The variation in amplitude of Δd thus apparently has the same characteristics as shown in Figure 4-4.

4.3. SMS Motion Relationships

Thus far we have examined the non-thrusted motion of an individual SMS and the motion of the antenna as a whole. Let us next consider this motion in relation to the desired precessional motion and to the associated control required to maintain this precession rate.

First we define a quantity which to avoid confusion we will call the "drift". The drift is the absolute value of maxima of the quantity $R-R_O$ where:

$R = \sqrt{x^2 + y^2 + z^2}$ = actual SMS position

R_D = radius vector to the desired SMS position

If the precession rate were zero, then

$$R_D = \sqrt{x_R^2 + y_R^2 + z_R^2}$$

Thus the drift, for zero precession is nothing but the amplitude of the motion shown in Figure 4-1. Furthermore, the drift rate will be of the same order of magnitude as given by Figure 4-4 (maximum rate of increase of amplitude).

Typical values for drift as shown in Figure 4-6 for four different sets of initial conditions. Three of the cases start at perigee (epoch = 0) and one starts 3- hours after perigee passage. The orientations of the plane of the antennas are shown in Figure 4-7. Also shown on this curve is the 25 meter boundary discussed previously.

Several important results which are significant in the design of the control system can be seen in Figure 4-5, even though the precession rates are zero.

The curve for i = 90°, epoch = 0, shows that within one-half hour the SMS will have drifted to the edge of the control region (i.e. the 25 meters boundary). Thus control actions will be required about every half hour to maintain the SMS within the boundaries in this period. However, some 12 hours later the drift rate, which is measured by the slope of the curve, has fallen to near zero. This implies two significant items, the first is that active control is required for at least a small portion of this orbit for stabilization, and the second is that there will be long periods, probably several hours, between required control actions over the vast portion of the orbit. It may also be inferred that for a 60,000 n mi circular orbit control actions would most likely not be required for keeping the antenna within the 50 meter boundary. The other two curves which start at perigee have the same characteristics but in both cases the drift rates reduce in a shorter period of time.

The fourth case, in which the KWOT is approaching apogee (epoch = 30 hours), shows a significant reduction in the control action. Extrapolation indicates a period of about 30 hours between firings. This result is not unexpected, since the gradient forces are appreciably less near apogee.

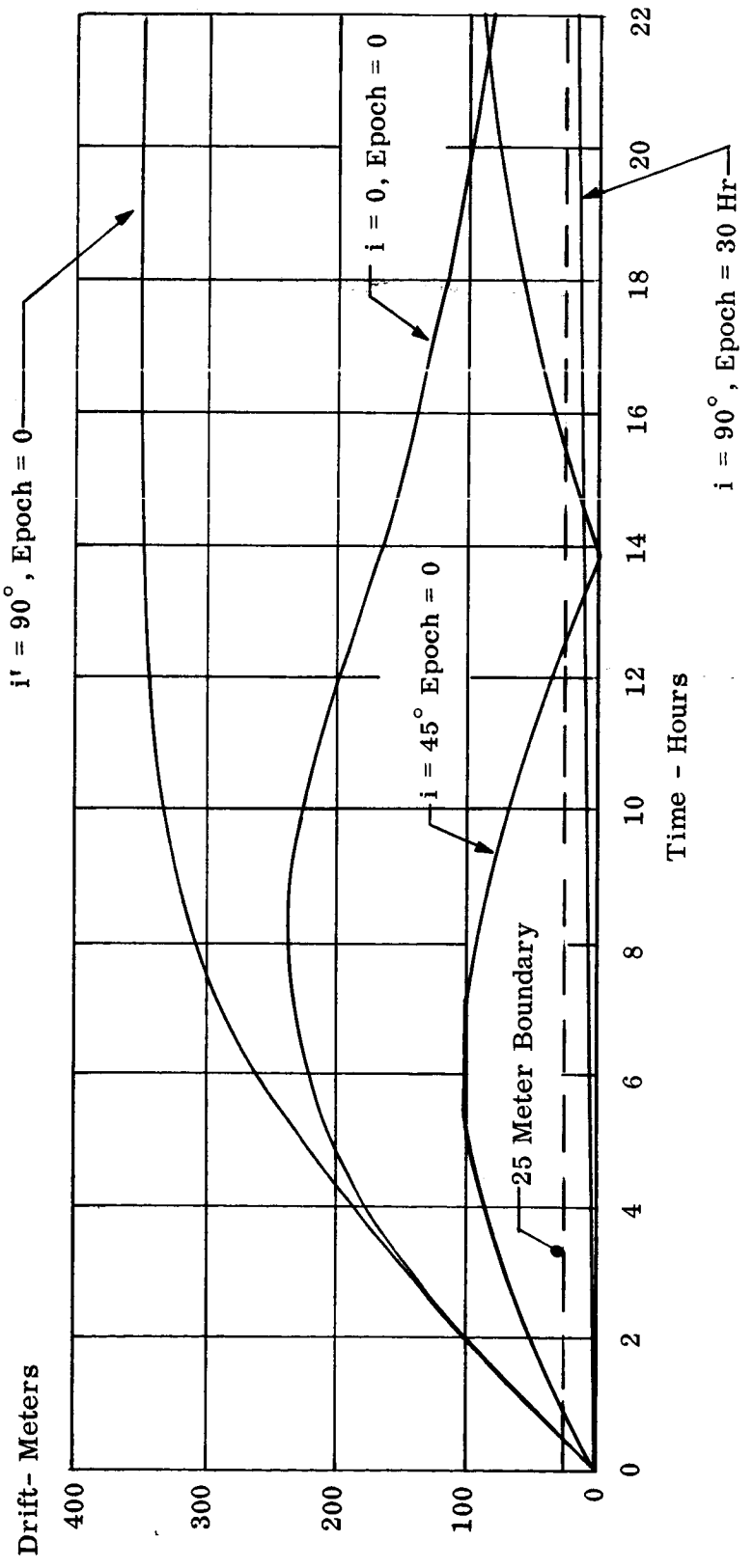

Figure 4-6. Typical KWOT Drift versus Time

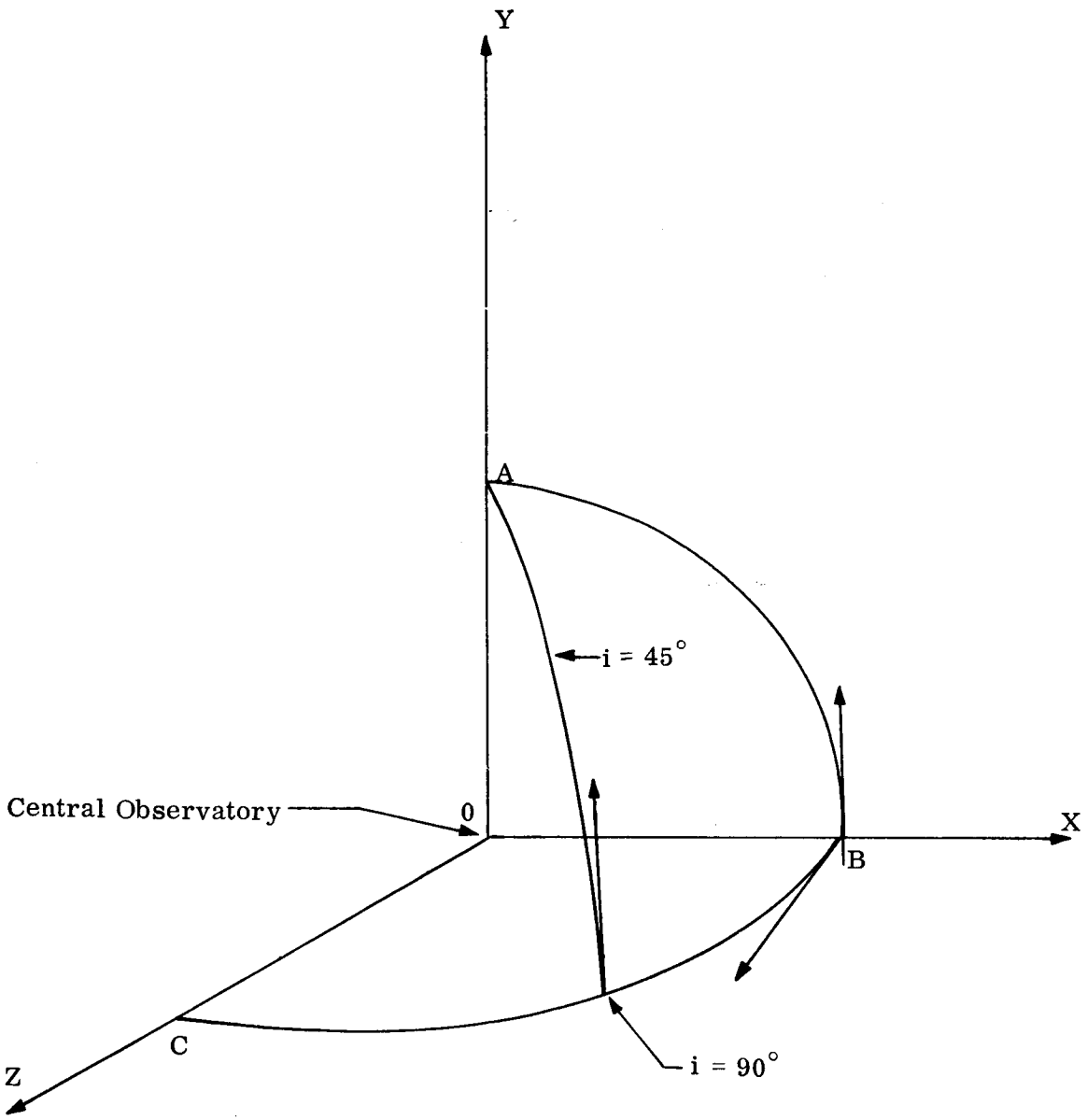

Figure 4-7. Sketch of Antenna Orientation

The effects caused by precession can be treated in a manner analogous to the perturbation effects. Consider the SMS in unperturbed position in the x-z plane (Figure 4-8). If the point, B, represents the desired position after some precession, i, has occurred, we can obtain expressions for the difference between A and B as a function of time.

We have for the unperturbed motion, point A:

$$x_R = r \cos \omega t$$

$$y_R = 0$$

$$z_R = r \sin \omega t$$

for the motion of the point P, we can write:

$$x_P = r \cos \omega t$$

$$y_P = r \sin \omega t \sin \delta_P$$

$$z_P = r \sin \omega t \cos \delta_P$$

The difference then is:

$$d = \sqrt{(x_P - x_R)^2 + (y_P - y_R)^2 + (z_P - z_R)^2}$$

$$d = \sqrt{0 + r^2 \sin^2 \omega t \left[\sin^2 \delta_P + \cos^2 \delta_P - 2 \cos \delta_P + 1 \right]} \qquad (4\text{-}7)$$

$$d = r \sin \omega t \sqrt{2(1 - \cos \delta_P)}$$

Using the half-angle relationship we have:

$$d = 2 r \sin \omega t \sin \left(\frac{\delta}{2} P\right) \qquad (4\text{-}8)$$

Equation 4-8 represents the distance between two points, one corresponds to the unperturbed motion and the other to the precessed motion and is sinusoidal in nature with an amplitude given by $\left[(2 r \sin \left(\frac{\delta}{2} P\right) \right]$. The rate of increase of this amplitude, for small δ_P (δ_P will always be small since the SMS is controlled to follow the control

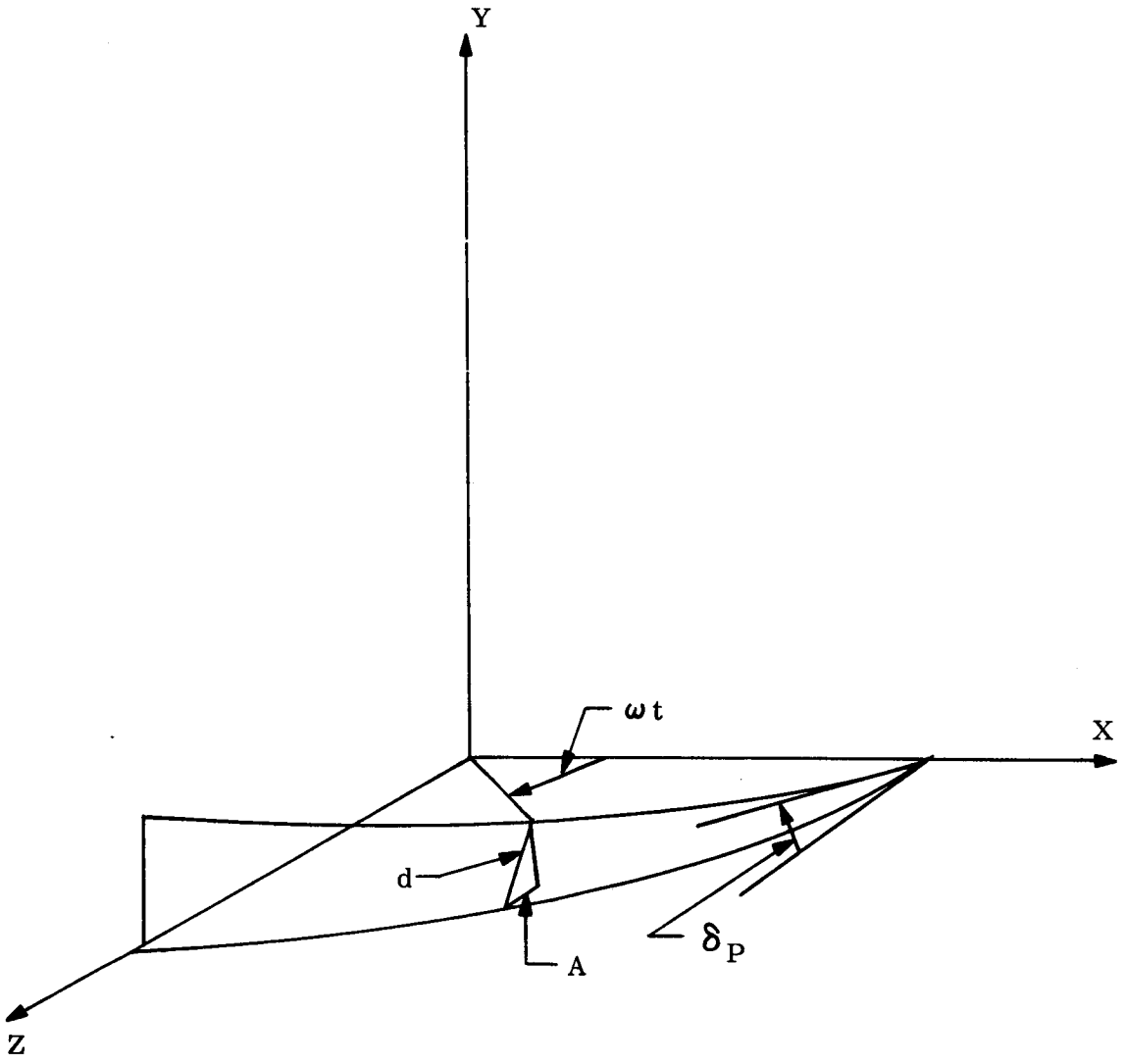

Figure 4-8. Schematic of SMS Precession

region) can be found as:

$$\frac{d\,(d)}{dt}\ (2\ r\ \sin\ \frac{\delta}{2}\ P)\ =\ r\ \frac{\dot{\delta}}{P}$$

For typical values of the precession rate, the rate increase of amplitude is:

Precession Rate	Rate of Amplitude Increase
1/4 deg/hr	43.6 meters/hr
1/2 deg/hr	21.8 meters/hr

Comparing, for example, the 1/2 deg/hr rates with the data of Figure 4-1 we can see that the precessional effects will be of the same order of magnitude as the perturbations rates at perigee, but will be many times larger than the perturbation effects at apogee (in fact, over a large portion of the KWOT orbit).

4.4. SUMMATION OF SMS MOTION

In this section we have considered the unpowered motion of a single SMS and the relative motions of the four subsatellites making up the KWOT antenna. We have shown that the motion in both cases is regular and well behaved.

It has also been shown that, in order to maintain the SMS within a 50 meter control region active control will be required. The frequency of control action will be a function of (a) the size of the perturbation forces, which depend on the KWOT orbit and the position in that orbit, and (b) the precession rate required for mapping the celestial sphere. The period between control actions will be a minimum near perigee, at which point they will be from one-half to one hour for a 25 meter boundary. Over a large part of the orbit, however, the precession rates will determine the period of the control actions.

It has been assumed in these studies that there are no connections between the subsatellites. One possible effect of connections would be to reduce the amplitude of the displacements between the antenna ends to less than the 25 meter boundary, which possibly

could affect a savings in Δ V for the case of zero precession. There would be little effect on the Δ V at the higher precession rates, however, since the corrections could be incorporated with that required for precession.

5.0 PRECESSION AND SKY COVERAGE

The immediate function of the KWOT is to provide a reliable map of the celestial sphere. As a consequence, this requires complete coverage of the sky at least once, and preferably several times for a reliable map. It may be desirable to have both complete and uniform coverage on a continuous basis, with selective observation gained only at time of successive passage.

In order to assess the magnitude of the problem, several alternative techniques are described in this section. All are consistent with the assumption that the entire system is being rotated at a nominal one revolution per hour. At any instant, one end of the rhombic antenna observes a $1/2^{\circ}$ wide cone whose axis is colinear with the major axis of the rhombus. It may be assumed that this cone will sweep out the entire sky 24 times per year. This results from 24, 180° rotations of the antenna. However, since the antenna is double ended, a 180° rotation completes a 360° circular coverage. In order to plan for an efficient and orderly sweep, it is first of all necessary to determine what the natural motions of the system will be. These natural motions are of three types: precession of the orbit, precession of the spin axis, and relative motion within the system. It is anticipated that these natural motions can be augmented by the expenditure of fuel to obtain any desired motion.

It was assumed for this element of the study that the combination of the spider web tension due to the spin motion and the stationkeeping activities of the individual RMU type vehicles will inhibit relative motion within the system and permit it to be treated as a rigid body.

5.1 PRECESSION

Due to the large diameter of the orbit, the usual perturbations due to Earth's oblateness are negligibly small. The nodal regression being 0.724 cos i deg/yr, and the advance of perigee 0.362 ($5 \cos^2 i - 1$) deg/yr. This latter term would, at its tangent point, (i.e., in equatorial orbit, 1.44 deg/yr) be only half that of the lowest planetary perturbance. The effect of other planetary bodies, noteably the sun and the moon, however, must be considered. Assuming, for convenience, an equatorial orbit, it was found that: the nodal regression rate about an axis perpendicular to the ecliptic due to solar attraction is approximately 3° per year. The nodal regression rates due to lunar attraction varies from about 15° per year at conjunction to about 3° per year at opposition with a value of nearly 7° per year under average conditions. The figures would increase less than 10% if the orbits were aligned with the ecliptic or the lunar orbit plane respectively, and decrease to zero for orbits passing through the ecliptic or lunar orbit pole. The rate of advance of the apsidal line due to solar and lunar perturbations would be double all of the values given for nodal regression, however, for circular orbits this would not be of great practical importance. The radial perturbations of the system would amount to as much as 12,000 feet due to the moon alone, and about 50% more due to sun and moon combined. The differential effect of this perturbation over a 10 km. distance from one side of the system to the other would tend to cause relative motions of not more than 25 to 30 feet. None of the above described motions are sufficient to be significantly useful, however, they are in general large enough that they must be considered a small non-negligible quantity in final system design.

Up to this point no mention has been made of the spacial orientation of the orbit. Although the precessional motions of the orbit will depend on its orientation, no compelling reasons are apparent for preferring any particular position. It is obvious that if the system is in an approximately ecliptic orbit, lunar conjunctions and oppositions will occur every six days, whereas if the orbit passes near the ecliptic pole, conjunctions and oppositions will occur on a semimonthly cycle. Similarly, but less important, the solar constellations will be influenced by orbit orientation. Further consideration should be given to the establishment of the desired orientation, and if the above becomes significant, then the desired solution should be correlated with the system booster sizing.

5.2 SKY COVERAGE

It is of interest to examine the various modes of sky coverage available through programming various precession modes, and the fuel (Δ V) requirements to achieve this precession. The results are, of course, independent of the spacial orientation of the orbit.

In order to facilitate discussion of the precessional motions, a coordinate system will be used for the plane of the antenna system similar to that used for an orbit. Let i' be the inclination angle between the system plane and an inertially fixed reference plane passing through the center of mass of the central observatory, and let Ω' be the angle to the line of nodes of these two planes from an inertially fixed reference direction. It is convenient to let the reference plane be parallel to the equatorial plane and let $\Omega' = 0°$.

In order to acquire a basic notion of sky coverage patterns and how they are affected by precession rates and initial conditions, a number of approaches were examined, and the results shown in the first four columns of Table 5-1. Since the unit of time during which it is assumed to provide complete sky coverage is fixed, precession rates can be more meaningfully represented as angular displacements, swept through during that time interval. For ease of analysis it will be assumed that actual precession occurs almost impulsively once each rotation of the antenna system (once per hour) rather than continuously, although it has not yet been determined which method will be used in actual practice. Thus, in the analysis, each rotation of the system may be considered as a great circle.

The accompanying sketches, Figures 5-1 to 5-4, illustrate the sky coverage patterns formed by those of the precession programs listed in Table 5-1, which give complete sky coverage. In each case, the "front view" is looking edge on at the reference plane from the reference direction. The initial node angle is zero. Positive precession of the node therefore proceeds from the center of the diagram counterclockwise toward the right. The "top view" is looking down on the reference plane with the reference direction pointing down the page. All zero inclination circles therefore appear as circles, regardless of node. In figure 5-1, top view, and figure 5-3, front view, the latter half of the coverage circles have been omitted because they require a reversal of the visible and hidden lines shown in the first half.

Since the area of the celestial sphere equals 4π steradians, whereas the antenna beam sweeps out $1/2^\circ \times 360^\circ = 0.0549$ steradians per revolution of 40 steradians per 1/24 of a year, assuming one revolution per hour, it is apparent that the sky will

TABLE 5-1

SKY COVERAGE

Rate of Incl. Change	Node Change	Initial Incl.	Sky Coverage		fps/ year/ SMS
$\Delta i'$	$\Delta\Omega'$	i'		$\Delta i'$ $\Delta\Omega'$	Δ V,fps
±180°	0°	any	complete, minimum uniformity	180°	1087
0°	±180°	±90°	complete, minimum uniformity	180°	1087
0°	±180°	0°	one great circle only	180°	0
0°	±180°	$-90° < \zeta' < 90°$	incomplete	-	-
±90°	±90°	any	incomplete	-	-
±90°	±180°	any	incomplete	-	-
±180°	±90°	±90°	incomplete	-	-
±180°	±90°	0°	complete	270°	1228
±180°	±180°	any	complete	360°	1390
±180°	±360°	0°	complete	540°	1817

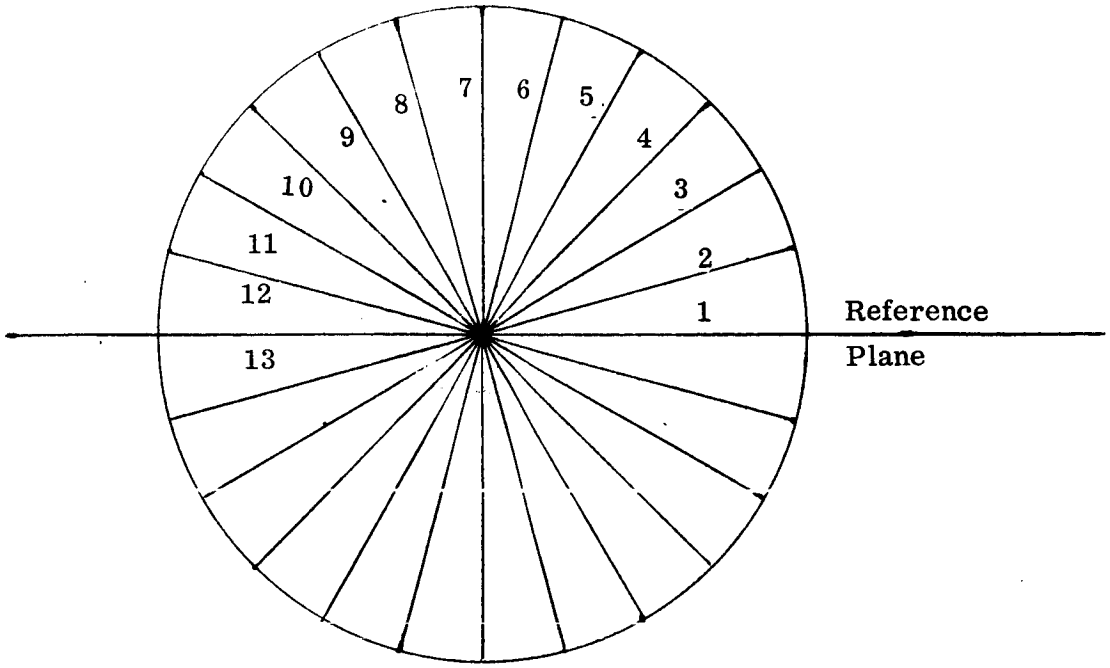

Front View

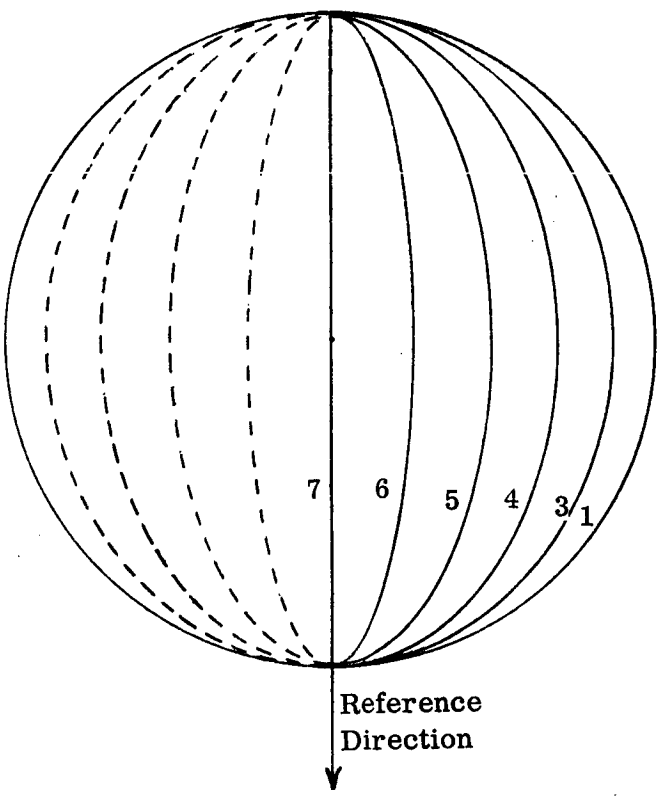

Top View

Figure 5-1. Sky Coverage Pattern Due to $\Delta\ '= 180°$, $\Delta\Omega' = 0^c$, $i_o' = 0°$ (also Due to $\Delta i' = 0°$, $\Delta\Omega' = 180°$, $i_o' = 90°$ if Front View and Top View are Interchanged and References Altered)

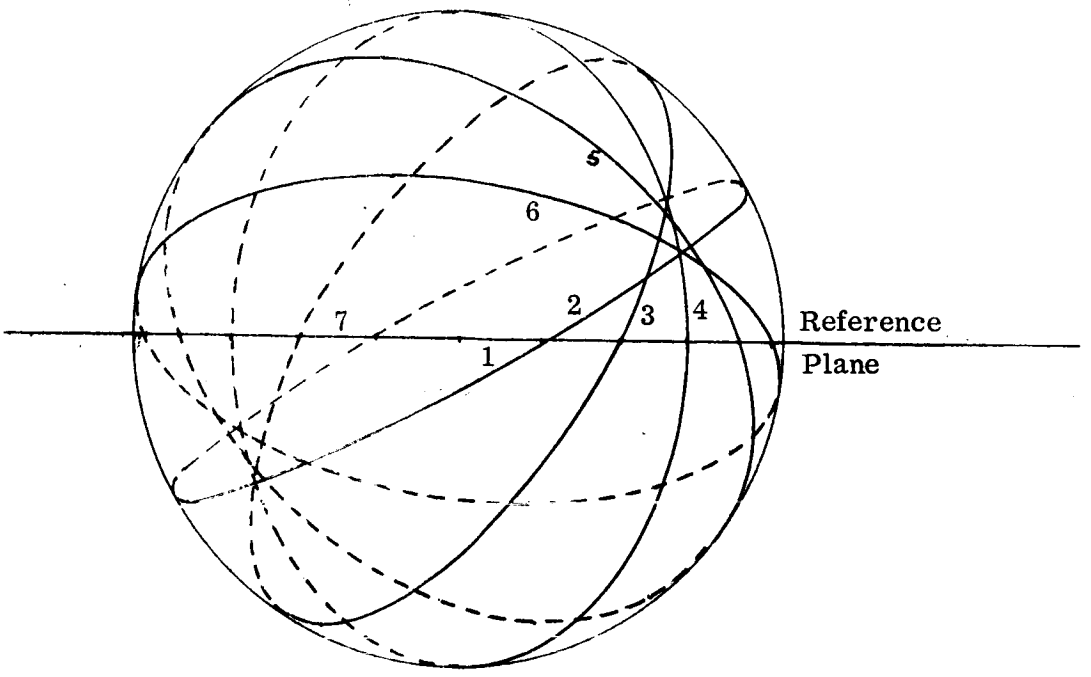

Front View

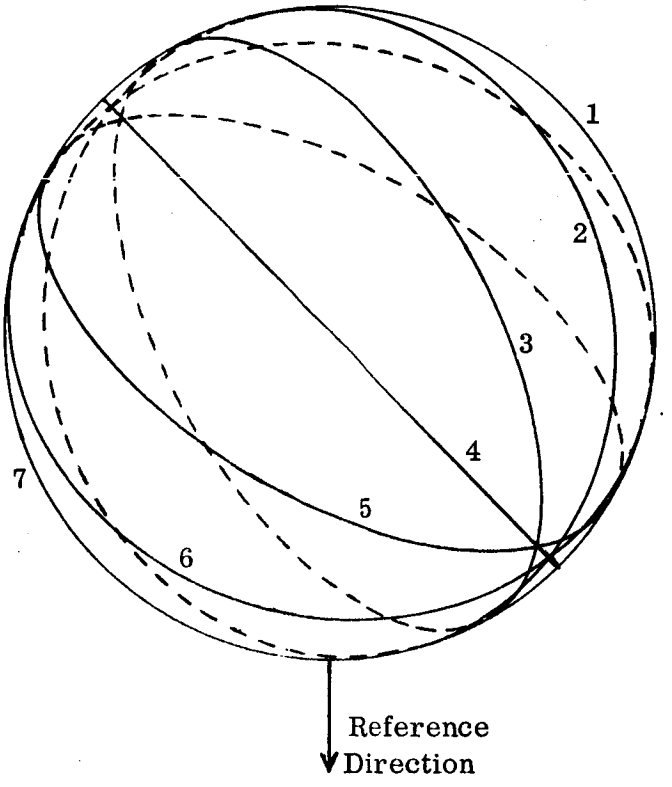

Top View

Figure 5-2. Sky Coverage Pattern Due to $\Delta i' = 180°$, $\Delta \Omega' = 90°$, $i_o' = 0°$

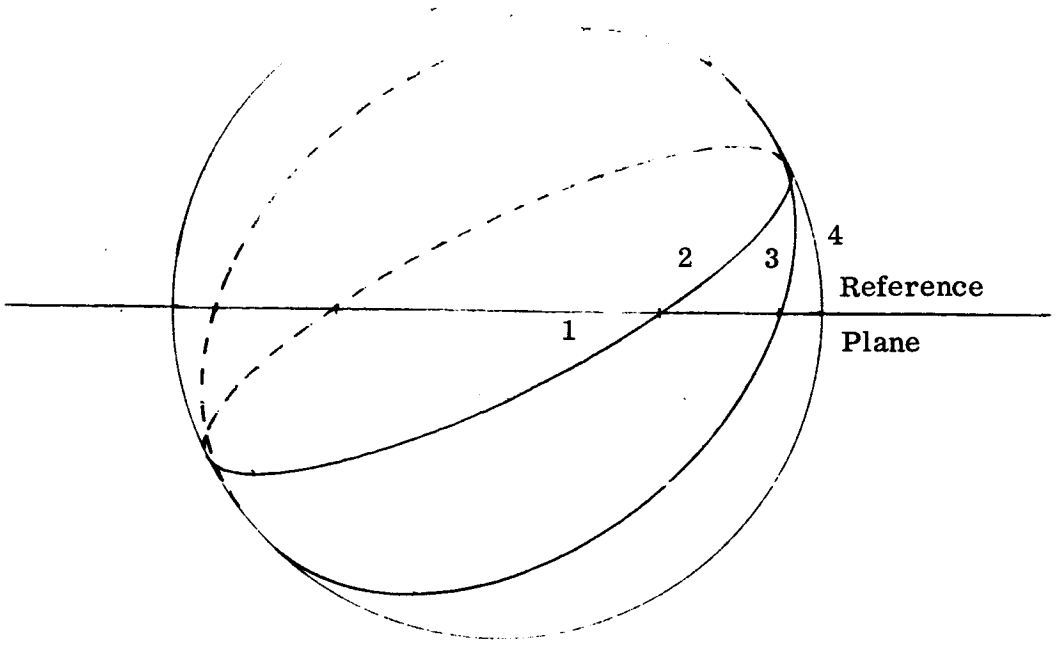

Front View

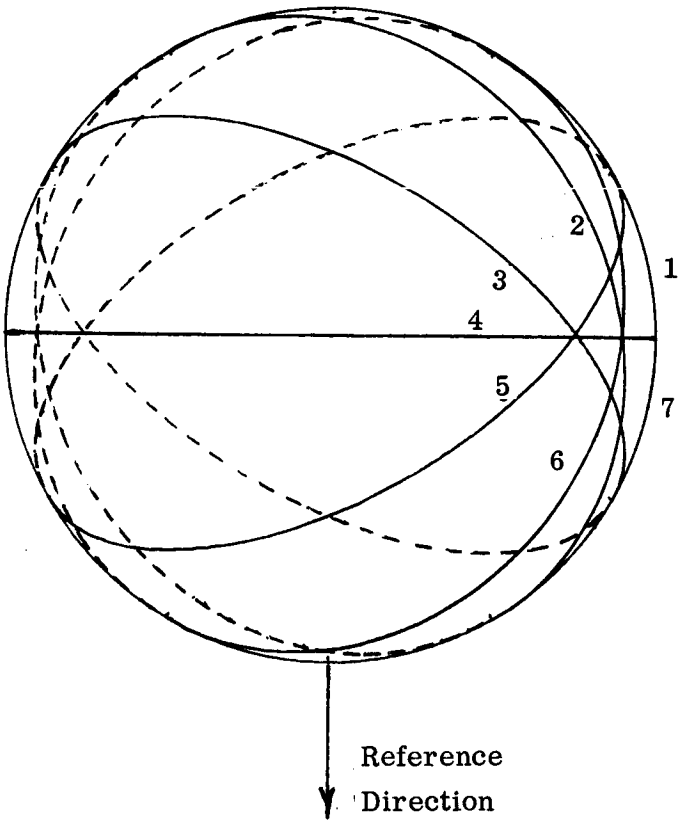

Top View

Figure 5-3. Sky Coverage Pattern Due to $\Delta i' = 180°$, $\Delta\Omega' = 180°$, $i_o' = 0°$

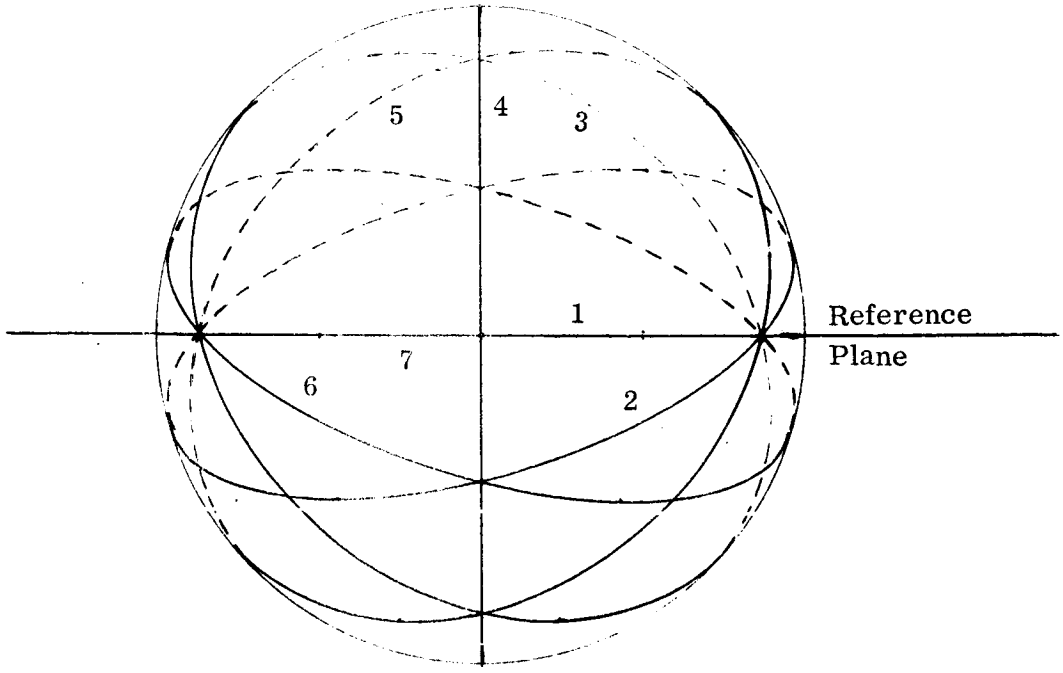

Front View

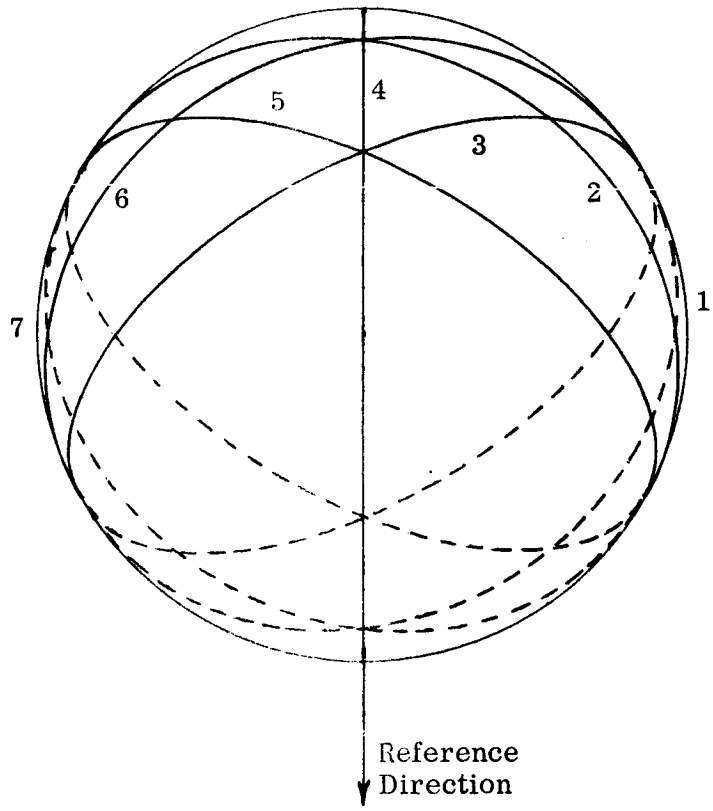

Top View

Figure 5-4. Sky Coverage Pattern Due to $\Delta i' = 180°$, $\Delta\Omega' = 360°$, $i_o' = 0°$

necessarily be overcovered by an average factor of 3.18. In order for this overcoverage to be distributed uniformly, the spin axis precession technique chosen must provide an overlap pattern wherein most of the areas are three layers of coverage thick and about one-fifth of them are four layers thick. Now it is obvious that very low precession rates (180° or less per month, see Table 5-1) will tend to cause successive strips of sky covered by successive rotations of the antenna to have a high degree of overlap and therefore build up far more than four layers in some areas. Since the average coverage must be 3.18 layers, an overabundance in one area will necessarily lead to a shortage elsewhere. It should be noted that completeness of coverage is not in question as long as at least one layer of coverage is provided in every area. This line of reasoning seems to indicate that as the inclination and nodal precession rates are increased from very low values, the sky coverage becomes more uniform, up to a point. Once precession rates are reached at which most of the sky is covered either three or four times, further increases may possibly upset the balance and actually decrease the uniformity.

The progressive buildup of a high degree of overcoverage in one area at the expense of other areas can be visualized as follows. Consider two successive strips of sky covered by successive rotations of the system. If the overlap is not continuous along their entire length, the intersection of these two strips forms a pair of rhombi with centroids on the line of nodes of the two antenna system planes. If the overlap is continuous these two "centroids" still retain their significance as the points where the instantaneous probability of overlap by succeeding strips is highest. If the precession rates are low, such that the inclination and node are displaced by perhaps one-half

revolution during the month, the centroids of all of the intersection areas will tend to lie in a restricted zone on the celestial sphere. This zone is clearly a region of excessive sky coverage at the expense of the rest of the celestial sphere where no centroids appear. Note again that the absence of centroids does not signify absence of coverage nor even absence of multiple coverage, but only an absence of a local maximum of coverage. It would appear that more uniform coverage could be obtained if the centroids were more uniformly distributed over the entire celestial sphere. This seems to require relatively high precession rates. Thus we are led to the same conclusion as before, namely, that increased uniformity requires higher precession rates than those considered in Table 5-1.

Note that if these higher precession rates are used, the sky can no longer be covered sequentially by strips which are either overlapping or adjacent to each other. Rather, the broad distribution of overlap areas sought, requires a relatively large displacement between successive strips which in turn require nonsequential coverage. For example, if a 720° displacement of one of the variables were to be used, perhaps alternate $1/2^\circ$ strips would be covered during the first half of the month and the in-between strips picked up during the second half.

If our reasoning thus far is valid, two consequences ensue. First of all, since higher precession rates require higher torque, therefore more thrust or ΔV, it follows that uniformity of sky coverage costs fuel. Second, the complex sequencing of covered sky strips that necessarily accompanies high precession rates may cause considerable increase in the complexity of data reduction.

It should be noted that it is possible to achieve a quasi-uniformity without recourse to high precession rates. This would involve accepting the relatively low uniformity associated with low precession rates during any 1/24 year period, but arranging for the high coverage areas to vary from period to period such that by the end of a year, a long term uniformity has been achieved.

The quantity of fuel required to produce these precession rates may be determined by use of the standard gyroscope equation, see figure 5-5.

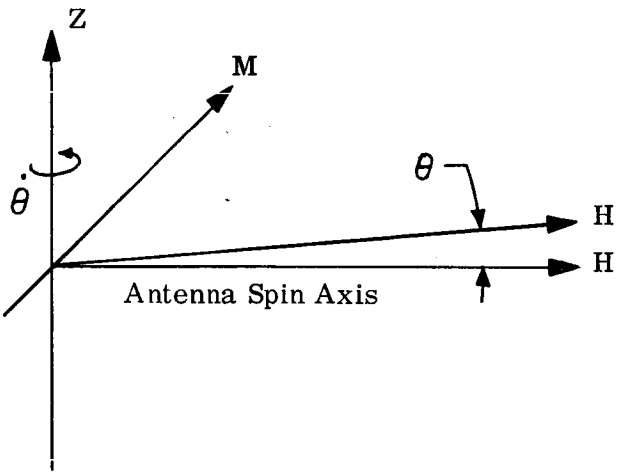

Figure 5-5

The angular momentum of the rotating antenna system

$$H = I\omega$$

where I is the polar moment of inertia and ω is the rotation rate. The torque available to precess the spin axis about the Z axis

$$M = Tr$$

where T is the combined thrust of two of the RMU type vehicles acting at a distance r equal to the radius of the antenna system from the Z axis. Since

$$M = \frac{d\ H}{d\ T}$$

$$Tr = I\omega\dot{\theta} \qquad (1)$$

where $\dot{\theta}$ is the precession rate, which has a component about the line of nodes equal to i' and a component about the line of antinodes equal to $\dot{\Omega}$ sin i. Thus

$$\dot{\theta} = \sqrt{(i')^2 + (\dot{\Omega}' \sin (i_o' + i' t))^2} \qquad (2)$$

where i_o' is the initial inclination.

The fuel requirements, expressed in terms of velocity capability of each RMU vehicle is

$$\Delta V = \int_o^t \frac{T}{4\ m}\ d\ t$$

where m is the mass of one RMU vehicle. Substituting equation (1) and expressing I as $4mr^2 + C$, where C is the polar moment of inertia of the spider web along we obtain:

$$\Delta V = r\omega \int_o^t (1 + \frac{C}{4mr^2})\ \dot{\theta}\ d\ t \qquad (3)$$

It should be pointed out that this C is a small, however non-negligible quantity. Should the mass of the antenna web grow this could become more significant. Note that the first term in equation (3), which represents the four RMU vehicles only, is independent of mass or specific impulse, reflecting the fact that mass changes cause proportionate changes in moment of inertia. The second term, however, is sensitive to mass and therefore specific impulse. Assuming that a one year supply of fuel is carried and that the same 30 day spin axis precession program is repeated 12 times, the quantity of fuel consumed each month will decrease but the monthly ΔV will remain constant, based on the first term only. If the second term is considered, the ΔV varies from month to month as fuel is consumed, as a function of specific impulse.

For typical values of specific impulse and precession rates shown in Table 5-1, the contribution of the second term of equation (3) is only a few percent. For higher precession rates it is still less. At this stage of the analysis the increased accuracy is hardly warranted, therefore only the first term will be used. The ΔV's associated with each of the spin axis precession programs shown in Table 5-1 that result in complete sky coverage have been computed and are shown in Table 5-1. Note first of all, that the fuel requirements do indeed increase with increasing precession rate as predicted and further that there appears to be a correlation between ΔV and $\Delta i' + \Delta \Omega'$. This correlation is not general but exists only due to the way in which the programs were selected.

Referring to equation (2) and recalling that the rates $\dot{i}'$ and $\dot{\Omega}'$ are assumed constant and therefore are linearly proportional to the angular displacements, it can be seen that if i_o' and the angular displacements are chosen so as to take advantage of the symmetry of $K^2 \sin^2 i$, the correlation will appear.

In conclusion, a number of techniques are feasible for obtaining complete sky coverage. The control of the degree of overlap through control of Δi and $\Delta \Omega$ imposes varying ΔV expenditures increasing with the increasing area of overlap. It therefore remains to examine the coverage techniques from the viewpoint of the astronomical objectives and the gathering of the radio source information.

6.0 STABILIZATION AND CONTROL

6.1 INTRODUCTION

The control problem consists of positioning the four subsatellites relative to the Central Observatory in such a manner that the five-mass-system corresponds closely to the desired system configuration and orientation. Control requirements, as they apply to station keeping of a subsatellite (SMS) operating under nominal environmental conditions and for a nominal antenna precession rate are estimated. The feasibility of a satisfactory SMS control system is demonstrated by showing one possible control concept to be basically workable. The control requirements associated with initial system deployment, large angle system reorientation, and possible short duration large magnitude disturbances are not considered here.

6.2 DESCRIPTION OF THE EXAMPLE CONTROL CONCEPT

In the selected system, the Central Observatory monitors, evaluates, and commands specific changes in the "state" of the four SMS vehicles--the "state" of the SMS, as used here, is that collection of variable and parameter values required to describe correctly the SMS's position and motion with respect to the Central Observatory. Figure 6-1 illustrates and defines the coordinates and the various symbols used in the following.

6.2.1 Control Equipment

The Central Observatory is equipped with the necessary sensing and computing devices to generate signals proportional to the position and rate in the three translations and the three attitudes of the SMS relative to the Central Observatory.

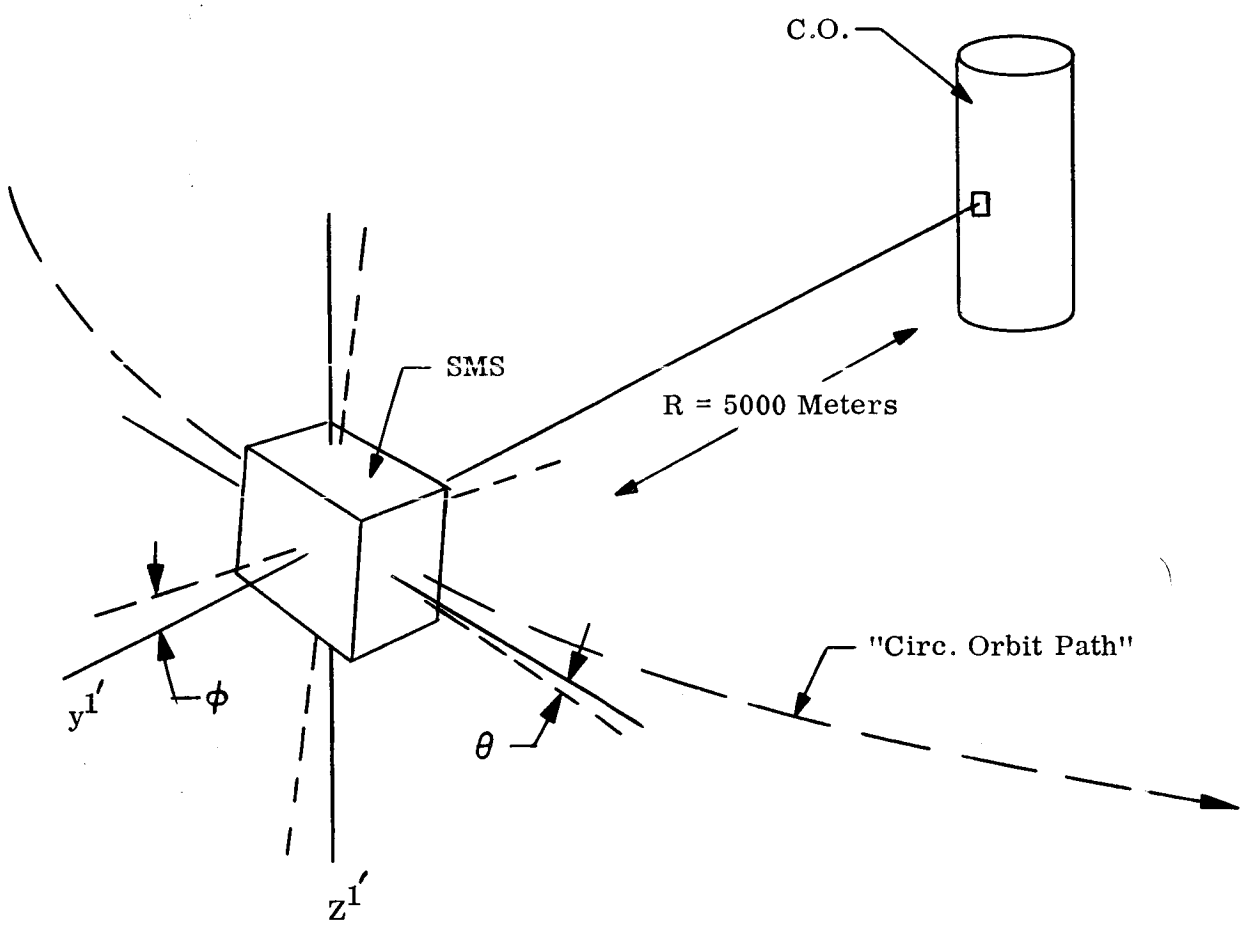

$y \cong \pm \Delta_R$ = Radial Error Velocity

$x \cong V_T \pm \Delta V_T$ = Tangential Velocity

$|\theta| \leq \phi_{D.B.}$ = Attitude Dead Band

$|\phi| \leq \phi_{D.B.}$ = Attitude Dead Band

Figure 6-1. Simplified Schematic of SMS – Central Observatory Relationship and Central Observatory Oriented Coordinate System

The system equipment aboard the Central Observatory and each SMS:

6.2.1.1 Central Observatory

(a) Radar and antenna - for ranging along the Y' axis and for determining rotations about the X' and Z' axis.

(b) Star Tracker (Also required by the navigation and guidance system) - for measuring position of the SMS along the X' and Z' axes, and for measuring rotation about the Y' axis.

(c) Computer (also required by the navigation and guidance system) - for computing the desired position of the SMS and for processing measured data and issuing translational and rotational commands to the SMS.

(d) Communication Link - for receiving measured data and for transmitting commands.

6.2.1.2 Small Manuevering Subsatellite

(a) Interferometer and radar receiver - used in conjunction with Item 1 of the Central Observatory's equipment.

(b) Rate gyros - used for stabilization of the SMS attitude loop.

(c) Beacon Lights - used in conjunction with item 2 of Central Observatory's equipment.

(d) Communication Link - used in conjunction with item 4 of Central Observatory's equipment.

A combination of precision radar and optical sensing devices are suitable for this purpose. Radial translation (Y' translation) is monitored by range radar, and roll and

yaw attitude is sensed by applications of radar interferometers on the SMS (state of the art radar equipment is capable to give accuracies better than ± 5 meters and ± 1 degree). X' and Z' translations and the pitch attitude of the SMS is obtained from optical sensors similar to state of the art star tracking devices; the SMS is equipped with special light sources (or reflectors on the SMS and light source on the Central Observatory) such that this light is distinguishable from the star and earth shine background--flashing light signals, colored lights and suitable filters, or a combination of these are possibilities. Processing of the output signals of these devices is accomplished in the Central Observatory computer, being connected to each of the four SMS vehicles either by "wire" or by some form of transmit-receiver communications link. The monitoring by the Central Observatory is in the form of periodic up-dating of the "state information" for each of the four SMS vehicles.

6.2.2 Control Technique

The control of the operation of the four SMS- antenna system is implemented by threshold-type controls that maintain the four SMS vehicles at all times within their prescribed "control regions"--where each control region is thought of as a volume in space, the center of each volume coinciding at any time to the exact desired position of the corresponding SMS (as determined by the computer in the Central Observatory), and the bounds of the volume formed by the specified permissible ± 25 meters in the X', Y' and Z' directions. The four control regions move in a regular pattern such that at any instant of time the Central Observatory and the centroids of the four control regions correspond to the desired antenna configuration and the orientation--i.e., circular orbit with respect to the Central Observatory of radius five Km, orbital period one hour, and precessing at 0.5 degree per hour.

Whenever the Central Observatory senses that a SMS has translated close to or past one of the bounds of its control region appropriate SMS thrusters are commanded by the Central Observatory. A guidance and control computer in the Central Observatory continually up-dates the control action requirements based on the monitored "state" of each SMS. The control action command will be in terms of three attitude angles and appropriate thrust pulse durations for the various thrusters of any one of the four SMS vehicles. Execution of the commanded control action will generally consist of first achieving the required attitudes. The attitude realignment action is then followed by translational thrusting to achieve the proper sub-orbit reorientation and any translation rate corrections as determined by the guidance and control computer of the Central Observatory such that the SMS's sub-orbit is closely aligned with the slowly precessing orbit of the control regions. The duration of any thrust application is generally very short in comparison to the sub-orbit period of one hour.

Precessing the antenna plane at a rate of 0.5 deg/hr is accomplished by thrusting normal to the desired plane each time an SMS passes the zero degree reference point (nodal point) as it orbits the Central Observatory, i.e., the translational thrust will be commanded at 0°, 360°, 720°, etc. The duration of the thrust firing is such that the tangential velocity of the SMS will be rotated about the radius vector through an angle of 0.5°. This is demonstrated by means of Figure 6-2 and 6-3; where Figure 6-2 presents a plot of the position of the control region centroid for about 1-3/4 revolutions of the antenna system, and Figure 6-3 presents a corresponding plot of the SMS position for two different sub-orbits. Each of the figures shows

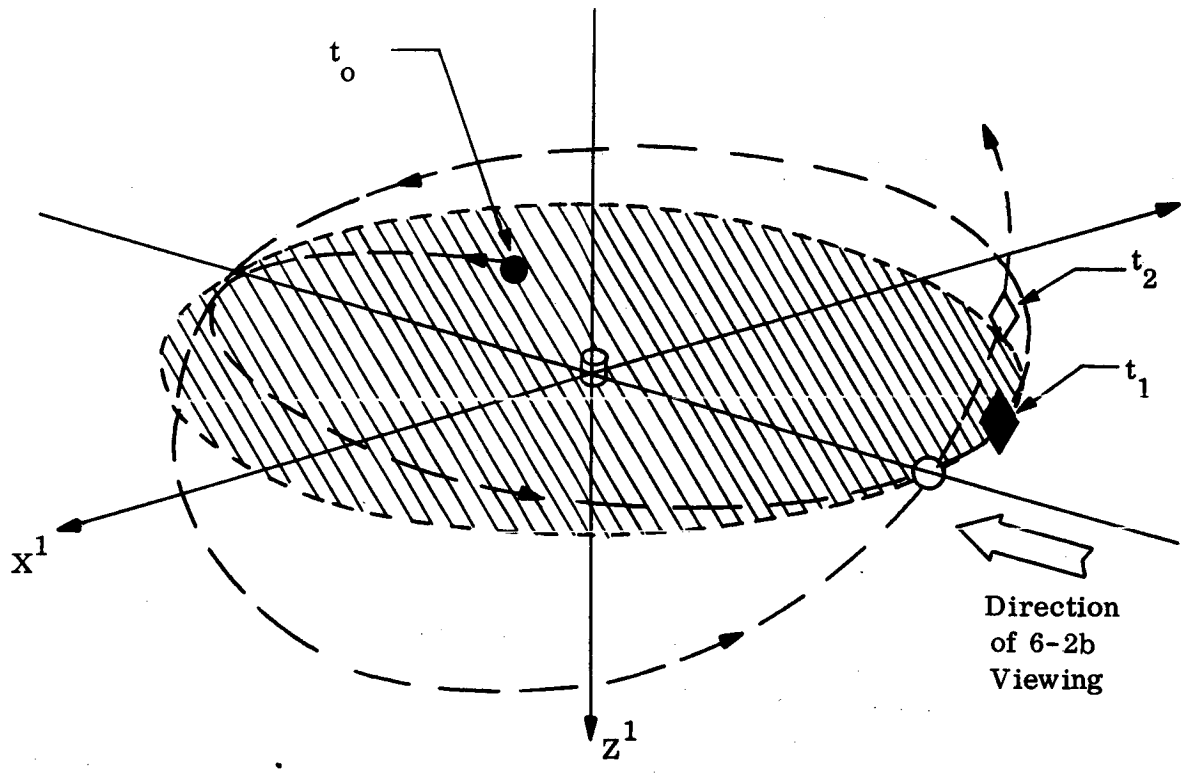

6-2a

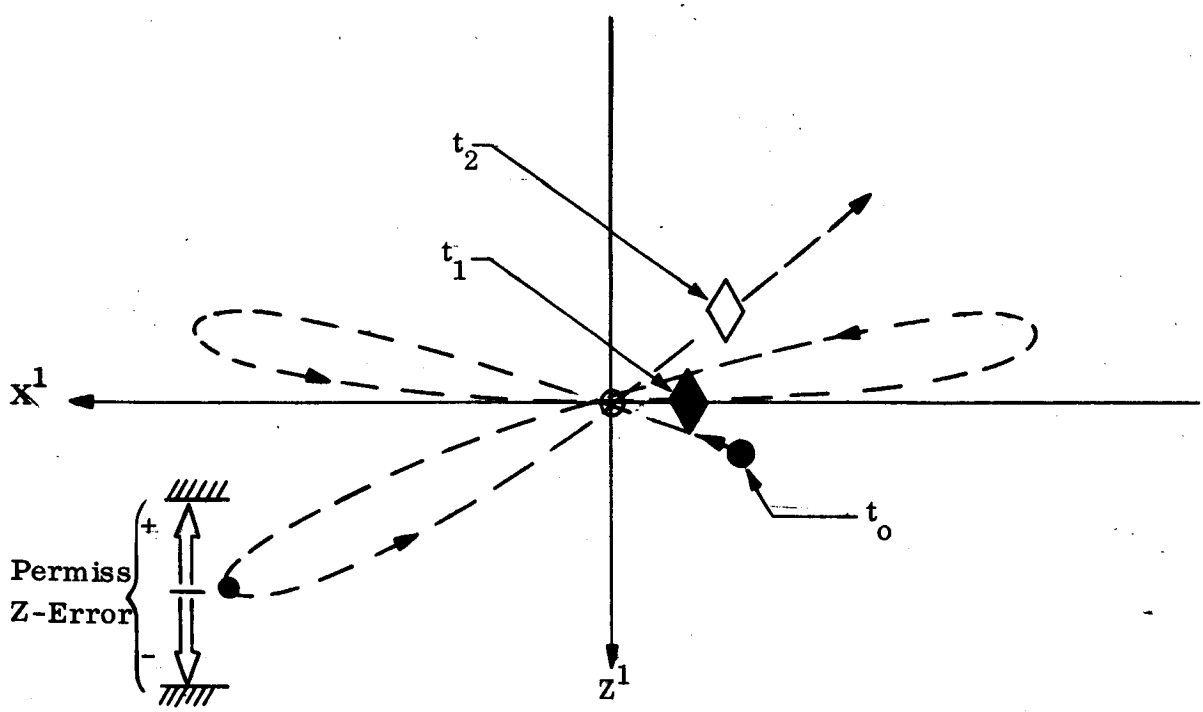

6-2b

Figure 6-2. "Control Region" for Precessing Orbital Motion

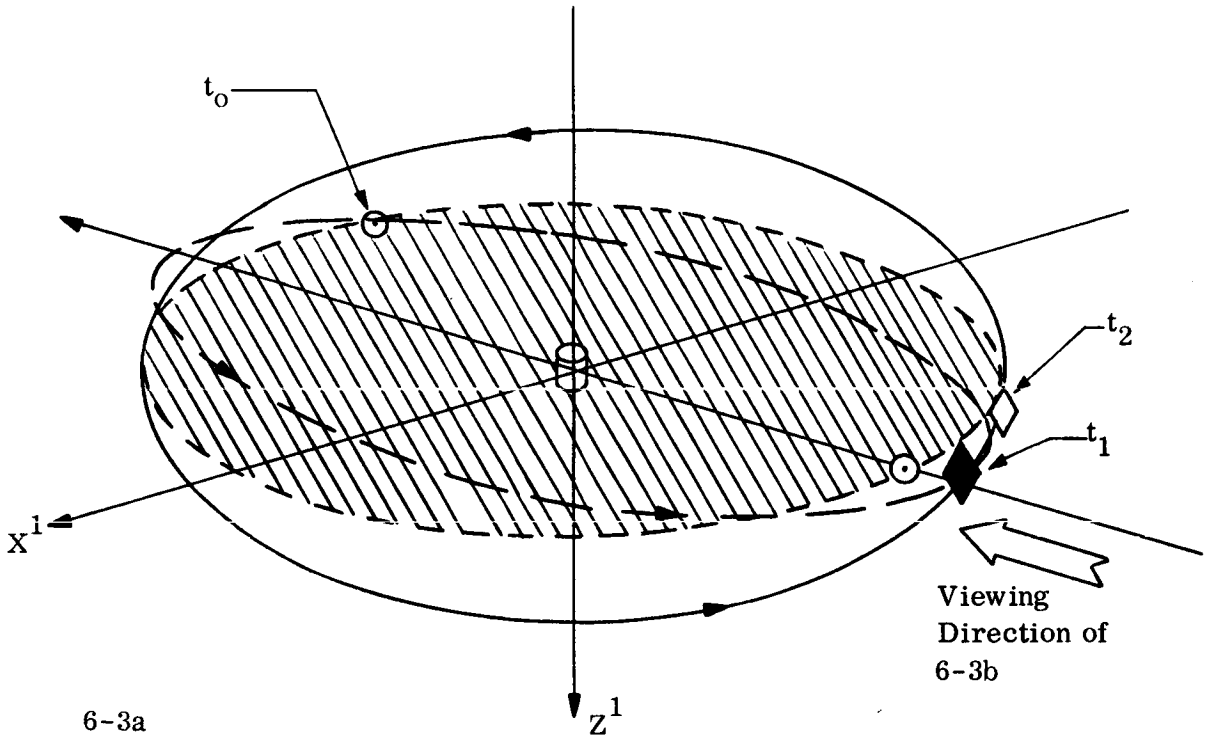

6-3a

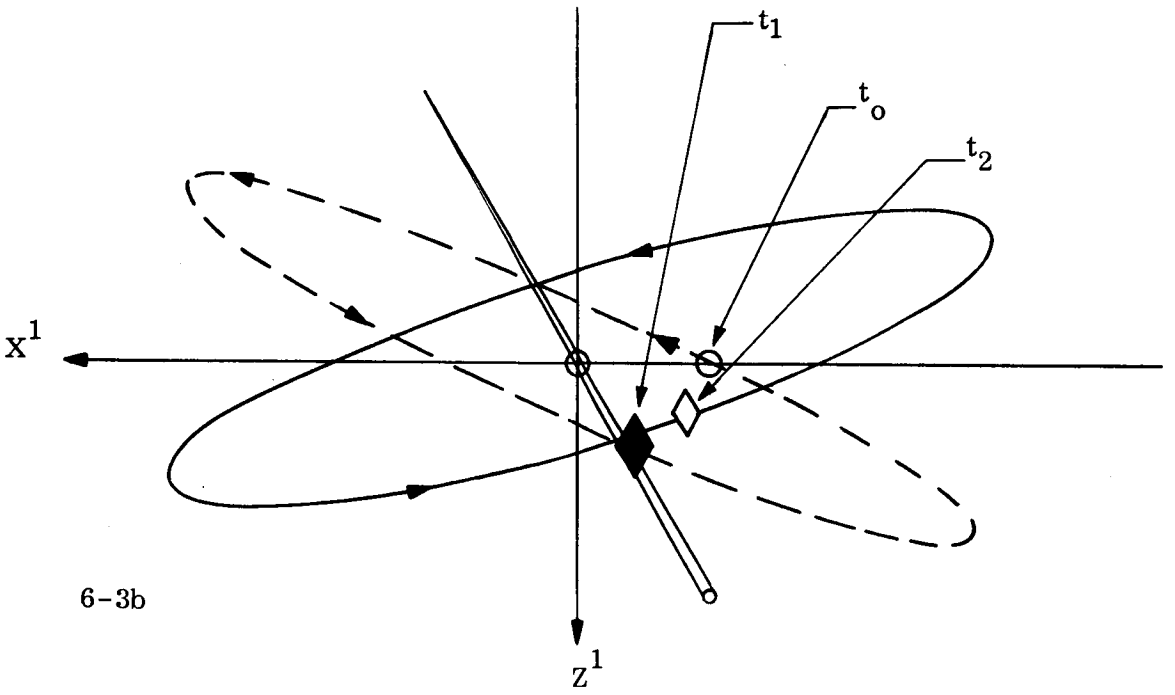

6-3b

Figure 6-3. Orbital Motion for Orbit Re-orientation of SMS

a perspective view and a corresponding X' - Z' plane projection; in each of the four curves' three positions are indicated which correspond to the control region and the SMS position at times t_0, t_1 and t_2. Relating corresponding points in Figures 6-2 and 6-3 and allowing for the indicated Z' error, it is seen that the Z' error band will generally be exceeded and thus a sub-orbit reorientation be commanded just past a nodal point as illustrated by the positions at time t_1. This may best be seen by superimposing the X' - Z' projections of Figures 6-2 and 6-3.

The case just illustrated corresponds to that of one sub-orbit reorientation per SMS per antenna system revolution, and was taken here as the nominal control mode applicable to the assumed antenna system operating characteristics--i.e., 5000 meter sub-orbit, period of one hour, antenna system precession of 1/2 degree per full revolution, and a permissable position error of $\pm$ 25 meters for the purpose of showing feasibility.

The number of required control actions per SMS per antenna revolution is in some approximate sense proportional to the antenna system precession rate and is inversely proportional to the size of the position error threshold. For position error threshold values less than about 25 m, the number of required control actions per SMS per revolution will rapidly increase ($>$ 2) in order for the SMS to follow the spiralling motion of the control region. The same kind of control action would also occur if the precession rate were increased substantially past the nominal 1/2 degree per hour.

6.3 SMS ΔV REQUIREMENTS

Proper control action will result in a change in the direction of the SMS velocity vector, such that it is rotated about a line connecting the SMS and the C.O., through the desired precession angle (resulting in an orbit reorientation as illustrated in Figure 6-3).

$$\bar{V}_{T_{(t_1^+)}} - \bar{V}_{T_{(t_1^-)}} = \Delta\bar{V}_{Pr}$$

where V_T is the tangential velocity at time t_1 - and time t_1^+, and ΔV_{Pr} is the precession velocity bit that is input.

Imparting a precession velocity bit may introduce small velocity errors ($\Delta V_{Pr} \pm \Delta\Delta V_{Pr}$). These errors may be resolved into tangential velocity and radial velocity errors of the SMS. These error velocities are caused by some attitude misalignment of the SMS at the time of the control action. It is desirable that the tangential and radial velocity errors (ΔV_T and ΔV_R respectively) will not exceed a value that would cause one SMS to drift beyond the permissible position threshold of ±25 meters during the time between successive control actions required for precession (t_{OFF}).

$$\therefore \Delta V_T \cong \Delta V_R \leq \frac{25}{t_{OFF}} \text{ m/sec.}$$

The maximum attitude misalignment at any time will be equal to some specified permissible attitude threshold value ($\phi_{D.B.}$), as defined in Figure 6-1

Therefore, the tangential velocity must also be less than the error in precession velocity times the sine of the threshold angle.

$$\therefore \Delta V_T \cong \Delta V_R \leq (\Delta V_{Pr} \pm \Delta\Delta V_{Pr}) \sin(\phi_{D.B.})$$

The total ΔV requirement per control action per subsatellite will consist of the nominal precession ΔV, the corrective ΔV's for the tangential and radial velocity, and the attitude $\Delta\dot{\phi}$ required for correction and alignment in pitch, roll, and yaw.

$$\sum \Delta V \cong \Delta V_{Pr} + \Delta V_T + \Delta V_R + 3(\Delta\dot{\phi})$$

An estimate of $\Delta\dot{\phi}$ is made based on the following:

In order to align the vehicle for inputting the precession thrust attitude repositionings will have to be made some time before the next ΔV_{Pr} input. The required attitude change will nominally be less than twice the selected threshold value ($\leq 2\phi_{D.B.}$), and the time available to execute this shift has been taken to be equal to or less than about 1/5 the time between ΔV_{Pr} inputs ($\leq 1/5\, t_{OFF}$).

These two conditions determine a required attitude correction velocity ($\dot{\phi}_c \geq \frac{2\phi_{D.B.}}{t_{OFF}/5}$), and $\Delta\dot{\phi} = 2(\dot{\phi}_c)$.

An equivalent $\Delta V\phi$ is defined as follows:

$$\Delta V\phi = (3\Delta\dot{\phi})\left(\frac{I}{(57.3)m_1}\right) \cong (0.56)\frac{\phi_{D.B.}}{t_{OFF}} \sim \text{Ft/Sec.}$$

where the various symbols are defined in front of this report.

Since the total ΔV required for position control may be defined as,

$$\sum \Delta V = \left[\Delta V_{Pr} + \Delta V_T + \Delta V_R + \Delta V_\phi \right] \sim \text{(Ft/sec)}$$

wherein that portion ascribed to precession and misalignment, (ΔV_{Pr}, Δ_K, and ΔV_R) may be referred to as the stationkeeping ΔV, i.e., that required to remain within the control corridor so that the total is the sum of the stationkeeping requirements and the attitude stabilization. Therefore considering control concept using one control action per SMS per antenna system revolution (Nominal System), we derive:

$$\Delta V_{Pr} \cong 0.232$$

$$\Delta V_R = \Delta V_T \cong 2(0.0227) \simeq 0.0454 \quad \text{Ft/sec}$$

Table 6-1, presents the stationkeeping requirements for various attitude dead bands for the single control action case.

For the operation of the KWOT for one year, considerations must also be given to deployment. Based upon Reference 1, it appears reasonable that the deployment ΔV for a single SMS is of the order of 28 ft/sec. Therefore for one year

TABLE 6-1

STATIONKEEPING ΔV REQUIREMENTS PER SMS VEHICLE (Single control action per revolution)			
$\Delta \Delta V_{Pr}$	ϕ D.B.	ΔV_ϕ Attitude Stabilization	$\Delta V_{ST.K}$ total per hour
% ΔV_{Pr}	Degrees	Ft/sec.	(Ft/sec)/hour
0	5.6	8.7×10^{-4}	
10	5.1	7.9×10^{-4}	
20	4.7	7.2×10^{-4}	0.278

a conservative estimate would be;

Mission Elements	ΔV Required
Deployment	28
Stationkeeping	2430
Attitude Stabilization	63
	2521

Applied to a typical SMS with an assumed mass of five slugs, Isp of 200 sec, the equivalent propellant would be 62.0 lb. If two control actions per antenna system revolution were assumed, then;

$$\Delta V_{Pr} \simeq 0.116 \text{ Ft/sec.}$$

$$\Delta V_R = \Delta V_T \simeq (0.0455) \simeq 0.0900 \text{ St/sec.}$$

Table 6-2 presents the stationkeeping requirements for the dual control action case.

TABLE 6-2

STATIONKEEPING ΔV REQUIREMENTS PER SMS VEHICLE (Dual control action per revolution)			
$\Delta \Delta V_{Pr}$	ϕ D.B.	ΔV_ϕ Attitude Stabilization	$\Delta V_{ST.K.}$ total per hour
% ΔV_R	Degrees	Ft/sec.	Ft/Sec./hour
0	23	7.1×10^{-3}	
10	21	6.5×10^{-3}	
20	19	5.9×10^{-3}	$\approx$ 0.426

For one year's operation, considering the same ΔV required for deployment, mission total would be

Mission Element	ΔV Required
Deployment	28
Stationkeeping	3609
Attitude Stabilization	52
	3689

For the same typical vehicle assumed previously, an equivalent amount of propellent is 94.0 lb.

There are several factors which should be noted here. The numbers computed for the two contol concepts are quite conservative for several reasons which will be given below.

First, the ΔV_R has been taken to be of the same order of magnitude as the ΔV_T. In light of the relatively stiff spring constant assumed for the webbing, this could probably be reduced substantially.

Secondly, the $\phi_{D.B.}$ limits for the concept using two control actions could be reduced without seriously complicating the attitude control system. This would tend to reduce the total ΔV for this concept, as can be seen by a comparison of the data shown in Figure 6-4. This line of reasoning could also be applied to the single action concept, however, in this case the dead band limits are already relatively small and the saving would be mitigated by the requirement for more attitude control propellant.

Lastly, the required number of firings will be reduced if the precession rate is less than the assumed value of 1/2 degree per hour. At this rate, one firing per revolution is necessary just to maintain the SMS in the control region. For a lesser rate say 1/4 degree per hour, it should be possible to maintain the antenna accuracy by firing once every second revolution over a major portion of the KWOT orbit. However, a still more accurate attitude system would then be required.

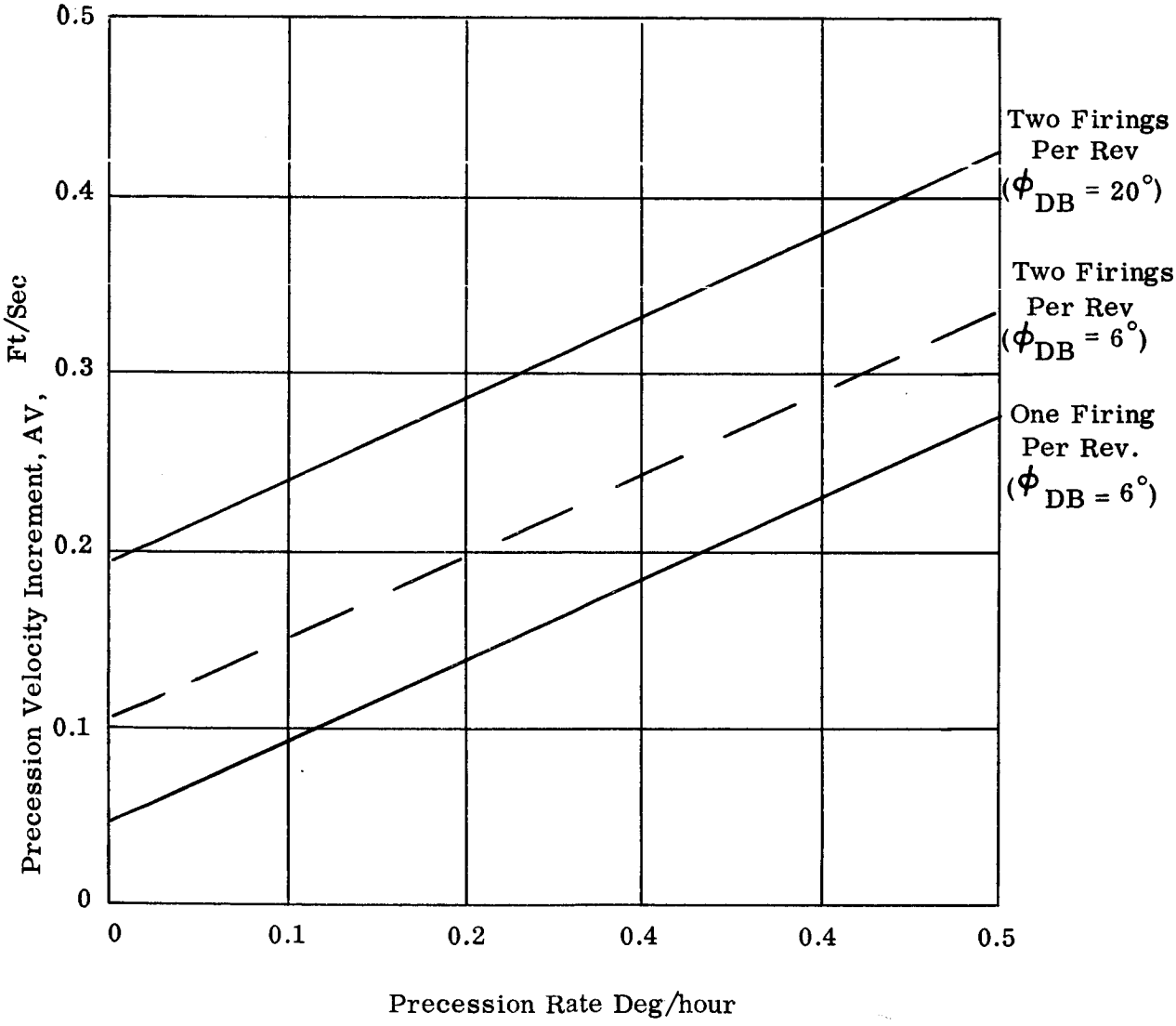

Figure 6-4. Precession Velocity Requirement versus Precession Rate

3.4 SMS THRUSTER SIZE

In order to estimate a suitable thrust level for the reaction control engines of the SMS vehicle the following arguments are used.

An upper bound for the thrust level is obtained from previously defined precession requirements and assuming a value for the minimum thrust pulse duration (t_{min} = 50 m.sec.) in addition to previously listed values of SMS parameters.

$$f < \frac{(\Delta V_{Pr})\,(m)}{(4)\,(t_{min})} = \frac{(0.232)\,(5)}{(4)\,(0.05)} \cong 5.9 \sim \text{lbs.}$$

The selection of a reasonable lower bound on F is not quite as straight forward. In order to achieve low attitude limit cycle drift rates very small thrust levels (of the order of milli-pounds) would be desirable, but on the other hand general maneuvering requirements are more easily met with thrust levels of about 0.1 pounds. A dual level attitude threshold would serve to reduce the above mentioned difficulty; the system is in "tight deadband" control during application of the precession ΔV inputs (corresponding to previously listed values of $\phi_{D.B.}$), and during t_{OFF} the attitude control would be a "very loose" threshold system ($\phi_{L.C.} \lesssim 10\phi_{D.B.}$) with a correspondingly long limit cycle period.

Under these assumptions an acceptable thrust level would be about 0.05 to 0.1 pound.

6.5 CONCLUSION

In conclusion, the active control concept investigated establishes the feasibility of utilizing active control, but not necessarily the optimum technique. Also it has been shown that the ΔV required to satisfy the SMS mission for one year under the assumed

conditions is reasonable ($\sim$ 2740 ft/sec). To achieve this control thrust levels of .003 to 5.9 are reasonable, however, the predominating requirement in establishing the low magnitude thrust is attitude stabilization, while the upper level is determined by achieving the total precession per revolution in a minimum bit firing. Since the latter condition can be readily achieved by burning for a longer time, considerations which would economize fuel should predominate in thrust selection. Therefore, the lowest reproducible thrust level practical should be selected, which for the current state of the art of monopropellant systems is between 0.01 and 0.1 lb.

7.0 SMS CONCEPT

7.1 CONCEPT CONSIDERATIONS

Based on the studies presented in the previous section, it is apparent that stabilization of the antenna by active control of an SMS system is feasible within a finely controlled corridor of ±25 meters for a period of one year for a nominal propellant load. It is appropriate therefore to look at what such would entail from a system design point of view, and the implications associated with the SMS concept.

Figure 7-1 presents a conceptual design of typical SMS as envisioned as a result of this feasibility study. Table 7-1 is an associated weight estimate. The principle subsystems required for the subsatellite are: (1) propulsion, consisting of propellant, tank and thrusters and associated plumbing; (2) stabilization and control, consisting of an attitude reference and a control logic, a reference system for range and range rate data, (3) a command and data link, (4) wire dispenser system for the antenna array elements, and (5) power supply and distribution system. It must be emphasized that a preliminary design study has not been conducted and this represents only conceptual thinking based on the results of the feasibility study.

7.2 PROPULSION

A propulsion system which would be suitable for a SMS would consist of nominally 16 thrusters of approximately 0.01-lb thrust. The system would be most probably a monopropellant, of the H_2O_2, or N_2H_4 class, preferably the latter because of the higher I_{sp} ($\sim$ 200 duty cycle), although the use of ion, and cold gas propulsion needs to be investigated. A blowdown system seems to be attractive because of its inherent

TABLE 7-1

SMALL MANEUVERING SUBSATELLITE WEIGHT STATEMENT

Rocket Propulsion System	(41.2)
Tank Blow Down	21.0
Fill Valve Pressurant	0.3
Pressure Transducer Pressurant	0.2
Fill Valve – Propellant	0.3
Filters – Propellant	0.1
Isolation Valves (2)	2.6
Thrust Chamber Assembly (16)	11.2
Lines and Fittings	2.0
Mounting Equipment	2.0
Instrumentation and Controls	1.5
Stabilization and Controls	(8.5)
Amplifiers/Flight Control Logic (SCS)	7.0
Wiring and Plugs	1.5
Command and Data Pack and Cables	8.3
Power Supplies and Distribution	(19.7)
Battery Pack	4.5
Solar Cell Assembly (20)	0.8
Dispenser and Wire (1)	1.9
Polarization Antenna	2.5
Interferometer Antenna	10.0
Structure and Insulation	19.0
One Dispenser Vehicle Total Dry Weight	96.7
Propellant	63.0
Pressurant	3.7
Total Wet Weight	162.4
One Dispenser Vehicle Wt (Wet)	162.4
Two Dispenser Vehicle Wt (Wet)	165.7

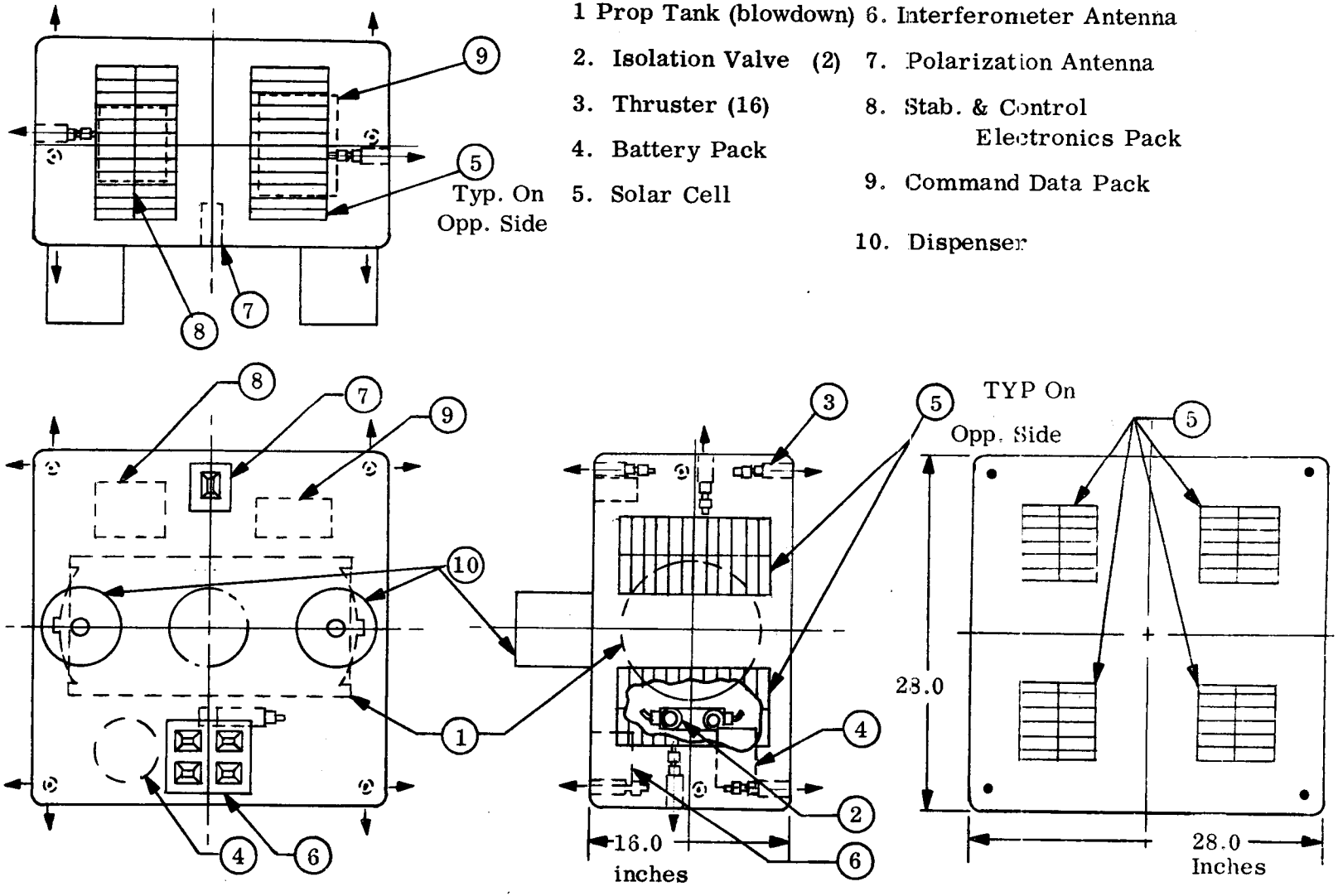

Figure 7-1. Small Maneuvering Satellite – KWOT

reliability, associated with the pressurant self contained in the propellant tank, and since the resultant thrust variations, would not be critical in this application.

7.3 STABILIZATION AND CONTROL

The SMS is to be attitude stabilized with reference to the Central Observatory so that its yaw, pitch and roll axes remain in essentially the same planes as the corresponding axes of the Central Observatory vehicle. Similarly, the control must be exercised by the stabilization and control system to precess the subsatellites; hence, the KWOT at the prescribed rate. The small reaction control thruster jets are used to accomplish this but for fuel conservation reasons, a corrective thrust firing will only be undertaken when the SMS reaches the control volume boundary and will then be a minimum impulse firing. This would only be done about once per hour or less according to the results of Section 6.0.

Attitude sensors are very often of the gyroscopic type but gyros drift with time and are mainly useful for taking out high frequency perturbing effects and for a short term attitude reference. Even if gyros were used, they would require updating frequently from some other reference. Furthermore, gyros have a limited life expectancy, and require a continuous application of significant electrical power. Therefore, a gyro attitude system is not recommended except possibly during the initial development of the SMS.

Since a command radio link (to be described subsequently) is used between the Central Observatory and the SMS, this radio signal arriving at the SMS may be used by the SMS to establish the direction of arrival by means of a phase measuring interferometer receiver system. It can thus sense its proper pitch and yaw attitude relative to the Central Observatory. Roll attitude is sensed by a right angle null sensing of the linearly polarized signal. Since all of this equipment is solid state electronic circuitry, its life expectancy

is well in excess of the one or two year operational requirements. Furthermore, for power conservation reasons, the equipment can be turned off (except for the command receiver/ decoder) between the hourly corrections which are expected to require less than five minutes including any warmup time.

The Central Observatory data processing equipment (computer) will probably control the time when corrective data word to the particular SMS being commanded (all SMS's may "hear" the radio transmission but only the correctly addressed SMS will respond to the code). The corrective position command will then be transmitted as a further coded data message. During this time the SMS interferometer and polarization sensitive receivers will operate on the received signal to determine if an attitude correction is required. The corrective position command will be stored momentarily in the SMS command decoder output section. When both the attitude and position (i.e. distance) command systems have had sufficient time to accumulate the required logical thruster firing data, an additional "execute" command will be sent from the Central Observatory to the particular SMS under control at that time. Only during and immediately following the "execute" command will the SMS fire the proper combination of thrusters. A confirming telemetry signal may be transmitted from the SMS to the Central Observatory both at the time of initial command data receipt and at the time of the command action execution.

Before the equipment is again returned to the quiescent state following the execution of a command, the Central Observatory will make a final measurement to assure that the desired command effects have been accomplished. Note that the actual corrections made occur over a time period following the application of the commanded thrust. At least after one or two minutes, the trends of the applied thrust should become

apparent, possibly in terms of arresting an undesirable drift tendency. After the final check is made, a return to quiescent state command is sent from the Central Observatory to the SMS. The SMS then shuts down all of its electrical equipment except for the radio telescope telemetry equipment and the command receiver/decoder unit which remains on standby operation.

The stabilization system contains all of the logical circuitry for accepting the decoder commands from the Central Observatory plus its own local attitude measuring system. It establishes the thruster firing duration and the combination of thrusters required for any given set of position command plus attitude stabilization commands. It then accepts the command execution signal from the Central Observatory and turns the proper thruster group on for the proper time period. The thruster valve driver circuits utilize power transistors and discrete components. All other circuits are low level signal type circuitry and are built up from interconnection of integrated micro circuits on small printed circuit boards.

One other promising technique would be to send commands from the Central Observatory directly to the thrusters in the SMS without any logical decision equipment in the SMS. Thus, all logic decisions would be made in the Central Observatory data processor and this one unit would serve all four SMS's. The equipment on the SMS would be made lighter, smaller, lower power and less costly. However, the attitude measurements made on the SMS would be telemetered to the Central Observatory and this might cause some degradation of the measurements. However, it would be expected that this data could be handled with the same error--free fidelity as will be typical of the command data. Therefore, this approach appears quite attractive.

7.4 ELECTRONIC SUBSYSTEMS

7.4.1 Command Receiver/Decoder

The radio command link from the Central Observatory to the SMS will probably operate in approximately the same frequency band as the telemetry system although offset sufficiently so as not to interfere with the telemetry signal. The bandwidth of the basic command information is so relatively narrow that no problem is foreseen with this link. It has already been shown that the telemetry link with a 10 MHZ bandwidth is operable with only a half watt power source while providing +30 db signal to noise ratio. The bandwidth of the command system is expected to be approximately 10 KHZ and could be reduced below this value if required.

Because the command system has such a high signal to noise ratio, the bit error probability is extremely low. However, to further ensure an error free system, the use of parity techniques and error correcting codes is recommended. The partial directivity of the antennas will further minimize the risk of interference as will the choice of a high microwave frequency band.

Since only one SMS is controlled at one time, the command system can be time shared between the four SMS units. The messages from the Central Observatory will carry a coded address which is different for each of the four SMS units. All of the SMS units would "hear" all of the command messages since all of them would be turned to a single common frequency, but would respond only to their particular individual address code.

Many of the commands are only single bit channels (ON-OFF discrete bi-level channels) and even in the case of the translation and attitude commands, the number of values to be transmitted are relatively finite since these commands represent thruster

turn-on time duration commands. The entire list of commands would never be sent within one command message sequence. After some preliminary analysis, it appears that a typical command message might contain about 30 binary bits of information. Assuming that adding the address code, parity bits and utilizing error correcting codes caused this bit count to rise to about 100 bits per message and assuming that every message is repeated twice, the count is still only 200 bits. Now assume that five such messages are sent per second at the highest probable rate, the information rate is still only 1000 bits per second.

7.4.2 Pitch/Yaw Interferometer Sensor

The pitch and yaw attitude sensor system would probably consist of a radio interferometer which senses the direction of arrival of the command signal from the Central Observatory command transmitter. Since the attitude stabilization thruster firing is only undertaken periodically, the attitude measurement is performed just prior to the thruster firing when the command signals are arriving. The phase front from the Central Observatory can be considered to be flat within the frame of reference of the SMS interferometer base line spacing (about eight inches nominal at an 8000 MHZ nominal frequency). The interferometer measures the relative phase of this signal at its reference element and at each of two other elements, one for the pitch axis and the other for the yaw axis.

The three interferometer antenna elements are arranged in the shape of an "L" with the reference unit in the corner of the "L". The pitch element is mounted vertically above the reference element while the yaw element is mounted to either side of the reference element. The antenna configuration is much like a monopulse radar antenna.

The three antennas are connected to three receiver channels. However, a common local oscillator is used for all of the receiver channels so that the signal containing the phase information will remain the same after amplification in the IF strips. A phase comparator between the reference channel and the pitch channel provides the pitch angle information while a similar comparator between the reference channel and the yaw channel yields the yaw angle information. The reference channel is also used as the command receiver channel. The interferometer system makes its angular measurements only when properly addressed coded commands are received.

The antennas used in the interferometer are linearly polarized in the same plane as the command transmitter antennas on the Central Observatory. Thus, there is no cross polarization loss in this system. Note however that a separate cross polarized antenna/receiver system is provided for sensing polarization null. This latter equipment is used for the roll attitude sensor system and is described in a subsequent paragraph.

All of the circuitry is solid state including the crystal controlled local oscillator for the receivers. The receiver IF strips are miniaturized, solid state units. All of the receiver equipment will weigh less than two pounds.

7.4 3 Roll Axis, Polarization Sensor

The roll axis attitude sensing is performed by measuring the polarization of the arriving command link radio signal, first in the normal linear (for example vertically polarized) mode and secondly, in a separate cross polarized (for example horizontal polarized) mode. The second sensor is installed solely for this purpose and its normal operating mode is to seek the cross polarized "null" whereas the regular command receiver looks for the correctly polarized signal maximum.

The roll axis attitude measurement is made at the same time as the pitch and yaw measurements. This is at the time of arrival of the command information from the Central Observatory. The equipment is all solid state and does not require any warm up time. The receiver uses the same local oscillator as the command receiver. The antenna is the same as the command receiver (interferometer reference element) antenna except that it is oriented 90° of angular rotation in relation to the command receiver antenna.

Since the polarization sensor is not required to decode any information, its bandwidth can be made relatively narrow which will give it an effectively greater signal to noise ratio capability. However, the signal which it seeks is the cross polarized null. Therefore, it operates close to its noise threshold but this is to be expected. While the regular command receiver is peaked up to its maximum signal level, the polarization sensor is seeking the lowest level null signal. The effect is that of the cosine function where the properly polarized signal is sensing a relatively broad peak maximum while the cross polarized sensor sees a fairly sharp 90° zero crossover null.

7.4.4 Radio Ranging

The distance of the SMS from Central Observatory must be measured to a high degree of accuracy. However, the SMS is size, weight and power limited and this suggests that one attractive means of measurement might be to make the SMS entirely passive in so far as the range measurement is concerned. Thus, one set of radar equipment on the Central Observatory could conceivably measure the range of each SMS (sequentially) by operating in a normal radar skin echo mode. A directive antenna system on the Central Observatory would be required in order that echos would be received from only one SMS

at a time. A passive signal enhance such as a corner reflector, luneberg lens reflector or Van Atta array reflector might be used to give each SMS an effectively large radar target cross section.

The alternative approach to the radio ranging system, is to make use of the command link from the Central Observatory to the SMS plus the telemetry link from the SMS to the Central Observatory for a radio ranging "couple". This system is somewhat like a radar with a transponder beacon at the far end. It is an active, cooperative radio ranging system. Its advantages include the elimination of the need for a directional antenna on the Central Observatory since the reply signals would only come from the properly addressed SMS (code message address enables the SMS telemetry range reply) and because the telemetry reply messages all come in on different frequencies from each different SMS. Furthermore, the transmitter power on the Central Observatory can be reduced from somewhere in the order of 1000 watts to a value of about half a watt. This is a significant power saving, even on the Central Observatory. Weight would also be reduced, perhaps by a factor of about 70 pounds approximately. The extra equipment required on the SMS to implement this system would amount to less than 0.5 lb and there would be virtually no increase in power required in the SMS.

A system of active transponder electronics offers a higher signal to noise ratio for a given power expenditure and therefore a theoretically more accurate system as compared with an active radar, passive reflector combination.

7.4.5 Telemetry

The telemetering system on the SMS is intended to return the primary radio telescope measurement data from the SMS (either the rhombic or the interferometer dipole signals) to the Central Observatory. However, this telemetry link may also serve

to return some SMS system status data from SMS to the Central Observatory. Furthermore, this telemetry link in conjunction with the command link to be described later, may serve as a round trip echo signal return in a cooperative radio ranging system. Thus, by using the command link and the telemetry link "couple", the Central Observatory can measure the range of the SMS from the Central Observatory.

The radio astronomy measurements are the prime purpose of the radio telecope satellite system and these measurements are of an essentially continuous nature. The other possible services which might be carried by the telemetry system are of an intermittant or sampled data type which can be sent in short bursts on a time sharing basis.

The primary radio telescope information consists of a set of signals which are much like radio galactic noise in the frequency band around one megahertz. Since the direction of arrival of the radio signals is of prime interest, the phase information from each of the radio telescope measurement sources (the rhombic plus the dipole interferometer antennas) must be preserved until the signals can be integrated in a correlator within the Central Observatory. Therefore, the telemetry link must not allow the phase information contained in the radio telescope signals to be lost or degraded in transit from the SMS to the Central Observatory.

Although an exact design implementation of the telemetery link is beyond the scope of this presentation, some of its characteristics can be presented. For several reasons it appears desirable to translate the fundamental radio signals from the radio telescope up to a much higher frequency band. The considerations involved here include several radio noise sources, antenna gain versus size, component availability, radio communication frequency band allocations and potential interference problems, required

bandwidth, power limitations of the SMS basic power source, modulation and frequency multiplication techniques, etc.

The frequency bands of interest here extend from the UHF range (300 MHZ) up through the high microwave region and on into the millimeter wave region. The latter choice might be somewhat limited at present by lack of suitable components, particularly solid state long life medium power transmitting hardware. If the choice were to be made today with the present state of the art components, the frequency band which appears most attractive are the S, C or X band segments (2000 to 10,000 MHz) of the microwave range.

In order to ensure the recovery of the phase information a wide bandwidth system is recommended. Although the basic signals are in the order of 1.0 MHz, a 10 bandwidth is recommended. Further, a high signal to noise ratio should be provided for good fidelity. A +20 db S/N is considered to be minimum for this service.

Since the transmitter operates continuously, an efficient solid state design is recommended. An RF power level of about a half watt now appears feasible in an all solid state source centered about a frequency of 8000 MHZ, with a nominal frequency distribution between each of the subsatellites. By using this high microwave frequency for telemetry, there is virtually no chance of radio interference with the basic radio telescope measurements.

One other major reason for the choice of the high microwave frequencies for the telemetry link, is the small size of the antennas on the SMS while yet providing significant gain and relative beam directivity. An initial survey of antenna types suggest that a slotted waveguide type may be preferable.

Because there are three dipole interferometer receivers adjacent to each of the side SMS units, three separate radio telescopes wide band transmitters will be required from each of these locations. The total frequency channel assignments for telemetry is therefore eight.

In considering the sources of phase error perturbation of the telemetered radio telescope signals, the velocity of the SMS along its roll axis (a line joining the SMS to the Central Observatory) must be considered. Although nominally at rest in a static position, the SMS may have some motion along this axis which might result in a doppler shift induced phase error. Therefore, position corrections along this axis should be made slowly.

7.5 POWER SOURCE

Since the SMS size is minimum and yet it must remain active for periods of time such as one or two years, the choice of primary power sources is limited to solar cells or nuclear types. Solar cells are suggested for simplicity reasons. A secondary battery system would be used for carrying over periods of darkness.

The power systems will be of a dual redundant type for reliability reasons and will have a 100 percent reserve factor so that either half of the power system could carry the entire load continuously.

In operation, the solar cells will power the SMS systems during most of its long elliptical orbit while the SMS is illuminated by the sun. During the approximate one hour time periods while the SMS is shadowed by the earth so that the solar cells are inoperative, the batteries will carry the SMS electrical load. As the SMS again emerges into the sun illumination, the solar cells will pick up the load and will also recharge the batteries.

It should be indicated, that in order to effect a true preliminary design, study must be conducted of both alternative mission modes and system hardware. For example, provision for deploying the antenna and control spin-up must be made, as well as a detailed analysis of the vehicle equipment, i.e., propulsion stabilization and control, etc., for the SMS. This section therefore, presents only an initial concept of the sub-satellites.

8.0 CONCLUSIONS

The approach taken in this study was to investigate the feasibility of a method to the keeping of a simple configuration radio astronomy antenna in the desired position in orbit for a period of one year. Should this, a single approach prove feasible, then the concept as a logical consequence is also feasible. Such has in fact proved to be the case. This does not mean to imply that through this technique that either an optimum radio astronomy configuration, subsatellite design or technique (i.e. active or passive) has been achieved. Rather it does imply that these items should, since they are now feasible, be studied from an engineering preliminary design point of view and a parametric evaluation conducted to determine the optimum subsatellite system, deployment technique, radio antenna configuration and subsatellite design.

It may therefore be concluded from the data presented in the previous section:

1. That the use of small maneuverable subsatellites for the maintenance of a radio astronomy antenna in prescribed position and with a fine degree of accuracy is feasible.
2. That the effects of the natural and induced environmental perturbative forces are negligible.
3. That the motion of the antenna system under the influence of the gravitational and environmental forces within the regime defined for operating tolerances (i.e. ±25 meters) retains planarity.
4. That the achievement of complete sky coverage through precession requires active control exerted by the SMS.

5. The motion of the antenna system under the influence of active control is regular and may be adequately described by a set of exact differential equations, which for this case may be reduced to simple closed form solutions.

6. That the energy expended to precess the antenna is an order of magnitude greater than that required to overcome the gravity gradient effects under the assumed set of conditions.

7. That conservative estimates of the system ΔV requirements (2500 ft/sec) and gross vehicle size, 16 in. x 28 in. x 28 in., are within reasonable limits for one year of operation.

Similarly, the following problems, while subjected to some preliminary study, remain unresolved.

1. The effect of larger permissible excursion of the ends of the antenna (SMS location); whether or not the system will become divergent, or sufficiently unstable for some periods to make accurate radio source measurement difficult or in error.

2. The technique to obtain relatively uniform as well as complete sky coverage, the definition of areas of overlap and interaction, and the tradeoff between ΔV required and overcoverage.

3. A number of parametric tradeoffs most notably between permissible excursion and ΔV required, variations in antenna configuration with SMS motion.

Based upon this study the items given below may be resumed as logical steps to be taken now with regard to the subsatellites. It should be pointed out that while some select items are listed here, the establishment of the feasibility of the use of SMS's in active control, warrants per se, further study of the SMS, the most logical of which would be comprehensive systems and preliminary design study. The items listed below, therefore, represent some unique points that need mention, and would constitute the "first steps" in any continued effort.

1. The investigation of SMS application to related missions or mission elements most notably – deployment, spin-up, and antenna calibration.
2. The determination of the techniques for deploying the array and the ΔV required for the various techniques.
3. The investigation of the interaction between the SMS, the array elements and the central observatory.
4. Investigation of the effects of distributed masses located at various points along the array axes particularly at the interferometer elements.

In addition, the items cited as unsolved problems certainly must be resolved. It is therefore recommended that a more detailed study be conducted to evaluate in a systematic and parametric fashion the Small Maneuverable Subsatellites in conjunction with a similar study of the Central Observatory.

REFERENCES
Sections 1.0-8.0

1. Seale, L. M., Economou, N., and Stewart, R. A., Remote Maneuvering Unit, Bell Aerosystems Company, Proceedings of National Conference on Space Maintenance and Extravehicular Activities, March 1966, Orlando, Florida.

2. Seale, L. M., Economou, N., and Stewart, R. A., et.al., MOL Experiment P-7 Extension Study (U), SSD-TR-65-28, May 1965 (S)

3. Smith, R. E., "Space Environment Criteria Conditions for Use in Space Vehicle Development", NASA TM-X-53273, May 1965

4. USAF AFSC, "Space Planners Guide", July 1965.

APPENDIX A

THE EFFECTS OF ENVIRONMENTAL AND INDUCED FORCES

ON

THE KWOT ANTENNA

APPENDIX A

This appendix describes an investigation conducted during the course of the study to describe the forces which may affect shape and motion of the antenna system. The following are the phenomena which would cause the forces:

1. Solar Wind
2. Solar radiation pressure
3. Solar flares
4. Charges in the Van Allen belt
5. Field of the magnetosphere

A sixth effect has been identified during the consideration of the above enumerated five phenomena: the electrodynamic interaction between current carrying conductors.

It is anticipated, at present, that the inertia effects, which are not objects of this note, would predominate. Consequently, some of the six above enumerated forces were given a summary treatment.

1.0 Solar Wind

The solar wind is a fairly steady flow of light nuclei originating in the sun. The effect of this wind will, in first approximation, be lumped with that of the solar radiation pressure.

2.0 Solar Radiation Pressure

The radiation pressure may be considered to be caused by the recoil of solar photons impinging on receivers. K. A. Ehricke, Reference 1, gives a value for the radiation pressure at the sun-earth distance:

$$P = 2.10^{-7} \text{ lb/ft}^2$$

This force may include the solar wind because it is the basis for the computation of solar sails. The direction of impingement is radial out from the sun. The receiving surface is the projected area of the members on a plane normal to the radius to the sun.

3.0 Solar Flares

The solar flares are not connected with significant increase of light emission; the particle flow can, however, become very intensive. It may be stated, as a rule of thumb, that the duration of a flare increases with its strength. We shall approximate, and assume that the flow direction is radially outward from the sun. Reference 2 gives some information on solar flares: the time for decay to half value of the flux is 10 to 20 hours, an extremely high value of the integrated proton flux with energies exceeding 30 Mev would be 6×10^9 protons/cm^2. The force may be estimated using these quoted data.

Assumptions:

1. duration of the flare: 10 hours
2. mean energy of one particle: 50 Mev. $= \frac{m}{2} V^2$ (2)

Connections:

1. the mass of one proton: $1.672 \cdot 10^{-24} g = m$ (3)
2. the connection between erg and electron volt:
   $1 \text{ ev} = 1.602 \cdot 10^{-12}$ erg (4)
3. the connection between energy and momentum:
   $mV = \sqrt{2 \left(\frac{m}{2} V^2\right) m}$

The momentum of one proton may be obtained by considering the equivalent in erg of 50 Mev:

$$mV = \sqrt{2 \left[(50)\, 10^6\, (1.602)\, 10^{-12}\right] (1.672)\, 10^{-24}}$$

$$= \sqrt{2 \left[(10^{-5})\right] 1.672\, (10^{-24}) = 1.63\, (10^{-14})} \text{ dynes} \cdot \text{sec.} \quad (5a)$$

It may be further assumed that the incidence is normal and that the reflection is complete; thus, the resulting change in momentum:

$$\Delta M = 2\ mV \tag{6}$$

$$\Delta M = 3.2\ (10^{-14})\ \text{dynes} \cdot \text{sec} \tag{6a}$$

The duration of the flare has been assumed to be 10 hours, or $3.6\ (10^{4})$ seconds. The number of protons incident on a square centimeter in one second is, then:

$$6\ (10^{9})\ \frac{1}{3.6\ (10^{4})} = 1.92\ (10^{5})\ \text{cm}^{-2}\ \text{sec}^{-1}. \tag{7}$$

The surface force becomes with the above values

$$3.2\ (10^{-4})\ 1.92\ (10^{5})\ \text{dynes/cm}^{2} = 6(10^{-9})\ \text{dynes/cm}^{2}$$

$$\doteq 6(10^{-9})\ 10^{-6}\ \text{Kg/cm}^{2} = 6\ (2.2)\ (6.5)\ 144\ (10^{-15})\ \text{psf} \tag{8}$$

$$P \doteq 1.2\ (10^{-11})\ \text{psf}$$

The pressure exerted by solar radiation greatly exceeds that caused by solar flare protons.

4.0 Effects of the Van Allen Belt

A distinction may be made between two kinds of effects: (1) the aerodynamic effects, these are not considered in this appendix; (2) the plasma effects, these will be discussed here. The Debye length is the yardstick measuring the importance of the existence of charges in the plasma. If the dimensions of the body immersed in plasma are larger than the Debye length, then "plasma effects" are important. The body dimension we consider is the diameter of the elements, i.e., 0.02 in. or 0.05 cm. (The SMS's are not treated in this first approximation.) The Debye-length is: (See Reference 3)

$$\lambda_{o} = \sqrt{k\ T_{e} / (4\pi)\ n_{e}\ e^{2}}\quad \text{cm.} \tag{9}$$

Gaussian units (cgs) are to be used in the above equation:

k Boltzmann constant
T_e electron temperature
n_e electron density

Based on Reference 4, the smallest value of the Debye length will be in the inner zone. On March 3, 1959, the following values existed at approximately 20000 Km on the geomagnetic equator:

Electrons of energy greater than 40 kev: omnidirectional intensity approximately 10^{11} cm^{-2} sec^{-1};

Electrons of energy exceeding 200 kev: omnidirectional intensity less than 10^{8} cm^{-2} sec^{-1}.

By referring the Debye length to the energetic particles quoted above rather large values for either of the cases would be obtained; however, if the data applicable to the ionosphere at 1000 Km height are used i.e., $n_e = 10^4/cm^3$ and $T_e \sim T_{gas} = 2000^{\circ}K$, even then the Debye length were 3cm, much in excess of the diameter. Based on these considerations the plasma effects may be judged negligible.

5.0 Forces in the Magnetosphere

Figure 1 is a schematic depicting the magnetosphere and the KWOT orbits under consideration.

The problems which fall in this section are fairly varied. The following may help to clarify.

1. Voltage is induced in a medium which is moving in a magnetic field. It is not necessary that the speed of displacement be variable, that the magnetic field be nonuniform or that the attitude between moving element and magnetic field lines be changed.

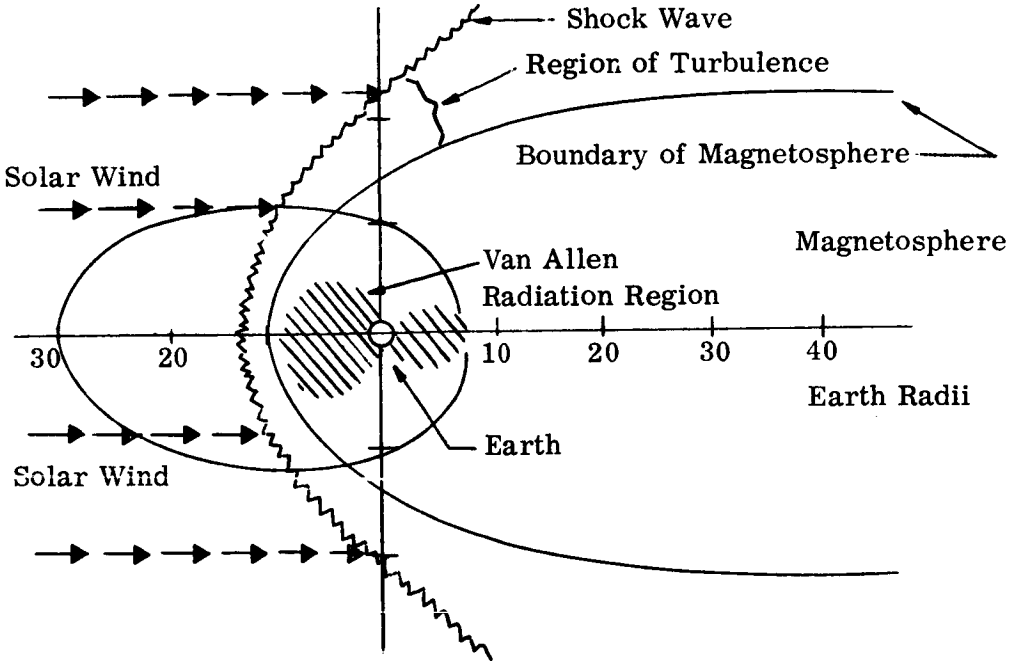

Figure 1. Orbit of KWOT

2. A current will develop in the above mentioned body if it is a conductor.

3. Charges will accumulate in the conducting elements if the flow of current was blocked.

4. The forces specific to the magnetosphere develop between the magnetic field and the currents in the members of the antenna. These currents may be impressed by external source or they may be induced by the magnetic field with which the interaction takes place.

5. The forces resulting from the interaction between current and magnetic field are external forces. These forces might change shape and velocity of the antenna.

6. Currents flowing in members of the antenna would generate forces acting between the members. The forces act within the system and cannot change the state of motion of the mass center, except by changing shape, attitude and, eventually, the drag.

The magnitude of the magnetic field and the direction of motion of each member with respect to the magnetic field should be known in order that the forces can be accurately computed. Anticipating that the prevalent forces are those caused by orbital motion, one may overestimate the effects of the magnetosphere force field. The magnitude of the magnetic field strength will be taken from Handbook of Geophysics and Space Environments, S. L. Valley, ed. 1965, (Reference 5) because no better data are available at this writing. It is necessary at this place to digress and to discuss peculiarities of the antenna and of its motion.

The antenna is designed in a manner that direct current cannot flow in it. Charges can, however, accumulate at blocking capacitors and along the members of the array. Twenty-five hours are required for one orbit. A second antenna motion is its rotation around the normal to its plane. This rotation has a period of one hour.

5.1 EQUATIONS FOR THE ESTIMATION OF THE FORCES

The equations have to be developed in four steps. The first is the collection of the equations describing the induced voltages which develop by displacements in the magnetic fields. The second is the computation of the resulting currents, the third the estimation of forces or moments, acting between the magnetic field and the currents. These latter may be conduction currents or convection currents, represented by charge separation on a moving system. All these ensuing forces are external. The fourth step is the computation of the internal forces, acting between current carrying elements of the antenna

system. The three first steps will be made for both the motions spelled out in the previous section. The effects of orbital motion will be presented in Paragraph 6.

5.1.1 Rotation around the normal to the plane of the antenna system.

a. Induced Voltage (U)

(See Reference 6 p. 433)

$$U = -\frac{1}{2}\,\omega\, B\,(r_1^{\,2} - r_2^{\,2}) \qquad (10)$$

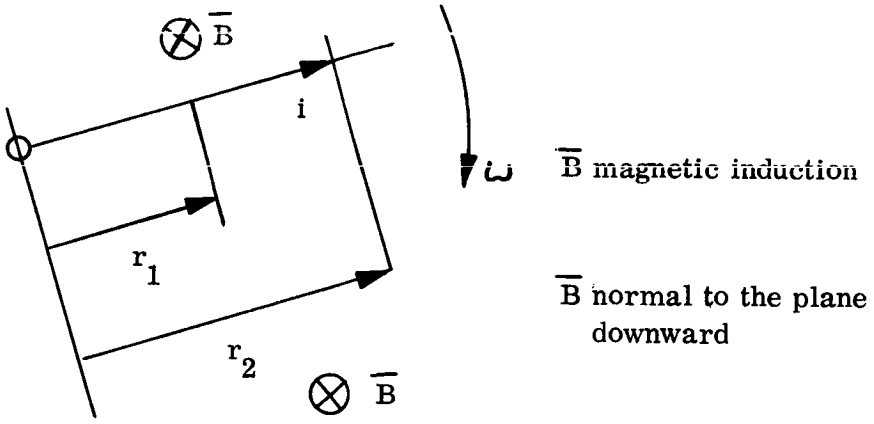

b. Resulting current (or charge)

Currents cannot circulate. Consequently, charges will separate in the legs. The separation would take place even if the antenna were not fitted with condensers. The charges may be written, in a general form:

$$Q = CU \qquad (11)$$

C is, at present, unknown, thus the numerical value of the charge is undetermined until C will be known. The charge must be of such a sign in the four points, where one may assume it to be concentrated, that the force between $\overline{B}$ and the rotating (convective) charges shall counteract the rotation.

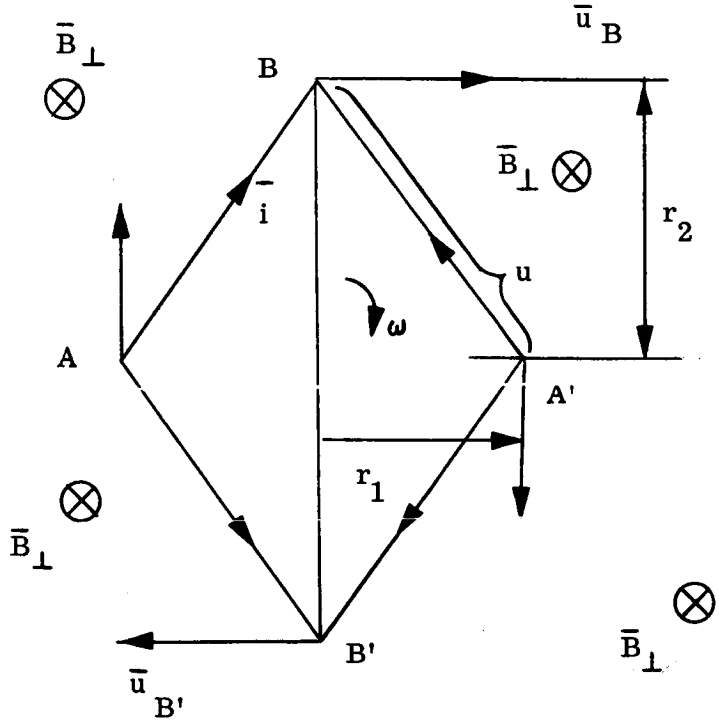

B is the component of the earth field normal to the plane of the antenna system. The component in the plane will be commented on in section 5.1.1.d.

c. Estimation of the forces

The force on a charge which moves in a magnetic field is as follows:

$$F = (\bar{u} \times \bar{B}) \qquad \text{(Reference 6 p. 376)} \qquad (12)$$

A positive charge may be put into the points B and B', and into the points A and A' an equal negative charge. The charges shall cause a drag, if they are well assumed. The force in B is vertically upward, in B' vertically downward. Consequently, these are opposite and do not result in a moment as long as the antenna is symmetrical, because they pass through the center of rotation. The force in A is horizontal and inward. The forces in A and A' are opposite and, as those in B and B', through the center.

The forces during charge separation can be found with the following equation:

$$d\bar{F} = (\bar{i} \times \bar{B})\, dl \qquad \text{(Reference 6 p. 391)} \qquad (13)$$

$\bar{i}$ current

$\bar{B}$ magnetic induction

dl element of conductor

The forces on the legs $\overline{A\,B}$ and $\overline{A'\,B'}$ are normal to them and point outward from the center, - they point inward for the leg $\overline{A'B}$, similarly for $\overline{A\,B'}$. The following picture is obtained:

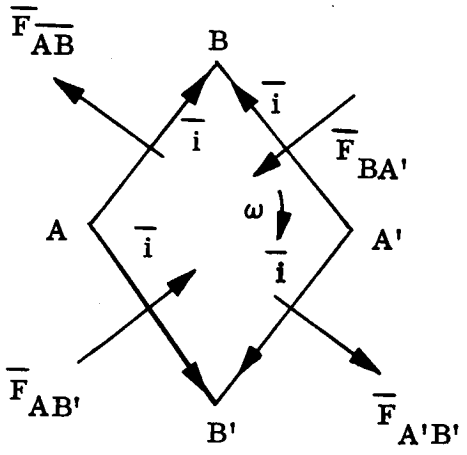

The four forces $\bar{F}$ are equal in absolute magnitude as the sides are of equal length. It is seen that a decelerating moment is obtained with the assumed direction of the current and sign of the charges. (Current = flow of ⊕ charge.)

d. Co-planar component

The co-planar component of the magnetic induction has a negligible effect on the forces generated by rotation around the axis of symmetry. The case may be different for the orbiting motion.

e. Forces between current carrying leads

As a memory refresher, the experiment on Page 293 of Westphal Physik, (Reference 6) (German), be referred to. The experiment shows that two parallel

currents attract each other, while two antiparallel currents repel. The following equation expresses the relationship between currents, geometry and the magnitude of the resulting force:

$$d^2F = \pm \frac{u_o (i_1 dl_1)(i_2 dl_2)}{4\pi r^2} \left[\cos (i_1, i_2) - \frac{3}{2} \cos (i_1 r) \cos (i_2 r)\right] \quad \text{Newtons} \qquad (14)$$

The sign is negative if the currents flow in the same direction because distance between them tends to decrease.

The above equation gives the force in Newtons. The currents shall be introduced in amperes, the distances in meters, the constant μo is 4π (10^{-7}) Volt sec/amp.meters. The symbols are defined as follows:

dl_1, dl_2	elements of the leads carrying the currents i_1 and i_2 respectively
i_1, i_2	the currents flowing in dl_1 and dl_2 resp.
r	the distance between dl_1 and dl_2
(i_1, i_2)	the angle between i_1 and i_2
(i_1, r), (i_2, r)	the angle between i_1 and r, and i_2 and r, resp.

Equation (14) may be used for the determination of the absolute value of the force acting between any two current carrying elements. It is well to remember that the force exerted by element (1) on element (2) is normal to element (2); the force exerted by element (2) on element (1) is, however, normal to element (1). The problem resolves itself for complete circuits (See Reference 8). Equation 14 may be written differently by deducing the interaction current-magnetic field--force between magnetic field and current, and the result is the differential form of the double line integral on p. 112, E (7-21) of Panofsky (Ref 18)):

$$d^2 \bar{F}_{12} = \frac{\mu_o}{4\pi r_{12}} i_2 dl_2 \times (i_1 dl_1 \times r_{12}) \qquad (15)$$

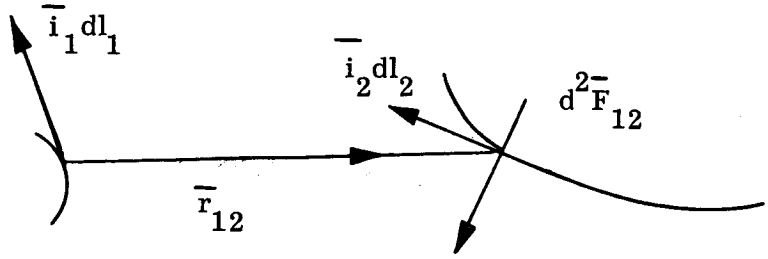

The forces F are internal forces and can change shape only. The currents to be used in Equation (14) or (15) are the algebraic sums of the impressed and induced currents. Currents are induced by motion in the earth magnetic field. The force between the earthfield and the currents in the members of the antenna system are external forces.

6.0 Electrodynamic Effects of the Orbital Motion

The study of the electrodynamic forces developed by the orbiting motion is more involved than the one concerned with those created by the rotation around the normal to the plane of the antenna. It is useful to introduce a system of co-ordinates.

The center of the antenna array, the surface normal, the velocity of the center of mass may be assumed to be in the plane of the orbit. The intensity of the earth's magnetic field is considered to be uniform within the boundary of the antenna array. The direction of the field lines is supposed to be known. The angle between the inward directed surface normal and the magnetic field lines be μ. (The field lines $\bar{B}$ and the surface normal $\bar{n}$ are not necessarily in the plane of the orbit.) The angle between the

orbital velocity and the surface normal be α. The surface normal points in the same direction as the vector of the angular velocity around the surface normal.

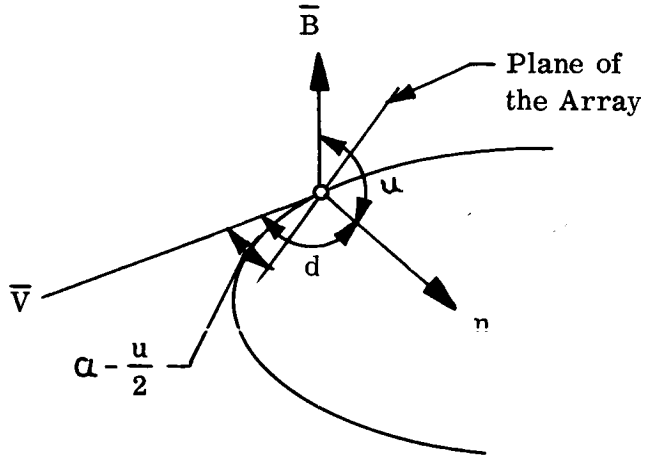

The component of the orbital velocity which lies in the plane of the array is V_{11}:

$$\bar{V}_{11} = \bar{V} \cos\left(\alpha - \frac{\pi}{2}\right) = \bar{V} \sin \alpha$$

Anticipating the statement of the following section, a second system of coordinates is introduced here. This system describes the attitude of the antenna system with respect to the velocity V_{11}. The coordinates are defined as shown on the following figure.

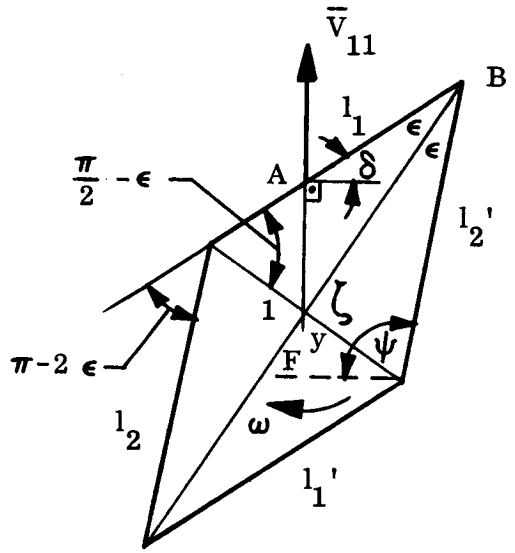

$$\beta = \omega t$$

The projections of the sides $1_1, 1_1'$ and $1_2, 1_2'$ on the normal to $\bar{V}_{11}$ are the quantities of interest.

6.1 Geometric relationships.

The projection of 1_1 or $1_1'$:

$$L_1 = 1_1 \cos \delta = 1_1' \cos \delta \qquad (18)$$

$$\delta + \frac{\pi}{2} + (\beta + \epsilon) = (\text{from } \Delta \text{ DAB}) = \pi$$

$$\delta \quad \frac{\pi}{2} - (\beta + \epsilon) = \frac{\pi}{2} - (\omega t + \epsilon) \tag{19}$$

$$L_1 = l_1 \sin(\omega t + \epsilon) = l_1' \sin 1\, \omega t + \epsilon) \tag{20, 20a}$$

The projection of 1_2 or $1_2'$:

$$L_2 = 1_2 \cos \psi = 1_2' \cos \psi \tag{21}$$

$$\zeta = \frac{\pi}{2} - \left[\psi - (\frac{\pi}{2} - \epsilon)\right] = \pi - (\psi + \epsilon) \tag{22}$$

$$\beta + \frac{\pi}{2} + \zeta = \pi = \beta + \frac{\pi}{2} + \left[\pi - (\psi + \epsilon)\right] \tag{23}$$

$$\psi = \frac{\pi}{2} + (\beta - \epsilon) = \frac{\pi}{2} + (\omega t - \epsilon) \tag{24}$$

$$\cos \psi = \sin(\epsilon - \omega t) \tag{25}$$

$$L_2 = 1_2 \sin(\epsilon - \omega t) = 1_2' \sin(\epsilon - \omega t) \tag{26, 26a}$$

$$1 = 1_1 = 1_2$$

6.2 Computation of the induced voltage

Panofsky, W.K.H., Classical Electricity and Magnetism, p. 149 gives the following equation for the voltage induced by the magnetic induction $\bar{B}$ in a strip of length 1 moving with the velocity $\bar{u}$, whereby the length is measured normal to $\bar{u}$:

$$U = \bar{1} \cdot (\bar{u} \times \bar{B}) \tag{27}$$

In the case under study $1 \rightarrow L_1$ or L_2, $\bar{u} \rightarrow \bar{V}_{11}$. The true direction of the magnetic field is not important for the estimation of the resulting effect. It is, however, of interest to know the direction of the induced current. The interaction between induced current, motion and magnetic field must be such that the motion be decelerated. This will be considered in the following sections. A comparison between the orbital and rotational velo-

cities will show that the change of the projected length (L_1 and L_2) is slow compared with the build-up of the induced voltage.

The orbital velocity V may be estimated from the following equation which expresses the equilibrium of inertial and gravitational forces. R is the radius of the earth, h the height of the (circular) orbit, g the gravitational acceleration at h = 0.

$$\frac{V^2}{R+h} = g \left(\frac{R}{R+h} \right)^2 \tag{28}$$

$$V = \sqrt{g \frac{R^2}{R+h}} = \sqrt{\frac{g R}{1 + \frac{h}{R}}} \tag{29}$$

The lower the altitude, the higher the velocity. One hundred thousand n. mi. may be the highest altitude or,

$$\frac{h}{R} = \frac{100}{3.45} = 29 \tag{30}$$

$$R = 6360 \text{ Km}, \quad g = 10 \text{ m/sec}^2$$

$$V \doteq \sqrt{\frac{10 \, (10^{-3}) \, 6.36 \, (10^3)}{1 + 29}} \doteq \sqrt{2.13 \text{ Km/sec}}$$

$$V \doteq 1.46 \text{ Km/sec} \tag{31}$$

The angular velocity which corresponds to one revolution per hour is

$$\omega = \frac{2\pi}{3600} = 1.745 \, (10^{-3}) \text{ rad/sec} \tag{32}$$

The circumferential velocity of any point of the rhombic antenna will not exceed the product of ω by the length of a leg, or

$$V_N < l\omega = 5.1 \text{ (Km)} \; 1.74 \, (10^{-3}) \text{ rad/sec} \doteq 0.009 \text{ Km/sec.} \tag{33}$$

$$\frac{V}{V_N} \quad \frac{1.46}{9} \, 10^3 \doteq 165 \tag{34}$$

Based on Equation (34), one may consider the problem of voltage induction according to Equation (27) to be a quasi-steady state case, i.e., the induced voltage follows from the instantaneous values of L, $\overline{cp}$, $\overline{u}$, and $\overline{B}$; the rate of change of any quantity is unimportant.

The complete equation for the induced voltage reads:

Legs 1_1 and $1_1'$ (from Eqq (27), (20) and (20a):

$$U_1 = 1 \sin(\omega t + \epsilon) \cdot (\overline{V}_{11} \times \overline{B}) \qquad (27a)$$

Legs 1_2 and $1_2'$ (from Eqq (27), (26) and (26a):

$$U_2 = 1 \sin(\epsilon - \omega t) \cdot (\overline{V}_{11} \times \overline{B}) \qquad (27b)$$

6.3 Computation of the induced currents (or charges)

The following figure helps to elucidate the case:

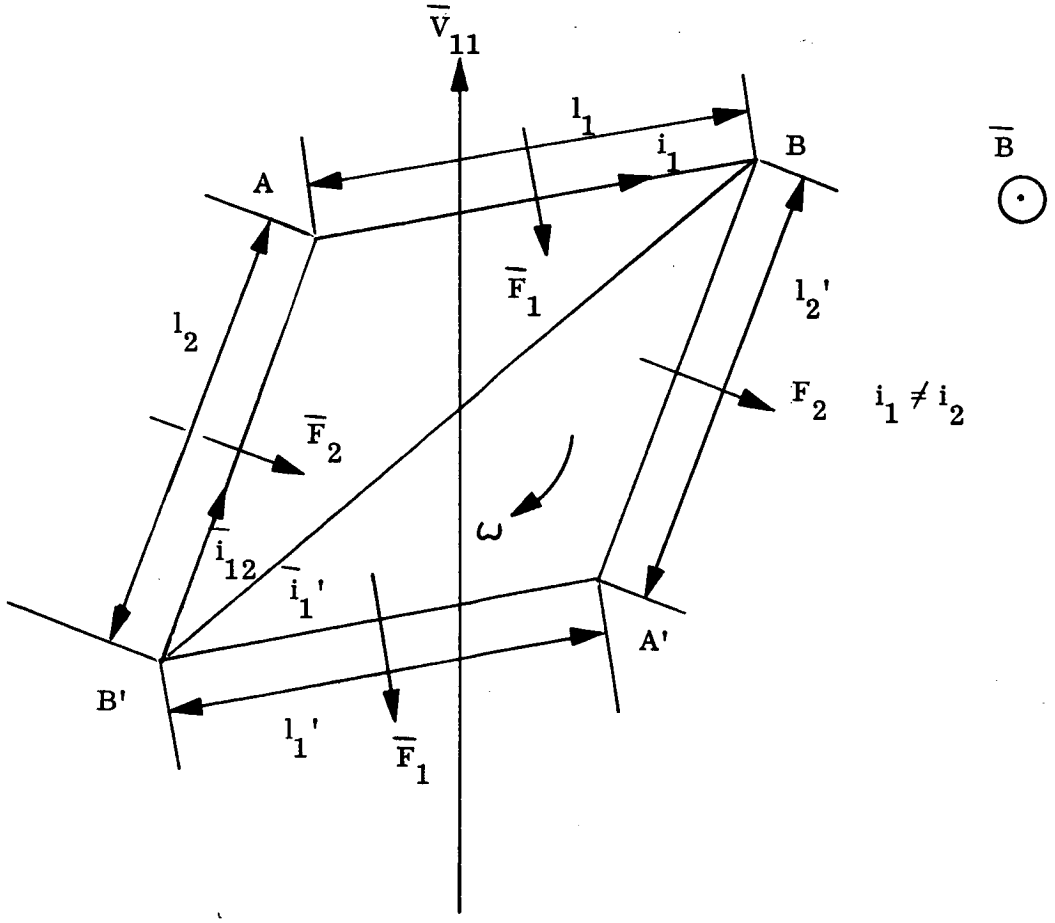

Charges in corners of the rhombus

Point / "Currents"	A	B	A'	B'	
A B	$-q_1$	$+q_1$			
B'A				$-q_1$ q_2	
B'A'			$+q_1$	$-q_1$	
A'B		$+q_2$	$-q_2$		
Net Charge	$-(q_1 - q_2)$	$+(q_1 + q_2)$	$+(q_1-q_2)$	$-(q_1+q_2)$	$-(q_1 + q_2)$

The preceding table shows that two dipoles would develop: A and A' form the one, B' and B the other. The charges can be found from Eq (27a) and (27b) and the, still unknown, effective capacitance of the legs of the antenna. (It is well to remember that forces may exist also on other members of the array, not on the rhombic only. Consequently, the effective capacitances of these members will have to be included.)

The consequence of charge accumulation in a structure moving in a magnetic field is that forces develop between the magnetic field and the moving charges. The forces on A and A' are equal in magnitude and opposite in direction because the charges are opposite. The charge in A' is positive and is displaced in direction of $\overline{V}$ (not $\overline{V}_{11}$). Thus, this force is to the right, and the resulting moment is counter clockwise. The moment resulting from the forces on the charges in B and B' is, however, clockwise.

6.5 Numerical example of an electrodynamic force.

It be assumed that direct current can flow in the rhombic, that the resistance is 80000 ohms, evenly distributed on the four legs, that the earth field is 10^{-2} Gauss. The area of the rhombic is 12 Km^2. The induced voltage will be estimated for a high rate of

change of the magnetic flux through the area enclosed by the antenna. The geometry of the earth-field suggests that the direction of the flux changes most rapidly when the antenna would pass over the magnetic poles. The time of ten hours for a complete reversal (vehicle in app. 45000 Km height) is reasonable. The field strength of 10^{-2} Gauss is a liberal overestimate for a height of 45000 Km because at five earth radii (35000 Km) the highest field strength is 0.028 Gauss.

The 10^{-2} Gauss correspond to $10^{-2}(10^{-4})$ Volt sec m^{-2} = B, the flux obtains with this value of the magnetic induction and with the area of 12 Km^2: $\phi = B \cdot A = 10^{-6}\ (10^{6})\ 12$; $\phi = 12$ Volt sec. The induced voltage, according to Faraday's law is:

$$U = \frac{-d\phi}{dt} = \frac{-12 \text{ Volt sec}}{36000} = 3.3\ (10^{-4}) \quad \text{Volts}$$

The resulting current is: $i = \frac{U}{R} = \frac{33(10^{-5})}{8.10^{4}} = 4\ (10^{-9})$ amp.

The rhombic of side length 5.15 Km is now replaced by a circle of equal perimeter of diameter d:

$$d = \frac{4\ (5.15)}{\pi} = 6.77 \text{ Km.}$$

The force per unit length on an element of current has to be radial for reasons of symmetry, see the figure below:

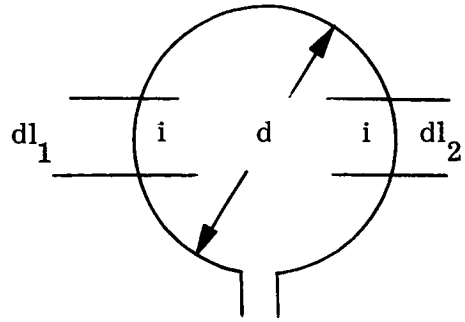

It will be shown in the next section that the assumed current direction satisfies Lenz's Law, namely that the motion (V_{11}) is decelerated by the interaction of the current with the earth field. One has to consider here that the current directions are in space, determined by magnetic field and vehicle velocity. The current flows in the leg 1_1 from A to B; when this leg will have turned in the position presently assumed by $1_2'$, the current will then be from B to A.

The flow of direct current is, however, blocked. Consequently, charges will develop. In the position sketched, positive charges will move in the direction of the arrows.

6.4 Estimation of the forces.

The internal forces, those connected with the interaction between current carrying elements are given by Eq (15). It can be stated that the elements repel each other.

The force acting in a field $\bar{B}$ on the elemental current $\bar{i}$ dl is given by the following equation:

$$d\bar{F} = dl\ (\bar{i} \times \bar{B}) \tag{36}$$

The component of the forces $\bar{F}_1$ which is antiparalled to $\bar{V}_{11}$ is greater than the parallel component of the forces $\bar{F}_2$. This is so because the projection of the sides $\overline{AB}$ and $\overline{A'B'}$ on the normal to V_{11} is larger than the corresponding projections of $\overline{AB'}$ and $\overline{A'B}$.

Convective currents will exist because charges develop in consequence of the blockage of direct currents. The charge distribution can be computed if effective capacitances of the elements of the antenna array are known. One may assume, for sake of illustration, that charges would collect in the corners of the rhombus. The following table illustrates the case:

The force per unit length is, according to Ampere's law:

$$\overline{F}/m = uo \frac{i^2}{\pi d^2} = (4\pi \cdot 10^{-7}) \frac{(4\pi \cdot 10^{-9})^2}{\pi (6.77)^2 10^{6-}} = 1.39\ (10^{-31})\ N/m$$

The force is negligibly small, even if reckoned for a 5 Km long side.

7.0 Conclusions

The magnitude has been estimated of the non-inertial forces which act on an antenna moving in the magnetic field of the earth. The analyses show that the internal force which exists between opposite elements of an antenna by virtue of currents induced by the earthfield are small.

Equations have been presented for the forces caused by interaction between induced currents or charges and the inducing earth-field.

The force exerted by solar wind and by the proton stream of a strong solar flare have also been estimated and was also found to be small. The specific, charge determined forces in the Van Allen belt have been considered, based on the ratio of Debye length to antenna element diameter, to be insignificant.

REFERENCES
Appendix A

1. K. A. Ehricke: "Solar Engine", in McGraw-Hill Encyclopedia of Science and Technology, Vol. 12, p. 470, Fig. 5, Editor in Chief, W. H. Crouse, McGraw-Hill Book Company, Inc., 1960.

2. Branigan, T. L., ed., TRW Space Log, Winter 1965-66.

3. R. F. Post: "Plasma Physics", in McGraw-Hill Encyclopedia of Science and Technology, Vol. 10, p 385ff Editor in chief. W. H. Crouse. McGraw-Hill Book Company, Inc., 1960.

4. J. A. Van Allen: "Van Allen Radiation", in McGraw-Hill Encyclopedia of Science and Technology, Vol. 14, p. 265ff Editor in Chief, W. H. Crouse, McGraw-Hill Book Company, Inc., 1960.

5. Valley, S. L., Ed.: Handbook of Geophysics and Space Environments, Macmillan, 1965.

6. Westphal, W. H., Physik, 16th and 17th edition (German), Springer Verlag, 1953.

7. Westphal, W. H., Physik, 2nd Ed. (German, Springer Verlag.)

8. Panofsky, W. K. H. and Phillips, Melba, "Classical Electricity and Magnetism", Addison-Wesley Publishing Co., Inc., 1955.

PHASE 1 FINAL REPORT

ENGINEERING FEASIBILITY STUDY OF A KILOMETER WAVE ORBITING TELESCOPE

NGR 23-005-131

Submitted by

Fred T. Haddock

University of Michigan
Radio Astronomy Observatory
Ann Arbor, Michigan

October 1966

TABLE OF CONTENTS

LIST OF FIGURES

APPENDICES

I. Summary of Phase I Engineering Feasibility Study

This is the final report of the first phase of an engineering feasibility study of a Kilometer Wave Orbiting Telescope (KWOT) by the University of Michigan Radio Astronomy Observatory (UM|RAO). A modest level of effort had been under way in this area since the latter of part of 1964. Professor Haddock made a presentation on large structures in space, which dealt primarily with the KWOT concept, to the President's Scientific Advisory Subcommittee on Space Science in August 1965. Recommendation that further study be made on such structures came out of the Woods Hole Summer Study Group of the National Academy of Sciences. The present study was initiated in November 1965 under NASA Grant NCR 23-005-131.

The principal results of the first phase study are as follows:

A. The possibility of mission feasibility appears favorable enough that we recommend continuing the study.

B. Engineering feasibility, in the usual sense of physical realizability within the constraints set down for one time operation, appears to be quite favorable. There does not appear to be any major state of the art problems in this regard. Excellent engineering design, construction and testing is the prime requirement.

C. Further study is needed in all the major areas of structure dynamics and control, antenna performance, and peripheral systems with special emphasis on long term reliability, which is the distinguishing difference between mission and engineering feasibility.

D. It appears likely that if man were made available with modest work capability, he could enhance the overall performance and reliability of such a system. His use in the deployment, repair and maintenance work appears to be his principal value. It is beyond the scope of this study to determine if the cost of providing this service is justifiable.

E. The following pertain to the KWOT system as illustrated in Fig. 1

1. A structure with relatively few structural elements seems preferable to a more complex structure from the points of view of stability, ease of erection, total weight, and tension available to keep the rhombic legs straight.

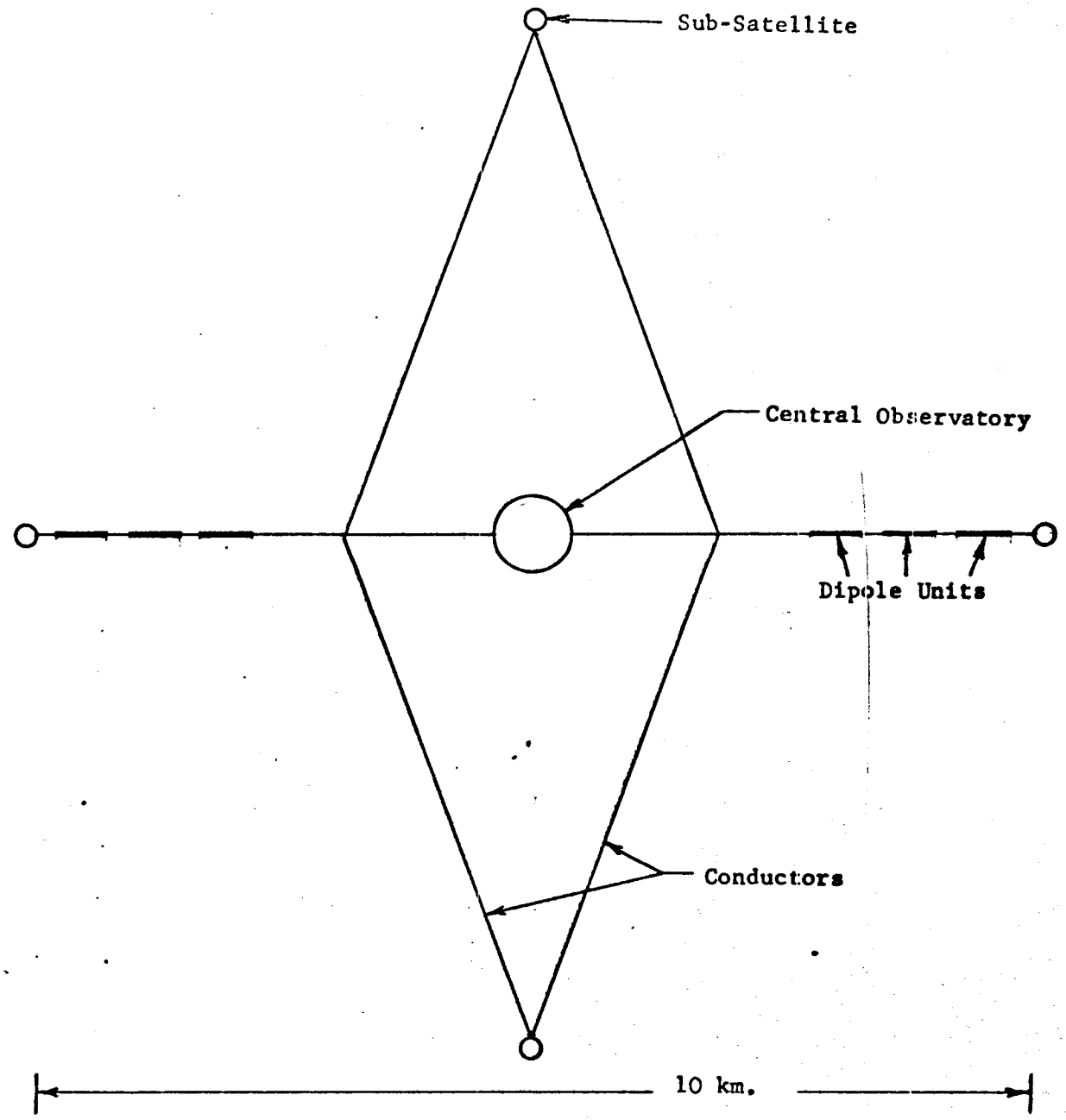

Figure 1 - KWOT Structure

Weight Estimates for KWOT

Sub-Systems and Components	Central Observatory (lb)	Sub-satellites Rhombic (lb)	Sub-satellites Interferometer (lb)	Dipole Unit (lb)
1. Sensors for attitude and position				
Antennas	12	2	2	-
RF (Transmitters and receivers)	10	3	3	-
Other electronics	8	2	2	-
2. Thrusters for attitude and position				
Valves, nozzles, etc.	16	16	16	-
Fuel	60	60	60	-
Control electronics	6	2	2	-
3. Pointing Sensors	12	-	-	-
4. Communications				
Internal to KWOT	14	1	1	1
KWOT to ground	30	-	-	-
5. Data Sub-system				
Computer	20	-	-	-
Other electronics	25	2	2	-
6. Radio Astronomy				
Pre-amp	-	2	-	1
Radiometers	50	-	-	-
7. Primary Power				
Solar cells	100	15	10	2
Batteries	50	10	10	2
8. Structure (includes thermal control	250	25	25	2.5
9. Deployment mechanism	100	25	25	2.0
10. Redundancy allowance	375	12	12	2.5
Total Each Unit	1138	177	170	13
Total All Units	1138	354	340	78

SUB-TOTAL FOR ALL ABOVE SUB-SYSTEMS..... 1910

- Antenna and Guy Lines 750

TOTAL KWOT SYSTEM 26601b

Electrical Power Estimates for KWOT Units

Sub-Systems and Components	Central Observatory (Watts)	Sub-Satellites Rhombic (Watts)	Sub-Satellites Interferometer (Watts)	Dipole Unit (Watts)
1. Sensors for attitude and position				
RF (transmitters and receivers)	5	2	2	-
Other electronics	5	1	1	-
2. Thrusters for attitude and position				
Control electronics	1	1	1	-
3. Pointing sensors	10	-	-	-
4. Communications				
Internal to KWOT	8	2	2	1
KWOT to ground	20	-	-	-
5. Data sub-system				
Computer	50	-	-	-
Other electronics	50	10	10	-
6. Radio Astronomy	20	5	-	5
Total power per unit, in watts	169	21	16	6
Deployment mechanism (only powered during deployment)	50	10	10	-
Total Average Power - All Units	169	42	32	36
Total Average Power			279 Watts	

2. Results from a study of a simplified model of KWOT indicate stability in that the oscillations do not continue to grow with time.

3. Gross weight of the central observatory is between 1000 and 3000 lb. The gross weight of each sub-satellite is between 100 and 200 lb. The total gross weight of the system is between 1400 and 4000 lb.

4. The sub-satellite thruster fuel required to deploy and to precess the spin axis of KWOT appears to be reasonable. Approximately 0.5 lb is required to spin up, and 1.5 lb to precess 180° in small steps, assuming 100 lb total weight per sub-satellite.

5. Position and attitude of sub-satellites may be sensed with sufficient accuracy.

6. Active control of sub-satellite position and attitude by thrusters is possible within a reasonable limitation of gross weight (<200 lb).

7. Gravity gradient is the largest perturbing force, and even it requires only a modest expenditure of thruster fuel to counteract if perigee is higher than about 10,000 nautical miles.

8. It is possible to make a complete sky survey in a relatively few days, if all frequencies are observed simultaneously.

9. A non-spinning mode seems possible for at least part of the KWOT lifetime.

10. Further analysis of the rhombic-interferometer antenna system has produced evidence that the initial approximate performance evaluations were not greatly in error. These indicate an elliptical beam, with angular dimensions (to half-power points) of 16° by 1.7°, and strongest sidelobes about 5 db below the main beam, unless the dipoles are so arranged to cancel the major sidelobes. There is no basis as yet for going to a non-real time system.

II. Study Background

A. Scientific Objectives

The broad scientific objectives of a high-resolution, low-frequency radio telescope are:

1. to measure the radio spectra of a large number of galactic and extragalactic radio sources in the frequency band from 10 kHz to 40 MHz;

2. to obtain complete high resolution maps of the galactic and extragalactic radio emission over the above frequency band;

3. to measure the character and variations of radio emission from the sun, planets and other sources, and to search for variable absorption and interplanetary scintillation effects;

4. to measure the brightness distribution over the above frequency band across individual radio sources by using lunar occultations when the circumstances are appropriate;

5. to determine the statistical parameters of the cosmic background noise fluctuations in order to test hypotheses regarding the distribution of radio sources in space.

The more specific objectives of the KWOT project are to:

1. measure the flux densities of several dozen extragalactic and galactic sources at a number of frequencies near 1 MHz;

2. map the cosmic background noise level of the full sky at a number of frequencies from 0.1 MHz to 10 MHz;

3. record variations of radio emission from the sun, Jupiter and other variable radio sources, including the variations due to inhomogeneities in the interplanetary medium at a number of frequencies between 0.1 MHz and 10 MHz;

4. measure the brightness distribution across individual radio sources which are occulted by the moon during the life of KWOT when the circumstances of the occultation are appropriate;

5. obtain data on the statistical parameters of cosmic background noise fluctuation at a few frequencies near 1 MHz.

B. Operational Requirements

An antenna with high directional gain (small beam area) is required to map the sky and measure the flux density of radio sources. In order to measure several dozen sources, a beam area of not more than about 80 square degrees is required. To achieve this resolution a large physical structure is required. A moderately broad-beam antenna is proposed for flux density measurements of discrete sources and contour mapping of the cosmic background noise. A compound interferometer can then be used to provide an estimate of source size for the larger and stronger sources and better data on the statistical character of the cosmic background due to many weaker sources.

Any high gain antenna must have a precisely controlled geometrical configuration. If the shape changes, the antenna properties change. Any deviation from the design shape degrades antenna gain and resolution, changes the pattern, and degrades system sensitivity. Since a rigid geometry is not practical, some limits must be set on allowable deviations.

It is desirable to have the satellite outside the earth's magnetosphere for at least a sizable fraction of its life. This appears to require an apogee of at least 60,000 nautical miles. Further study of a synchronous orbit is necessary. The choice of orbit will be influenced by studies of the dynamics of the large antenna and the distortions produced by internal and external perturbing forces and by radio propagation effects due to the ionosphere and the solar corona.

The stabilization and the scanning of the antenna are mutually related. Ideally, one would like to have complete control over the pointing of the antenna. If the structure were to be spinning then precession of the spin axis by 180° can provide full sky coverage. The precessional rate may be chosen so that any zone of the sky can be scanned slowly enough to obtain adequate sensitivity and complete coverage.

The pointing of the antenna should be known to an accuracy of at least 0.1 degree. The required pointing accuracy is a function of the antenna beamwidth and the accuracy to which the pattern of the antenna is known or can be determined. Knowledge of the pattern and beamwidth may be obtained by monitoring the relative positions of the elements of the antenna and should be checked by a specially designed pattern-measuring space vehicle.

The cosmic background noise near 1 MHz is relatively intense, so that the cosmic noise power fed into the receivers will be several orders greater than the internally generated receiver noise. Therefore receiver noise is not a serious problem. The confusion between sources will be the limiting factor in measuring individual radio source flux densities.

C. Proposed Structure

As a vehicle for the present feasibility study, a KWOT structure is proposed which consists of a central observatory surrounded by four sub-satellites, with all five bodies connected by a set of conducting and non-conducting filaments. The overall diameter of the structure is about 10 kilometers. The conducting portions of the connecting elements form a rhombic antenna and an interferometer array of dipoles. The signals from the rhombic and interferometer are combined in such a way that an antenna pattern is generated which combines the resolution of the interferometer with the unidirectional properties of the rhombic.

The entire structure spins about an axis perpendicular to its plane with a period of approximately one hour. This spinning motion serves to scan the antenna array over the sky and with the precession of the spin axis, which is brought about by the active thruster control system, will provide complete sky coverage. The spinning motion also aids in maintaining the shape of the structure for this mode of operation. It may be desirable for some types of observing programs to have the antenna array stopped from spinning but still controlled with regard to pointing the beam.

D. Aims of Present Study

Because of the modest funding and the limited time of this first phase feasibility study, it was decided to concentrate the greater portion of the effort on two aspects of the rhombic-interferometer structure. These aspects are the dynamics of the structure and the electrical properties of the antenna. The ultimate objective of these studies is to obtain an estimate of the amount of distortion which might be experienced by the structure when in orbit, and to determine the effect of this distortion on the antenna pattern. Both of these problems can be completely solved only through extremely complex theoretical analysis. There is little prior theoretical work which is applicable, and even less practical experience.

The primary objectives of this phase of the study are to develop analysis techniques in each of the areas of structural dynamics and electrical properties of the antenna, and to apply these techniques as far as possible in a preliminary evaluation of the system performance. Secondary objectives of the present study include a preliminary survey of deployment methods and an analysis of various sub-systems for the rhombic-interferometer system, and a survey of orbital effects. About 90% of the effort has been devoted to the primary objectives and about 10% to the secondary objectives.

III. Systems Studies

A. Introduction

This area concerns the peripheral systems considerations to the KWOT and has included refinement and revision of the KWOT concept, correlation of the studies of antenna properties with the studies of structure dynamics, consideration of system requirements for several possible observing modes, identification of sub-systems and preliminary performance requirements, choice of orbit, and the possible role of man in KWOT.

B. Description of the System

1. System Layout

The KWOT structure is shown in Fig. 1. This structure includes a rhombic antenna ten kilometers long, consisting of thin, lightweight conductors, with a thin, lightweight cross member, also ten kilometers long, crossing the rhombic along its minor diagonal. Along most of its length, this cross member is non-conducting, but six or eight conducting lengths are provided which act as dipole elements of the interferometer array. There may be or may not be a second member extending along the major diagonal of the rhombic, from apex to apex. Four bodies, or sub-satellites, are attached to these lines, one at each end of the major diagonal of the rhombic, and one at each end of the cross member. These sub-satellites control the shape and orientation of the structure by means of thrusters actuated by a control system and partly by exerting centrifugal force on the lines. A detailed study of these units and their use is found in Appendix D. A Central Observatory in the center of the structure houses instrumentation for controlling the sub-satellites, processing the data, and communicating with the sub-satellite and ground stations. A dipole unit located in the center of each dipole relays the signal collected in that dipole to the Central Observatory for processing.

The correlation of the results of the studies of antenna properties with the result of the studies of structural dynamics has been looked upon as the key to the feasibility question. Obviously, if the present KWOT concept is to be feasible, it must be shown that the physical configuration of the components of the structure can be maintained within sufficiently narrow limits that the antenna performance is not intolerably degraded. Preliminary analysis of the rhombic performance has enabled us to place a value of ± 50 meters on this position tolerance, so the studies of structural dynamics have been carried out subject to the ground rule that no part of the antenna structure was to deviate more than 50 meters from its prescribed position relative to the rest of the structure. The studies of structural dynamics have indicated that this tolerance can be achieved with reasonable expenditure of thruster fuel if a judicious choice of orbit is made.

Some parts of the structure can deviate more than 50 meters from their proper positions without seriously hampering the antenna performance, while for other parts a 50 meter displacement is enough to cause concern. Hence a more detailed study of structure distortions is indicated. We have developed the mathematical techniques required to carry out a more rigorous and detailed study during the next phase of the feasibility study.

To provide the necessary background for system analysis, a set of astronomical observing programs have been generated which are representative of those which might be performed with KWOT. These programs include radio source flux density measurement, sky mapping, a search for variable sources, lunar occultation observations, and a search for noise bursts from such bodies as the sun and Jupiter.

To accomplish these observations, three observing modes are postulated: mapping mode, a repeat scan mode, and a non-scan mode. Each mode imposes different requirements on KWOT, especially with respect to fuel consumption. Estimates of these requirements are worked out, and a typical fuel budget is present in Appendix A.

Several sub-systems of KWOT have been defined, and preliminary statements of the functional requirements on these systems are presented in Appendix A. All of these requirements seem to be within the present state of the art. So far, there is no indication that any new and exotic techniques are required to implement KWOT. It appears as though the major engineering effort in the design of KWOT will be devoted to the question of reliability and probable lifetime.

Several factors enter into the choice of orbit for KWOT. Major factors are the scientific requirements and the requirements for structural stability, launch vehicle considerations, and coverage by ground stations. The scientific requirements and the requirements for structural stability both favor high orbits. It is required that the KWOT orbit be well above the earth's ionosphere, and it is desirable that a large portion of the observations be made outside the earth's magnetosphere.

Our present studies of structural dynamics indicate that if perigee is above about 18,500 km, there should be no significant distortions

due to gravitational effects. More refined studies may permit us to set this limit somewhat lower, but if apogee is above 110,000 km, there would be no great reduction in launch thrust requirements if perigee were reduced below 18,500 km.

As presently conceived KWOT does not include accommodations for man. It does take account of equipment and sub-system design factors which allow repair and maintenance by man, if he is available.

2. Deployment

A possible deployment sequence is shown symbolically in Fig. 2. The lines could be paid out from reels mounted either on the central body or on the sub-satellites, or perhaps both. Thrusters on the sub-satellites would maintain tension upon the lines until the structure is spinning fast enough to generate significant centrifugal force. It is not obvious whether the spin-up of the structure should be started while the sub-satellites are moving out, or deferred until they have reached their final radius. Either way appears possible.

3. Frequency Coverage

The optimum frequency for a rhombic antenna depends upon the dimensions, and particularly upon the apex angle. The KWOT antenna could be tuned over a quite wide frequency range by simply reeling the cross-member in and out from the Central Observatory. Fig. 3 illustrates the change in configuration with frequency. The radius of rotation of the sub-satellites also changes, of course, and some thrust would be required to compensate for the changes in angular momentum. Only a fraction of a pound of fuel would be required in each sub-satellite for this maneuver. No detailed studies of the dynamics of this operation have been performed as yet, but the technique promises to broaden the effective frequency range of KWOT by a considerable factor.

4. Calibration

The value of radio astronomy observations depends not only upon the performance characteristics of the antenna system, but also upon the degree of certainty with which these characteristics are known. Of particular import are the beam profile, and the location and strength

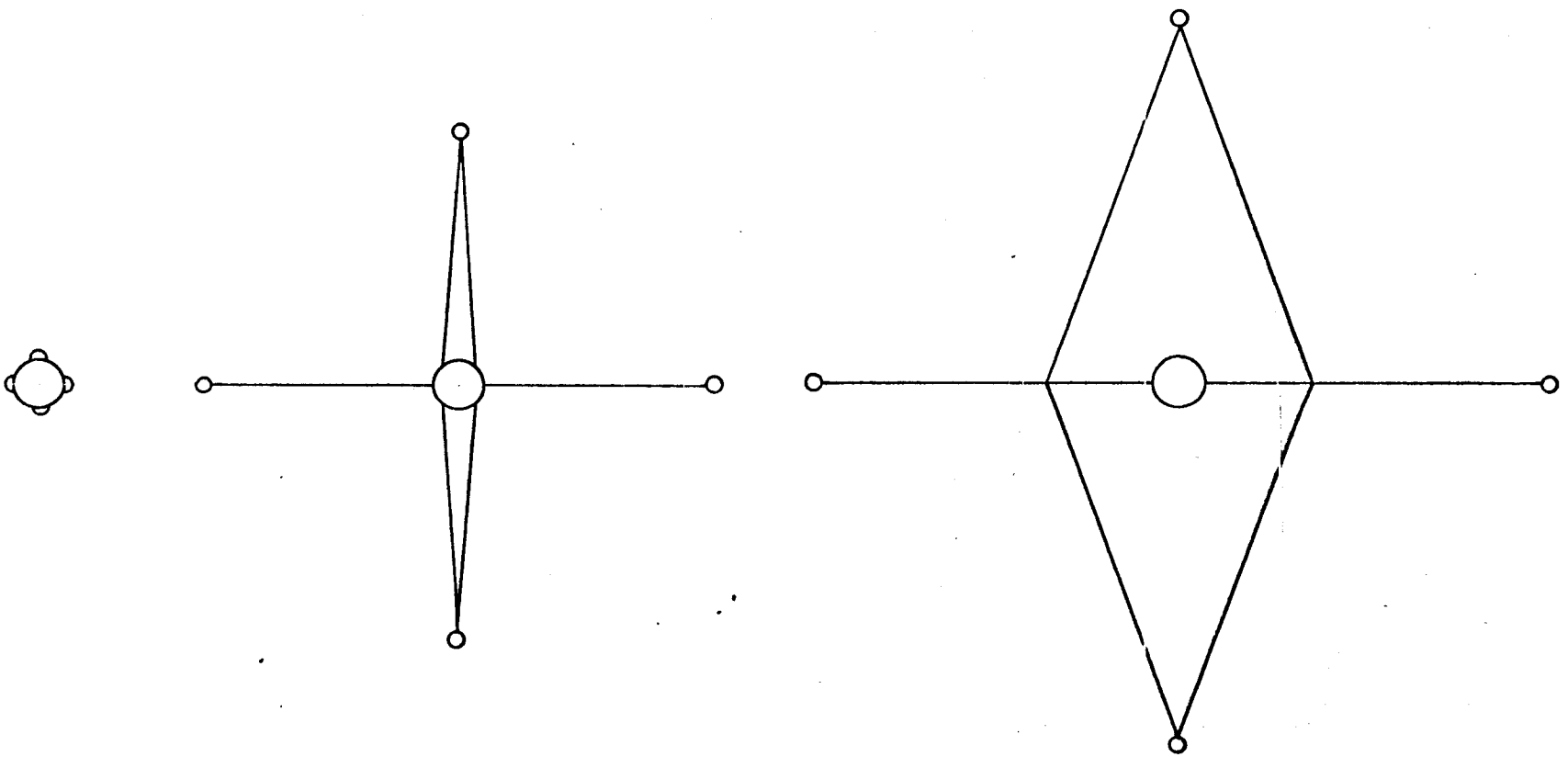

DEPLOYMENT SEQUENCE

Figure 2

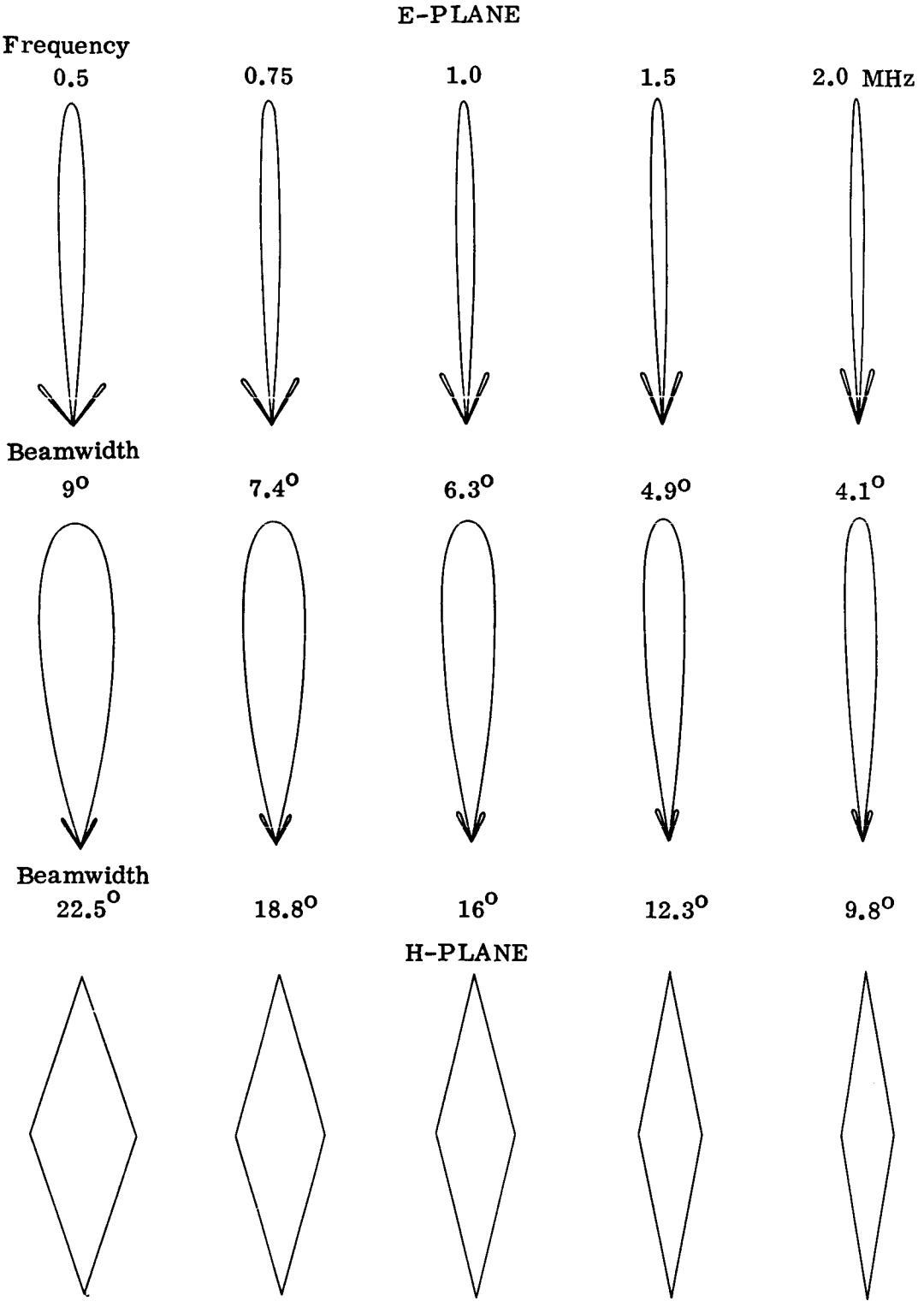

SHAPE AND PATTERNS OF A RHOMBIC AT VARIOUS FREQUENCIES

Figure 3

of antenna sidelobes. As the KWOT antenna is of unprecendented nature, it is particularly important we obtain confirmation of the antenna pattern. The pattern will be calculated using the best theory available, and confirmed with scale models on an antenna test range, but there will still be enough uncertainty to warrant an in-flight calibration of the antenna pattern. Our present concept of this in-flight calibration requires a separate calibrator spacecraft which is in an orbit with the same period as KWOT, but with slightly different parameters, so that it accompanies KWOT in its orbit, but generally at distances of a few hundred kilometers. Such a distance is required to place the calibrator in the "far field" of the KWOT antenna, so that a valid calibration is obtained. The relative motion of the calibrator with respect to KWOT would describe some sort of a loop around KWOT once each orbit. This motion, combined with the scanning of KWOT, would allow the "mapping" of the KWOT antenna pattern to any desired level of detail.

The calibrator spacecraft would carry calibration transmitters of relatively low power at one or more selected frequencies in the KWOT spectrum, as well as a tracking beacon transmitter and a simple command receiver for turning the calibration transmitters on and off by ground command. It is, therefore, a very small payload, and could be launched "piggyback" with KWOT and then injected into its own orbit with a small thrust. Other backup calibrator spacecraft could be carred in KWOT, to be ejected by ground command if the initial calibrator fails.

Detailed information on this section is found in Appendix A.

IV. Structural Dynamics

A. Introduction

The design of very large flexible structures for orbital space applications is a relatively new field and very little experience is available as background for this study. Of primary concern are the stability of the structure in its orbital environment and the degree of geometric distortion it suffers from the perturbing forces acting upon it.

A sizeable portion of the effort in this area was devoted to the development of techniques for analyzing such structures. These techniques

have been developed to the point that the completely modeled KWOT can be analyzed using numerical analysis techniques on a computer. The results from simplified models of KWOT, which are somewhat easier to analyze, are presented here to give approximate answers to the questions of dynamics. We plan to complete the full model analysis in the next phase of the feasibility study.

B. Techniques Used in First Phase Analysis

In the course of this study, several techniques of analysis have been used. A brief discussion and summary of these techniques is given below and references to the appropriate appendix made:

1. To derive the equations of motion for the continuous description of KWOT, the Lagrangian functional can be formulated. The application of Hamilton's principle of stationary action will then generate the appropriate equations of motion and associated boundary conditions. (Appendix B and C)

2. The Lagrangian method for deriving equations of motion for a lumped mass model was found to be highly effective. This approach can handle any order discrete system and hence may be used for the more complicated dynamic systems to be studied in the next phase (Appendix D and E)

3. Digital computer solution of the lumped mass equations by a Runge-Kutta technique provides the response of the system for a finite time interval. This method can handle a much more complicated lumped model. (Appendix E)

4. The numerical application of Floquete theory with appropriate matrix operations can be used to determine stability for a certain class of linear equation which result when the lumped mass equations are linearized about a certain type of motion. (Appendix E)

5. For complex elastic structures, the stiffness matrix approach allows one to systematically write the force-deformation relations for the discrete approximation to the system. (Appendix F)

C. Dynamics of Simplified Model Structure

The KWOT structure may be thought of as an assembly of rigid bodies interconnected by elastic lines. Insight into the dynamics of such a structure may be gained by studying the mathematical equations for various models in which the rigid bodies are represented as point masses and the interconnecting elastic lines as springs. The dynamic equations of motion may be written for the point masses assuming the model is spinning in orbit. A computer can be used to determine the motion of the point masses under various conditions.

The remainder of the section discusses the results obtained from one such investigation. The complete report of the investigation is contained in Appendix E.

The basic structure of the KWOT system consists of four sub-satellites connected to a Central Observatory by thin flexible wires. The Central Observatory as originally conceived, is an order of magnitude heavier than a sub-satellite so it may be assumed that the motion of the center of mass is uncoupled from the sub-satellite or relative motion. The equations of motion for the sub-satellite in this basic structure were investigated by examining a simple model of two point masses connected by a spring. The model was assumed to be spinning in orbit at a nominal rate of one revolution per hour. All disturbing forces except those due to the gradient in the earth's gravitational were considered negligible.

The linearized equations so derived are ordinary, second order, forced, linear differential equations with periodic coefficients. The solution of a set of simultaneous equations of this type is a formidible task. Since an analytic approach did not appear to be fruitful, the equations were programmed for a computer. Part of the work was done on an analog computer and part was done on a digital computer. Time on the digital machines costs about 10 times that on the analog machine so only the cases that were too complex for the analog machine were done on the digital machine.

Analog computer runs were made for various circular orbits with the plane of the KWOT structure always in the orbital plane. The spring constant was varied. This investigation did not reveal any geometric distortion of the model that continue to grow with time. Distortions to the model were of two kinds. First the point masses (sub-satellites) oscillate

radially about the nominal stretched length of the supporting spring. This distortion means that the distance from the Central Observatory to the sub-satellite would not remain fixed but would go through periodic variations. The maximum amplitude of this oscillation is on the order of inches as shown in Figure 4, [redacted] and is considered negligible. The second type of geometric distortion for this model was such that the angle formed by two sub-satellites and the Central Observatory would not remain at 90° but would go through periodic variations. This distortion may be thought of as one sub-satellite catching up to or dropping behind the one in front of it and so is called a variation in the spin rate. The amplitude of this variation for a 30,000 nautical mile orbit is less than 0.1% of the basic 1 revolution per hour spin rate as shown in Figure 5, [redacted] The amplitude of the variation is even less for higher orbits.

The equation of motion for elliptic orbits when the plane of the KWOT structure was out of the orbital plane could not be handled on the analog computer. Computations for this case were done digitally.

The results of the digital runs confirmed the result obtained on the analog computer in that no geometric distortions were found that continue to grow with time. The digital runs clearly showed the nature of the geometric distortions as the structure passes through perigee. The distortions of the KWOT model were of three kinds when the plane of the structure is not in the orbital plane. First, the sub-satellites oscillate radially about the nominal stretched length of the supporting line; second the spin rate of the sub-satellites go through periodic variations; and third the plane of the KWOT structure is tilted a slight amount following each pass through perigee.

The axial oscillations shown in Figure 6 contain a high frequency component like that found for circular orbits, and in addition a low frequency component near perigee. This low frequency component has a peak amplitude of 6 inches for a perigee of 10,000 nautical miles. The amplitude of this oscillation decays after the system passes through perigee. Distortions of this level will cause no measurable change in the antenna beam pattern.

The periodic variations in spin rate shown in Figure 7 also go through their maximum amplitude at perigee and then decay. For orbits with perigees as low as 10,000 nautical miles from the center of the earth this variation

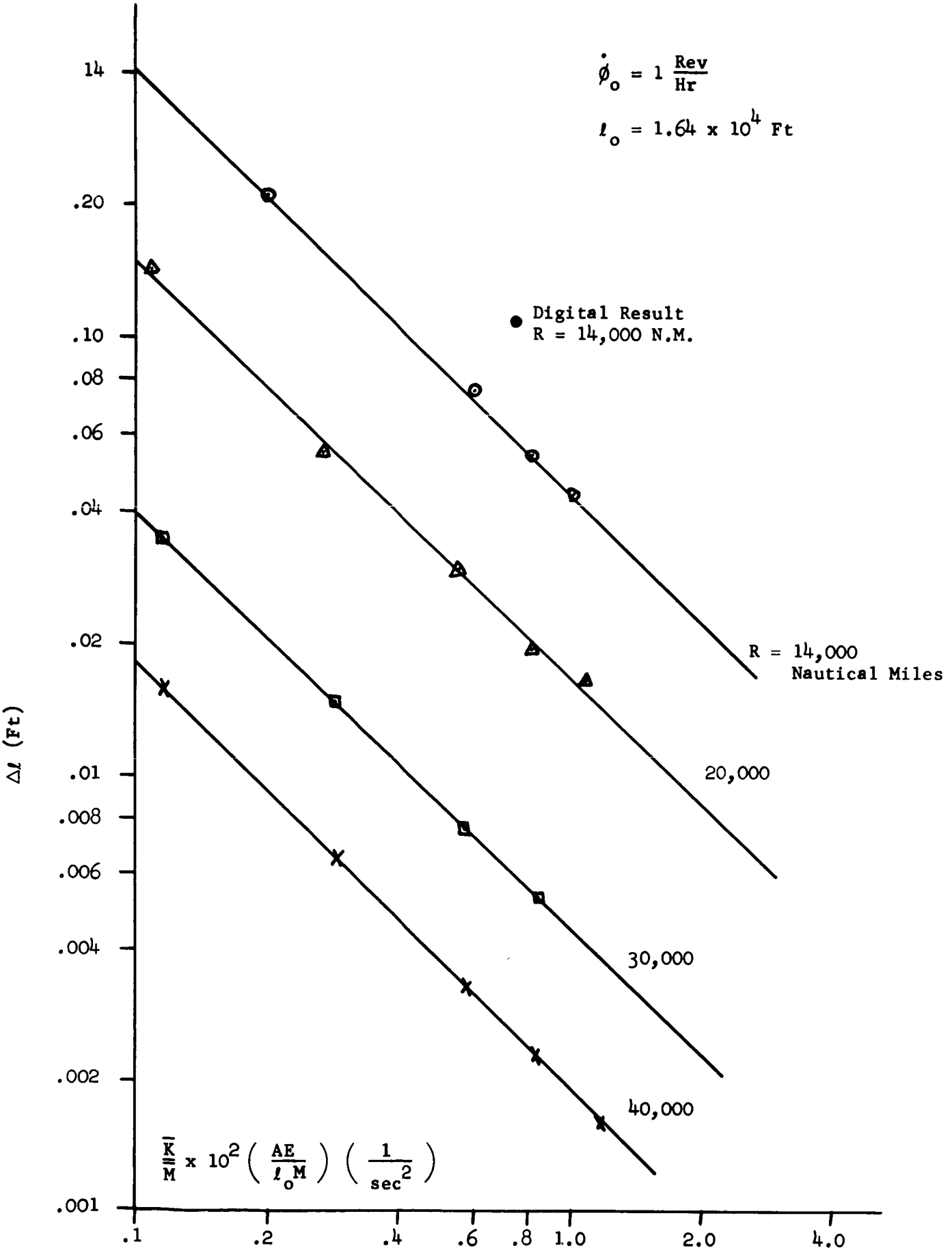

Figure 4 - Axial Deviation vs. Spring Stiffness (planar motion)

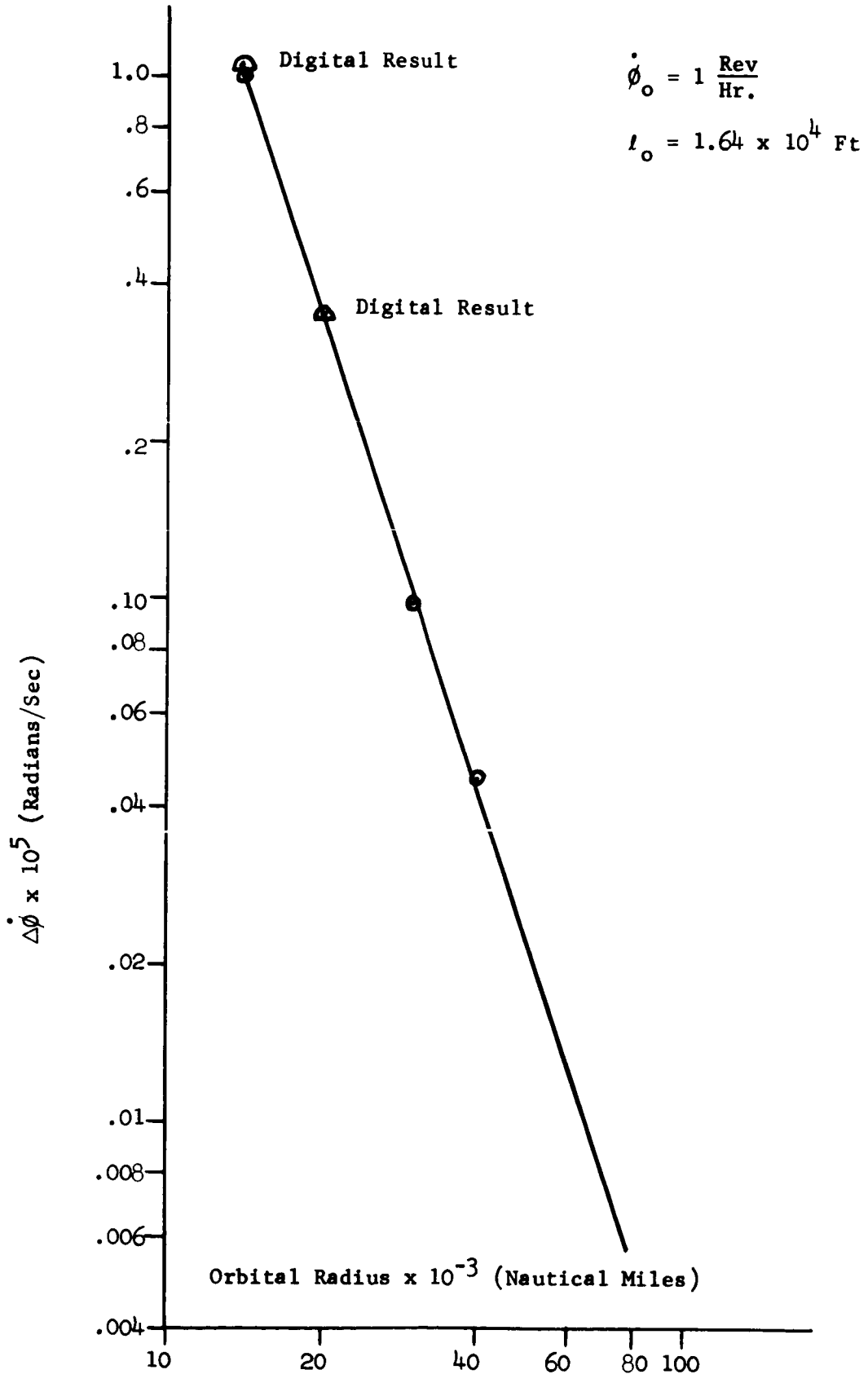

Figure 5 - Spin Rate Deviation vs. Orbital Radius (planar motion)

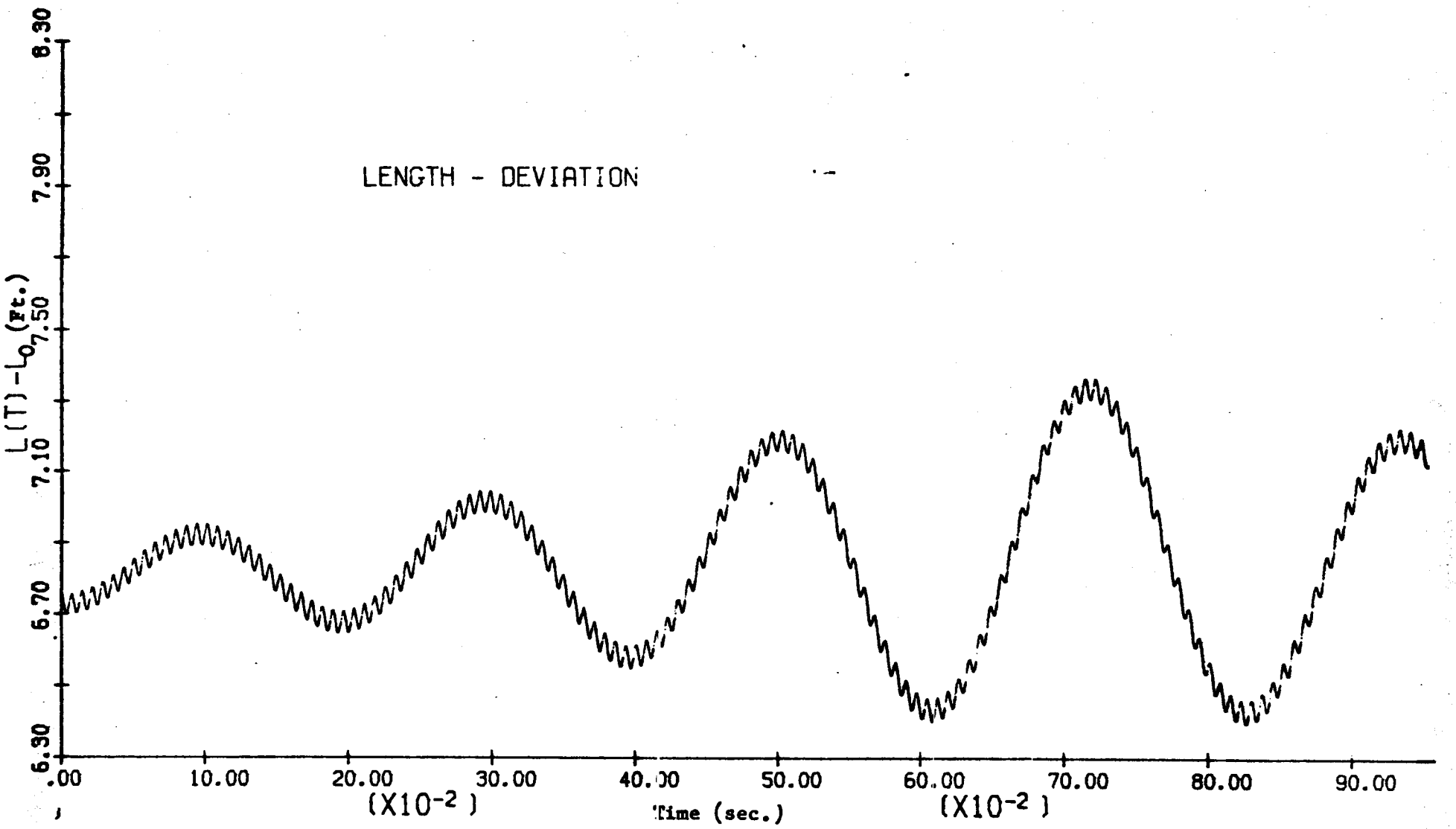

Figure 6 - Axial Deviation vs. Time, 10,000 x 60,000 N.M. (planar motion)

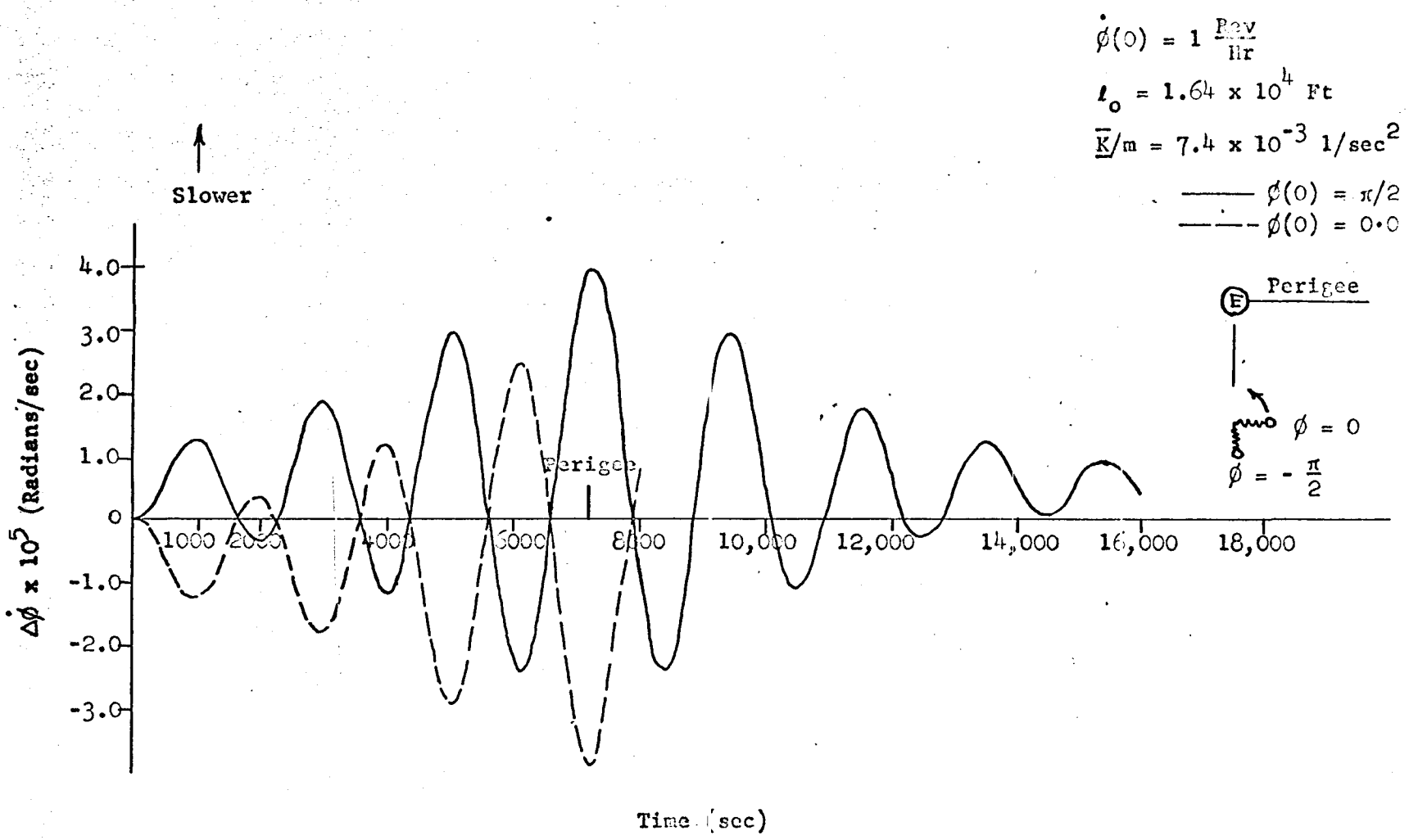

Figure 7 - Spin Rate Deviation for 10,000 x 60,000 N.M. Orbit (planar motion)

in sub-satellite spin rate is on the order of 2% and will thus cause some changes in the antenna beam pattern. The altered antenna pattern will have to be accounted for when processing the data taken near perigee.

This effect may be considerably reduced by going to a higher perigee or a higher spin rate. Conversely, the effect is aggravated by going to a lower perigee or lower spin rate.

The third effect is that the plane of the KWOT structure is tilted a slight amount following each pass through perigee. See Figure 8 for orbits with a perigee of 10,000 nautical miles or more, this motion represents a precession of the plane of KWOT toward the orbital plane. This type of precession is identical to that required to get full sky coverage for the radio telescope. For orbits with perigees below 10,000 nautical miles an additional nutation of the plane of the KWOT structure results. Data from the analog and digital computer runs for these linearized equations, consistently indicated that the four sub-satellites would remain planar.

D. Dynamics of Structure with Active Position Control of the Sub-Satellites

Three tasks which must be performed on the KWOT structure require active position control over the sub-satellites. These tasks are the initial deployment of the structure, structure spin up, and precession of the plane of the radio astronomy antenna while observing so that the antenna beam will scan the full sky. Obviously this same active position control system could be used to reduce the magnitude of the geometric distortions in the structure caused by the gravity gradient.

A study was conducted to determine the feasibility of controlling the position of the KWOT structure by the use of small thrusters located in each of the sub-satellites. One control concept investigated was that of a simple threshold system maintaining the sub-satellite position within a given volume surrounding the desired location. Under this control assumption as soon as any sub-satellite reaches the limit of the control volume, the thrusters fire to bring it back within the boundary. The equations of motion were written for the sub-satellites and approximate solutions obtained. Details of the study will be found in Appendix E. This motion was investigated for KWOT in a 60,000 nautical mile circular orbit and in a 20,000 - 60,000 nautical mile elliptical orbit. This analysis showed that even for the elliptic orbit the

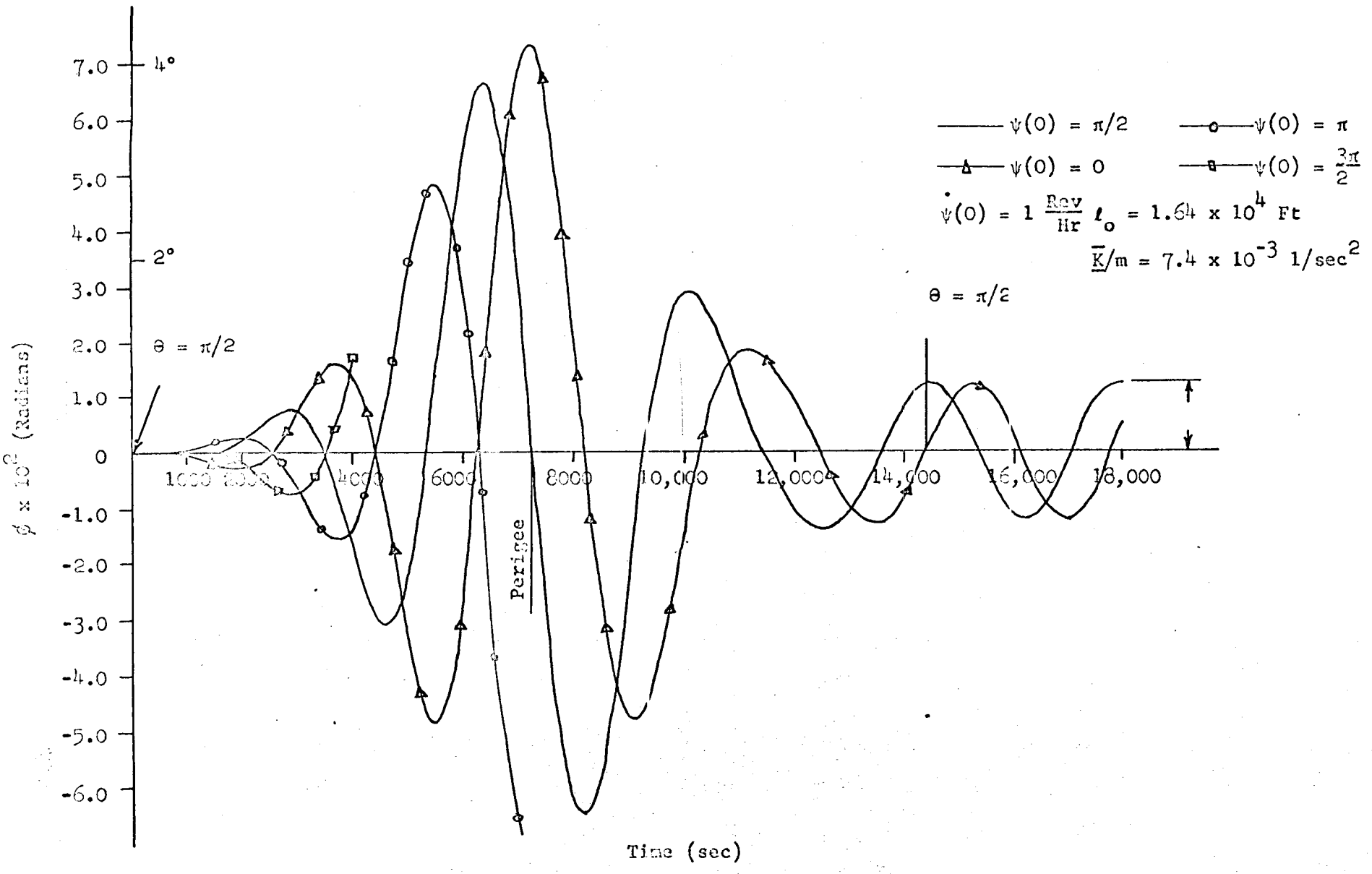

Figure 8- Angular Deviation from Reference Plane for 10,000 x 60,000 N.M. Orbit (motion out of orbital plane)

amount of thruster fuel required to overcome the distortion effects due to the gravity gradient and maintain the sub-satellites within ±50 meters of the desired location was small when compared to the fuel required to precess the plane of the radio astronomy antenna for full sky coverage.

The study indicated that active control is required for only a small portion of the orbit and there are long periods of many hours between required control actions over the vast portion of the orbit. The amount of fuel required for control is a function of the size of the perturbation forces which depend on the KWOT orbit and the tolerance to which the position of the sub-satellites are maintained. For the assumed model, control fuel would last a minimum of one year.

The major function of the sub-satellite position control system then, is to precess the plane of the structure to obtain the proper scan modes and sky coverage. A calculation was made of the fuel required to completely scan the sky once by incremental changes in the plane of the radio astronomy antenna. Details of this investigation will be found in Appendix G entitled "Incremental Thrust Bursts for Precessing the KWOT Scan Plane". It is shown that an expenditure of about 1.5 pounds of fuel is required for each of the four sub-satellites. One year of observing would be equivalent to about 24 such complete sky scans and would require 36 pounds of fuel in each sub-satellite. This amount of fuel is very compatible with the assumed size and weight of the sub-satellite.

E. Conclusions from the Dynamics Investigations

1. The simplified equations of motion for the spring-mass models of KWOT proved to be dynamically stable in that the geometric distortions of the structure caused by the gravity gradient do not continue to grow with time.

2. The continuous or complete model for KWOT bears a further investigation to determine if there are possible modes of energy transfer which should be avoided by proper choice of design parameters.

3. The gravity gradient produces the dominant distortion force. Forces such as those resulting from induced currents or charges on the structure, solar radiation pressure or particle drag are all negligible.

4. The use of small maneuverable sub-satellites for the orientation of the radio astronomy antenna in the prescribed position is possible and reasonable.

5. The amount of fuel required to counteract the distortions caused by the gravity gradient force will be small compared to that required to precess the structure to obtain complete sky coverage.

6. The major function of the position control system will be pointing control for controlled observing.

7. Each sub-satellite can reasonably carry enough fuel to maintain position control for one year.

8. More complex models of KWOT should be analyzed using the techniques developed in this study phase.

V. Radio Telescope Antenna Studies

A. Introduction

The class of high directional gain antennas required to obtain an adequate coverage of the sky and measure the flux density of a few dozen sources may be subdivided into two major subsections. This division is based on the time duration required for the construction of an antenna pattern which will meet the specifications of beamwidth, gain, etc.

On one hand we have systems which operate on a real time basis, such as filled arrays and long traveling wave structures. These antennas are scanned across the source by virtue of their orbiting motions and the flux densities received by these devices may be obtained directly from their receiver outputs. On the other hand we have systems which construct (or synthesize) their pattern over a long duration of time by the appropriate motion of two or more small elements. The data obtained by these synthetic arrays must first be processed before a suitable radiation pattern is obtained. Suitable data processing allows one to point the beam in any desired direction so that in principle we may simultaneously scan the whole sky from one set of data. It should be noted that in order to accomplish this goal with an array of N elements it is necessary to obtain N^2 independent power measurements from the array at each element position.

While each of the two classes of antennas mentioned have obvious advantages and disadvantages, it is necessary to study representative systems from each class in detail in order to make a judgement on the type of structure best suited for the task at hand.

In order to accomplish this comparison, we must first set practical restrictions on the complexity of the structures and their auxiliary equipment. Since the scientific objectives of the mission require a highly directive antenna at low frequencies (1 MHz), it is necessary to resort to structures whose linear dimensions range on the order of several miles. This imposes severe practical limitations on a large three-dimensional structure in orbit unless men in space are used to help erect the antenna. For this reason, our primary studies to this date have been limited to two-dimensional antenna systems, although the concept of using men to aid in the deploying and maintenance of the structure is under consideration.

Thus, restricting attention at present to two-dimensional systems, we first consider the class of "real time" antennas. As a result of our preliminary studies we have chosen a rhombic antenna with an interferometer system as being a feasible structure for the performance of radio astronomy in space. The rhombic antenna has a unidirectional pattern with a fairly narrow beam and moderate sidelobes, and can be easily terminated. Both the rhombic and the interferometer can operate at several frequencies simultaneously. Since the rhombic antenna is electrically symmetrical, receivers capable of receiving a number of discrete frequencies may be placed at each apex to effect a unidirectional beam in opposite directions. This also provides system redundancy and greater flexibility and capacity. Each subsatellite at the apices of the rhombic and at each interferometer dipole location can also contain a ranging and positioning system and a transmitter to relay the data to the main satellite. This arrangement has intrinsic mechanical symmetry. The rhombic and interferometer may be used separately and also together as a compound system, resulting in a variety of antenna patterns.

Although the rhombic antenna has been used extensively since 1931, and many papers have been written on various parameters of the rhombic, there are several areas of interest to space applications which have not been considered at all. One of the primary effects which has not been studied

is the resultant change in rhombic pattern due to the use of lossy conductors. This factor is of interest since the weight requirements of the system necessitate the utilization of thin conductors. The cosmic noise signals are expected to be so large that quite lossy conductors could be used if this loss did not affect the antenna pattern.

In order to determine the effect of using long, resistive wires for the rhombic construction, we must first be able to determine the current distribution on the antenna. The difficulty of this problem can be easily seen when one considers that studies concerned with obtaining a useful approximate analytic solution for the current distribution on a long, straight, perfectly conducting wire have only recently yielded results (see the papers of Vainshtein referenced in Appendix K). There have also been contributions in the area of determining the current distribution on straight lossy conductors, but those published to date have neglected many of the important physical aspects of the problem. We have initiated a program with the purpose of developing techniques suitable to obtaining a solution to the current distribution problem. The details of the work done are presented in Appendix K. In general, we have concluded that a quadratic convergence approximation scheme will provide results in the most efficient manner, and have therefore derived variational principles for the solution of the required integral equations. Although these techniques have the decided advantage of providing results which are independent of the scale factor used in the trial functions, we are also actively considering other quadratic convergence schemes which will have the additional benefit of faster convergence and will require less computer time. We plan to investigate the possibility of combining the variational principle with one of these techniques to obtain a scheme which will contain the desired properties of both.

Another area of great importance to the study of large traveling wave structures in space is the sensitivity of the antenna performance to perturbations of the structures. We have established the mathematical tools necessary for the solution of this problem, including the determination of the effect of these perturbations on the current distribution. We have also studied the problem of out of plane perturbations on the structure using these techniques. (See Appendix H).

There are several other studies essential to the design and evaluation of the rhombic-interferometer system which will be undertaken in future work. Among these are an investigation of the operation of the combined system including the manner in which the outputs from the two antennas should be compounded, the amount of beam sharpening that data processing might give, and the amount of precision needed in the cosmic noise measurements to do satisfactory beam sharpening. We also intend to consider the implementation of modified rhombic antennas for the purpose of improving the basic radiation pattern over the frequencies of interest. This result is shown in Fig. 3.

We have initiated some work on the study of generalized symmetrical two wire traveling wave structures or modified rhombic antennas. The work to date (see Appendix I) has shown that in general one must require the length of each wire on the structure to be greater by approximately one wavelength than the direct distance between the two vertices of the antenna. This property should allow one to extend the frequency range of the antenna by varying the vertex spacing. Some general results concerning the reduction of sidelobe levels have by suitable spatial tapering been obtained.

The rotating two element array with variable inter-element spacing has been chosen as a representative system of the synthetic aperture class of antennas. The efficient utilization of a system of this type requires extensive data processing equipment. Its effectiveness is contingent upon the time stationarity properties of the signals being processed, as temporal variations occurring during the construction time of the antenna pattern will lead to errors in the observed brightness distributions. A brief study of a system of this type (see Appendix M) has indicated that although the resultant antenna pattern affords narrow beamwidths, and sidelobe levels comparable to the rhombic, these properties are quite sensitive to random phase errors (such as would be induced by the random motion of the elements) and to the other temporal variations mentioned above. We have not, however, considered methods of weighting or filtering the received data in order to improve the pattern or decrease the sensitivity of the system to external perturbations. These studies along with considerations of collecting areas, data processing capacity requirements, and more detailed investigations of the sensitivity of the system to other types of errors should be initiated in order to perform a final judgement on the most effective antenna system for the performance of the required mission.

B. KWOT Antenna Studies

1. General

The effort in the area of electromagnetic studies of the KWOT antenna has been mainly devoted to the consideration of long wire rhombic antennas in free space and to a lesser degree to the optimization of the compounding of the rhombic-interferometer combination.

Two major efforts have been initiated in the analysis of the rhombic antenna. The first has consisted of studies of the antenna performance based on assumed zeroth order current distributions, while the second has been devoted to obtaining the correct current distribution and using the same to predict the performance of the antenna system. The motivation of the former effort was an immediate need for reasonable approximations to the antenna performance as we realized that the latter study would require a great deal of time and would probably not yield results by the end of this first phase study.

2. Antenna Study Utilizing Zeroth Order Current Distribution

This study was initiated by assuming that the current distribution on the rhombic takes the form of uniform traveling waves when the conductors are lossless and exponentially attenuated waves when the conductors are resistive. It is then possible to obtain the resultant radiation patterns in each case by integrating the appropriate current distribution over the structure. These results allow us to evaluate the effects of conductor losses on the antenna performance and the same technique may be employed to determine the effects of geometrical distortions of the structure.

The choice of the zeroth order current distributions described above was dictated by their use in all the literature to date on the rhombic antenna. Furthermore, there have been very few experimental measurements of the current on this structure and the measurements that have been performed are subject to question because the antenna was operating over a lossy ground. It was, therefore, impossible to use experimental results to aid in improving this approximation. There are several reasons for feeling that the results obtained by employing these approximations won't be radically different from the more

rigorous results. In the case of the low-loss antenna elements, the radiation pattern is relatively insensitive to errors in the assumed form of current distribution, being determined chiefly by the antenna configuration. Errors in current distribution become important only in those directions where the contributions from the various parts of the antenna tend to cancel, as in the nulls and minor lobes of the rhombic pattern. Furthermore, the losses which will be present on the rhombic should dampen the reflections from the discontinuities, and since the reflections from the corners are neglected in the assumed current distribution, the effect of this phenomenon will be decreased by the presence of losses. This same argument is applicable in the problem of determining the input impedance of the rhombic, which is usually assumed to be that of an infinitely long Vee antenna. The condition of infinite length implies no reflected wave from discontinuities such as the corners or termination of the rhombic. With a lossy rhombic this condition should be a better approximation since the reflected waves are highly attenuated.

As a prelude to the analysis of the rhombic, a study was made of the characteristics of long wire radiators because the rhombic can be considered as a suitable spatial placement of four long wires. Calculations were made showing the effect of attenuation on the radiation pattern of the long wire and showing the effect of curving the wire into a shallow parabolic shape. In both cases the effect is to increase the strength of the sidelobes with respect to the main lobe and to fill in the nulls between the sidelobes. The analysis shows that a parabolic curve which departs from a straight line by no more than 1% of the length increases the amplitude of the sidelobes by about 10% as compared to their amplitude on a straight wire. A reasonable assumption for the attenuation has about the same effect.

The positions and amplitudes of the rhombic sidelobes have been obtained under the assumption of a uniform current distribution. Since the rhombic has two planes of symmetry, the sidelobes generally come in sets of four. This analysis shows, for example, that the four sidelobes of the strongest set have amplitudes which are more than 5 db below the

amplitude of the main beam. When the effects of lossy antenna elements are introduced, the sidelobes tend to become somewhat larger in amplitude but remain in the same spatial location or direction.

The polarization of the rhombic is not constant throughout the antenna pattern. This polarization pattern is known and is being considered whenever it will affect the results of various antenna performance calculations. The polarization effect is small in the main beam of the rhombic and becomes more pronounced in the sidelobes.

3. Rhombic Current Distribution Studies and Related Perturbation Investigation

The study of the current distribution on the rhombic is motivated by the fact that we are dealing with a structure that is quite long and lossy. The rhombics which have been treated in the literature to date do not have quite these properties so that we feel it is important to verify that the usual assumptions concerning the current on the rhombic are still valid.

This problem was attacked by the consideration of various canonical problems whose solutions could then be applied to the rhombic itself. The first of these problems to be considered was that of the resistive "Vee" antenna. This structure is simpler than the rhombic since it consists of only two wires, however it still incorporates the basic problem of determining the current distribution on a thin wire structure with sharp corners. An attempt was made to obtain a "direct" solution to this problem by using Vainshtein's method of slowly varying coefficients [1, 2]. This attack failed because the current varied too rapidly in the vicinity of the corner. It then became apparent that the utilization of a variational principle would probably be the most effective method for obtaining a solution.

The current distribution on a long straight resistive wire was subsequently considered by utilizing a variational principle in conjunction with a successive approximation scheme [3, 4]. An analytic expression for the first order approximation to this current was obtained in reference [3], along with a prescription for obtaining higher order approximations. The results of reference [4] indicate

that the first order approximation will most likely give sufficient accuracy over the entire structure.

This same technique was then applied to the resistive "Vee" antenna [5]. In this case it was convenient to divide the current into its symmetric and antisymmetric components and obtain a variational principle for each component. The result of this work is a solution for the current distribution on the structure in terms of some well behaved definite integrals which must be evaluated by numerical techniques. The results indicate that the current distribution on the rhombic can most likely be obtained by utilizing the same methods.

The next problem to be considered was a determination of the effects of configurational and/or material variations on the antenna performance. The purpose of this consideration is to enable one to obtain the changes in the far field pattern, power dissipated and antenna efficiency for prescribed variations in the antenna geometry and/or material due to the dynamic characteristics of the structure. This investigation was conducted by considering an arbitrary thin wire antenna and performing a perturbation about this equilibrium configuration [6]. This procedure enables one to determine the variation in the current distribution on the structure and subsequently the change in the performance characteristics mentioned above. At present this method is being utilized to determine the change in the far field pattern when the rhombic is subjected to an out-of-plane displacement. This technique should also be most effective in determining the manner in which the antenna performance is affected by spatial oscillations on the legs of the rhombic.

4. Experimental Verification of Theoretical Studies

The KWOT antenna is large physically and electrically and the conductors used for the elements are lossy, adding parameters to the theoretical and experimental analysis which are usually neglected. The full-size rhombic has a total length of about six miles. Because the resistive components of the antenna do not scale with frequency while most of the other properties do, it would be best to scale the KWOT rhombic antenna by as small a factor as possible. However, a scaling of 100:1 would still give dimensions of 300 feet.

There are very few companies in the U.S. or Canada with a sufficiently large antenna range to make adequate radiation pattern measurements on the KWOT rhombic. So the best approach seems to be that of doing as much of the study of the rhombic in a theoretical form, and doing experimental measurements on those parameters which are impossible to calculate analytically or which should be verified.

5. The Compound Interferometer System

In the combined rhombic-dipole array antenna system the dipole array plays two general roles. The dipole array will narrow the effective beam from that yielded by the rhombic alone, and serve to cancel or at least reduce the effect of some of the stronger rhombic sidelobes. Studies are in progress to choose the optimum spacing and amplitude distribution of the dipole elements which will yield the best compound antenna pattern when combined with the rhombic antenna pattern. No definite results are available from the studies yet because we must obtain a better description of the rhombic radiation pattern.

REFERENCES

1. L. A. Vainshtein, Soviet Phys. Tech. Phys., 4, 601, (1959).

2. L. A. Vainshtein, Soviet Phys. Tech. Phys., 4, 617, (1959).

3. W. H. Schoendorf, "The Current Distribution on a Resistive Cylindrical Antenna".

4. L. A. Vainshtein, Soviet Phys. Tech. Phys., 6, 19, (1961).

5. W. H. Schoendorf, "The Current Distribution on the Vee Antenna".

6. W. H. Schoendorf, "The Effects of Configuration and Material Variations on Antenna Performance".

APPENDIX A

SYSTEMS STUDY

I. Operation of System

A. Observing Programs

In order to arrive at a first-order approximation for the thruster fuel assume the following radio astronomy observing programs might be carried out in approximately one year:

1. Initial sky survey

   Scan the entire sky, stepping the scan plane 3° each scan. Total integration time: 17 sec at each point in the sky.

2. Detailed survey

   Make a complete survey in about 30 days observing time, and repeat as many times as possible. Step the scan plane 3° every 12 hours. Effective integration time: 100 to 200 sec at each point at each frequency.

3. Variable source study

   Make careful measurements of the flux from perhaps a dozen sources which might show variability over a period of a year. Repeat these measurements three times in the course of a year, with frequent calibration measurements interspersed. Less precise measurements of these sources will also be available from the sky survey programs.

   Each source will be observed for several hours at each epoch in the repeat scan mode, with the scan plane slowly rotating about an axis passing through the source, so that it is scanned from various angles. This rotation can serve the additional purpose of bringing the next source to be observed into the scan plane.

4. Occultation studies

   Observe the occultation of selected sources by the moon. Since the KWOT beam subtends a considerably greater angle than the moon (even when seen at the closest approach in a 185,000 km. orbit), it is necessary to keep the beam approximately centered on the moon during the occultation. The apparent motion of the moon will never be greater than a few degrees per hour.

5. Noise bursts from sun and Jupiter

Observe the sun, Jupiter, and possibly other planets in the non-scan mode, looking for short-term variations in flux.

B. Observing Modes

Three different observing modes are possible with the KWOT structure: (1) Mapping mode, (2) Repeat scan mode, and (3) Non-scan mode.

In the mapping mode, the beam is swept around a given great circle on the celestial sphere for enough rotations to build up the required integration time at each point. Then the plane of rotation is tipped a few degrees, and the process repeated on another great circle. Eventually, the entire sky will be scanned.

In the repeat-scan mode, the scan plane is held in such a position as to pass through an object of special interest. The object is thus scanned twice for each rotation of KWOT, for as many scans as may be required. During this time, the scan plane may be rotated about an axis passing through the object of interest, so that this object is scanned at different angles, and so that another object is brought within the scan plane. The repeat-scan mode would be useful for investigating time-varying phenomena whose period is of the order of several hours, or for building up a long effective integration time on objects of special interest.

In the non-scan mode, the rotation of the KWOT structure is stopped with one of the beams directed toward an object of interest. The dimensional integrity of the antenna is preserved by controlled thrusters in the sub-satellites. The non-scan mode would be useful in studying time-varying phenomena where the time-scale of the variations is less than a few hours. It is a necessary mode of operation for observing occultations of sources by the moon and earth, and would be extremely valuable in observing Jovian and solar noise bursts.

C. Representative KWOT Schedule of Operations

A typical schedule for the launch, deployment and operation of a KWOT mission might be as follows:

Day 0	Launch to parking orbit, then thrust to transition orbit
Day 1-3	Inject into final orbit. Separate from launch vehicle. T/M status.
Day 4-6	Track KWOT, and compute actual orbit. Command any necessary thrust to correct orbit.

Day 7	Deploy
Day 8-10	Tests to check deployment
Day 11	Make initial run with calibrator to confirm operation (survey mode)
Day 12-16	Make initial sky survey (survey mode)
Day 17-27	Make first-epoch observations of suspected variable sources (repeat-scan mode)
Day 28-60	Make first detailed sky survey (survey mode)
Day 61-71	Observe Jupiter, sun, earth, other planets (repeat-scan and non-scan)
Day 72-160	Make second detailed sky survey, but interrupt survey for occultation observations when favorable (survey and non-scan mode)
Day 161-171	Make second-epoch observations of suspected variable sources (repeat scan mode)
Day 171-300	Continue survey and occultations (survey and non-scan mode)
Day 300-311	Make third-epoch observations of suspected variable sources (repeat scan mode)
Day 312-Failure	Continue to alternate survey, occultations, and suspected variable source observations

D. Thruster Fuel for Operational Modes

The thruster fuel consumed in the various modes of observation can be computed from approximate results of dynamic studies. If the mass of each sub-satellite is assumed to be 100 lbs., the rotation period of the structure one hour, the specific impulse of the thrusters 200 sec, and the moment of inertia of the central body and the connecting lines neglected, one arrives at the following figures for fuel consumption due to various maneuvers:

1. Spin-up structure to one rotation per hour, or stop rotation from one rotation per hour: 0.5 lbs per sub-satellite.

2. Change the plane of rotation by 180° in small steps: 1.5 lbs per sub-satellite.

3. Maintain precise sub-satellite position in non-rotating mode: 1.0 lb per week per sub-satellite (upper limit estimate).

A complete sky survey requires that the scan plane be rotated through 180° and therefore costs 1.5 lbs of fuel, regardless of whether it is a coarse survey, where the scan plane is rotated several degrees each time, or a fine survey, where the scan plane is only rotated a degree or so each time.

When a series of objects are observed in the repeat-scan mode, it is never necessary to rotate the scan plane more than 90° to move from one object to another. The maximum expenditure of fuel, therefore, is 0.75 lbs per object observed.

To observe in the non-scan mode, it is necessary to stop the rotation of the structure and to spin it up again when returning to one of the scanning modes, which costs 1.0 lbs of fuel for each period in the non-scan mode. If more than one object is observed in the non-scan mode, additional fuel is required to move from one to another. If we assume that the average change of direction from one object to the next is 90°, and require that the beam move from one object to the next in 15 minutes, then the rotation rate becomes one rotation per hour, the same as the scan rate, and 1.0 lbs of fuel are required to accelerate and decelerate. Thus we add 1.0 lb for each additional object observed, bringing the total to 1.0 lbs per object for the non-scan mode. It is estimated that a typical observing program, as described in Section IA above, the thruster fuel required would be on the order of 4.6 pounds for each remote maneuvering satellite.

II. KWOT System and Sub-System Description

Referring to Fig. 1 in the main text, the KWOT is seen to consist of a rhombic antenna with an array of dipoles along the minor diagonal but external to the rhombic forming an interferometer array. There are nine or more system units involved which are:

1. One Central Observatory.
2. Two Sub-Satellites at each acute apex of the rhombic.
3. Two Sub-Satellites, one at each end of the minor axis of the rhombic.
4. Six Dipole Units, one for each dipole of the interferometer array.

For the normal sky survey mode of operation this entire assemblage is rotating about the center with a period of about one hour. The dipole units not shown previously are much simpler than the others and serve to relay the dipole signals to the Central Observatory. The functions of these units are outlined below:

A. Central Observatory

1. House entire system during launch.

2. Deploy other components and lines.

3. Receive commands from ground, interpret them, and relay to other units when appropriate.

4. Receive data (radiometer, status, orientation, position, etc.) from other units. Store, process, encode, and transmit it to ground.

5. Track the positions of the other system components, with respect to the system frame of reference.

6. Determine the orientation of the system frame of reference with respect to the celestial sphere.

7. Generate all primary power needed within the unit.

B. Rhombic Sub-Satellite

1. Measure the R.F. energy delivered by the rhombic.

2. Integrate, encode, and transmit these measurements to the Central Observatory.

3. Receive control signals from Central Observatory to control both radiometers and thrusters.

4. Return proper transponder signals to central body tracking system.

5. Measure its own orientation with respect to the system frame of reference, correct by thrusters and/or reaction wheels.

6. Generate all primary power needed in the unit.

7. Sense all necessary housekeeping data, and transmit to the Central Observatory.

C. Interferometer Sub-Satellite

1. Receive control signals from the Central Observatory to control thrusters.

2. Return proper transponder signals to Central Observatory tracking system.

3. Measure its own orientation with respect to the system frame of reference, and correct by thrusters and/or reaction wheels.

4. Generate all primary power needed in the unit.

5. Sense all necessary housekeeping data, and transmit it to the Central Observatory.

D. Dipole Unit Functions

1. Amplify the RF signal appearing at the dipole terminals, modulate a carrier, and transmit it to the Central Observatory.

2. Receive control signals from Central Observatory to control its pre-amp.

3. Generate all primary power needed in the unit.

4. Sense all necessary housekeeping data, and transmit it to the Central Observatory.

The shape of the antenna, and hence the characteristics of the beam, is controlled by controlling the positions of the outer units with respect to the Central Observatory. These positions are sensed from the Central Observatory and corrected by firing appropriate thrusters on these units.

In order for the action of these thrusters to be properly directed, the attitude of each sub-satellite must also be controlled. This control can best be accomplished through the use of attitude sensors in each sub-satellite, and thrusters to correct the attitude.

All sub-satellite units generate attitude data and housekeeping data which must be transmitted to the Central Observatory, and all but the two interferometer sub-satellite units generate scientific data as well. Furthermore, all sub-satellite units receive thruster control commands, and most of them receive other command signals as well. Therefore, two-way communications is required from each sub-satellite to the Central Observatory, or perhaps direct to ground.

Obviously, each sub-satellite will use electric power, and will require some form of long-lived source of primary power, such as solar cells. Each sub-satellite must be independent, since each is separated by kilometers from its neighbors.

Thorough study of dynamics of the structure may show that the dimensions of the spinning web are adequately stable and predictable. More likely, it will appear that some use of thrusters will improve the position accuracy of the antenna elements enough to narrow the beam significantly. In any event, some use of thrusters is required during erection, and whenever it is desired to change the axis of rotation to allow the antenna to scan a different band of sky.

Until the results of a complete study of the dynamics are available, it seems safest to assume that complete active control of attitude and position is required in each sub-satellite, and study the feasibility of such a system. If full active control can be provided within reasonable limits of weight, power consumption, and reliability, then any system with partial active control is certainly within these limits.

E. Assumed Accuracy Requirements

In this study, it is assumed that the beam pattern of the antenna array will not be significantly degraded if each sub-satellite remains within 50 meters of its prescribed position, relative to the system frame of reference. This figure is based upon the study reported in the proposal which showed that elongation or compression of the major diagonal of the rhombic by 1 percent produced a distortion of the beam that was about as much as could be tolerated. A 1 percent change in the length of this diagonal would displace each of the end points by 50 meters. In Appendix H, it is shown that this criterion is more than adequate for out-of-plane perturbations. To get better figures, a thorough study must be made of the effect of various distortions and displacements on the rhombic beam, and on the beam synthesized from the rhombic and interferometer signals. Such a study will no doubt show that the position tolerance on some sub-satellites can be relaxed considerably, while perhaps some may be tightened.

F. System Frame of Reference

All measurements of position and attitude, and all calculations of beam position are made with respect to a frame of reference, called the system frame of reference, which rotates with the system, and is based upon some sort of a mean position of the active bodies. Tentatively, we have chosen to define this frame of reference as follows:

The origin of the system frame of reference is the center of mass of the Central Observatory.

The x axis points along the desired direction of the beam center.

The z axis is perpendicular to the desired plane of the KWOT system.

Normally, the system frame of reference rotates about its z axis at a uniform angular velocity. The direction of the z axis will also change with respect to the celestial sphere, but much more slowly. The whole frame of reference moves along the orbital path, but has no direct relationship to the orbital elements.

III. Definitions of KWOT Sub-Systems

The sub-systems of KWOT which are covered in this report perform the following general functions:

A. Attitude Sub-System:

Measures the attitude, or orientation, of each of the bodies in the KWOT structure, relative to the system frame of reference.

B. Position Sub-System:

Measures the position of each of the units in the KWOT structure relative to the system frame of reference.

C. Pointing Sub-System:

Measures the orientation of the system frame of reference with respect to the celestial sphere.

D. Communications Sub-System:

Provides all necessary communications between the units of the KWOT structure, and between KWOT and ground stations.

E. Command and Control Sub-System:

Receives, stores, and interprets commands received from ground control, and generates the necessary thruster command signals to maintain the attitude and position of the structural elements within limits.

F. Data Sub-System:

Collects, stores, processes, and prepares for transmission all data gathered in the KWOT system, both scientific and housekeeping.

G. Radio Astronomy Sub-System

H. Ground Support System:

Includes the ground portions of the communications, command, and data systems, and perhaps other sub-systems as well.

IV. Sub-System Requirements

In this section are presented the key requirements on the various sub-systems, and the basic reasoning behind them.

A. <u>Attitude Sub-System</u>

The primary importance of measuring and controlling the attitude of the sub-satellites is to assure that, when the thrusters are commanded to fire, the thrust vector is directed in the proper direction. If a thrust burst is

applied in an erroneous direction, the result is an extraneous velocity component in an orthogonal direction. This spurious velocity adds to all the other sources of spurious velocity components, increasing the net velocity error, and hence shortening the time interval between velocity corrections. If this spurious velocity component is no more than 10 percent of the desired change in velocity, it should not materially degrade the position control. This standard will be achieved if the direction of the applied thrust is controlled with an accuracy of $\pm 5°$. The direction of the applied thrust can be controlled either by controlling the attitude of the sub-satellite when the thrusters are fired, or by knowing the attitude and computing the thrust component required in each of a set or orthogonal thrusters to generate the required thrust vector. In either case, the attitude of the sub-statelite must be known to within $\pm 5°$.

The only time when the attitude of a sub-satellite is critical is when a thrust burst is about to be commanded. Since it is anticipated that under typical operating conditions, such bursts may not occur with a frequency greater than once per hour, the attitude sub-system can remain inactive most of the time to conserve power.

B. Position Sub-System

The primary importance of measuring and controlling the positions of the remote units is to maintain the proper configuration of the antenna elements; the rhombic and the dipoles which make up the interferometer. Early studies of the electrical properties indicated that the positions of each antenna element should be maintained within an accuracy of ± 50 meters, with respect to a common frame of reference. To control the position with this accuracy, we should be able to measure it with still more accuracy, perhaps ± 5 meters.

The positions of the sub-satellites will probably be sensed by some sort of radar or optical device located in the Central Observatory. If so, the accuracy requirement of ± 5 meters implies a range accuracy of ± 5 meters at 5 kilometers, or ± 0.1 percent, and an angular accuracy of 0.001 radian, or 0.058 degress (3.44 minutes arc). Such accuracies are feasible by a variety of techniques.

C. Pointing Sub-System

The pointing sub-system must supply the necessary coordinate transformation data to permit the antenna beam position, as calculated in the system

frame of reference from the measured positions of the sub-satellites, to be transformed into conventional celestial coordinates, such as right ascension and declination. The beam position must ultimately be determined with an error which is a small fraction of the smallest dimension of the narrowest beam that can be anticipated, or about $\pm$0.1 degree. About half of this error has been assigned to the position measuring sub-system, so only about $\pm$0.05 degree can be allowed in the pointing sub-system.

The implementation of the pointing sub-system may be based upon measuring the apparent positions of any two celestial bodies whose actual positions with respect to KWOT are known. Optical measuring techniques seem most obvious.

D. Communications Sub-System

The communications sub-system consists of internal data links between the various units of KWOT, and external data-links between KWOT and the ground stations. Each link carries different sorts of data, and hence has its own specifications. All communications pass through the Central Observatory. There are no communications direct from sub-satellite to sub-satellite, or from sub-satellite to ground. In general, command and control information flows from ground to Central Observatory, and from Central Observatory to sub-satellite, while status and scientic information flows from sub-satellite to Central Observatory and from Central Observatory to ground.

All KWOT units generate basic status information, such as temperatures, and solar cell and battery parameters.

The dipole units generate scientific information, which must be relayed to the Central Observatory along with the basic status information. An information bandwidth of two to ten MHz will be required for each dipole unit with the information carried in analog modulation, probably amplitude modulation. The dipole units probably receive no command and control information, except possibly for simple on-off signals.

The rhombic sub-satellites generate scientific information and basic status information, similar to that generated in the dipole units. In addition, they generate attitude information and status information concerning the attitude control and propulsion systems. They must accept command and control signals to control the thrusters and possibly the attitude sensors.

The interferometer sub-satellites have no scientific information, but otherwise have the same requirements as the rhombic sub-satellites.

The Central Observatory receives all scientific information from the sub-satellites and dipole units in broadband analog form, processes it, converting it to narrow-band digital form, and relays it to the ground. In addition, it receives commands from the ground and status information from the sub-satellites and generates command and control signals to the sub-satellites and relays the status information to ground.

E. Command and Control Sub-system

The command and control sub-system accepts inputs in the form of commands from the ground, error signals from the attitude and position-sensing sub-systems, signals from the pointing system, and status signals from the various sub-satellites. From this information, it generates control signals to the thrusters throughout the structure, so that the proper attitude and positon of each body is maintained, and the antenna beam is pointed and moved as commanded from the ground. This task requires sufficient precision that digital techniques are indicated, and is of sufficient magnitude and complexity that services of a general purpose, stored program digital computer on board the spacecraft are probably required. This computer will be shared with the data sub-system.

Backup control loops of a simple analog nature should also be provided, to be switched in the event of computer failure. These analog control loops could control the attitude, position, and pointing with sufficient accuracy to permit continued operation of the system in the basic scanning modes, but at the cost of a much more rapid consumption of thruster fuel, and hence a shorter useful life for the system.

F. Data Sub-System

The basic function of the data sub-system is the processing of all data collected in KWOT system, including scientific, housekeeping, status, attitude, position and pointing data. The data sub-system must prepare information for transmission to ground, and for the use of the command and control sub-system.

The scientific information, as it is presented to the data sub-system, will consist of several analog voltage signals, perhaps ten, representing the output of several radiometers. The data sub-system must sample some or all of these channels according to a sequence which is specified by ground command, convert these values to digital numbers, store and encode them for transmission to earth. Very likely it will also be called upon to perform some

numeric processing upon this information, also under control of ground commands. This processing might be no more than simple averaging, but it might be as complex as correlations.

The status and housekeeping information will be handled in the data sub-system in a number of ways. First, certain key parameters will be tested to detect conditions which present a hazard to the system. Out-of-limit temperatures or power-supply voltages would be in this category. Any condition that might lead to a runaway condition in the control system should also be monitored closely. Such conditions might include malfunction of the thruster valves in any sub-satellites, or noise in the transmission of the control signals.

Second, enough status and housekeeping information must be sent to the ground to permit the performance of all KWOT sub-systems to be monitored, including the data sub-system.

Third, some of the status and housekeeping information will be analyzed in the on-board computer, and the computer will modify the mode of operation of various sub-systems to adopt to changing conditions, either internal or external. For example, if it is found that the present mode of operation is depleting the charge on the batteries, the system might change to a mode that will use less current until the charge is built up again.

G. Radio Astronomy Sub-System

The radio astronomy sub-system consists of pre-amplifier and relay units located in the dipole units and rhombic sub-satellites and radiometer units located in the Central Observatory.

The pre-amplifier and relay units must amplify the radio-frequency signals appearing at the terminals of the antenna elements, both dipoles and rhombic, and transform them to some high frequency for the transmission to the Central Observatory. The simplest implementation would be a broad-band pre-amplifier, covering the entire range over which KWOT is to operate (perhaps 0.1 MHz to 10 MHz), whose output is modulated upon a carrier in the microwave frequency region. Transmission in the microwave region is desirable not only because of the broad bandwidth requirements, but also because of the small size of the directive antennas, and because of the shielding effect of molecular absorption in the atmosphere, which will prevent interference from transmitters located on earth. The actual transmitters, receivers, and

antennas for relaying the radio astronomy information from the dipole units and rhombic sub-satellites to the Central Observatory are included in the communications system.

The facility for combining the signals from the various antenna elements is located in the Central Observatory. After the broad-band signal from each element is recovered by demodulation of the signals relayed to the Central Observatory, and the particular frequency bands upon which KWOT is operating at the moment are selected by filters, these signals must be combined to synthesize two or more beams. The phase of each dipole signal must be corrected for the propagation delay introducted in transmission from the sub-satellite to the Central Observatory, and then all dipole signals are linearly mixed to synthesize the interferometer signal. The interferometer signal is then correlated independently with each of the two rhombic signals to synthesize two narrow beams, one pointing each direction along the major axis of the rhombic. A simple signal multiplication may suffice for this correlation, or a more complex process may be required. Probably the two rhombic signals and the interferometer signal will be independently rectified, filtered, and telemetered to earth in addition to the composite signal from the correlator.

Some form of internal noise calibration will be required, and it will probably be desirable to periodically switch one or more noise sources into the signal path. Many alternatives exist, but no choice has been made as yet.

Various alternative modes exist for the radiometer system. For instance, it is possible to move the interferometer beam about within the broad rhombic beam by appropriately shifting the phases of the dipole signals. If the interferometer beam were scanned in this way at a rate equal and opposite to the KWOT spin, the composite beam could be made to dwell upon one object for several minutes, considerably increasing the integration time on that object.

Another alternative would be to synthesize two or more interferometer beams, all contained within the broad rhombic beam, and correlate each of these independently with each rhombic signal. The result would be a series of narrow fan beams, sweeping one after another across each point in the sky, each gathering data independently.

V. Orbit and Launch Vehicle

From a scientific point of view, the preferred orbit would be a circular one, with a radius of the order of 100,000 to 185,000 kilometers. However, an elliptic orbit with an apogee in the range of 100,000 to 185,000 kilometers, and perigee at least 40,000 kilometers is almost as attractive.

The minimum apogee is determined by the scientific requirement that KWOT spend an appreciable portion of its life beyond the magnetosphere, and the minimum perigee is determined by the gravity gradient distorting forces experienced near perigee, and which increase very rapidly as perigee is lowered (distortion force varies as the inverse cube of distance from the earth's center).

The earliest weight estimates for the KWOT structure indicated that a Saturn V launch vehicle would be required to achieve an acceptable orbit. However, as the KWOT study has proceeded, and out concepts of the structure and methods of implementation have advanced, it has been possible to revise the weight estimates downward, until it now appears probable that the entire KWOT structure will weigh less than 4000 lbs. It has therefore become possible to consider the Saturn 1B, or one of the suggested configurations of Saturn components with capability between that of the Saturn 1B and Saturn V.

VI. Reliability, Man's Role

A matter of principal concern in the study of KWOT or any other large, complex system is it's reliability. In general this means the system's ability to perform the task for which it was designed for some prescribed period of time. The task in this case is the set of scientific goals set down as the mission objective, not the performing of some specific technical function.

It appears that an appropriate measure of performance might be the returned data in comparison to the ideal design objective. This criterion allows for different degrees of system degradation and measures the effect on the returned data for a realistic measure of the system performance. This leads to the Figure of Merit (FOM) approach to reliability.

(See Ref. "A Realistic Measure of Spacecraft Reliability", 9th Nat'l Symposium on Reliability and Quality Control, by G. R. Grainger, W. E. Faragher, L. I. Philipson, Planning Research Corporation, Los Angeles)

With this measure one can have spacecraft which have "failed" and yet are still returning data which is degraded by some lesser degree. It also allows for changing the state of the system in the event they can be repaired.

As systems grow larger and more complex the reliability of course goes down unless steps are taken to prevent this trend. The present state of numerical treatment of reliability in this area is very unsatisfactory. Experience has shown that the numbers attached to various systems for reliability have little meaning. It is generally conceded by people working in reliability that no absolute measure exists, only relative measures in comparing one system to another.

There is a further weakness because of inability to make proper models of a large system. Failures have occured because of interactions between various parts of a large system which were not known a priori or were not properly taken into account. In this sense it is very important to know how the reliability model was constructed from the real system.

If we are faced with a situation of low reliability, what can we do about it? This question is best examined by listing the areas of concern. These areas in a system development are:

1. System design, sub-system design, "black box" designation.
2. Circuit, sub-assembly design.
3. Component, parts selection, TESTING.
4. Circuit, sub-assembly fabrication, TESTING.
5. "Black box", sub-system fabrication, TESTING.
6. System fabrication, TESTING.
7. Flight, the real TEST.

Volumes have been written on good, acceptable and otherwise practice in all these various areas for improving reliability. Some general observations at this point seem to be in order.

Obviously for any given system one should be able to show that good practice was followed as far as balance between single line and redundant design. In some of the other areas listed above there is an especially heavy emphasis on testing, to the point where there seems to be some imbalance. There is a very heavy emphasis on testing at the lower levels of component selection and up through the "black box" level. There appears to be inadequate testing at the systems level. Of course in some cases it is not possible to realistically test a system until it is in orbit, however it appears that this area could be given more attention than it has in some cases. This area may be sometimes slighted because, by the time the project progresses past the "black box" level, all the slack time in the schedule has been used up and there is heavy pressure (due to other boundary conditions) to meet the

launch schedule. Coupled closely to this is the problem that, in general, systems testing is much more difficult to design and carry out than any of the other tests and therefore more expensive and time consuming. A proper and complete testing program should be designed into the operation from the beginning and will likely add considerably to the cost.

It is impossible to simulate closely some space systems performance on earth. In these cases work is needed in structuring model tests so that they better bring out those intrinsic properties which may lead to the large system performance properties. This testing would, to the best of our ability, bring out the interactions between basic system properties as manifested by the key sub-system performances characteristics. This is the approach advocated for a system such as KWOT; to design an appropriate model which will bring out the key interactions, then allocate the time and resources to properly test the model. In addition to this, more testing should be done as far beyond the "black box" level as is possible on the real system as it is being prepared for flight. These two efforts will give the best possible expectation of a successful flight.

Man may serve several roles which include:

1. Observer (In the role of scientist).
2. Monitor, semi-builder (In the role of technician).
3. Builder.
4. Maintenance and Repair.

Our present feeling regarding KWOT is that he would be most useful in categories 2 and 4. This would bring him into play during erection of the telescope and later for repair work. Our findings as to the potential for man to do these tasks have generally been quite pessimistic. For this and other reasons we are proceeding with our KWOT conceptual design as though man were not in the picture, with one exception. The system will be designed so that it can be serviced by a man. This has merit for other reasons and if man were to be made available in orbit for repair and maintenance he could readily carry out his tasks. It is generally felt that if man were available and could perform satisfactorily the necessary repair and service functions, this would no doubt upgrade the long term reliability or figure of merit. In considering a manned vs. un-manned approach to such a mission in the broad sense, one must compare the cost of perhaps fewer units with man in the picture, compared to more units with him out of the picture. This assumes lower overall reliability with him out. It is not at all clear at present

which might prove to be the most economical in the end, and it is quite beyond the scope of this study to make such an evaluation. Our knowledge about costs for putting a man in orbit and providing him with the tools necessary to do a given job is very limited but the cost appears to be quite high.

APPENDIX B

KWOT DYNAMICS

I. A. Description of the physical system

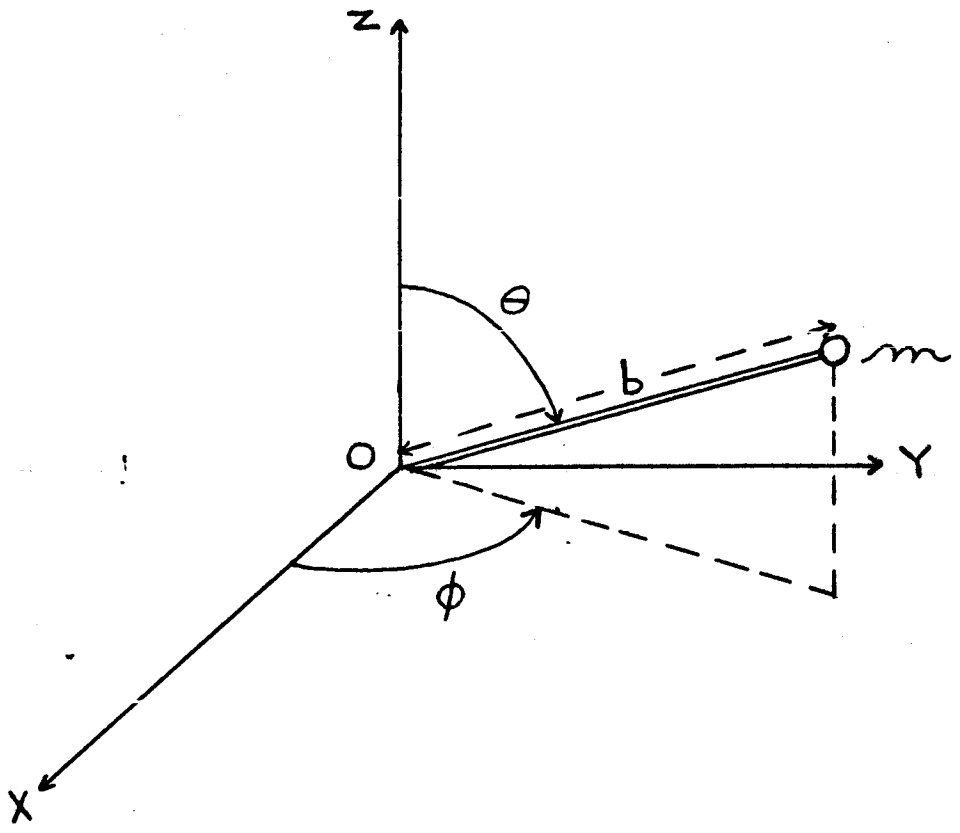

Assume the following conditions:

1. The XYZ-set of axes is an inertial system of coordinates.
2. The point mass is constrained by a massless rod to a spherical surface with radial length b.
3. The system is situated in free space.

B. Kinematical considerations

Let θ and ϕ be the generalized coordinates.

C. Dynamical considerations[1]

The system is spherically symmetric. Therefore, any polar rotational coordinate is cyclic in a Lagrangian description so that any conjugate angular momentum is a constant of the motion. Since every component of the angular momentum is constant, the total angular momentum is a constant of the motion. Let $\vec{r}$ be the radial vector from the origin to the point mass. The total angular momentum (relative to the origin 0)

$$\vec{J} = m\vec{r} \times \vec{v}$$

Since $\vec{J}$ is a constant vector, it follows that $\vec{r}$ is always perpendicular to the fixed direction of $\vec{J}$. The rigidity of the rod constrains the point mass to a sphere with radial length b. These facts imply directly that the point mass always moves on a great circle of the spherical surface.

It is shown now that the point mass moves with constant speed on a great circle. When the cartesian coordinates of the point mass are expressed as functions of the generalized coordinates θ and ϕ, the resulting equations obviously do not contain the time explicitly. Also, by assumption I-A-3, the potential energy of the system vanishes. Therefore, the Lagrangian function cannot be an explicit function of time so that the associated Hamiltonian function H is a constant of the motion. Furthermore, the Hamiltonian reduces to the usual sum of the kinetic energy T plus the potential energy V. Since V = 0 in this case,

$$H = T = \frac{1}{2} mv^2$$

Thus, the magnitude of the velocity of the point mass is a constant of the motion. In summary the general motion of the point mass is such that it moves with constant speed on a great circle.

---

[1] The first two paragraphs of this section employ the dynamical theory presented in Herbert Goldstein, Classical Mechanics, Addison-Wesley Publishing Co., Inc., Massachusetts, 1959, section 2-6.

The fact that the point mass moves on a great circle can be seen also in another, more elegant fashion.[2] Since the Hamiltonian function of the system is a constant in time, the motion of the point mass satisfies the principle of least action. For a single body in free space this principle implies that the body traverses a geodesic on the surface which is determined by the constraints of the problem. The radial constraint in this case generates a spherical surface and the associated geodesics are great circles.

D. Determination of θ, ϕ [3]

Let the Euler angles be denoted by θ_e, ϕ_e and ψ_e. Suppose that the point mass is traversing a great circle such that:

1. The associated total angular momentum vector is directed along the Z' - axis of Fig. 4-6c.
2. At time t = 0 the point mass is located along the line of nodes.
3. For simplicity let $\phi_e = \psi_e = 0$.

Let θ', ϕ' be respectively the colatitude and azimuthal angles in the primed coordinate system and let J denote the magnitude of the total angular momentum of the system.

$$\theta'(t) = \frac{\pi}{2}$$

$$J = m b^2 \dot{\phi}'(t) = \text{constant}$$

Referring to p. 109,

$$\vec{X} = A^{-1} \vec{X}'$$

---

[2] This paragraph uses the dynamical theory discussed in Herbert Goldstein, ---, section 7-5.

[3] This section employs the diagram, notation, and results of Goldstein, ---, section 4-4.

$$\vec{X}' = b\begin{bmatrix}\sin\theta'\cos\phi'\\ \sin\theta'\sin\phi'\\ \cos\theta'\end{bmatrix} = b\begin{bmatrix}\cos\phi'\\ \sin\phi'\\ 0\end{bmatrix}$$

$$A^{-1} = b\begin{bmatrix}1 & 0 & 0\\ 0 & \cos\theta_e & -\sin\theta_e\\ 0 & \sin\theta_e & \cos\theta_e\end{bmatrix}$$

$$\vec{X} = b\begin{bmatrix}\sin\theta\cos\phi\\ \sin\theta\sin\phi\\ \cos\theta\end{bmatrix}$$

Thus, $\sin\theta\cos\phi = \cos\phi'$

$\sin\theta\sin\phi = \cos\theta_e \sin\phi'$

$\cos\theta = \sin\theta_e \sin\phi'$

$\sin^2\theta = \cos^2\theta_e \sin^2\phi' + \cos^2\phi'$

$\tan\phi = \cos\theta_e \tan\phi'$

Therefore, $\theta(t) = \text{Arcsin}\left[1 + (\cos^2\theta_e - 1)\sin^2\phi'\right]^{1/2}$

$\phi(t) = \text{Arctan}\left[\cos\theta_e \tan\phi'\right]$

$\dot{\phi}'(t) = \frac{J}{mb^2} \Rightarrow \phi'(t) = \frac{Jt}{mb^2}$

Summary of Results

$$\theta(t) = \text{Arcsin}\left[1 + (\cos^2\theta_e - 1)\sin^2\frac{Jt}{mb^2}\right]^{1/2}$$

$$\phi(t) = \text{Arctan}\left[\cos\theta_e \tan\frac{Jt}{mb^2}\right]$$

where θ_e is the angle between the Z-axis and the angular momentum $\vec{J}$ and where the line of nodes of the Euler angles, the X-axis and the X'-axis are chosen to be coincident.

II.

A. Description of the physical system

The system in section I is modified to include radial oscillations.[4]

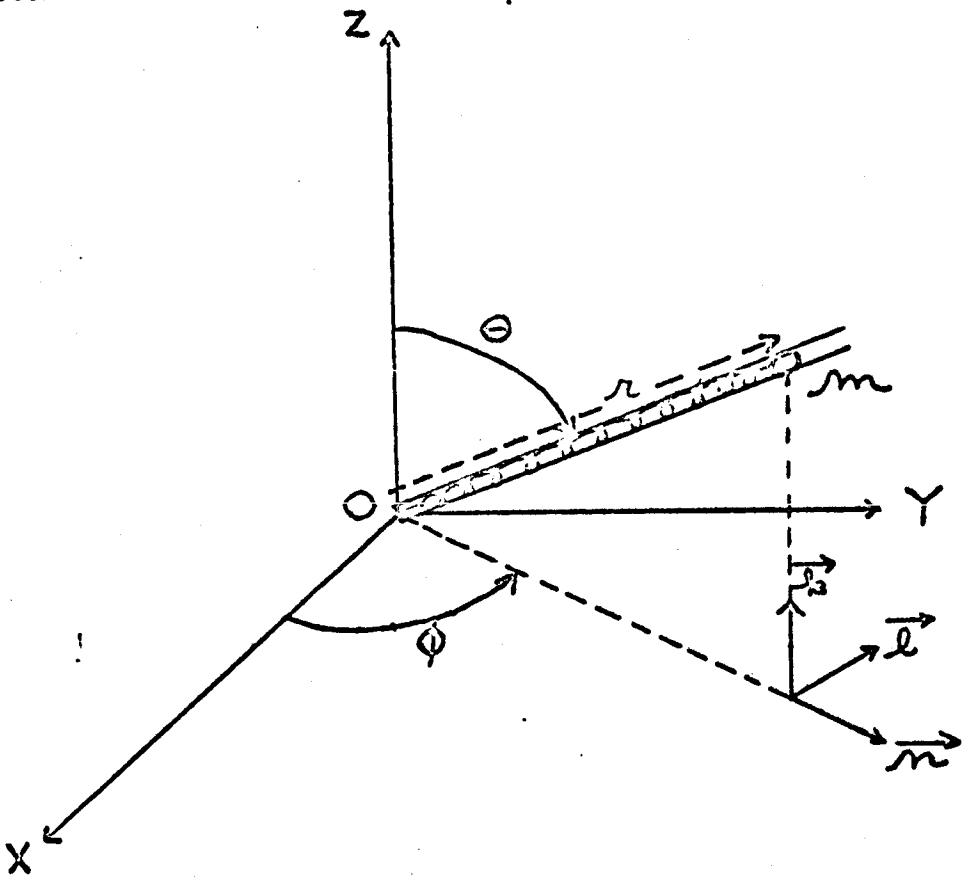

Assume the following conditions:

1. The XYZ-set of axes is an inertial system of coordinates.
2. The point mass is connected to a massless spring which obeys Hooke's law under tension and compression. Both the spring and the point mass are constrained inside a massless cylinder. The unstressed length of the spring is b and the spring constant is K.
3. The system is located in free space.

---

[4] This is essentially the problem of the "space oscillator." Refer to L.D. Landau and E. M. Lifshitz, Mechanics, Addison-Wesley Publishing Co., Inc., Massachusetts, 1960, section 14.

B. Kinematical considerations

Let r, θ, ϕ be the generalized coordinates.

C. Dynamical considerations

The dynamical considerations in section I-C have an analogous application in this case. The system is spherically symmetric so that the total angular momentum is constant. This implies that the point mass moves in a plane perpendicular to the direction of the constant total angular momentum vector. However, the point mass is no longer constrained to a constant radial distance from the origin. The Hamiltonian function H again is a constant of the motion. H equals the sum of the kinetic energy T plus the potential energy V which is stored in the spring.

D. Determination of r, θ, and ϕ

For simplicity let the total angular momentum vector point along the Z axis of the diagram in section II-A. Then,

$$\theta(t) = \frac{\pi}{2}$$

and the position vector $\vec{r}$ of the point mass is

$$\vec{r} = r\vec{n}$$

The velocity vector

$$\vec{v} = \frac{d\vec{r}}{dt} = \dot{r}\vec{n} + r\dot{\phi}\vec{l}$$

$$v^2 = \dot{r}^2 + r^2\dot{\phi}^2$$

Also, the constant total angular momentum $\vec{J}$ is

$$\vec{J} = m\vec{r} \times \vec{v} = mr^2\dot{\phi}\vec{k}$$

$$J = mr^2\dot{\phi} = \text{constant}$$

Substituting this result into the expression for v^2,

$$v^2 = \dot{r}^2 + \frac{J^2}{m^2 r^2}$$

The potential energy V of the spring is

$$V = \frac{1}{2}K(r-b)^2$$

The constant Hamiltonian H is

$$H = T + V = \frac{1}{2}mv^2 + \frac{1}{2}K(r-b)^2$$

$$= \frac{1}{2}m\left(\dot{r}^2 + \frac{J^2}{m^2 r^2}\right) + \frac{1}{2}K(r-b)^2$$

$$\dot{r}^2 = \frac{2H}{m} - \frac{K}{m}(r-b)^2 - \frac{J^2}{m^2 r^2}$$

The remainder of the calculation can be found in Goldstein's text.[5] Let $r(t=0) = r_o$, $\phi(t=0) = \phi_o$

$$\phi(r) = \phi_o + \int_{r_o}^{r} \frac{dr}{r^2\sqrt{\frac{2mH}{J^2} - \frac{mK(r-b)^2}{J^2} - \frac{1}{r^2}}}$$

This integral may be evaluated explicitly to obtain an "orbit" equation.[6] The dependence of r and ϕ upon the time may be deduced from the previous result which expressed the conservation of angular momentum:

$$J = mr^2\dot{\phi}$$

$$\frac{Jt}{m} = \int_{\phi_o}^{\phi} r^2(\phi)\,d\phi$$

---

[5] See Goldstein, ---, section 3-5.

[6] See Goldstein, ---, p.74.

Summary of Results

1. $\theta(t) = \frac{\pi}{2}$

2. $$\phi(r) = \phi_o + \int_{r_o}^{r} \frac{dr}{r^2\sqrt{\frac{2mH}{J^2} - \frac{mK(r-b)^2}{J^2} - \frac{1}{r^2}}}$$

3. $$\int_{\phi_o}^{\phi} r^2(\phi)\,d\phi = \frac{Jt}{m}$$

III. A. Description of the physical system

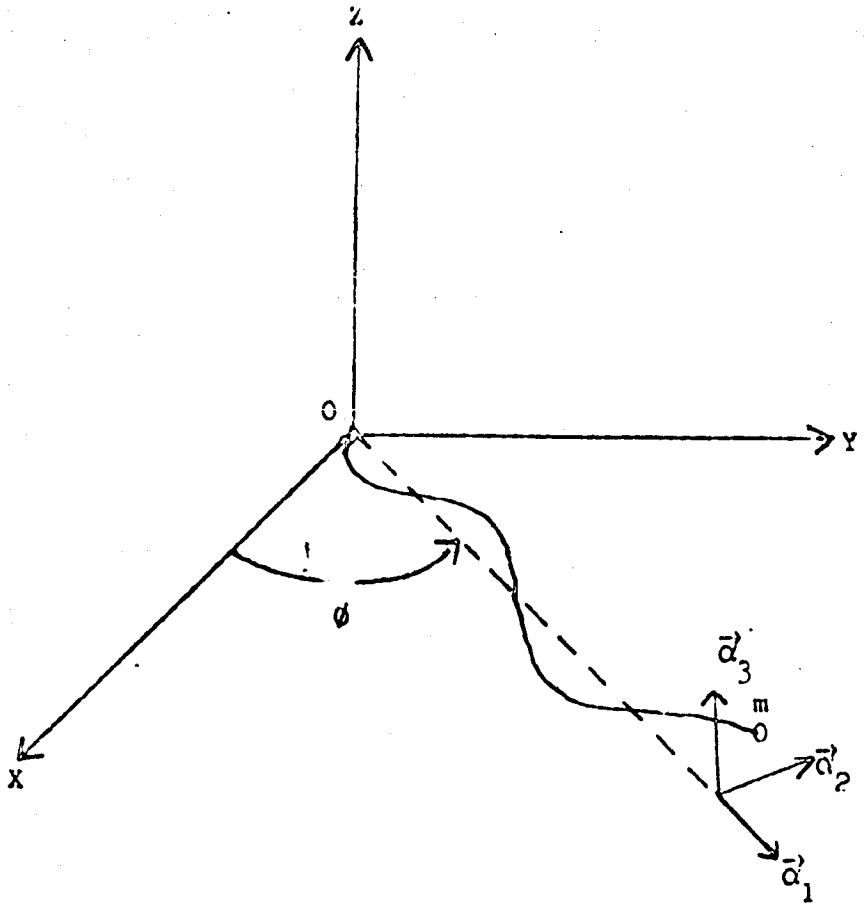

Assume the following conditions:

1. The XYZ-set of axes is an inertial system of coordinates.
2. The system is located in free space.
3. The "string" obeys a Hooke's law under <u>both</u> tension and compression. Let Y be the Young's modulus such that the local tension or compression force is expressed by a relation

$$\text{force} = Y\zeta$$

where ζ is the local elongation per unit length.

4. The string is perfectly elastic so that a potential energy can be associated with any instantaneous configuration. (See section III-C-2.)

5. The unstretched length of the string is b; the unstretched linear mass density has the constant value ρ; and the point mass at the end of the string has the value m.

B. Kinematical considerations

1. The displacements of the string will be measured from a radial direction which rotates with a constant angular velocity $\omega = \dot{\phi}$. $\vec{\alpha}_3$ is a fixed unit vector which is parallel to the Z-axis while $\vec{\alpha}_1$ and $\vec{\alpha}_2$ are unit vectors in the XY-plane. $\vec{\alpha}_1$ and $\vec{\alpha}_2$ rotate at the constant angular rate ω.

2. Consider the points $r\vec{\alpha}_1$ where $0 \leq r \leq b$. The reference configuration of the string is defined by the following conditions:

   a. Every string element lies along the radial direction.

   b. The string has length b.

   c. No portion of the string is either elongated or compressed.

3. The displacement (relative to the origin 0) of the string elements from the reference configuration is described by the following vector function:

$$\vec{D}(r,t) = [r + \eta(r,t)]\vec{\alpha}_1 + \theta(r,t)\vec{\alpha}_2 + Z(r,t)\vec{\alpha}_3$$

For each r $(0 \leq r \leq b)$ $\vec{D}(r,t)$ is the vector displacement of a string element which is located at $r\vec{\alpha}_1$ in the reference configuration. Therefore, the coordinate r is a label for the nondenumerable, triply infinite set of generalized coordinates $\eta(r,t)$, $\theta(r,t)$, $Z(r,t)$.

C. Dynamical considerations

1. The kinetic energy of the system.

Consider the mass point which is labeled by any particular value of $r(0 \leq r \leq b)$. The displacement of this point is $\vec{D}(r,t)$. The square of the velocity (measured relative to the inertial frame of coordinates) is computed below. Note that r is a time-independent labeling index.

$$\vec{v}(r,t) = \frac{d}{dt}\vec{D}(r,t) = \frac{d}{dt}\left[(r+\eta)\vec{\alpha}_1\right] + \frac{d}{dt}(\theta\vec{\alpha}_2) + \frac{d}{dt}(z\vec{\alpha}_3)$$

$$= \left(\frac{\partial\eta}{\partial t}\right)\vec{\alpha}_1 + (r+\eta)\omega\vec{\alpha}_2 + \left(\frac{\partial}{\partial t}\theta\right)\vec{\alpha}_2 - \omega\theta\vec{\alpha}_1 + \left(\frac{\partial}{\partial t}z\right)\vec{\alpha}_3$$

$$v^2(r,t) = (\eta_t - \omega\theta)^2 + \left[(r+\eta)\omega + \theta_t\right]^2 + z_t^2$$

v^2 is the square of the velocity of the mass point which in the reference configuration is located at $r\vec{\alpha}_1$.

The kinetic energy of the string (not including the mass m) is given by the relation

$$T_S(t) = \int_0^b \frac{1}{2}\Delta v^2(r,t)\,dr,$$

where Δ is the linear mass density function which remains to be determined. Note that the integral extends over the reference configuration. Each mass point labeled by the radial distance r in the reference configuration has velocity $v^2(r,t)$ in the instantaneous configuration at time t. Since the relation $T_S(t)$ for the kinetic energy integral is actually a line integral over the reference configuration, it is necessary to use the linear mass density for the reference configuration, i.e. $\Delta = \rho$. Alternatively, if the integral for the kinetic energy extended along the arc length of the string in its instantaneous configuration, then Δ would display a complicated dependence upon the instantaneous configuration. Moreover, the limits of integration would be variable, etc. Furthermore, if the string has a variable linear mass density $\rho(r)$ in its reference configuration, then $\Delta = \rho(r)$ in the expression for $T_S(t)$. Writing the expression for $T_S(t)$ in detail,

$$T_S = \int_0^b \frac{1}{2}\rho\left\{(\eta_t - \omega\theta)^2 + \left[(r+\eta)\omega + \theta_t\right]^2 + z_t^2\right\}dr$$

The determination of the correct mass density can be visualized from the following obvious limit argument:

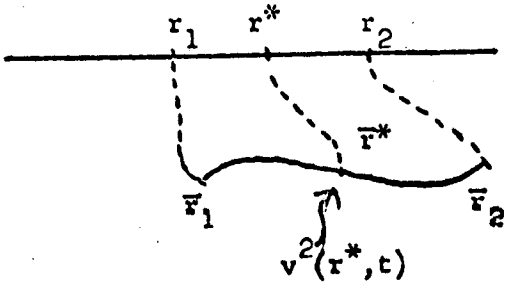

static configuration

dynamic configuration

Clearly, as $(r_2 - r_1)$ approaches zero about the point r^*, $(\bar{r}_2 - \bar{r}_1)$ approaches zero about the point $\bar{r}^*$. In the limit $r_2 - r_1 = \delta r$, the kinetic energy of the mass segment is $\frac{1}{2}\rho\, \delta r\, v^2(r^*,t)$ and the total kinetic energy for the string minus the mass m is given by the previous integral. The kinetic energy associated with the mass m is

$$T_m = \frac{1}{2} m \left\{ \left[\eta_t(b,t) - \omega\theta(b,t) \right]^2 + \left[b\omega + \omega\eta(b,t) + \theta_t(b,t) \right]^2 + z_t^2(b,t) \right\}$$

Thus, the total kinetic energy of the system is

$$T = T_S + T_m = \int_0^b \frac{1}{2}\rho \left\{ \left(\eta_t - \omega\theta \right)^2 + \left[\left(r + \eta \right)\omega + \theta_t \right]^2 + z_t^2 \right\} dr$$

$$+ \frac{1}{2} m \left\{ \left[\eta_t(b,t) - \omega\theta(b,t) \right]^2 + \left[b\omega + \omega\eta(b,t) + \theta_t(b,t) \right]^2 + z_t^2(b,t) \right\}$$

2. The potential energy of the system.

It is assumed that it is possible to define a potential energy function. Thus, this quantity must depend only upon the instantaneous configuration of the string. There must be no implicit physical dependence upon the "past history" or "path" which the system has followed to arrive at the instantaneous configuration. Such conditions will be satisfied if there exist no heat losses to friction during expansion and compression, etc. The reference configuration defined in section II-B-2 will be used as the reference for the definition of the potential energy of the string.

Consider first the work ΔW expended in stretching a spring a distance Δb from a position where the spring is just taut. Let the spring be massless and have a spring constant K.

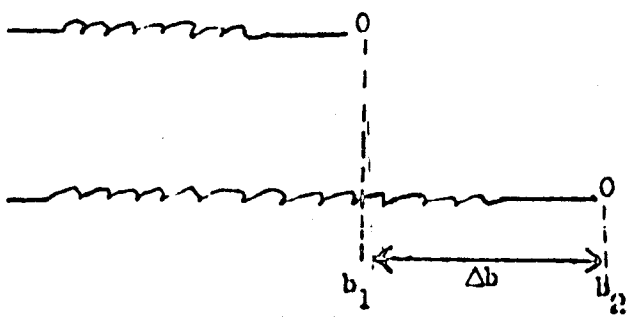

$$\Delta W = \int_{b_1}^{b_2} K(X - b_1)\,dX = \frac{1}{2} K (b_2 - b_1) \times (b_2 - b_1)$$

$$= \text{(average tension)} \times \text{(increase in length)}$$

where the (average tension) is $\frac{1}{2}$ the sum of the initial tension (= 0 here) plus the final tension. This result will be applied to each element δr of the string and the total potential energy of the string is obtained then by summing over all elements of the string. Consider a segment δr in the reference configuration. In the instantaneous configuration the segment has length

$$\delta S = \delta r \sqrt{(1 + \eta_r)^2 + \theta_r^2 + z_r^2}$$

where the functions are evaluated at some point lying in δr.

Proof:

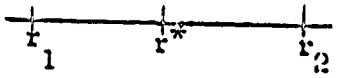

δr

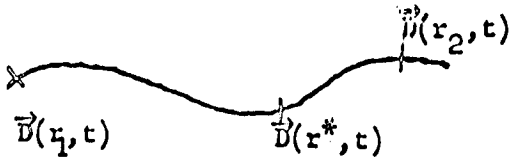

δS

$$\delta S \cong \left| \vec{D}(r_2,t) - \vec{D}(r_1,t) \right|$$

$$= (r_2 - r_1)\sqrt{\left[1 + \frac{\eta(r_2,t) - \eta(r_1,t)}{r_2 - r_1}\right]^2 + \left[\frac{\theta(r_2,t) - \theta(r_1,t)}{r_2 - r_1}\right]^2 + \left[\frac{Z(r_2,t) - Z(r_1,t)}{r_2 - r_1}\right]^2}$$

Clearly, in the limit $r_2 - r_1 = \delta r$, an infinitesimal quantity,

$$\delta S = \delta r\sqrt{(1 + \eta_r)^2 + \theta_r^2 + z_r^2} \qquad \text{and}$$

increase in length per unit length

$$= \sqrt{(1 + \eta_r)^2 + \theta_r^2 + z_r^2} - 1,$$

where the last result is exact; i.e. if the expression is evaluated at point r, the result gives the exact increase in length per unit length at the point r. Assumption II-3 implies that the tension (or compression)

$$\tau(r,t) = Y\left[\sqrt{(1 + \eta_r)^2 + \theta_r^2 + z_r^2} - 1\right]$$

The mass point located by the coordinate r in the reference configuration has tension $\tau(r,t)$ in the instantaneous configuration. The potential energy of a segment which has length δr in the reference configuration is

$$\delta V = \frac{1}{2} Y\left[\sqrt{(1 + \eta_r)^2 + \theta_r^2 + z_r^2} - 1\right]^2 \delta r,$$

so that the potential energy V of the system is

$$V(t) = \int_0^b \frac{1}{2} Y\left[\sqrt{(1 + \eta_r)^2 + \theta_r^2 + z_r^2} - 1\right]^2 dr$$

3. The Lagrangian and the action integral.[7]

The Lagrangian $L = T - V$

$$= \int_0^b \left\{\frac{1}{2}\rho\left[(\eta_t - \omega\vartheta)^2 + (\omega r + \omega\eta + \theta_t)^2 + z_t^2\right]\right.$$

$$\left. - \frac{1}{2} Y\left[\sqrt{(1 + \eta_r)^2 + \theta_r^2 + z_r^2} - 1\right]^2\right\} dr$$

$$+ \frac{1}{2} m\left\{\left[\eta_t(b,t) - \omega\vartheta(b,t)\right]^2 + \left[b\omega + \omega\eta(b,t) + \theta_t(b,t)\right]^2 + z_t^2(b,t)\right\}$$

[7] Gelfand, I. M. and Fomin, S. V., Calculus of Variations, Prentice-Hall, Inc.: New Jersey, 1963, Chap. 7, Sec. 36.

The action integral

$$J(\eta,\theta,Z) = \int_{t_1}^{t_2} L\,dt = \int_{t_1}^{t_2}\int_0^b \ell_1\,dx\,dt + \int_{t_1}^{t_2} \ell_2\,dt$$

where

$$\ell_1(r,\ \eta,\ \eta_r,\ \eta_t,\ \theta,\ \theta_r,\ \theta_t,\ Z_r,\ Z_t)$$

$$= \frac{1}{2}\rho\left[(\eta_t - \omega\theta)^2 + (\omega r + \omega\eta + \theta_t)^2 + Z_t^2\right] - \frac{1}{2}Y\left[\sqrt{(1+\eta_r)^2 + \theta_r^2 + Z_r^2} - 1\right]^2$$

$$\ell_2(t) = \frac{1}{2}m\left\{\left[\eta_t(b,t) - \omega\theta(b,t)\right]^2 + \left[b\omega + \omega\eta(b,t) + \theta_t(b,t)\right]^2 + Z_t^2(b,t)\right\}$$

4. Application of Hamilton's principle (principle of stationary action).[8] The boundary conditions determined by the constraints of the problem are obviously

$$\eta(0,t) = 0$$
$$\theta(0,t) = 0$$
$$Z(0,t) = 0$$

Consider the varied functions

$$\eta^*(r,t) = \eta(r,t) + \epsilon\mu(r,t) + \ldots$$
$$\theta^*(r,t) = \theta(r,t) + \epsilon\gamma(r,t) + \ldots$$
$$Z^*(r,t) = Z(r,t) + \epsilon\delta(r,t) + \ldots$$

---

[8] Gelfand, I. M. and Fomin, S. V., Calculus of Variations, Prentice-Hall, Inc.: New Jersey, 1963, Chap. 7, Sec. 36.

The 1st variation of the action integral is

$$\delta J = \epsilon \int_{t_1}^{t_2} \int_0^b \left(\ell_{1_\eta} - \frac{\partial}{\partial r} \ell_{1_{\eta_r}} - \frac{\partial}{\partial t} \ell_{1_{\eta_t}} \right) \mu(r,t)\, dr\, dt$$

$$+ \epsilon \int_{t_1}^{t_2} \int_0^b \left(\ell_{1_\theta} - \frac{\partial}{\partial r} \ell_{1_{\theta_r}} - \frac{\partial}{\partial t} \ell_{1_{\theta_t}} \right) \gamma(r,t)\, dr\, dt$$

$$+ \epsilon \int_{t_1}^{t_2} \int_0^b \left(\ell_{1_z} - \frac{\partial}{\partial r} \ell_{1_{z_r}} - \frac{\partial}{\partial t} \ell_{1_{z_t}} \right) \delta(r,t)\, dr\, dt$$

$$+ \epsilon \int_{t_1}^{t_2} \int_0^b \frac{\partial}{\partial t} \left(\ell_{1_{\eta_t}} \mu + \ell_{1_{\theta_t}} \gamma + \ell_{1_{z_t}} \delta \right) dr\, dt$$

$$+ \epsilon \int_{t_1}^{t_2} \int_0^b \frac{\partial}{\partial r} \left(\ell_{1_{\eta_r}} \mu + \ell_{1_{\theta_r}} \gamma + \ell_{1_{z_r}} \delta \right) dr\, dt$$

$$+ \epsilon \int_{t_1}^{t_2} \left(\ell_{2_\eta} - \frac{\partial}{\partial t} \ell_{2_{\eta_t}} \right) \mu(b,t)\, dt + \epsilon \int_{t_1}^{t_2} \frac{\partial}{\partial t} \left(\ell_{2_{\eta_t}} \mu(b,t) \right) dt$$

$$+ \epsilon \int_{t_1}^{t_2} \left(\ell_{2_\theta} - \frac{\partial}{\partial t} \ell_{2_{\theta_t}} \right) \gamma(b,t)\, dt + \epsilon \int_{t_1}^{t_2} \frac{\partial}{\partial t} \left(\ell_{2_{\theta_t}} \gamma(b,t) \right) dt$$

$$+ \epsilon \int_{t_1}^{t_2} \left(\ell_{2_z} - \frac{\partial}{\partial t} \ell_{2_{z_t}} \right) \delta(b,t)\, dt + \epsilon \int_{t_1}^{t_2} \frac{\partial}{\partial t} \left(\ell_{2_{z_t}} \delta(b,t) \right) dt$$

Hamilton's principle requires that the varied functions vanish at the extremities of the time interval. Thus, for $(0 \le r \le b)$

$$\mu(r,t_1) = \mu(r,t_2) = \gamma(r,t_1) = \gamma(r,t_2) = \delta(r,t_1) = \delta(r,t_2) = 0$$

The constraints imply

$$\mu(0,t) = \gamma(0,t) = \delta(0,t) = 0$$

Thus,

$$\epsilon \int_{t_1}^{t_2} \int_0^b \frac{\partial}{\partial t} \left(\ell_{1_{\eta_t}} \mu + \ell_{1_{\theta_t}} \gamma + \ell_{1_{z_t}} \delta \right) dr\, dt \equiv \epsilon \int_{t_1}^{t_2} \frac{\partial}{\partial t} \left(\ell_{2_{\eta_t}} \mu(b,t) \right) dt$$

$$\equiv \epsilon \int_{t_1}^{t_2} \frac{\partial}{\partial t} \left(\ell_{2_{\theta_t}} \gamma(b,t) \right) dt \equiv \epsilon \int_{t_1}^{t_2} \frac{\partial}{\partial t} \left(\ell_{2_{z_t}} \delta(b,t) \right) dt \equiv 0$$

$$\epsilon \int_{t_1}^{t_2} \int_0^b \frac{\partial}{\partial r} \left(\ell_{1_{\eta_r}} \mu + \ell_{1_{\theta_r}} \gamma + \ell_{1_{z_r}} \delta \right) dr\, dt$$

$$\equiv \epsilon \int_{t_1}^{t_2} \left(\ell_{1_{\eta_r}} \mu + \ell_{1_{\theta_r}} \gamma + \ell_{1_{z_r}} \delta \right) \Big|_{r=b} dt$$

The vanishing of the 1st variation over the restricted class of admissible functions such that $\mu(b,t) \equiv \gamma(b,t) \equiv \delta(b,t) \equiv 0$ implies the following Euler equations of motion:

$$\ell_{1_\eta} - \frac{\partial}{\partial r} \ell_{1_{\eta_r}} - \frac{\partial}{\partial t} \ell_{1_{\eta_t}} = 0$$

$$\ell_{1_\theta} - \frac{\partial}{\partial r} \ell_{1_{\theta_r}} - \frac{\partial}{\partial t} \ell_{1_{\theta_t}} = 0$$

$$\ell_{1_z} - \frac{\partial}{\partial r} \ell_{1_{z_r}} - \frac{\partial}{\partial t} \ell_{1_{z_t}} = 0$$

If we remove these restrictions on the class of admissible functions so that $\mu(b,t)$, $\gamma(b,t)$, and $\delta(b,t)$ are arbitrary admissible functions on $[t_1,t_2]$; the vanishing of the 1st variation implies also the following boundary conditions:

$$\ell_{1_{\eta_r}}\Big|_{r=b} + \ell_{2_\eta} - \frac{\partial}{\partial t}\ell_{2_{\eta_t}} = 0$$

$$\ell_{1_{\theta_r}}\Big|_{r=b} + \ell_{2_\theta} - \frac{\partial}{\partial t}\ell_{2_{\theta_t}} = 0$$

$$\ell_{1_{Z_r}}\Big|_{r=b} + \ell_{2_Z} - \frac{\partial}{\partial t}\ell_{2_{Z_t}} = 0$$

5. Computation of derivatives in section III-C-4.

$$\ell_{1_\eta} = \rho\,\omega\,(\omega x + \omega\eta + \theta_t)$$

$$\ell_{1_{\eta_r}} = \frac{-Y\left[\sqrt{(1+\eta_r)^2 + \theta_r^2 + z_r^2} \quad -1\right](1+\eta_r)}{\sqrt{(1+\eta_r)^2 + \theta_r^2 + z_r^2}}$$

$$\frac{\partial}{\partial r}\ell_{1_{\eta_r}} = \frac{-Y\,(1+\eta_r)\left[(1+\eta_r)\,\eta_{rr} + \theta_r\,\theta_{rr} + z_r\,z_{rr}\right]}{\left[(1+\eta_r)^2 + \theta_r^2 + z_r^2\right]^{3/2}}$$

$$\frac{-Y\left[\sqrt{(1+\eta_r)^2 + \theta_r^2 + z_r^2} \quad -1\right]\eta_{rr}}{\sqrt{(1+\eta_r)^2 + \theta_r^2 + z_r^2}}$$

$$\ell_{1_{\eta_t}} = \rho(\eta_t - \omega\theta)$$

$$\frac{\partial}{\partial t}\,\ell_{1_{\eta_t}} = \rho(\eta_{tt} - \omega\theta_t)$$

$$\ell_{1_{\theta}} = -\rho\omega(\eta_t - \omega\theta)$$

$$\ell_{1_{\theta_r}} = \frac{-Y\left[\sqrt{(1+\eta_r)^2 + \theta_r^2 + z_r^2} - 1\right]\theta_r}{\sqrt{(1+\eta_r)^2 + \theta_r^2 + z_r^2}}$$

$$\frac{\partial}{\partial r}\,\ell_{1_{\theta_r}} = \frac{-Y\,\theta_r\left[(1+\eta_r)\,\eta_{rr} + \theta_r\,\theta_{rr} + z_r\,z_{rr}\right]}{\left[(1+\eta_r)^2 + \theta_r^2 + z_r^2\right]^{3/2}} + \frac{-Y\left[\sqrt{(1+\eta_r)^2 + \theta_r^2 + z_r^2} - 1\right]\theta_{rr}}{\sqrt{(1+\eta_r)^2 + \theta_r^2 + z_r^2}}$$

$$\ell_{1_{\theta_t}} = \rho(\omega r + \omega\eta + \theta_t)$$

$$\frac{\partial}{\partial t}\,\ell_{1_{\theta_t}} = \rho(\omega\eta_t + \theta_{tt})$$

$$\ell_{1_z} = 0$$

$$\ell_{1_{Z_r}} = \frac{-Y\left[\sqrt{(1+\eta_r)^2 + \theta_r^2 + Z_r^2} - 1\right] Z_r}{\sqrt{(1+\eta_r)^2 + \theta_r^2 + Z_r^2}}$$

$$\frac{\partial}{\partial r}\ell_{1_{Z_r}} = \frac{-Y Z_r\left[(1+\eta_r)\,\eta_{rr} + \theta_r\,\theta_{rr} + Z_r\,Z_{rr}\right]}{\left[(1+\eta_r)^2 + \theta_r^2 + Z_r^2\right]^{3/2}}$$

$$\frac{-Y\left[\sqrt{(1+\eta_r)^2 + \theta_r^2 + Z_r^2} - 1\right] Z_{rr}}{\sqrt{(1+\eta_r)^2 + \theta_r^2 + Z_r^2}}$$

$$\ell_{1_{Z_t}} = \rho\, Z_t$$

$$\frac{\partial}{\partial t}\ell_{1_{Z_t}} = \rho\, Z_{tt}$$

$$\ell_{2_\eta} = m\omega\left[b\omega + \omega\eta(b,t) + \theta_t(b,t)\right]$$

$$\ell_{2_{\eta_t}} = m\left[\eta_t(b,t) - \omega\theta(b,t)\right]$$

$$\frac{\partial}{\partial t}\ell_{2_{\eta_t}} = m\left[\eta_{tt}(b,t) - \omega\theta_t(b,t)\right]$$

$$\ell_{2_\theta} = -m\omega\left[\eta_t(b,t) - \omega\theta(b,t)\right]$$

$$\ell_{2_{\theta_t}} = m\left[b\omega + \omega\eta(b,t) + \theta_t(b,t)\right]$$

$$\frac{\partial}{\partial t}\ell_{2_{\theta_t}} = m\left[\omega\eta_t(b,t) + \theta_{tt}(b,t)\right]$$

$$\ell_{2_Z} = 0$$

$$\ell_{2_{Z_t}} = m\, Z_t(b,t)$$

$$\frac{\partial}{\partial t}\,\ell_{2_{Z_t}} = m\, Z_{tt}(b,t)$$

6. Summary of Results

D.E. 1

$$-\rho\omega(\omega r + \omega\eta + \theta_t) - \frac{Y\left[\sqrt{(1+\eta_r)^2 + \theta_r^2 + Z_r^2} - 1\right]\eta_{rr}}{\sqrt{(1+\eta_r)^2 + \theta_r^2 + Z_r^2}}$$

$$- \frac{Y(1+\eta_r)\left[(1+\eta_r)\,\eta_{rr} + \theta_r\,\theta_{rr} + Z_r\,Z_{rr}\right]}{\left[(1+\eta_r)^2 + \theta_r^2 + Z_r^2\right]^{3/2}} + \rho(\eta_{tt} - \omega\theta_t) = 0$$

D.E. 2

$$\rho\omega(\eta_t - \omega\theta) - \frac{Y\left[\sqrt{(1+\eta_r)^2 + \theta_r^2 + Z_r^2} - 1\right]\theta_{rr}}{\sqrt{(1+\eta_r)^2 + \theta_r^2 + Z_r^2}}$$

$$- \frac{Y\,\theta_r\left[(1+\eta_r)\,\eta_{rr} + \theta_r\,\theta_{rr} + Z_r\,Z_{rr}\right]}{\left[(1+\eta_r)^2 + \theta_r^2 + Z_r^2\right]^{3/2}} + \rho(\omega\eta_t + \theta_{tt}) = 0$$

D.E. 3

$$- \frac{Y\left[\sqrt{(1+\eta_r)^2+\theta_r^2+z_r^2} - 1\right] z_{rr}}{\sqrt{(1+\eta_r)^2+\theta_r^2+z_r^2}}$$

$$- \frac{Y\, z_r\left[(1+\eta_r)\,\eta_{rr} + \theta_r\,\theta_{rr} + z_r\, z_{rr}\right]}{\left[(1+\eta_r)^2+\theta_r^2+z_r^2\right]^{3/2}} + \rho\, z_{tt} = 0$$

B.C. 1 $\quad \eta(0,t) = 0$

B.C. 2

$$\left\{ - \frac{Y\left[\sqrt{(1+\eta_r)^2+\theta_r^2+z_r^2} - 1\right](1+\eta_r)}{\sqrt{(1+\eta_r)^2+\theta_r^2+z_r^2}} + m\omega(r\omega + \omega\eta + \theta_t) - m(\eta_{tt} - \omega\theta_t) \right\}\Bigg|_{r=b} = 0$$

B.C. 3 $\quad \theta(0,t) = 0$

B.C. 4

$$\left\{ - \frac{Y\left[\sqrt{(1+\eta_r)^2+\theta_r^2+z_r^2} - 1\right]\theta_r}{\sqrt{(1+\eta_r)^2+\theta_r^2+z_r^2}} - m\omega(\eta_t - \omega\theta) - m(\omega\eta_t + \theta_{tt}) \right\}\Bigg|_{r=b} = 0$$

B.C. 5 $\quad z(0,t) = 0$

B.C. 6

$$\left\{ + \frac{Y\left[\sqrt{(1+\eta_r)^2 + \theta_r^2 + Z_r^2} - 1\right] Z_r}{\sqrt{(1+\eta_r)^2 + \theta_r^2 + Z_r^2}} + m Z_{tt} \right\}\Bigg|_{r=b} = 0$$

NOTE: It is clear that, if the linear mass density in the reference configuration is given by a function $\rho = \rho(r)$, the net effect on the results listed above can be obtained by replacing ρ everywhere by $\rho(r)$. This conclusion is established easily by examining the steps of the derivation.

IV.

A. Description of the physical system

1. Diagram A

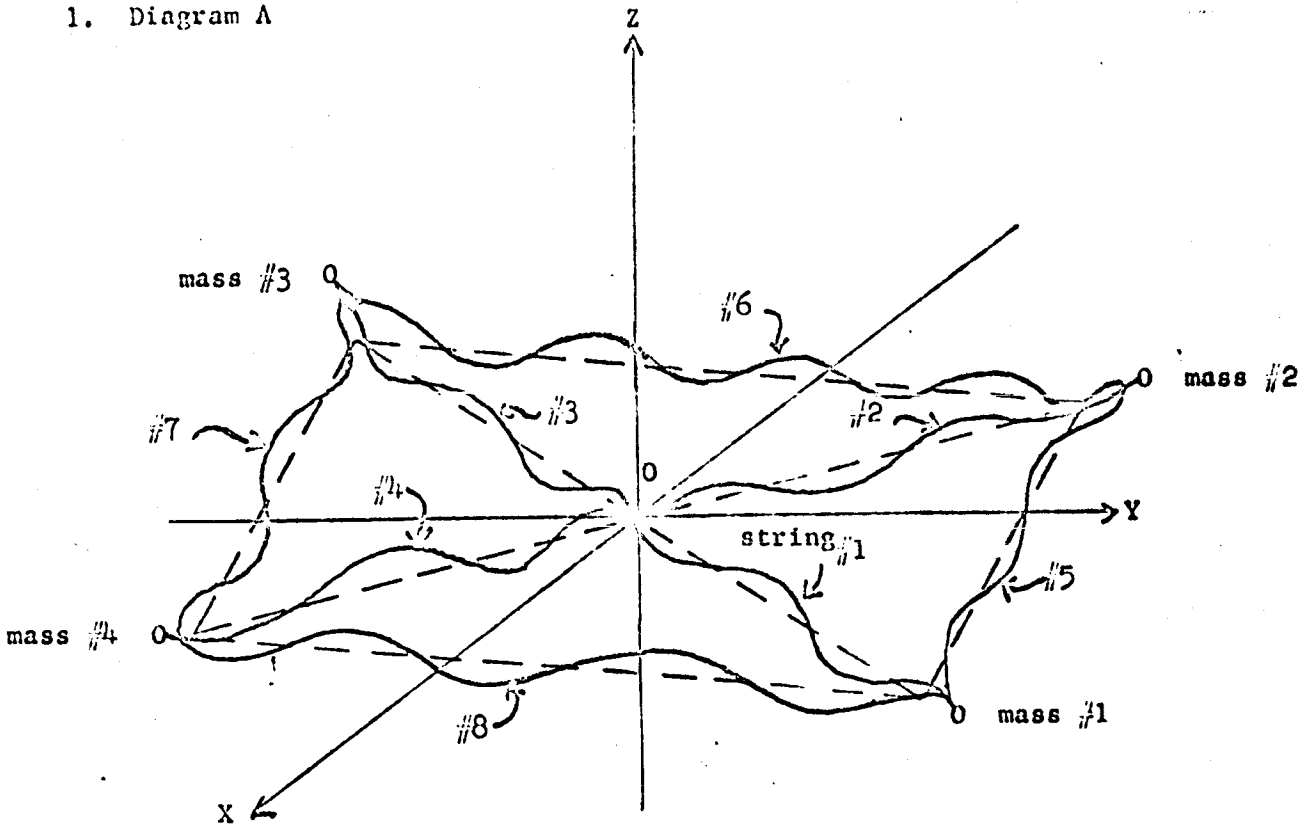

2. Diagram B

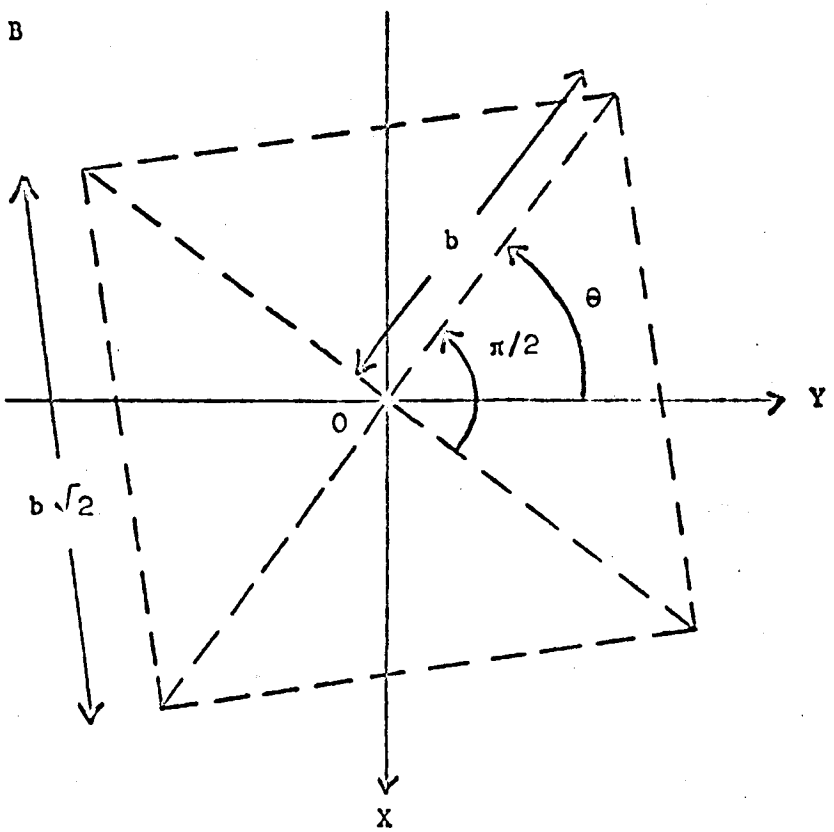

where $\dot{\theta} = \omega$ = constant.

3. Diagram C

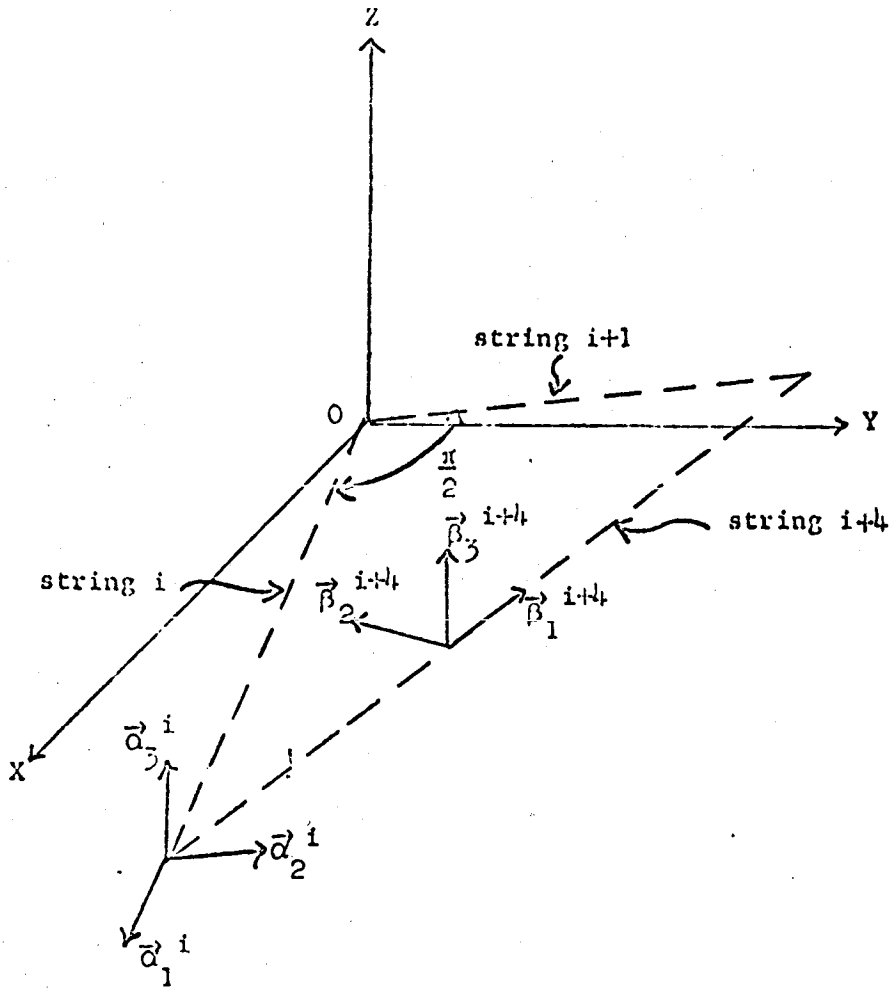

4. Diagram D

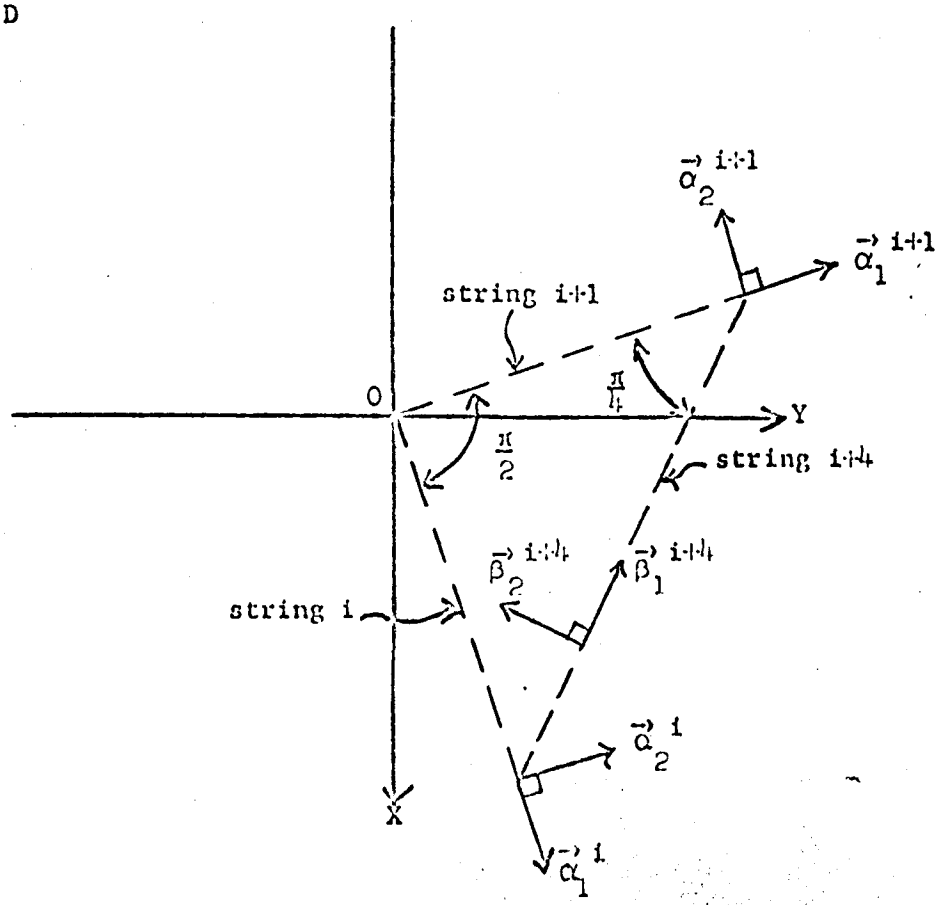

5. Assume the following conditions:

a. The XYZ-set of axes is an inertial system of coordinates.

b. The system is located in free space.

c. Each "string" obeys Hooke's law under <u>both</u> tension and compression. Let Y be the Young's Modulus such that the local tension or compression force is expressed by a relation

$$\text{force} = Y\zeta$$

where ζ is the local elongation per unit length.

d. The strings are perfectly elastic so that a potential energy can be associated with any instantaneous configuration. (See section IV-C-2.)

e. The unstressed length of the radial strings (i.e. strings #1, #2, #3 and #4) is b; the unstressed length of the tangential strings (i.e. strings #5, #6, #7 and #8) is $b\sqrt{2}$; the unstressed linear mass density of each string has the constant value ρ; and each point mass has the constant value m.

B. <u>Kinematical considerations</u>

1. The displacements of the strings will be measured relative to the rigid mesh which is illustrated in section IV-A-2. This mesh rotates with the constant angular velocity ω. Note that $\vec{\alpha}_3^{\,i}$ and $\vec{\beta}_3^{\,i+4}$ are equal, fixed unit vectors which are parallel to the Z-axis. $\vec{\alpha}_1^{\,i}$, $\vec{\alpha}_2^{\,i}$ and $\vec{\beta}_1^{\,i+4}$, $\vec{\beta}_2^{\,i+4}$ are pairs of orthogonal unit vectors in the XY plane. The $\vec{\alpha}_j^{\,i}$ unit vectors refer to a radial string while the $\vec{\beta}_j^{\,i}$ unit vectors refer to a tangential string. Sections IV-A-3 and IV-A-4 illustrate these unit vectors.

2. Consider the points $r^i\vec{\alpha}_1^{\,i}$ where i = 1,2,3 or 4 and $0 \leq r^i \leq b$. The reference configuration of this radial string is defined by the following conditions:

a. Every string element lies along the radial direction $\vec{\alpha}_1^{\,i}$.

b. The string has length b.

c. No portion of the string is either elongated or compressed.

Consider the points $r^i\vec{\beta}_1^{\,i}$ where i = 5, 6, 7 or 8 and $0 \leq r^i \leq b\sqrt{2}$. The reference configuration of this tangential string is defined by analogous conditions:

d. Every string element lies along the tangential direction $\vec{\beta}_1^{\,i}$.

e. The string has length $b\cdot\sqrt{2}$.

f. No portion of the string is either elongated or compressed.

3. The displacement (relative to the origin 0) of the radial string elements from the reference configuration is described by the following vector function:

$$\vec{D}^i(r^i,t) = \left[r^i + \eta^i(r^i,t)\right]\vec{\alpha}_1^{\,i} + \theta^i(r^i,t)\vec{\alpha}_2^{\,i} + z^i(r^i,t)\vec{\alpha}_3^{\,i}$$

where $i = 1, 2, 3$ or 4. For each r^i $(0 \le r^i \le b)$ $\vec{D}^i(r^i,t)$ is the vector displacement of a radial string element which is located at $r^i\vec{\alpha}_1^{\,i}$ in the reference configuration. Therefore, the coordinate r^i is a label for the nondenumerable, triply infinite set of generalized coordinates $\eta^i(r^i,t)$, $\theta^i(r^i,t)$, $z^i(r^i,t)$.

The displacement (relative to the origin 0) of the tangential string elements from the reference configuration is described by the following vector function:

$$\vec{D}^i(r^i,t) = b\,\vec{\alpha}_1^{\,i-4} + \left[r^i + \eta^i(r^i,t)\right]\vec{\beta}_1^{\,i} + \theta^i(r^i,t)\vec{\beta}_2^{\,i} + z^i(r^i,t)\vec{\beta}_3^{\,i}$$

where $i = 5, 6, 7$ or 8. Referring to sections IV-A-3 and IV-A-4,

$$\vec{\beta}_3^{\,i+4} = \vec{\alpha}_3^{\,i-4}$$

$$\vec{\beta}_1^{\,i} = -\cos\tfrac{\pi}{4}\,\vec{\alpha}_1^{\,i-4} + \cos\tfrac{\pi}{4}\,\vec{\alpha}_2^{\,i-4} = \frac{-1}{\sqrt{2}}\left(\vec{\alpha}_1^{\,i-4} - \vec{\alpha}_2^{\,i-4}\right)$$

$$\vec{\beta}_2^{\,i} = -\cos\tfrac{\pi}{4}\,\vec{\alpha}_1^{\,i-4} - \cos\tfrac{\pi}{4}\,\vec{\alpha}_2^{\,i-4} = \frac{-1}{\sqrt{2}}\left(\vec{\alpha}_1^{\,i-4} + \vec{\alpha}_2^{\,i-4}\right)$$

Thus,

$$\vec{D}^i(r^i,t) = \frac{1}{\sqrt{2}}\left[b\sqrt{2} - r^i - \eta^i(r^i,t) - \theta^i(r^i,t)\right]\vec{\alpha}_1^{\,i-4} + \frac{1}{\sqrt{2}}\left[r^i + \eta^i(r^i,t) - \theta^i(r^i,t)\right]\vec{\alpha}_2^{\,i-4}$$
$$+ z^i(r^i,t)\vec{\alpha}_3^{\,i-4}$$

where $0 \le r^i \le b\cdot\sqrt{2}$ and $i = 5, 6, 7$ or 8.

Dynamical considerations

1. The kinetic energy of the system.

Consider any radial string along with the associated point mass m. The computation of the kinetic energy of this portion of the system is identical to the procedure used in section III-C-1. Therefore, if T_R denotes the kinetic energy of the four radial strings plus the four associated point masses, the result on page 4 implies that

$$T_R(t) = \sum_{i=1}^{4} \int_0^b \frac{1}{2} \rho \left\{ \left(\eta_t^i - \omega\theta^i \right)^2 + \left[\left(r^i + \eta^i \right)\omega + \theta_t^i \right]^2 + z_t^{i\,2} \right\} dr^i$$

$$+ \sum_{i=1}^{4} \frac{1}{2} m \left\{ \left[\eta_t^i(b,t) - \omega\theta^i(b,t) \right]^2 + \left[b\omega + \omega\eta^i(b,t) + \theta_t^i(b,t) \right]^2 + z_t^{i\,2}(b,t) \right\}$$

Consider any tangential string. The mass point labelled by the index r^i $(0 \le r^i \le b\sqrt{2})$ has the displacement

$$\vec{D}^i(r^i,t) = \frac{1}{\sqrt{2}} \left(b\sqrt{2} - r^i - \eta^i - \theta^i \right) \vec{\alpha}_1^{\,i-4} + \frac{1}{\sqrt{2}} \left(r^i + \eta^i - \theta^i \right) \vec{\alpha}_2^{\,i-4} + z^i \vec{\alpha}_3^{\,i-4}$$

where i = 5, 6, 7 or 8. The square of the velocity (measured relative to the inertial frame of coordinates) is computed below. Recall that r^i is a time-independent labelling index.

$$\vec{v}(r^i,t) = \frac{d}{dt} \vec{D}^i(r^i,t) = \frac{d}{dt} \left[\frac{1}{\sqrt{2}} \left(b\sqrt{2} - r^i - \eta^i - \theta^i \right) \vec{\alpha}_1^{\,i-4} \right]$$

$$+ \frac{d}{dt} \left[\frac{1}{\sqrt{2}} \left(r^i + \eta^i - \theta^i \right) \vec{\alpha}_2^{\,i-4} \right] + \frac{d}{dt} \left(z^i \vec{\alpha}_3^{\,i-4} \right)$$

$$= -\frac{1}{\sqrt{2}} \left(\eta_t^i + \theta_t^i \right) \vec{\alpha}_1^{\,i-4} + \frac{1}{\sqrt{2}} \left(b\sqrt{2} - r^i - \eta^i - \theta^i \right) \omega \vec{\alpha}_2^{\,i-4}$$

$$+ \frac{1}{\sqrt{2}} \left(\eta_t^i - \theta_t^i \right) \vec{\alpha}_2^{\,i-4} - \frac{1}{\sqrt{2}} \left(r^i + \eta^i - \theta^i \right) \omega \vec{\alpha}_1^{\,i-4} + z_t^i \vec{\alpha}_3^{\,i-4}$$

$$= -\frac{1}{\sqrt{2}}\left[\eta_t^i + \theta_t^i + \omega\left(r^i + \eta^i - \theta^i\right)\right]\vec{\alpha}_1^{\,i-4}$$

$$+\frac{1}{\sqrt{2}}\left[\eta_t^i - \theta_t^i + \omega\left(b\sqrt{2} - r^i - \eta^i - \theta^i\right)\right]\vec{\alpha}_2^{\,i-4} + z_t^i\,\vec{\alpha}_3^{\,i-4}$$

$$v^{i2} = \frac{1}{2}\left[\eta_t^i + \theta_t^i + \omega\left(r^i + \eta^i - \theta^i\right)\right]^2 + \frac{1}{2}\left[\eta_t^i - \theta_t^i + \omega\left(b\sqrt{2} - r^i - \eta^i - \theta^i\right)\right]^2$$

$$+ z_t^{i2}$$

The kinetic energy T_T of the tangential strings is given by the relation

$$T_T(t) = \sum_{i=5}^{8} \int_0^{b\sqrt{2}} \frac{1}{2}\,\Delta_i\, v^{i2}\,(r^i,t)\,dr^i \quad ,$$

where Δ_i is the linear mass density function for the reference configuration. The arguments of section III-C-1 may be repeated to conclude that

$$\Delta_i = \rho = \text{constant for } i = 5,\ 6,\ 7 \text{ or } 8$$

Writing the expression for $T_T(t)$ in detail,

$$T_T(t) = \sum_{i=5}^{8} \int_0^{b\sqrt{2}} \frac{1}{2}\,\rho\left\{\frac{1}{2}\left[\eta_t^i + \theta_t^i + \omega\left(r^i + \eta^i - \theta^i\right)\right]^2\right.$$

$$\left. + \frac{1}{2}\left[\eta_t^i - \theta_t^i + \omega\left(b\sqrt{2} - r^i - \eta^i - \theta^i\right)\right]^2 + z_t^{i2}\right\} dr^i$$

Thus, the total kinetic energy of the system is

$$T = T_R + T_T = \sum_{i=1}^{4} \int_0^b \frac{1}{2} \rho \left\{ \left(\eta_t^i - \omega\theta^i \right)^2 + \left[\left(r^i + \eta^i \right) \omega + \theta_t^i \right]^2 + z_t^{i\,2} \right\} dr^i$$

$$+ \sum_{i=1}^{4} \frac{1}{2} m \left\{ \left[\eta_t^i(b,t) - \omega\theta^i(b,t) \right]^2 + \left[b\omega + \omega\eta^i(b,t) + \theta^i(b,t) \right]^2 + z_t^{i\,2}(b,t) \right\}$$

$$+ \sum_{i=5}^{8} \int_0^{b\sqrt{2}} \frac{1}{2} \rho \left\{ \frac{1}{2} \left[\eta_t^i + \theta_t^i + \omega \left(r^i + \eta^i - \theta^i \right) \right]^2 \right.$$

$$+ \frac{1}{2} \left[\eta_t^i - \theta_t^i + \omega \left(b\sqrt{2} - r^i - \eta^i - \theta^i \right) \right]^2$$

$$\left. + z_t^{i\,2} \right\} dr^i$$

2. The potential energy of the system.

The arguments of section III-C-2 may be repeated verbatim to conclude that the potential energy of the system is

$$V(t) = \sum_{i=1}^{4} \int_0^b \frac{1}{2} Y \left[\sqrt{\left(1 + \eta_r^i \right)^2 + \theta_r^{i\,2} + z_r^{i\,2}} - 1 \right]^2 dr^i$$

$$+ \sum_{i=5}^{8} \int_0^{b\sqrt{2}} \frac{1}{2} Y \left[\sqrt{\left(1 + \eta_r^i \right)^2 + \theta_r^{i\,2} + z_r^{i\,2}} - 1 \right]^2 dr^i$$

3. The Lagrangian and the action integral.

The Lagrangian L = T - V and the action integral

$$J\left(\eta^1, \eta^2, \cdots, \eta^8;\ \theta^1, \theta^2, \cdots, \theta^8;\ z^1, z^2, \cdots, z^8\right) = \int_{t_1}^{t_2} L\, dt$$

$$= \int_{t_1}^{t_2}\int_0^b \sum_{i=1}^{4} \ell_1^i\left(r^i, \eta^i, \theta^i, z^i, \eta_r^i, \eta_t^i, \theta_r^i, \theta_t^i, z_r^i, z_t^i\right) dr^i\, dt.$$

$$+ \int_{t_1}^{t_2}\int_0^{b\sqrt{2}} \sum_{i=5}^{8} \ell_2^i\left(r^i, \eta^i, \theta^i, z^i, \eta_r^i, \eta_t^i, \theta_r^i, \theta_t^i\, z_r^i, z_t^i\right) dr^i\, dt$$

$$+ \int_{t_1}^{t_2} \sum_{i=1}^{4} \ell_3^i\left[\eta^i(b,t);\ \theta^i(b,t);\ \eta_t^i(b,t);\ \theta_t^i(b,t);\ z_t^i(b,t)\right] dt$$

where $\ell_1^i\left(r^i, \eta^i, \theta^i, z^i, \eta_r^i, \eta_t^i, \theta_r^i, \theta_t^i, z_r^i, z_t^i\right)$

$$= \frac{1}{2}\rho\left[\left(\eta_t^i - \omega\theta^i\right)^2 + \left(\omega r^i + \omega\eta^i + \theta_t^i\right)^2 + z_t^{i2}\right] - \frac{1}{2}Y\left[\sqrt{\left(1+\eta_r^i\right)^2 + \theta_r^{i2} + z_r^{i2}} - 1\right]^2$$

$$\ell_2^i\left(r^i, \eta^i, \theta^i, z^i, \eta_r^i, \eta_t^i, \theta_r^i, \theta_t^i, z_r^i, z_t^i\right)$$

$$= \frac{1}{2}\rho\left[\frac{1}{2}\left(\eta_t^i + \theta_t^i + \omega r^i + \omega\eta^i - \omega\theta^i\right)^2 + \frac{1}{2}\left(\eta_t^i - \theta_t^i + \omega b\sqrt{2} - \omega r^i - \omega\eta^i - \omega\theta^i\right)^2\right.$$

$$\left. + z_t^{i2}\right] - \frac{1}{2}Y\left[\sqrt{\left(1+\eta_r^i\right)^2 + \theta_r^{i2} + z_r^{i2}} - 1\right]^2$$

$$\ell_3^i\left[\eta^i(b,t);\ \theta^i(b,t);\ \eta_t^i(b,t);\ \theta_t^i(b,t);\ z_t^i(b,t)\right]$$

$$= \frac{1}{2}m\left\{\left[\eta_t^i(b,t) - \omega\theta^i(b,t)\right]^2 + \left[b\omega + \omega\eta^i(b,t) + \theta^i(b,t)\right]^2 + z_t^{i2}(b,t)\right\}$$

4. Application of Hamilton's principle (principle of stationary action). The constraints of the problem determine 36 boundary conditions (see sections IV-A-1, IV-A-3 and IV-A-4) which are listed below:

1, 2, 3, 4: $\eta^i(r^i = 0,t) = 0$ for $i = 1, 2, 3, 4$

5, 6, 7, 8: $\theta^i(r^i = 0,t) = 0$ " "

9, 10, 11, 12: $z^i(r^i = 0,t) = 0$ " "

13, 14, 15, 16: $z^i(r^i = 0,t) = z^{i-4}(r^{i-4} = b,t)$ for $i = 5, 6, 7, 8$

17, 18, 19: $z^i(r^i = b\sqrt{2},t) = z^{i-3}(r^{i-3} = b,t)$ for $i = 5, 6, 7$

20: $z^8(r^8 = b\sqrt{2},t) = z^1(r^1 = b,t)$

$$\eta^i\left(r^i = 0,t\right)\vec{\beta}_1^{\,i} + \theta^i\left(r^i = 0,t\right)\vec{\beta}_2^{\,i} = \eta^{i-4}\left(r^{i-4} = b,t\right)\vec{\alpha}_1^{\,i-4} + \theta^{i-4}\left(r^{i-4} = b,t\right)\vec{\alpha}_2^{\,i-4}$$

for $i = 5, 6, 7, 8$. From section IV-A-4

$$\vec{\alpha}_1^{\,i-4} = -\frac{1}{\sqrt{2}}\left(\vec{\beta}_1^{\,i} + \vec{\beta}_2^{\,i}\right)$$

$$\vec{\alpha}_2^{\,i-4} = \frac{1}{\sqrt{2}}\left(\vec{\beta}_1^{\,i} - \vec{\beta}_2^{\,i}\right)$$

so that

21,22,23,24: $\eta^i(r^i=0,t) = -\frac{1}{\sqrt{2}}\left[\eta^{i-4}\left(r^{i-4}=b,t\right) - \theta^{i-4}\left(r^{i-4}=b,t\right)\right]$ for $i = 5,6,7,8$

25,26,27,28: $\theta^i(r^i=0,t) = -\frac{1}{\sqrt{2}}\left[\eta^{i-4}\left(r^{i-4}=b,t\right) + \theta^{i-4}\left(r^{i-4}=b,t\right)\right]$ " "

$$\eta^i\left(r^{i=b\sqrt{2}},t\right)\vec{\beta}_1^{\,i} + \theta^i\left(r^{i=b\sqrt{2}},t\right)\vec{\beta}_2^{\,i} = \eta^{i-3}\left(r^{i-3=b},t\right)\vec{\alpha}_1^{\,i-3} + \theta^{i-3}\left(r^{i-3=b},t\right)\vec{\alpha}_2^{\,i-3}$$

for i = 5, 6, 7, 8. From section IV-A-4

$$\vec{\alpha}_1^{\,i-3} = \frac{1}{\sqrt{2}}\left(\vec{\beta}_1^{\,i} - \vec{\beta}_2^{\,i}\right)$$

$$\vec{\alpha}_2^{\,i-3} = \frac{1}{\sqrt{2}}\left(\vec{\beta}_1^{\,i} + \vec{\beta}_2^{\,i}\right)$$

so that

29,30,31: $$\eta^i\left(r^{i=b\sqrt{2}},t\right) = \frac{1}{\sqrt{2}}\left[\eta^{i-3}\left(r^{i-3=b},t\right) + \theta^{i-3}\left(r^{i-3=b},t\right)\right] \text{ for } i = 5,6,7$$

32: $$\eta^8\left(r^{8=b\sqrt{2}},t\right) = \frac{1}{\sqrt{2}}\left[\eta^1\left(r^{1=b},t\right) + \theta^1\left(r^{1=b},t\right)\right]$$

33,34,35: $$\theta^i\left(r^{i=b\sqrt{2}},t\right) = -\frac{1}{\sqrt{2}}\left[\eta^{i-3}\left(r^{i-3=b},t\right) - \theta^{i-3}\left(r^{i-3=b},t\right)\right] \text{ for } i = 5,6,7$$

36: $$\theta^8\left(r^{8=b\sqrt{2}},t\right) = -\frac{1}{\sqrt{2}}\left[\eta^1\left(r^{1=b},t\right) - \theta^1\left(r^{1=b},t\right)\right]$$

Consider the varied functions

$$\eta^{i^*}(r^i,t) = \eta^i(r^i,t) + \epsilon\,\mu^i(r^i,t) + \ldots$$

$$\theta^{i^*}(r^i,t) = \theta^i(r^i,t) + \epsilon\,\gamma^i(r^i,t) + \ldots$$

$$Z^{i^*}(r^i,t) = Z^i(r^i,t) + \epsilon\,\delta^i(r^i,t) + \ldots$$

where i = 1, 2, ---, 8. The 1st variation of the action integral is

$$\delta J = \epsilon \int_{t_1}^{t_2} \int_0^b \sum_{i=1}^{4} \left(\ell^i_{1_{\eta^i}} - \frac{\partial}{\partial r^i} \ell^i_{1_{\eta^i_r}} - \frac{\partial}{\partial t} \ell^i_{1_{\eta^i_t}} \right) \mu^i(r^i,t)\, dr^i\, dt$$

$$+ \epsilon \int_{t_1}^{t_2} \int_0^b \sum_{i=1}^{4} \left(\ell^i_{1_{\theta^i}} - \frac{\partial}{\partial r^i} \ell^i_{1_{\theta^i_r}} - \frac{\partial}{\partial t} \ell^i_{1_{\theta^i_t}} \right) \gamma^i(r^i,t)\, dr^i\, dt$$

$$+ \epsilon \int_{t_1}^{t_2} \int_0^b \sum_{i=1}^{4} \left(\ell^i_{1_{Z^i}} - \frac{\partial}{\partial r^i} \ell^i_{1_{Z^i_r}} - \frac{\partial}{\partial t} \ell^i_{1_{Z^i_t}} \right) \delta^i(r^i,t)\, dr^i\, dt$$

$$+ \epsilon \int_{t_1}^{t_2} \int_0^{\sqrt{2}} \sum_{i=5}^{8} \left(\ell^i_{2_{\eta^i}} - \frac{\partial}{\partial r^i} \ell^i_{2_{\eta^i_r}} - \frac{\partial}{\partial t} \ell^i_{2_{\eta^i_t}} \right) \mu^i(r^i,t)\, dr^i\, dt$$

$$+ \epsilon \int_{t_1}^{t_2} \int_0^{\sqrt{2}} \sum_{i=5}^{8} \left(\ell^i_{2_{\theta^i}} - \frac{\partial}{\partial r^i} \ell^i_{2_{\theta^i_r}} - \frac{\partial}{\partial t} \ell^i_{2_{\theta^i_t}} \right) \gamma^i(r^i,t)\, dr^i\, dt$$

$$+ \epsilon \int_{t_1}^{t_2} \int_0^{\sqrt{2}} \sum_{i=5}^{8} \left(\ell^i_{2_{Z^i}} - \frac{\partial}{\partial r^i} \ell^i_{2_{Z^i_r}} - \frac{\partial}{\partial t} \ell^i_{2_{Z^i_t}} \right) \delta^i(r^i,t)\, dr^i\, dt$$

$$+ \epsilon \int_{t_1}^{t_2} \sum_{i=1}^{4} \left(\ell^i_{3_{\eta^i}} - \frac{\partial}{\partial t} \ell^i_{3_{\eta^i_t}} \right) \mu^i(b,t)\, dt + \epsilon \int_{t_1}^{t_2} \sum_{i=1}^{4} \left(\ell^i_{3_{\theta^i}} - \frac{\partial}{\partial t} \ell^i_{3_{\theta^i_t}} \right) \gamma^i(b,t)\, dt$$

$$+ \epsilon \int_{t_1}^{t_2} \sum_{i=1}^{4} \left(\ell^i_{3_{Z^i}} - \frac{\partial}{\partial t} \ell^i_{3_{Z^i_t}} \right) \delta^i(b,t)\, dt$$

$$+ \epsilon \int_{t_1}^{t_2} \int_0^b \sum_{i=1}^{4} \frac{\partial}{\partial r^i} \left(\ell^i_{1_{\eta^i_r}} \mu^i + \ell^i_{1_{\theta^i_r}} \gamma^i + \ell^i_{1_{Z^i_r}} \delta^i \right) dr^i\, dt$$

$$+ \epsilon \int_{t_1}^{t_2} \int_0^b \sum_{i=1}^{4} \frac{\partial}{\partial t} \left(\ell^i_{1_{\eta^i_t}} \mu^i + \ell^i_{1_{\theta^i_t}} \gamma^i + \ell^i_{1_{z^i_t}} \delta^i \right) dr^i \, dt$$

$$+ \epsilon \int_{t_1}^{t_2} \int_0^{b\sqrt{2}} \sum_{i=5}^{8} \frac{\partial}{\partial r^i} \left(\ell^i_{2_{\eta^i_r}} \mu^i + \ell^i_{2_{\theta^i_r}} \gamma^i + \ell^i_{2_{z^i_r}} \delta^i \right) dr^i \, dt$$

$$+ \epsilon \int_{t_1}^{t_2} \int_0^{b\sqrt{2}} \sum_{i=5}^{8} \frac{\partial}{\partial t} \left(\ell^i_{2_{\eta^i_t}} \mu^i + \ell^i_{2_{\theta^i_t}} \gamma^i + \ell^i_{2_{z^i_t}} \delta^i \right) dr^i \, dt$$

$$+ \epsilon \int_{t_1}^{t_2} \sum_{i=1}^{4} \frac{\partial}{\partial t} \left(\ell^i_{3_{\eta^i_t}} \mu^i + \ell^i_{3_{\theta^i_t}} \gamma^i + \ell^i_{3_{z^i_t}} \delta^i \right) dt$$

Hamilton's principle requires that the varied functions vanish at the extremities of the time interval. Therefore, for i = 1, 2, ---, 8

$$\mu^i(r^i,t_1) = \mu^i(r^i,t_2) = \gamma^i(r^i,t_1) = \gamma^i(r^i,t_2) = \delta^i(r^i,t_1) = \delta^i(r^i,t_2) = 0$$

where $0 \le r^i \le b$ for i = 1, 2, 3, 4 and $0 \le r^i \le b\sqrt{2}$ for i = 5, 6, 7, 8. These relations imply

$$\epsilon \int_{t_1}^{t_2} \int_0^b \sum_{i=1}^{4} \frac{\partial}{\partial t} \left(\ell^i_{1_{\eta^i_t}} \mu^i + \ell^i_{1_{\theta^i_t}} \gamma^i + \ell^i_{1_{z^i_t}} \delta^i \right) dr^i \, dt = 0$$

$$\epsilon \int_{t_1}^{t_2} \int_0^{b\sqrt{2}} \sum_{i=5}^{8} \frac{\partial}{\partial t} \left(\ell^i_{2_{\eta^i_t}} \mu^i + \ell^i_{2_{\theta^i_t}} \gamma^i + \ell^i_{2_{z^i_t}} \delta^i \right) dr^i \, dt = 0$$

$$\epsilon \int_{t_1}^{t_2} \sum_{i=1}^{4} \frac{\partial}{\partial t} \left(\ell^i_{3_{\eta^i_t}} \mu^i + \ell^i_{3_{\theta^i_t}} \gamma^i + \ell^i_{3_{z^i_t}} \delta^i \right) dt = 0$$

The constraints (see boundary conditions 1, 2, ---, 12 in this section) imply

$$\mu^i(r^i = 0,t) = 0 \quad \text{for } i = 1, 2, 3, 4$$

$$\gamma^i(r^i = 0,t) = 0 \qquad "$$

$$\delta^i(r^i = 0,t) = 0 \qquad "$$

so that

$$\epsilon \int_{t_1}^{t_2} \int_0^b \sum_{i=1}^{4} \frac{\partial}{\partial r^i} \left(\ell^i_{1_{\eta^i_r}} \mu^i + \ell^i_{1_{\theta^i_r}} \gamma^i + \ell^i_{1_{z^i_r}} \delta^i \right) dr^i \, dt$$

$$= \epsilon \int_{t_1}^{t_2} \sum_{i=1}^{4} \left(\ell^i_{1_{\eta^i_r}} \mu^i + \ell^i_{1_{\theta^i_r}} \gamma^i + \ell^i_{1_{z^i_r}} \delta^i \right) \Bigg|_{r^i = b} dt$$

Also,

$$\epsilon \int_{t_1}^{t_2} \int_0^{b\sqrt{2}} \sum_{i=5}^{8} \frac{\partial}{\partial r^i} \left(\ell^i_{2_{\eta^i_r}} \mu^i + \ell^i_{2_{\theta^i_r}} \gamma^i + \ell^i_{2_{z^i_r}} \delta^i \right) dr^i \, dt$$

$$= \epsilon \int_{t_1}^{t_2} \sum_{i=5}^{8} \left(\ell^i_{2_{\eta^i_r}} \mu^i + \ell^i_{2_{\theta^i_r}} \gamma^i + \ell^i_{2_{z^i_r}} \delta^i \right) \Bigg|_{r^i = 0}^{r^i = b\sqrt{2}} dt$$

Consider the restricted class of admissible functions such that

$$\mu^i(r^i = b,t) = 0 \quad \text{for } i = 1, 2, 3, 4$$

$$\gamma^i(r^i = b,t) = 0 \qquad "$$

$$\delta^i(r^i = b,t) = 0 \qquad "$$

$$\mu^i(r^i = 0,t) = \mu^i(r^i = b\sqrt{2},t) = 0 \quad \text{for } i = 5, 6, 7, 8$$

$$\gamma^i(r^i = 0,t) = \gamma^i(r^i = b\sqrt{2},t) = 0 \qquad "$$

$$\delta^i(r^i = 0,t) = \delta^i(r^i = b\sqrt{2},t) = 0 \qquad "$$

The vanishing of the 1st variation over this restricted class of admissible functions implies the following Euler equations of motion:

$$\ell^i_{1_{\eta^i}} - \frac{\partial}{\partial r^i}\ell^i_{1_{\eta^i_r}} - \frac{\partial}{\partial t}\ell^i_{1_{\eta^i_t}} = 0 \quad \text{where } i = 1, 2, 3, 4 \text{ and } 0 \le r^i \le b$$

$$\ell^i_{1_{\theta^i}} - \frac{\partial}{\partial r^i}\ell^i_{1_{\theta^i_r}} - \frac{\partial}{\partial t}\ell^i_{1_{\theta^i_t}} = 0 \qquad " \qquad " \qquad "$$

$$\ell^i_{1_{Z^i}} - \frac{\partial}{\partial r^i}\ell^i_{1_{Z^i_r}} - \frac{\partial}{\partial t}\ell^i_{1_{Z^i_t}} = 0 \qquad " \qquad " \qquad "$$

$$\ell^i_{2_{\eta^i}} - \frac{\partial}{\partial r^i}\ell^i_{2_{\eta^i_r}} - \frac{\partial}{\partial t}\ell^i_{2_{\eta^i_t}} = 0 \quad \text{where } i = 5, 6, 7, 8 \text{ and } 0 \le r^i \le b\sqrt{2}$$

$$\ell^i_{2_{\theta^i}} - \frac{\partial}{\partial r^i}\ell^i_{2_{\theta^i_r}} - \frac{\partial}{\partial t}\ell^i_{2_{\theta^i_t}} = 0 \qquad " \qquad " \qquad "$$

$$\ell^i_{2_{Z^i}} - \frac{\partial}{\partial r^i}\ell^i_{2_{Z^i_r}} - \frac{\partial}{\partial t}\ell^i_{2_{Z^i_t}} = 0 \qquad " \qquad " \qquad "$$

Now, remove the previous restrictions on the class of admissible functions so that $\mu^i(r^i,t)$, $\gamma^i(r^i,t)$, and $\delta^i(r^i,t)$ are arbitrary admissible functions (on $[t_1,t_2]$) which satisfy the 36 boundary conditions specified by the constraints. The vanishing of the 1st variation over the expanded class of admissible functions implies all previous results so that

$$\delta J = 0 = \epsilon \int_{t_1}^{t_2} \sum_{i=1}^{4} \left(\ell^i_{3_{\eta^i}} - \frac{\partial}{\partial t} \ell^i_{3_{\eta^i_t}} \right) \mu^i(b,t)\, dt$$

$$+ \epsilon \int_{t_1}^{t_2} \sum_{i=1}^{4} \left(\ell^i_{3_{\theta i}} - \frac{\partial}{\partial t} \ell^i_{3_{\theta^i_t}} \right) \gamma^i(b,t)\, dt + \epsilon \int_{t_1}^{t_2} \sum_{i=1}^{4} \left(\ell^i_{3_{Zi}} - \frac{\partial}{\partial t} \ell^i_{3_{Z^i_t}} \right) \delta^i(b,t)\, dt$$

$$+ \epsilon \int_{t_1}^{t_2} \sum_{i=1}^{4} \left(\ell^i_{1_{\eta^i_r}} \mu^i + \ell^i_{1_{\theta^i_r}} \gamma^i + \ell^i_{1_{Z^i_r}} \delta^i \right) \Big|_{r^i = b} dt$$

$$+ \epsilon \int_{t_1}^{t_2} \sum_{i=5}^{8} \left(\ell^i_{2_{\eta^i_r}} \mu^i + \ell^i_{2_{\theta^i_r}} \gamma^i + \ell^i_{2_{Z^i_r}} \delta^i \right) \Big|_{r^i = 0}^{r^i = b\sqrt{2}} dt$$

$$= \epsilon \int_{t_1}^{t_2} \sum_{i=1}^{4} \left(\ell^i_{1_{\eta^i_r}} \Big|_{r^i = b} + \ell^i_{3_{\eta^i}} - \frac{\partial}{\partial t} \ell^i_{3_{\eta^i_t}} \right) \mu^i(b,t)\, dt$$

$$+ \epsilon \int_{t_1}^{t_2} \sum_{i=1}^{4} \left(\ell^i_{1_{\theta^i_r}} \Big|_{r^i = b} + \ell^i_{3_{\theta i}} - \frac{\partial}{\partial t} \ell^i_{3_{\theta^i_t}} \right) \gamma^i(b,t)\, dt$$

$$+ \epsilon \int_{t_1}^{t_2} \sum_{i=1}^{4} \left(\ell^i_{1_{Z^i_r}} \Big|_{r^i = b} + \ell^i_{3_{Zi}} - \frac{\partial}{\partial t} \ell^i_{3_{Z^i_t}} \right) \delta^i(b,t)\, dt$$

$$+ \epsilon \int_{t_1}^{t_2} \sum_{i=5}^{8} \left(\ell^i_{2_{\eta^i_r}} \mu^i + \ell^i_{2_{\theta^i_r}} \gamma^i + \ell^i_{2_{Z^i_r}} \delta^i \right) \Big|_{r^i = 0}^{r^i = b\sqrt{2}} dt$$

Boundary conditions 13, 14, ---, 36 imply

$$\mu^i(r^i = 0,t) = -\frac{1}{\sqrt{2}}\left[\mu^{i-4}(r^{i-4} = b,t) - \gamma^{i-4}(r^{i-4} = b,t)\right] \quad \text{for } i = 5, 6, 7, 8$$

$$\mu^i(r^i = b\sqrt{2},t) = \frac{1}{\sqrt{2}}\left[\mu^{i-3}(r^{i-3} = b,t) + \gamma^{i-3}(r^{i-3} = b,t)\right] \quad \text{for } i = 5, 6, 7$$

$$\mu^8(r^8 = b\sqrt{2},t) = \frac{1}{\sqrt{2}}\left[\mu^1(r^1 = b,t) + \gamma^1(r^1 = b,t)\right]$$

$$\gamma^i(r^i = 0,t) = -\frac{1}{\sqrt{2}}\left[\mu^{i-4}(r^{i-4} = b,t) + \gamma^{i-4}(r^{i-4} = b,t)\right] \quad \text{for } i = 5, 6, 7, 8$$

$$\gamma^i(r^i = b\sqrt{2},t) = -\frac{1}{\sqrt{2}}\left[\mu^{i-3}(r^{i-3} = b,t) - \gamma^{i-3}(r^{i-3} = b,t)\right] \quad \text{for } i = 5, 6, 7$$

$$\gamma^8(r^8 = b\sqrt{2},t) = -\frac{1}{\sqrt{2}}\left[\mu^1(r^1 = b,t) - \gamma^1(r^1 = b,t)\right]$$

$$\delta^i(r^i = 0,t) = \delta^{i-4}(r^{i-4} = b,t) \quad \text{for } i = 5, 6, 7, 8$$

$$\delta^i(r^i = b\sqrt{2},t) = \delta^{i-3}(r^{i-3} = b,t) \quad \text{for } i = 5, 6, 7$$

$$\delta^8(r^8 = b\sqrt{2},t) = \delta^1(r^1 = b,t)$$

Thus,

$$\epsilon\int_{t_1}^{t_2}\sum_{i=5}^{8}\left(\ell^i_{2\eta^i_r}\,\mu^i + \ell^i_{2\theta^i_r}\,\gamma^i + \ell^i_{2z^i_r}\,\delta^i\right)\Bigg|_{r^i=0}^{r^i=b\sqrt{2}} dt$$

$$= \epsilon\int_{t_1}^{t_2}\sum_{i=5}^{7}\left[\frac{1}{\sqrt{2}}\,\ell^i_{2\eta^i_{r^i}}\Big|_{r^i=b\sqrt{2}}\left(\mu^{i-3}+\gamma^{i-3}\right)\Big|_{r^{i-3}=b} + \frac{1}{\sqrt{2}}\,\ell^8_{2\eta^8_{r^8}}\Big|_{r^8=b\sqrt{2}}\left(\mu^1+\gamma^1\right)\Big|_{r^1=b}\right] dt$$

$$- \epsilon \int_{t_1}^{t_2} \sum_{i=5}^{8} \left[\frac{1}{\sqrt{2}} \ell^i_{2\eta^i_r} \Big|_{r^i=0} \left(-\mu^{i-4} + \gamma^{i-4} \right) \Big|_{r^{i-4}=b} \right] dt$$

$$+ \epsilon \int_{t_1}^{t_2} \sum_{i=5}^{7} \left[\frac{1}{\sqrt{2}} \ell^i_{2\theta^i_r} \Big|_{r^i=b\sqrt{2}} \left(-\mu^{i-3} + \gamma^{i-3} \right) \Big|_{r^{i-3}=b} + \frac{1}{\sqrt{2}} \ell^8_{2\theta^8_r} \Big|_{r^8=b\sqrt{2}} \left(-\mu^1 + \gamma^1 \right) \Big|_{r^1=b} \right] dt$$

$$- \epsilon \int_{t_1}^{t_2} \sum_{i=5}^{8} \left[\frac{1}{\sqrt{2}} \ell^i_{2\theta^i_r} \Big|_{r^i=0} \left(-\mu^{i-4} - \gamma^{i-4} \right) \Big|_{r^{i-4}=b} \right] dt$$

$$+ \epsilon \int_{t_1}^{t_2} \left[\sum_{i=5}^{7} \left(\ell^i_{2\chi^i_r} \Big|_{r^i=b\sqrt{2}} s^{i-3} \Big|_{r^{i-3}=b} \right) + \ell^8_{2\chi^8_r} \Big|_{r^8=b\sqrt{2}} s^1 \Big|_{r^1=b} \right] dt$$

$$- \epsilon \int_{t_1}^{t_2} \sum_{i=5}^{8} \left[\ell^i_{2\chi^i_r} \Big|_{r^i=0} s^{i-4} \Big|_{r^{i-4}=b} \right] dt$$

$$= \epsilon \int_{t_1}^{t_2} \frac{1}{\sqrt{2}} \left[\left(\ell^8_{2\eta^8_r} - \ell^8_{2\theta^8_r} \right) \Big|_{r^8=b\sqrt{2}} + \left(\ell^5_{2\eta^5_r} + \ell^5_{2\theta^5_r} \right) \Big|_{r^5=0} \right] \mu^1(b,t)\, dt$$

$$+ \epsilon \int_{t_1}^{t_2} \sum_{i=2}^{4} \frac{1}{\sqrt{2}} \left[\left(\ell^{i+3}_{2\eta^{i+3}_r} - \ell^{i+3}_{2\theta^{i+3}_r} \right) \Big|_{r^{i+3}=b\sqrt{2}} + \left(\ell^{i+4}_{2\eta^{i+4}_r} + \ell^{i+4}_{2\theta^{i+4}_r} \right) \Big|_{r^{i+4}=0} \right] \mu^i(b,t)\, dt$$

$$+ \epsilon \int_{t_1}^{t_2} \frac{1}{\sqrt{2}} \left[\left(\ell^8_{2\eta^8_r} + \ell^8_{2\theta^8_r} \right) \Big|_{r^8=b\sqrt{2}} + \left(-\ell^5_{2\eta^5_r} + \ell^5_{2\theta^5_r} \right) \Big|_{r^5=0} \right] \gamma^1(b,t)\, dt$$

$$+ \epsilon \int_{t_1}^{t_2} \sum_{i=2}^{4} \frac{1}{\sqrt{2}} \left[\left(\ell^{i+3}_{2\eta^{i+3}_r} + \ell^{i+3}_{2\theta^{i+3}_r} \right) \Big|_{r^{i+3}=b\sqrt{2}} + \left(-\ell^{i+4}_{2\eta^{i+4}_r} + \ell^{i+4}_{2\theta^{i+4}_r} \right) \Big|_{r^{i+4}=0} \right] \gamma^i(b,t)\, dt$$

$$+ \epsilon \int_{t_1}^{t_2} \left(\ell^{3}_{2_{\eta^{3}_{r}}} \Big|_{r^3 = b\sqrt{2}} - \ell^{5}_{2_{\eta^{5}_{r}}} \Big|_{r^5 = 0} \right) \delta^1(b,t)\, dt$$

$$+ \epsilon \int_{t_1}^{t_2} \sum_{i=2}^{4} \left(\ell^{i+3}_{2_{\eta^{i+3}_{r}}} \Big|_{r^{i+3} = b\sqrt{2}} - \ell^{i+4}_{2_{\eta^{i+4}_{r}}} \Big|_{r^{i+4} = 0} \right) \delta^i(b,t)\, dt$$

so that the expression for δJ becomes

$$\delta J = 0 = \epsilon \int_{t_1}^{t_2} \left[\ell^{1}_{1_{\eta^{1}_{r}}} \Big|_{r^1 = b} + \ell^{1}_{3_{\eta^1}} - \frac{\partial}{\partial t} \ell^{1}_{3_{\eta^{1}_{t}}} + \frac{1}{\sqrt{2}} \left(\ell^{8}_{2_{\eta^{8}_{r}}} - \ell^{8}_{2_{\theta^{8}_{r}}} \right) \Big|_{r^8 = b\sqrt{2}} \right.$$

$$\left. + \frac{1}{\sqrt{2}} \left(\ell^{5}_{2_{\eta^{5}_{r}}} + \ell^{5}_{2_{\theta^{5}_{r}}} \right) \Big|_{r^5 = 0} \right] \mu^1(b,t)\, dt$$

$$+ \epsilon \int_{t_1}^{t_2} \sum_{i=2}^{4} \left[\ell^{i}_{1_{\eta^{i}_{r}}} \Big|_{r^i = b} + \ell^{i}_{3_{\eta^i}} - \frac{\partial}{\partial t} \ell^{i}_{3_{\eta^{i}_{t}}} + \frac{1}{\sqrt{2}} \left(\ell^{i+3}_{2_{\eta^{i+3}_{r}}} - \ell^{i+3}_{2_{\theta^{i+3}_{r}}} \right) \Big|_{r^{i+3} = b\sqrt{2}} \right.$$

$$\left. + \frac{1}{\sqrt{2}} \left(\ell^{i+4}_{2_{\eta^{i+4}_{r}}} + \ell^{i+4}_{2_{\theta^{i+4}_{r}}} \right) \Big|_{r^{i+4} = 0} \right] \mu^i(b,t)\, dt$$

$$+ \epsilon \int_{t_1}^{t_2} \left[\ell^{1}_{1_{\theta^{1}_{r}}} \Big|_{r^1 = b} + \ell^{1}_{3_{\theta^1}} - \frac{\partial}{\partial t} \ell^{1}_{3_{\theta^{1}_{t}}} + \frac{1}{\sqrt{2}} \left(\ell^{8}_{2_{\eta^{8}_{r}}} + \ell^{8}_{2_{\theta^{8}_{r}}} \right) \Big|_{r^8 = b\sqrt{2}} \right.$$

$$\left. + \frac{1}{\sqrt{2}} \left(-\ell^{5}_{2_{\eta^{5}_{r}}} + \ell^{5}_{2_{\theta^{5}_{r}}} \right) \Big|_{r^5 = 0} \right] \gamma^1(b,t)\, dt$$

$$+\epsilon\int_{t_1}^{t_2}\sum_{i=2}^{4}\left[\ell_{1_{\theta_r^i}}^{i}\Big|_{r^i=b}+\ell_{3_{\theta i}}^{i}-\frac{\partial}{\partial t}\,\ell_{3_{\theta_t^i}}^{i}+\frac{1}{\sqrt{2}}\left(\ell_{2_{\eta_r^{i+3}}}^{i+3}+\ell_{2_{\theta_r^{i+3}}}^{i+3}\right)\Big|_{r^{i+3}=b\sqrt{2}}\right.$$

$$\left.+\frac{1}{\sqrt{2}}\left(-\ell_{2_{\eta_r^{i+4}}}^{i+4}+\ell_{2_{\theta_r^{i+4}}}^{i+4}\right)\Big|_{r^{i+4}=0}\right]\gamma^i(b,t)\,dt$$

$$+\epsilon\int_{t_1}^{t_2}\left[\ell_{1_{z_r^1}}^{1}\Big|_{r^1=b}+\ell_{3_{z1}}^{1}-\frac{\partial}{\partial t}\,\ell_{3_{z_t^1}}^{1}+\ell_{2_{z_r^8}}^{8}\Big|_{r^8=b\sqrt{2}}\right.$$

$$\left.-\ell_{2_{z_r^5}}^{5}\Big|_{r^5=0}\right]\delta^1(b,t)\,dt$$

$$+\epsilon\int_{t_1}^{t_2}\sum_{i=2}^{4}\left[\ell_{1_{z_r^i}}^{i}\Big|_{r^i=b}+\ell_{3_{zi}}^{i}-\frac{\partial}{\partial t}\,\ell_{3_{z_t^i}}^{i}+\ell_{2_{z_r^{i+3}}}^{i+3}\Big|_{r^{i+3}=b\sqrt{2}}\right.$$

$$\left.-\ell_{2_{z_r^{i+4}}}^{i+4}\Big|_{r^{i+4}=0}\right]\delta^i(b,t)\,dt$$

Since $\mu^i(b,t)$, $\gamma^i(b,t)$, and $\delta^i(b,t)$ (for $i = 1, 2, 3, 4$) are arbitrary admissible functions on $[t_1,t_2]$, the vanishing of the 1st variation implies that each integrand separately vanishes. This result gives 12 more boundary conditions in addition to the previous 36 boundary conditions which are specified by the constraints.

5. Computation of derivatives in section IV-C-4.

Most of the required computations have been performed already in section III-C-5. ℓ_1^i ($i = 1, 2, 3, 4$) is identical to the function ℓ_1 in section III-C-3; ℓ_3^i ($i = 1, 2, 3, 4$) is identical to the functions $\ell_2(t)$ in section III-C-3; and ℓ_2^i ($i = 5, 6, 7, 8$) is <u>almost</u> identical to the function ℓ_1 in section III-C-3.

Therefore, the only new computations are those associated with the four functions ℓ_2^i ($i = 5, 6, 7, 8$) and these computations are facilitated by comparing the functions ℓ_2^i with the function ℓ_1 in section III-C-3.

$$\ell^i_{2_{\eta^i}} = \rho\omega\left(\omega r^i + \omega\eta^i + \theta^i_t - \frac{\omega\, b\sqrt{2}}{2}\right)$$

$$\ell^i_{2_{\eta^i_r}} = -\frac{\gamma\left[\sqrt{(1+\eta^i_r)^2 + \theta^{i2}_r + Z^{i2}_r} - 1\right](1+\eta^i_r)}{\sqrt{(1+\eta^i_r)^2 + \theta^{i2}_r + Z^{i2}_r}}$$

$$\frac{\partial}{\partial r^i}\,\ell^i_{2_{\eta^i_r}} = -\frac{\gamma(1+\eta^i_r)\left[(1+\eta^i_r)\,\eta^i_{rr} + \theta^i_r\,\theta^i_{rr} + Z^i_r\,Z^i_{rr}\right]}{\left[(1+\eta^i_r)^2 + \theta^{i2}_r + Z^{i2}_r\right]^{3/2}}$$

$$-\frac{\gamma\left[\sqrt{(1+\eta^i_r)^2 + \theta^{i2}_r + Z^{i2}_r} - 1\right]\eta^i_{rr}}{\sqrt{(1+\eta^i_r)^2 + \theta^{i2}_r + Z^{i2}_r}}$$

$$\ell^i_{2_{\eta^i_t}} = \rho\left(\eta^i_t - \omega\theta^i + \frac{\omega\, b\sqrt{2}}{2}\right)$$

$$\frac{\partial}{\partial t}\,\ell^i_{2_{\eta^i_t}} = \rho\left(\eta^i_{tt} - \omega\theta^i_t\right)$$

$$\ell^i_{2_{\theta^i}} = -\rho\omega\left(\eta^i_t - \omega\theta^i + \frac{\omega\, b\sqrt{2}}{2}\right)$$

$$\ell^i_{\theta^i_r} = -\frac{\gamma\left[\sqrt{(1+\eta^{i2}_r+\theta^{i2}_r+z^{i2}_r}-1\right]\theta^i_r}{\sqrt{(1+\eta^i_r)^2+\theta^{i2}_r+z^{i2}_r}}$$

$$\frac{\partial}{\partial r^i}\ell^i_{\theta^i_r} = -\frac{\gamma\,\theta^i_r\left[(1+\eta^i_r)\,\eta^i_{rr}+\theta^i_r\,\theta^i_{rr}+z^i_r\,z^i_{rr}\right]}{\left[(1+\eta^i_r)^2+\theta^{i2}_r+z^{i2}_r\right]^{3/2}}$$

$$-\frac{\gamma\left[\sqrt{(1+\eta^i_r)^2+\theta^{i2}_r+z^{i2}_r}-1\right]\theta^i_{rr}}{\sqrt{(1+\eta^i_r)^2+\theta^{i2}_r+z^{i2}_r}}$$

$$\ell^i_{\dot{\theta}^i_t} = \rho\left(\omega r^i+\omega\eta^i+\theta^i_t-\frac{\omega\,b\sqrt{2}}{2}\right)$$

$$\frac{\partial}{\partial t}\ell^i_{\dot{\theta}^i_t} = \rho\left(\omega\eta^i_t+\theta^i_{tt}\right)$$

$$\ell^i_{\dot{z}^i} = 0$$

$$\ell^i_{\dot{z}^i_r} = -\frac{\gamma\left[\sqrt{(1+\eta^i_r)^2+\theta^{i2}_r+z^{i2}_r}-1\right]z^i_r}{\sqrt{(1+\eta^i_r)^2+\theta^{i2}_r+z^{i2}_r}}$$

$$\frac{\partial}{\partial r^i}\ell^i_{\dot{z}^i_r} = -\frac{\gamma\,z^i_r\left[(1+\eta^i_r)\,\eta^i_{rr}+\theta^i_r\,\theta^i_{rr}+z^i_r\,z^i_{rr}\right]}{\left[(1+\eta^i_r)^2+\theta^{i2}_r+z^{i2}_r\right]^{3/2}}$$

$$- \frac{Y\left[\sqrt{(1+\eta_r^i)^2+\theta_r^{i2}+z_r^{i2}}-1\right] z_{rr}^i}{\sqrt{(1+\eta_r^i)^2+\theta_r^{i2}+z_r^{i2}}}$$

$$l_{2_{z_t^i}}^i = \rho\, z_t^i$$

$$\frac{\partial}{\partial t}\, l_{2_{z_t^i}}^i = \rho\, z_{tt}^i$$

6. Summary of Results

D.E. 1, 2, 3, 4

$$- \rho\omega(\omega r^i + \omega\eta^i + \theta_t^i) \quad - \frac{Y\left[\sqrt{(1+\eta_r^i)^2+\theta_r^{i2}+z_r^{i2}}-1\right]\eta_{rr}^i}{\sqrt{(1+\eta_r^i)^2+\theta_r^{i2}+z_r^{i2}}}$$

$$- \frac{Y\,(1+\eta_r^i)\left[(1+\eta_r^i)\,\eta_{rr}^i + \theta_r^i\,\theta_{rr}^i + z_r^i\,z_{rr}^i\right]}{\left[(1+\eta_r^i)^2+\theta_r^{i2}+z_r^{i2}\right]^{3/2}} + \rho(\eta_{tt}^i - \omega\theta_t^i) = 0$$

where $0 \le r^i \le b$ and $i = 1, 2, 3, 4$.

D.E. 5, 6, 7, 8

$$\rho\omega(\eta_t^i - \omega\theta^i) \quad - \frac{Y\left[\sqrt{(1+\eta_r^i)^2+\theta_r^{i2}+z_r^{i2}}-1\right]\theta_{rr}^i}{\sqrt{(1+\eta_r^i)^2+\theta_r^{i2}+z_r^{i2}}}$$

$$- \frac{Y\,\theta_r^i\left[(1+\eta_r^i)\,\eta_{rr}^i + \theta_r^i\,\theta_{rr}^i + z_r^i\,z_{rr}^i\right]}{\left[(1+\eta_r^i)^2+\theta_r^{i2}+z_r^{i2}\right]^{3/2}} + \rho(\omega\eta_t^i + \theta_{tt}^i) = 0$$

where $0 \le r^i \le b$ and $i = 1, 2, 3, 4$.

D.E. 9, 10, 11, 12

$$- \frac{\gamma \left[\sqrt{(1 + \eta_r^i)^2 + \theta_r^{i2} + z_r^{i2}} - 1 \right] z_{rr}^i}{\sqrt{(1 + \eta_r^i)^2 + \theta_r^{i2} + z_r^{i2}}}$$

$$- \frac{\gamma z_r^i \left[(1 + \eta_r^i) \eta_{rr}^i + \theta_r^i \theta_{rr}^i + z_r^i z_{rr}^i \right]}{\left[(1 + \eta_r^i)^2 + \theta_r^{i2} + z_r^{i2} \right]^{3/2}} + \rho z_{tt}^i = 0$$

where $0 \leq r^i \leq b$ and $i = 1, 2, 3, 4$.

D.E. 13, 14, 15, 16

$$- \rho\omega\left(\omega r^i + \omega\eta^i + \theta_t^i - \frac{\omega b\sqrt{2}}{2}\right) - \frac{\gamma \left[\sqrt{(1 + \eta_r^i)^2 + \theta_r^{i2} + z_r^{i2}} - 1 \right] \eta_{rr}^i}{\sqrt{(1 + \eta_r^i)^2 + \theta_r^{i2} + z_r^{i2}}}$$

$$- \frac{\gamma(1 + \eta_r^i) \left[(1 + \eta_r^i) \eta_{rr}^i + \theta_r^i \theta_{rr}^i + z_r^i z_{rr}^i \right]}{\left[(1 + \eta_r^i)^2 + \theta_r^{i2} + z_r^{i2} \right]^{3/2}} + \rho(\eta_{tt}^i - \omega\theta_t^i) = 0$$

where $0 \leq r^i \leq b\sqrt{2}$ and $i = 5, 6, 7, 8$.

D.E. 17, 18, 19, 20

$$\rho\omega\left(\eta_t^i - \omega\theta^i + \frac{\omega b\sqrt{2}}{2}\right) - \frac{\gamma \left[\sqrt{(1 + \eta_r^i)^2 + \theta_r^{i2} + z_r^{i2}} - 1 \right] \theta_{rr}^i}{\sqrt{(1 + \eta_r^i)^2 + \theta_r^{i2} + z_r^{i2}}}$$

$$- \frac{\gamma \theta_r^i \left[(1 + \eta_r^i) \eta_{rr}^i + \theta_r^i \theta_{rr}^i + z_r^i z_{rr}^i \right]}{\left[(1 + \eta_r^i)^2 + \theta_r^{i2} + z_r^{i2} \right]^{3/2}} + \rho(\omega\eta_t^i + \theta_{tt}^i) = 0$$

where $0 \leq r^i \leq b\sqrt{2}$ and $i = 5, 6, 7, 8$.

D.E. 21, 22, 23, 24

$$-\frac{Y\left[\sqrt{(1+\eta_r^i)^2+\theta_r^{i2}+z_r^{i2}}-1\right]z_{rr}^i}{\sqrt{(1+\eta_r^i)^2+\theta_r^{i2}+z_r^{i2}}}$$

$$-\frac{Y\,z_r^i\left[(1+\eta_r^i)\,\eta_{rr}^i+\theta_r^i\,\theta_{rr}^i+z_r^i\,z_{rr}^i\right]}{\left[(1+\eta_r^i)^2+\theta_r^{i2}+z_r^{i2}\right]^{3/2}}+\rho\,z_{tt}^i=0$$

where $0 \le r^i \le b\sqrt{2}$ and $i = 5, 6, 7, 8$.

B.C. 1, 2, 3, 4

$$\eta^i(r^i=0,t)=0 \quad \text{where } i=1,2,3,4$$

B.C. 5, 6, 7, 8

$$\left\{-\frac{Y\left[\sqrt{(1+\eta_r^1)^2+\theta_r^{1^2}+z_r^{1^2}}-1\right](1+\eta_r^1)}{\sqrt{(1+\eta_r^1)^2+\theta_r^{1^2}+z_r^{1^2}}}\right.$$

$$\left.+m\omega(\omega r^1+\omega\eta^1+\theta_t^1)-m(\eta_{tt}^1-\theta_{tt}^1)\right\}\Bigg|_{r^1=b}$$

$$+\frac{1}{\sqrt{2}}\left\{-\frac{Y\left[\sqrt{(1+\eta_r^8)^2+\theta_r^{8^2}+z_r^{8^2}}-1\right](1+\eta_r^8-\theta_r^8)}{\sqrt{(1+\eta_r^8)^2+\theta_r^{8^2}+z_r^{8^2}}}\right\}\Bigg|_{r^8=b\sqrt{2}}$$

$$+\frac{1}{\sqrt{2}}\left\{-Y\left[\sqrt{(1+\eta_r^5)^2+\theta_r^{5^2}+z_r^{5^2}}-1\right](1+\eta_r^5+\theta_r^5)\right\}\Bigg|_{r^5=0}=0\,,$$

$$\left\{-\frac{Y\left[\sqrt{(1+\eta_r^i)^2+\theta_r^{i^2}+z_r^{i^2}}-1\right](1+\eta_r^i)}{\sqrt{(1+\eta_r^i)^2+\theta_r^{i^2}+z_r^{i2}}}\right.$$

$$\left.+m\omega(\omega r^i+\omega\eta^i+\theta_t^i)-m(\eta_{tt}^i-\theta_{tt}^i)\right\}\Bigg|_{r^i=b}$$

$$+\frac{1}{\sqrt{2}}\left\{-\frac{Y\left[\sqrt{(1+\eta_r^{i+3})^2+\theta_r^{i+3^2}+z_r^{i+3^2}}-1\right](1+\eta_r^{i+3}-\theta_r^{i+3})}{\sqrt{(1+\eta_r^{i+3})^2+\theta_r^{i+3^2}+z_r^{i+3^2}}}\right\}\Bigg|_{r^{i+3}=b\sqrt{2}}$$

$$+\frac{1}{\sqrt{2}}\left\{-\frac{Y\left[\sqrt{(1+\eta_r^{i+4})^2+\theta_r^{i+4^2}+z_r^{i+4^2}}-1\right](1+\eta_r^{i+4}+\theta_r^{i+4})}{\sqrt{(1+\eta_r^{i+4})^2+\theta_r^{i+4^2}+z_r^{i+3^2}}}\right\}\Bigg|_{r^{i+4}=0}=0$$

where i = 2, 3, 4.

B.C. 9, 10, 11, 12

$$\theta^i(r^i=0,t)=0 \quad \text{where } i=1,\ 2,\ 3,\ 4$$

B.C. 13, 14, 15, 16

$$\left\{-\frac{Y\left[\sqrt{(1+\eta_r^1)^2+\theta_r^{1^2}+z_r^{1^2}}-1\right]\theta_r^1}{\sqrt{(1+\eta_r^1)^2+\theta_r^{1^2}+z_r^{1^2}}}\right.$$

$$\left.-m\omega(\eta_t^1-\omega\theta^1)-m(\omega\eta_t^1+\theta_{tt}^1)\right\}\Bigg|_{r^1=b}$$

$$+\frac{1}{\sqrt{2}}\left\{-\frac{Y\left[\sqrt{(1+\eta_r^3)^2+\theta_r^{3^2}+z_r^{3^2}}-1\right](1+\eta_r^3+\theta_r^3)}{\sqrt{(1+\eta_r^3)^2+\theta_r^{3^2}+z_r^{3^2}}}\right\}\Bigg|_{r^3=b\sqrt{2}}$$

$$+\frac{1}{\sqrt{2}}\left\{+\frac{Y\left[\sqrt{(1+\eta_r^5)^2+\theta_r^{5^2}+z_r^{5^2}}-1\right](1+\eta_r^5-\theta_r^5)}{\sqrt{(1+\eta_r^5)^2+\theta_r^{5^2}+z_r^{5^2}}}\right\}\Bigg|_{r^5=0}=0,$$

$$\left\{-\frac{Y\left[\sqrt{(1+\eta_r^i)^2+\theta_r^{i^2}+z_r^{i^2}}-1\right]\theta_r^i}{\sqrt{(1+\eta_r^i)^2+\theta_r^{i^2}+z_r^{i^2}}}\right.$$

$$\left.-m_0(\dot{\eta}_t^i-\omega\theta^i)-m(\omega\eta_t^i+\theta_{tt}^i)\right\}\Bigg|_{r^i=b}$$

$$+\frac{1}{\sqrt{2}}\left\{-\frac{Y\left[\sqrt{(1+\eta_r^{i+3})^2+\theta_r^{i+3^2}+z_r^{i+3^2}}-1\right](1+\eta_r^{i+3}+\theta_r^{i+3})}{\sqrt{(1+\eta_r^{i+3})^2+\theta_r^{i+3^2}+z_r^{i+3^2}}}\right\}\Bigg|_{r^{i+3}=b\sqrt{2}}$$

$$+\frac{1}{\sqrt{2}}\left\{+\frac{Y\left[\sqrt{(1+\eta_r^{i+4})^2+\theta_r^{i+4^2}+z_r^{i+4^2}}-1\right](1+\eta_r^{i+4}-\theta_r^{i+4})}{\sqrt{(1+\eta_r^{i+4})^2+\theta_r^{i+4^2}+z_r^{i+4^2}}}\right\}\Bigg|_{r^{i+4}=0}=0$$

where i = 2, 3, 4.

B.C. 17, 18, 19, 20

$$z^i(r^i=0,t)=0 \quad \text{where } i=1,2,3,4$$

B.C. 21, 22, 23, 24

$$\left\{ + \frac{Y\left[\sqrt{(1+\eta_r^1)^2 + \theta_r^{1^2} + z_r^{1^2}} - 1\right] z_r^1}{\sqrt{(1+\eta_r^1)^2 + \theta_r^{1^2} + z_r^{1^2}}} + m\, z_{tt}^1 \right\}\Bigg|_{r^1 = b}$$

$$+ \left\{ + \frac{Y\left[\sqrt{(1+\eta_r^8)^2 + \theta_r^{8^2} + z_r^{8^2}} - 1\right] z_r^8}{\sqrt{(1+\eta_r^8)^2 + \theta_r^{8^2} + z_r^{8^2}}} \right\}\Bigg|_{r^8 = b\sqrt{2}}$$

$$+ \left\{ - \frac{Y\left[\sqrt{(1+\eta_r^5)^2 + \theta_r^{5^2} + z_r^{5^2}} - 1\right] z_r^5}{\sqrt{(1+\eta_r^5)^2 + \theta_r^{5^2} + z_r^{5^2}}} \right\}\Bigg|_{r^5 = 0} = 0 \ ,$$

$$\left\{ + \frac{Y\left[\sqrt{(1+\eta_r^i)^2 + \theta_r^{i^2} + z_r^{i^2}} - 1\right] z_r^i}{\sqrt{(1+\eta_r^i)^2 + \theta_r^{i^2} + z_r^{i^2}}} + m\, z_{tt}^i \right\}\Bigg|_{r^i = b}$$

$$+ \left\{ + \frac{Y\left[\sqrt{(1+\eta_r^{i+3})^2 + \theta_r^{i+3^2} + z_r^{i+3^2}} - 1\right] z_r^{i+3}}{\sqrt{(1+\eta_r^{i+3})^2 + \theta_r^{i+3^2} + z_r^{i+3^2}}} \right\}\Bigg|_{r^{i+3} = b\sqrt{2}}$$

$$+ \left\{ - \frac{Y\left[\sqrt{(1+\eta_r^{i+4})^2 + \theta_r^{i+4^2} + z_r^{i+4^2}} - 1\right] z_r^{i+4}}{\sqrt{(1+\eta_r^{i+4})^2 + \theta^{i+4^2} + z^{i+4^2}}} \right\}\Bigg|_{r^{i+4} = 0} = 0$$

where i = 2, 3, 4.

B.C. 25, 26, 27, 28

$$\eta^i(r^i = 0,t) = -\frac{1}{\sqrt{2}}\left[\eta^{i-4}(r^{i-4} = b,t) - \theta^{i-4}(r^{i-4} = b,t)\right]$$

where i = 5, 6, 7, 8.

B.C. 29, 30, 31, 32

$$\eta^i(r^i = b\sqrt{2},t) = \frac{1}{\sqrt{2}}\left[\eta^{i-3}(r^{i-3} = b,t) + \theta^{i-3}(r^{i-3} = b,t)\right]$$

where i = 5, 6, 7.

$$\eta^8(r^8 = b\sqrt{2},t) = \frac{1}{\sqrt{2}}\left[\eta^1(r^1 = b,t) + \theta^1(r^1 = b,t)\right]$$

B.C. 33, 34, 35, 36

$$\theta^i(r^i = 0,t) = -\frac{1}{\sqrt{2}}\left[\eta^{i-4}(r^{i-4} = b,t) + \theta^{i-4}(r^{i-4} = b,t)\right]$$

where i = 5, 6, 7, 8.

B.C. 37, 38, 39, 40

$$\theta^i(r^i = b\sqrt{2},t) = -\frac{1}{\sqrt{2}}\left[\eta^{i-3}(r^{i-3} = b,t) - \theta^{i-3}(r^{i-3} = b,t)\right]$$

where i = 5, 6, 7.

$$\theta^8(r^8 = b\sqrt{2},t) = -\frac{1}{\sqrt{2}}\left[\eta^1(r^1 = b,t) - \theta^1(r^1 = b,t)\right]$$

B.C. 41, 42, 43, 44

$$z^i(r^i = 0,t) = z^{i-4}(r^{i-4} = b,t) \quad \text{where } i = 5, 6, 7, 8.$$

B.C. 45, 46, 47, 48

$$z^i(r^i = b\sqrt{2},t) = z^{i-3}(r^{i-3} = b,t) \quad \text{where } i = 5, 6, 7.$$

$$z^8(r^8 = b\sqrt{2},t) = z^1(r^1 = b,t)$$

Note: It is clear that, if the linear mass density of the ith string in the reference configuration is given by a function $\rho_i = \rho_i(r^i)$, the net effect on the results listed above can be obtained by replacing ρ everywhere by $\rho_i(r^i)$ $(i = 1, 2, ---, 8)$. This conclusion is established easily by examining the steps of the derivation.

APPENDIX C

Stable Configurations of Nonrigid Structures in Force-free Rotational Motion

This report discusses the passive stability properties of KWOT configurations. Thus, it is assumed throughout that no external forces are applied to the KWOT system, so that the center of mass of the system moves at a constant velocity relative to any inertial frame of coordinates.[1] There is no loss in generality for the analysis of the relative motion of the KWOT system if all dynamical quantities are measured relative to an inertial frame of coordinates with origin located at the position of the center of mass. Such a coordinate system is used henceforth. Let the vectors $\vec{r}_i$ locate the positions of mass elements in the KWOT system.[2] The total kinetic energy of the system is a function of internal coordinates $\vec{r}_i$:

$$T = T(\vec{r}_i, \dot{\vec{r}}_i)$$

The internal forces in the system are not exactly conservative since the

---

[1] The dynamical theory in this paragraph is presented, e.g. in Herbert Goldstein, Classical Mechanics, Addison-Wesley Publishing Co., Inc., Massachusetts, 1959, section 1-2.

[2] Since the KWOT system has both continuous and discrete mass distributions, the index i in principle should assume both continuous and discrete values. Discrete indices are used throughout for notational convenience.

frictional forces provide a mechanism for the conversion of mechanical energy into heat energy. However, it is physically obvious that the frictional forces are very much smaller than the other internal forces. The frictional forces exist only when mass elements of the system are in relative motion.[3] We conceptually can stretch the flexible elements of the system into any given configuration at a rate slow enough so that the effect of the frictional forces is negligible. It is possible then to associate a potential energy which is a function only of the internal coordinates $\vec{r}_i$:

$$V = V(\vec{r}_i)$$

The total mechanical energy of the system then satisfies the usual relation.

$$E(\vec{r}_i, \overset{\circ}{\vec{r}}_i) = T(\vec{r}_i, \overset{\circ}{\vec{r}}_i) + V(\vec{r}_i).$$

E is not a constant of the motion, since the very small frictional forces gradually damp any relative motion in the system. Thus, we can associate a total energy with any arbitrary dynamical state of the KWOT system and in all passive situations this total energy will decrease until all relative motion ceases, i.e. until all distances between mass elements become constants. Since frictional forces satisfy Newton's third law of action and reaction, the total angular momentum $\vec{L}$ of the system is a constant of the motion. It is emphasized that only a passive, completely mechanical system is under consideration. The preceding elementary physical arguments are essential to the subsequent analysis.

Definition 1 A rigid geometry of a mechanical system is any configuration such that all distances between mass elements of the system are constants during some specified motion.

The fact that all mass elements of KWOT are linked dissipatively implies that KWOT always will attain a rigid geometry when there are no external forces. A rigid body is characterized by a rigid geometry for all possible motions.

---

[3] We eliminate from consideration those frictional forces which would be generated by stationary contact between surfaces of mass distributions. It is obvious that only velocity-dependent frictional forces are required to model the damping mechanisms in the KWOT system.

Of course, not all possible motions of KWOT correspond to a rigid geometry. But, whenever KWOT executes a motion associated with a rigid geometry, then that motion is described exactly by the usual formulae from rigid body theory.[4] The most general force-free motion of a rigid body can be described in the center-of-mass coordinate frame as a rotation about a fixed point which is the center of mass. The energy relation has the following general form:

$$E(\vec{r}_i, \dot{\vec{r}}_i) = \frac{\vec{\omega} \circ \vec{L}}{2} + V(\vec{r}_i) = \frac{\vec{\omega} \circ \overleftrightarrow{I} \circ \vec{\omega}}{2} + V(\vec{r}_i)$$

where

$\overleftrightarrow{I}$ = moment-of-inertia tensor

$\vec{\omega}$ = angular velocity vector

$\vec{L}$ = relative angular momentum

It can be established from Poinsot's construction for the force-free motion of a rigid body that all possible rigid geometries of a structure with flexible cables can be established only when the angular velocity vector $\vec{\omega}$ is parallel to the angular momentum $\vec{L}$.[5] This circumstance occurs only when the system is spinning about one of the principal axes of the rigid geometry. Any precessional motion of $\vec{\omega}$ about $\vec{L}$ implies a variable distortion in flexible cable elements. Thus,

$$\frac{\vec{\omega} \circ \vec{I} \circ \vec{\omega}}{2} = \frac{1}{2}\omega^2 I \quad \text{and} \quad \vec{L} = I\omega\frac{\vec{\omega}}{\omega}$$

where I is the moment of inertia about the axis of rotation:

$$I = \sum_i m_i \left[r_i^2 - \left(\vec{r}_i \circ \frac{\vec{\omega}}{\omega}\right)^2 \right]$$

Elementary physical considerations imply that a rigid geometry for a system with flexible cables must be planar if the structure cannot support compressions.[6] Any flexible cable not located on the rotation axis will be

---

[4] Force-free motion of a rigid body is treated, e.g., in Chapter 5 of Goldstein, op. cit.

[5] The essential inference is that motion of the spin vector $\vec{\omega}$ relative to the body axes implies that any flexible mass element experiences a variable acceleration relative to the body axes.

[6] The only exception is the circumstance $\vec{\omega} = 0$. This possibility is trivial, so it is excluded from consideration.

bowed outward by the centrifugal forces. The resulting tension forces are such that a three-dimensional rigid geometry can be maintained only with compression members. The KWOT system does not support compressions, so all possible KWOT rigid geometries are planar:

$$\vec{r}_i \cdot \underset{\omega}{\vec{\omega}} = 0$$

$$I = \sum_i m_i r_i^2 = I(\vec{r}_i)$$

$$E = E(\vec{r}_i) = \frac{L^2}{2I(\vec{r}_i)} + V(\vec{r}_i)$$

Since the KWOT system always dissipates energy via frictional forces until a rigid geometry is attained, the energy of an initially non-planar system must be greater than the energy of the final rigid geometry. Since the angular momentum vector $\vec{L}$ is a constant of the motion, the plane of the rigid geometry is perpendicular to the angular momentum vector $\vec{L}$ of the initial state.

The coordinate set $(\vec{r}_i)$ requires some discussion. A specification of all $\vec{r}_i$ uniquely determines the geometry of the system. However, some parts of the system may be rigid so that a unique specification of geometry may be possible with knowledge of only a subset of all the $\vec{r}_i$.

Definition 2 A coordinate set $(\vec{r}_i)$ is complete if, and only if, a specification of all coordinates in the set uniquely fixes the geometry of the system.

The previous arguments have established the following result:

Theorem 1. A passive KWOT system always attains a final state in which the configuration is a planar rigid geometry. This plane is perpendicular to the constant angular momentum vector $\vec{L}$ of the system. If the initial state of the system is non-planar, then this final energy is less than the initial energy. If the initial state is planar, then this final energy is less than or equal to the initial energy. If $(\vec{r}_i)$ denotes a complete coordinate set, the energy of this final state is given by the basic energy relation

$$E(\vec{r}_i) = \frac{L^2}{2I(\vec{r}_i)} + V(\vec{r}_i)$$

where $I(\vec{r}_i)$ is the moment of inertia of the planar mass distribution about the center of mass.

The basic energy relation in theorem 1 is defined for all allowed values of the complete coordinate set $(\vec{r}_i)$. However, since the KWOT system has flexible components, a rigid geometry does not correspond to each set of values for the $(\vec{r}_i)$. Consider an arbitrary, planar KWOT geometry $(\vec{r}_i)$ and suppose we wish to determine if this geometry is rigid at some specified angular velocity $\vec{\omega}$. The specification of $\vec{\omega}$ and of the particular geometry $(\vec{r}_i)$ determines the angular momentum $\vec{L}$ to be used in the basic energy relation. In Figure 1 an arbitrary planar rigid geometry is depicted.

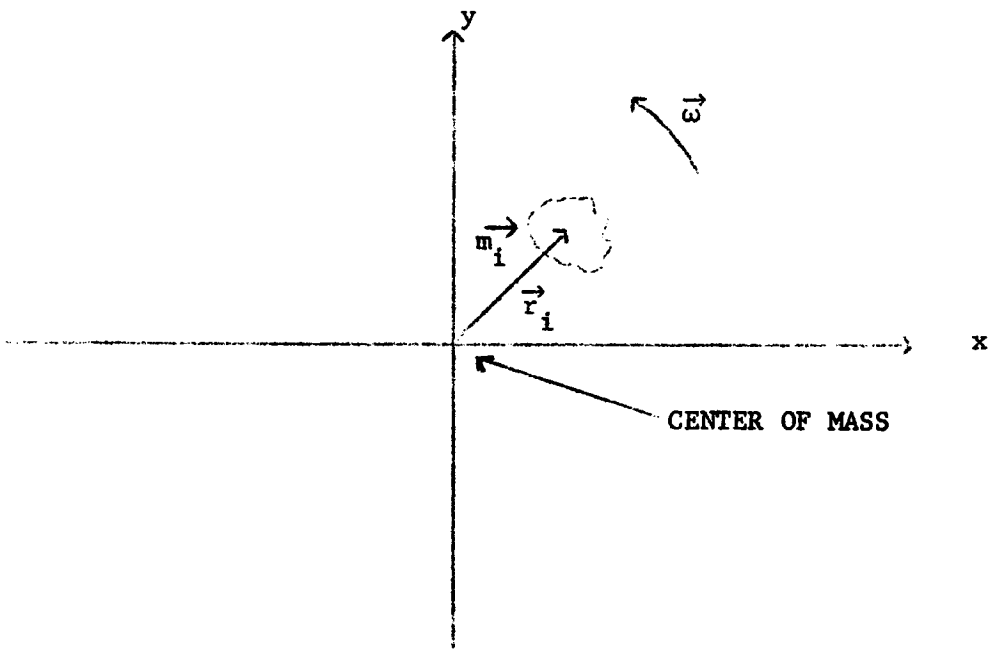

FIGURE 1. A RIGID GEOMETRY ROTATING AT ANGULAR RATE $\vec{\omega}$.

Since the system is a rigid geometry, the total force $\vec{F}_T^{\,i}$ on the mass element m_i satisfies the usual expression for circular motion at rate ω:

$$\vec{F}_T^{\,i} = -m_i \omega^2 \vec{r}_i$$

where the total force $\vec{F}_T^{\,i}$ is exerted on m_i by the rest of the system. Consider a small virtual displacement $\delta\vec{r}_i$ of the system.[7]

$$\vec{F}_T^{\,i} \circ \delta\vec{r}_i + m_i\omega^2 \vec{r}_i \circ \delta\vec{r}_i = 0$$

$$\sum_i \vec{F}_T^{\,i} \circ \delta\vec{r}_i + \omega^2 \sum_i m_i \vec{r}_i \circ \delta\vec{r}_i = 0$$

$$\vec{F}_T^{\,i} = \vec{F}_e^{\,i} + \vec{F}_c^{\,i}$$

where $\vec{F}_e^{\,i}$ = sum of elastic forces on m_i

$\vec{F}_c^{\,i}$ = sum of rigid body constraint forces

The virtual work of the rigid body constraint forces always vanishes, so

$$\sum_i \vec{F}_T^{\,i} \circ \delta\vec{r}_i = \sum_i \vec{F}_e^{\,i} \circ \delta\vec{r}_i + \sum_i \vec{F}_c^{\,i} \circ \delta\vec{r}_i = \sum_i \vec{F}_e^{\,i} \circ \delta\vec{r}_i$$

Thus, $$\sum_i \vec{F}_e^{\,i} \circ \delta\vec{r}_i + \omega^2 \sum_i m_i \vec{r}_i \circ \delta\vec{r}_i = 0$$

This last relation is merely an expression of D'Alembert's principle. The increase in potential energy δV in the virtual displacement $\delta\vec{r}_i$ is

$$\delta V = -\sum_i \vec{F}_e^{\,i} \circ \delta\vec{r}_i,$$

while

$$\omega^2 \sum_i m_i \vec{r}_i \circ \delta\vec{r}_i = \frac{1}{2}\omega^2 \delta \sum_i m_i r_i^2 = \frac{1}{2}\omega^2 \delta I(\vec{r}_i)$$

$$= \frac{1}{2}\frac{L^2}{I^2}\delta I = -\frac{\delta(L^2)}{2I}$$

---

[7] The concept of a virtual displacement and D'Alembert's principle are discussed, e.g., in section 1-4 of Goldstein, op. cit.

Therefore, D'Alembert's principle in this case is the relation

$$\delta\left(\frac{L^2}{2I} + V\right) = 0$$

We have established the following result:[8]

Theorem 2 The rigid geometries $(\vec{r}_i)$ of KWOT are the stationary values of the functional

$$E(\vec{r}_i) = \frac{L^2}{2I(\vec{r}_i)} + V(\vec{r}_i)$$

where $(\vec{r}_i)$ is a complete coordinate set.[9]

It is emphasized that only these stationary values correspond to rigid KWOT geometries. Thus, suppose that the system is prepared in a state which corresponds to a non-stationary value of the functional E. Since such a state cannot be a rigid geometry, subsequent relative motion occurs and the system dissipates this relative motion until a planar rigid geometry is attained via the preceding arguments.

Definition 3 An arbitrary rigid geometry is stable if, and only if, the system has intrinsic, self-restoring tendencies toward this geometry for all possible sufficiently small, finite geometrical perturbations which conserve the angular momentum $\vec{L}$ of the rigid geometry.

This definition of stability corresponds precisely to the operational

---

[8] In general the KWOT system has continous distributions of mass as well as lumped masses. Therefore, the expression for E will contain integrals over the continuous distributions so that E appears as a functional of the geometry. E solely depends upon functions of the geometry when the KWOT model has only lumped masses.

[9] Theorem 2 may be inferred from a rather general theorem about the motion of mechanical systems which are constrained to rotate uniformly about a fixed axis. Refer to E.T. Whittaker, A Treatise on the Analytical Dynamics of Particles and Rigid Bodies, 4th. ed., Cambridge University Press, 1937, p. 40. In particular, the complete coordinate set $(\vec{r}_i)$ of definition 2 is the set of generalized coordinates $q_1, q_2, \ldots, q_n$ which appear in Whittaker's discussion. Note that theorems 2 and 3 remain valid for three-dimensional systems if the expression for $I(\vec{r}_i)$ has the previously listed three - dimensional form:

$$I(\vec{r}_i) = \sum_i m_i\left[r_i^2 - (\vec{r}_i \circ \frac{\vec{\omega}}{\omega})^2\right]$$

Also, the restrictive assumption in Whittaker's development is superfluous for the inference of theorem 2.

requirements of KWOT. Consider now the problem of determining the stability of a rigid geometry. The rigid geometry is specified by a set of values for a complete coordinate set $(\vec{r}_i)$. An arbitrary change in this geometry can be specified by assigning finite increments $(\Delta\vec{r}_i)$ to the values of the complete coordinate set $(\vec{r}_i)$. We conceptually can introduce additional internal constraints so that the perturbed geometry $(\vec{r}_i + \Delta\vec{r}_i)$ is rigid at an angular rate which is selected so that the angular momentum of the rigid geometry $(\vec{r}_i + \Delta\vec{r}_i)$ is identical with the angular momentum of the rigid geometry $(\vec{r}_i)$. Now let these additional constraints be relaxed. The subsequent relative motion will dissipate relative energy until the system attains a rigid geometry $(\vec{r}_i)$ via the previously discussed arguments. The angular momentum is conserved during this process. If the rigid geometry $(\vec{r}_i)$ is stable, then by definition 3 there exist finite bounds $N_i > 0$ such that the conditions $|\Delta r_i| \leq N_i$ guarantee that the rigid geometry $(\vec{r}_i)$ is identical to the original rigid geometry $(\vec{r}_i)$.[10] Thus,

$$E(\vec{r}_i) < E(\vec{r}_i + \Delta\vec{r}_i) \quad \text{if} \quad |\Delta r_i| \leq N_i$$

so that the following result has been verified:

Theorem 3 The stable rigid geometries of KWOT are the relative minimum values of the functional

$$E(\vec{r}_i) = \frac{L^2}{2I(\vec{r}_i)} + V(\vec{r}_i)$$

where $(\vec{r}_i)$ is a complete coordinate set.

One can formulate a practical classification for those rigid geometries which are not associated with the relative minima discussed in theorem 1. When the mechanical system is perturbed arbitrarily about such rigid geometries in a manner such that the relative angular momentum $\vec{L}$ is unchanged by the perturbation, the system in general dissipates into a new rigid geometry with the same relative angular momentum. The new rigid geometry may differ radically from the original rigid geometry, or the two rigid geometries

[10] It is important to note that the changes $(\Delta\vec{r}_i)$ conserve the magnitude of the angular momentum, since this condition is necessary in order that the deviated system $(\vec{r}_i + \Delta\vec{r}_i)$ can return to the original configuration $(\vec{r}_i)$.

may differ slightly. The following two definitions state these notions precisely.

Definition 5 Denote the given rigid geometry by the complete set $(\vec{r}_i)$ and consider arbitrary perturbations $\Delta\vec{r}_i$ which conserve the angular momentum of the given rigid geometry. The given rigid geometry is neutrally stable if, and only if, there exists a neighborhood of the geometry $(\vec{r}_i)$, defined by constants ϵ_i so that $|\Delta\vec{r}_i| < \epsilon_i$, such that all values of the complete set $(\vec{r}_i)$ lying within this neighborhood are rigid geometries.

Thus, a neutrally stable rigid geometry can be characterized as a rigid geometry belonging to a region where the functional $E(\vec{r}_i)$ is constant, since by theorem 2 all rigid geometries must belong to stationary values of $E(\vec{r}_i)$. Alternatively, any sufficiently small perturbation of a rigid geometry obtains another rigid geometry, so that the system remains fixed in the new configuration. There is no tendency for the system to regain the original rigid geometry, but also the perturbation has no tendency to grow larger.

Definition 6 The given rigid geometry is unstable if, and only if, it is neither stable nor neutrally stable.

An unstable rigid geometry is characterized by the fact that every neighborhood of the rigid geometry $(\vec{r}_i)$ contains a configuration which is not a rigid geometry. Thus, theorem 2 implies that every neighborhood of an

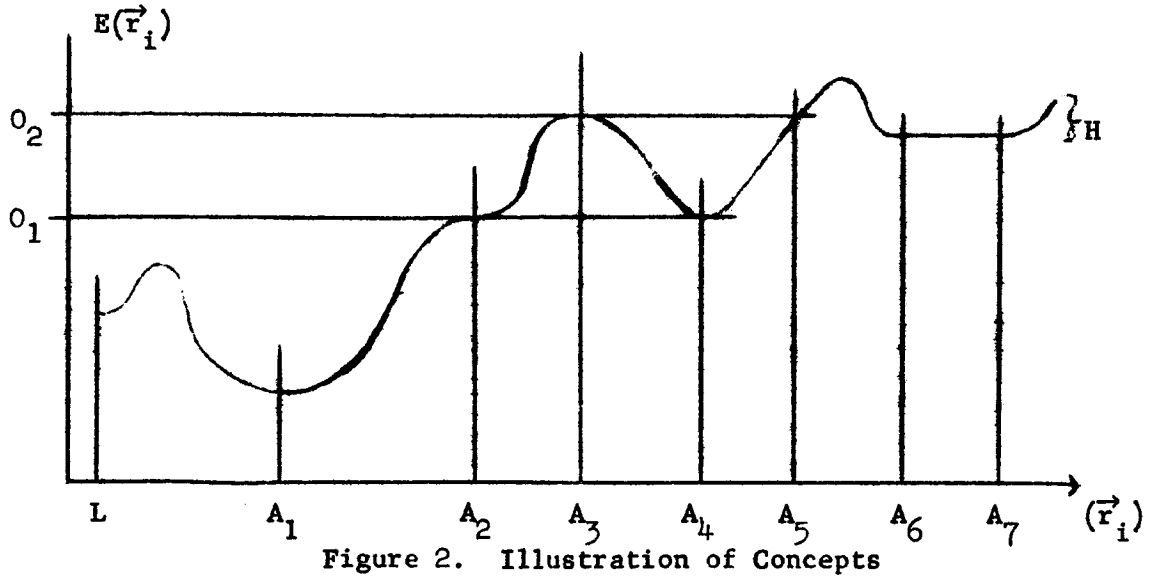

Figure 2. Illustration of Concepts

unstable rigid geometry contains at least one configuration of lower energy. Any perturbation toward these configurations results in subsequent growth of the perturbation. The utility of the preceding classifications of rigid geometries will be apparent in the presentation of examples.

Figure 2 illustrates the previously discussed concepts. The abscissa represents the range of values of a complete set of coordinates, while the ordinate scales the values of the associated relative total energy. Point A_1 is a stable rigid geometry which is an absolute minimum, e.e. it has the lowest possible energy. Since point A_1 lies in the deepest energy sink, it would be the best operational geometry for KWOT if the geometry $(\vec{r}_i) = A_1$ has a satisfactory shape.[11] Point A_2 is an unstable rigid geometry which appears as a "saddle point," while point A_3 is an unstable rigid geometry which is a relative maximum. Point A_4 is a stable rigid geometry because it is a relative minimum. The height $\Delta E = (0_2 - 0_1)$ of the energy sink defines the finite bounds $N_{1,2} = \{(A_4 - A_3), (A_5 - A_4)\}$ which appeared in the proof of theorem 3. The open interval $(A_6\ A_7)$ represents a collection of adjacent, neutrally stable rigid geometries. Consider an energy perturbation $\Delta E > 0$ from any one of these neutrally stable rigid geometries such that the angular momentum is not changed. If ΔE is less than the minimum height H of the energy sink which bounds this region of neutrally stable rigid geometries, then the system point must return to a configuration in this region via a process which dissipates the extra energy ΔE. It is worthwhile at this point to note also that the domain of the complete set $(\vec{r}_i)$ may be bounded in some or all of the variables. If one of these bounds corresponds to a stationary value then this bound is a rigid geometry. Thus, configuration L in Figure 2 is a stable rigid geometry.

Theorem 1 established the fact that the passive KWOT system always tends toward a planar rigid geometry such that the conserved angular momentum vector $\vec{L}$ is perpendicular to this plane. All subsequent analysis implicitly is restricted to planar perturbations. Suppose that the KWOT system has a configuration which is a rigid geometry with angular momentum $\vec{L}$ and consider a

[11] If the geometry $(\vec{r}_i) = A_1$ represents, e.g., a linear distribution of mass, then the KWOT rhombic in such a geometry would be collapsed. Such a geometry obviously is unacceptable.

general non-planar perturbation which conserves the angular momentum $\vec{L}$. By theorem 1 the system must tend toward a rigid geometry in the plane perpendicular to $\vec{L}$. A general conclusion is that the final rigid geometry must have energy $E < E_i + \Delta E_i$ where E_i is the initial energy and ΔE_i is the perturbation in the initial energy. The arguments leading to theorem 1 indicate that any planar rigid geometry is a relative minimum relative to non-planar perturbations in the geometry. Thus, if ΔE_i is small enough, any rigid geometry is stable toward non-planar perturbations. It is conceivable, also, that the response to non-planar perturbations depends in detail on the particular KWOT geometry. Thus, a neutrally stable rigid geometry may be more sensitive to non-planar perturbations than a stable rigid geometry.

Applications of the preceding theory are presented below. Some comparisons with other techniques are included either to demonstrate the equivalence of the methods or to illustrate the advantages of this theory.

Example 1

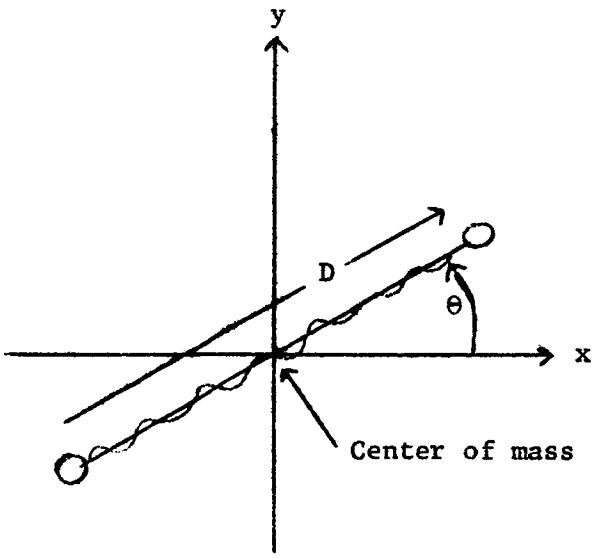

Figure 3. Example of a stable rigid geometry.

Assume the following conditions:

(a) The spring is massless.

(b) The spring obeys Hooke's law.

(c) The spring is constrained to a line through the two point masses.

(d) The spring is damped by frictional forces which depend upon the

relative motion of the two point masses. These forces vanish when there is no relative motion.

Assume the following numerical constants:

(a) Spring constant = k.

(b) Natural spring length = ℓ.

(c) Value of each point mass = m.

Let the conserved angular momentum vector $\vec{L}$ be perpendicular to the xy-plane. The problem is the computation of the separation of the two masses after the relative motion has been dissipated completely.

Let

D_{eq} = equilibrium separation

ω = equilibrium angular velocity

A. Common method of solution

Centripetal force = $\frac{m\omega^2 D}{2}$

Spring restoring force = $k(D-\ell)$

D_{eq} is the solution of the equation

$$\frac{m\omega^2 D}{2} = k(D-\ell)$$

B. Method of solution presented in this report

Moment of inertia $I = 2m\left(\frac{D}{2}\right)^2 = \frac{mD^2}{2}$

Potential energy $V(D) = \frac{1}{2}k(D-\ell)^2$

Kinetic energy $T(D) = \frac{L^2}{2I} = \frac{L^2}{mD^2}$

$$E(D) = T + V = \frac{L^2}{mD^2} + \frac{1}{2}k(D-\ell)^2$$

$$\frac{dE}{dD} = \frac{-2L^2}{mD^3} + k(D-\ell)$$

$$\frac{d^2E}{dD^2} = \frac{6L^2}{mD^4} + k > 0 \text{ for all real values of D.}$$

D_{eq} is the solution of the equation $\frac{dE}{dD} = 0$.

$$\frac{2L^2}{mD^3} = k(D-\ell)$$

$$L^2 = I^2\omega^2 = \frac{m^2\omega^2D^4}{4}$$

$$\frac{m\omega^2D}{2} = k(D-\ell)$$

Since this last equation is identical to the equation listed in part A, the methods are equivalent. Also, $\frac{d^2E}{dD^2} > 0 \Rightarrow D_{eq}$ is a stable rigid geometry. This fact, of course, is obvious. It may be objected that $\frac{dE}{dD} = 0$ has in principle four nonzero roots, but it is easy to show that this equation has only one positive real root.

Example 2

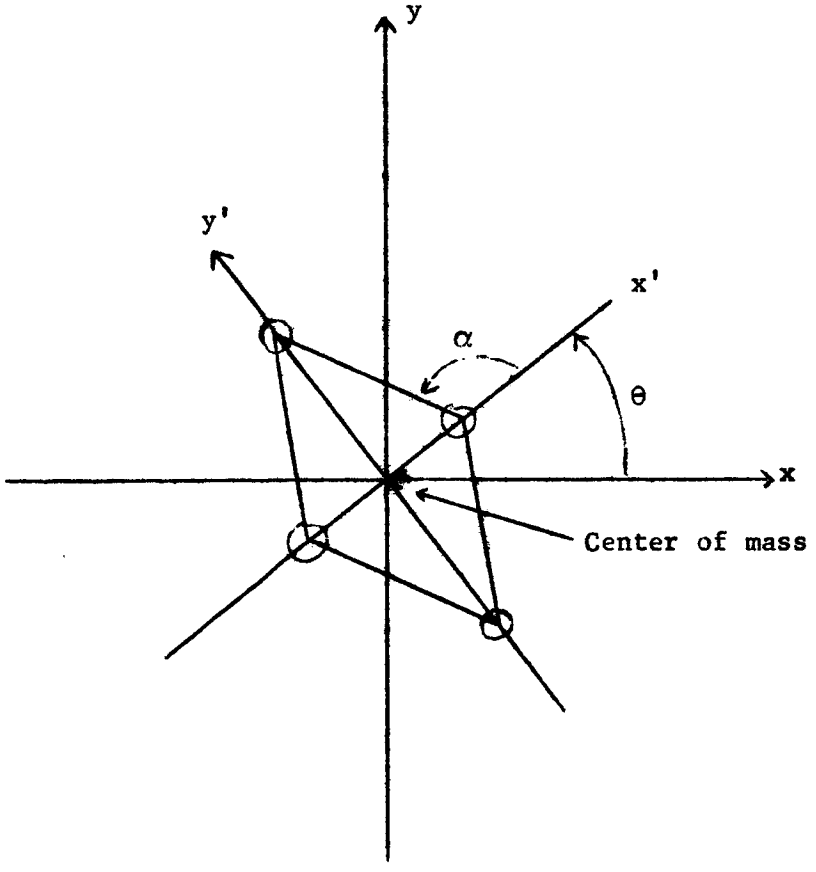

Figure 4. Example of neutrally stable rigid geometry

Assume the following conditions:

(a) The four masses are connected by massless, rigid rods.

(b) Each mass is constrained to displacements only along its respective primed axis. Thus, $\frac{\pi}{2} < \alpha < \pi$.

(c) The system is damped by frictional forces which depend upon motion relative to the primed axes. These forces vanish when there is no such relative motion.

Assume the following numerical constants:

(a) Length of each rod = ℓ.

(b) Value of each point mass = m.

Let the conserved angular momentum vector $\vec{L}$ be perpendicular to the xy-plane. The problem is the computation of the angle α after the relatave motion has been dissipated completely. Let

α_{eq} = equilibrium value of α

ω = equilibrium value of $\dot{\theta}$

A. Common method of solution

Symmetry considerations imply that each connecting rod has a common tension τ.

Tension restoring force = $2\tau \cos \alpha$

Centripetal force = $m \omega^2 \ell \cos \alpha$

α_{eq} is the solution of the equation

$$m \omega^2 \ell \cos \alpha = 2\tau \cos \alpha$$

This equation is satisfied for all α in the allowed range $\frac{\pi}{2} < \alpha < \pi$, so all configurations are possible.

B. Method of solution presented in this report

Moment of inertia $I(\alpha) = 2m\ell^2 =$ constant

Potential energy $V \equiv 0$

Kinetic energy $T(\alpha) = \frac{L^2}{2I(\alpha)} = \frac{L^2}{4m\ell^2} =$ constant

$E(\alpha) = \frac{L^2}{4m\ell^2} =$ constant $\Rightarrow$ the range $\frac{\pi}{2} < \alpha < \pi$ is a set of neutrally stable rigid geometries. For completeness note that

$$\omega = \frac{L}{I} = \frac{L}{2m\ell^2}$$

Example 4

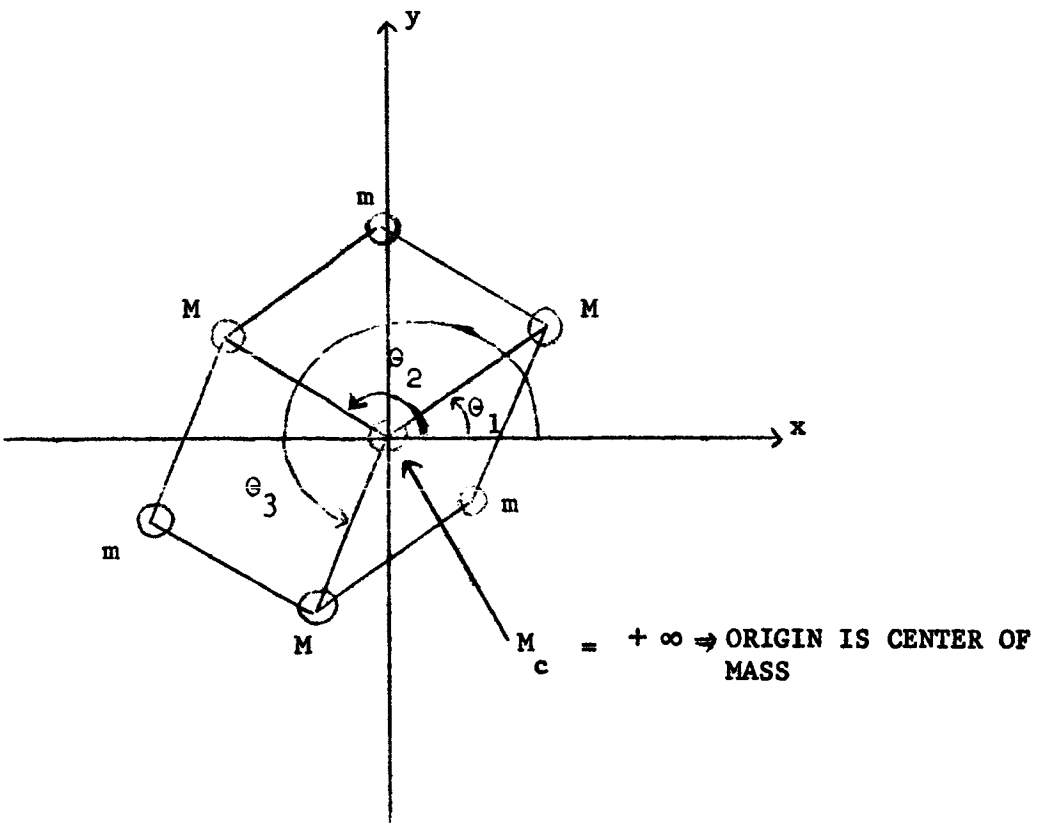

Figure 5. Example of unstable rigid geometry

Assume the following conditions:

(a) All masses are connected by massless, rigid rods.

(b) The central body M_c has infinite mass so that the center of mass coincides with the origin for all the allowed values of Θ_1, Θ_2, and Θ_3. Alternatively, one can assume that the system is attached firmly to the origin.

(c) There are no frictional forces applied at the oigin when one considers the second alternative of the preceding condition (b).

(d) The system is damped by frictional forces at the peripheral joints. These forces depend upon relative motion of mass elements in the system. When there is no relative motion, these forces vanish.

Assume the following numerical constants:

(a) Each rod has length ℓ.

(b) The mass values for the peripheral masses are indicated in figure 5.

The conserved angular momentum vector $\vec{L}$ is perpendicular to the xy-plane.

The problem is to determine the rigid body configurations and the associated stability. Let the equilibrium angular rate be ω.

A. Common method of solution

The standard stability technique is applied to investigate the first approximation stability characteristics of the symmetrical configuration defined by the relations[12]

$$\dot{\theta}_1 = \dot{\theta}_2 = \dot{\theta}_3 = \omega$$

$$\theta_2 - \theta_1 = \theta_3 - \theta_2 = \theta_1 + (2\pi - \theta_3) = \frac{2\pi}{3}$$

The nature of the assumed frictional forces is such that we can neglect them for this stability consideration, if we determine as a result of this assumption that the symmetrical configuration is an unstable rigid geometry. Neglect of these frictional forces permits the formulation of the conservative Lagrangian function.

$$L(\theta_1, \theta_2, \theta_3, \dot{\theta}_1, \dot{\theta}_2, \dot{\theta}_3) = \frac{1}{2} M\ell^2(\dot{\theta}_1^2 + \dot{\theta}_2^2 + \dot{\theta}_3^2)$$

$$+ m\ell^2\Big[\dot{\theta}_1^2 + \dot{\theta}_2^2 + \dot{\theta}_3^2 + \dot{\theta}_1\dot{\theta}_2 \cos(\theta_2 - \theta_1) + \dot{\theta}_2\dot{\theta}_3 \cos(\theta_3 - \theta_2)$$

$$+ \dot{\theta}_1\dot{\theta}_3 \cos(\theta_3 - \theta_1)\Big]$$

The equations of motion

$$\frac{d}{dt}\frac{\partial L}{\partial \dot{\theta}_i} - \frac{\partial L}{\partial \theta_i} = 0 \quad \text{for } i = 1, 2, 3$$

are satisfied by the symmetrical configuration. The appropriate linearized variational equations in the deviation variables δ_1, δ_2, and δ_3 are generated by the substitutions

$$\theta_1 = \omega t + \delta_1$$

$$\theta_2 = \omega t + \frac{2\pi}{3} + \delta_2$$

$$\theta_3 = \omega t + \frac{4\pi}{3} + \delta_3$$

The linearized variational equations can be written in the 6x6 matrix form.

---

[12] The standard treatment of stability encompasses the following steps: (a) Formulation of dynamical equations of motion. (b) Determination of relevant equilibrium solution. (c) Construction of variational equations about this equilibrium solution. (d) First approximation analysis via linearized variational equations. (e) Estimations of effects of nonlinearities in the variational equations.

$$\dot{\vec{\zeta}}_6 = M_6 \vec{\zeta}_6$$

where $\zeta_6^T = (\delta_1, \delta_2, \delta_3, \dot{\delta}_1, \dot{\delta}_2, \dot{\delta}_3)$

$$\begin{bmatrix} 0 & 0 & 0 & 1 & 0 & 0 \\ 0 & 0 & 0 & 0 & 1 & 0 \\ 0 & 0 & 0 & 0 & 0 & 1 \\ 2\beta & -\beta & -\beta & 0 & \alpha & -\alpha \\ -\beta & 2\beta & -\beta & -\alpha & 0 & \alpha \\ -\beta & -\beta & 2\beta & \alpha & -\alpha & 0 \end{bmatrix}$$

$$\alpha = \frac{2\sqrt{3}\, K\, \omega}{(1 + 5K)} > 0$$

$$\beta = \frac{K\, \omega^2}{(1 + 5K)} > 0$$

$$K = \frac{m}{2\, m}$$

For all allowed values of these parameters the Jordan canonical form M_6^J has the form

$$\begin{bmatrix} 0 & 1 & 0 & 0 & 0 & 0 \\ 0 & 0 & 0 & 0 & 0 & 0 \\ 0 & 0 & \lambda_1 & 0 & 0 & 0 \\ 0 & 0 & 0 & \lambda_1^* & 0 & 0 \\ 0 & 0 & 0 & 0 & \lambda_2 & 0 \\ 0 & 0 & 0 & 0 & 0 & \lambda_2^* \end{bmatrix}$$

where $R_e\lambda_1$, $I_m\lambda_1$, $R_e\lambda_2$, $I_m\lambda_2$ are all nonvanishing and $\lambda_2 = -\lambda_1$, so that the linearized variational equations have unstable solutions.[13]

[13] The stability theory in these arguments is treated, e.g., in L.A. Pars, A Treatise on Analytical Dynamics, Heinemann Educational Books Ltd., London, 1965, Chpaters 19 and 23.

Since some of the eigenvalues have positive real parts, this instability is also characteristic of the solutions of the exact, nonlinear variational equations.

It may be objected that this instability is spurious, since the linearized theory must reflect the fact that the system can be rotated rigidly at a different rate than that which was selected for the definition of the symmetrical equilibrium configuration. The rotational invariance of the system implies that the angular momentum $\vec{L}$ is an arbitrary integration constant so that equations of motion always admit solutions which correspond to different equilibrium angular rotation rates. Such solutions must appear as instabilities in terms of the perturbations δ_1, δ_2, δ_3 which are measured relative to some selected equilibrium angular rotation rate.[14] This undesirable situation can be eliminated by specifying that the perturbations δ_1, δ_2, δ_3 conserve the angular momentum of the selected equilibrium to a linear approximation in these variables. Such a specification furnishes an additional linear relationship between the perturbations δ_1, δ_2, δ_3:

Total angular momentum A =

$$\sum_{i=1}^{3} \frac{\partial L}{\partial \dot{\theta}_i} = A(\theta_1, \theta_2, \theta_3, \dot{\theta}_1, \dot{\theta}_2, \dot{\theta}_3)$$

$$A\left(\omega t + \delta, \omega t + \delta_2 + \frac{2\pi}{3}, \omega t + \frac{4\pi}{3} + \delta_3, \omega + \dot{\delta}_1, \omega + \dot{\delta}_2, \omega + \dot{\delta}_3\right) =$$

$$A_{eq} + A_{\ell} + \phi(\delta^2)$$

where $A_{eq} = A\left(\omega t, \omega t + \frac{2\pi}{3}, \omega t + \frac{4\pi}{3}, \omega, \omega, \omega\right)$

$$A_{\ell} = (M + m)\ell^2 (\dot{\delta}_1 + \dot{\delta}_2 + \dot{\delta}_3)$$

$\phi(\delta^2)$ = terms of quadratic and higher order in δ_1, δ_2, δ_3

[14] Note also that the system is translationally invariant so that the linear momentum $\vec{P}$ of the system is an arbitrary integration constant. This fact can lead also to a spurious instability. The fact that all dynamical quantities are measured in the center-of-mass coordinate frame eliminates this possibility. Reduction of the system of variational equations with these invariances yields a system of equations which describe only the relative motion of the system.

$$A_\ell = 0 \Rightarrow (\dot{\delta}_1 + \dot{\delta}_2 + \dot{\delta}_3) = 0$$

When this relationship is applied to reduce the order of the system of variational equations, one obtains the 5x5 matrix equation

$$\dot{\vec{\zeta}}_5 = M_5 \vec{\zeta}_5$$

where $\zeta_5^T = (\delta_1, \delta_2, \delta_3, \dot{\delta}_1, \dot{\delta}_2)$

$$M_5 = \begin{bmatrix} 0 & 0 & 0 & 1 & 0 \\ 0 & 0 & 0 & 0 & 1 \\ 0 & 0 & 0 & -1 & -1 \\ 2\beta & -\beta & -\beta & \alpha & 2\alpha \\ -\beta & 2\beta & -\beta & -2\alpha & -\alpha \end{bmatrix}$$

For all allowed values of the parameters α, β the Jordan canonical form M_5^J has the form

$$M_5^J = \begin{bmatrix} 0 & 0 & 0 & 0 & 0 \\ 0 & \lambda_1 & 0 & 0 & 0 \\ 0 & 0 & \lambda_1^* & 0 & 0 \\ 0 & 0 & 0 & \lambda_2 & 0 \\ 0 & 0 & 0 & 0 & \lambda_2^* \end{bmatrix}$$

where

$$M_6^J \quad \begin{bmatrix} 0 & 1 & 0 & 0 & 0 & 0 \\ 0 & & & & & \\ 0 & & & & & \\ 0 & & & M_5^J & & \\ 0 & & & & & \\ 0 & & & & & \end{bmatrix}$$

The reduced system of linearized variational equations retains the same unstable eigenvalues which have positive real parts. The reduced system of exact, nonlinear variational equations also must have unstable solutions, since the stability character of the linear approximation persists when the eigenvalues of the linear approximation have positive real parts. Therefore, the symmetrical equilibrium configuration is an unstable rigid geometry. It is physically obvious, also, that the neglect of relative velocity-dependent frictional forces does not obviate the validity of this conclusion.

B. Method of solution presented in this report.

Let

$$\alpha = \theta_2 - \theta_1$$

$$\beta = \theta_3 - \theta_2$$

The nature of the system is such that all possible configurations are realized with the following restrictions on α, β:

$$0 < \alpha, \beta < \pi$$

$$\pi < (\alpha + \beta) < 2\pi$$

These inequalities define the closed region indicated in figure 6.

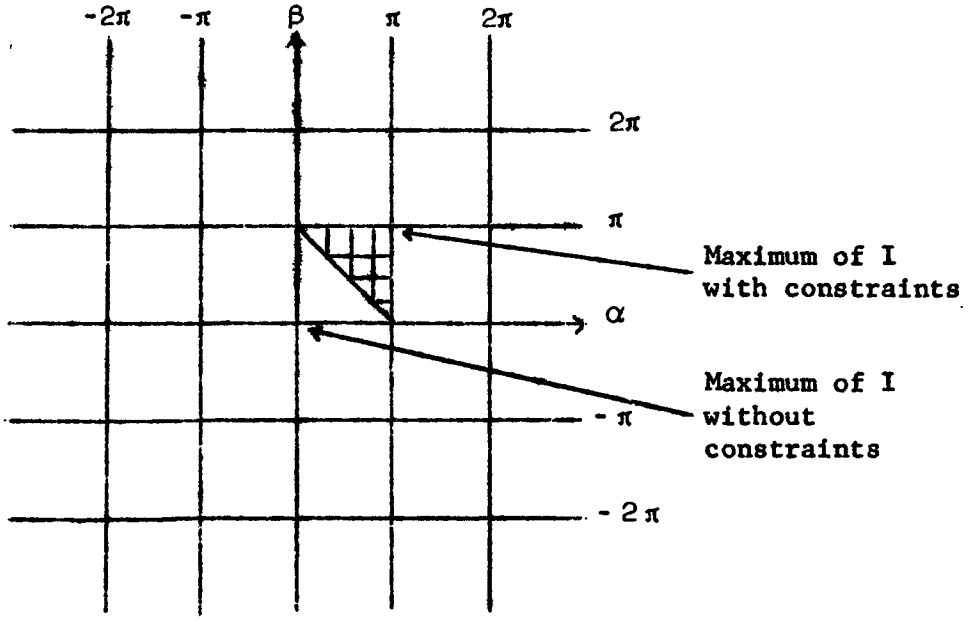

Figure 6. Values of α, β Allowed by Constraints

Moment of inertia $I(\alpha,\beta) = 3Ml^2 + 4ml^2\left[\cos^2\frac{\alpha}{2} + \cos^2\frac{\beta}{2} + \cos^2\frac{(\alpha+\beta)}{2}\right]$

Potential energy $V = 0$

Kinetic energy $T(\alpha,\beta) = \frac{L^2}{2I(\alpha,\beta)}$

$$E(\alpha,\beta) = \frac{L^2}{2I(\alpha,\beta)}$$

This last inverse relationship between E and I implies the following properties:

(a) The rigid geometries of the system correspond to the stationary values of I.

(b) The stable rigid geometries of the system correspond to the relative maximum values of I.

(c) The neutrally stable rigid geometries of the system correspond to the regions of constant I.

(d) The unstable rigid geometries of the system correspond to the relative minimum values of I.

The following computations investigate the extrema of $I(\alpha,\beta)$.[15]

$$\frac{\partial I}{\partial \alpha} = -2ml^2[\sin\alpha + \sin(\alpha+\beta)]$$

$$\frac{\partial I}{\partial \beta} = -2ml^2[\sin\beta + \sin(\alpha+\beta)]$$

$$\frac{\partial^2 I}{\partial \alpha^2} = -2ml^2[\cos\alpha + \cos(\alpha+\beta)] = A(\alpha,\beta)$$

$$\frac{\partial^2 I}{\partial \alpha \partial \beta} = -2ml^2\cos(\alpha+\beta) = B(\alpha,\beta)$$

$$\frac{\partial^2 I}{\partial \beta^2} = -2ml^2[\cos\beta + \cos(\alpha+\beta)] = C(\alpha,\beta)$$

$$B^2 - AC = -4m^2l^4[\cos\alpha\cos\beta + (\cos\alpha + \cos\beta)\cos(\alpha+\beta)]$$

$$A + C = -2ml^2[\cos\alpha + \cos\beta + 2\cos(\alpha+\beta)]$$

---

[15] The usual theory about the extrema of a function of two variables is applied in the analysis. Refer, for example, to Wilfred Kaplan, Advanced Calculus, Addison-Wesley Publishing Company, Inc., Massachusetts, 1959, p. 126.

The stationary values of I satisfy the following two equations simultaneously:

$$\frac{\partial I}{\partial \alpha} = \frac{\partial I}{\partial \beta} = 0$$

$$\Rightarrow \sin\alpha + \sin(\alpha+\beta) = 0$$

$$\sin\beta + \sin(\alpha+\beta) = 0$$

$$\Rightarrow \sin\alpha = \sin\beta$$

$$\Rightarrow \alpha = \beta \quad \text{since} \quad 0 < \alpha, \beta < \pi$$

$$\Rightarrow \sin\alpha + \sin 2\alpha = 0$$

$$\sin\alpha\,(1 + \cos 2\alpha) = 0$$

$$\Rightarrow \alpha = \beta = 0, \frac{2}{3}\pi, \pi$$

The restriction $\pi \leqslant (\alpha + \beta) \leqslant 2\pi$ implies that the value $\alpha = \beta = 0$ must be rejected. This value has an important significance which is discussed further below. The only possible rigid geometries for the specified constraining restrictions correspond to the remaining two values.

$$B^2 - AC\Big|_{\alpha=\beta=\frac{2\pi}{3}} = -3m^2\ell^4 < 0$$

$$A + C\Big|_{\alpha=\beta=\frac{2\pi}{3}} = 4m\ell^2 > 0$$

Therefore, $\alpha = \beta = \frac{2\pi}{3}$ is a relative minimum of I so that the symmetrical configuration is an unstable rigid geometry.

$$B^2 - AC\Big|_{\alpha=\beta=\pi} = 4m^2\ell^4 > 0$$

Therefore, $\alpha = \beta = \pi$ is a saddle point of I. The value $\alpha = \beta = \pi$ corresponds to the allowed linear configuration of the system. At first glance there appears to be a contradiction. The value $\alpha = \beta = \pi$ should correpond to a relative maximum so that the linear configuration is the state of lowest energy. However, the constraints in the problem prevent the system from assuming the geometry of lowest energy. The point $\alpha = \beta = \pi$ is a stationary value of E such that this point lies on the boundary of the closed region of allowed values of α,β.

Thus, $\alpha = \beta = \pi$ is an example of point L in Figure 2 so that the linear geometry is indeed a stable rigid geometry. It remains to ascertain the significance of the maximum value of $I(\alpha,\beta)$. This value is $\alpha = \beta = 0$ which was rejected temporarily above. The system can attain a configuration corresponding to $\alpha = \beta = 0$ only if one of the small masses m is allowed to move through the origin in the above linear configuration so that the linear configuration indicated in Figure 7 is attainable.

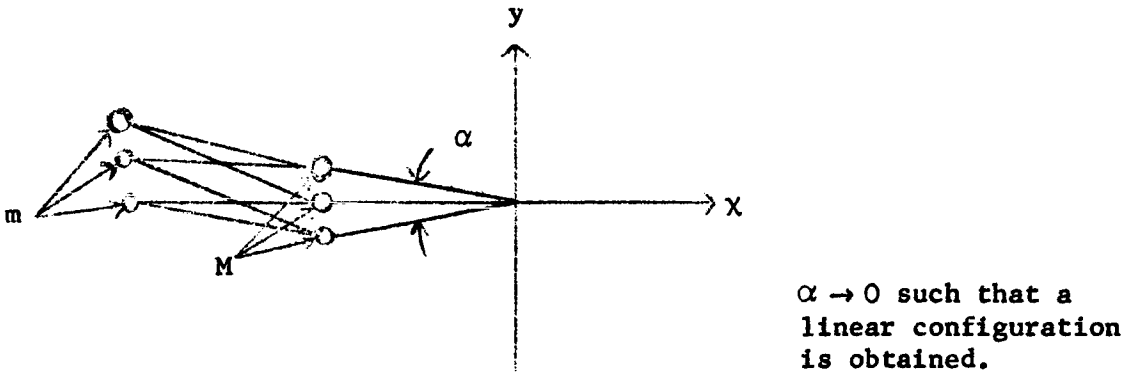

Figure 7. The Minimum Energy State $I(0,0) = 3M\ell^2 + 12m\ell^2$

$$B^2 - AC\Big|_{\alpha = \beta = 0} = -12m^2\ell^4 < 0$$

$$A + C\Big|_{\alpha = \beta = 0} = -8m\ell^2 < 0$$

Thus, $\alpha = \beta = 0$ is a relative maximum of I, so that the relaxation of constraints in the original problem would allow the absolute minimum energy state to be attained. This state, of course, would be a stable rigid geometry.

JG/sk

APPENDIX E

THE MOTION AND STABILITY OF A SPINNING SPRING-MASS IN ORBIT WITH RESULTS PERTAINING TO THE FEASIBILITY OF KWOT

TABLE OF CONTENTS

LIST OF SYMBOLS

A	Wire cross-sectional area
E	Young's modulus of elasticity
K	Product of universal gravitational constant and mass of Earth
$\bar{K}$	Spring constant $\left(\frac{AE}{\ell_o}\right)$
$\bar{K}_i$	Spring constant of i^{th} spring in multi-mass model
ℓ	Length of spring
ℓ_o	Unstretched length of spring
ℓ_s	Stretched equilibrium length of spring for nominal spin rate
L	Lagrangian function
m	Mass of sub-satellite
m_i	Mass of i^{th} particle in multi-mass model
q_i	Generalized coordinate
q_1	Deviation of spring length from ℓs
q_2	Deviation from nominal or steady state angular position
R	Radial distance from center of mass of the Earth to the center of spin of the model
t	Time
$\Delta( )$	Deviation of quantity following it
θ	Angular position of center of spin of spring-mass model

θ_i	Initial angular position
$\dot{\theta}$	Angular rate of center of spin
$\dot{\theta}_o$	Angular rate for circular orbit
λ_i	i^{th} eigenvalue of monodromy matrix
τ	Period of cyclic motion
ϕ	Angular position of model for motion in orbital plane or angular deviation from initial spin plane for motion out of orbital plane
ϕ_i	Initial angular position of spring-mass model
$\dot{\phi}$	Angular rate of spring-mass model
$\dot{\phi}_o$	Nominal angular rate of spring-mass model
ψ	Angular position of the projection of the model in the initial spin plane for motion out of orbital plane
$\dot{(\ )}$	Denotes derivative with respect to time

Matrices

[A]	Square matrix of constant coefficients for a linear system of differential equations
[A(t)]	Square matrix of time variant coefficients for a linear system of differential equations
$\{b(t)\}$	Column matrix of forcing functions
[F(t)] or $[F^1(t)]$	Fundamental matrix of linear system of differential equations
[I]	Identity matrix
[J]	Jordan normal form of monodromy matrix

$[M]$	Monodromy matrix
$\{q\}$ and $\{\dot{q}\}$	Column matrices of dependent variables and associated derivatives

LIST OF FIGURES

THE MOTION AND STABILITY OF A SPINNING SPRING-MASS IN ORBIT WITH RESULTS PERTAINING TO THE FEASIBILITY OF KWOT

1.0.0 Introduction

The KWOT system presents some very challenging structural dynamics problems (see bibliography). The dimensions range from thousands of miles for the orbit radius to a few thousandths of an inch diameter for the connecting wires. The very size of the system can cause one's intuition, based on more common structures, to be misleading. For these reasons, we must move carefully into the problem of analysis of such a system to insure that a consistent degree of sophistication is maintained at each level of work. In essence, one must start at the very foundations of mechancis to build the appropriate analysis for a system such as KWOT.

1.1.0 KWOT Problem Areas

Two problem areas have been defined and are treated in this report. These areas are basic to any attempt to ascertain the feasibility and to gain insight into the properties of a large, flexible, spinning structure in a gravity gradient field. These problem areas are:

1. Stability of motion of a large elastic system spinning in orbit. Specifically, a small sub-satellite attached to and spinning at some large distance around a much heavier body. Here, the center of mass (C.M.) of the spinning system is approximately at the C.M. of the large body and moves in a Keplerian orbit.

2. Motion of such a system in the gravity gradient. If stability can be shown for the system then the actual motion must be calculated to further verify the feasibility (i.e., not only must motion be stable, but its amplitude must be reasonable in some sense).

It is the questions implied in the above two problem areas that the following sections attempt to answer.

2.0.0 Derivation of Equations of Motion

2.1.0 Spring-mass Model (Planar Motion)

The simplest model to be treated which has the basic characteristics of KWOT is the model shown in Fig. 1. The point mass represents the sub-satellite and the linear massless spring represents the interconnecting wire.

2.1.1 Coordinate System for Spring-mass Model (Planar Motion)

The coordinate system for this model when it is restrained to rotate only in the plane of the orbit is shown in Fig. 2. Polar coordinates provide a convenient system by which to describe the motion. Plane motion (i.e., in the orbit plane) is analyzed first to demonstrate gravity gradient effects.

The independent variable is time, t, and the four dependent variables are R, Θ, ℓ, ϕ. The radius vector to the sub-satellite from the origin of the Earth centered inertial frame is

$$\hat{r} = (R\cos\Theta + \ell\cos\phi)\hat{i} + (R\sin\Theta + \ell\sin\phi)\hat{j} \tag{1}$$

The kinetic energy of the sub-satellite is given by

$$\text{K.E.} = \frac{1}{2} m \left| \dot{\hat{r}} \right|^2 \tag{2}$$

and the potential energy has two contributions, one from the gravity potential and one from the elastic energy.
Thus

$$\text{P.E.} = \frac{-K m}{|\hat{r}|} + \frac{1}{2} \bar{K} (\ell - \ell_o)^2 \tag{3}$$

where K is the product of the universal gravitation constant and the mass of the Earth, $\bar{K}$ is the spring constant, and ℓ_o is the natural length of the spring.

The Lagrangian is defined as L = K.E. - P.E. The equations of motion are generated from the following equation:

$$\frac{d}{dt}\left[\frac{\partial L}{\partial \dot{q}_i}\right] - \frac{\partial L}{\partial q_i} = 0 \qquad i = 1,2,3,4 \qquad (4)$$

where the q_i's are the dependent variables R, θ, ℓ, ϕ. If we assume the sub-satellite is attached to a much heavier body whose motion is unaffected by the much lighter sub-satellite the equations for the heavy body are the standard equations for a Keplerian orbit, namely

$$\ddot{R} - R\dot{\theta}^2 + \frac{K}{R^2} = 0 \qquad (5)$$

and

$$R\ddot{\theta} + 2\dot{R}\dot{\theta} = 0 \qquad (6)$$

the two equations for the relative motion of the sub-satellite

$$\ddot{\ell} - \ell\dot{\phi}^2 + \frac{K[\ell + R\cos(\phi - \theta)]}{[R^2 + \ell^2 + 2R\ell\cos(\phi - \theta)]^{3/2}} + \frac{\bar{K}}{m}(\ell - \ell_o) =$$

$$-(\ddot{R} - R\dot{\theta}^2)\cos(\phi - \theta) - (R\ddot{\theta} + 2\dot{R}\dot{\theta})\sin(\phi - \theta) \qquad (7)$$

and

$$\ell^2\ddot{\phi} + 2\ell\dot{\ell}\dot{\phi} - \frac{KR\ell\sin(\phi - \theta)}{[R^2 + \ell^2 + 2R\ell\cos(\phi - \theta)]^{3/2}} =$$

$$+ (\ddot{R} - R\dot{\theta}^2)\,\ell\sin(\phi - \theta) - (R\ddot{\theta} + 2\dot{R}\dot{\theta})\,\ell\cos(\phi - \theta) \qquad (8)$$

Note that the last terms in both (7) and (8) are identically zero because of (6). If we expand the radical in (7) and (8) in terms of $\frac{\ell}{R}$ (a very small number), we will see that the second to last terms in (7) and (8) are also zero. For example, the expansion of

$$\frac{K[\ell + R\cos(\phi - \theta)]}{[R^2 + \ell^2 + 2R\ell\cos(\phi - \theta)]^{3/2}}$$

yields

$$\frac{-K\ell}{2R^3}\left[1 + 3\cos 2(\phi - \theta)\right] + \frac{K}{R^2}\cos(\phi - \theta)$$

Putting this expression back into (7) and combining terms with $\cos(\phi - \theta)$ is (5) and hence zero.

Thus, the equations of motion (keeping only the leading term in the expansion) are

$$\ddot{\ell} - \ell\dot{\phi}^2 - \frac{K\ell}{2R^3}\left[1 + 3\cos 2(\phi - \theta)\right] + \frac{\bar{K}}{m}(\ell - \ell_o) = 0 \qquad (9)$$

and

$$\ell\ddot{\phi} + 2\dot{\ell}\dot{\phi} + \frac{3K\ell}{2R^3}\sin 2(\phi - \theta) = 0 \qquad (10)$$

2.1.2 Spring-mass Model (Motion Out of Orbital Plane)

If the spring-mass model in Fig. 2 is given an additional degree of freedom, motions out of the plane of the orbit may be analyzed. The coordinate system is shown in Fig. 3. By using the Lagrangian approach outlined above, the equations of motion for the system with 3 degrees of freedom may be found to be

$$\ddot{\ell} = \ell(\dot{\phi}^2 + \cos^2\phi\dot{\psi}^2) - \frac{K\ell}{R^3}\left[1 - 3(\cos\theta\sin\phi + \sin\theta\cos\phi\sin\psi)^2\right] - \frac{\bar{K}}{m}(\ell - \ell_o) \quad (11)$$

$$\ddot{\phi} = -\frac{2\dot{\ell}\dot{\phi}}{\ell} - \frac{\sin 2\phi}{2}\dot{\psi}^2 + \frac{3K}{2R^2}\left\{\sin 2\phi\,[\cos^2\theta - \sin^2\theta\sin^2\psi] + \sin 2\theta\sin\psi\cos 2\phi\right\} \quad (12)$$

$$\ddot{\psi} = \frac{-2\dot{\ell}\dot{\psi}}{\ell} + \frac{\sin 2\phi}{\cos^2\phi}\dot{\phi}\dot{\psi} + \frac{3K}{R^3}\left[\frac{\sin 2\theta}{2}\frac{\sin 2\phi}{2}\frac{\cos\psi}{\cos\phi} + \frac{\sin^2\theta\sin 2\psi}{2}\right] \quad (13)$$

2.2.0 Multi-mass Model (Planar Motion)

The three models described above do not take into account the line dynamics of the connecting wire. In order to account for this, the equations for the 3-mass model shown in Fig. 4 were derived. The equations were derived assuming that the origin of the x,y system is prescribed to move in a Keplerian orbit given by the solution of (5) and (6). The six equations for the six degrees of freedom for the system relative to the x,y system are

$$\ddot{\ell}_1 = \ell_1\dot{\phi}_1^2 - \frac{K\ell_1}{R^3}[1 - 3\cos^2(\phi_1 - \theta)] - \frac{\bar{K}_1}{m_1}(\ell_1 - \ell_{10}) - \frac{\bar{K}_2}{m_1}\frac{\sqrt{\ell_1^2 + \ell_2^2 - 2\ell_1\ell_2\cos(\phi_1 - \phi_2)} - \ell_{20}}{\sqrt{\ell_1^2 + \ell_2^2 - 2\ell_1\ell_2\cos(\phi_1 - \phi_2)}}[\ell_1 - \ell_2\cos(\phi_1 - \phi_2)] \quad (14)$$

$$\ddot{\phi}_1 = -\frac{2\dot{\ell}_1\dot{\phi}_1}{\ell_1} - \frac{3K}{2R^3}\sin 2(\phi_1 - \theta)$$

$$- \frac{\bar{K}_2}{m_1}\frac{\left[\sqrt{\ell_1^2 + \ell_2^2 - 2\ell_1\ell_2\cos(\phi_1-\phi_2)} - \ell_{20}\right]}{\sqrt{\ell_1^2 + \ell_2^2 - 2\ell_1\ell_2\cos(\phi_1-\phi_2)}} \times \left[\frac{\ell_2}{\ell_1}\sin(\phi_1-\phi_2)\right] \qquad (15)$$

$$\ddot{\ell}_2 = \ell_2\dot{\phi}_2^2 - \frac{K\ell_2}{R^3}\left[1 - 3\cos^2(\phi_2 - \theta)\right]$$

$$- \frac{\bar{K}_2}{m_2}\frac{\left[\sqrt{\ell_1^2 + \ell_2^2 - 2\ell_1\ell_2\cos(\phi_1 - \phi_2)} - \ell_{20}\right]}{\sqrt{\ell_1^2 + \ell_2^2 - 2\ell_1\ell_2\cos(\phi_1 - \phi_2)}}\left[\ell_2 - \ell_1\cos(\phi_1 - \phi_2)\right]$$

$$- \frac{\bar{K}_3}{m_2}\frac{\left[\sqrt{\ell_2^2 + \ell_3^2 - 2\ell_2\ell_3\cos(\phi_2 - \phi_3)} - \ell_{30}\right]}{\sqrt{\ell_2^2 + \ell_3^2 - 2\ell_2\ell_3\cos(\phi_2 - \phi_3)}}\left[\ell_2 - \ell_3\cos(\phi_2-\phi_3)\right] \qquad (16)$$

$$\ddot{\phi}_2 = -\frac{2\dot{\ell}_2\dot{\phi}_2}{\ell_2} - \frac{3K}{2R^3}\sin 2(\phi_2 - \theta)$$

$$+ \frac{\bar{K}_2}{m_2}\frac{\left[\sqrt{\ell_1^2 + \ell_2^2 - 2\ell_1\ell_2\cos(\phi_1 - \phi_2)} - \ell_{20}\right]}{\sqrt{\ell_1^2 + \ell_2^2 - 2\ell_1\ell_2\cos(\phi_1 - \phi_2)}}\left[\frac{\ell_1}{\ell_2}\sin(\phi_1 - \phi_2)\right]$$

$$- \frac{\bar{K}_3}{m_2}\frac{\left[\sqrt{\ell_2^2 + \ell_3^2 - 2\ell_2\ell_3\cos(\phi_2-\phi_3)} - \ell_{3.0}\right]}{\sqrt{\ell_2^2 + \ell_3^2 - 2\ell_2\ell_3\cos(\phi_2-\phi_3)}}\left[\frac{\ell_3}{\ell_2}\sin(\phi_2-\phi_3)\right] \qquad (17)$$

$$\ddot{\ell}_3 = \ell_3\dot{\phi}_3^2 - \frac{K\ell_3}{R^3}\left[1 - 3\cos^2(\phi_3 - \theta)\right]$$

$$- \frac{\overline{K}_3}{m_3}\frac{\left[\sqrt{\ell_2^2 + \ell_3^2 - 2\ell_2\ell_3\cos(\phi_2 - \phi_3)} - \ell_{20}\right]}{\sqrt{\ell_2^2 + \ell_3^2 - 2\ell_2\ell_3\cos(\phi_2 - \phi_3)}}\left[\ell_2 - \ell_3\cos(\phi_2 - \phi_3)\right] \qquad (18)$$

$$\ddot{\phi}_3 = -\frac{2\dot{\ell}_3\dot{\phi}_3}{\ell_3} - \frac{3K}{2R^3}\sin 2(\phi_3 - \theta)$$

$$+ \frac{\overline{K}_3}{m_3}\frac{\left[\sqrt{\ell_3^2 + \ell_2^2 - 2\ell_2\ell_3\cos(\phi_2 - \phi_3)} - \ell_{30}\right]}{\sqrt{\ell_3^2 + \ell_2^2 - 2\ell_2\ell_3\cos(\phi_2 - \phi_3)}}\left[\frac{\ell_2}{\ell_3}\sin(\phi_2 - \phi_3)\right] \qquad (19)$$

The above system (14)-(19) contains only the first non-canceling entry in the expansion of the term which came from the gravity potential. The above equations do allow for arbitrarily large deflections of the connecting wire (represented by masses 1 and 2 in Fig. 4).

3.1.0 Linearization of Nonlinear Equations for Spring-mass Model (Planar Motion)

The equations of motion (9) and (10) for the mass on a spring attached to a heavy body, Fig. 1, are nonlinear and do not yield readily to analytic solution or even a rigorous stability analysis. Equations (9) and (10) were thus linearized in an attempt to get a better understanding of the nature of the motion.

The usual procedure of linearizing around a stationary point of the nonlinear equations is not possible here since there is no stationary point solution of (9) and (10) for a spinning system in orbit. Thus if any

linearization is to be made, it must be around some specified solution which is close to the expected motion. Such a motion does exist.

As the orbital radius, R, goes to ∞, (9) and (10) become

$$\ddot{\ell} = \ell\dot{\phi}^2 - \frac{\overline{K}}{m}(\ell - \ell_o) \tag{20}$$

and

$$\ddot{\phi} = \frac{-2\dot{\ell}\dot{\phi}}{\ell} \qquad \text{or} \qquad \frac{d}{dt}\left[\ell^2\,\dot{\phi}\right] = 0 \tag{21}$$

These are the equations for a system spinning in free space. Here a stationary solution does exist where $\ddot{\ell} \equiv 0$ and $\ddot{\phi} \equiv 0$. This motion is when

$$\ell\dot{\phi}^2 = \frac{\overline{K}}{m}(\ell - \ell_o)$$

or the centrifugal force is balanced by the elastic restoring force and when

$$\frac{-2\,\dot{\ell}\,\dot{\phi}}{\ell} \equiv 0$$

This is satisfied if $\dot{\ell} \equiv 0$. Thus we have a so-called "free space" solution of (9) and (10), namely

$$\dot{\phi} = \text{const.} = \dot{\phi}_o \tag{22}$$

$$\ell = \frac{\frac{\overline{K}}{m}\,\ell_o}{\left(\frac{\overline{K}}{m} - \dot{\phi}_o^{\,2}\right)} = \ell_s \tag{23}$$

Note $\ell_s \to \infty$ as $\frac{\overline{K}}{m} \to \dot{\phi}_o^{\,2}$ or when the centrifugal force approaches the elastic restoring force.

Since the stationary solution of (9) and (10) approach (22) and (23) as $R \to \infty$, the natural motion to linearize around is that for free space.

Defining deviations from the desired free space motion as follows

$$\ell(t) = \ell_s + q_1(t) \qquad \text{and} \qquad \phi(t) = (\dot{\phi}_o t + \phi_i) + q_2(t)$$

where ℓ_s and $\dot{\phi}_o$ are constants, we may linearize (9) and (10). The equations in terms of the linearized quantities are

$$\ddot{q}_1 = \left[\frac{\bar{K}}{m} - \dot{\phi}_o^2 - \frac{K}{2R^3} - \frac{3K}{2R^3} \cos 2(\dot{\phi}_o t + \phi_i - \theta) \right] q_1$$

$$+ 2\dot{\phi}_o \ell_s q_2 - \frac{3K}{R^3} \ell_s \sin 2(\dot{\phi}_o t + \phi_i - \theta) q_2$$

$$+ \frac{3K\ell_s}{2R^3} \cos 2(\dot{\phi}_o t + \phi_i - \theta) \tag{24}$$

and

$$\ddot{q}_2 = \frac{3K}{R^3} \cos 2(\dot{\phi}_o t + \phi_i - \theta)\, q_2 - \frac{2\dot{\phi}_o}{2R^3} \dot{q}_1$$

$$- \frac{3K}{2R^3} \sin 2(\dot{\phi}_o t + \phi_o - \theta) \tag{25}$$

As $R \to \infty$, the natural frequency of the system approaches

$$\sqrt{\frac{\bar{K}}{m} + 3\dot{\phi}_o^2}$$

as pointed out in Ref. 1. Note that even in the linearized form, (9) and (10) (now (24) and (25)) are still rather intractable. In matrix notation, (24) and (25) may be written as

$$\{\dot{q}\} = [A(t)] \{q\} + \{b(t)\} \tag{26}$$

Equation (26) is the general form for a system of first order, linear, ordinary, forced differential equations with periodic coefficients. The matrix [A(t)] is made up of the coefficients of (24) and (25). b(t) is the column matrix of forcing functions. It is the time dependence of [A(t)] that necessitates use of other than the standard techniques normally used in linear differential equation.

4.1.0 Stability of Linear Differential Equations with Periodic Coefficients

Once the equations of motion have been derived, the next step is to use them to determine the feasibility of a system such as KWOT in the gravity field in a passive or uncontrolled mode. A firm understanding of the passive motion must be at hand before any attempt is made to control the system through active means. The inherent stability of such a system must be ascertained if at all possible.

Before the question of stability is explored in great detail, the definition to be used must be spelled out. Ref. 1 has pointed out that a system such as the spring-mass model, mentioned above, is moving in a conservative force field. The total energy of the system is finite and the worst possible case would be if all the energy of the various modes of motion transferred into a single mode (for example, elastic vibrational energy). The coupling of the modes is such that this is certainly a possibility. The question of stability, therefore, is not whether various dependent variables grow without bound, but whether energy can feed continuously from one mode of motion into some other mode, thus destroying the configuration necessary for KWOT's scientific mission.

In view of this, a linearization about some desirable (and hopefully stable) reference motion may be analyzed for stability. The obvious motion to linearize around (as mentioned in 3.1.0) is the free space motion which is both stable in the sense discussed above and desirable for the scientific objectives of KWOT. Thus, a stability study of (24) and (25) will provide useful information about the gross feasibility of a spinning, spring-mass type system in orbit.

4.2.0 Floquet Theory

Equations of the form of (26) may be readily analyzed for the stability properties by matrix operations as outlined in Chapter 6 of Ref. 2 if $[A(t)]$ is a constant matrix and not time variant. This is not the case for systems in orbit which are not axisymmetric with respect to their spin axis. The linearized equations for the non-axisymmetric configurations contain periodic coefficients.

A theory which does apply to a system of the form

$$\left\{\dot{q}\right\} = [A(t)] \left\{q\right\} \tag{27}$$

where $[A(t)]$ is periodic with period τ is given by Floquet as reported in Ref. 3, pp. 55-59 (see also Ref. 4, pp. 461-463). $[A(t)]$ is periodic if

$$[A(t + \tau)] = [A(t)] \qquad t > 0$$

A matrix $[F(t)]$ whose columns are linearly independent solutions of (27) is called a fundamental matrix. Thus $[F(t)]$ satisfies (27). Also if $[F(t)]$ is a fundamental matrix, so is $[F(t + \tau)]$ and there exists a non-singular matrix $[M]$ (sometimes called the monodromy matrix) such that

$$[F(t + \tau)] = [F(t)][M] \tag{28}$$

$[M]$ may be reduced to the Jordan normal and eigenvalues $\lambda_1 \ldots, \lambda_m$ are called multipliers. None of the multipliers vanish since

$$\lambda_1\lambda_2 \ldots \lambda_m = \det[M] \neq 0$$

since $[M]$ is non-singular. In particular if

$$[F(0)] = [I]$$

then

$$[F(\tau)] = [I]\,[M] \tag{29}$$

We may choose $[F(0)] = [I]$ and by numerical integration of (27) over one period, generate $[F(\tau)]$ which will be $[M]$ which in turn will yield the desired multipliers. Thus if the Jordon normal form of $[M]$ is diagonal we may write

$$[C]^{-1}\,[F(\tau)][C] = [C^{-1}][F(0)][C][C]^{-1}[M][C]$$

$$[F'(\tau)] = [F'(0)][J] = [F'(0)] \begin{Bmatrix} \lambda_1 & 0 & \dots & 0 \\ 0 & \lambda_2 & \dots & 0 \\ \dot{0} & \dot{0} & \dots & \lambda_m \end{Bmatrix} \tag{30}$$

where $[F'(\tau)]$ is still a fundamental matrix of (27). Taking the first column of $[F'(\tau)]$ we get

$$\left\{q_1(\tau)\right\} = \lambda_1 \left\{q_1(0)\right\} \text{ or in general } \left\{q_1(t+\tau)\right\} = \lambda_i \left\{q_i(t)\right\}$$

From this, we can see that if $\lambda_i < 1.0$ the vector decreases in length exponentially. If $\lambda_i = 1.0$ it remains the same and if $\lambda_i > 1.0$ it grows exponentially with time. Thus stability can be determined by calculating all the λ's and checking their absolute values against 1.0. In other words, if any λ is greater than 1.0, there exists at least one unstable solution to (27).

There does exist a case where stability is not found merely from the λ's alone. This case arises when at least two of the λ's are equal to 1.0. This case may be either neutrally stable or grow linearly with time. This ambiguity may be resolved by determining the Jordan normal form of the monodromy matrix $[M]$. If it has only diagonal entries and no off-diagonal 1.0's, the solutions associated with the unitary λ's are neutrally stable. If, however, there are off-diagonal, non-zero entries, the associated solution vectors will grow at least linearly with time but not exponentially. Repeated values of λ other than 1.0 are of no consequence because the behavior of the associated solution vectors is dominated by an exponential growth or decay.

In summary, if the system of m equations, (27), can be integrated m times over period τ for initial conditions which in matrix form constitute the identity matrix, the monodromy matrix [M] will be generated. The roots and Jordan normal form of [M] completely determine the stability properties of the system of equations.

4.3.0 Extension of Floquet to Forced Equations

Floquet theory as described above does not apply to forced systems such as (26). However, an extension to the theory to allow analysis of forced systems was made by L. Ceasari (Ref. 5). A variable Z is defined, and $\dot{Z} \equiv 0$. This allows (26) to be written as follows

$$\begin{Bmatrix} \dot{q}_1 \\ \vdots \\ \dot{q}_m \\ \dot{Z} \end{Bmatrix} = \left[\begin{array}{c|c} [A(t)] & b(t) \\ \hline [0] & 0 \end{array}\right] \begin{Bmatrix} q_1 \\ \vdots \\ q_m \\ Z \end{Bmatrix} \qquad (31)$$

System (31) is now in proper form and Floquet theory may be applied as outlined previously.

4.3.1 Application of Floquet Theory to Equation for a Forced Harmonic Oscillator

As an example of the application of this extension to Floquet theory, the simple forced harmonic oscillator may be analyzed. The equation is

$$\ddot{X} + \omega_o^2 X = \cos \omega t$$

The matrix equation is found if we define $\dot{X} = Y$, namely

$$\begin{Bmatrix} \dot{Y} \\ \dot{X} \\ \dot{Z} \end{Bmatrix} = \begin{bmatrix} 0 & -\omega_o^2 & \cos \omega t \\ 1 & 0 & 0 \\ 0 & 0 & 0 \end{bmatrix} \begin{Bmatrix} Y \\ X \\ Z \end{Bmatrix} \qquad (32)$$

The fundamental matrix at t = 0 is selected as the identity matrix so that the associated initial conditions on y,x, and z for column vectors are as follows:

$$\begin{Bmatrix} 1 \\ 0 \\ 0 \end{Bmatrix} \quad , \quad \begin{Bmatrix} 0 \\ 1 \\ 0 \end{Bmatrix} \quad \text{and} \quad \begin{Bmatrix} 0 \\ 0 \\ 1 \end{Bmatrix}$$

Since $[A(t)]$ has period $\tau = \frac{2\pi}{\omega}$, the corresponding column vectors for the monodromy matrix, $[M]$, are found by solving (32) using the three vectors above for the initial conditions. For $\omega \neq \omega_o$ the monodromy matrix in Jordan form is

$$[M] = \begin{bmatrix} 1 & 0 & 0 \\ 0 & 1 & 0 \\ 0 & 0 & 1 \end{bmatrix}$$

when $\omega = \omega_o$ we get

$$[M] = \begin{bmatrix} 1 & 0 & 0 \\ 0 & 1 & 1 \\ 0 & 0 & 1 \end{bmatrix}$$

where the off diagonal element indicates a linear growth of one solution with respect to time. It should be noted that the Jordan form need not be calculated. By knowing the rank of the matrix

$$\left[[M] - [I]\right] \tag{33}$$

one can obtain the nullity and in turn the number of linearly independent eigenvectors. Knowing the eigenvalues and the number of linearly independent eigenvectors associated with each eigenvalue, we can infer what the entries of the Jordan normal matrix must be.

4.3.2 Application of Floquet Theory to Spring-mass Linearized Equations

We now turn to the application of the modified Floquet theory to the stability analysis of the spring-mass model in Fig. 1 when the orbit is circular. A computer program was written which calculates the fundamental matrix for the linear system of equations (24) and (25) at the end of a period. The eigenvalues (which are the multipliers) are found and the rank of the matrix (32) is calculated.

The monodromy matrix is fifth order (four from (24) and (25) and one form the z variable for the forcing function) and the rank for all the cases considered was three. This implies that these are 5-3 or 2 linearly independent eigenvectors. However the root 1.0 is repeated three times. The other two roots (making the expected total of five) are complex conjugates with absolute value of 1.0. This means the fifth order monodromy matrix has only four linearly independent eigenvectors and that its Jordan normal form has one off diagonal element which is non-zero. In other words, the system has a linear growth in time!

A closer look reveals that this is in fact a trivial instability. This apparent instability merely reflects the fact that the system can be given an initial angular momentum different than the reference level. The linear growth is in the angular position relative to the free space motion. In other words, if the system were started a little faster or slower than the reference spin rate, a linear growth in the angular position of the actual motion relative to the reference motion would be observed. One can also argue that the angular position is the only variable that can grow linearly with time and not affect any of the other three variables.

5.1.0 Analog Solution of Linearized Spring-mass Equations (Planar Motion)

To obtain some insight into the behavior of the linearized equations of motion for the mass on a spring model, Fig. 1, (24) and (25) were programmed. The orbit was chosen as circular so the orbital variables were easily handled. For a circular orbit one gets

$$R = \text{const.},\ \Theta = \text{const.},\ \text{and}\ \dot{\Theta} = \Theta t + \Theta_i$$

The results of the analog study are summarized in graphical form in Figs. 5 - 7.

Fig. 5 shows the axial deviation of the spring about the nominal free space stretched length. This is the axial deviations caused by the changing gravity field that a given sub-satellite "sees" as it rotates about the central mass. Note that the curves are essentially straight. The appearance of the data suggested an empirical formula for the axial deviation that has been shown to represent the data in Fig. 5 to within a few percent, namely

$$\Delta \ell = (115)\ \frac{K}{R^3}\ \frac{\ell_o}{\frac{\bar{\bar{K}}}{m} - \dot{\phi}_o^2 - \frac{\dot{\theta}^2}{2}} \tag{34}$$

This equation has only been verified by comparison with Fig. 5 and its validity for spin rates other than one revolution per one hour has not been demonstrated. It should be pointed out that the axial deviations are less than one foot, even for a 14,000 nautical mile orbit and hence presents no problems to KWOT feasibility.

Fig. 6 shows that the spin rate deviation from the nominal rate of one rev./hour is considerably less than ±1% for orbits above 14,000 nautical miles. Fig. 7 is the transverse deviation of a sub-satellite due to gravity effects. The curve shows that the oscillations are quite small compared to the size of the overall system. This indicates that active control of this mode of motion is not needed, since the deviation for most orbits is easily within the ±50 meter criterion initially set up as allowable.

It is interesting to note that if a new nondimensional variable is defined as

$$m_1 = \frac{q_1}{\ell_s}$$

then (24) and (25) are independent of ℓ_s or ℓ_o if the effective spring constant $\frac{\bar{K}}{m}$ is specified. This means the angular rate deviation is independent of the length of the spring. This also implies that the angular position deviation (not plotted) is independent of the spring length.

6.0.0 Numerical Solution of Nonlinear Equations

The nonlinear equations of motion derived in 2.1.0 and 2.2.0 were also numerically integrated on an IBM 7090 digital computer. A fourth order Runge-Kutta method was used (see Ref. 6). The optimum step size was determined through trial and error. It appears that about twenty steps over the smallest period of motion is the best compromise between accuracy and round-off errors. This conclusion was based on several integrations of the spinning "free space" equations (20) and (21) for which the solution is known analytically for the linearized equations.

6.1.0 Spring-mass Model (Planar Motion)

The first model to be treated numerically was the spring-mass model for motion in the orbital plane only. The system of equations for this model consists of (5), (6), (9) and (10). These four second order equations were reduced to a system of eight first order differential equations. They were then integrated numerically on a digital computer (IBM 7090) using a fourth order Runge-Kutta scheme.

The effect of the nonlinearities can be seen by comparing the point marked "digital" of Figs. 5 - 7. The axial and transverse deviations are 47 and ~0% respectively. The 47% is not significant when the magnitude of the deviations are considered. The spin rate deviation is not affected by nonlinearities of the equations as may be seen in Fig. 5. From these results we can conclude that the linear equations are not available, the importance of this conclusion is diminished.

The stability that was indicated in 4.3.2 for a spring-mass in orbit is further substantiated by numerical integration of its equations of motion. This is an important point since only neutral stability was

found for the linearized equations and that does not imply stability of the nonlinear equations. The effects of the nonlinearities could be such as to cause a growth or a decay of the motion. Therefore, the fact that the linear equations seem to adequately describe the nonlinear motion indicates that the linear stability (namely neutral) is probably the same as that for the nonlinear motion.

The effects of eccentric orbits is quite a different matter. For other than circular orbits, the orbital radius, R, is not constant and the angular rate of the orbit, $\dot{\theta}$, is not constant. The coefficients of (9) and (10) are still time variant but they are not necessarily periodic any more. Only when

$$\frac{1}{R^3} \qquad \text{and} \qquad \frac{\cos 2(\phi - \theta)}{R^3}$$

have periods which are integer multiples of each other would (9) and (10) have periodic coefficients. Floquet theory only treats linear equations with periodic coefficients, so in general, the stability of motion of elliptic orbits cannot be determined directly. For this reason, several cases were integrated to indicate the type of motion one should expect for elliptic orbits. Fig. 7 shows the axial deviation for a spring-mass passing through perigee of a 10,000 by 60,000 N.M. orbit. Note that this deviation at perigee (10,000 N.M.) is ±0.5 feet, which is close to what we would find from Fig. 4 for a 10,000 N.M. circular orbit. This implies the axial deviation is still given by expression (30) if the instantaneous orbital radius is used.

The angular or transverse deviation (transverse = angular x spring length) however, is affected by the eccentricity of the orbit. Compare Figs. 8 and 9. Fig. 8 shows the angular deviation for a 14,000 N.M. circular orbit. The corresponding transverse displacement about the linearily increasing angle is ±53 feet. The linear growth is the "trivial" instability discussed in 4.3.2. It merely indicates that the system is spinning at a constant angular rate which is slightly different from $\dot{\phi}_o$. The angular deviation for a 10,000 x 60,000 N.M. elliptic orbit

is shown in Fig. 9. Note again that the "trivial" instability occurs even for the highly elliptic orbits shown.

One additional phenomenon should be noted. As was seen for the 10,000 x 60,000 N.M. orbit, the motion of the system remained near "free space" motion. However, if the perigee is dropped to 5,000 N.M. the motion deviated quite markedly. Axial deviations are relatively unaffected but the spin rate and hence angular deviation can be greatly affected. Fig. 10 shows the effect of starting position on the spin rate deviation. Note that the system can either gain or loose spin rate while passing through perigee of a low perigee elliptic orbit. This implies that energy may be put into or taken out of the spinning spring-mass.

For the 10,000 x 60,000 N.M. orbit, the ratio of the spin rate to the orbital angular rate at perigee was 5.43 while it was only 1.82 for the 5,000 x 60,000 N.M. orbit. The frequency of the gravity perturbation is essentially $2(\dot{\phi} - \dot{\theta})$. When this is near zero (or the ratio near one), gravity gradient has effectively "captured" the spring-mass. Following this reasoning, Fig. 10 shows the cases where the spring-mass is slowed down or partially "captured" or is speeded up because of its position relative to the earth while passing perigee. We therefore can conclude that there is some orbit which is too low to passively maintain the desired geometry (5,000 N.M. for a spin rate of one hour is one example).

6.2.0 Spring-mass Model (Motion Out of Orbital Plane)

The spring-mass treated in the previous section had only two degrees of freedom relative to the center of rotation which was restrained to move in a Keplerian orbit. This section allows the spring-mass an additional degree of freedom and hence allows it to freely spin out of the orbital plane. The coordinate system is shown in Fig. 2 and the equations of motion for the three degrees of freedom relative to the center of rotation are (11), (12) and (13). The orbital equations are still (15) and (16).

The only results obtained to date have been for the spin vector of the spring-mass lying in the orbital plane. This puts the spin plane of the spring-mass perpendicular to the orbital plane. The system was started so that the plane of the spring-mass was either perpendicular to or coincident with the orbital radius vector. Thus, initially, there was no torque acting to precess the spin plane of the spring-mass. However, as the system moves around in the orbit, a torque develops due to its position relative to the Earth and the spin plane precesses. The torque vector tending to precess the plane is perpendicular to the orbital plane, hence the plane precesses toward the orbital plane. A typical precession for a 10,000 x 60,000 N.M. orbit with the spin plane initially coincident with the radius vector at $\Theta = -\pi/2$ is 0.7° after passing perigee. This is the toatl precession induced in the spin plane of the spring-mass from an originally vertical position.

The "capture" effect described in 6.1.0 is also apparent in the out of plane motion for a 5,000 x 60,000 N.M. orbit. The change in spin rate for two spring-masses initially started 90° apart would cause them to collide near perigee and hence a discussion of precession is meaningless.

The long term behavior of the out of orbital plane motion has not been considered in this phase of study. An active control system could remove any of the long term motions that are undesirable. It may be possible to augment active control of the sky scan mode of operation by careful use of the natural precession available at perigee. However, this is a question for the second phase of study.

6.3.0 Multi-mass Model (Planar Motion)

The third model treated was a three mass model developed to account for line dynamics. This model is shown in Fig. 3. Here again, the center of rotation is restrained to move in a Keplerian orbit. The equations of motion relative to the orbit are given by (14) through (19). This system has only 6 relative degrees of freedom since only motion in the orbital plane is allowed.

This model indicated that certain situations could be undesirable. One such case occured when the axial oscillation frequency of the larger mass given by

$$\sqrt{\frac{\bar{\bar{K}}}{m} + 3\dot{\phi}_o^2}$$

was near the first natural transverse frequency of the wire. A parametric excitation was observed and a large amplitude (±300 feet) motion was started. When the lowest axial frequency was higher than the transverse, the motion remained bounded around (±10 feet) which is quite acceptable for maintaining the electrical properties of the dipole array. Again, the purpose here was only to point out feasibility and not to do a detailed study. Such a study could be carried out at a later time using the numerical techniques mentioned and employing a more complicated model such as Fig. 11.

7.1.0 Conclusions

The following conclusions have been drawn from the work performed concerning the gross feasibility of KWOT.

(1) The Lagrangian may be effectively used to generate the equations of motion for all discrete models.

(2) A fourth order Runge-Kutta integrating technique is will suited to the type of equations derived for KWOT.

(3) The numerical application of Floquet theory with appropriate matrix operations can be used to determine stability for a certain class of linearized equations which apply to KWOT in a gravity field.

(4) The spring-mass approximation for a part of the KWOT structure is neutrally stable in the linear sense and numerical integration indicates neutral stability of the nonlinear motion as well. Hence, some active control will be needed for long term operation in a space environment.

(5) The gravity gradient induced axial oscillations of the spring-mass model, and by implication the rhombic's major axis, are much less than 1% of the major axis.

(6) For the range of stiffnesses applicable to the KWOT system the spin rate deviations are predominantly due to gravity gradient effects.

(7) For sufficiently high spin-rates or orbits, the gravity gradient disturbances do not produce undesirable motions.

(8) The natural precession of the system may be used to increase life time by aiding the active control system.

(9) A multi-mass, discrete model of KWOT can be realistically used to furnish design information in the later phases.

REFERENCES

1. Pittman, D. L., Hall, B. M., "The Inherent Stability of Counterweight Cable Connected Space Stations", Douglas Paper No. 3051, Douglas Missile and Space Systems Division, July 1964.

2. Kaplan, W., Ordinary Differential Equations, Addison-Wesley Co., Inc., Reading, Mass., 1958.

3. Cesari, L., Asymptotic Behavior and Stability Problems in Ordinary Differential Equations, Academic Press Inc., New York, 1963.

4. Pars, L. A., A Treatise on Analytical Dynamics, Heinemann Educational Books Ltd., London, 1965.

5. Private communication with L. Cesari, Spring 1966.

6. Hamming, R. W., Numerical Methods for Scientists and Engineers, McGraw-Hill, New York, 1962.

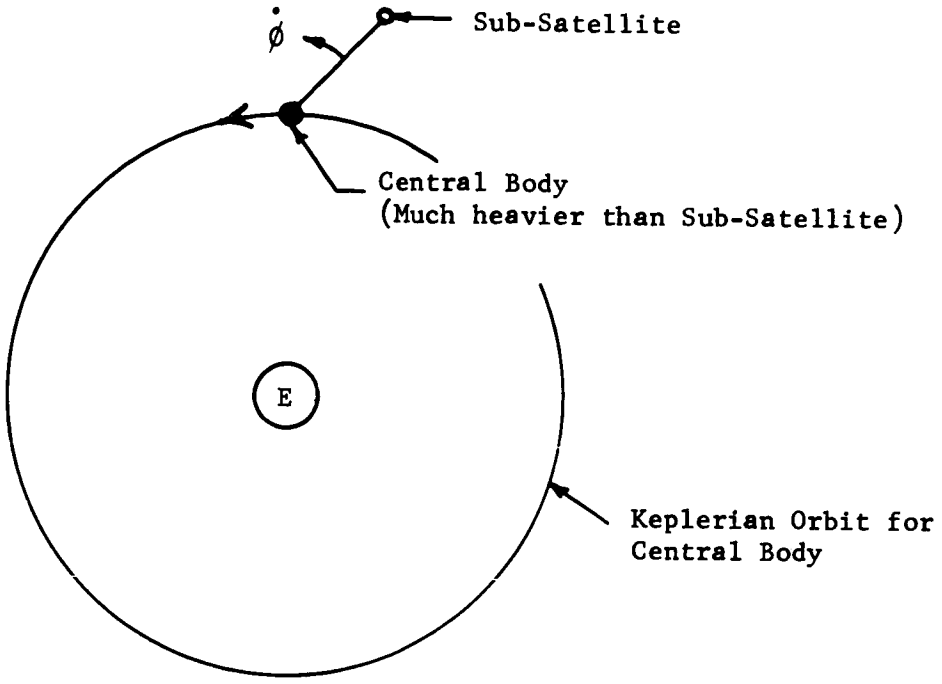

Figure 1 - Schematic of Sub-satellite-central body in Earth Orbit

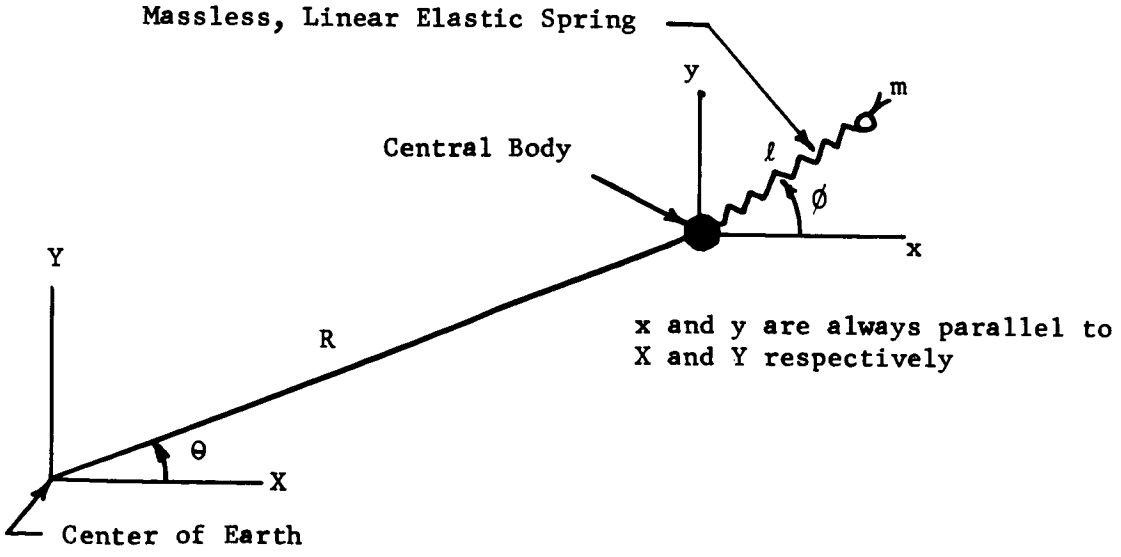

Figure 2 - Coordinate System for Spring-mass Model Restrained to Orbital Plane

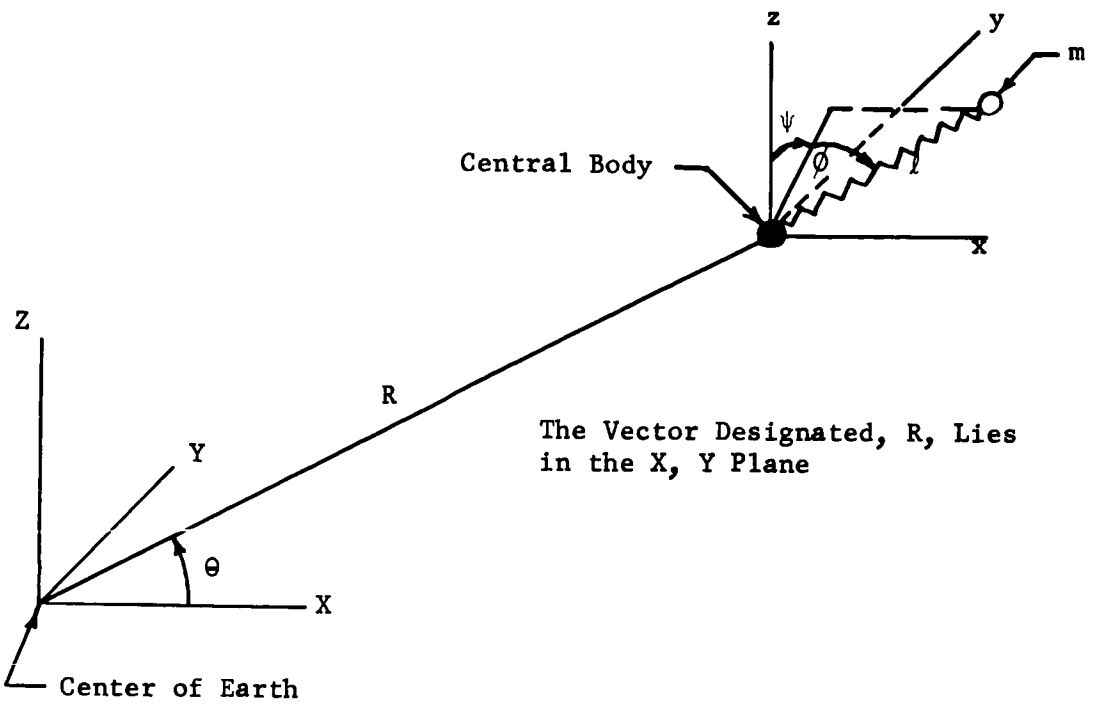

Figure 3 - Coordinate System for Motion Out of Orbital Plane

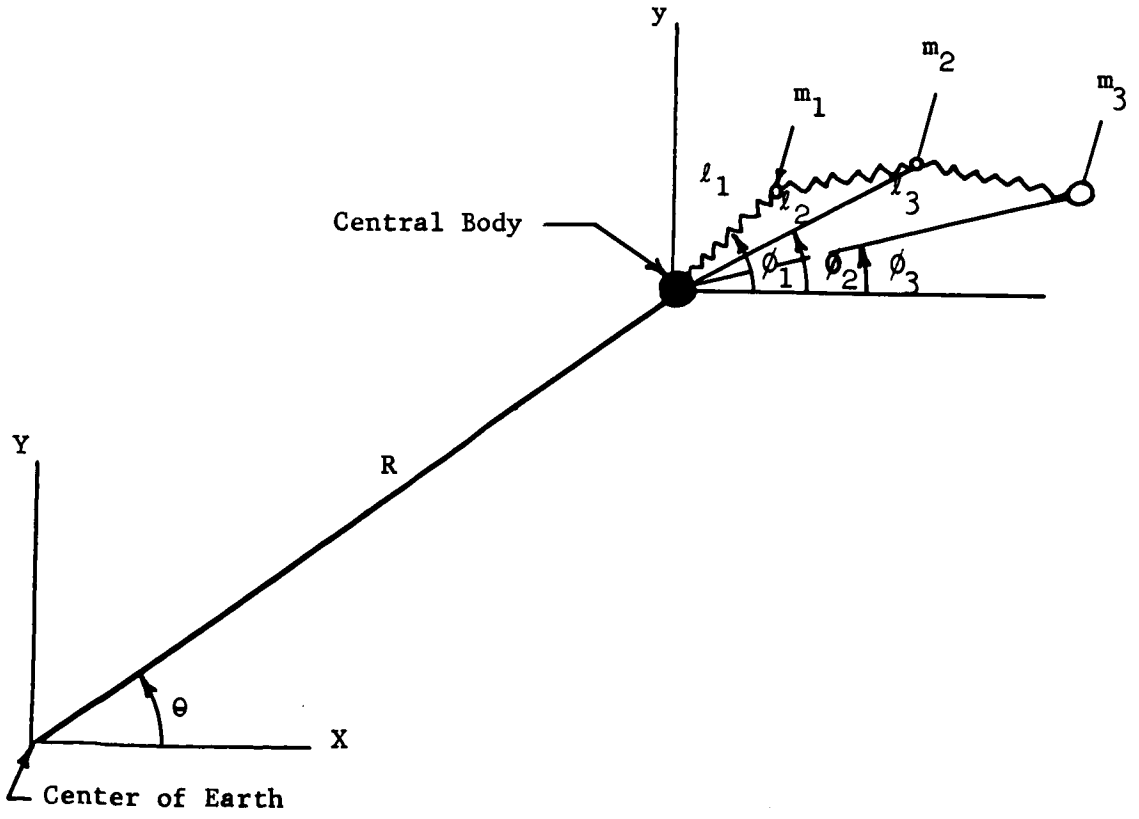

Figure 4 - Coordinate System for Motion in Orbital Plane for Multi-Mass Model

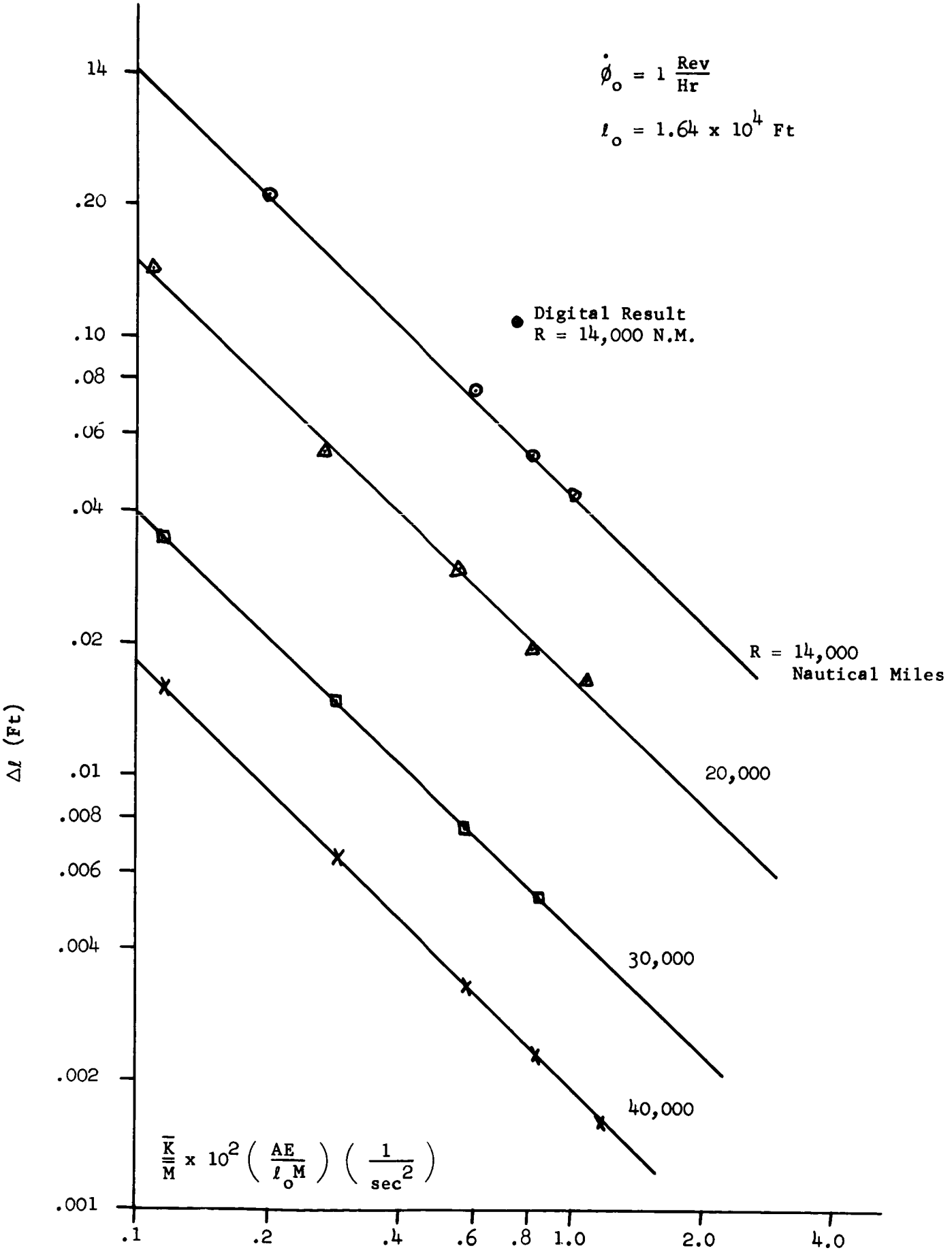

Figure 5 - Axial Deviation vs. Spring Stiffness (planar motion)

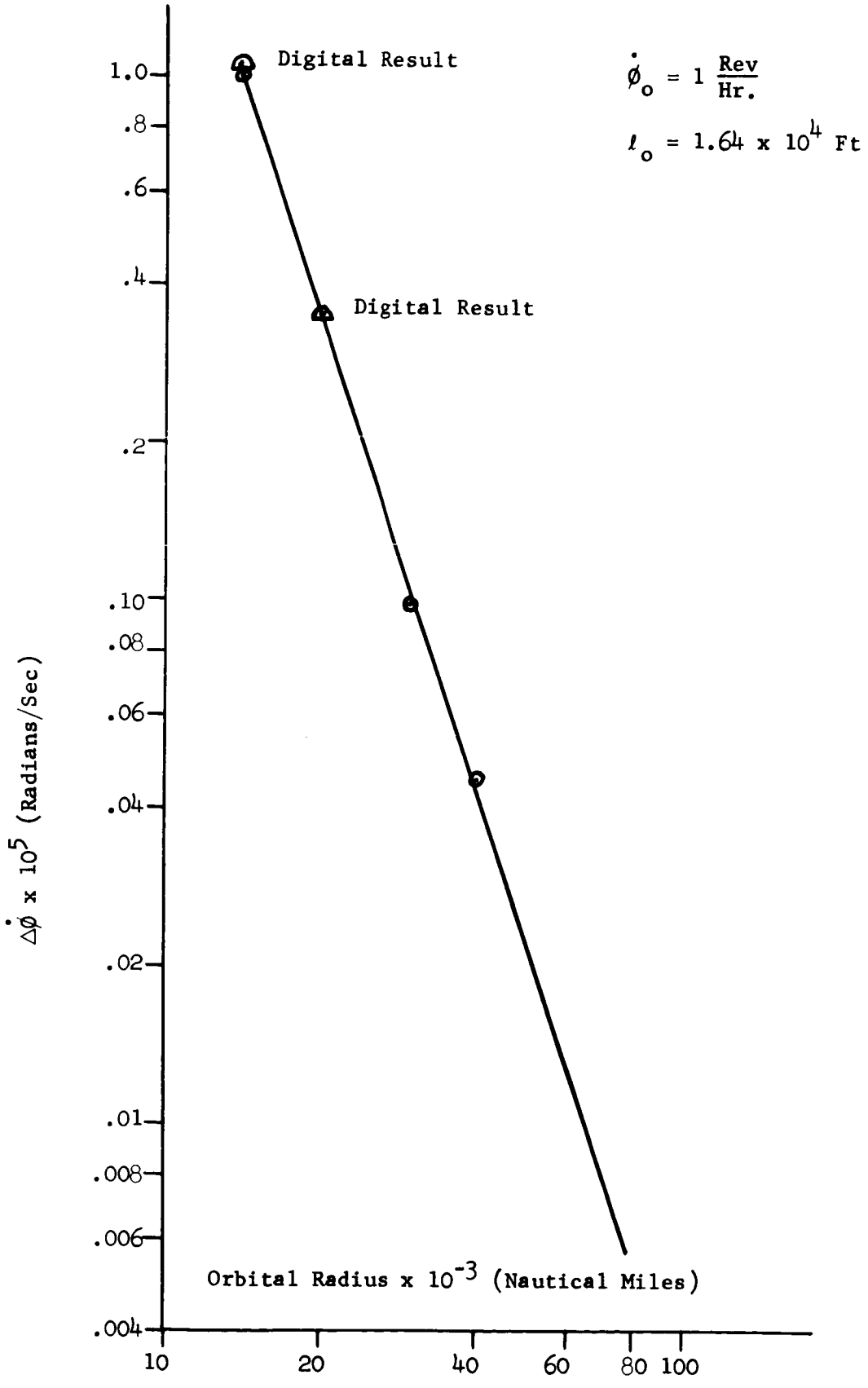

Figure 6 - Spin Rate Deviation vs. Orbital Radius (planar motion)

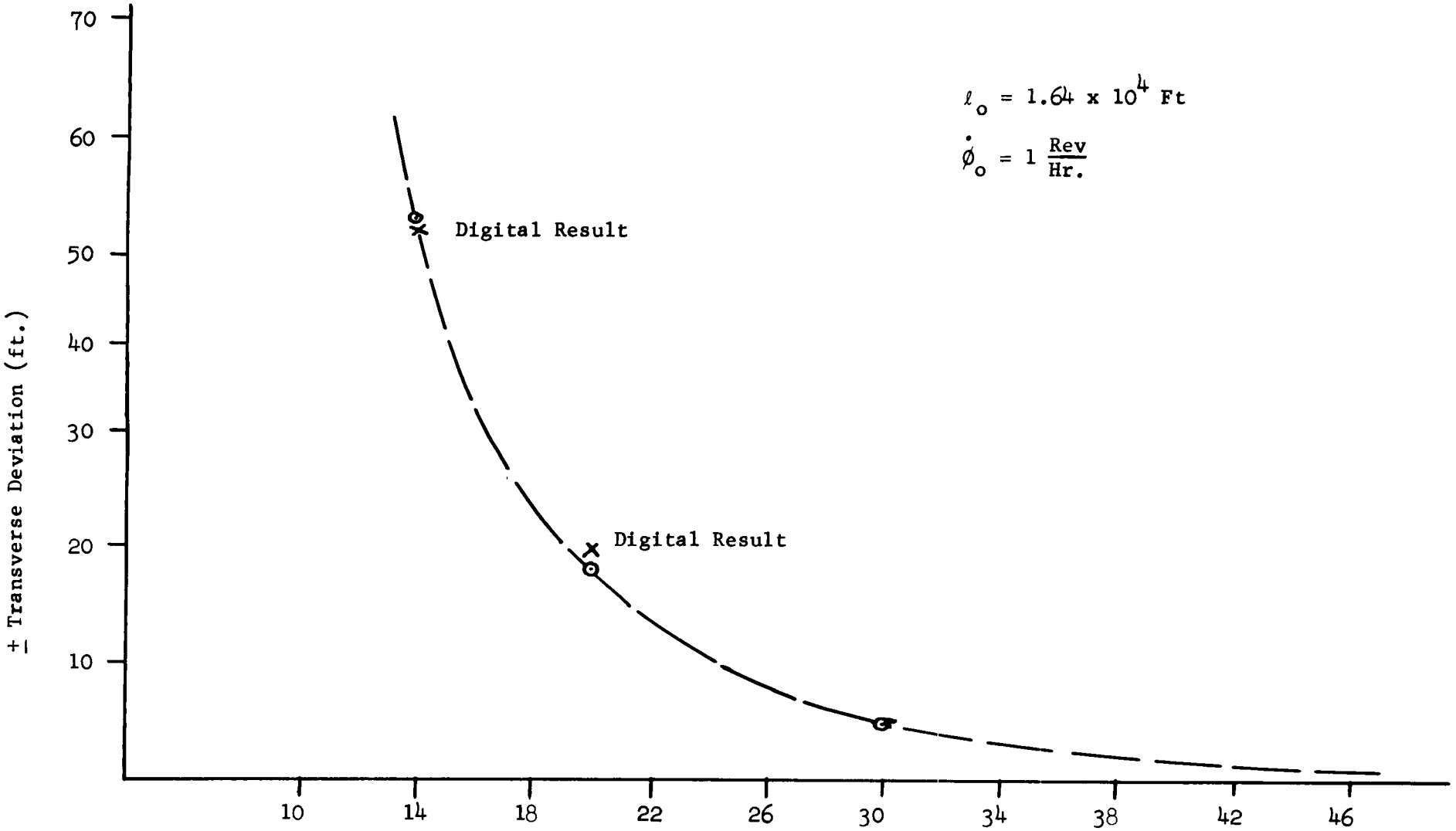

Figure 7 - Transverse Deviation vs. Orbital Radius (planar motion)

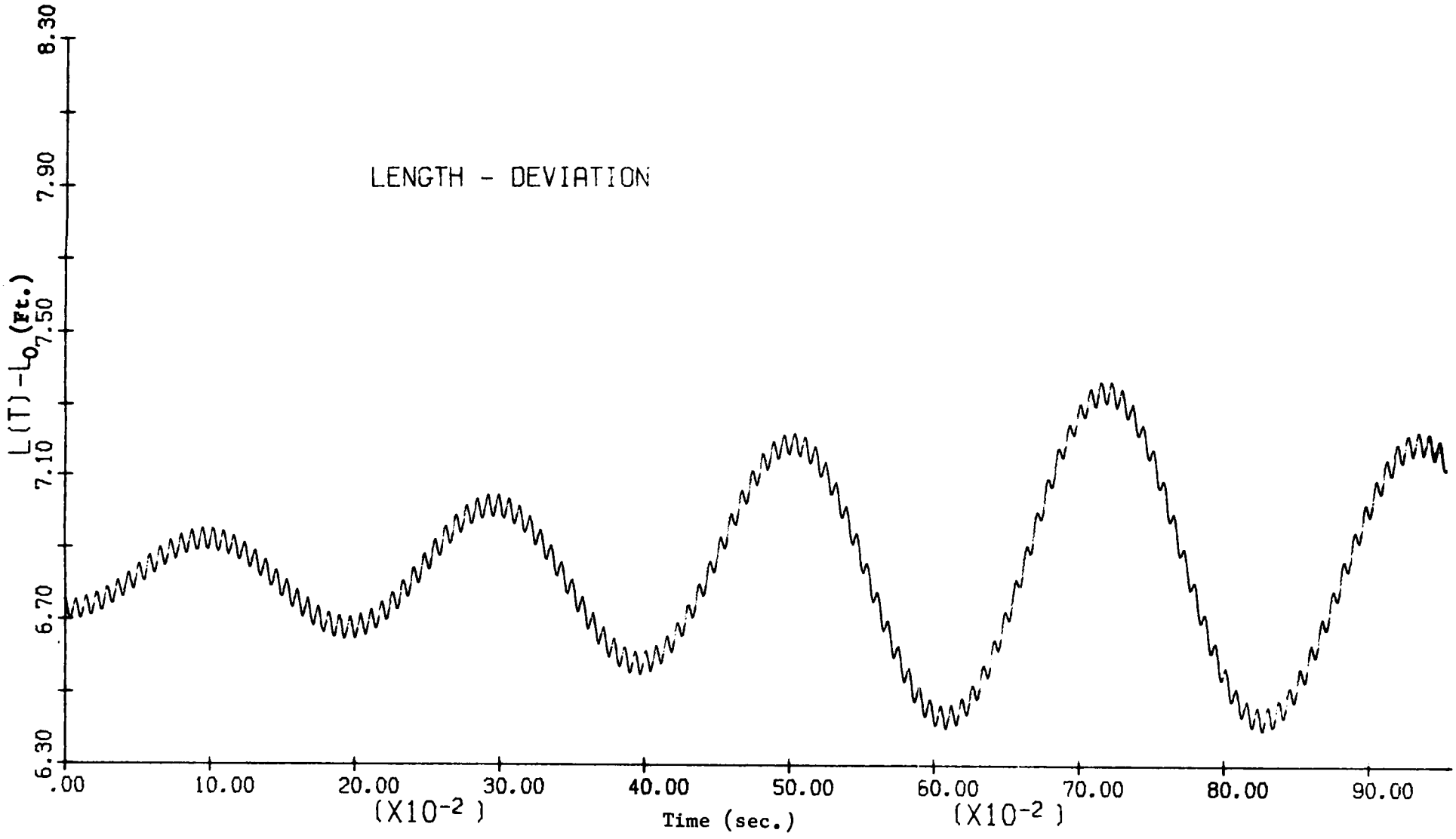

Figure 8 - Axial Deviation vs. Time, 10,000 x 60,000 N.M. (planar motion)

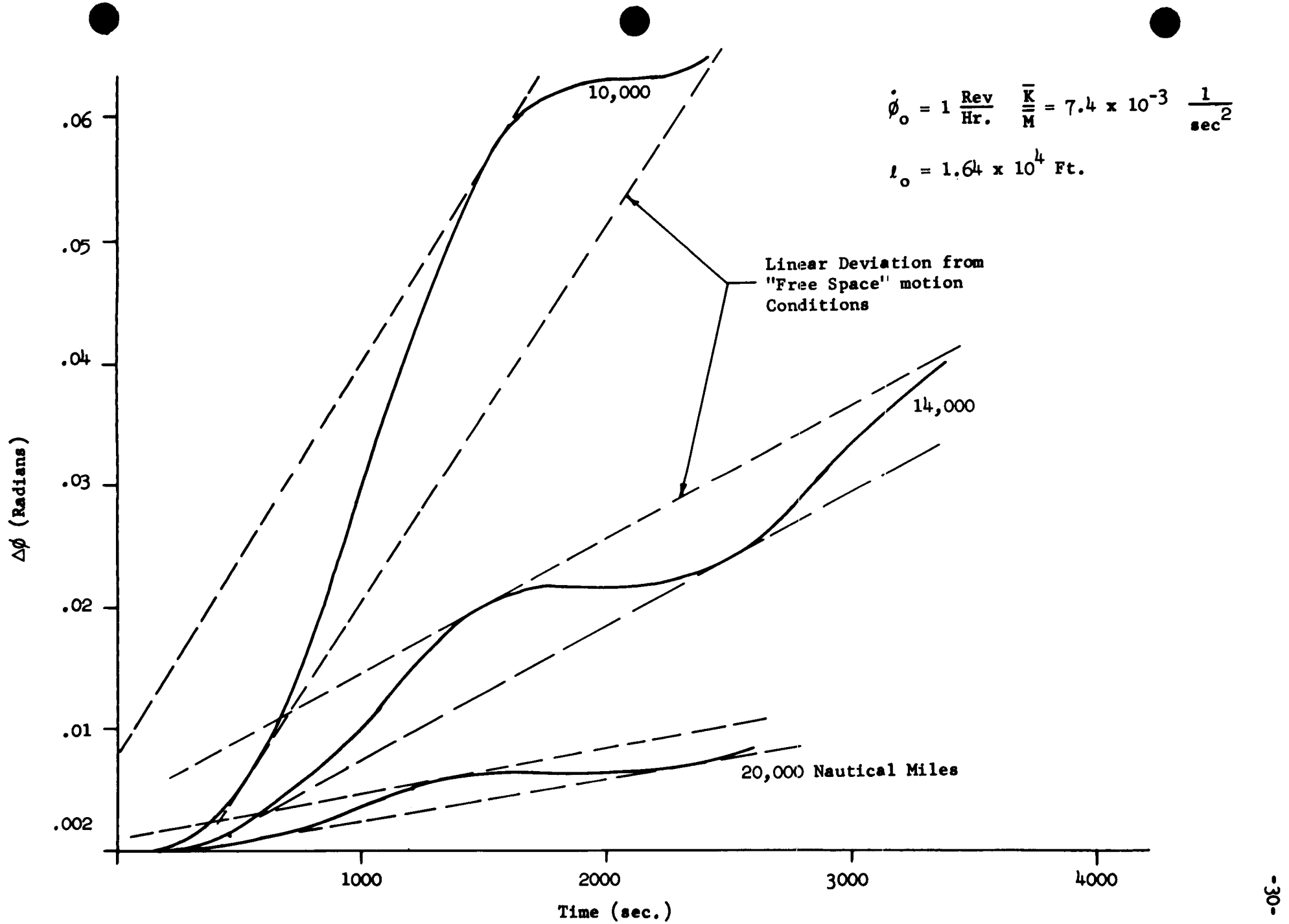

Figure 9 - Angular Deviation vs. Time, Circular Orbits (planar motion)

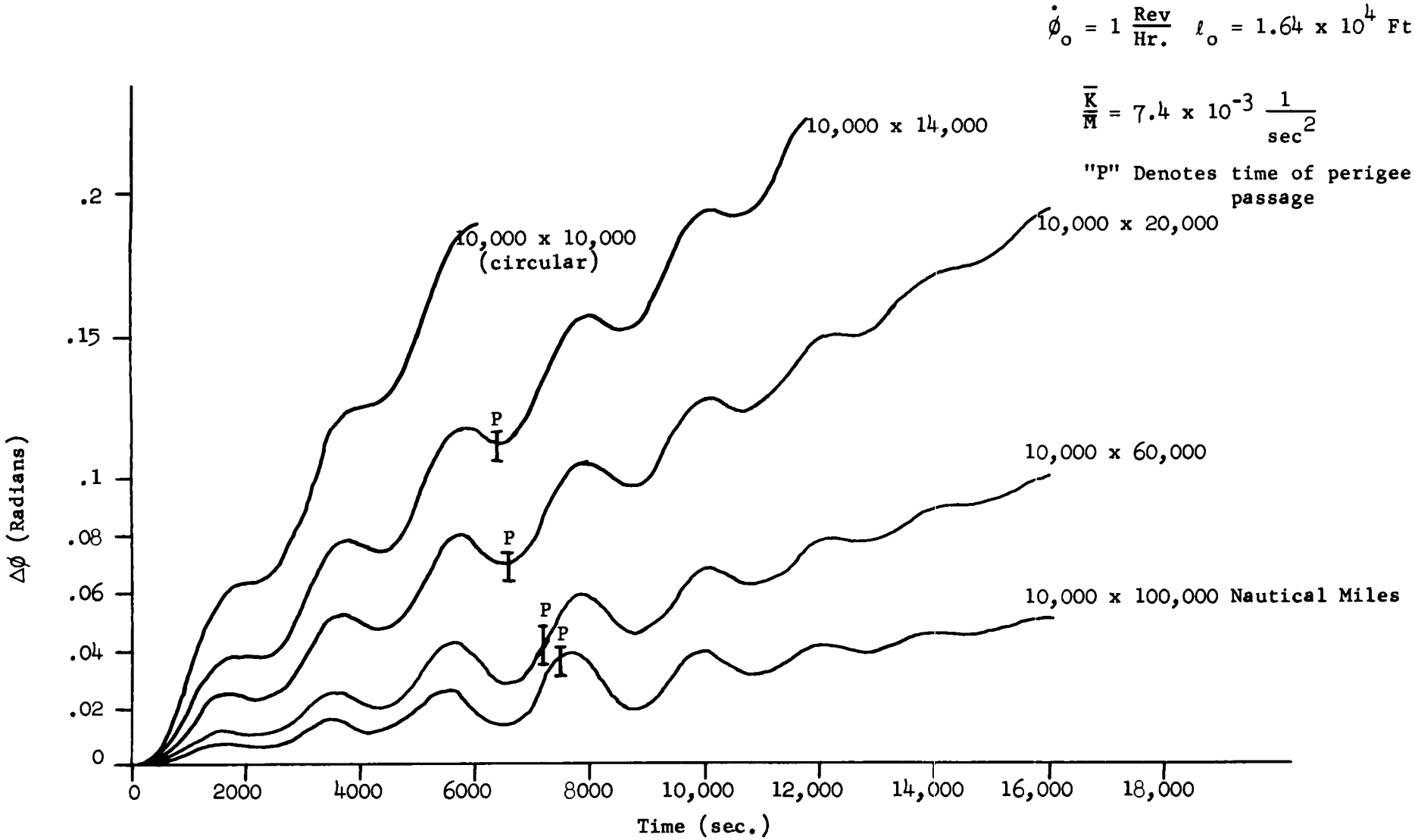

Figure 10 - Angular Deviation vs. Time, Eccentric Orbits (planar motion)

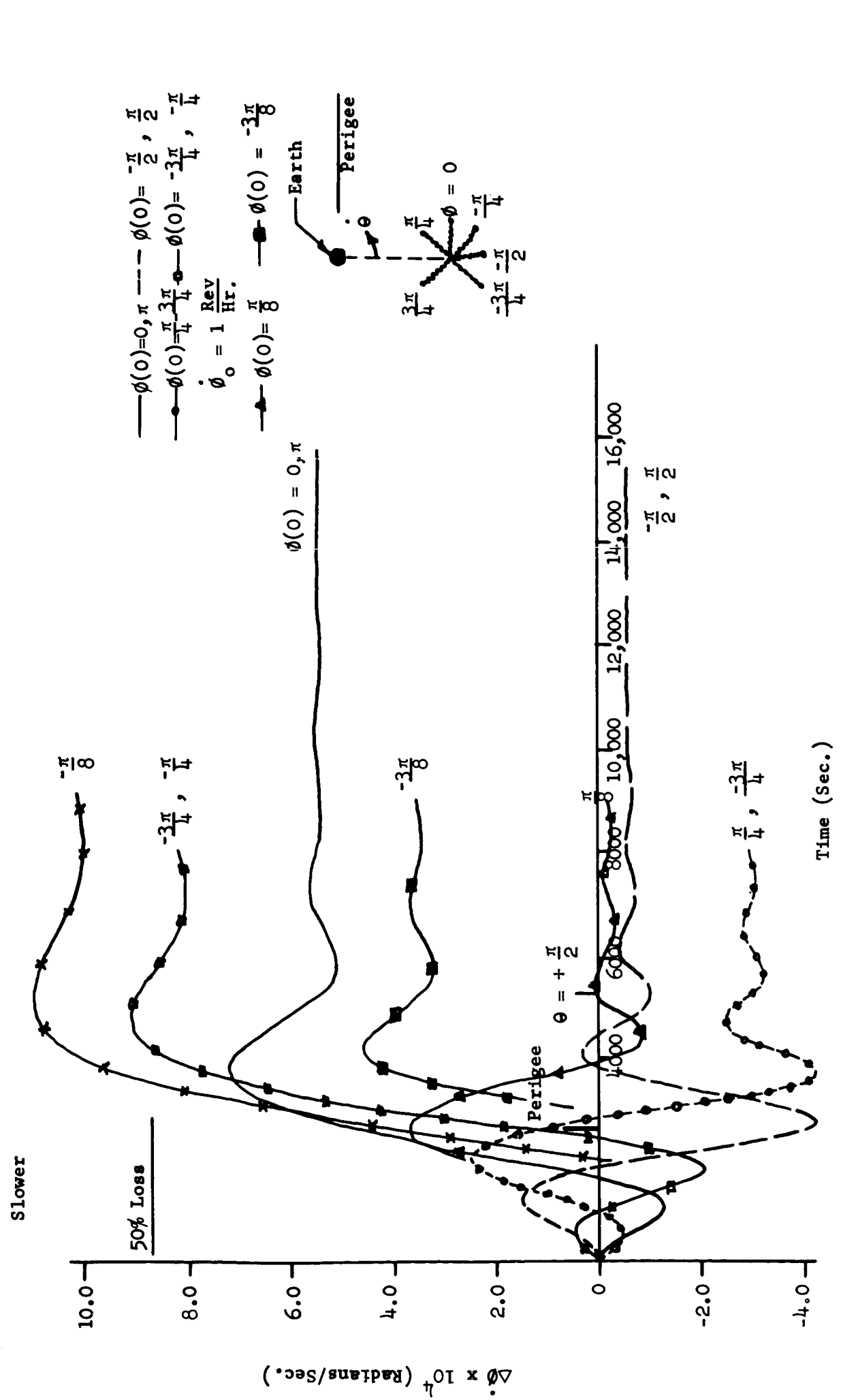

Figure 11 - Angular Rate Deviation vs. Time, 5,000 x 60,000 (plane motion)

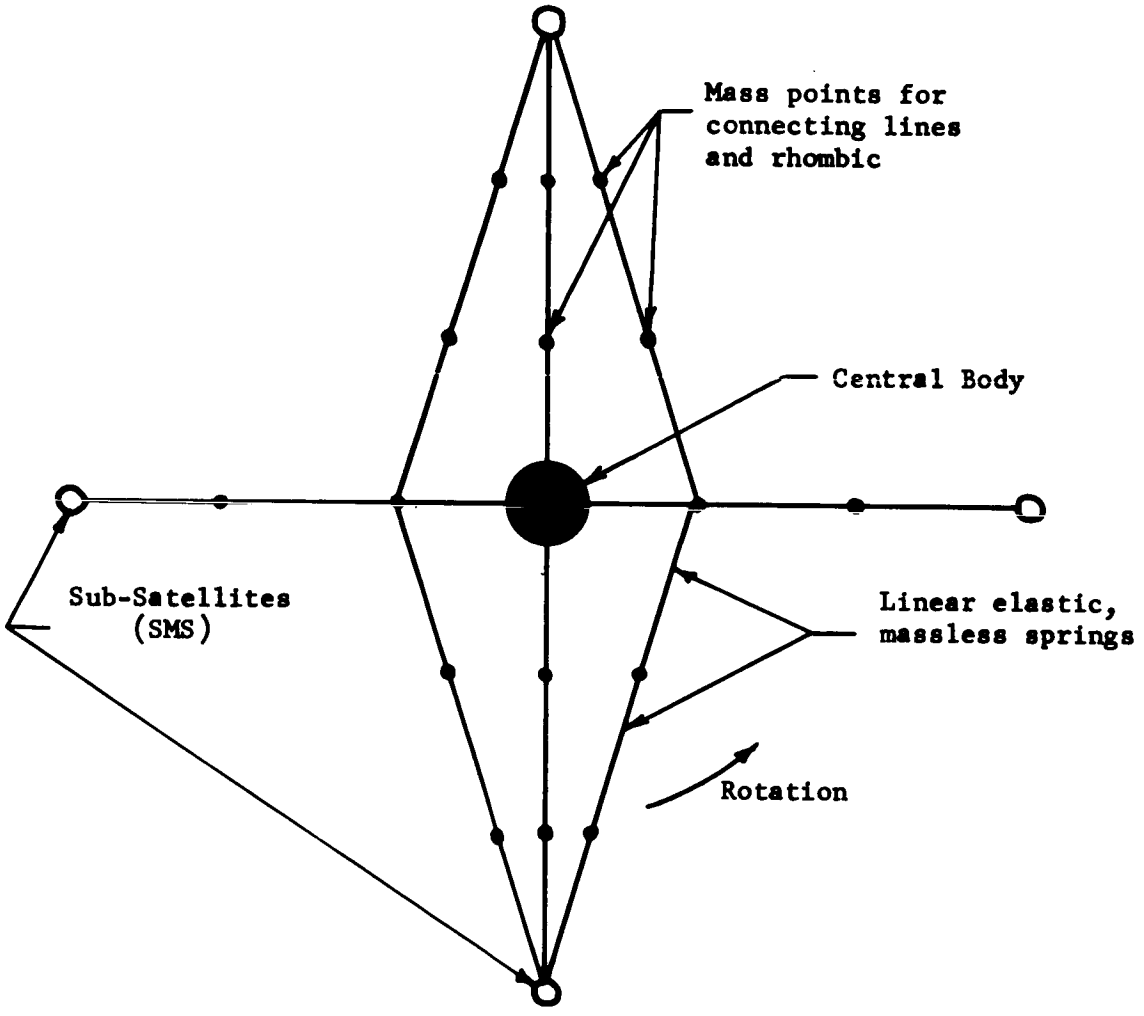

Figure 12 - Example of Complete Lumped Mass Model for KWOT Design Study (62 degrees of freedom)

BIBLIOGRAPHY

1. Garber, T. B., "A Preliminary Investigation of the Motion of a Long Flexible Wire in Orbit", RAND Rep. RM-2705-ARPA, March 23, 1961.

2. Chobotov, V., "Gravity-Gradient Excitation of a Rotating Cable-Counterweight Space Station in Orbit", J. Appl. Mech. December 1963, pp. 547-554.

3. Pittman, D. L., Hall, B. M., "The Inherent Stability of Counterweight Cable Connected Space Stations", Douglas Paper No. 3051, Douglas Missile and Space Systems Division, July 1964.

4. Tai, C. L., Andrew, L. V., Loh, M. M. H., Kamrath, P. C., "Transient Dynamic Response of Orbiting Space Stations", U.S.A.F. Systems Command, Flight Dynamics Lab., TDR-64-25, May 1964.

5. Tai, C. L., Loh, M. M. H., "Planar Motion of a Rotating Cable-Connected Space Station in Orbit", J. Spacecraft, Vol. 2, No. 6, November-December 1965, pp. 889-894.

6. Pengelly, C. D., "Preliminary Survey of Dynamic Stability of a 'tassel concept' Space Station", AIAA Structural Dynamics and Aeroelasticity Symposium, August 1965.

7. Austin, F., "Nonlinear Dynamics of a Free-Rotating Flexibly Connected Double-Mass Space Station", J. Spacecraft, Vol. 2, No. 6, November-December 1965, pp. 901-906.

8. Targoff, W., "On the Lateral Vibration of Rotating, Orbiting Cables", AIAA Paper No. 66-98, January 25, 1966.

9. Green, J. W., "KWOT Dynamics", January 1966.

10. Ordway, D. E., "The Two-Dimensional Dumbbell Satellite", National Academy of Science, Air Research and Development Command, Special Study at Woods Hole, Mass. COMI-T25, August 1958.

11. Robinson, A. C., "On the Three-Dimensional Libration of a Dumbbell Shaped Satellite over a Oblate Earth", WCLJY, Internal Memo 58-54, Wright-Patterson Air Force Base, September 1958.

12. Moran, J. P., "The Effects of Plane Librations on the Orbital Motion of a Dumbbell Satellite", Therin Advanced Research, Inc., New York, TN603, August 1960.

13. Paul, B., "Planar Librations of an Extensible Dumbbell Satellite", AIAA J., Vol. 1, pp. 411-418, 1963.

14. Simmonds, J. G., "The In-Plane Vibrations of a Flat Spinning Disk", NASA TN D-521, December 1962.

15. Huston, R. L., "Wave Propagation in Rotating Elastic Media", AIAA J., Vol. 2, July 1964, pp. 575-576.

16. Kyser, A. C., "Uniform Stress Spinning Filamentary Disk", AIAA J., Vol. 3, No. 7, July 1965, pp. 1313-1316.

17. Huston, R. L., "In-Plane Vibration of Spinning Disks", AIAA J., Vol. 3, No. 8, August 1965, p. 1519.

18. Frick, R. H., Garber, T. B., "General Equations of Motion of Satellite in a Gravitational Field", RAND Rep. RM 2527, December 9, 1959.

19. Langer, R. M., "Mechanics of Flexible Lines", AIAA Paper No. 66-99, January 25, 1966.

20. Gluck, R., Gale, E. H., "Motion of a Spinning Satellite During the Deployment of N Asymmetrical Appendages", AIAA Paper No. 66-100, January 25, 1966.

21. Pringle, R., "On the Stability of a Body with Connected Moving Parts", AIAA Paper No. 66-101, January 25, 1966.

PA-66-U/M-1 CFR
15 July 1966

APPENDIX F

Final Report

FEASIBILITY STUDY ON THE DYNAMIC ANALYSIS OF A KILOMETER WAVE ORBITING TELESCOPE

Purchase Order No. R-67057

Radio Astronomy Observatory
University of Michigan
Ann Arbor, Michigan

Phoenix Associates Inc. 1211 Stewart Ave., Bethpage, N. Y.

ERRATA

Correct sequence of pages in Section II is: 1-38, 53,54,55,56,57, 39-52.

Page II-8 is deleted.

Page IV-33 line 6 should read: ---denoted by P andδ ---, add δ.

Page IV-33 Equation 4.3-1 should read $P=k\,\delta$.

Page IV-35 line 6 should read:---allowable δ displacement---, add δ.

Remove page IV-37 and add page IV-37R in its place.

Page IV-45 change equation 4.3-25 to read

$$-\omega^2 \begin{bmatrix} M & 0 & 0 & m_r & 0 \\ 0 & M & 0 & 0 & m_r \\ 0 & 0 & I & (-Z_m)_r & (Y_m)_r \\ m_c & 0 & (-Z_m)_c & m & 0 \\ 0 & m_c & (Y_m)_c & 0 & m \end{bmatrix} \begin{bmatrix} Y_o \\ Z_o \\ \phi_o \\ Y \\ Z \end{bmatrix} + \left[\begin{array}{c|cc} 0 & 0 & \\ \hline 0 & E_{YY} & E_{YZ} \\ & E_{ZY} & E_{ZZ} \end{array}\right] \begin{bmatrix} Y_o \\ Z_o \\ \phi_o \\ Y \\ Z \end{bmatrix} = [0]$$

Page IV-45 change equation 4.3-26 to read

$$-\omega^2 \begin{bmatrix} M & 0 & 0 \\ 0 & M & 0 \\ 0 & 0 & I \end{bmatrix} \begin{bmatrix} Y_o \\ Z_o \\ \phi_o \end{bmatrix} - \omega^2 \begin{bmatrix} m_r & 0 \\ 0 & m_r \\ (-Z_m)_r & (Y_m)_r \end{bmatrix} \begin{bmatrix} Y \\ Z \end{bmatrix} = [0]$$

$$\begin{bmatrix} Y_o \\ Z_o \\ \phi_o \end{bmatrix} = - \begin{bmatrix} M & 0 & 0 \\ 0 & M & 0 \\ 0 & 0 & I \end{bmatrix}^{-1} \begin{bmatrix} m_r & 0 \\ 0 & m_r \\ (-Z_m)_r & (Y_m)_r \end{bmatrix} \begin{bmatrix} Y \\ Z \end{bmatrix}$$

Thus

$$-\omega^2 \left\{ - \begin{bmatrix} m_c & 0 & (-Z_m)_c \\ 0 & m_c & (Y_m)_c \end{bmatrix} \begin{bmatrix} M & 0 & 0 \\ 0 & M & 0 \\ 0 & 0 & I \end{bmatrix}^{-1} \begin{bmatrix} m_c & 0 & (-Z_m)_c \\ 0 & m_c & (Y_m)_c \end{bmatrix}^T + \begin{bmatrix} m & 0 \\ 0 & m \end{bmatrix} \right\} \begin{bmatrix} Y \\ Z \end{bmatrix}$$

$$+ \begin{bmatrix} E_{YY} & E_{YZ} \\ E_{ZY} & E_{ZZ} \end{bmatrix} \begin{bmatrix} Y \\ Z \end{bmatrix} = [0]$$

ABSTRACT

This final report presents the results of the engineering feasibility study of the Dynamic Analysis of a Kilometer Wave Orbiting Telescope (KWOT). First order linearized analyses are presented for a planar structural model of KWOT. The control system dynamics are formulated in general and a control law defined for the main spacecraft as determined by the maneuver and orbital requirements. Disturbance torques are considered and their general effects presented. Results of various aspects of the structural dynamic characteristics of KWOT are analyzed and presented.

TABLE OF CONTENTS

TABLE OF CONTENTS (continued)

SECTION III

PRECESSION-SPIN DYNAMICS CONSIDERATIONS

TABLE OF CONTENTS (continued)

SECTION IV

EFFECTS OF EXTERNAL FORCES

SECTION V

LINEARIZED DEPLOYMENT CONSIDERATIONS

TABLE OF CONTENTS (continued)

SECTION I

INTRODUCTION

1.1 PURPOSE, OBJECTIVES AND SCOPE

The purpose of the engineering study presented in this report is to evaluate certain aspects of the feasibility of a Kilometer Wave Orbiting Telescope (KWOT). The KWOT was conceived by the University of Michigan Radio Astronomy Obeservatory as an instrument for mapping background missions and determining the radio spectra of discrete sources in the frequency band centered on 1 Mhz. The initial configuration used as a point of departure for this study consist of a central hub 20 feet in diameter by 50 feet in length, weighing 20,000 lbs., and four 100-lb. subsatellites deployed at a distance of 5 km. Interconnecting structure includes the elements of a rhombic antenna and two linear dipole arrays, as shown in Figure I-1. A scan of the entire celestial sphere is to be accomplished by a combination of spin and precession of the entire structure.

In this study, the conceptual model of the KWOT is used to develop the linearized dynamic equations needed for structural and control system determination. As a consequence of these equations and the maneuver requirements, the optimum mode of precessing the spin axis is seen to be that in which the precession rate is equal to the orbital angular velocity,

KWOT

Figure I-1.

such that the spin axis remains directed at the center of the earth. External sources of disturbance are evaluated and consideration is given to the effects of perturbations including those due to deployment and spin. A linearized evaluation of deployment parameters is given.

1.2 PROPOSED SYSTEM

The basic assumptions made for the study are summarized as follows:

Orbital Data:

Altitude: 60,000 km - circular orbit in equatorial plane.

Satellite Dimensions:

10 km by 15.24 m

Antenna Configurations:

Rhombic 10 km on major axis - 28° apex angle.

Spin Rate:

0.5 to 3 rph

Spin Axis Precession Rate:

0.1 to 1 revolution per orbit

Weight:

Central hub - 20,000 lbs.

Four subsatellites - 100 lb. each.

Hub Body Inertia

I_x (about spin axis)	6.2×10^4 slug-ft.^{2}
I_y, I_z	1.6×10^5 slug-ft.^{2}

1.3 SUMMARY OF SALIENT FEATURES

1.3.1 System Concept

A conceptual sketch of the deployed KWOT is shown in Figure I-1. By considering the mission requirements with respect to inertial space, the required coordinate systems are defined, and the equations of motion of the antenna and its support system are derived. The circular equatorial orbit considered for this study functionally defined the maneuver requirements for a 6° antenna beam width and a 3° overlap per spin rotation, the required spin rate being 120 times the precession rate. The use of the circular orbit, at this time, enables system definition in terms of mission requirements, and qualitative calculations of the system characteristics.

Since KWOT is a large system which must function under various orientations, it was decided in the early stages of the study to concentrate on defining an active control system while considering only briefly a passive control concept. However, the requirement for stability under either active or passive control is that KWOT spin about an axis of maximum inertia. The control concept simply stated, is to use the central hub as the orbit reference and to control the subsatellites relative to the central hub dynamics.

1.3.2 Dynamic Equations

The structural, structural dynamic and KWOT dynamic equations used in this feasibility study were derived and are

presented in Section II. The dynamic system is formulated in six "rigid-body" degrees of freedom plus translational motion of the various components of the satellite with respect to the cylindrical center body. By linearizing the equations of the KWOT model it was possible to perform the necessary small deflection theory stress analysis for the preliminary design of the antenna and support structure.

1.3.3 Control System

In considering the question of KWOT position and attitude control, the greatest attention was given to an active rather than a passive type of control system. A basic concept for the latter type was evolved and is described in a qualitative manner; however, active control is more likely to produce an acceptable level of performance since it expands the tolerable limits of error in computed system dynamics. In addition, a requirement for active stability augmentation would necessitate the same studies; and a comparison of physical characteristics vs. performance levels will be of interest at the detailed design stage.

In defining the control law for the active system, the central hub is taken as the subsatellite position reference, and maneuver requirements are founded on the hub dynamics. A prominent feature emerging from each area of study is that the desirable mode of precession is that produced by maintaining the spin axis in alignment with a geocentric radial, i.e.,

by a precession rate equal to the orbital angular velocity. Open loop considerations for the hub control system include gravity gradient effect, spin stability, torquing methods, and parametric trade-off of spin rate, spin axis inertia, precession and required control torques. Orbital position control (station keeping) of the hub was not considered since the necessary techniques are numerous and well-known.

The dynamic equations for subsatellite relative position control were derived and the required forces computed, for a worst-case condition in which the subsatellites are treated as free bodies requiring independent control. Subsatellite orientation control is expected to follow the design of the hub attitude controller with appropriate simplifications.

1.3.4 External Forces

The effects of solar electromagnetic radiation, gravity gradient, magnetic moment, meteoroids and solar flare particles on KWOT were considered and numerical values were derived. Various aspects of the structural dynamic characteristics of KWOT were investigated under certain simplifying assumptions. The constraints on deployment velocity and the cable sag due to centrifugal force were analyzed in terms of the structural characteristics. The frequencies of the normal modes of lateral vibration of the cables in response to an external disturbance of the structure are given. The response of the extremely flexible KWOT structure to the complete perturbation environment was

not considered since a computerized study is required.

1.3.5 Deployment

Certain elements of desirable deployment operations follow naturally from control system and structural requirements, especially the optimum deployment orientation and maximum deployment velocity. A parametric investigation of deployment rates and fuel consumption for self-ferrying operation of the subsatellites is given, together with parametric curves for subsatellite relative motion.

1.3.6 Out-of-Plane Structural Stability

Consideration was given to means of enhancing the out-of-plane stiffness of the KWOT system, and a preliminary design for a feasible structure was generated. At this time, external stiffening is not specifically recommended; the information generated during this study is presented as an appendix for possible future use.

SECTION II

DYNAMIC EQUATIONS

2.1 GENERAL

The general problem of analyzing a system depends upon the reference frame considered. Therefore in order to develop the dynamic equations used in the feasibility study and to precisely determine the manuever requirements which are implied by the mission requirements, appropriate coordinate systems must be defined at the outset. The first part of this section defines a coordinate system that is useful in studying a KWOT spacecraft which maneuvers in such a way as to cause an essentially body-fixed sensor to sweep out a spherical volume in some specified time.

A study of the feasibility of stabilizing and controlling a satellite with the degree of flexibility of the KWOT involves formidable problems in the fields of control system synthesis and structural dynamics.

Initial feasibility studies have necessitated a number of simplifications of the equations of motion of the satellite. Subsequent design studies however will take into account the effects of the numerous degrees of freedom chosen to represent the flexible excursions of the elements of the satellite system.

For this reason it was felt that the control system studies should be defined in two separate areas.

1. Dynamic equations for a control system which will generate the required precessions of a rigid body satellite having the same deployed shape as the actual satellite which is presented as the second part of this section, and

2. Further studies on a control system which will stabilize the flexible satellite and maintain the shape of the rhombic antenna within specified limits.

This part of the control system study necessitated a mathematical definition of the flexible satellite and it is this particular aspect of the total problem which is the subject of the third part of this section.

A structural model of KWOT was conceived for the purpose of this study. The underlying principle guiding the preliminary design effort was the desire to generate a structure which, although tenuous, would behave as nearly linearly as possible in response to forces. The development of the structural equations are presented in part four of this section.

2.2 COORDINATE SYSTEMS DEFINITION

In order to determine maneuver requirements which are implied by mission requirements, appropriate coordinate systems must be defined at the outset. This is required so that the above requirements may be stated with precision. The coordinate systems to be defined subsequently are based on the following assumed ground rules:

a) The spacecraft is to be spin stabilized.

b) The orbit considered is circular, earth-equatorial, and at an altitude of 60,000 km.

c) The spacecraft is to maneuver in such a way as to cause an essentially body-fixed sensor to sweep out a spherical volume in some specified time.

A sketch of the orbit-earth-sun geometry over the course of a year is presented in Figure 2.2-1.

Coordinate Sets

(1) Inertial Frame (Figure 2.2-2)

A preliminary inertial frame is first defined as follows:

$\underline{Z}_1'$ - A unit vector originating at the spacecraft c.g. and pointing in the direction of the first point in Aries.

$\underline{X}_1'$ - A unit vector normal to $\underline{Z}_1'$ and in the ecliptic.

EARTH YEARLY MOTION

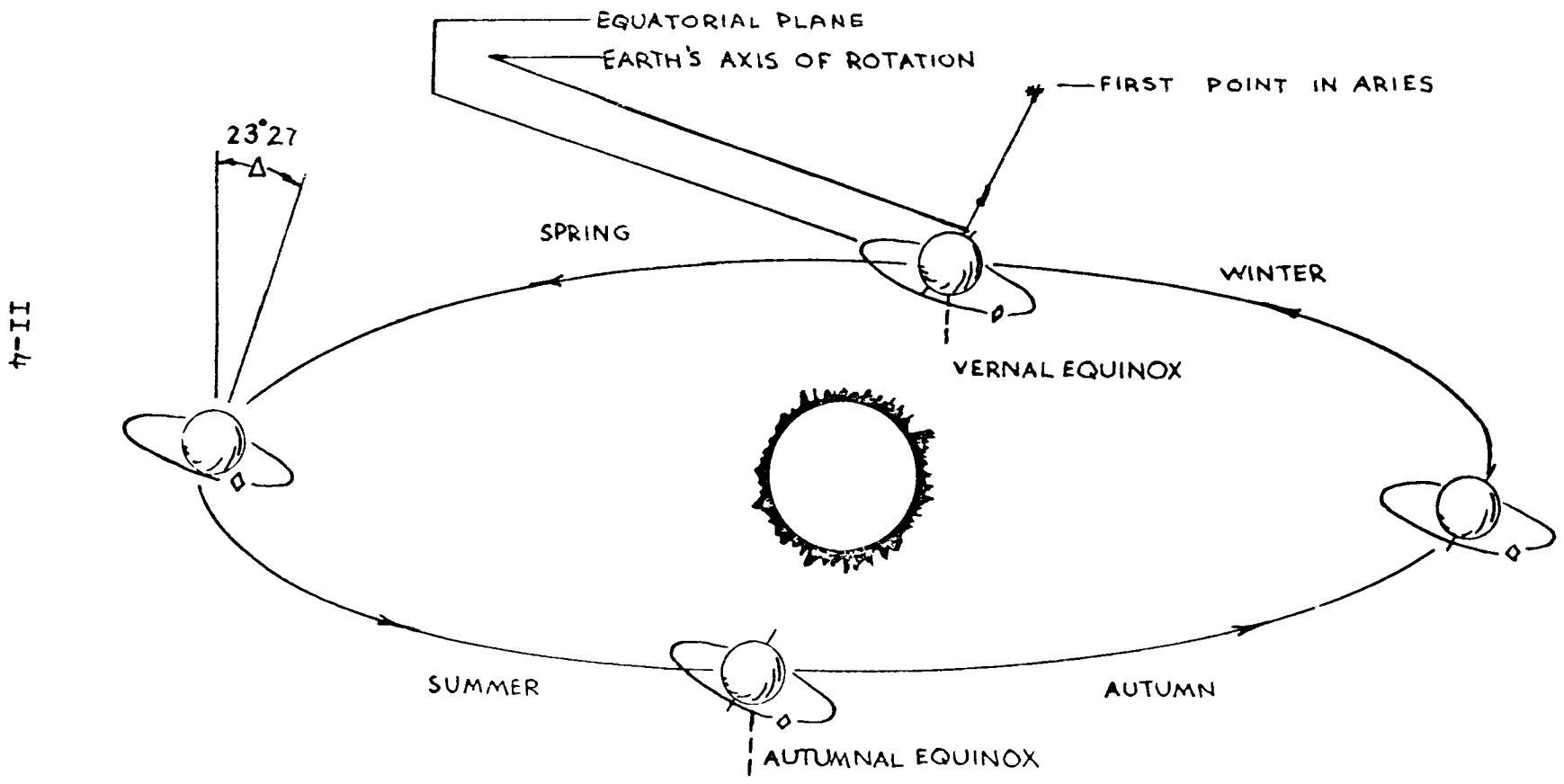

II-4

Figure 2.2-1

$\underline{Y}_1'$ - A unit vector in such a direction as to complete a right handed system.

(2) Primary Inertial Frame

The primary inertial frame may now be defined as that frame resulting from a positive rotation about the $\underline{Z}_1'$ axis through an angle $\Delta = 23^{\circ}27'$ so that the $\underline{X}_1$ axis lies in the equatorial plane. This primary inertial frame, shown in Figure 2.2-2, is defined as $\underline{X}_1$, $\underline{Y}_1$, $\underline{Z}_1$.

(3) Reference Frame (Figure 2.2-3)

A reference frame ($\underline{X}_r$, $\underline{Y}_r$, $\underline{Z}_r$) is defined with respect to the inertial frame. Both of these frames are shown in Figure 2.2-3. The reference frame is related to the inertial frame by two conventional Euler rotations. The first (yaw) rotation is about the $\underline{Z}_1$ axis through an angle ψ_r. The second (roll) rotation is about the displaced $\underline{X}_1$ axis through an angle ϕ_r. The reference frame is that frame which traces out the desired scan pattern with zero error, i.e., ψ_r and ϕ_r take on all values and their time derivatives $\dot{\psi}_r$ and $\dot{\phi}_r$ are constant.

(4) Body Frame (Figure 2.2-4)

The body axis frame is embedded in the spacecraft with its center at the nominal vehicle c.g. It is

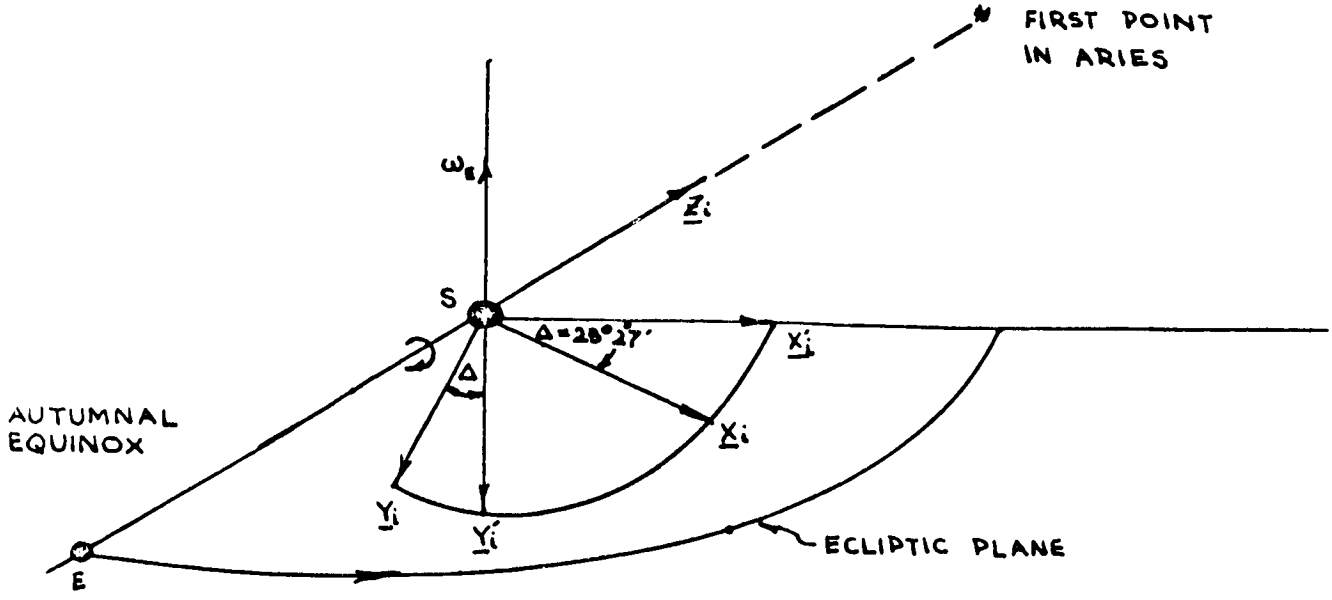

Figure 2.2-2

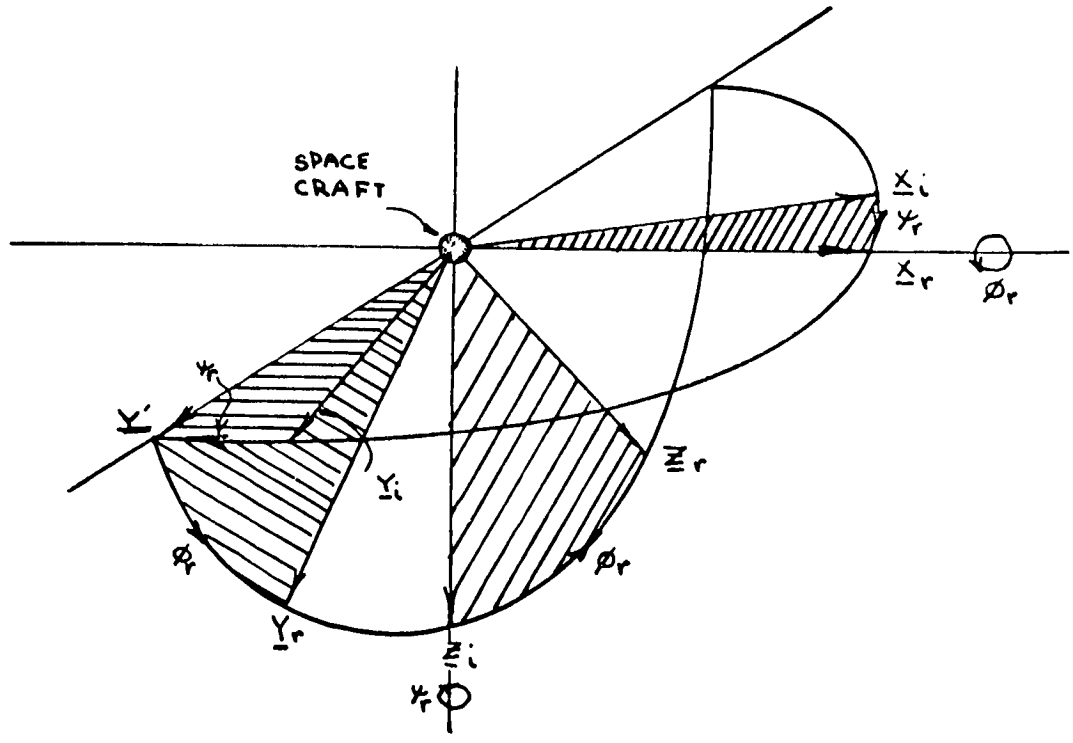

Figure 2.2-3

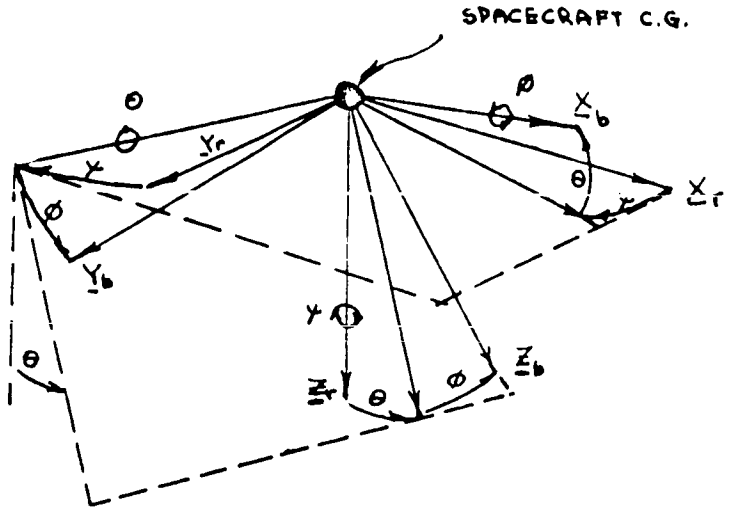

Figure 2.2-4

related to the reference frame by a conventional set of Euler rotations, i.e., the standard sequence of yaw-pitch-roll rotations is utilized. The pertinent geometry is defined in Figure 2.2-4 and the orientation of the satellite in the body frame is shown in Figure 2.2-1. The Euler angles ψ, θ, and ϕ therefore are error angles, the amount by which the satellite deviates from its desired position.

Transformation Matrices

The transformation of a vector quantity expressed in terms of one of the coordinate systems defined previously to another coordinate system is given by the relationships indicated diagrammatically in Figure 2.2-5. The subscript outside of the bracket indicates the instantaneous axis about which the rotation takes place. The signed quantity inside the bracket is the positive angle through which the coordinate set is rotated to reach the coordinate set, going in the direction indicated by the sense of the arrow. Reversal of direction is accompanied by a reversal of the quantity inside the brackets.

The matrices corresponding to these transformations in the direction indicated are given by

$$[\Delta]_{z_i'} = \begin{bmatrix} C\Delta & S\Delta & 0 \\ -S\Delta & C\Delta & 0 \\ 0 & 0 & 1 \end{bmatrix} \qquad (2.2\text{-}1)$$

$$[\psi_r]_{z_i} = \begin{bmatrix} C\psi_r & S\psi_r & 0 \\ -S\psi_r & C\psi_r & 0 \\ 0 & 0 & 1 \end{bmatrix} \qquad (2.2\text{-}2)$$

$$[\phi_r]_{x_r} = \begin{bmatrix} 1 & 0 & 0 \\ 0 & C\phi & S\phi \\ 0 & -S\phi & C\phi \end{bmatrix} \qquad (2.2\text{-}3)$$

$$[\psi]_{z_r} = \begin{bmatrix} C\psi & S\psi & 0 \\ -S\psi & C\psi & 0 \\ 0 & 0 & 1 \end{bmatrix} \qquad (2.2\text{-}4)$$

$$[\theta]_{y_c} = \begin{bmatrix} C\theta & 0 & -S\theta \\ 0 & 1 & 0 \\ S\theta & 0 & C\theta \end{bmatrix} \qquad (2.2\text{-}5)$$

$$[\phi]_{x_b} = \begin{bmatrix} 1 & 0 & 0 \\ 0 & C\phi & S\phi \\ 0 & -S\phi & C\phi \end{bmatrix} \qquad (2.2\text{-}6)$$

where

$Sx = \sin x$ and $Cx = \cos x$

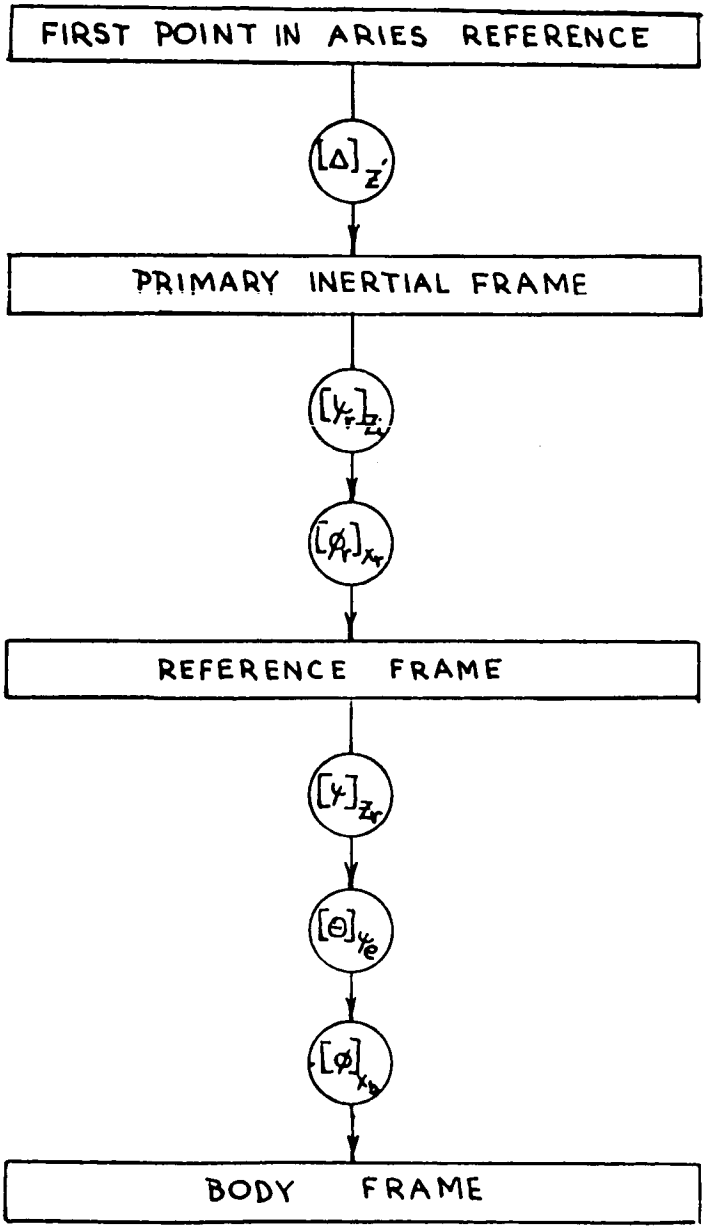

Figure 2.2-5 Schematic Representation of Coordinate Transformation.

2.3 CONTROL SYSTEM EQUATIONS

Main Spacecraft Equations of Motion

The purpose of this section is to develop the equations of motion for the main spacecraft and to examine these equations so as to determine, on a preliminary basis, the simplifications which are permissible.

It is well known that the equations of motion of a rigid body may be written in the form:

(2.3-1)

$$\underline{T}_{(\omega)b} = \begin{bmatrix} T_x \\ T_y \\ T_z \end{bmatrix} = \begin{bmatrix} I_x & -I_{xy} & -I_{xz} \\ -I_{xy} & I_y & -I_{yz} \\ -I_{xz} & -I_{yz} & I_z \end{bmatrix} \begin{bmatrix} \dot{\omega}_x \\ \dot{\omega}_y \\ \dot{\omega}_z \end{bmatrix} + \begin{bmatrix} 0 & -I_{yz} & I_{yz} \\ I_{xz} & 0 & -I_{xz} \\ -I_{xy} & I_{xy} & 0 \end{bmatrix} \begin{bmatrix} \omega_x^2 \\ \omega_y^2 \\ \omega_z^2 \end{bmatrix} + \begin{bmatrix} -I_{xz} & \Delta I_{zy} & I_{xy} \\ I_{yz} & -I_{xy} & \Delta I_{xz} \\ \Delta I_{yz} & I_{xz} & -I_{yz} \end{bmatrix} \begin{bmatrix} \omega_x \omega_y \\ \omega_y \omega_z \\ \omega_z \omega_x \end{bmatrix}$$

Where:

$\begin{pmatrix} T_x \\ T_y \\ T_z \end{pmatrix} = \underline{T}_{(\omega)_b}$ = torque about point "o" fixed in the body, expressed in body coordinates

$\begin{pmatrix} \omega_x \\ \omega_y \\ \omega_z \end{pmatrix} = \underline{\omega}_{(b)_b}$ = angular velocity of the body (b) frame with respect to an inertial frame as seen in the body axis system and expressed in body coordinates.

Considering the main spacecraft geometry and the desire to spin the vehicle about its $\underline{X}_b$ axis, the following simplifying assumptions are made:

$$I_x > I_y, I_z$$

$$I_y \approx I_z \quad (\Delta I_{zy} = 0)$$

In addition it is assumed that the mass is distributed in the main spacecraft in such a way that the products of inertia with respect to the chosen orthogonal body axis vanish. With these assumptions Equation 2.3-1 may be rewritten:

(2.3-2)

$$\begin{bmatrix} T_x \\ T_y \\ T_z \end{bmatrix} = \begin{bmatrix} I_x & 0 & 0 \\ 0 & I_y & 0 \\ 0 & 0 & I_z \end{bmatrix} \begin{bmatrix} \dot{\omega}_x \\ \dot{\omega}_y \\ \dot{\omega}_z \end{bmatrix} + \begin{bmatrix} 0 & 0 & 0 \\ 0 & 0 & \Delta I_{xz} \\ \Delta I_{yx} & 0 & 0 \end{bmatrix} \begin{bmatrix} \omega_x \omega_y \\ \omega_y \omega_z \\ \omega_z \omega_x \end{bmatrix}$$

The next step in the analysis is the evaluation of $\underline{\omega}_{(bi)_b}$ This angular velocity may be written as:

(2.3-3)

$$\underline{\omega}_{(bi)_b} = \underline{\omega}_{(br)_b} + \underline{\omega}_{(ri)_b}$$

where:

$\underline{\omega}_{(ri)_b}$ = angular velocity of the reference (r) frame with respect to the inertial (i) frame expressed in body coordinates.

$\underline{\omega}_{(br)_b}$ = angular velocity of the body (b) frame with respect to the reference frame expressed in body coordinates.

Equation 2.3-3 may be rewritten in expanded form as:

$$\underline{\omega}_{(bi)b} = Q_{eb}[\underline{\omega}_{(br)e}] + Q_{rb}[\underline{\omega}_{(ri)r}] \qquad (2.3\text{-}4)$$

$$= Q_{eb}[\underline{\omega}_{(br)e}] + Q_{rb}Q_{er}[\underline{\omega}_{(ri)e'}]$$

where, from the definitions of coordinate frames previously given:

(2.3-5)

$$\underline{\omega}_{(br)e} = \begin{bmatrix} \dot{\phi} \\ \dot{\theta} \\ \dot{\psi} \end{bmatrix} \quad , \quad \underline{\omega}_{(ri)e'} = \begin{bmatrix} \dot{\phi}_r \\ 0 \\ \dot{\psi}_r \end{bmatrix}$$

Letting S = Sine

C = Cosine

The transformation matrices may be written:

(2.3-6)

$$Q_{eb} = \begin{bmatrix} 1 & 0 & -S_\theta \\ 0 & C_\phi & S_\phi C_\theta \\ 0 & -S_\phi & C_\phi C_\theta \end{bmatrix}$$

$$Q_{er} = \begin{bmatrix} 1 & 0 & 0 \\ 0 & C_{\phi_r} & S\phi_r \\ 0 & -S\phi_r & C\phi_r \end{bmatrix}$$

$$Q_{rb} = \begin{bmatrix} C_\theta C_\psi & C_\theta S_\psi & -S_\theta \\ S_\phi S_\theta C_\psi - C_\phi S_\psi & C_\phi C_\psi + S_\phi S_\theta S_\psi & S_\phi C_\theta \\ S_\phi S_\psi + C_\phi S_\theta C_\psi & C_\phi S_\theta S_\psi - S_\phi C_\psi & C_\phi C_\theta \end{bmatrix}$$

Substituting Equations 2.3-5 and 2.3-6 into 2.3-4:

(2.3-7)

$$\omega_{(b/i)_b} = \begin{bmatrix} C_\theta C_\psi \dot{\phi}_r + (C_\theta S_\psi S_{\phi_r} - S_\theta C_{\phi_r})\dot{\psi}_r + \dot{\phi} - S_\theta \dot{\psi} \\ (S_\phi S_\theta C_\psi - C_\phi S_\psi)\dot{\phi}_r + [(C_\phi C_\psi + S_\phi S_\theta S_\psi)S_{\phi_r} + S_\phi C_\theta C_{\phi_r}]\dot{\psi}_r + C_\phi \dot{\theta} + S_\phi C_\theta \dot{\psi} \\ (S_\phi S_\psi + C_\phi S_\theta C_\psi)\dot{\phi}_r + [(C_\phi S_\theta S_\psi - S_\phi C_\psi)S_{\phi_r} + C_\phi C_\theta C_{\phi_r}]\dot{\psi}_r - S_\phi \dot{\theta} + C_\phi C_\theta \dot{\psi} \end{bmatrix}$$

The time derivative of Equation 2.3-7, as seen in the body frame is:

(2.3-8)

$$\mathring{\omega}_{(b/i)_b} = \begin{bmatrix} -(C_\theta S_\psi \dot{\psi} + S_\theta \dot{\theta} C_\psi)\dot{\phi}_r + [(C_\theta C_\psi \dot{\psi} - S_\theta \dot{\theta} S_\psi)S_{\phi_r} + C_\theta S_\psi \dot{\phi}_r C_{\phi_r} + S_\theta \dot{\phi}_r S_{\phi_r} - C_\theta \dot{\theta} C_{\phi_r}]\dot{\psi}_r \\ \quad + \ddot{\phi} - S_\theta \ddot{\psi} - C_\theta \dot{\theta}\dot{\psi} \\ [(S_\phi C_\theta \dot{\theta} + C_\phi \dot{\phi} S_\theta)C_\psi - S_\phi S_\theta S_\psi \dot{\psi} + S_\phi \dot{\phi} S_\psi - C_\phi C_\psi \dot{\psi}]\dot{\phi}_r + \{[-C_\phi S_\psi \dot{\psi} - S_\phi \dot{\phi} C_\psi + (S_\phi C_\theta \dot{\theta} + C_\phi \dot{\phi} S_\theta)S_\psi \\ \quad + S_\phi S_\theta C_\psi \dot{\psi}]S_{\phi_r} + (C_\phi C_\psi + S_\phi S_\theta S_\psi)\dot{\phi}_r C_{\phi_r} + (C_\phi \dot{\phi} C_\theta - S_\phi S_\theta \dot{\theta})C_{\phi_r} - S_\phi C_\theta S_{\phi_r}\dot{\phi}_r\}\dot{\psi}_r \\ \quad + C_\phi \ddot{\theta} - S_\phi \dot{\phi}\dot{\theta} + (C_\phi \dot{\phi} C_\theta - S_\phi S_\theta \dot{\theta})\dot{\psi} + S_\phi C_\theta \ddot{\psi} \\ [S_\phi C_\psi \dot{\psi} + C_\phi \dot{\phi} S_\psi + (C_\phi C_\theta \dot{\theta} - S_\phi \dot{\phi} S_\theta)C_\psi - C_\phi S_\theta S_\psi \dot{\psi}]\dot{\phi}_r + \{[(C_\phi C_\theta \theta - S_\phi \dot{\phi} S_\theta)S_\psi + C_\phi S_\theta C_\psi \dot{\psi} \\ \quad + S_\phi S_\psi \dot{\psi} - C_\phi \dot{\phi} C_\psi]S_{\phi_r} + (C_\phi S_\theta S_\psi - S_\phi C_\psi)\dot{\phi}_r C_{\phi_r} - (S_\phi \dot{\phi} C_\theta + C_\phi \dot{\theta} S_\theta)C_{\phi_r} \\ \quad - C_\phi C_\theta \dot{\phi}_r S_{\phi_r}\}\dot{\psi}_r - S_\phi \ddot{\theta} - C_\phi \dot{\phi}\dot{\theta} + (-C_\phi S_\theta \dot{\theta} - S_\phi \dot{\phi} C_\theta)\dot{\psi} + C_\phi C_\theta \ddot{\psi} \end{bmatrix}$$

For the proper operation of the control system, angles ψ, ϕ and θ remain small. Hence, a considerable simplification can be effected by making appropriate approximations to the above expressions. Equations 2.3-7 and 2.3-8 may be reduced to:

$$\underline{\omega}_{(bi)_b} = \begin{bmatrix} \dot{\phi}_r + (\psi S_{\phi_r} - \theta C_{\phi_r})\dot{\psi}_r + \dot{\phi} - \theta\dot{\psi} \\ (\phi\theta - \psi)\dot{\phi}_r + [(1 - \phi\theta\psi)S_{\phi_r} + \phi C_{\phi_r}]\dot{\psi}_r + \dot{\theta} + \phi\dot{\psi} \\ (\phi\psi + \theta)\dot{\phi}_r + [(\theta\psi - \phi)S_{\phi_r} + C_{\phi_r}]\dot{\psi}_r - \phi\dot{\theta} + \dot{\psi} \end{bmatrix} \qquad (2.3\text{-}9)$$

$$\dot{\underline{\omega}}_{(bi)_b} = \begin{bmatrix} -(\psi\dot{\psi} + \theta\dot{\theta})\dot{\phi}_r + [(\dot{\psi} - \theta\dot{\theta}\psi)S_{\phi_r} + \psi\dot{\phi}_r C_{\phi_r} + \theta\dot{\phi}_r S_{\phi_r} - \dot{\theta}C_{\phi_r}]\dot{\psi}_r + \ddot{\phi} - \theta\ddot{\psi} - \dot{\theta}\dot{\psi} \\ [(\phi\dot{\theta} + \dot{\phi}\theta) - \phi\theta\psi\dot{\psi} - \dot{\psi}\psi + \phi\dot{\phi}\psi]\dot{\phi}_r + \{[-\psi\dot{\psi} - \phi\dot{\phi} + (\phi\dot{\theta} + \dot{\phi}\theta)\psi + \phi\theta\dot{\psi}]S_{\phi_r} \\ \quad + (1 + \phi\theta\psi)\dot{\phi}_r C_{\phi_r} + (\dot{\phi} - \phi\theta\dot{\theta})C_{\phi_r} - \phi S_{\phi_r}\dot{\phi}_r\}\dot{\psi}_r + \ddot{\theta} - \phi\dot{\phi}\dot{\theta} \\ \quad + (\dot{\phi} - \phi\theta\dot{\theta})\dot{\psi} + \phi\ddot{\psi} \\ [\phi\dot{\psi} + \dot{\phi}\psi + (\dot{\theta} - \phi\dot{\phi}\theta) - \theta\psi\dot{\psi}]\dot{\phi}_r + \{[(\dot{\theta} - \phi\dot{\phi}\theta)\psi + \theta\dot{\psi} + \phi\psi\dot{\psi} - \dot{\phi}]S_{\phi_r} \\ \quad + (\theta\psi - \phi)\dot{\phi}_r C_{\phi_r} - (\phi\dot{\phi} + \theta\dot{\theta})C_{\phi_r} - \dot{\phi}_r S_{\phi_r}\}\dot{\psi}_r - \phi\ddot{\theta} - \dot{\phi}\dot{\theta} \\ \quad - (\theta\dot{\theta} + \phi\dot{\phi})\dot{\psi} + \ddot{\psi} \end{bmatrix} \qquad (2.3\text{-}10)$$

If products of Euler rate and angles characterizing the main spacecraft matrix are ignored, Equation 2.3-10 may be simplified to the form:

$$\dot{\underline{\omega}}_{(bi)_b} = \begin{bmatrix} \dot{\psi}_r\dot{\psi}S_{\phi_r} + \dot{\psi}_r(\dot{\phi}_r\psi - \dot{\theta})C_{\phi_r} + \ddot{\phi} + \theta S_{\phi_r}\dot{\phi}_r\dot{\psi}_r \\ \dot{\psi}_r(\dot{\phi}_r + \dot{\phi})C_{\phi_r} - \dot{\psi}_r\dot{\phi}_r\phi S_{\phi_r} - \dot{\psi}\dot{\phi}_r + \ddot{\theta} \\ \dot{\theta}\dot{\phi}_r - \dot{\psi}_r(\dot{\phi} + \dot{\phi}_r)S_{\phi_r} - \dot{\phi}\dot{\psi}_r\phi C_{\phi_r} + \ddot{\psi} \end{bmatrix} = \begin{bmatrix} \dot{\omega}_x \\ \dot{\omega}_y \\ \dot{\omega}_z \end{bmatrix} \qquad (2.3\text{-}11)$$

Similarly, Equation 2.3-9 reduces to:

$$\underline{\omega}_{(bi)_b} = \begin{bmatrix} \dot{\psi}_r\psi S_{\phi_r} - \dot{\psi}_r\theta C_{\phi_r} + \dot{\phi}_r + \dot{\phi} \\ \dot{\psi}_r S_{\phi_r} + \dot{\psi}_r\phi C_{\phi_r} - \psi\phi_r + \dot{\theta} \\ \dot{\psi}_r C_{\phi_r} - \dot{\psi}_r\phi S_{\phi_r} + \theta\dot{\phi}_r + \dot{\psi} \end{bmatrix} = \begin{bmatrix} \omega_x \\ \omega_y \\ \omega_z \end{bmatrix} \qquad (2.3\text{-}12)$$

Substituting Equations 2.3-11 and 2.3-12 into Equation 2.3-2 yields the simplified equation of motion for the main spacecraft.

(2.3-13)

$$\begin{bmatrix} T_x \\ T_y \\ T_z \end{bmatrix} = \left[\begin{array}{c|c|c} I_x p^2 & I_x \dot{\psi}_r(-C_{\phi_r} p + \dot{\phi}_r S_{\phi_r}) & I_x \dot{\psi}_r(S_{\phi_r} p + \dot{\phi}_r C_{\phi_r}) \\ -(I_x+I_y-I_z)\dot{\psi}_r(-C_{\phi_r} p + \dot{\phi}_r S_{\phi_r}) & I_y p^2 + (I_x-I_z)(\dot{\phi}_r^2 - \dot{\psi}_r^2 C_{\phi_r}^2) & (I_x-I_y-I_z)\dot{\phi}_r p + (I_x-I_z)\dot{\psi}_r^2 C_{\phi_r} S_{\phi_r} \\ -(I_x-I_y+I_z)\dot{\psi}_r(S_{\phi_r} p + \dot{\phi}_r C_{\phi_r}) & -[(I_x-I_y-I_z)\dot{\phi}_r p + (-I_x+I_y)\dot{\psi}_r^2 C_{\phi_r} S_{\phi_r}] & I_z p^2 + (-I_x+I_y)(\dot{\psi}_r^2 S_{\phi_r}^2 - \dot{\phi}_r^2) \end{array}\right] \begin{bmatrix} \phi \\ \theta \\ \psi \end{bmatrix}$$

$$+ \begin{bmatrix} 0 \\ (I_x+I_y-I_z)\dot{\phi}_r \dot{\psi}_r C_{\phi_r} \\ (-I_x+I_y-I_z)\dot{\phi}_r \dot{\psi}_r S_{\phi_r} \end{bmatrix}$$

Equation 2.3-13 represents the simplified equation of motion for the main spacecraft and will serve as a point of departure for dynamical studies leading to synthesis of the main spacecraft attitude controller.

2.4 STRUCTURAL - DYNAMIC EQUATIONS

The dynamic system has been formulated in six "rigid-body" degrees of freedom plus translational motion of the various components of the satellite with respect to the cylindrical center body. The rigid body motion will be defined as rotations about and translations along the body axes of the satellite (Figure 2.4-1) and the flexible degrees of freedom will consist of additional motion of the satellite components defined in the form of modes of distortion.

KWOT satellite can be represented as a structure having linear stiffness characteristics providing the assumed deformations are small and providing no "slack" occurs in any of the interconnecting cables. These assumptions put some limitations on subsequent analysis but any more sophisticated approach would result in equations of unmanageable size. It will be shown that the structural potential energy of the satellite may be expressed in terms of a stiffness matrix which relates the displacements of the satellite components from their stabilized position to the restoring force arising from tensions in the restraining cables. The fact that the cables are already in a state of tension in the initially "stabilized and spinning" configuration is accounted for.

The choice of structural degrees of freedom requires some explanation. The structural degrees of freedom could be

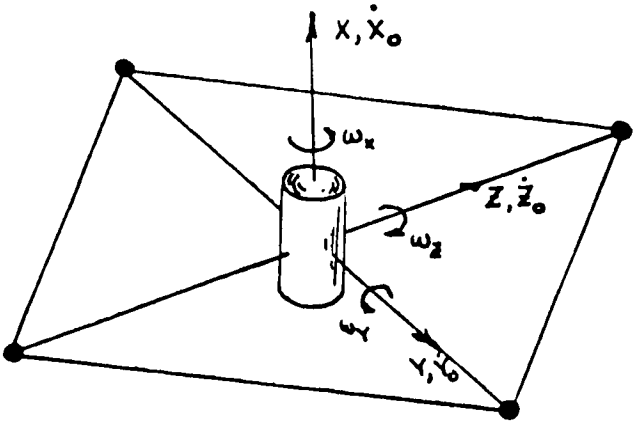

X, Y, Z BODY AXIS COORDINATES

$\dot{X}_o$, $\dot{Y}_o$, $\dot{Z}_o$ - Components of Inertial Velocity of Body Axis Origin Along Body Axes X, Y, and Z.

Figure 2.4-1 Satellite in Undisturbed Configuration

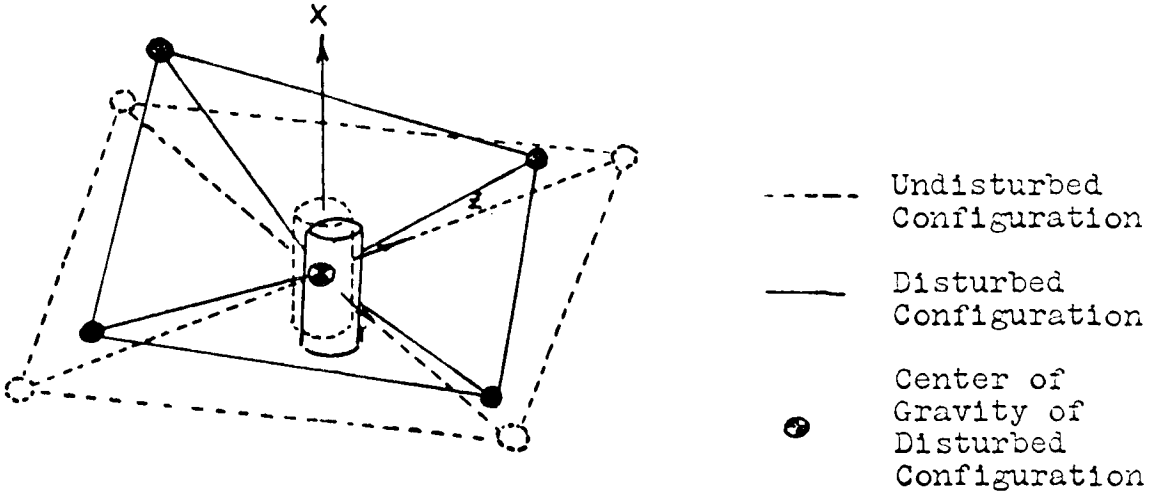

Figure 2.4-2 Satellite in Disturbed Configuration

defined as displacements of each "lumped mass" element of the satellite with respect to the satellite centerbody in the X, Y, and Z directions. Such a choice would however result in equations of motion complicated by the inclusion of cross inertias and cross stiffnesses occurring in both the rigid body and flexible equations. The orthogonality properties of normal modes offer a beneficial simplification to the dynamic equations of motion often used in this type of problem. Therefore the generalized coordinates of the flexibility degrees of freedom are defined in terms of free body normal modes. With such a choice of modes the origin of the body axes will always be at the center of gravity of the flexible satellite, and the inertial position of the cylindrical center body at any time will be a function of the six rigid body degrees of freedom plus the generalized coordinates of the flexible modes. (Figure 2.4-2)

It will be noted that exclusion of the flexibility degrees of freedom from the dynamic equations of motion will result in the familiar Euler equations of motion for principal axes (due to the symmetry of the satellite's initial deployed shape).

The Lagrangian expression in body axis variables (as opposed to inertial coordinates) is unwieldy and the equations of motion in the six rigid body degrees of freedom are more conveniently derived by equating external forces to a summation of mass x acceleration assuming the internal forces are self

equilibrating. These resulting expressions are as follows:

$$F_x = \sum_v \partial m a_x \qquad (2.4\text{-}1)$$
$$F_y = \sum_v \partial m a_y$$
$$F_z = \sum_v \partial m a_z$$

and

$$M_x = \sum_v \partial m (a_z Y - a_y Z) \qquad (2.4\text{-}2)$$
$$M_y = \sum_v \partial m (a_x Z - a_z X)$$
$$M_z = \sum_v \partial m (a_y X - a_x Y)$$

The equations of motion of the flexible degrees of freedom are conveniently derived using the Lagrange equation

$$\frac{d}{dt}\left(\frac{\partial L}{\partial \dot{q}_i}\right) - \frac{\partial L}{\partial q_i} = Q_i \qquad (2.4\text{-}3)$$

where Q_1 is a generalized force

For gravity gradient the generalized force in the structural mode can be written as $Q_i(r, \phi_o, \theta_o) = \sum_v \underline{F} \cdot \underline{h}_i$. (Q_1 for rigid body degrees of freedom are identical to those in Section 4.2.2.)

Formulation of Dynamic Equations of Motion

The general expression of velocity of point (X, Y, Z) in the satellite structural system may be written as

$$\underline{V} = \underline{V}_o + \underline{\omega} \times \underline{r} + \frac{\partial \underline{r}}{\partial t} \qquad (2.4\text{-}4)$$

where the components are:

$$V_x = \dot{X}_o + \dot{X} + (\omega_y Z - \omega_z Y)$$

$$V_y = \dot{Y}_o + \dot{Y} + (\omega_z X - \omega_x Z)$$

$$V_z = \dot{Z}_o + \dot{Z} + (\omega_x Y - \omega_y X)$$

Where $\dot{X}_o$, $\dot{Y}_o$ and $\dot{Z}_o$ are the inertial velocity components of the body axis origin in the body axis directions and $\dot{X}$, $\dot{Y}$ and $\dot{Z}$ are velocities of structural elements in body axis directions.

The Kinetic Engergy (T) is:

$$T = \frac{1}{2} \Sigma \partial m (V_x^2 + V_y^2 + V_z^2) \qquad (2.4\text{-}5)$$

and consequently:

$$\begin{aligned} 2T = \Sigma \partial m \{ & \dot{X}_o^2 + \dot{X}^2 + (\omega_y Z - \omega_z Y)^2 + 2[\dot{X}\dot{X}_o + \dot{X}(\omega_y Z - \omega_z Y) + \dot{X}_o(\omega_y Z - \omega_z Y)] \\ & + \dot{Y}_o^2 + \dot{Y}^2 + (\omega_z X - \omega_x Z)^2 + 2[\dot{Y}\dot{Y}_o + \dot{Y}(\omega_z X - \omega_x Z) + \dot{Y}_o(\omega_z X - \omega_x Z)] \\ & + \dot{Z}_o^2 + \dot{Z}^2 + (\omega_x Y - \omega_y X)^2 + 2[\dot{Z}\dot{Z}_o + \dot{Z}(\omega_x Y - \omega_y X) + \dot{Z}_o(\omega_x Y - \omega_y X)] \} \end{aligned} \qquad (2.4\text{-}6)$$

Now the position of any elements as shown in Figure 2.4-3, in the body axis system may be written as:

$$X = X_r + \Sigma h_{iX} \xi_i(t) \qquad (2.4\text{-}7)$$

$$Y = Y_r + \Sigma h_{iY} \xi_i(t)$$

$$Z = Z_r + \Sigma h_{iZ} \xi_i(t)$$

where (X_r, Y_r and Z_r) are the rigid body coordinates of the element and h_{iX} is the structural displacement in the X direction in the i^{th} normal mode and h_{iY} and h_{iZ} have similar

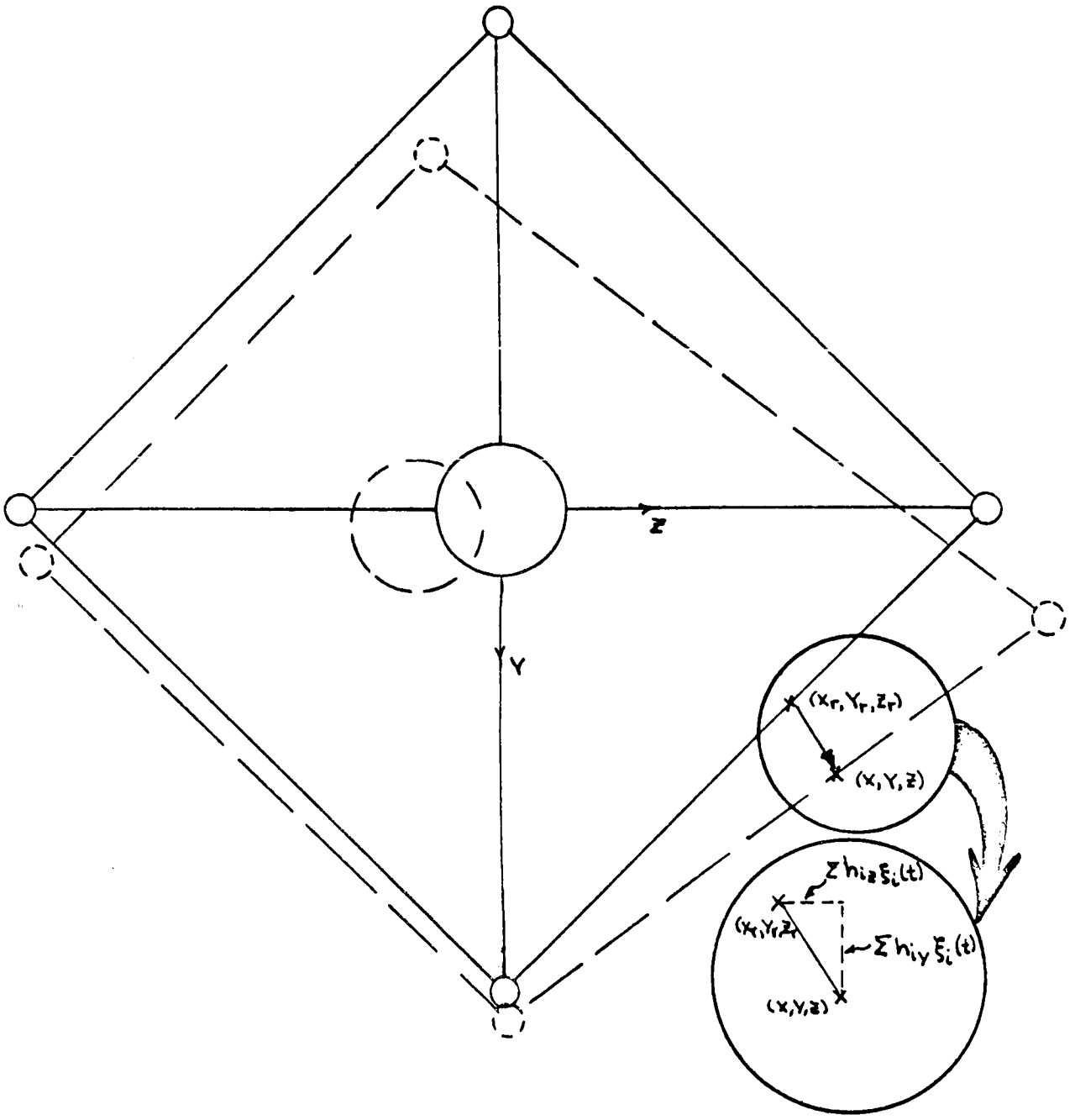

Figure 2.4-3 Deformation of Satellite in Y-Z Plane.

definitions. ξ_i is the generalized coordinate of the i^{th} flexibility mode.

Differentiating Equation 2.4-7 one obtains:

$$\dot{x} = \Sigma h_{ix} \dot{\xi}_i(t)$$
$$\dot{y} = \Sigma h_{iy} \dot{\xi}_i(t) \qquad (2.4\text{-}8)$$
$$\dot{z} = \Sigma h_{iz} \dot{\xi}_i(t)$$

It should be noted that if the structural degrees of freedom are free-free normal modes of vibration, then the body axis origin will be at the deformed body c.g., and

$$\sum_{body} \partial m x = \sum_{body} \partial m y = \sum_{body} \partial m z = 0 \qquad (2.4\text{-}9)$$

Also

$$\sum_{b} \partial m \dot{x} = \sum_{b} \partial m \dot{y} = \sum_{b} \partial m \dot{z} = \sum_{b} \partial m \ddot{x} = \sum_{b} \partial m \ddot{y} = \sum_{b} \partial m \ddot{z} = 0 \qquad (2.4\text{-}10)$$

Using the modal orthogonality condition

$$\Sigma \partial m \dot{x}^2 = I_{1x} \dot{\xi}_1^2 + I_{2x} \dot{\xi}_2^2 + I_{3x} \dot{\xi}_3^2 + \cdots + I_{nx} \dot{\xi}_n^2 \qquad (2.4\text{-}11)$$

where I_{ix} is the contribution of the displacements in the X direction to the total inertia of the i^{th} normal mode

$$I_{ix} = \Sigma \partial m h_{ix}^2 \qquad (2.4\text{-}12)$$

$$I_i = \Sigma \partial m (h_{ix}^2 + h_{iy}^2 + h_{iz}^2) \qquad (2.4\text{-}13)$$

Summations of $\sum_v \delta m \dot{y}^2$ and $\sum_v \delta m \dot{z}^2$ will result in similar expressions to Equations 2.4-11, 2.4-12 and 2.4-13.

In addition, if the flexibility mode system is divided into three sets of modes, each set having displacements of the structural elements in one body axis direction only, (i.e., a set of X deflection, Y deflection, and Z deflection modes) then it is possible to make further simplifications to the dynamic problem.

We have

$$I_i = \sum_v \delta m (h_{ix}^2 + h_{iy}^2 + h_{iz}^2) \tag{2.4-14}$$

where for the i^{th} mode there are only values for h_{ix} or h_{iy} or h_{iz}.

Also if the i^{th} mode is an 'X deflection' mode then

$$I_{iy} = I_{iz} = 0 \tag{2.4-15}$$

and

$$\sum \delta m \dot{x}^2 = \sum \delta m (\dot{x}_r + \sum h_{ix} \dot{\xi}_i(t))^2 \tag{2.4-16}$$

which expands to

$$\sum \delta m \dot{x}^2 = \sum_v \delta m \dot{x}_r^2 + I_{1x} \dot{\xi}_1^2 + I_{2x} \dot{\xi}_2^2 + \cdots + I_{nx} \dot{\xi}_n^2 + 2 \sum_v \delta m \sum_{i=1}^{n} h_{ix} \dot{x}_r \dot{\xi}_i(t) \tag{2.4-17}$$

Also

$$\sum_v \delta_m X Y = \sum_v \delta_m X_r Y_r + \sum_v \delta_m \sum_{i=1}^{n} h_{iy} X_r \xi_i(t) \tag{2.4-18}$$

$$+ \sum_v \delta_m \sum h_{ix} Y_r \xi_i(t)$$

$$+ \sum_v \delta_m \sum_i \sum_j h_{ix} h_{iy} \xi_i(t) \xi_j(t)$$

It should be noted that

$$\sum_v \delta_m X_r Y_r = \sum_v \delta_m Y_r Z_r = \sum_v \delta_m X_r Z_r = 0 \tag{2.4-19}$$

since the body axes will lie along the principal axes of the satellite in the undisturbed configurations. The expansions of $\Sigma \delta_m Y^2$, $\Sigma \delta_m Z^2$, $\Sigma \delta_m YZ$, and $\Sigma \delta m XZ$ have been omitted since they follow the same pattern as the ones given in full above.

The above equations may now be substituted into the expression for kinetic energy (2.4-6) which results in:

(2.4-20)

$$\begin{aligned}
2T = {} & \Sigma \delta m \dot{x}_o^2 + \Sigma \delta m \dot{x}^2 + \Sigma \delta m (\omega_y^2 z^2 - 2\omega_y \omega_z yz + \omega_z^2 y^2) + 2\Sigma \delta m \dot{x} \dot{x}_o \\
& + 2\Sigma \delta m \dot{x} \omega_y z - 2\Sigma \delta m \dot{x} \omega_z y + 2\Sigma \delta m \dot{x}_o \omega_y z - 2\Sigma \delta m \dot{x}_o \omega_z y \\
& + \Sigma \delta m \dot{y}_o^2 + \Sigma \delta m \dot{y}^2 + \Sigma \delta m (\omega_z^2 x^2 - 2\omega_z \omega_x zx + \omega_x^2 z^2) + 2\Sigma \delta m \dot{y} \dot{y}_o \\
& + 2\Sigma \delta m \dot{y} \omega_z x - 2\Sigma \delta m \dot{y} \omega_x z + 2\Sigma \delta m \dot{y}_o \omega_z x - 2\Sigma \delta m \dot{y}_o \omega_x z \\
& + \Sigma \delta m \dot{z}_o^2 + \Sigma \delta m \dot{z}^2 + \Sigma \delta m (\omega_x^2 x^2 - 2\omega_y \omega_x yx + \omega_y^2 x^2) + 2\Sigma \delta m \dot{z} \dot{z}_o \\
& + 2\Sigma \delta m \dot{z} \omega_x y - 2\Sigma \delta m \dot{z} \omega_y x + 2\Sigma \delta m \dot{z}_o \omega_x y - 2\Sigma \delta m \dot{z}_o \omega_y x
\end{aligned}$$

$$
\begin{aligned}
2T = {} & M\dot{X}_o^2 + (I_{1x}\dot{\xi}_1^2 + I_{2x}\dot{\xi}_2^2 + \cdots + I_{nx}\dot{\xi}_n^2) + \omega_y^2\Big[\Sigma \delta m Z_r^2 + 2\Sigma \delta m (Z_r)\Sigma h_{iz}\xi_i(t) \\
& + I_{1z}\xi_1(t)^2 + I_{2z}\xi_2(t)^2 + \cdots + I_{nz}\xi_n(t)^2\Big] - 2\omega_y\omega_z\Big[\delta_m Y_r \Sigma h_{iz}\xi_i(t) + \Sigma \delta m Z_r \Sigma h_{iy}\xi_i(t) \qquad (2.4\text{-}21) \\
& + \Sigma \delta m \sum_i \sum_j h_{iy} h_{jz}\xi_i(t)\xi_j(t)\Big] + \omega_z^2\Big[\delta m Y_r^2 + 2\Sigma \delta m (Y_r)\Sigma h_{iy}\xi_i(t) + I_{1y}\xi_1(t)^2 \\
& + I_{2y}\xi_2(t)^2 + \cdots + I_{ny}\xi_n(t)^2\Big] + 2\Sigma \delta m \dot{X} Z \omega_y - 2\Sigma \delta m \dot{X} Y \omega_z \\
& + M\dot{Y}_o^2 + (I_{1y}\dot{\xi}_1^2 + I_{2y}\dot{\xi}_2^2 + \cdots + I_{ny}\dot{\xi}_n^2) + \omega_z^2\Big[\Sigma \delta m X_r^2 + 2\Sigma \delta m (X_r)\Sigma h_{ix}\xi_i(t) \\
& + I_{1x}\xi(t)^2 + I_{2x}\xi_2(t)^2 + \cdots + I_{nx}\xi_n(t)^2\Big] - 2\omega_x\omega_z\Big[\Sigma \delta m X_r \Sigma h_{iz}\xi_i(t) + \Sigma \delta m X_r \Sigma h_{iz}\xi_i(t) \\
& + \Sigma \delta m \sum_i \sum_j h_{ix} h_{jz}\xi_i(t)\xi_j(t)\Big] + \omega_x^2\Big[\Sigma \delta m Z_r^2 + 2\Sigma \delta m (Z_r)\Sigma h_{iz}\xi_i(t) + I_{1z}\xi_1(t)^2 + \\
& + I_{2z}\xi_2(t)^2 + \cdots + I_{nz}\xi_n(t)^2\Big] + 2\Sigma \delta m \dot{Y} X \omega_z - 2\Sigma \delta m \dot{Y} Z \omega_x \\
& + M\dot{Z}_o^2 + (I_{1z}\dot{\xi}_1^2 + I_{2z}\dot{\xi}_2^2 + \cdots + I_{nz}\dot{\xi}_n^2) + \omega_x^2\Big[\Sigma \delta m Y_r^2 + 2\Sigma \delta m (Y_r)\Sigma h_{iy}\xi_i(t) \\
& + I_{1y}\xi_1(t)^2 + I_{2y}\xi_2(t)^2 + \cdots + I_{ny}\xi_n(t)^2\Big] - 2\omega_x\omega_y\Big[\Sigma \delta m X_r \Sigma h_{iy}\xi_i(t) + I_{1y}\xi_1(t)^2 \\
& + I_{2y}\xi_2(t)^2 + \cdots + I_{ny}\xi_n(t)^2\Big] + \omega_y^2\Big[\Sigma \delta m X_r^2 + 2\Sigma \delta m (X_r)\Sigma h_{ix}\xi_i(t) + I_{1x}\xi_1(t)^2 \\
& + I_{2x}\xi_2(t)^2 + \cdots + I_{nx}\xi_n(t)^2\Big] + 2\Sigma \delta m Z \omega_x Y - 2\Sigma \delta m \dot{Z} \omega_y X
\end{aligned}
$$

The required expression for the Lagrange equation of each flexible mode is:

$$\frac{d}{dt}\left(\frac{\partial T}{\partial \dot{\xi}_p}\right) - \frac{\partial T}{\partial \xi_p} \qquad (2.4\text{-}22)$$

Before this expression is expanded it should be noted that the terms appearing in the expression for kinetic energy as $\Sigma \delta m \dot{x} z$, $\Sigma \delta m \dot{x} y$ etc. may be expanded in the form

$$\sum_v \delta m \dot{x} z = \sum_v \delta m \sum_{i=1}^{n} Z_r h_{ix}\dot{\xi}_i(t) + \sum_v \delta m \sum_i \sum_j h_{ix} h_{jz}\dot{\xi}_i\xi_j \qquad (2.4\text{-}23)$$

Also

$$\frac{d}{dt}\left(\frac{\partial}{\partial \dot{\xi}_p}\right)\left(\sum_v \delta m \dot{x} z\right) = \sum_v \delta m \sum_{j=1}^{n} h_{px} h_{jz} \dot{\xi}_j \tag{2.4-24}$$

$$\left(\frac{\partial}{\partial \xi_p}\right)\left(\sum_v \delta m \dot{x} z\right) = \sum_v \delta m \sum_{i}^{n} h_{ix} h_{pz} \dot{\xi}_i \tag{2.4-25}$$

It should also be noted that

$$\frac{\partial}{\partial \xi_p}\left(\sum_v \delta m \sum_i \sum_j h_{ix} h_{jz} \xi_i \xi_j\right) \tag{2.4-26}$$

$$= \sum_v \delta m \sum_{i}^{n} h_{px} h_{jz} \xi_j + \sum_v \delta m \sum_{i}^{n} h_{pz} h_{ix} \xi_i \tag{2.4-27}$$

Using the above equations, the Lagrange expression (2.4-22) for the p^{th} mode becomes

$$\{I_{px}\ddot{\xi}_p + \omega_y \sum_j \delta m\, h_{px} h_{jz} \dot{\xi}_j - \omega_z \sum_j \delta m\, h_{px} h_{jy} \dot{\xi}_j + I_{py}\ddot{\xi}_p + \omega_z \sum_j \delta m\, h_{py} h_{jx} \dot{\xi}_j \qquad (2.4\text{-}28)$$

$$+ I_{pz}\ddot{\xi}_p - \omega_x \sum_j \delta m\, h_{py} h_{jz} \dot{\xi}_j + \omega_x \sum_j \delta_m h_{pz} h_{jy} \dot{\xi}_j - \omega_y \Sigma \delta m\, h_{pz} h_{jx} \dot{\xi}_j\}$$

$$+\{\omega_y^2 (I_{pz}\xi_p + \Sigma \delta m\, z_r h_{pz}) - \omega_y \sum_i \delta m h_{pz} h_{ix} \dot{\xi}_i - \omega_z \sum_i \delta m h_{py} h_{ix} \dot{\xi}_i$$

$$+\omega_z^2 (I_{py}\xi_p + \Sigma \delta m\, y_r h_{py}) - 2\omega_y\omega_z [(\Sigma \delta m y_r h_{pz} + \Sigma \delta m z_r h_{py}$$

$$+ \Sigma \delta m (h_{py} \Sigma h_{jz} \xi_j + h_{pz} \Sigma h_{iy} \xi_i)] + \omega_z \sum_i \delta m h_{px} h_{iy} \dot{\xi}_i$$

$$- \omega_x \sum_i \delta m h_{pz} h_{iy} \dot{\xi}_i + \omega_z^2 (I_{px}\xi_p + \Sigma \delta m x_r h_{px})$$

$$+ \omega_x^2 (I_{pz} + \Sigma \delta m z_r h_{pz}) - \omega_x\omega_z [(\Sigma \delta m x_r h_{pz} + \Sigma \delta m z_r h_{px}$$

$$+ \Sigma \delta m (h_{pz} \Sigma h_{jx} \xi_j + h_{px} \Sigma h_{iz} \xi_i)] + \omega_x \sum_i \delta m h_{py} h_{iz} \dot{\xi}_i$$

$$- \omega_y \sum_i \delta m h_{px} h_{iz} \dot{\xi}_i + \omega_x^2 (I_{py}\xi_p + \Sigma \delta m y_r h_{py}).$$

$$+ \omega_y^2 (I_{px}\xi_p + \Sigma \delta m\, x_r h_{px}) - \omega_x\omega_y [(\Sigma \delta m x_r h_{py} + \Sigma \delta m y_r h_{px}$$

$$+ \Sigma \delta m (h_{px} \Sigma h_{jy} \xi_j + h_{py} \Sigma h_{ix} \xi_i)]\}$$

The above expression gives the inertial contribution to the equation of motion of the p^{th} structural degree of freedom in the most general case. In a particular problem it will be realized that a large number of expressions may be eliminated on the grounds that they are second order terms.

It is felt however that the initial formulation of the dynamic problem should include all second order terms since it is possible that a certain number of them will be significant due to the extreme flexibility of the KWOT configuration.

The "rigid body" equations of motion will be derived from more basic concepts using Equations 2.4-1 and 2.4-2.

From Equation 2.4-4:

$$\underline{V} = \underline{V}_o + \underline{\omega} \times \underline{r} + \frac{\partial \underline{r}}{\partial t} \tag{2.4-29}$$

$$\underline{A} = \dot{\underline{V}}_o + \frac{d}{dt}\left(\frac{\partial \underline{r}}{\partial t} + \underline{r} \times \underline{\omega}\right) + \underline{\omega} \times \left(\frac{\partial \underline{r}}{\partial t} + \underline{r} \times \underline{\omega}\right) \tag{2.4-30}$$

$$\underline{A} = \underline{A}_o + \frac{\partial \underline{r}}{\partial t} \times \underline{\omega} + \underline{r} \times \dot{\underline{\omega}} + \underline{r} \times \underline{\omega} \times \underline{\omega} + \frac{\partial^2 \underline{r}}{\partial t^2} + \underline{r} \times \underline{\omega} + \underline{\omega} \times \underline{r} \tag{2.4-31}$$

Expanding Equation 2.4-31 yields:

$$A_x = \ddot{X}_o + 2\omega_y \dot{Z} - 2\omega_z \dot{Y} + Y(\omega_x \omega_y) - Y\dot{\omega}_z + Z\dot{\omega}_y + Z(\omega_x \omega_z) + X(-\omega_y^2 - \omega_z^2) + \ddot{X} \tag{2.4-32}$$

Similarly

$$A_y = \ddot{Y}_o + 2\omega_z \dot{X} - 2\omega_x \dot{Z} + X(\omega_x \omega_y + \dot{\omega}_z) + Z(\omega_y \omega_z - \dot{\omega}_x) - Y(\omega_x^2 + \omega_z^2) + \ddot{Y} \tag{2.4-33}$$

and

$$A_z = \ddot{Z}_o + 2\omega_x \dot{Y} - 2\omega_y \dot{X} + X(\omega_x \omega_z - \dot{\omega}_y) + Y(\omega_y \omega_z + \dot{\omega}_x) - Z(\omega_x^2 + \omega_y^2) + \ddot{Z} \tag{2.4-34}$$

Consider the equation:

$$\Sigma F_x = \Sigma \partial m a_x \tag{2.4-35}$$

Then

$$\Sigma F_{x(external)} + \Sigma F_{x(internal)} = \Sigma \partial m a_x \tag{2.4-36}$$

$$\text{but } \Sigma F_{x(internal)} = 0$$

since the resultant internal forces of a structure free in space can only equate to zero.

Consequently by substituting 2.4-32 in 2.4-36

$$\Sigma \partial m a_x = M \ddot{X}_o = \Sigma f_{x(ext.)} \tag{2.4-37}$$

and in similar fashion

$$\Sigma \partial m a_y = M \ddot{Y}_o = \Sigma F_{y(ext.)} \tag{2.4-38}$$

and

$$\Sigma \partial m a_z = M \ddot{Z}_o = \Sigma F_{z(ext.)} \tag{2.4-39}$$

Rigid body translation equations

The absence of coupling terms with the flexibility modes is due to the choice of free-free normal modes plus an origin which is always at the c.g. of the total system.

Consider equation

$$M_x = \Sigma \partial m (a_z y - a_y z) \tag{2.4-40}$$

therefore

$$M_x = \sum \delta m [\ddot{Z}_o Y + 2\omega_x \dot{Y} Y - 2\omega_y \dot{X} Y + (\omega_x \omega_z - \dot{\omega}_y) XY + Y^2(\omega_y \omega_z + \dot{\omega}_x) \quad (2.4\text{-}41)$$

$$- ZY(\omega_x^2 + \omega_y^2) + \ddot{Z} Y - \ddot{Y}_o Z - 2\omega_z \dot{X} Z + 2\omega_x \dot{Z} Z$$

$$- XZ(\omega_x \omega_y + \dot{\omega}_z) - Z^2(\omega_y \omega_z - \dot{\omega}_x) + YZ(\omega_x^2 + \omega_z^2)$$

$$- Z\ddot{Y}]$$

The Moment equation about the X axis is:

$$M_{x_{inertial}} = 2\omega_x(\sum_i \delta m Y_r \Sigma h_{iy} \dot{\xi}_i + \sum_i I_{yi} \dot{\beta}_i \xi_i) + (\Sigma \delta m \sum_i \sum_j h_{ix} h_{iy} \xi_i \xi_j + \delta m X_r \sum_i h_{iy} \xi_i \quad (2.4\text{-}42)$$

$$+ \Sigma \delta m Y_r \sum_i h_{ix} \xi_i)(\omega_x \omega_z - \dot{\omega}_y) - 2\omega_y(\Sigma \delta m Y_r \sum_i h_{ix} \dot{\xi}_i + \Sigma \delta m \sum_i \sum_j h_{ix} h_{jy} \dot{\xi}_i \xi_j)$$

$$+ (\omega_y \omega_z + \dot{\omega}_x)[(\Sigma \delta m Y_r^2 + I_{1y} \xi_1^2 + I_{2y} \xi_2^2 + \cdots + I_{ny} \xi_n^2) + 2\Sigma \delta m Y_r \sum_i h_{ix} \xi_i]$$

$$- (\omega_x^2 + \omega_y^2)(\Sigma \delta m Z_r \Sigma h_{iz} \xi_i + \Sigma \delta m Y_r \sum_i h_{iz} \xi_i + \Sigma \delta m \sum_i \sum_j h_{iz} h_{jy} \xi_i \xi_j)$$

$$+ \Sigma \delta m Y_r \Sigma h_{iz} \ddot{\xi}_i + \sum_i \sum_j h_{iz} h_{jz} \ddot{\xi}_i \xi_j - 2\omega_z(\Sigma \delta m Z_r \Sigma h_{ix} \dot{\xi}_i + \Sigma \delta m \sum_i \sum_j h_{ix} h_{jz} \dot{\xi}_i \xi_j)$$

$$+ 2\omega_x(\Sigma \delta m Z_r \Sigma h_{iz} \dot{\xi}_i + \Sigma I_{iz} \dot{\xi}_i \xi_i) - (\omega_x \omega_y + \dot{\omega}_z)(\Sigma \delta m X_r \sum_i h_{iz} \xi_i$$

$$+ \Sigma \delta m Z_r \sum_i h_{ix} \xi_i + \Sigma \delta m \sum_i \sum_j h_{ix} h_{jz} \xi_i \xi_j) - (\omega_y \omega_z - \dot{\omega}_x)(\Sigma \delta m Z_r^2 \cdot$$

$$+ I_{1z} \xi_1^2 + I_{2z} \xi_2^2 + \cdots I_{nz} \xi_n^2 + 2\Sigma \delta m Z_r \Sigma h_{iz} \xi_i) + (\omega_x^2 + \omega_z^2)(\Sigma \delta m Y_r \Sigma h_{iz} \xi_i$$

$$+ \Sigma \delta m Z_i \Sigma h_{iy} \xi_i + \Sigma \delta m \sum_i \sum_j h_{iy} h_{jz} \xi_i \xi_j) - \Sigma \delta m Z_r \Sigma h_{iy} \ddot{\xi}_i - \Sigma \delta m \sum_i \sum_j h_{iz} h_{jy} \xi_i \xi_j$$

This expression gives the inertial contribution to the moment equation about the X axis. It will be noted that we could separate the following expression out of the total expression

$$\dot{\omega}_x(\Sigma \delta m Y_r^2 + \Sigma \delta m Z_r^2) \quad (2.4\text{-}43)$$

which is of course, $I_{XX}\dot{\omega}_X$ where I_{XX} is the rigid body inertia about the X axis and $\dot{\omega}_X$ is the rigid body accelleration.

Derivation of Structural Potential and Formulation of Structural Degrees of Freedom

The potential part of the Lagrange expression must now be considered. The general form of the potential expression occurring in the Lagrange equation is

$$\frac{\partial U}{\partial q_r} \qquad (2.4\text{-}44)$$

where q_r is any generalized coordinate.
At present considering only the derivation of the above expression (2.4-44) we will restrict ourselves to deriving the structural potential alone.

In any flexible system one is faced with the problem of assigning degrees of freedom to the structure. It is obvious that there are an infinite number of degrees of freedom of any continuous structure and that the choice of a limited number of these degrees of freedom is a necessary simplification of the true facts.

In the Lagrangean concept the total configuration at any time (t) is represented as a superposition of the various generalized coordinates of the system. One may write this as

$$\underline{r} = \underline{r}\big(\overbrace{x, y, z, \phi, \theta, \psi}^{\text{rigid body}}, \overbrace{\xi_1, \xi_2, \xi_3, \xi_4, \cdots \xi_n}^{\text{flexible body}}\big) \qquad (2.4\text{-}45)$$

$$\underbrace{\qquad\qquad\qquad\qquad\qquad\qquad}_{\text{all functions of time}}$$

It will be noted that the particular choice of coordinates results in the following expression for structural potential.

$$U = U(\xi_1, \xi_2, \xi_3, \cdots \xi_n) \qquad (2.4\text{-}46)$$

The "rigid body" condition defined previously may be described as the initial stabilized structural state in the fully deployed, spinning configuration. Since the structure is already in a state of strain in this stabilized state it is possible to define the potential energy as

$$U = U_0 + \delta U \qquad (2.4\text{-}47)$$

where δU is the perturbation in structural potential energy due to structural distortion from the initial stabilized configuration.

For small deformations from the original shape, no slack will develop in the load carrying cables since these cables are in an initial strained state. It is therefore possible to consider the satellite as a linear structural system under this condition.

A stiffness matrix for the initially strained structure may be defined in the following manner. Figure 2.4-4 illustrates the definition of the stiffness at point P in the body axis

direction Z. It will be noted that cables A and B are in a state of tension in the initial configuration resulting in a net force acting on element P in the -Z direction. In displacing element P through Δ_z there will be an increase in the force acting on P in the -Z direction. This increment in force may be considered as a restoring force ΔF_z where ΔF_z and Δ_z are related through

$$\Delta F_z = E_{pz} \Delta_z \tag{2.4-48}$$

where E_{pz} is the stiffness of the structure at point P in the Z direction.

It is possible in this manner to define a stiffness matrix for the complete structure.

$$\begin{bmatrix} \Delta F_x \\ \Delta F_y \\ \Delta F_z \end{bmatrix} = \begin{bmatrix} E_{xx} & E_{xy} & E_{xz} \\ E_{yx} & E_{yy} & E_{yz} \\ E_{zx} & E_{zy} & E_{zz} \end{bmatrix} \begin{bmatrix} \Delta_x \\ \Delta_y \\ \Delta_z \end{bmatrix} \tag{2.4-49}$$

Consider any element P of the satellite structure. The total work done on P in taking it from its initial position through a distance Δ_z (see figure 2.4-4) can be written as

$$\text{work done} = F_{oz} \Delta_z + \tfrac{1}{2} \Delta F_z \Delta_z \tag{2.4-50}$$

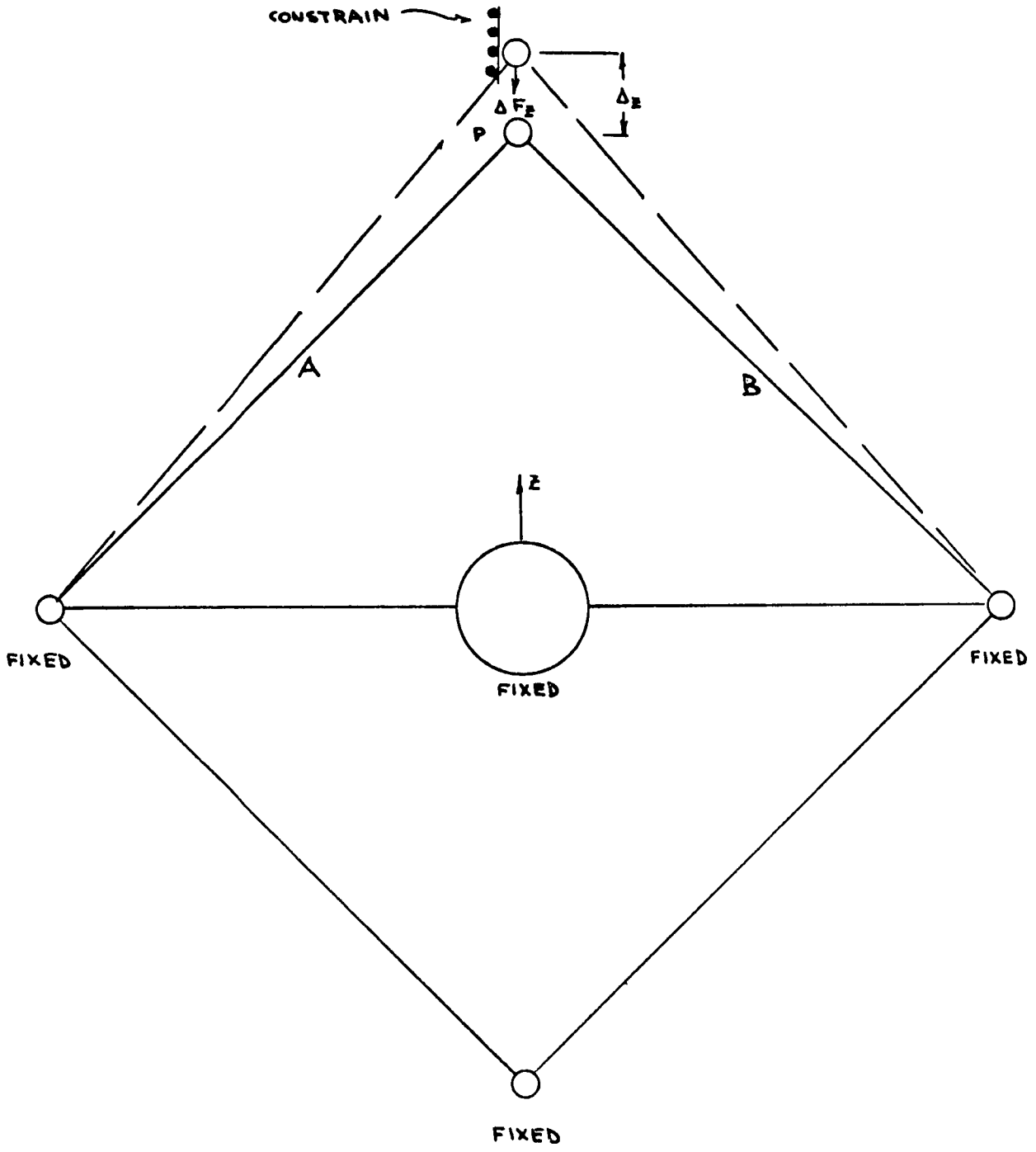

Figure 2.4-4 Definition Structural Stiffness in P Direction.

where F_{oz} is the cable restraining force acting on P in the Z negative direction in the initial configuration. Thus the increase in potential energy associated with a displacement Δ_z is

$$\delta U_p = F_{oz}\Delta_z + \tfrac{1}{2}\Delta F_z \Delta_z \qquad (2.4\text{-}51a)$$

$$= F_{oz}\Delta_z + \tfrac{1}{2} F_{pz}\Delta_z^2 \qquad (2.4\text{-}51)$$

It follows, therefore, that the total potential energy of the structure may be expressed in the form

$$U = U_o + \tfrac{1}{2}\Delta^T E \Delta + \Delta^T F_o \qquad (2.4\text{-}52)$$

where Δ is a column vector of element displacements in the body axis X, Y, and Z directions, E is the structure stiffness matrix defined in Equation 2.4-49 and F_o is a column vector of structural forces acting on each element of the satellite in the initial configuration. The latter terms may be derived from static load considerations at the prescribed satellite spin rate.

Equation 2.4-52 exhibits the general form of the potential energy expression for a linear structure with certain additions due to the particular definition of the stiffness matrix used in this study. It is now possible to transform from the relative displacements Δ to the generalized coordinates of the

structural modes. This transformation will take the form

$$[\Delta] = [h][\xi] \tag{2.4-53}$$

or for the particular modes selected for this problem

$$\begin{bmatrix} \Delta_x \\ \Delta_y \\ \Delta_z \end{bmatrix} = \begin{bmatrix} h_x & 0 & 0 \\ 0 & h_y & 0 \\ 0 & 0 & h_z \end{bmatrix} \begin{bmatrix} \xi_x \\ \xi_y \\ \xi_z \end{bmatrix} \tag{2.4-54}$$

where h_x is a set of column vectors of displacements of the satellite elements in the X direction for the "X" type modes and ξ_x is the corresponding column vector of generalized coordinates for these modes, etc.

Thus the potential energy of the structure may be expressed in terms of the generalized coordinates of the structure in the form

$$U = U_o + \tfrac{1}{2}[\xi]^T[h]^T[E][h][\xi] + [\xi]^T[h]^T[F_o] \tag{2.4-55}$$

Differentiating partially with respect to the generalized coordinates

2.5 STRUCTURAL EQUATIONS

A structural model of KWOT was conceived for the purpose of an engineering feasibility study. The underlying principle guiding the preliminary design effort was the desire to generate a structure which, although tenuous, would behave as nearly linearly as possible in response to forces. The precise nature and magnitude of some forces such as solar pressure, gravity gradient, and guying wire body forces, were not accounted for at this stage of analysis. However initial estimates were established of the limitations of forces under which the structure could be assumed to behave linearly.

Under these linearized conditions, it was possible to perform the necessary small deflection theory stress analysis for the preliminary design of the guying wires used to maintain the peripheral satellites' relative positions.

The initial phase of this investigation was limited to a simplified planar model of the conceptual KWOT. The system's stiffness matrix was calculated and is given later in this section.

Analysis - General Approach

In order to restrict the obviously tenuous KWOT structure to a regime of linear response, the most compelling geometrical layout of the structure is that of a pin-jointed truss with straight members. In order to maintain such a shape,

many guying wires will be required. The conceptual study is given later. A structure of this type is statically indeterminate, having more force-carrying members than independent equations of statics from which to determine member forces caused by the loads applied to the structure.

The stiffness method of analysis was used to solve this problem. The deflections of the joints of the structure are given by

$$[k]\{\Delta\} = \{w\} \qquad (2.5\text{-}1)$$

in which $[K]$ is the stiffness matrix, $\{\Delta\}$ represents the unknown deflection and $\{w\}$ represents the externally applied forces or the mechanical forces equivaltent to their effect to thermal distortion.[1] The individual stiffness matrices of the structural elements are multiplied by the pertinent deflections after they are obtained from the solution of 2.5-1. The result is the set of internal forces required to bring about the compatible and equilibrated state-of-being defined by 2.5-1.

The element deflections are related to the common independent displacements of the structure by the kinematic relations:

$$\{\Delta_{el}\} = [b]\{\Delta\} \qquad (2.5\text{-}2)$$

Applying the Principle of Virtual Work, results in:

$$[K] = [b]^T [K_{el}] [b] \qquad (2.5\text{-}3)$$

where $[K_{el}]$ consists of the structural element stiffness matrices arranged along the diagonal of a square matrix. However, $[K]$ may also be generated by the suitable addition of element stiffness matrices after they have been transformed to the common coordinate system. This has been done for the simplified problem presently under study.

Finally, one obtains the element forces $\{F_m\}$:

$$\{F_m\} = [K_{el}] \{\Delta_{el}\} \qquad (2.5\text{-}4a)$$

$$= [K_{el}] [b] \{\Delta\} \qquad (2.5\text{-}4)$$

The rigidly supported degrees of freedom of the structure do not appear in any of the Equations 2.5-1 through 2.5-4, for simplicity of exposition.

Conceptual Model

The basic configuration of the antenna, hub structure, and four peripheral control satellites was stabilized by a truss-like system of interconnected ribbons shown in Figure 2.5-1. A solid web of 0.0005 in. "Mylar" plastic, for the plane of the antenna, was also considered. However, the

weight of the required quantity of the Mylar material was prohibitive. An attempt was made to make all members as short as possible in order to maximize the stiffness of the system for the least amount of weight. It has been assumed throughout this study that the ribbons cannot take compression loadings, and therefore the centrifugal forces on the satellites are depended upon to generate the necessary pre-tension in the ribbons.

Figure 2.5-1 shows the basic ties used to maintain the in-plane rhomboid shape of the antenna. Opposing centrifugal forces maintain the positions of many points along the antenna in a straight line through the medium of the guying ribbons. Only a limited number of ribbons are shown to illustrate the basic arrangement. The final configuration should have connecting points spaced approximately 50 meters apart. If wires, of ordinary circular cross-section, were used the probability of kinking and tangling during deployment would be very great. The more practical scheme therefore is the use of a set of ribbons instead. The joints would be formed by predetermined spot heat sealing or a suitable adhesive during assembly, similar to the manufacture of honeycomb core. The ribbon assembly would then be folded into a suitable package to fit into the central hub. Deployment would then cause expansion of the ribbon structure, similar to the expansion of honeycomb core.

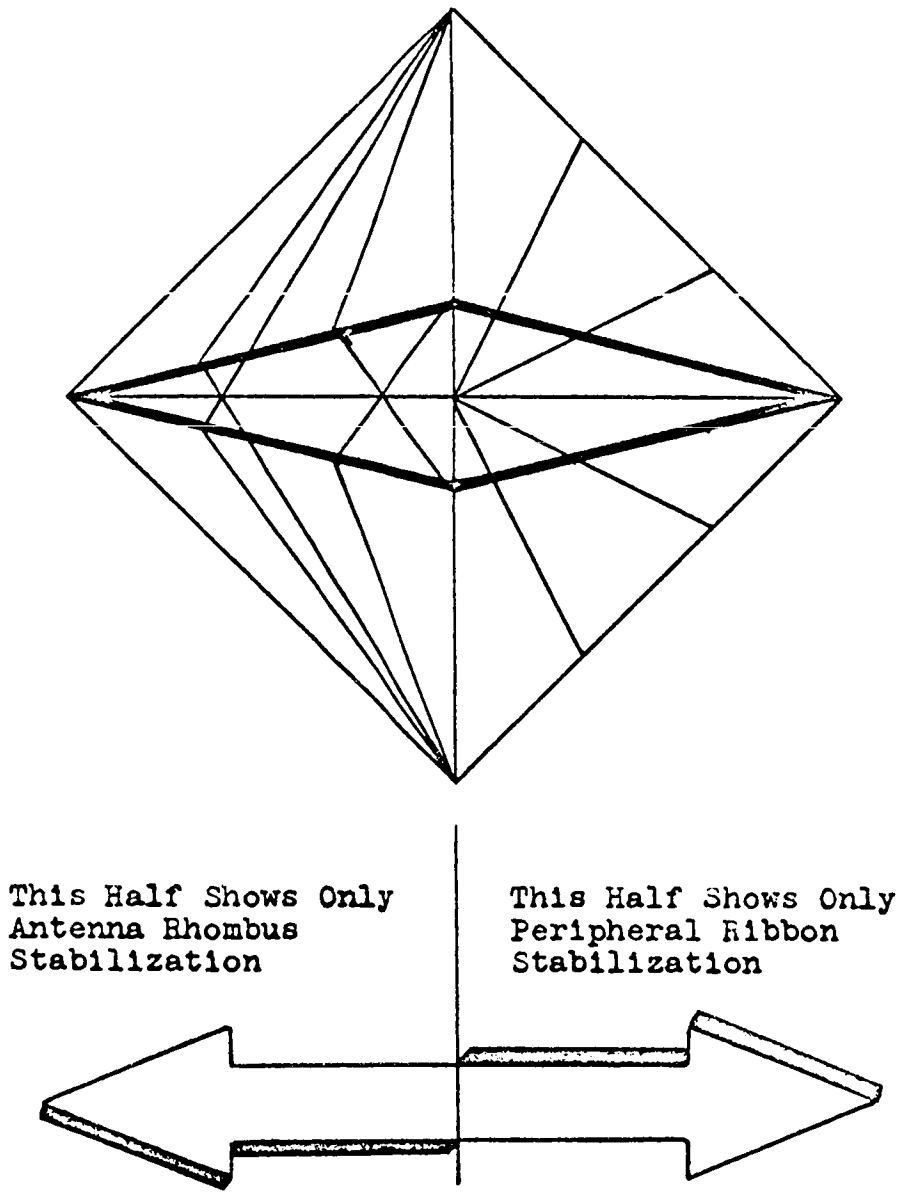

Figure 2.5-1 KWOT Conceptual Model Structure

The Simplified Planar Model

For the purpose of a planar dynamic analysis, a simplified planar model of the antenna has been used to define initial stiffness characteristics of the KWOT. This model is shown in Figure 2.5-2. The design, i.e., the cross-sectional areas of the guying ribbons is based upon standard load criteria and the loads in the deployed steady state condition.

Assume that the tension is established suddenly at the moment of incipient tension during deployment. The resulting conservative dynamic load factor is 2. Linear behavior is required. Assume Mylar type A coated, so that room temperature (about 65°F) will prevail in the ribbon. The material properties are then the stress at 2% offset, $F_{2\% \text{ offset}}$, and the ultimate stress, $F_{(\text{ultimate})}$

$F_{2\% \text{ offset}} = 12000$ psi

$F_{ult} = 25000$ psi

$E = 0.55 \times 10^6$ psi

Design of Guying Ribbons

Design condition 1:

Rotational velocity $\omega = 2\pi$/hr.

Design condition 2:

Rotation velocity $\omega = 2\pi$/hr.

Tangential control force nullifying centrifugal tension in the peripheral ribbon.

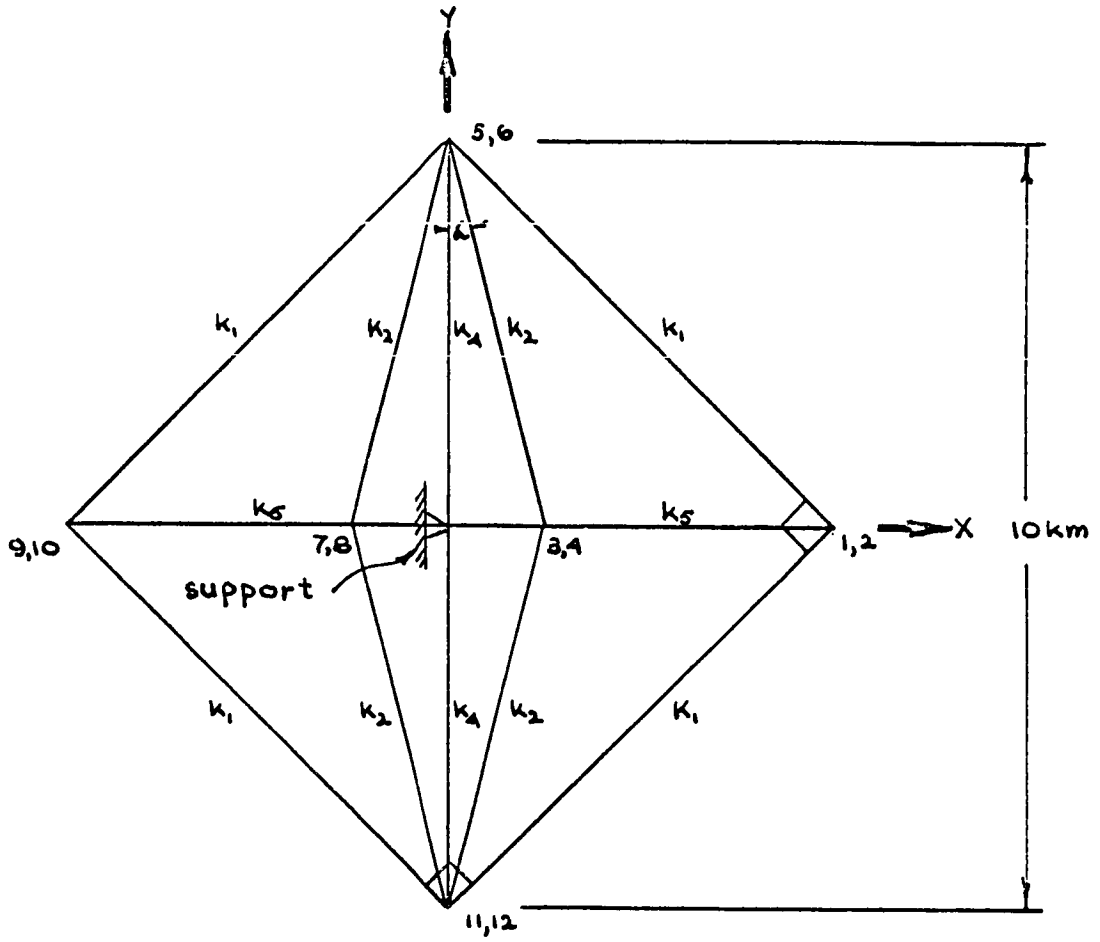

Figure 2.5-2 KWOT Simplified Structural Model

CONDITION 1

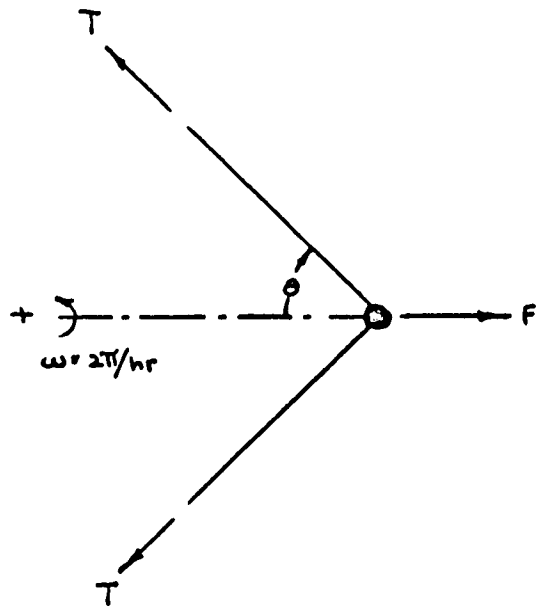

$$F = m\omega^2 r$$

$$T = \frac{F}{2\cos\theta}$$

Centrifugal force F causes tension T in circumferential ribbon. Assume only the circumferential ribbon is tensioned, where:

$$m = \frac{100}{32.2}\left(\frac{\#\cdot sec^2}{ft}\right)$$

$\omega = \frac{2\pi}{3600}\left(\frac{1}{sec}\right)$

$r = 5\ km (\approx 16400 ft)$

$\theta = 45°$

CONDITION 2

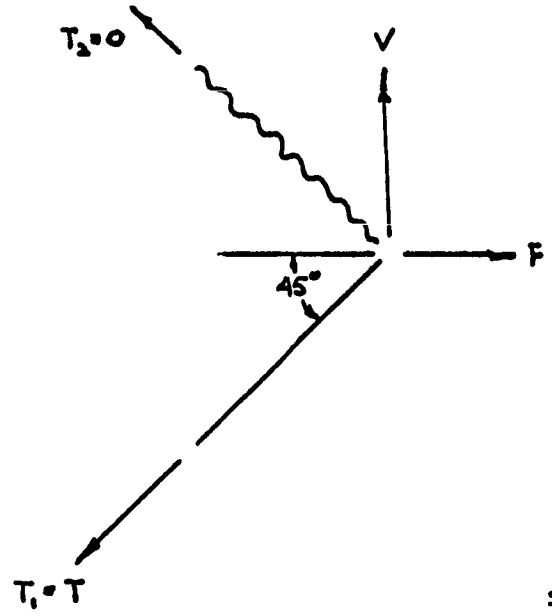

$T \sin 45° = V$

$T \cos 45° = F$

$\therefore V_{max} = F$

$$\therefore T_{max} = \frac{F}{\cos 45°}$$

This is therefore the design condition and thus

$$T_{max} = 2 \cdot 0.872 \qquad (2.5\text{-}5)$$

$$= 1.744\ lb. \qquad (2.5\text{-}5a)$$

$$A_{reqd} = \frac{T_{max}}{\sigma_{2\%\ offset}} \qquad (2.5\text{-}6)$$

$$= \frac{1.744}{12000} = 0.1452 \times 10^{-3}\ in^2 \qquad (2.5\text{-}6a)$$

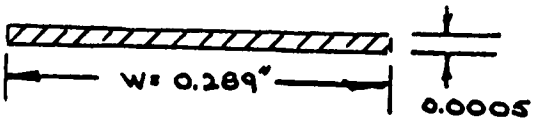

Assume t = .0005

Then $W = \frac{A}{t} = \frac{0.0726}{0.0005} \times 10^{-3}$

$= 0.289$ in.

Ultimate Load = 1.5 x Design Limit

Design Limit = 1.1 x Design Load

Ultimate Load = 1.65 x 1.744

= 2.88 lb.

$= \frac{2.88 \times 10^3}{.1452}$ psi

= 19800 psi

$$M.S. = \frac{F_{ult}}{\sigma_{ult}} - 1 = 26\%$$

By making all ribbons this size, the actual structure is overstrength by inspection.

Check on Applicability of Small Deflection Theory

Consider the displacements of the outer satellite due to a combination of tangential and radial forces as shown in diagram below.

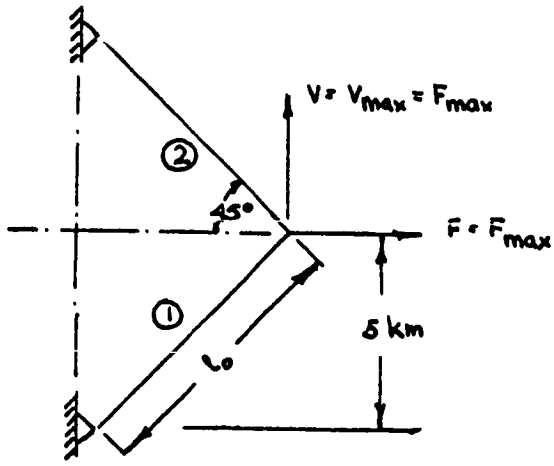

Then

$$T_{①} = 1.744 \text{ lbs.}$$

$$T_{②} = 0$$

Elongation of

$$T_{①} = \Delta\ell$$

$$\Delta\ell = \epsilon\ell_0 = \frac{\sigma}{E}\ell_0$$

$$\sigma = \frac{T_1}{A_1} = 12000 \text{ psi}$$

Thus

$$\Delta\ell = 505 \text{ ft.}$$

$$\frac{\Delta\ell}{\ell} = 0.0218$$

This is in the elastic range, and the geometric change is negligible. Hence linear behavior of the structure may be assumed.

The KWOT Stiffness Matrix

The stiffness matrix is shown in its literal form in Figure 2.5-3 and numerically in Figure 2.5-4 for certain assumed section properties. The final matrix of the simplified planar model will reflect necessary changes in the antenna material and section properties.

As an initial estimate, sufficient ribbons will be assumed in the actual structure to give the effect of 100 times the design area of the peripheral ribbon to the simplified model members. The simplified model members are assumed to sustain only positive forces.

Simplified Model Bar Stiffnesses

Member	Lengths	Area	$k = \frac{AE}{L}$ $\frac{lb.}{in.}$
1 - 5	23,196 ft.	1.45×10^{-2}	.0286
3 - 5	16,907 ft.	↓	.0392
0 - 3	4,090 ft.	↓	.1675
0 - 5	16,405 ft.	↓	.0405
1 - 3	12,315 ft.	↓	.0536

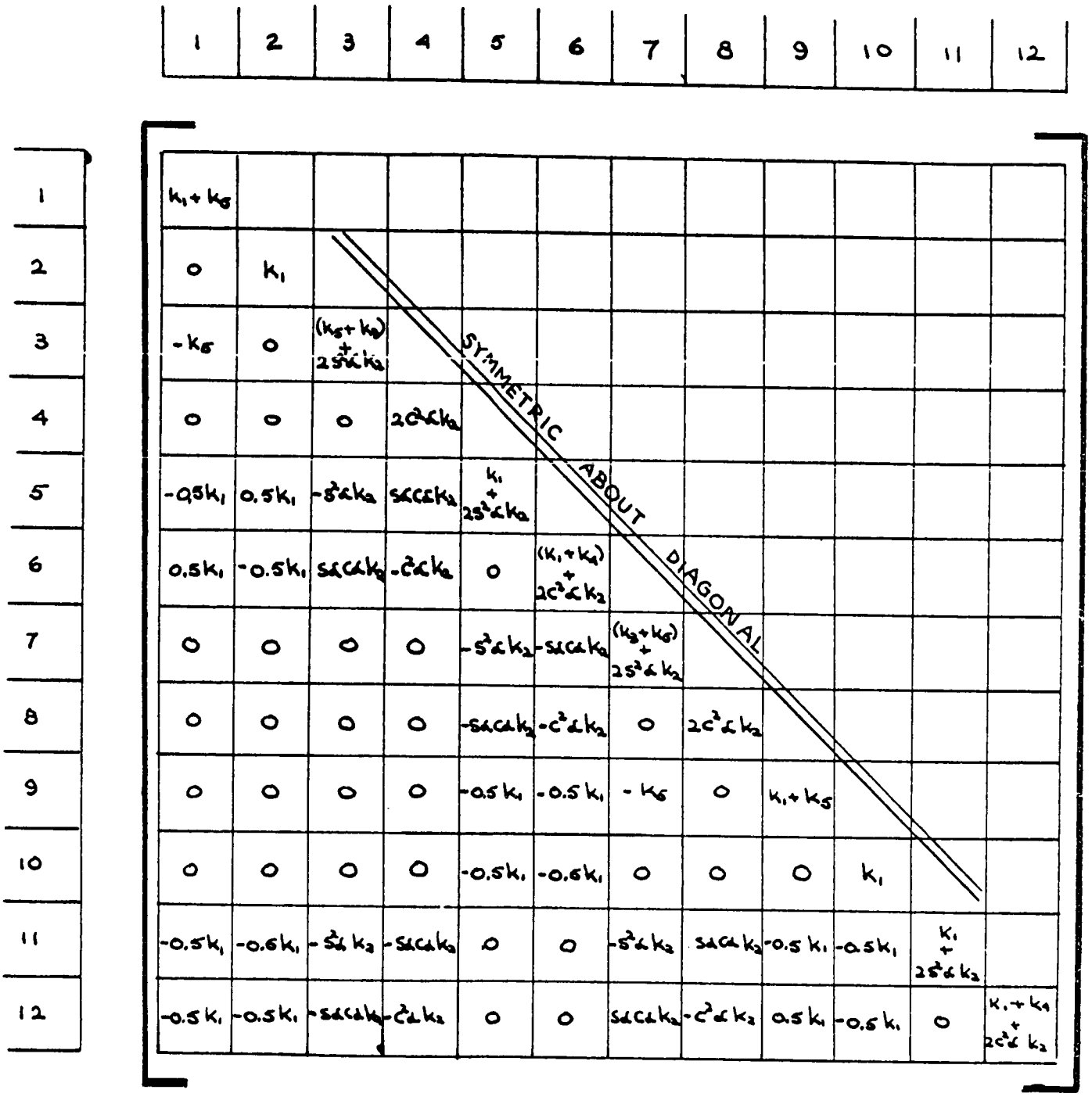

Figure 2.5-3 KWOT Literal Planar Stiffness Matrix

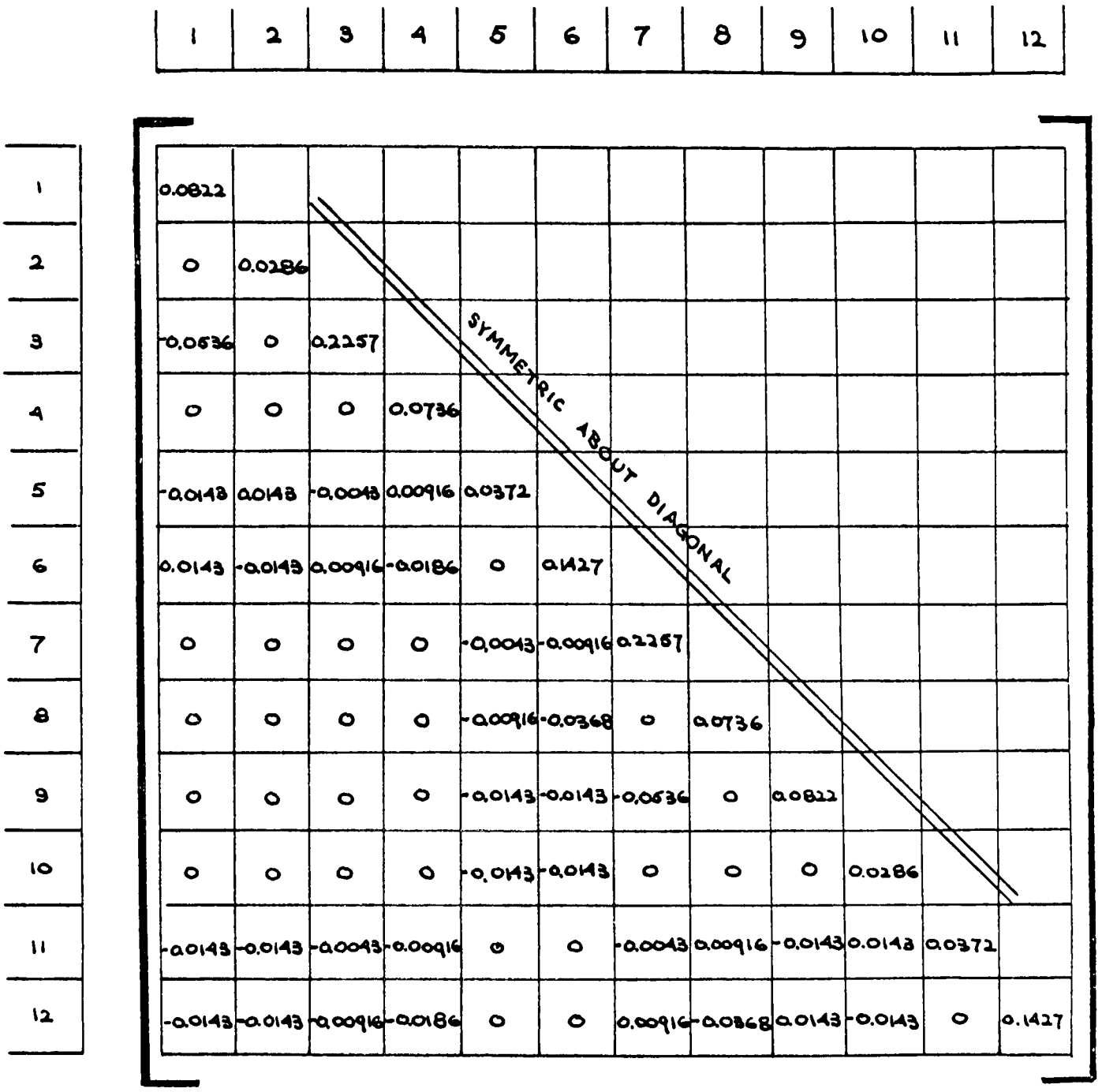

Figure 2.5-4 KWOT Simplified Planar Model Stiffness Matrix in lb./in.

$$\begin{bmatrix} \frac{\partial U}{\partial \xi_1} \\ \vdots \\ \frac{\partial U}{\partial \xi_n} \end{bmatrix} = [h]^T[E][h][\xi] + [h]^T[F_o] \qquad (2.4\text{-}56)$$

The above equation will yield, in matrix form, the required Lagrange expressions for structural stiffness. Operation $[h]^T[E][h]$ will yield a stiffness matrix of the form

$$\begin{bmatrix} K_{xx} & K_{xy} & K_{xz} \\ K_{yx} & K_{yy} & K_{yz} \\ K_{zx} & K_{zy} & K_{zz} \end{bmatrix} \qquad (2.4\text{-}57)$$

where the K_{XX}, K_{YY} and K_{ZZ} portions will have a diagonal form due to orthogonalization but the partitioned cross stiffness matrices will be non-zero due to the restraints imposed on the elements in the X, Y, or Z type modes.

Procedure for Determining Orthogonal Modes

The general procedure for orthogonalizing the structural degrees of freedom of the satellite is routine.

The eigenvectors of the satellite for the "center body fixed" configuration must be determined. The general equation takes the form

$$-\omega^2 [M][\Delta] + [E][\Delta] = [0] \qquad (2.4\text{-}58)$$

where $[E]$ is the stiffness matrix of the elements of the satellite in the X, Y, or Z directions in the "center body fixed" configuration and $[M]$ is the corresponding diagonal mass matrix. Solutions to this equation give a set of eigenvalues and corresponding eigenvectors.

Each set of modes determined in the above manner can be "freed" by releasing the appropriate translational constraint which was imposed on the center body. It will be noted that the rotational constraints on the satellite center body are not released and it follows that this procedure will lead to cross inertia terms between the rigid body rotations and modes determined in the above manner.

The restraint imposed on the center body such that it is permitted to translate, but not rotate about its own axes implies that the inertial angular orientation of any measuring system installed within the center body would only be a function of the 'rigid body' rotation coordinates whose rates are $\omega_X, \omega_Y, \omega_Z$.

The KWOT configuration is structurally symmetric about 3 planes. This property may be used to effect economies in the computation of normal modes of vibration. This economy

is achieved by computing a stiffness matrix for one half of the structure and calculating a flexibility matrix (by inversion of the stiffness matrix) for symmetric and antisymmetric motion of the component elements on either side of a plane of symmetry. (Figure 2.4-5)

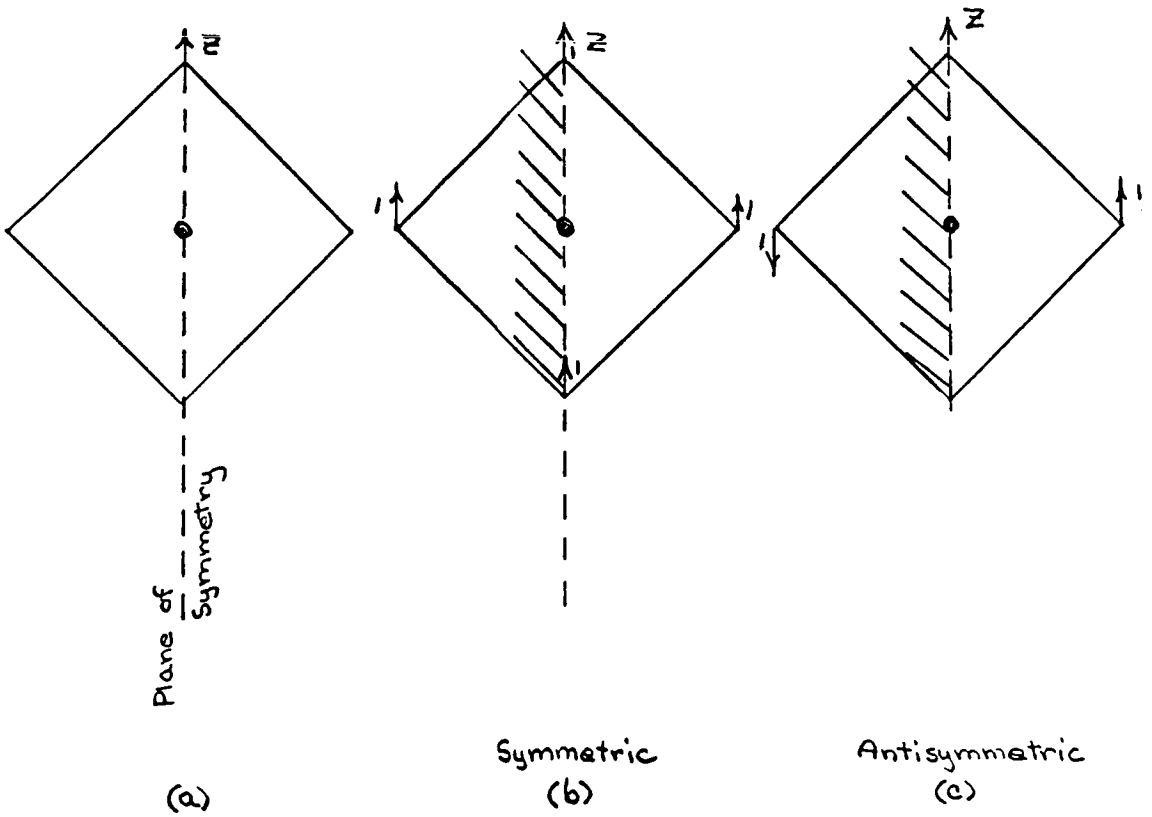

Figure 2.4-5 Symmetric and Antisymmetric Geometry

For computational purposes the masses and flexibilities of elements for one half of the structure will be considered and the elements lying in the plane of symmetry for the anti-symmetric case will be neglected since they will have no motion.

For the example indicated in Figure 2.4-5 one would have three degrees of freedom in case b (see figure) and only one degree of freedom in case c (see figure).

The subdivision of each set of X, Y, or Z type modes into symmetric and antisymmetric modes results in a further economy in the dynamic equations since the symmetric modes will have no inertial coupling with rigid body rotations ($\omega_X, \omega_Y, \omega_Z$) and the antisymmetric modes will have no cross inertias with rigid body translation ($\dot{X}_o, \dot{Y}_o, \dot{Z}_o$).

A great number of terms occurring in the dynamic equations of motion involve summation of the products of masses and rigid body coordinates and/or model displacements, e.g. $\Sigma \delta_m Y_r h_{mx}$. Terms of this type may be readily computed by matrix operations after the mode displacements (h_{i_X}) have been computed.

A stiffness matrix for the basic KWOT structure has been defined previously. In this particular example it has been assumed that the connecting cables remain straight. Therefore the use of this stiffness matrix in calculating the orthogonal modes of the structure implies that the following assumptions have been made on the dynamic characteristics of

the structure. These assumptions are as follows.

a. All cables remain in a continuous state of tension.

b. There is no cable sag, i.e., the lateral stiffness of the cables due to axial tension is large compared with the inertial loads occurring on the cables (function of cable mass).

c. Relative motions of the subsatellites cause no significant curvature in the cables.

If studies show that the cable tension forces are low enough and the inertial force high enough to cause significant distortion of the interconnecting cables it will be necessary to incorporate the elastic and inertial properties of the cables into the structural mode analysis.

REFERENCES

1. Meissner, C. J., "Direct Beam Stiffness Matrix Calculations Including Shear Effects," J. of Aerospace Sciences, Vol. 29, No. 2, Feb. 1962.

2. Materials Data: Dupont Bulletin M2-C
Dupont Mylar Polyester Film.

SECTION III

PRECESSION - SPIN DYNAMICS CONSIDERATIONS

3.1 GENERAL

3.1.1 Introduction

The material which follows describes the results of initial efforts in the area of KWOT position and attitude control. Two distinct approaches to this problem are possible. These approaches may be differentiated by the relative emphasis given to either passive or active control. The approach taken in the effort described here was to concentrate heavily on active control while considering passive control in a somewhat brief manner. This approach was taken for a number of reasons. The first and most important is that active control is more likely to be able to produce an acceptable level of performance since it permits much wider limits on allowable ignorance of exact system dynamics. In addition, future studies may well show the need for active stability augmentation and, therefore, substantially the same ground would have to be covered in any event. Finally, it is ultimately of interest to compare physical characteristics (size - weight - power) requirements with achievable performance levels when the detailed preliminary design stage of the project is reached.

3.1.2 Active Control

There are, basically, four subsystems which may be regarded as comprising the KWOT active control system. These systems are defined as follows:

a. Hub Absolute Position Control System

This system has not been considered since it is, essentially, a station keeping system and the techniques for accomplishing this function are both numerous and well known. In addition, depending on the final orbit selection, as well as mission analysis, the KWOT drift rates may be found to remain within acceptable limits without any control.

b. Hub Attitude Control System

This subsystem has been investigated in some detail with the results being presented in a subsequent paragraph.

c. Subsatellite Relative Position Control System

Preliminary studies have been initiated with regard to the synthesis of this control system. These studies are also described in a subsequent paragraph.

d. Subsatellite Orientation Control System

The purpose of this control system is to maintain the orientation of the four subsatellites fixed with respect to the hub. The design of the system should closely parallel the design of the hub attitude controller, which will be described in some detail. The attitude sensing problems for the subsatellites will, however, be somewhat simpler than those encountered in the hub attitude controller design.

3.1.3 Flexibility

In order to simplify the control design problem, the effects of the structure have initially been omitted, i.e.,

the control system design efforts have been aimed at synthesis of a system which could function without any structure connecting the subsatellites to each other and to the hub. This approach was taken because, as stated previously, inclusion of the structural dynamics complicates the problem to the point where it is very difficult to obtain the physical insight required for intelligent control system design. In addition, if the structure is subsequently determined to be incapable of providing useful adequate restraints on subsatellite motion the same ground would have to be covered to obtain a computation scheme for providing required force and torque increments. In future studies, however, complete structural-rigid dynamics of the KWOT will be considered. The conceptual diagram of Figure 3.1-1 shows the manner in which the interface will probably be handled. The outputs of one rigid body dynamics will be used to define the inertial motions of the points of attachment of the structure to the hubs and subsatellites. The structural dynamic model will, in turn, have as an output the reaction forces applied by the interconnecting structure to their points of attachment.

3.1.4 Passive Control

A substantial amount of thought has been devoted to passive means for controlling the KWOT vehicle. A basic concept for a passive control system has been evolved. This concept is described in a qualitative manner below. It is to be

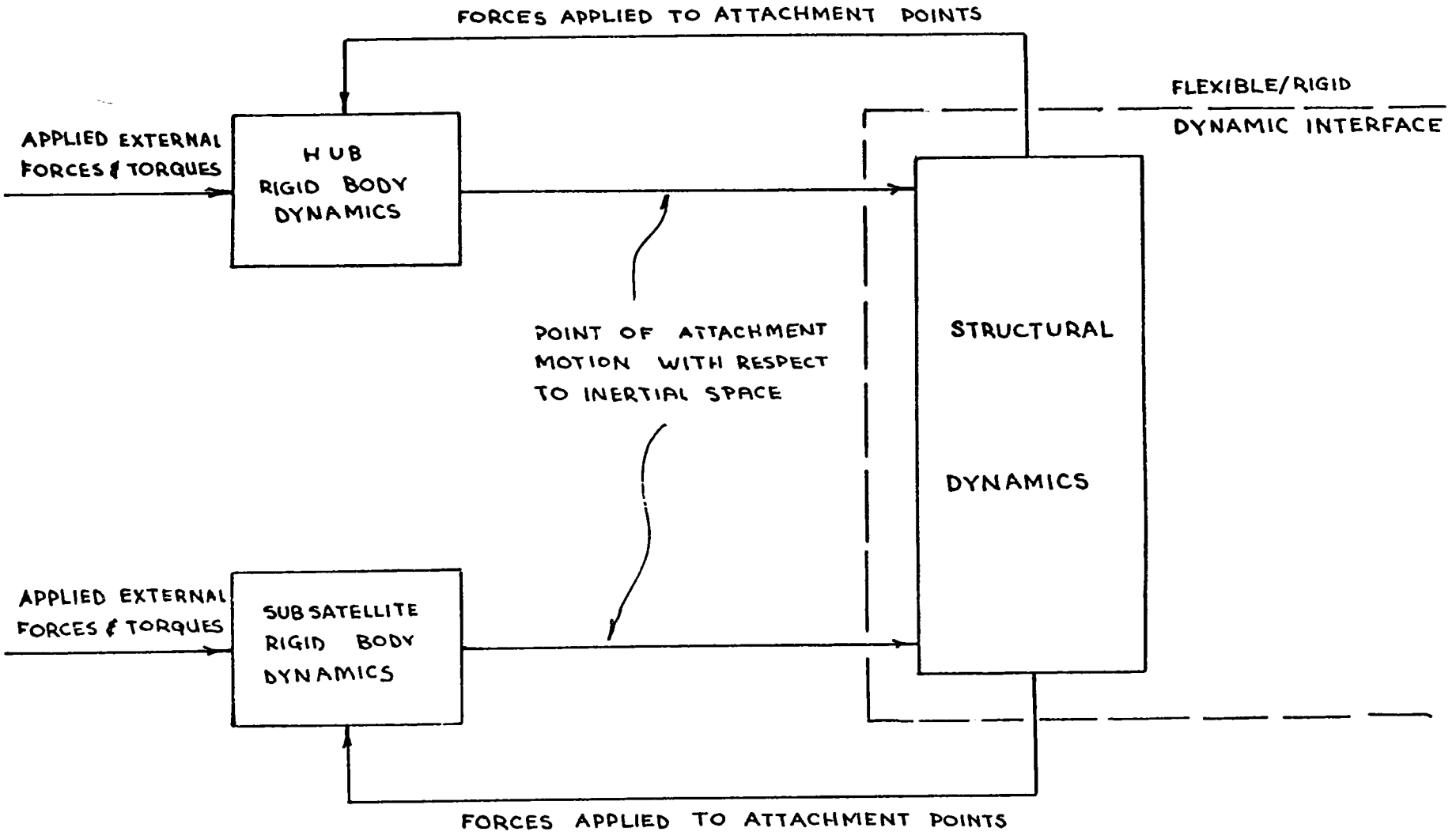

Figure 3.1-1 Conceptual Dynamic Interface

emphasized, however, that the feasibility of such a system can only be established by detailed dynamical studies, which are well beyond the scope of the present effort, so that it can only be said, at this time, that the concept appears to be worthy of more intensive study.

This control technique utilizes gravity gradient torques to achieve control of KWOT. If complete observation of a spherical volume once every orbit is satisfactory then an orbit may be chosen where the hub spin vector is precessed in the orbit plane and at the negative of orbital rate so that the hub spin vector always points along the local vertical towards the Earth's center. In addition, it is assumed that the centrifugal force resulting from the spinning hub is sufficient to cause the plane of the subsatellites to remain essentially normal to the hub spin axis. Finally, it is assumed that hub-axial inertia rods may be used to enhance gravity gradient torques so that they will be able to overcome the gyroscopic forces induced by the spinning hub to a point that acceptable hub pointing accuracy may be achieved. Another possibility might be the addition of an axial mounted wheel in the hub which spins at such a rate that the hub-wheel combination has a zero set spin angular momentum and, therefore, no set gyroscopic torque due to spin.

It is reiterated, however, that extensive studies including the effects of interim and thermal bending and induced

loadings would have to be very carefully studied in order to validate this concept.

3.2 MANEUVER REQUIREMENTS

3.2.1 Introduction

In this section a set of maneuver requirements are to be derived. These requirements will be evolved from the mission requirements in terms of motion of the reference frame with respect to the inertial frame. The object of subsequent attitude control subsystem synthesis efforts will then be the evaluation of a system which will cause the body axis system to be maintained in alignment with the reference frame within specified tolerances.

3.2.2 Sensor Geometry and Mission Requirement

The primary goal of the KWOT spacecraft is to completely scan the heavens periodically. The sensor to be used for this scanning may be defined, for purposes of control requirement definition, in terms of its field of view.

The spacecraft is sketched in Figure 3.2.1 while Figure 3.2.2 presents a schematic of the sensor field of view which is assumed to be essentially fixed with respect to the body axis frame.

From the sketch of Figure 3.2.3 it is easy to see that the sensor boresight direction nominally taken along $\underline{Y}_r$, may be expressed in the inertial frame as:

(3.2.1)

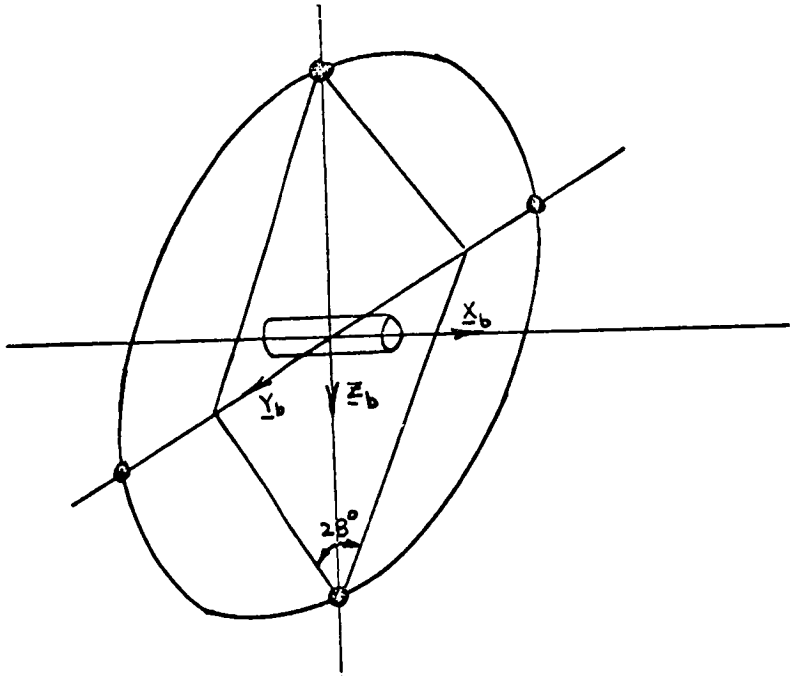

Figure 3.2.1

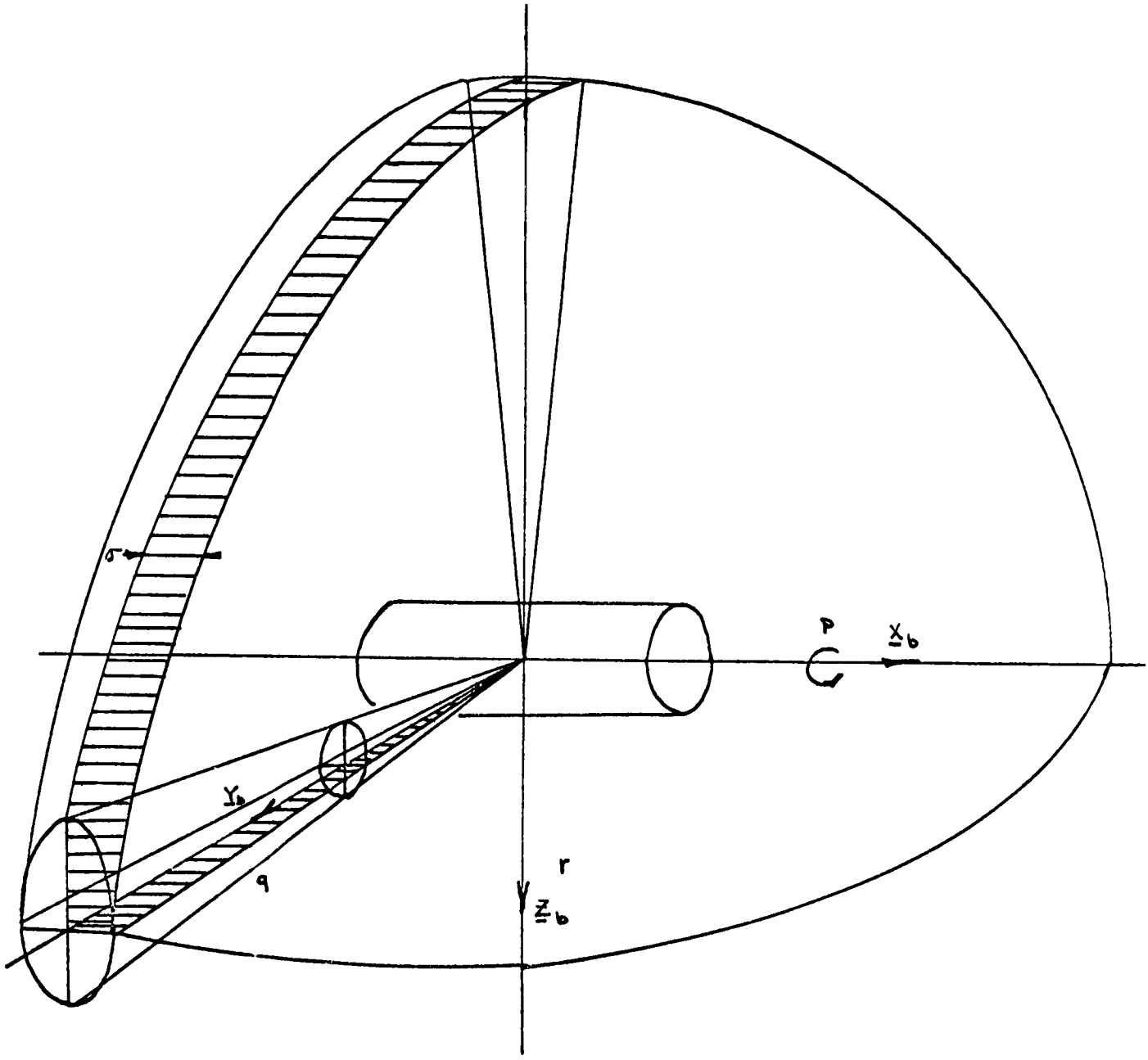

Figure 3.2.2

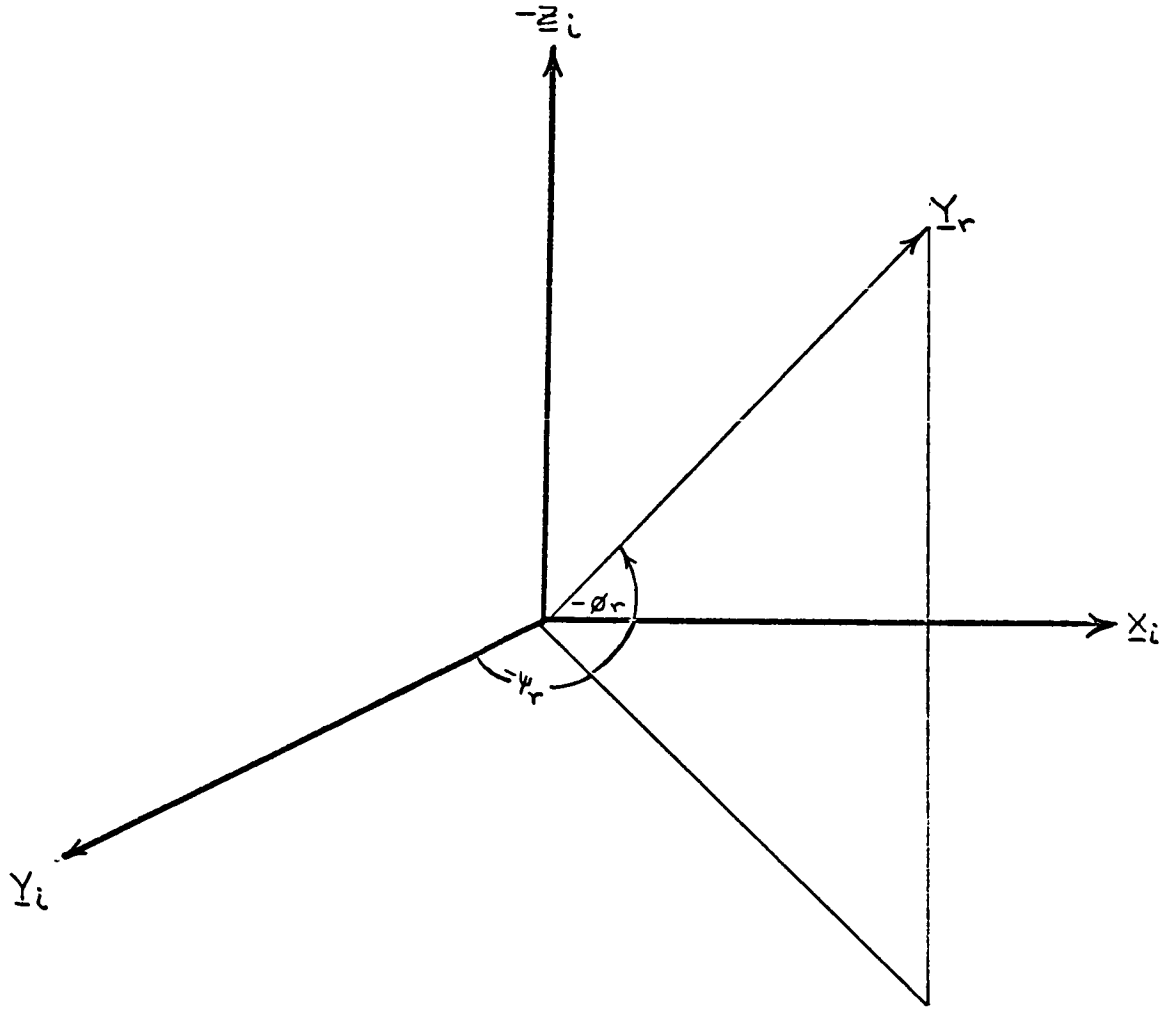
$-\underline{Z}_i$
$\underline{Y}_r$
$-\phi_r$
$\underline{X}_i$
$-\psi_r$
$\underline{Y}_i$

Figure 3.2.3

In order to establish the spacecraft maneuver requirements it now remains only to specify $\underline{Y}_r$ in terms of desired functions of ϕ_r and Ψ_r.

These requirements may be obtained, on a preliminary basis in an intuitive fashion. It is easy to see that the $\underline{Y}_r$ trajectory presented in Figure 3.2.4 will produce adequate spatial coverage. This trajectory corresponds to the angle functions:

$$\text{Yaw} \quad \dot{\Psi}_r = \dot{\Psi}_o \tag{3.2.2}$$

$$\text{Roll} \quad \dot{\phi}_r = \dot{\phi}_o \tag{3.2.3}$$

where $\dot{\Psi}_o$ and $\dot{\phi}_o$ are the desired precession and spin rates respectively. If σ is the conical scan angle then the maneuver requirement is approximately:

$$\frac{\dot{\Psi}_o}{\dot{\phi}_o} = \frac{2\sigma}{K\pi} \qquad \text{where } K(>1) \text{ depends on the desired minimum overlap.} \tag{3.2.4}$$

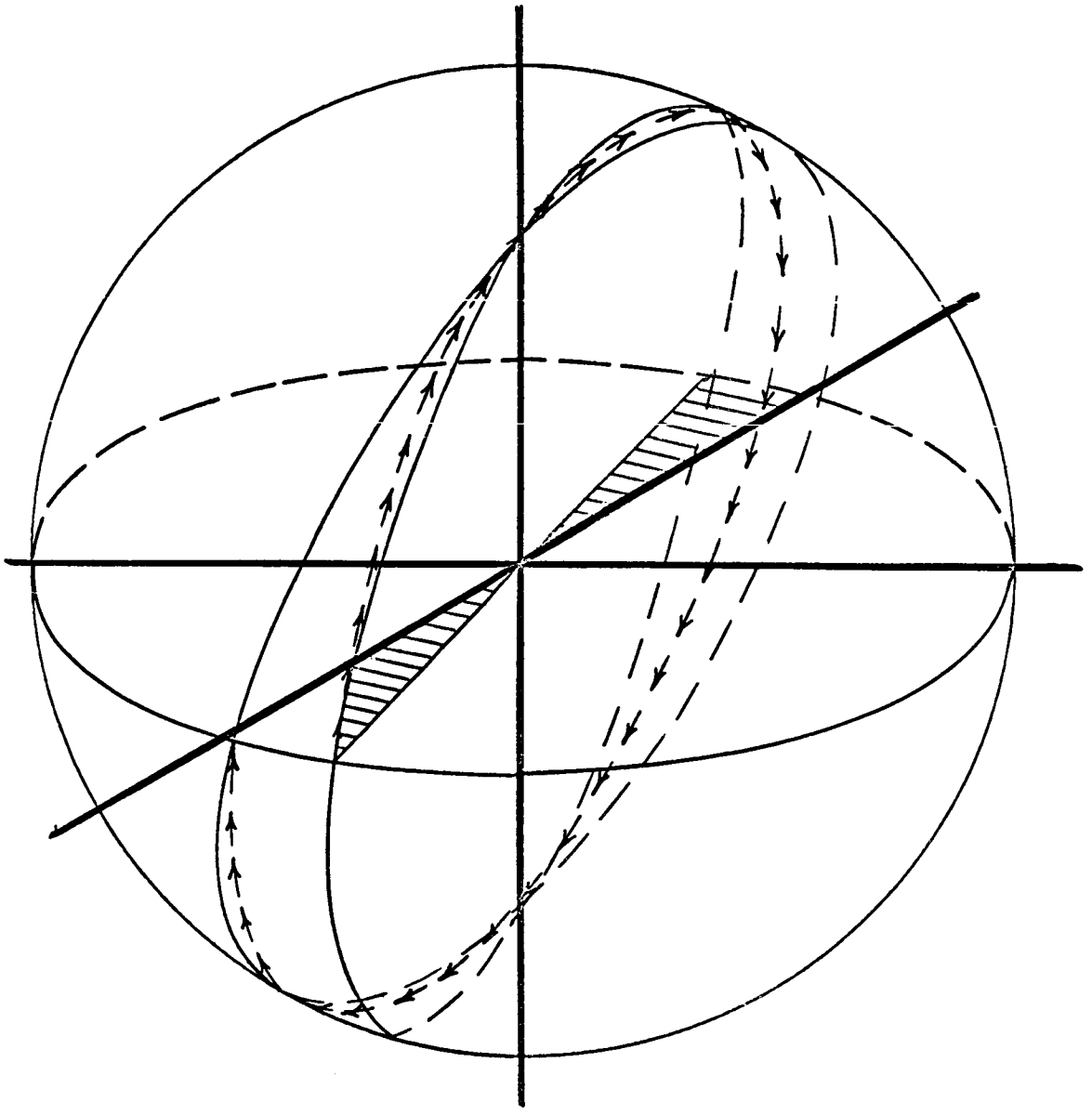

Figure 3.2.4

3.3 HUB CONSIDERATIONS (OPEN LOOP)

3.3.1 Introduction

The recommended concept for KWOT control requires that a central body, at the hub of the overall configuration, be utilized as a reference base for control of the subsatellites. In this initial study it is considered that the supporting structure provides no stiffness, thus the central body and subsatellites are treated as free bodies requiring independent control. The inclusion of cable forces on the individual bodies must be included eventually, but is considered to be beyond the scope of this phase of the study.

This section of the study provides a first order evaluation of the open loop characteristics of the central vehicle, considered here to be a free body. The object here is to provide recommendations regarding open loop characteristics such that well behaved dynamics suitable to this application are provided to ease the problem of closed loop control.

3.3.2 Precession at Orbital Angular Velocity

The presently conceived KWOT concept requires that the central axis spin at a particular rate to provide a circular scan. The spin axis is then precessed to provide coverage of the complete celestial sphere. A precession rate well suited to the problem is that of orbital rate. It is well suited in the sense that it considerably relieves the difficulty in

sensing the direction of the spin axis. By precessing at orbital angular velocity, the spin axis will be directed at the earth under ideal conditions. By employing earth sensors one has a measure of the spin axis misorientation by means of error signals generated in tracking the earth's horizon.

In the following section, the orbital period and angular velocity are computed for the altitude of KWOT.

The orbital period for a circular orbit may be obtained from the following expression:

$$\tau = \frac{2\pi}{\omega} = \frac{2\pi}{R_e}\sqrt{\frac{R^3}{g_o}} \qquad (3.3.1)$$

where $g_o = 9.83$ m/sec^2 (equatorial)

R_e = earth equatorial radius = 6.378×10^6 m

R = geocentric satellite altitude - 6.6378×10^7m

Solving (3.3.1) one obtains the period to be 1.696×10^5 sec. or 47.1 hrs.

The purpose of this section is to obtain a comparison of gravitational torques with the torques required to precess the spinning central vehicle at a rate equal to the orbital angular velocity.

With a vehicle having its "long" axis directed toward the local vertical, the gravitational torques about the cross

body axes of maximum inertia are approximately:

$$\tau = 3\,\omega_o^2\,(\Delta I)\sin\alpha \qquad (3.3.2)$$

where:

$\Delta I = (I_{max} - I_{long})$

α = angle off local vertical

ω_o = orbital angular velocity.

For the case of interest:

$\Delta I \cong 100{,}000$ slug ft.^{2}

$\omega_o = 3.7 \times 10^{-5}$ rad/sec.

and $\tau_{\substack{grav. \\ grad.}} = 4.11 \times 10^{-4} \sin$ (lb.-ft.)

3.3.3 Torque Required to Precess at Orbital Angular Velocity

Based on an antenna beam width of 6° and a desire for 3° overlap per spin rotation, a spin rate of 120 times the precession rate is required.

For precession at orbital frequency then, the required spin rate is:

$\omega_{spin} = 120 \times 3.7 \times 10^{-5}$ rad/sec.

$\omega_{spin} = 4.44 \times 10^{-3}$ rad/sec.

From Section II the body torque equations representing motion of the control body with respect to the reference frame are rewritten as:

$$T_x = I_x \ddot{\phi} + \dot{\psi}_r I_x \sin\phi_r \dot{\psi} + \dot{\psi}_r \dot{\phi}_r I_x \cos\phi_r \psi \qquad (3.3.3)$$
$$- \dot{\psi}_r I_x \dot{\theta} \cos\phi_r + \dot{\psi}_r \dot{\phi}_r I_x \sin\phi_r \theta$$

$$T_y = I_y \ddot{\theta} + \Delta I_{xz} \dot{\phi}_r^2 \theta + (I_x - 2I_z) \dot{\phi}_r \dot{\psi} \qquad (3.3.4)$$
$$+ (I_x - I_z) \frac{\dot{\psi}_r^2}{2} \sin 2\phi_r \psi + \dot{\psi}_r I_x \cos\phi_r \dot{\phi}$$
$$- \dot{\psi}_r \dot{\phi}_r I_x \sin\phi_r \phi + \dot{\psi}_r \dot{\phi}_r I_x \cos\phi_r$$

$$T_z = I_z \ddot{\psi} + \Delta I_{xy} \dot{\phi}_r^2 \psi - (I_x - 2I_z) \dot{\phi}_r \dot{\theta} \qquad (3.3.5)$$
$$+ \Delta I_{xy} \frac{\dot{\psi}_r^2}{2} \sin 2\phi_r \theta - \dot{\psi}_r I_x \sin\phi_r \dot{\phi}$$
$$- \dot{\psi}_r \dot{\phi}_r I_x \cos\phi_r \phi - \dot{\psi}_r \dot{\phi}_r I_x \sin\phi_r$$

From equations (3.3.4) and (3.3.5) it is seen that the last two terms represent the control torques required to cause the body frame to rotate with the reference frame. This is seen by letting the Euler angles and their rates equal zero. The remaining terms in the y and z equations respectively are:

$$+ \dot{\psi}_r \dot{\phi}_r I_x \cos\phi_r \qquad (3.3.6)$$

$$- \dot{\psi}_r \dot{\phi}_r I_x \sin\phi_r \qquad (3.3.7)$$

Equations (3.3.6) and (3.3.7) when expressed in inertial coordinates provide the following resultant torque:

$$\sigma_{Precess} = \dot{\psi}_r \dot{\phi}_r I_x$$

$$\text{for } \dot{\psi} = \omega_o \text{ , } \& \ \dot{\phi} = \omega_{spin} \text{ , } \& \ I_x = 10^5 \text{ slug-ft}^2 \qquad (3.3.8)$$

$$\sigma_{Precess} = 1.64 \times 10^{-2} \text{ Ft-lb.}$$

It is seen from the previous calculations in this section that gravitational torques are several orders of magnitude smaller (for any appreciable angle of the long axis off the local vertical) than that required for precession at orbital frequency.

Orientation of the cylinder along the local vertical is a preferred orientation from the point of view of sensing vehicle orientation. For the configuration under study with the desired spin and precession rates, local vertical orientation does not however provide sufficient torque to further consider gravity gradient stabilization.

It is not considered feasible to utilize the entire antennas/subsatellite configuration due to the extreme non-rigidity of the connecting structure. Further study may show that gravity stabilization is a feasible technique for the KWOT configuration only if sufficient stiffness is inherent in the connecting structure. For the structure presently under study it is not felt that this is the case.

3.3.4 Stability of the Central Spinning Body

a. Stability During Precession

The purpose of this section is to investigate

stability aspects of the central body during combined rotational and precessional motion. The object here is to provide as stable a motion as possible during precession and rotation so that the control system can perform its task more easily in establishing the central vehicle as a reference for control of the subsatellites.

Moment equations of the central vehicle in terms of body axes are:

$$M_x = \dot{h}_x + \omega_y h_z - \omega_z h_y \tag{3.3.9}$$

$$M_y = \dot{h}_y + \omega_z h_x - \omega_x h_z \tag{3.3.10}$$

$$M_z = \dot{h}_z + \omega_x h_y - \omega_y h_x \tag{3.3.11}$$

Torques required for precession expressed in terms of body axes are:

$$T_y = \omega_x \omega_p I_x \cos \phi \tag{3.3.12}$$

$$T_z = - \omega_x \omega_p I_x \sin \phi \tag{3.3.13}$$

Assuming external moments are zero and that $I_y = I_z \triangleq I_o$, equations 3.3.9, 3.3.10, and 3.3.11 are expressed

as follows when torques required for precession are included:

$$I_x \dot{\omega}_x = 0 \tag{3.3.14}$$

$$I_o \dot{\omega}_y + \omega_z \omega_x (I_x - I_o) - \omega_x \dot{\psi}_r I_x \cos \omega_x t = 0 \tag{3.3.15}$$

$$I_o \dot{\omega}_z + \omega_y \omega_x (I_o - I_x) + \omega_x \dot{\psi}_r I_x \sin \omega_x t = 0 \tag{3.3.16}$$

Body rates expressed in terms of reference frame rates are the following:

$$\omega_x = \dot{\phi}_r \tag{3.3.17}$$

$$\left.\begin{aligned} \omega_y &= \dot{\psi}_r \sin \phi_r \\ \omega_z &= \dot{\psi}_r \cos \phi_r \end{aligned}\right\} \quad \dot{\psi}^2 = \omega_y^2 + \omega_z^2 \tag{3.3.18}$$

$$\tag{3.3.18}$$

"Stability" in the sense used here means the ability of the central satellite to maintain the body velocities expressed in equations 3.3.17, 3.3.18, and 3.3.19. This implies that the body will precess in the desired manner.

Therefore, we wish to examine equations 3.3.15 and 3.3.16 and its parameters to obtain the velocities of equations 3.3.18 and 3.3.19 as closely as possible when under the in-

fluence of the appropriate forcing function. Equations 3.3.18 and 3.3.19 are exact solutions to equations 3.3.15 and 3.3.16 which can be verified by differentiating 3.3.18 and 3.3.19 and substituting into equations 3.3.15 and 3.3.16. The question of stability during forced precession by application of control torques is not a significant one, when the exact forcing function is applied. How exact the applied control torques are is a function of control systems implementation. Since any physical system will not be perfect, certain degradations in performance are to be expected. To determine actual system performance closed loop analysis of the final control system configuration is required.

A further question regarding stability of the central vehicle exists which bears some discussion. That is the nutation of the central body during spin either without precession or during precession. If the spinning body is subjected to extraneous torques or if the control torques are not perfect, nutation will occur. Nutation is most clearly discussed for the case of spin without precession. The nutation frequency for this case is, however, identical for the precessional case.

b. Spin Stability Without Precession

Rewriting equations 3.3.15 and 3.3.16, but without the precessional torque term, will provide the required equations for stability examination of the spinning central body.

$$I_o \dot{\omega}_y + \omega_z \omega_x (I_x - I_o) = 0 \qquad (3.3.20)$$

$$I_o \dot{\omega}_z + \omega_y \omega_x (I_o - I_x) = 0 \qquad (3.3.21)$$

differentiating equation 3.3.20

$$I_o \ddot{\omega}_y + \dot{\omega}_z \omega_x (I_x - I_o) = 0 \qquad (3.3.22)$$

and substituting equation 3.3.21 into equation 3.3.22

$$\ddot{\omega}_y + \left[\omega_x^2 \left(\frac{I_x - I_o}{I_o} \right)^2 \right] \omega_y = 0 \qquad (3.3.23)$$

This equation is seen to be stable (non divergent) regardless of whether the spin axis inertia (I_x) is greater or less than I_o. It is well known, however, that if the body is not rigid and energy dissipation takes place through structural deformation that the system is stable only if spinning about an axis of maximum inertia.

It is therefore recommended that the central body be configured such that the cylinder axis is one of maximum inertia.

Note that the term in brackets (equation 3.3.23) defines the nutation frequency (sometimes called coning or wobble).

Therefore

$$\omega_N = \omega_x \left(\frac{I_x - I_o}{I_o}\right) \tag{3.3.24}$$

Depending on whether I_x is greater or less than I_o, the resulting nutation is either in opposition or in the same direction as vehicle spin velocity.

If the total angular momentum is initially in the direction of the vehicle X axis, no coning will exist. If, however, an impulsive torque or other extraneous or improper control torques are applied coning motion will occur.

The coning effect will be considered during the subsequent discussion on pulse torquing. The influence of coning on performance and means for damping this undesirable motion are implicitly considered in the analysis and design of a proper control system.

c. Precessional Torque Requirement

The last terms of equations 3.3.16 and 3.3.17 are the torques required to precess the central vehicle. These are rewritten as

$$T_y = -\omega_x \dot{\psi}_r I_x \cos \omega_x t \tag{3.3.25}$$

$$T_z = \omega_x \dot{\psi}_r I_x \sin \omega_x t \tag{3.3.26}$$

Total torque as expressed in inertial coordinates is the following

$$T = \left(T_y^2 + T_z^2\right)^2 = \omega_x \dot{\psi}_r I_x \qquad (3.3.27)$$

Since a spin rate of 120 times the precession rate is required due to antenna beam width and a desirable scan pattern as discussed previously, equation 3.3.27 may be re-written as:

$$T = 120\, \dot{\psi}_r^2\, I_x \qquad (3.3.28)$$

This equation is plotted in figure 3.3.1 to provide a ready reference to the tradeoffs between spin rate, precession and required control torque. It shows the total precessional torque required as a function of precession rate ($\dot{\psi}_r$), spin axis inertia, and spin rate.

3.3.5 Precessional Torque Devices

To achieve a steady precession rate by means of continuous torquing it is felt that gyroscopic devices hold more promise than mass expulsion devices which require a continuous expenditure of consumables. In the case of pulse torques, serious timing and nutation synchronization problems exist which must be overcome. On the other hand, gyroscopic rotary reaction devices require continuous power but do have the advantage of cyclic operation for the KWOT application. Cyclic

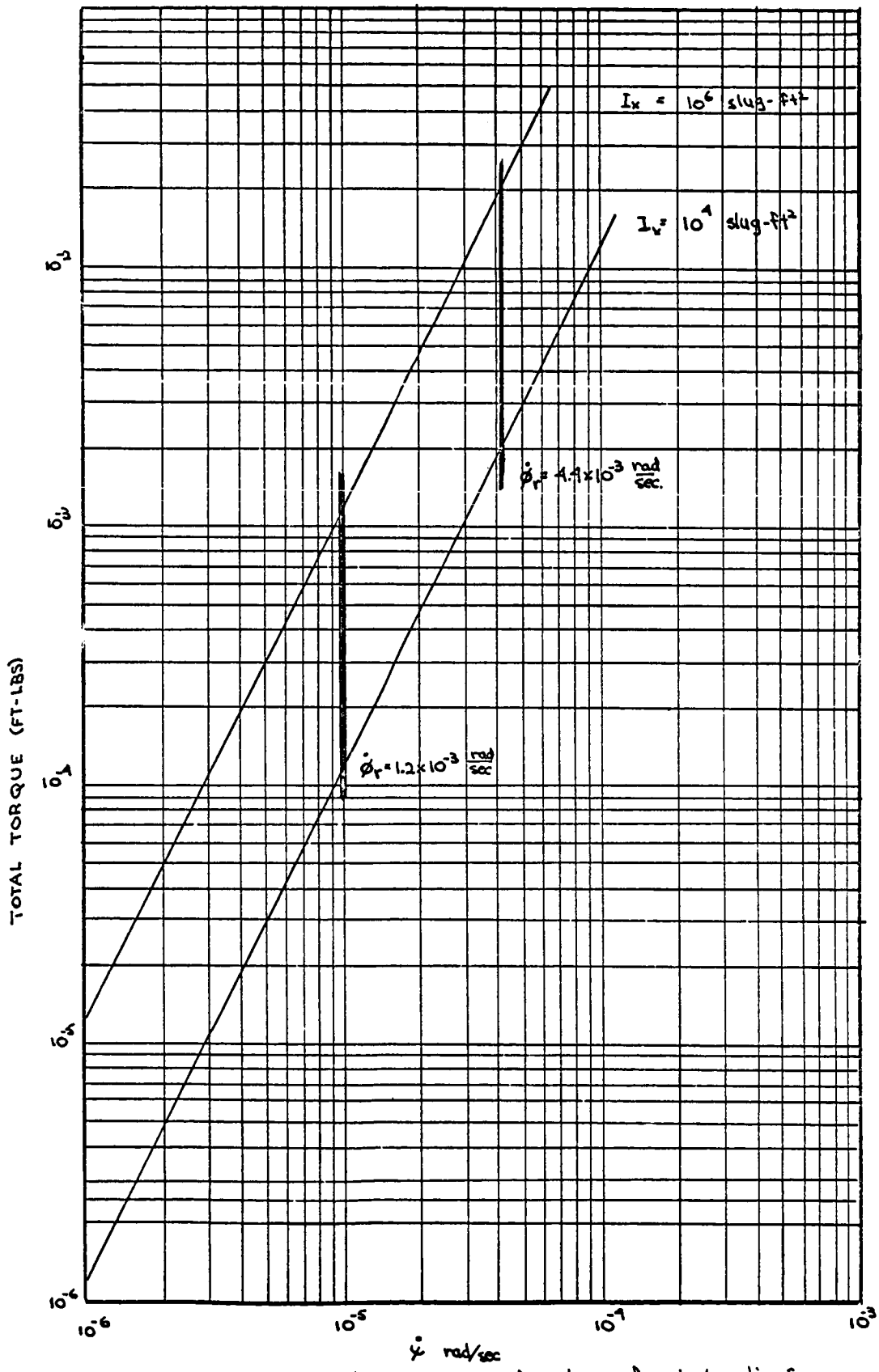

Figure 3.3.1 Precessional torque as a function of spin inertia and precession rate

operation does not require secondary devices for momentum unloading of the gyroscopic elements. A possible disadvantage to gyroscopic or rotary reaction devices is that of deleterous cross coupling effects, which are investigated in the next few paragraphs.

a. Reaction Wheel Torquers

For a reaction wheel control system which possesses gyroscopic coupling terms, the body rotational equations are the following. (Once again $I_y = I_z = I_o$ and external moments are zero).

$$I_x \dot{\omega}_x + \omega_y h_{cz} - \omega_z h_{cy} = 0 \qquad (3.3.29)$$

$$I_o \dot{\omega}_y + \dot{h}_{cy} + \omega_z \omega_x (I_x - I_o) - \omega_x h_{cz} = 0 \qquad (3.3.30)$$

$$I_o \dot{\omega}_z + \dot{h}_{cz} + \omega_y \omega_x (I_o - I_x) + \omega_x h_{cy} = 0 \qquad (3.3.31)$$

where

Reaction Control Torques

$$\begin{cases} h_{cy} = -\omega_x \dot{\psi}_r I_x \cos \omega_x t \\ h_{cz} = +\omega_x \dot{\psi}_r I_x \sin \omega_x t \end{cases}$$

Control Element Momentum

$$\left.\begin{cases} h_{cy} = -\dot{\psi} I_x \sin \omega_x t \\ h_{cz} = -\dot{\psi} I_x \cos \omega_x t \end{cases}\right\} \text{considering } \omega_x \text{ is constant}$$

for the desired precessional motion we know from equation e.e.18 and equation 3.3.19 that

$$\omega_y = \dot{\psi}_r \sin \omega_x t$$

$$\omega_z = \dot{\psi}_r \cos \omega_x t$$

Substituting these desired values of ω and h into equation 3.3.29 we can determine if the body spin rate is influenced by gyroscopic coupling terms when the vehicle precesses in the desired manner.

$$I_x \dot{\omega}_x - (\dot{\psi})^2 I_x \sin \omega_x t \cos \omega_x t + (\dot{\psi})^2 I_x \sin \omega_x t \cos \omega_x t = 0 \qquad (3.3.32)$$

This equation indicates that the vehicle spin rate, ω_x, will not be affected by gyroscopic coupling if it can be now shown that the other two axes are not adversely influenced.

Substitute desired ω's and h's into equation 3.3.30 where the desired $\dot{\omega}_y$ and $\dot{\omega}_z$ are obtained by differentiating equations 3.3.18 and 3.3.19.

$$I_o \dot{\psi} \omega_x \cos \omega_x t - \omega_x \dot{\psi} I_x \cos \omega_x t + \omega_x I_x \dot{\psi} \cos \omega_x t - I_o \omega_x \dot{\psi} \cos \omega_x t + \omega_x \dot{\psi} I_x \cos \omega_x t = 0 \qquad (3.3.33)$$

Since complete cancellation of terms is not obtained it is evident that gyroscopic coupling of a standard reaction control wheel precludes achieving the desired central vehicle motion. It is interesting to note that the control term and

the gyroscopic coupling term in equation 3.3.33 are of identical form. If the control torque term were minimized, the gyroscopic coupling term would provide an effective control. It may be fruitful to explore this further.

b. Single Axis Control Moment Gyro

If a single axis gyro is used to provide vehicle control torques, the control torque is

$$T_c = h_g \left(\frac{d\theta}{dt} \right) \tag{3.3.34}$$

where

θ = gyro gimbal angle

h_g = wheel momentum.

For the y axis the control torque required for precession is substituted into equation 3.3.34

$$\omega_x \dot{\psi}^{\circ} I_x \cos \omega_x t = h_g \frac{d\theta}{dt} \tag{3.3.35}$$

Solving for θ

$$\theta = \frac{I_x \dot{\psi}^{\circ}}{h_g} \sin \omega_x t \tag{3.3.36}$$

If θ is kept small, the cross coupling into other vehicle axes will also be small. To get a feel for the magnitude of gyro momentum required, consider the magnitude of θ to be one degree

which presumably would keep coupling effects small. The gyro momentum would then be

$$h_g = 57.3\ I$$

$$\approx 21.2 \text{ ft.-lb.-sec.}$$

for $I_x = 10{,}000$ slug ft.^{2}

$\dot{\psi}^\circ = 3.7 \times 10^{-5}$ rad/sec.

Such a momentum can be obtained in a gyro wheel at relatively little cost in weight (estimated at 20-25 pounds). Note that wheel momentum is directly related to vehicle spin axis inertia. This provides additional reason for minimizing the moment of inertia of the spin axis. Previously it was recommended that the spin axis inertia be a maximum. If single axis control moment gyros are used to provide precessional torques, the central vehicle configuration should resemble a thin disk.

c. Pulse Torquing

This method of torquing would ideally provide an impulsive torque once per rotation of the spin axis by means of firing a reaction control jet.

Equation 3.3.27 represents the total continuous torque required to achieve precession. In the case of a pulse torquer we would like to achieve an average equal to the continuous case. It is also desirable to minimize pulse width in order to keep vehicle wobble at a minimum. State of the art pulse rocket technology can provide approximately 10 milli. sec. pulse widths.

For continuous torquing, the torque-time product can be expressed as $2\pi I_x \dot{\psi}$. The impulsive torque which provides the appropriate time average is expressed as

$$T_{imp} = 200\pi I_x \dot{\psi} \quad (ft\text{-}lbs) \tag{3.3.37}$$

Once again to obtain a feel for magnitudes we will compute T_{imp} for the minimum inertia (10,000 slug ft.^{2}) and orbital angular velocity. For this case T_{imp} would be approximately 74 ft-lbs. Considering a 10 foot moment arm, this would require approximately a 23.2 pounds of thrust, which is not unreasonable.

For a specific impulse of 270 seconds, an expenditure of 10^{-3} pounds of propellant would be required per pulse or once per spin revolution. If precessing at orbital angular velocity and providing 100% scan coverage overlap, the required vehicle spin rate would be 4.44×10^{-3} rad/sec which implies approximately 2.5 pulses per hour would be required to maintain precession. Thus a $2.5 \cdot x\ 10^{-3}$ lbs/hour propellant consumption is required in order to utilize a pulse torquer.

A serious disadvantage exists with the pulse torquing method. Nutation or coning occurs as a result of applying an impulsive torque, the frequency of nutation being dependent on the vehicle inertia configuration and spin rate. The difficulty with this method exists in timing the applica-

tion of the torque impulse. The torque should be applied (in order to achieve the desired average precession) every half cycle of nutation. Simultaneously the body mounted impulse torquers must be in the proper position to fire with respect to the spin rotation. The time to apply the torque as well as synchronization of nutation and spin rates, are difficult problems to implement and at times lead to dubious system performance. Such techniques are used for very coarse control of spin vehicles, but are unsuitable for precise control.

3.3.6 Conclusions

We have attempted to show some fundamental open loop considerations in regard to control of the central spinning vehicle. The more significant points of the previous discussions are summarized below.

a. Gravity gradient stabilization of the central vehicle in its presently conceived configuration (20 x 50 ft. cylinder) would not provide sufficient restoring torques to precess at orbital angular velocity. The gradient torques are several orders of magnitude less than that required for precession.

Orientation of the spin axis along the local vertical (precession at orbital rate) does however provide ease of sensing spin axis orientation by observing the relative position of the earth. This will be further discussed in the control system section.

b. The intent of stability discussions was to obtain insight into preferential configurations and desirable spin and precession rates in order to establish a dynamically well behaved central vehicle prior to considering closed loop control. Along these lines the following recommendations are made.

The spin axis of the control vehicle should be an axis of maximum inertia. This is required to provide inherent stability when energy dissipation occurs due to structural elasticity. This stability requirement is necessary after deployment of subsatellites, during and after completion of spin up prior to the start of precession.

From the point of view of minimizing torques required for precession, the spin axis inertia should be as small as possible. To satisfy this and the previous requirement the control vehicle should resemble a thin disk.

c. Section 3.3 has shown that continuous sinusoidal body torques as shown, provide an exact solution to the body rotational equations of motion. The problem of implementing such a precessional torque is a problem requiring considerable study (to be discussed in the section on control systems).

It has been shown that rotary control elements such as reaction wheels, control moment gyros and the like, provide a unique advantage: since the precessional torques in body axes are cyclical in nature, cyclic operation of these devices does not require momentum unloading.

It has also been shown that gyroscopic cross coupling provides undesirable terms in the equations of motion. How undesirable these are requires detailed analysis. It is clear however that the direction to go in is to implement a technique where coupling terms are minimized (e.g., maintaining a small gimbal angle for a single axis gyro).

Preliminary investigation of a pulse torquer has shown this technique to be not unreasonable from the point of view of thrust level and propellant consumption. Factors which detract from this technique are pulse timing and syncronization of nutation and spin frequencies. The resulting coarse vehicle control due to nutational motion would have a serious adverse effect on the use of the central vehicle as a reference base for control of the subsatellites.

3.4 HUB CONSIDERATIONS (CLOSED LOOP)

This section describes the closed loop attitude control of the central vehicle. It has been previously shown that a continuous torque application to the central body is required to achieve a desired precession rate. This section will describe how corrective torques are obtained if the central vehicle motion strays from the ideal.

A control system will be described for the case where precession rate is set equal to orbital angular velocity. Figure 3.4.1 illustrates the instantaneous orientation of the central body axes. The spin axis (the x axis) is directed

along the local vertical, and the precessional torque (T_c) is nominally in the plane of the orbit in the direction of the

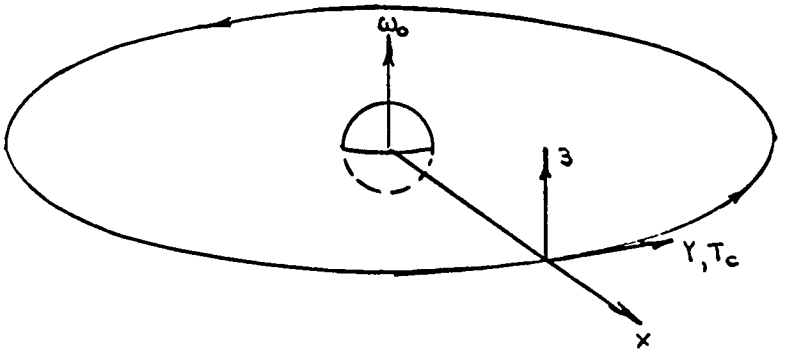

Figure 3.4.1

satellite velocity vector. For this nominal situation the precession rate vector is seen to be colinear with the orbital rate vector. If an error exists between the spin axis and the local vertical vehicle correction can be obtained by adjusting the direction and/or magnitude of the control torque vector.

Figure 3.4.2 shows the implementation of this control scheme. The earth sensor output is $(\varepsilon_\psi^2 + \varepsilon_\theta^2)^{1/2} \sin\omega_x t$. Corrective action is obtained by changing the magnitude of the control torque if an in plane error exists and by rotation of the torque vector if an out of plane error exists. This may be obtained by use of a gradient control technique.

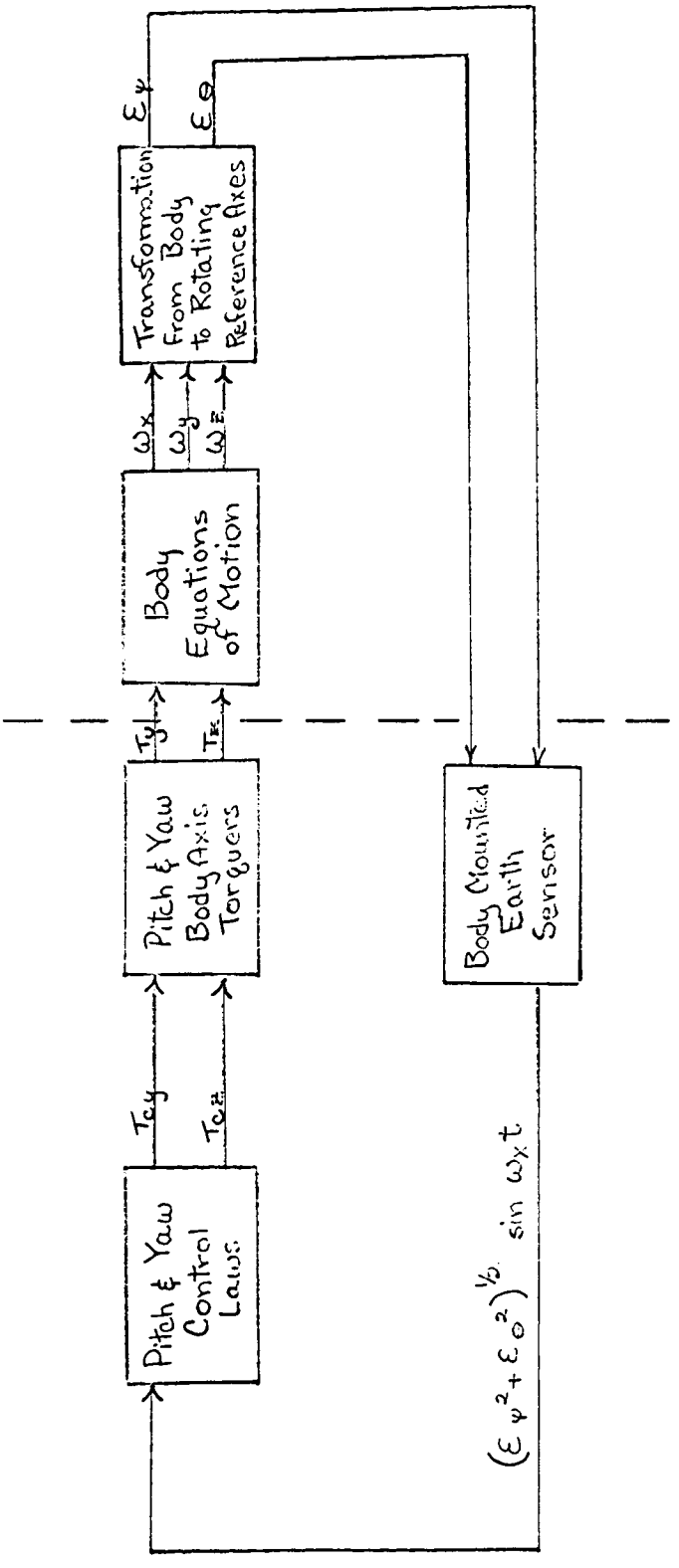
Pitch & Yaw Control Laws
Pitch & Yaw Body Axis Torquers
Body Equations of Motion
Transformation From Body to Rotating Reference Axes
Body Mounted Earth Sensor
T_{ay}
T_{ax}
T_y
T_x
ω_x
ω_y
ω_z
ε_ψ
ε_θ
$(\varepsilon_\psi^2 + \varepsilon_\theta^2)^{1/2} \sin \omega_x t$

Figure 3.4.2

Another possible hub attitude controller implementation is presented in figure 3.4-3. The attitude reference package senses the three error angles, ϕ, θ, and ψ. This package might consist of a horizon scanner, four to six sun sensors, and required coordinate transformation electronics. It's outputs are the sensed angles.

The control torques for pitch and yaw aces are obtained by gating the error angle signals through switches which fire at twice the natural frequency of the pitch and yaw loops. These switch outputs are applied to bang-bang torques which supply the required control torques. In addition, periodic proportional torques are supplied which establish the nominal spacecraft motion.

In this system concept the closed altitude control loops may be viewed as functioning in a supervisory manner, i.e., supplying small corrections to compensate for errors in the generation of the nominal maneuvering torques.

3.5 RELATIVE POSITION CONTROL (SUBSATELLITES)

In this section, the problem of relative position control of the subsatellites will be formulated and some problem areas will be given preliminary consideration. The problem will not be solved since, as will be shortly seen, the dynamical situation, even when framed in simplified terms, is quite complex. The analytical machinery necessary for its solution will, however, be set up in enough detail so that the effort

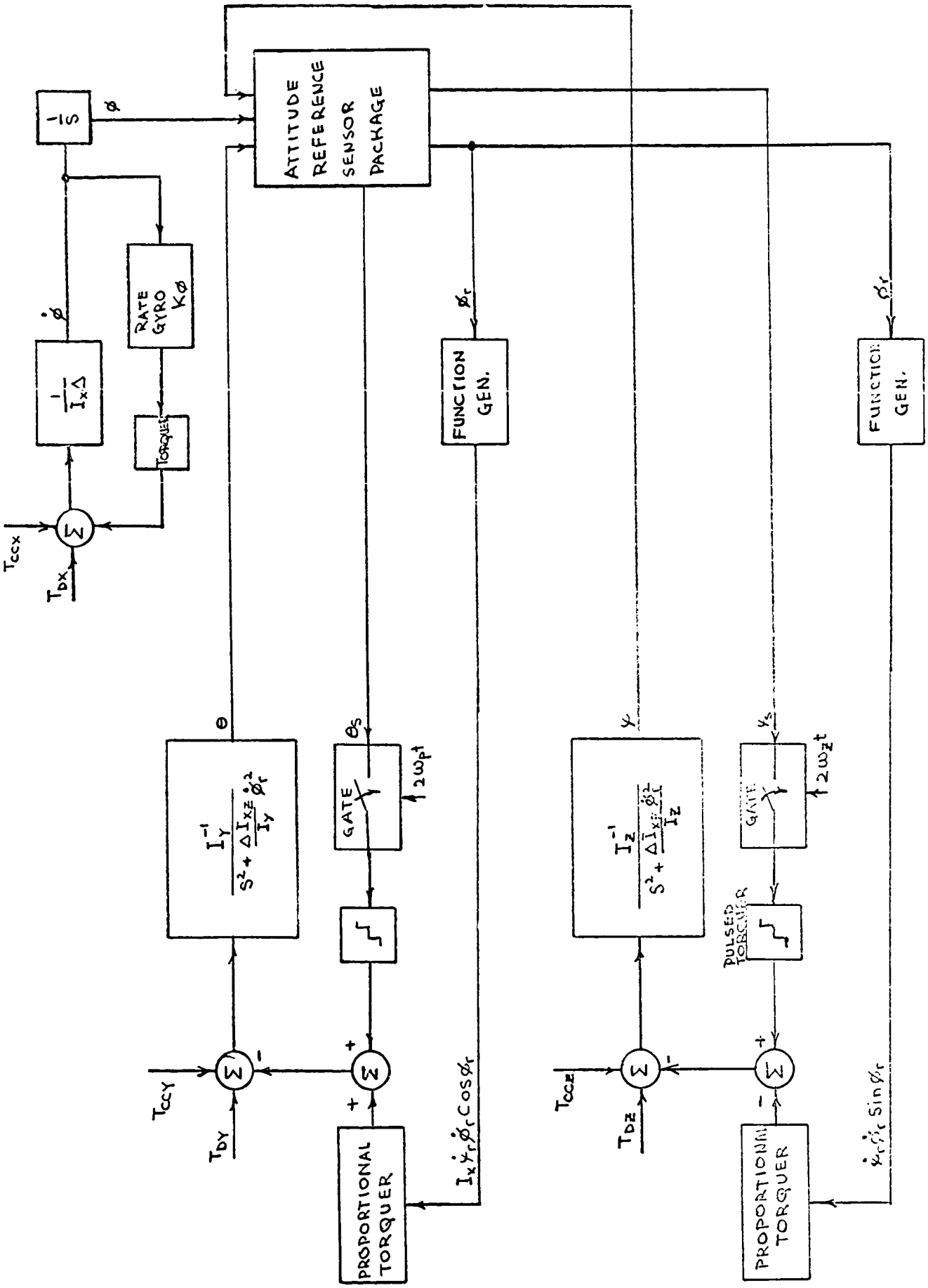

Figure 3.4.3 Hub Attitude Controller - Conceptual Block Diagram

required for a complete colution will be quite clear.

In the problem statement, notation defined in Figure 3.5-1 will be used, i.e., 0 denotes the origin of the inertial reference frame, 0'denotes the subsatellite c.g. and 0" denotes the hub c.g. (nominally at the origin of the reference and hub body frames).

In order for the formulation of the translational equations of motion to be of maximum use in control system synthesis, they should be expressed in terms of vectors which are relatively easy to measure. Referring to Figure 3.5-1, the relative position vector, $\underline{R}_{(0'0")}$, when expressed in hub coordinates is relatively easy to measure. Figure 3.5-2a illustrates the measurement. The angles α_{11} and α_{12} may be measured with sun sensor type devices, while ℓ_s, may be measured in a variety of ways such as by active ranging or optical triangulation techniques. If centrifugal forces on the subsatellite are adequate, it may simply be assumed that ℓ_s, is constant.

Measurement of $\underline{R}_{(00")}$ expressed in an Earth fixed system will probably be accomplished "for free" since the communication antenna may have to be pointed at the spacecraft in order to minimize transmitter power. It is, however, not expected that any sort of station keeping, except for initial error correction, will be required. It is, however, convenient to express this vector in terms of the inertial frame, as illustrated in Figure 3.5-2b.

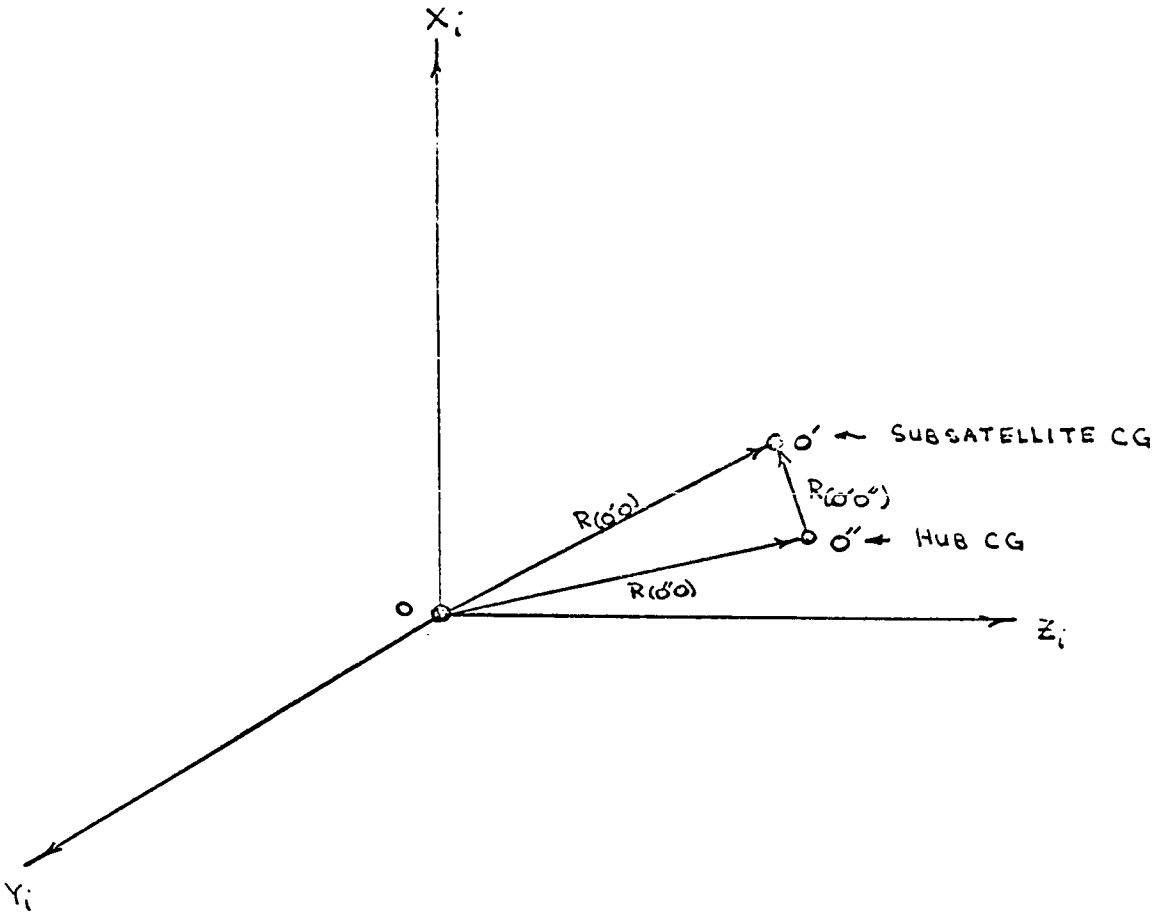

Figure 3.5-1 Vector Definitions

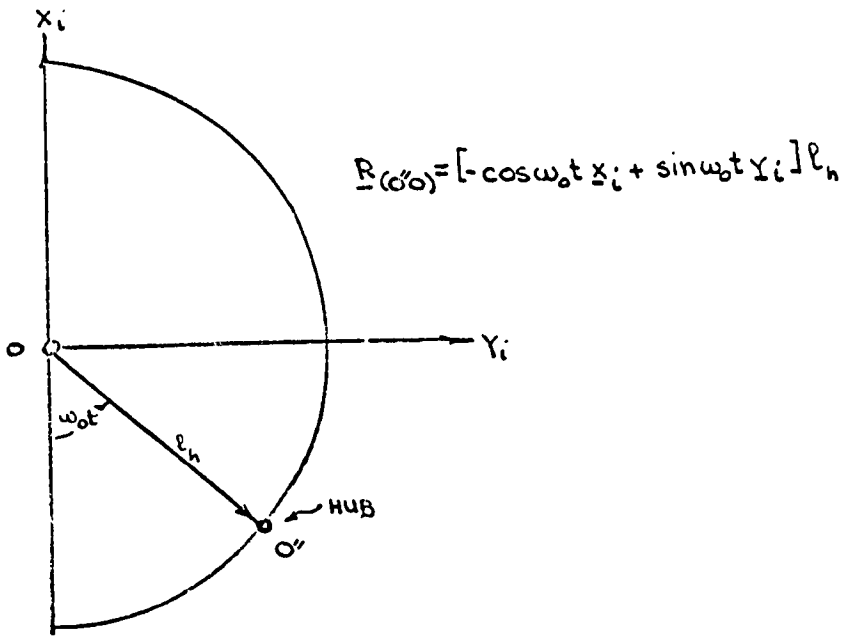

Figure 3.5.2a Satellite Position Relative to Hub

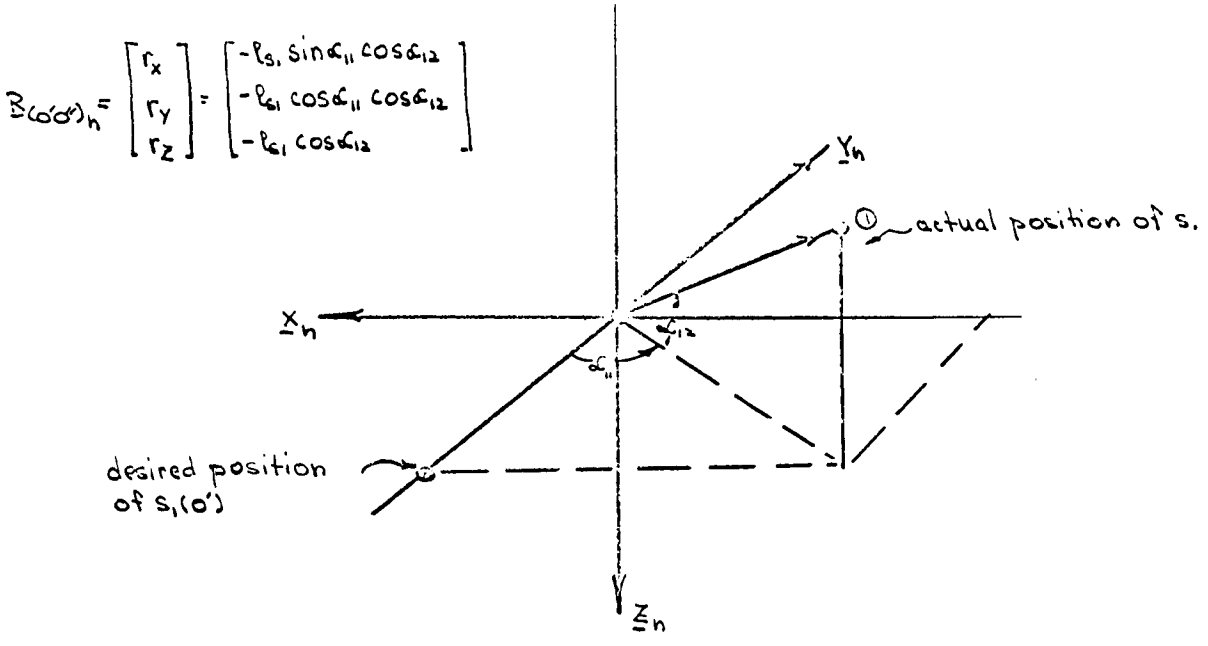

Figure 3.5.2b Hub Position Relative to i-Frame

The coordinate systems to be used in the formulation of this problem are defined in Figure 3.5-3. These frames are:

Inertial (i) frame with unit vectors ($\underline{X}_i$, $\underline{Y}_i$, $\underline{Z}_i$)

Reference (r) frame with unit vectors ($\underline{X}_r$, $\underline{Y}_r$, $\underline{Z}_r$)

Hub (h) frame with unit vectors ($\underline{X}_h$, $\underline{Y}_h$, $\underline{Z}_h$)

Subsatellite 1 (S_1) frame with unit vectors ($\underline{X}_{S1}$, $\underline{Y}_{S1}$, $\underline{Z}_{S1}$)

In addition, the notation:

Q_{ab} = transformation matrix transforming a vector expressed in the a frame to a vector expressed in the b frame.

Since unnecessary complexity is to be avoided in these initial studies, so that any fundamental problems which exist will emerge with maximum clarity, it is initially assumed that the hub attitude controller maintains the h and r frames in alignment (perfect hub attitude control). In addition it is assumed that the hub is in a circular reference orbit so that its velocity with respect to the r frame is zero. The final basic assumption made is that the subsatellite attitude controller keeps the S_1 frame aligned with the h frame, i.e., that the hub attitude is perfectly controlled.

It can be seen that these simplifying assumptions are all quite reasonable and have the major effect of suppressing unwanted, detailed complexities which are not required at this preliminary stage.

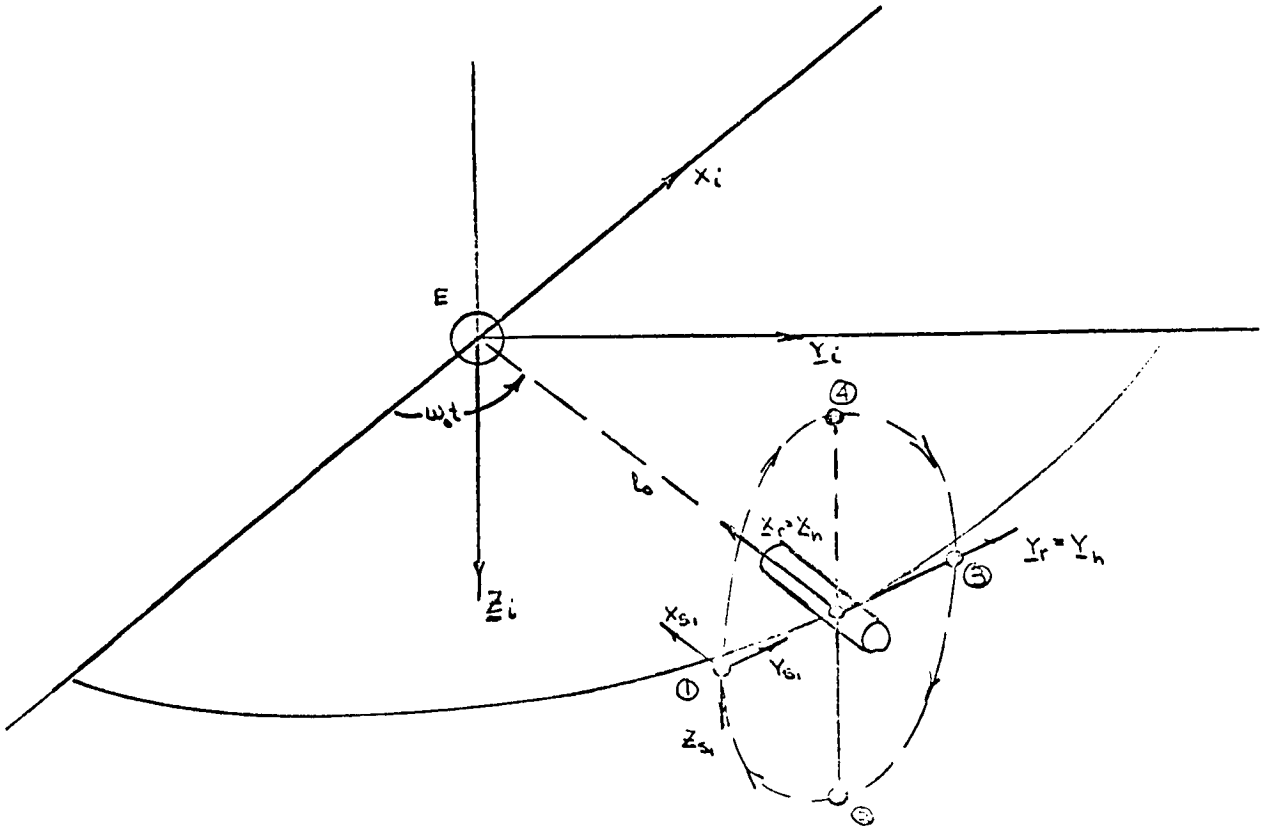

Figure 3.5-3 Coordinate System and Orbit Definition

The derivation of the equations of motion now becomes straightforward. The basic equation is

$$\underline{F} = m_{s1} \frac{d^2}{dt^2} \underline{\overset{\circ\circ}{R}}_{(o'o)} \tag{3.5-1}$$

Where:

m_{s1} = mass of satellite s_1

If $\underline{R}_{(o'o)}$ is expressed as:

$$\underline{R}_{(o'o)} = \varphi_{ir}\, \underline{R}_{(o''o)i} + \underline{R}_{(o'o'')h} \tag{3.5-2}$$

Equation 3.5-1 becomes:

$$\begin{aligned} \underline{F}_{(o')h} = {} & \underline{\overset{\times\times}{R}}_{(o''o)h} + \underline{\overset{\times\times}{R}}_{(o'o'')h} + 2\,\underline{\omega}_{(hi)h} \times \left[\underline{\overset{\times}{R}}_{(o''o)h} + \underline{\overset{\times}{R}}_{(o'o'')h}\right] \\ & + \underline{\omega}_{(hi)h} \times \left[\underline{\omega}_{(hi)h} \times \left(\underline{R}_{(o''o)h} + R_{(o'o'')h}\right)\right] \\ & + \underline{\overset{\times}{\omega}}_{(hi)h} \times \left[\underline{R}_{(o''o)h} + \underline{R}_{(o'o'')h}\right] \end{aligned} \tag{3.5-3}$$

Where, from previous assumptions:

$$\underline{\overset{\times\times}{R}}_{(o'o'')h} = 0$$

$$\underline{\overset{\times}{R}}_{(o'o'')h} = 0$$

$$\underline{\overset{\times}{\omega}}_{(hi)h} = 0 \quad .$$

So that 3.5-3 may be simplified to:

$$\begin{aligned} \underline{F}_{(o')h} = {} & \underline{\overset{\times\times}{R}}_{(o''o)h} + 2\,\underline{\omega}_{(hi)h} \times \underline{\overset{\times}{R}}_{(o''o)h} \\ & + \underline{\omega}_{(hi)h} \times \left[\underline{\omega}_{(hi)h} \times \left(\underline{R}_{(o''o)h} + R_{(o'o'')h}\right)\right] \end{aligned} \tag{3.5-4}$$

where:

$$\underline{R}_{(o''o)h} = \varphi_{ir}\, \underline{R}_{(o''o)i} \tag{3.5-4a}$$

$$\Phi_{ir} = \begin{bmatrix} c\psi_r & s\psi_r & 0 \\ -c\phi_r s\psi_r & c\phi_r c\psi_r & s\dot{\psi}_r \\ s\phi_r s\psi_r & -s\phi_r c\psi_r & c\phi_r \end{bmatrix} \qquad (3.5\text{-}4b)$$

$$\underline{R}_{(o'o)i} = \ell_h \begin{bmatrix} -\cos\omega_o t \\ \sin\omega_o t \\ 0 \end{bmatrix} \qquad (3.5\text{-}4c)$$

$$\underline{\omega}_{(hi)h} = \Phi_{eh}\, \underline{\omega}_{(hi)e} \qquad (3.5\text{-}4d)$$

$$\underline{\omega}_{(hi)e} = \begin{bmatrix} \phi_r' \\ 0 \\ \psi_r' \end{bmatrix} \qquad (3.5\text{-}4e)$$

$$\Phi_{eh} = \begin{bmatrix} 1 & 0 & 0 \\ 0 & c\dot{\phi}_r & s\dot{\phi}_r \\ 1 & -s\phi_r & c\phi_r \end{bmatrix} \qquad (3.5\text{-}4f)$$

$$R_{(o'o'')h} = \begin{bmatrix} 0 \\ -\ell_{s1} \\ 0 \end{bmatrix} \qquad (3.5\text{-}4g)$$

The gravity force on the vehicle is:

$$\underline{F}_{(d)h} = \frac{-GM_e}{\left|\underline{R}_{(o''o)h} + \underline{R}_{(o'o'')h}\right|^3}\left[\underline{R}_{(o''o)h} + \underline{R}_{(o'o'')h}\right] \qquad (3.5\text{-}5)$$

Equations 3.5-4 through 3.5-4g and 3.5-5 comprise the initial model of the translational dynamics to be used for the study of translational control and for determination of the nominal relative position control laws. These equations are to be studies analytically in order to determine force magnitudes and wave forms. Computer studies would then be required to obtain performance runs and parameter sensitivities.

Equation 3.5-3 has been expanded and, based on preliminary force estimates, it appears that the largest force required for relative position control is one associated with precessing the subsatellite spin plane. This force is:

$$F = m_{s1}\, \ell_{s1}\, \dot{\phi}_r\, \dot{\psi}_r \sin \dot{\phi}_r t \qquad (3.5\text{-}6)$$

where:

m_{s1} = 3 slugs

ℓ_{s1} = 16,400 ft.

$\dot{\psi}_r = \omega_o = 3.7 \times 10^{-5}$ rad/sec.

$\dot{\phi}_r = 120\dot{\psi} = 4.43 \times 10^{-3}$ rad/sec (100% overlap)

The average force level is, therefore:

$$\bar{F} = 5.65 \times 10^{-3} \text{ lbs.}$$

The total impulse per year is:

$$I_T = 17.8 \times 10^4 \text{ lb/sec.}$$

If a mass expulsion thruster system with a propellant specific impulse of 300 seconds is assumed then the propellant weight is

$$\omega_p/\text{year/satellite} = 593 \text{ lbs.}$$

which is considered excessive. This analysis, however, neglects the effects of the structure. It is believed that most of this force will be supplied by centrifugal force loading of the sub-satellites. In the event that this effect does not diminish or, possibly, obviate the need for this force to be applied by an active system, there are other alternatives. For any fixed overlap, $\dot{\phi}_r = K\dot{\psi}_r$ so that (3.5-6) may be written in the form:

$$\bar{F} = .7\, m_{s1}\, \ell_{s1}\, K \dot{\psi}_r^2 \qquad (3.5\text{-}7)$$

The heavens are swept out once every T_ℓ time units where:

$$T_\ell = \frac{2\pi}{\dot{\psi}_o} \qquad (3.5\text{-}8)$$

so that for a time period t_y (nominally 1 year) the propellant weight is:

$$\omega_p = \frac{2.8\, m_{s1}\, \ell_{s1}\, K \pi^2}{T_\ell^2} = \frac{A}{T_e^2} \quad (A = \text{constant}) \qquad (3.5\text{-}9)$$

for example, previous calculations considered $\dot{\psi}_o = -\omega_o$ so that

$$T_L = \text{orbital period} = 47.1 \text{ hrs.} \approx 2 \text{ days}$$

If mission requirements permit a complete scan of the heavens once a month then the propellant weight would be:

$$W_p = 593 \left(\frac{2}{30}\right)^2 = \frac{593}{225} = 2.64 \text{ lbs.}$$

If one "loop" per week were required:

$$W_p = 593 \left(\frac{2}{7}\right)^2 = 48.5 \text{ lbs.}$$

It can therefore be seen that, if actively produced forces are required, the propellant weight is quite sensitive to mission requirements in terms of T_L.

Any "detuning" of $\dot{\psi}_r$ from it's present value of $-\omega_o$ will however complicate sensor problems since the hub will no longer point continuously at the Earth.

SECTION IV

EFFECTS OF EXTERNAL FORCES

4.1 GENERAL

The attitude of the KWOT will be to some extent affected by small disturbance forces, specifically those due to solar electromagnetic radiation, gravity gradient, magnetic moment, meteoroids, solar flare particles and moving parts, if any, within the satellite. The most significant of these disturbances will be the first two and possibly the last. It will be seen that the disturbances due to magnetic moment and to meteoroids are relatively small. The disturbance due to solar flare particles may, during an especially severe outburst, equal or exceed that due to solar electromagnetic radiation; however, such events are rare and no statistical approach has been made. Interior moving parts are not treated since present configurations do not conceive the use of any moving parts.

Various aspects of the structural dynamic characteristics of KWOT are investigated under certain simplifying assumptions. The constraints on deployment velocity and the cable sag due to centrifugal force are analyzed in terms of the structural characteristics; it is shown that the light structural element considered in Section II is desirable. The frequencies of normal modes of lateral vibration of the cables in response to an

external disturbance of the structure are given. The response of the extremely flexible KWOT structure to the complete perturbation environment will require a computerized study.

4.2 DISTURBANCE TORQUES

An estimate of the magnitude of the various disturbance torques acting upon the KWOT is given in the following paragraphs. A fairly complete presentation of the development of the necessary equations is given in order that subsequent KWOT configurations may be easily evaluated. Numerical calculations are made for the simplified model used in the present study.

4.2.1 Solar Electromagnetic Radiation

The force per unit area on a flat absorbing surface normal to the sun's radiation is S/C where S is the incident solar energy per unit time per unit area and C is the velocity of propagation.

The solar constant at the mean distance of the earth from the sun is 2.00 cal/cm^2 min (reference 4). Then

$$S/C = E/A\dot{c}C = 1.65 \cdot 10^{-5} \text{ dyne/cm}^2 \cong 10^{-7} \text{ lb}_f/\text{ft}^2$$

If solar radiation is incident at some angle φ to the normal to the surface, and if in addition there is specular reflection of some fraction R of the incident radiation, the area irradiated by a beam of unit cross-section is proportional to $1/\cos\varphi$; the force exerted on this area has a normal com-

ponent proportional to $\cos\varphi$ and a tangential component proportional to $\sin\varphi$. Then for unit surface area, the normal force is

$$F_{incident} + F_{reflected} = S/c\,(1+R)\cos^2\varphi \qquad (4.2\text{-}1)$$

and the tangential force equals

$$S/c\,(1-R)\cos\varphi\sin\varphi \qquad (4.2\text{-}2)$$

The solar energy is either converted to electrical energy and stored, or reradiated diffusely. If the surface temperatures on the body in question are constant, the reradiated energy will produce zero net force. If the value of R is not high, and if portions of the surface are at much higher temperatures than others, then diffuse reradiation will add to the net force.

Given an element of surface area which is reradiating absorbed energy, the intensity of radiation in the half-space above the surface is given by Lambert's cosine law

$$I = I_o \cos\psi \qquad (4.2\text{-}3)$$

where I_o is the intensity of radiation along the normal to the surface and ψ is the angle to the normal.

The total emitted pressure (normal and tangential components) is given by

$$P = \int I \, dA \qquad (4.2\text{-}4)$$

where

$$dA = 2\pi (r \sin\psi)\, ds \qquad ds = r\, d\psi$$

$$dA = 2\pi r^2 \sin\psi \, d\psi$$

therefore

$$P = \int_0^{\pi/2} I_0 \cos\psi \, 2\pi r^2 \sin\psi \, d\psi \qquad (4.2\text{-}5)$$

$$= \pi r^2 I_0$$

The component of I normal to the emitting surface at the band dA is

$$I_N = I_0 \cos^2\psi \qquad (4.2\text{-}6)$$

so the normal component of pressure is

$$\int I_N \, dA = \int_0^{\pi/2} I_0 \cos^2\psi \, 2\pi r^2 \sin\psi \, d\psi \qquad (4.2\text{-}7)$$

$$= \frac{2}{3} \pi r^2 I_0$$

Hence if the incident pressure is

$$P = S/c \cos\varphi \qquad (4.2\text{-}8)$$

and the fraction reflected is R, the fraction absorbed is (1-R). If the fraction of absorbed energy that is stored is γ', then the total pressure of the reradiated energy is

$$(1-\gamma)(1-R)\ S/c\ \cos\varphi \qquad (4.2\text{-}9)$$

of which the normal component is

$$2/3\ (1-\gamma)(1-R)\ S/c\ \cos\varphi \qquad (4.2\text{-}10)$$

and the tangential components cancel.

Then the total pressure on a unit surface due to incidence, reflection and reradiation of solar energy is

$$P_{normal} = S/c\ \cos\varphi\left[(1+R)\cos\varphi + \tfrac{2}{3}(1-R)(1-\gamma)\right] \qquad (4.2\text{-}11)$$

The tangential pressure remains

$$P_{tan} = S/c\ (1-R)\cos\varphi\sin\varphi \qquad (4.2\text{-}12)$$

a. <u>Forces on a Circular Cylinder, Axis Normal to Incident Radiation.</u>

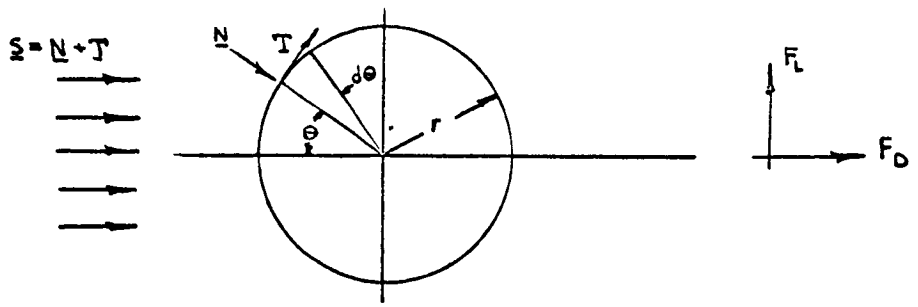

Figure 4.2-1

The normal and tangential forces on a differential area of the surface of the cylinder are:

$$dN = dA\ S/C\ \cos\Theta\left[(1+R)\cos\Theta + \tfrac{2}{3}(1-R)(1-\gamma)\right] \qquad (4.2\text{-}13)$$

$$dT = dA\ S/C\ (1-R)\cos\Theta\sin\Theta \qquad (4.2\text{-}14)$$

where

$$dA = r\,l\,d\Theta \qquad (4.2\text{-}15)$$

then

$$F_D = \int \cos\Theta\, dN + \int \sin\Theta\, dT \qquad (4.2\text{-}16)$$

$$= 2\,\frac{S}{C}\,r\,l\left\{\int_0^{\pi/2}\left[(1+R)\cos^3\Theta + \tfrac{2}{3}(1-R)(1-\gamma)\cos^2\Theta\right]d\Theta + \int_0^{\pi/2}(1-R)\cos\Theta\sin^2\Theta\,d\Theta\right\}$$

$$= 2\,\frac{S}{C}\,r\,l\left\{\frac{1+R}{3}\sin\Theta(\cos^2\Theta+2) + \tfrac{2}{3}(1-R)(1-\gamma)\left(\frac{\Theta}{2} + \sin\frac{2\Theta}{4}\right) + (1-R)\frac{\sin^3\Theta}{3}\right.$$

$$F_D = 2\,S/c\,r\,l\left[\frac{2(1+R)}{3} + \frac{2}{3}(1-R)(1-\kappa)\frac{\pi}{4} + \frac{1-R}{3}\right]$$

$$= 2\,S/c\,r\,l\left[1 + \frac{R}{3} + \frac{\pi}{6}(1-R)(1-\kappa)\right]$$

By symmetry, $F_L = 0$

b. Forces on an Inclined Cylinder

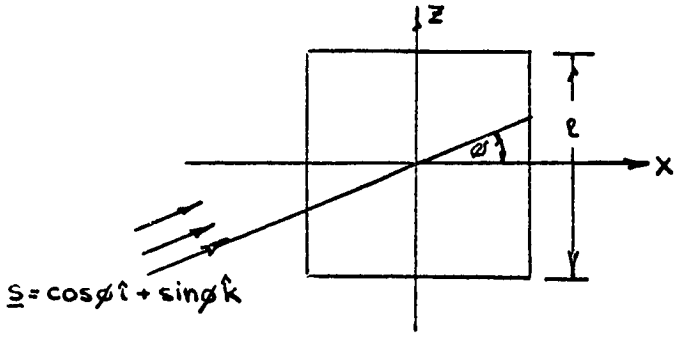

Figure 4.2-3

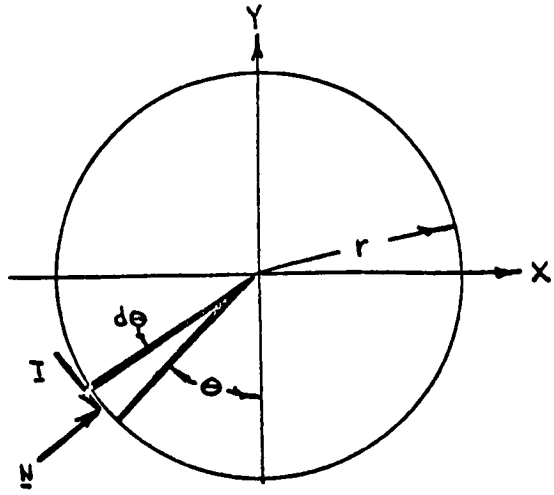

Figure 4.2-4

Let ψ be the angle between $\underline{N}$ and $\underline{S}$ then

$$\cos\psi = \cos\varphi \sin\Theta \qquad (4.2\text{-}17)$$

$\underline{S}$ the incident solar radiation

$\underline{N}$ the force normal to the surface element $da = rd\Theta dz$

$\underline{T}$ the force tangent to the surface element $da = rd\Theta dz$

$$\underline{T} = \underline{N} \times (\underline{S} \times \underline{N}) \qquad (4.2\text{-}18)$$

Then the components of ($\underline{S}$ x $\underline{N}$) are

$$\frac{\hat{i}}{\frac{-\sin\varphi\cos\Theta}{\sqrt{1-\cos^2\varphi\sin^2\Theta}}} \quad \frac{\hat{j}}{\frac{\sin\varphi\sin\Theta}{\sqrt{1-\cos^2\varphi\sin^2\Theta}}} \quad \frac{\hat{k}}{\frac{\cos\varphi\cos\Theta}{\sqrt{1-\cos^2\varphi\sin^2\Theta}}} \qquad (4.2\text{-}19)$$

whence the components of $\underline{T}$ are

$$\frac{\hat{i}}{\frac{\cos^2\varphi\cos^2\Theta}{\sqrt{1-\cos^2\varphi\sin^2\Theta}}} \quad \frac{\hat{j}}{\frac{-\sin\Theta\cos\Theta\cos\varphi}{\sqrt{1-\cos^2\varphi\sin^2\Theta}}} \quad \frac{\hat{k}}{\frac{\sin\varphi}{\sqrt{1-\cos^2\varphi\sin^2\Theta}}} \tag{4.2-20}$$

The forces on each surface element are:

$$dN = dA\, S/c \cos\psi\left[(1+R)\cos\psi + (1-R)\tfrac{2}{3}(1-\sigma)\right] \tag{4.2-21}$$

$$dT = dA\, S/c \cos\psi\left[(1-R)\sin\psi\right] \tag{4.2-22}$$

$$dA = r\, d\Theta\, dz \tag{4.2-23}$$

since the only term in z is dz and $\int dz = \ell$, and substituting for $\cos\psi$,

$$dN = r\ell\, d\Theta\, S/c\left[(1+R)\cos^2\varphi\sin^2\Theta + \tfrac{2}{3}(1-R)(1-\sigma)\sin\Theta\cos\varphi\right] \tag{4.2-24}$$

$$dT = r\ell\, d\Theta\, S/c\left[(1-R)\sqrt{1-\cos^2\varphi\sin^2\Theta}\;\cos\varphi\sin\Theta\right. \tag{4.2-25}$$

$$d\underline{N} = dN\,(n_x\hat{i}, n_y\hat{j}, n_z\hat{k}) = dN\,\hat{n} \tag{4.2-26}$$

The unit normal vector is

$$\hat{n} = \cos\alpha\,\hat{i} + \cos\beta\,\hat{j} + \cos\gamma\,\hat{k} \qquad (4.2\text{-}27)$$

$$\alpha = 90 - \Theta \qquad \cos\alpha = \sin\Theta$$

$$\beta = \Theta \qquad \cos\beta = \cos\Theta$$

$$\gamma = \pi/2 \qquad \cos\gamma = 0$$

$$N_x = r\ell\, S/c\,(1+R)\cos^2\varphi \int_0^{\pi} \sin^2\Theta \sin\Theta\, d\Theta \qquad (4.2\text{-}28)$$

$$+ r\ell\, S/c^2/3\,(1-R)(1-\gamma)\cos\varphi \int_0^{\pi} \sin^2\Theta\, d\Theta$$

$$= r\ell\, S/c \left[4/3\,(1+R)\cos^2\varphi + \pi/3\,\cos\varphi\,(1-R)(1-\gamma)\right]$$

$$N_y = r\ell\, S/c\,\cos^2\varphi\,(1+R) \int_0^{\pi} \sin^2\Theta \cos\Theta\, d\Theta \qquad (4.2\text{-}29)$$

$$+ r\ell\, S/c^2/3\,(1-R)(1-\gamma)\cos\varphi \int_0^{\pi} \sin\Theta\cos\Theta\, d\Theta$$

$$= 0$$

$$N_z = 0 \qquad (4.2\text{-}30)$$

Similarly,

$$T_x = r\ell\, S/c\,(1-R)\,2/3\,\cos^2\varphi \qquad (4.2\text{-}31)$$

$$T_y = 0 \qquad (4.2\text{-}32)$$

$$T_z = \pi \ell \, S/c \, (1-R) \, 2 \sin\varphi \cos\varphi \qquad (4.2\text{-}33)$$

Then the force normal to the axis of the cylinder is

$$F_x = N_x + T_x = 2\pi\ell \, S/c \cos^2\varphi \left(1 + R/3\right) + 2\pi\ell \, S/c \cos\varphi \, \pi/6 \, (1-R)(1-\sigma) \qquad (4.2\text{-}34)$$

where the second term is the reradiation term. The force parallel to the axis of the cylinder is

$$F_z = 2\pi\ell \, S/c \cos\varphi \, (1-R) \sin\varphi \qquad (4.2\text{-}35)$$

These forces act on the center of pressure of the cylinder, taken to be the geometric center of its projected area. The above result is applicable to a cylinder the length of which is large compared with its diameter. When the ends of the cylinder must be taken into consideration, an additional force acts on the c.p. of the exposed end. If this end is taken to be a uniform flat surface, then the force acting normal to the axis of the cylinder (tangential to the end) is

$$F_{ET} = \pi r^2 \, S/c \cos\varphi \, (1-R) \sin\varphi \qquad (4.2\text{-}36)$$

and the force acting parallel to the axis (normal to the end) is

$$F_{EN} = \pi r^2 S/c \sin^2\varphi (1+R) + \pi r^2 S/c \sin\varphi \, 2/3 (1-R)(1-\gamma) \quad (4.2\text{-}37)$$

where the force acts on the center of the (circular) end.

c. Force on a Sphere

Given a spherical satellite, the normal and tangential components of the force due to solar irradiation are

$$dN = P_N dA = S/c \cos\varphi\left[(1+R)\cos\varphi + \tfrac{2}{3}(1-R)(1-\gamma)\right] \quad (4.2\text{-}38)$$

$$dT = P_T dA = S/c \cos\varphi (1-R) \sin\varphi \, dA \quad (4.2\text{-}39)$$

The element of area of a sphere is

$$dA = r^2 \sin\Psi \, d\Psi \, d\Theta \quad (4.2\text{-}40)$$

Suppose the solar radiation is incident in the y direction (see figure 4.2-5)

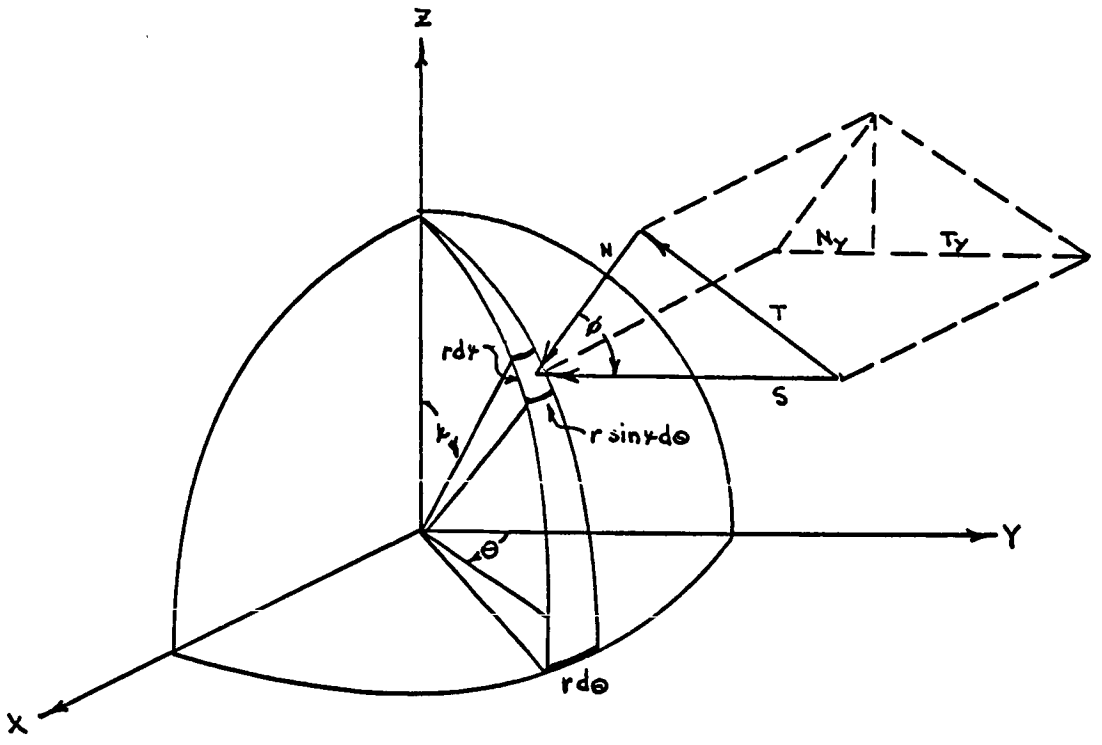

Figure 4.2-5

$$dN_y = dN\cos\varphi = dN\cos\Theta\sin\psi \qquad (4.2\text{-}41)$$

$$dT_y = dT\sin\varphi = dT\sqrt{1-\cos^2\Theta\sin^2\psi} \qquad (4.2\text{-}42)$$

$$F_y = \int dN_y + \int dT_y$$

$$F_y = \int \cos\varphi \; {}^{5}/_{c} \cos\varphi \left[(1+R)\cos\varphi + {}^{2}/_{3}(1-R)(1-\gamma) \right] dA$$

$$+ \int \sin\varphi \; {}^{5}/_{c} \cos\varphi (1-R) \sin\varphi \, dA$$

$$= {}^{5}/_{c} \int \cos^3\Theta \sin^4\Psi (1+R) r^2 d\Psi d\Theta$$

$$+ {}^{5}/_{c} \int \cos^2\Theta \sin^3\Psi r^2 \tfrac{2}{3} (1-R)(1-\gamma) d\Psi d\Theta$$

$$+ {}^{5}/_{c} \int r^2 (1 - \cos^2\Theta \sin^2\Psi)(\cos\Theta \sin\Psi)(1-R) \sin\Psi d\Psi d\Theta$$

$$= {}^{5}/_{c} \, r^2 (1+R) \, {}^{\pi}/_{2}$$

$$+ {}^{5}/_{c} \, r^2 (1-R)(1-\gamma) \, {}^{4}/_{9}$$

$$+ {}^{5}/_{c} \, r^2 (1-R) \, {}^{\pi}/_{2}$$

$$F_y = {}^{5}/_{c} \, \pi r^2 + {}^{4}/_{9} \, {}^{5}/_{c} \, \pi r^2 (1-R)(1-\gamma) \qquad (4.2\text{-}43)$$

$$F_x = F_z = 0$$

d. Sample Calculations

Given that the force on a sphere due to solar radiation is

$$F = S/c\ \pi r^2 \left[1 + 4/9 (1-R)(1-\gamma) \right] \qquad (4.2\text{-}43)$$

and the forces on a cylinder are

$$F_N = S/c\ 2r\ell \left[\cos^2\varphi + R/3 \cos^2\varphi + \frac{\pi}{6} \cos\varphi (1-R)(1-\gamma) \right] \qquad (4.2\text{-}44)$$

$$F_T = S/c\ 2r\ell \left[(1-R) \sin\varphi \cos\varphi \right] \qquad (4.2\text{-}45)$$

normal and parallel to the cylinder axis respectively, plus

$$F_{ET} = S/c\ \pi r^2 \left[(1-R) \sin\varphi \cos\varphi \right] \qquad (4.2\text{-}46)$$

$$F_{EN} = S/c\ \pi r^2 \left[\sin^2\varphi + R \sin^2\varphi + \frac{2}{3} \sin\varphi (1-R)(1-\gamma) \right] \qquad (4.2\text{-}47)$$

acting on the (flat) end, tangential and normal to the cylinder end respectively.

The case considered is:

Hub dimensions: 20' diameter by 50' long

Subsatellites: 3' diameter

Satellite skin: 50% aluminum, 50% solar cells

Reflectivity: Al $R = .9$ $\bar{R} = .5$ average

Solar cells $R = .1$

Conversion efficiency: = 12% (solar cells)

= 0 (aluminum)

= .06 average

It should be noted that an exact calculation would require an integration over the surface of Fresnel's expression for the variation of R with angle of incidence and polarization. This approach was felt to be unnecessarily complicated for the present study.

The force on each subsatellite from (4.2-43) is then

$$F = 10^{-7}\ \text{lbs}/\text{ft}^2\ \pi (1.5)^2\ \text{ft}^2 \left[1 + \frac{4}{9}(1-.5)(1-.06)\right]$$

$$= 7.06 \cdot 10^{-7}(1 + .21)\ \text{lbs}$$

$$= 1.5 \cdot 10^{-7}\ \text{lbs}$$

The torque on the hub is given by

$$F_T\, r - F_{ET}\, \ell/2 \qquad (4.2\text{-}48)$$

where r = hub radius

ℓ = hub length

This torque is shown for a complete orbit in figure 4.2-6. It should be noted that, while the net torque over the orbit is zero for the simplified case considered (c.g. at the geometric

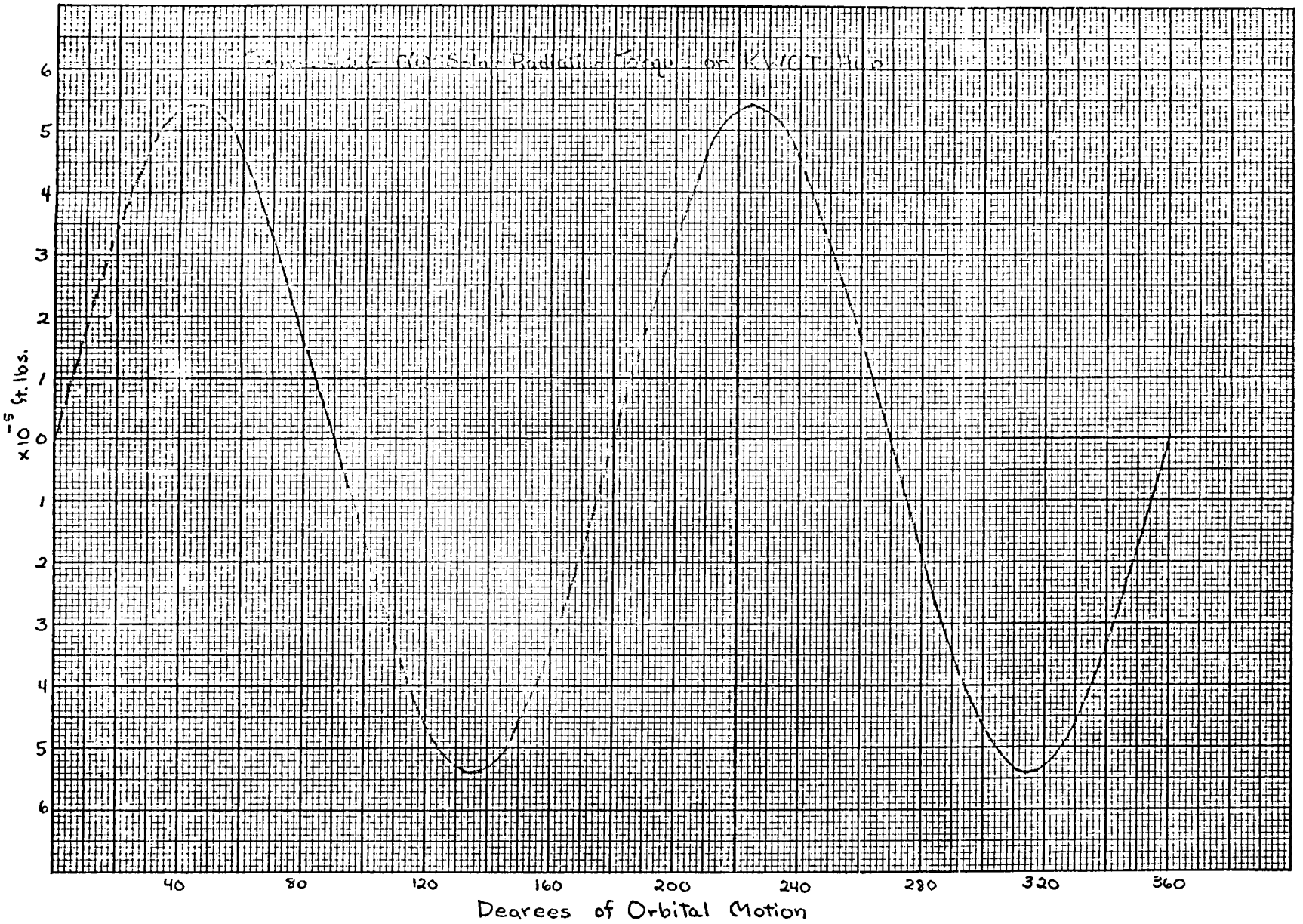
6
5
4
3
2
1
0
1
2
3
4
5
6
$\times 10^{-5}$ ft. lbs.
40
80
120
160
200
240
280
320
360
Degrees of Orbital Motion

center, right circular cylinder with flat ends) a departure from symmetry would result in a d.c. level of torque over the orbit and an attitude correction would be required.

The normal and tangential forces on the cylinder as a function of φ are shown in figure 4.2-7.

4.2.2 Gravity-Gradient Forces

a. Coordinates

For the purpose of deriving the expression for gravity-gradient torques, we define two coordinate reference frames, the orbital and body frames, and the coordinate transformation between them. The orbital reference frame is defined by origin at the vehicle's center of mass, z_o axis directed toward the earth's center in the plane of the orbit, x_o axis tangent to the orbital path in the direction of the vehicle's orbital motion, and y_o axis normal to z_o and x_o for a right-handed coordinate system.

The body reference frame is fixed in the vehicle with its origin at the vehicle's center of mass and its axes X, Y, Z defined along the vehicle's principal body axes. The vehicle's orientation in space is then defined with respect to the orbital reference frame by an ordered sequence of rotations about z_o, y_o and x_o axes through the angles ψ, θ and φ respectively (Figure 4.2-8). The transformation relating orbital coordinates to body coordinates is then

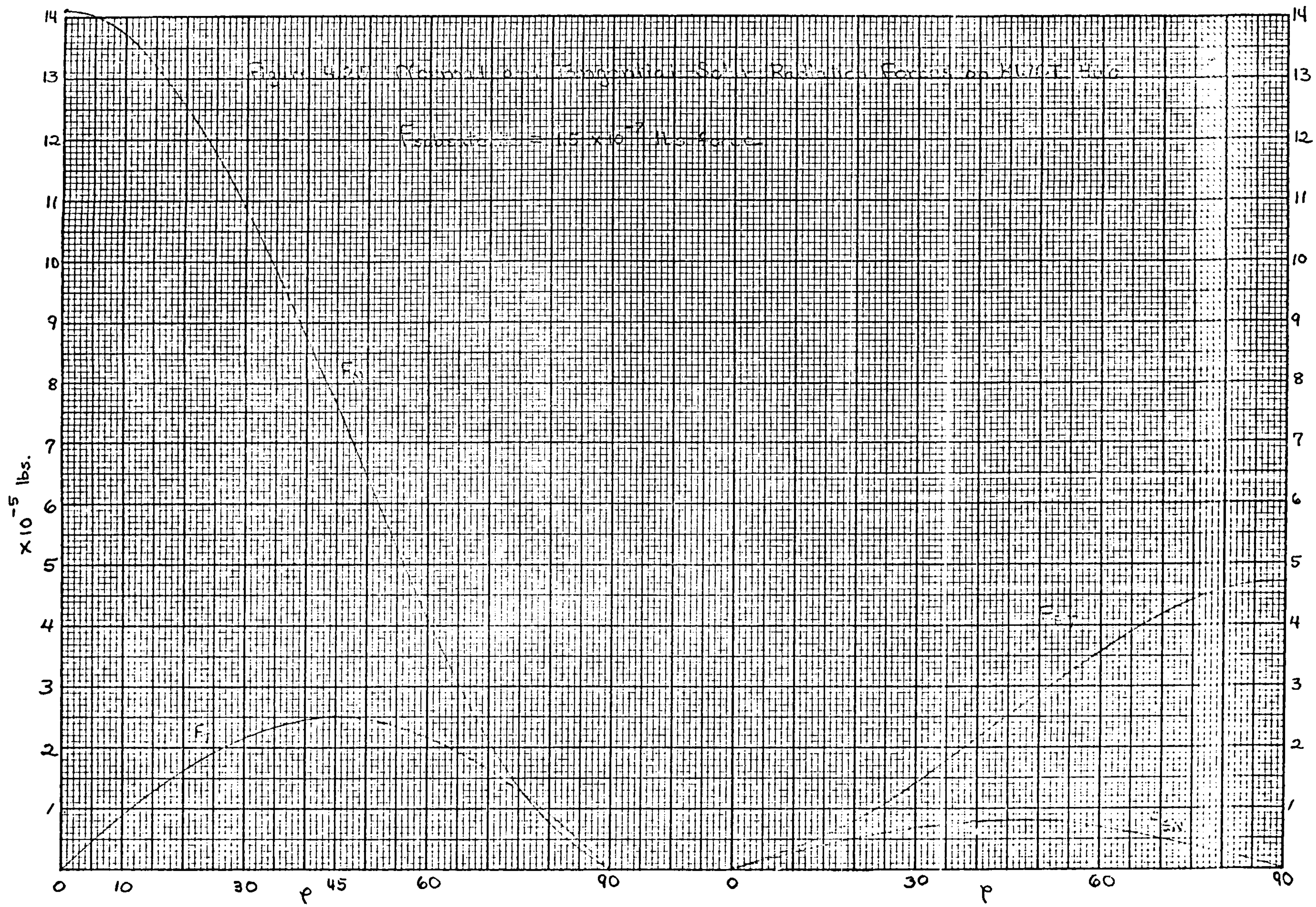
Solar Radiation Forces
x10^-7
14
13
12
11
10
9
8
7
6
5
4
3
2
1
x10^-5 lbs.
F
0
10
30
45
60
90
30
60
90
ρ
ρ

$$\begin{bmatrix} C_\theta C_\psi & C_\theta S_\psi & -S_\theta \\ S_\varphi S_\theta C_\psi - C_\varphi S_\psi & C_\varphi C_\psi + S_\varphi S_\theta S_\psi & S_\varphi C_\theta \\ S_\varphi S_\psi + C_\varphi S_\theta C_\psi & C_\varphi S_\theta S_\psi - S_\varphi C_\psi & C_\varphi C_\theta \end{bmatrix} \qquad (4.2\text{-}49)$$

where

$$S_\alpha = \sin\alpha \quad \text{and} \quad C_\alpha = \cos\alpha$$

b. Forces

The force dF acting on an element of mass dm due to the earth's gravitational attraction is given by

$$dF = -G M_\oplus \frac{dm}{r^3} \underline{r} \qquad (4.2\text{-}50)$$

where

G = univeral gravitational constant

M_e = mass of the earth

$\underline{r}$ = position vector from the center of the earth to the element of mass dm.

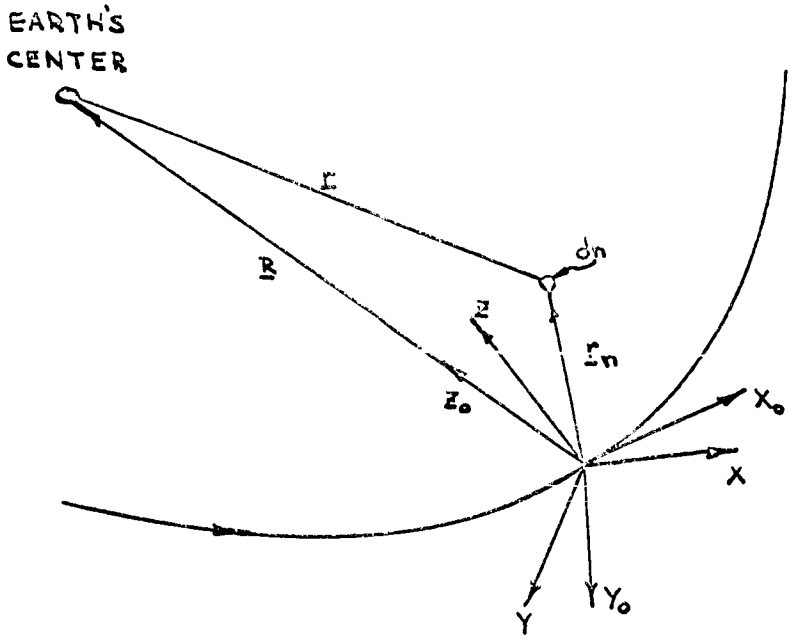

Figure 4.2-8

From Figure 4.2-8 it can be seen that

$$\underline{\rho} = \underline{r}_m - \underline{R} \qquad (4.2\text{-}51)$$

where

$$\underline{R} = R\,\underline{z}_o \tag{4.2-52}$$

and

$$\underline{r}_m = x\,\underline{x} + y\,\underline{y} + z\,\underline{z} \tag{4.2-53}$$

Then from Equation 4.2-49

$$\underline{R} = -R\sin\theta\,\underline{x} + R\sin\varphi\cos\theta\,\underline{y} + R\cos\varphi\cos\theta\,\underline{z} \tag{4.2-54}$$

and

$$\underline{r} = (x + RS_\theta)\underline{x} + (y - RS_\varphi C_\theta)\underline{y} + (z - RC_\varphi C_\theta)\underline{z} \tag{4.2-55}$$

$$|r|^2 = r^2 = (x + RS_\theta)^2 + (y - RS_\varphi C_\theta)^2 + (z - RC_\varphi C_\theta)^2$$

$$= R^2 + 2R(xS_\theta - yS_\varphi C_\theta - zC_\varphi C_\theta) + x^2 + y^2 + z^2$$

$$= R^2 + 2Rb + (x^2 + y^2 + z^2)$$

$$= R^2 + \chi \tag{4.2-56}$$

Then r^{-3} may be written

$$r^{-3} = (r^2)^{-3/2} \tag{4.2-57}$$

$$= (R^2 + \chi)^{-3/2}$$

Since $X^2 < R^4$, the series expansion is

$$(R^2+\chi)^{-3/2} = R^{-3} - \frac{3}{2}R^{-5}\chi + \frac{15}{8}R^{-7}\chi^2 + \cdots \tag{4.2-58}$$

$$\approx R^{-3} - \frac{3}{2}R^{-5}\chi$$

$$= R^{-3} - 3R^{-4}\mathcal{L} - \frac{3}{2} R^{-5}(x^2+y^2+z^2) \qquad (4.2\text{-}59)$$

$$(R^2+\chi)^{-3/2} \cong R^{-3}(1-3R^{-1}\mathcal{L}) \qquad (4.2\text{-}60)$$

Substituting Equations 4.2-60 and 4.2-53 into 4.2-50

$$\underline{dF} = \frac{-GM_e\, dm\,(x+RS_\Theta)\underline{x} + (y-RS_\varphi C_\Theta)\underline{y} + (z-RC_\varphi C_\Theta)\underline{z}}{R^3(1-3R^{-1}\mathcal{L})^{-1}} \qquad (4.2\text{-}61)$$

For a circular orbit,

$$\frac{GM_e}{R^3} = \omega_o^2 \qquad (4.2\text{-}62)$$

where ω_o is the orbital angular velocity.

Then

$$dF_x = -\omega_o^2 (x + RS_\Theta)(1-3R^{-1}\mathcal{L})\,dm \qquad (4.2\text{-}63)$$

$$dF_y = -\omega_o^2 (y - RS_\varphi C_\Theta)(1-3R^{-1}\mathcal{L})\,dm \qquad (4.2\text{-}64)$$

$$dF_z = -\omega_o^2 (z - RC_\varphi C_\Theta)(1-3R^{-1}\mathcal{L})\,dm \qquad (4.2\text{-}65)$$

c. Rigid-Body Torques

The moment $d\underline{M}$ due to the force $d\underline{F}$ acting on the mass element dm is

$$\underline{dM} = \underline{r}_m \times \underline{dF} \qquad (4.2\text{-}66)$$

$$= (y\,dF_z - z\,dF_y)\,\underline{x} + (z\,dF_x - x\,dF_z)\,\underline{y} + (x\,dF_y - y\,dF_x)\,\underline{z}$$

or

$$dM_x = \omega_o^2 R C_\Theta (y C_\varphi - z S_\varphi)\,dm - 3\omega_o^2 b C_\Theta (y C_\varphi - z S_\varphi)\,dm \qquad (4.2\text{-}67)$$

$$dM_y = -\omega_o^2 R (z S_\Theta + x C_\varphi C_\Theta)\,dm + 3\omega_o^2 b (z S_\Theta + x C_\varphi C_\Theta)\,dm \qquad (4.2\text{-}68)$$

$$dM_z = \omega_o^2 R (x S_\varphi C_\Theta + y S_\Theta)\,dm - 3\omega_o^2 b (x S_\varphi C_\Theta + y S_\Theta)\,dm \qquad (4.2\text{-}69)$$

Since the origin of $\underline{r}_n$ is at the center of mass,

$$\int x\,dm = \int y\,dm = \int z\,dm = 0 \qquad (4.2\text{-}70)$$

and Equations 4.2-67, 68 and 69 reduce to:

$$dM_x = -3\omega_o^2 b C_\Theta (y C_\varphi - z S_\varphi)\, dm \qquad (4.2\text{-}71)$$

$$dM_y = 3\omega_o^2 b (z S_\Theta + x C_\varphi C_\Theta)\, dm \qquad (4.2\text{-}72)$$

$$dM_z = -3\omega_o^2 b (x S_\varphi C_\Theta + y S_\Theta)\, dm \qquad (4.2\text{-}73)$$

Substituting for b,

$$b = x S_\Theta - y S_\varphi C_\Theta - z C_\varphi C_\Theta \qquad (4.2\text{-}74)$$

$$M_x = -3\omega_o^2 \left[S_\Theta C_\Theta C_\varphi \int xy\, dm - S_\Theta C_\Theta C_\varphi \int xz\, dm \right. \qquad (4.2\text{-}75)$$
$$\left. + C_\Theta^2 S_\varphi C_\varphi \int (z^2 - y^2)\, dm + C_\Theta^2 (S_\varphi^2 - C_\varphi^2) \int yz\, dm \right]$$

$$M_y = 3\omega_o^2 \left[S_\Theta^2 \int xz\, dm + C_\varphi S_\Theta C_\Theta \int (x^2 - z^2)\, dm \right. \qquad (4.2\text{-}76)$$
$$- S_\varphi S_\Theta C_\Theta \int yz\, dm - C_\Theta^2 S_\varphi C_\varphi \int xy\, dm$$
$$\left. - C_\varphi^2 C_\Theta^2 \int xz\, dm \right]$$

$$M_z = -3\omega_o^2 \left[S_\varphi S_\Theta C_\Theta \int (x^2 - y^2)\, dm + S_\Theta^2 \int xy\, dm \right. \qquad (4.2\text{-}77)$$
$$- S_\varphi^2 C_\Theta^2 \int xy\, dm - C_\Theta^2 S_\varphi C_\varphi \int xz\, dm$$
$$\left. - C_\varphi S_\Theta C_\Theta \int yz\, dm \right]$$

The moments of inertia about the body axes X, Y, Z are

$$I_x = \int (y^2 + z^2)\, dm \qquad (4.2\text{-}78)$$

$$I_y = \int (x^2 + z^2)\, dm \qquad (4.2\text{-}79)$$

$$I_z = \int (x^2 + y^2)\, dm \qquad (4.2\text{-}80)$$

and the products of inertia are

$$I_{xy} = \int xy\, dm \qquad (4.2\text{-}81)$$

$$I_{xz} = \int xz\, dm \qquad (4.2\text{-}82)$$

$$I_{yz} = \int yz\, dm \qquad (4.2\text{-}83)$$

Since we have chosen as our axes X, Y and Z, the principal axes of the body, the products of inertia are zero. Then Equations 4.2-75, 76, and 77 reduce to:

$$M_x = -3\omega_o^2 C_\theta^2 S_\varphi C_\varphi (I_y - I_z) \qquad (4.2\text{-}84)$$

$$M_y = -3\omega_o^2 C_\varphi S_\theta C_\theta (I_x - I_z) \qquad (4.2\text{-}85)$$

$$M_z = -3\omega_o^2 S_\varphi S_\theta C_\theta (I_y - I_x) \qquad (4.2\text{-}86)$$

or by the use of trigonometric identities

$$M_x = -\frac{3}{2}\omega_o^2 (I_y - I_z) \cos^2\theta \sin 2\varphi \qquad (4.2\text{-}87)$$

$$M_y = -\frac{3}{2}\omega_o^2 (I_x - I_z) \cos\varphi \sin 2\theta \qquad (4.2\text{-}88)$$

$$M_z = -\frac{3}{2}\omega_o^2 (I_y - I_x) \sin\varphi \sin 2\theta \qquad (4.2\text{-}89)$$

d. Orbital Period, Moments of Inertia and Typical Values

The orbital velocity ω_o as indicated in Section III is $3.7 \cdot 10^{-5}$ rad/sec. The hub (as originally indicated) is considered to be an annular cylinder 20 feet in diameter by 50 feet in length, so that the moment of inertia about the

cylinder axis is

$$M r^2 = 8.42 \cdot 10^4 \text{ kg m}^2 = 6.21 \cdot 10^4 \text{ slug ft}^2 \qquad (4.2\text{-}90)$$

and about the other two axes is

$$\frac{M}{2}\left(r^2 + \frac{h^2}{6}\right) = 2.2 \cdot 10^5 \text{ kg m}^2 = 1.6 \cdot 10^5 \text{ slug ft}^2 \qquad (4.2\text{-}91)$$

These moments are larger by approximately a factor of 2 than if the hub were considered a homogeneous mass. Then if the KWOT hub axis lies on an earth radial or perpendicular to it, the gravity gradient moments on the hub are zero. The gravity gradient moments are maximum if the axis lies at 45° to the earth radial; if $\Theta = 45^\circ$, $\varphi = 0$, then $M_y = 2.5 \cdot 10^{-4}$ nt. meters = $3.4 \cdot 10^{-4}$ ft.lbs.

4.2.3 Magnetic Torques

It is expected that magnetic torques will be small in comparison with the radiation pressures; hence only an idealized (perfect dipole) representation of the earth's field will be made here. (At the altitude of the KWOT orbit ($\sim$ 11 R_e), the distorting effect of the solar wind becomes significant so that the earth's field departs even further than was previously believed from that of a magnetic dipole). The small additional effect of the non-coincidence of the magnetic and geographic equator (where the KWOT is taken to be in equatorial

orbit) is also ignored.

Given that the earth's field is $3.5.10^{-5}$ webers/m^2 horizontal at the equator (7.10^{-5} weber/m^2 vertical at the poles) the equivalent dipole magnetic moment is $M = 9 \times 10^{15}$ amp.m^2 from

$$\underline{B} = -\nabla \frac{\underline{M} \cdot \underline{r}}{r^3} \qquad (4.2\text{-}92)$$

$B = M/r^3$ in the equatorial plane

$B = 2M/r^3$ on the axis

Then at the orbital altitude of 60,000 km, r = 66,380 km, B = $3.2.10^{-8}$ webers/m^2 in the equatorial plane. The direction of B is perpendicular to the orbit.

The torque on a current-carrying loop is

$$L = BIA \sin\Theta \qquad (4.2\text{-}93)$$

where

I = current

A = area of the loop

Θ = angle between B and plane of loop.

As sample calculations, suppose 1 μ amp flows in the outer perimeter of the KWOT (10 x 10 km), and suppose the KWOT lies initially in the orbital plane (worst case). Then the torque is

$$L_{max} = 3.2 \cdot 10^{-8} \text{ webers/m}^2 \cdot 10^{-6} \text{ amp} \cdot 10^{8} \text{ m}^2$$

$$= 3.2 \cdot 10^{-6} \text{ nt m} = 4.3 \cdot 10^{-6} \text{ ft lbs}$$

Alternatively, suppose 1 amp flows around the periphery of the central hub (A = 20 x 50 feet = 1000 feet^2 = 93 m^2) Then

$$L_{max} = 3 \cdot 10^{-6} \text{ nt m} = 4 \cdot 10^{-6} \text{ ft lbs}$$

4.2.4 Meteoroids

The angular disturbance ω due to the (inelastic) impact of a meteoroid is

$$\omega = \frac{m v \ell}{I} \quad \text{rad/sec} \qquad (4.2\text{-}94)$$

where

m = mass of meteoroid

v = velocity of meteoroid

ℓ = moment arm about vehicle c.g.

I = moment of inertia.

In the calculations below, it has been assumed that:

a) meteoroid impact takes place at the maximum lever arm (periphery of the vehicle).

b) velocity vector of meteoroid is normal to lever arm

c) all momentum of meteoroid is transferred to vehicle as angular momentum

d) meteoroid velocity is 45 km/sec

e) at the altitude of the KWOT, shielding due to the earth is small enough to be neglected (the effective area of the satellite is equal to its actual area).

Table 4.2-1 shows the angular disturbance of the center hub about the spin axis and about (either of) the other two axes, and the angular disturbance of the subsatellites.

The figures on average number of impacts are computed from reference 1:

$$N = 2.53 \cdot 10^{-9} \cdot 10^{0.4M} \qquad (4.2\text{-}95)$$

where

N = number of impacts per square meter per day

M = apparent visual magnitude

Other expressions in the literature include

$$N = 2.5 \cdot 10^{-15}\, m^{-1.34}\, m^{-2} sec^{-1} \quad \text{Ref. 2} \qquad (4.2\text{-}96)$$

and

$$N = 1.26 \cdot 10^{-17} \cdot m^{-1.7} \quad (10^{-10} \leqq m \leqq 10^{-7}) \qquad (4.2\text{-}97)$$

$$N = 10^{-12} \cdot m^{-1} \quad (10^{-7} \leqq m \leqq 10) \quad \text{Ref. 3}$$

where

m = mass in grams

The latter expression yields significantly higher flux densities, especially at the smaller masses; it will be seen, however, that disturbances due to meteoroids are either sufficiently small or sufficiently rare that they may be neglected.

TABLE 4.2-1 ANGULAR DISTURBANCE OF KWOT

Meteroid vis. mag.	Mass gm.	Avg. no. of Impacts $m^{-2} yr^{-1}$	ω_x rad/sec	$\omega_y = \omega_z$ rad/sec	Avg. time between impacts hub	$\omega_{subsatellites}$ rad/sec	Avg. time between impacts subsats.
0	25	9.24×10^{-7}	4.35×10^{-2}	4.2×10^{-2}	2700 yr.	134	41,000 yr
1	10	2.32×10^{-6}	1.74×10^{-2}	1.68×10^{-2}		53.7	
2	4	5.84×10^{-6}	6.96×10^{-3}	6.71×10^{-3}		21.4	
3	1.6	1.46×10^{-5}	2.78×10^{-3}	2.68×10^{-3}		8.6	
4	.6	3.68×10^{-5}	1.04×10^{-3}	1.01×10^{-3}		3.21	
5	.25	9.24×10^{-5}	4.35×10^{-4}	4.2×10^{-4}	27 yr	1.34	410 yr
6	.1	2.32×10^{-4}	1.74×10^{-4}	1.68×10^{-4}		.54	
7	4×10^{-2}	5.84×10^{-4}	6.96×10^{-5}	6.71×10^{-5}		.21	
8	1.6×10^{-2}	1.46×10^{-3}	2.78×10^{-5}	2.68×10^{-5}		8.6×10^{-2}	
9	6×10^{-3}	3.68×10^{-3}	1.04×10^{-5}	1.01×10^{-5}		3.2×10^{-2}	
10	2.5×10^{-3}	9.24×10^{-3}	4.35×10^{-6}	4.2×10^{-6}	98 days	1.34×10^{-2}	4.1 yr.
11	10^{-3}	2.32×10^{-2}	1.74×10^{-6}	1.68×10^{-6}		5.4×10^{-3}	
12	4×10^{-4}	5.84×10^{-2}	6.96×10^{-7}	6.71×10^{-7}		2.1×10^{-3}	
13	1.6×10^{-4}	1.46×10^{-1}	2.78×10^{-7}	2.68×10^{-7}		8.6×10^{-4}	
14	6×10^{-5}	3.68×10^{-1}	1.04×10^{-7}	1.01×10^{-7}		3.2×10^{-4}	
15	2.5×10^{-5}	9.24×10^{-1}	4.35×10^{-8}	4.2×10^{-8}	1 day	1.34×10^{-4}	15 day
16	10^{-5}	2.32	1.74×10^{-8}	1.68×10^{-8}		5.4×10^{-5}	
17	4×10^{-6}	5.84	6.96×10^{-9}	6.71×10^{-9}		2.1×10^{-5}	
18	1.6×10^{-6}	14.6	2.78×10^{-9}	2.68×10^{-9}		8.6×10^{-6}	
19	6×10^{-7}	36.8	1.04×10^{-9}	1.01×10^{-9}		3.2×10^{-6}	
20	2.5×10^{-7}	92.4	4.35×10^{-10}	4.2×10^{-10}	14 min.	1.34×10^{-6}	3.6 hr
21	10^{-7}	2.32×10^{2}	1.74×10^{-10}	1.68×10^{-10}		5.4×10^{-7}	
22	4×10^{-8}	5.84×10^{2}	6.96×10^{-11}	6.71×10^{-11}		2.1×10^{-7}	
23	1.6×10^{-8}	1.46×10^{3}	2.78×10^{-11}	2.68×10^{-11}		8.6×10^{-8}	
24	6×10^{-9}	3.68×10^{3}	1.04×10^{-11}	1.01×10^{-11}		3.2×10^{-8}	
25	2.5×10^{-9}	9.24×10^{3}	4.35×10^{-12}	4.2×10^{-12}	8.6 sec	1.34×10^{-8}	2.2 min.
26	10^{-9}	2.32×10^{4}	1.74×10^{-12}	1.68×10^{-12}		5.4×10^{-9}	
27	4×10^{-10}	5.84×10^{4}	6.96×10^{-13}	6.71×10^{-13}		2.1×10^{-9}	
28	1.6×10^{-10}	1.46×10^{5}	2.78×10^{-13}	2.68×10^{-13}		8.6×10^{-10}	
29	6×10^{-11}	3.68×10^{5}	1.04×10^{-13}	1.01×10^{-13}		3.2×10^{-10}	
30	2.5×10^{-11}	9.24×10^{5}	4.35×10^{-14}	4.2×10^{-14}	8.6×10^{-2} sec.	1.34×10^{-10}	1.3 sec.

KWOT $I_x = 6.21\times10^4$ SLUG-FT^2 $= 8.42\times10^4$ KG-M^2

$I_Y = I_Z = 1.6\times10^5$ SLUG-FT^2 $= 2.18\times10^5$ KG-M^2

$I_{SUBSAT.} = 3.85$ KG-M^2

Surface area = 400 M^2 (HUB), 2.66 M^2 (SUBSATELLITE)

References

1. White, J.B., "Meteoric Effects on Attitude Control of Space Vehicles," ARS Journal, January 1962.

2. Whipple, F.L., J. Astro, Sci. 10, 92, 1963.

3. McCracken, C.W., and W.M. Alexander, "The Distribution of Small Interplanetary Dust Particles in the Vicinity of the Earth," NASA TND 1349.

4. Handbook of Chemistry and Physics, 40th edition, Chemical Rubber Publishing Company, Cleveland, Ohio, 1958.

4.3 EFFECTS OF FORCES ON STRUCTURE

The following section is devoted to various aspects of the dynamic characteristics of the KWOT structure. The response of the structure to certain inherent and external perturbations is given, under a number of simplifying assumptions. The response of the extremely flexible KWOT system to the complete perturbation environment given in Section 4.2 will require a computerized study and is outside the scope of this feasibility report.

It will be assumed that the KWOT structure consists of strands of mylar ribbon (referred to as cable in subsequent discussion) having the elastic properties defined on page II-44

Two thicknesses of mylar ribbon have been considered, one having a cross sectional area of 1.452×10^{-4} in.^{2} (referred to on page II-48) and the other having a cross sectional area of 1.452×10^{-2} in.^{2} (used to define the stiffness matrix on page II-52 It is felt that these thicknesses represent the two extremes for a feasible structure and these two types of ribbon will be used in the subsequent analysis. In order to avoid constant repetition of the cross sectional properties they will be referred to as thin and thick cable. In this section the KWOT satellite will be considered to have a spin rate of 2 revs/hr. about its own axis.

4.3.1 Deployment Velocities

The deployment technique will inevitably result in some system whereby the subsatellites are propelled from the center

body in a radial direction. The purpose of this section is to determine the maximum permissible radial velocity component of the subsatellites at the point at which the cables come into tension. It is assumed that the subsatellites are propelled from the non-spinning center body and remain approximately equidistant from the center body as they move away from it. It follows that as the slack in the cables disappears, structural restraining forces will occur simultaneously on all four subsatellites, bringing them to rest. The structure considered is a rather more elementary version (Figure 4.3-1) of the one shown in Figure 2.5-2. It has the same geometry and the same structural stiffnesses for the members which are common to both structural representations.

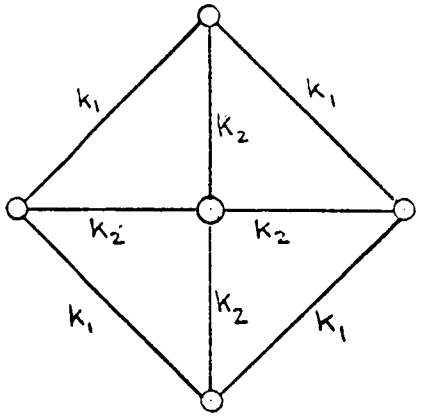

Figure 4.3-1 KWOT Structural Model

The stiffnesses of the peripheral and radial structural members will be denoted by K_1 and K_2 respectively and the structural stiffness at the four radial corners of the structure due to simultaneous radial displacements of the subsatellites will be calculated. If the simultaneously applied forces and displacements are denoted by P and (see Figure 4.3-2) respectively, then

$$P = KS \qquad \text{where K is the structural stiffness at a subsatellite in the radial direction} \qquad (4.3\text{-}1)$$

For thick cable

$$K_1 = .0286 \text{ lb/in.} \qquad (4.3\text{-}2)$$

$$K_2 = .0405 \text{ lb/in.}$$

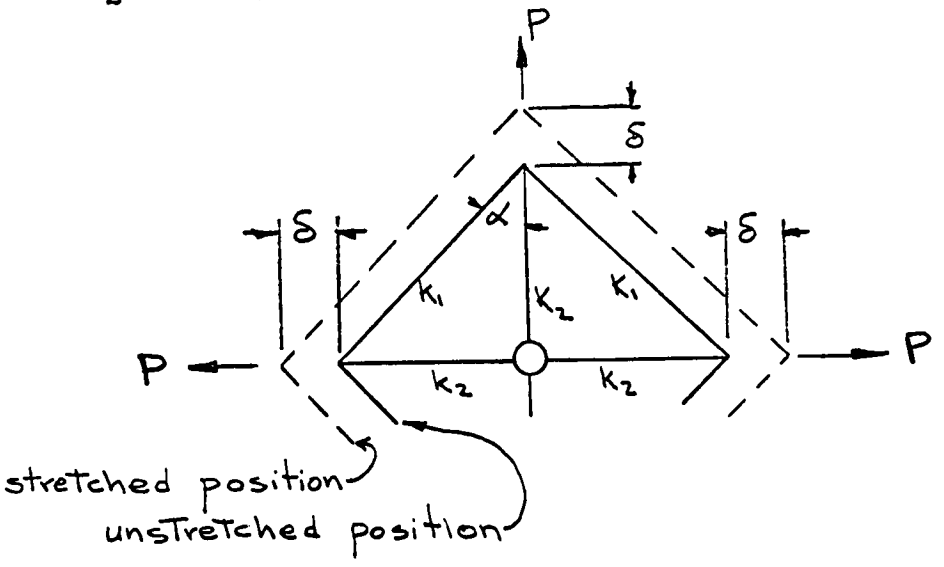

Figure 4.3-2 KWOT Displacement Model

In a condition of static equilibrium

$$P = K_2 \delta + 2K_1 (2\delta \cos\alpha) \cos\alpha \qquad (4.3\text{-}3)$$
$$= [K_2 + 4K_1 \cos^2\alpha]\,\delta$$

Thus

$$K = K_2 + 4K_1 \cos^2\alpha \qquad (4.3\text{-}4)$$

It is assumed that the outer structure of KWOT is in the form of a square, i.e., $\alpha = 45°$.

Hence

$$K = K_2 + 2K_1 \qquad (4.3\text{-}5)$$
$$= 0.0977 \text{ lb/in}$$

Assuming the subsatellites have a radial velocity V with respect to the center body at the point that the structure tensions then

$$\frac{mV^2}{2} = \int_0^{\delta_o} K\delta\, d\delta = \frac{1}{2} K \delta_o^2 \qquad (4.3\text{-}6)$$

where: δ_o is the displacement when the subsatellite comes to rest.
m is the mass of a subsatellite.

It will be noted that when $\delta = 1''$ then the tension in a peripheral member is given by

$$K_1 \times 2\cos 45° \qquad (4.3\text{-}7)$$
$$= 0.0405 \text{ lb.}$$

and the tension in a peripheral member will be K_2 (= .0405 lb.). Thus, the loads induced in the peripheral and radial members will be equal for unit radial displacement. From equations 2.5-6 and 2.5-6a it will be noted that the maximum allowable tension in the thick mylar cable is 174.4 lbs. Therefore the maximum allowable displacement is given by

$$\delta_{max.} = \frac{174.4"}{.0405} \qquad (4.3\text{-}7)$$

$$= 359 \text{ ft.}$$

Therefore from Equation 4.3-6

$$\frac{1}{2} m V_{max.}^2 = \frac{1}{2} K \delta_{max}^2 \qquad (4.3\text{-}8)$$

$$m = \frac{100}{32.2} = 3.1 \text{ slugs} \qquad \delta_{max} = 359 \text{ ft}$$

$$K = 12 \times 0.0977 = 1.17 \text{ lb/ft.}$$

Where V_{max} is the maximum permissible radial velocity of each subsatellite at deployment.

Substituting in the above yields

$$V_{max.} = 220 \text{ ft/sec} \qquad (4.3\text{-}9)$$

Since V_{max} is proportional to the square root of cross section area of the mylar cable then for thin cable

$$V_{max} = 22 \text{ ft/sec} \qquad (4.3\text{-}10)$$

It appears that the permissible radial velocity of deployment is not unduly restrictive the cable thicknesses considered.

4.3.2 Structural Deflection Due to Spin Rate

It has been determined that the centrifugal force due to spin acting at each corner of the KWOT structure is 0.621 lb. for a spin rate of 2 revolutions per hour (100 lb. subsatellites). Thus the radial elastic displacement in the spinning configuration (δ_s) is given by

$$\delta_s = \frac{.621}{.0977} = 6.37 \text{ inches for thick cable} \qquad (4.3\text{-}11)$$

$$\delta_s = 637 \text{ inches} = 53 \text{ feet for thin cable} \qquad (4.3\text{-}12)$$

Since the subsatellite radial position control will be incapable of maintaining station within $\pm$ 6" then it follows that use of thick cable would result in a structure alternating between a state of 'slack' and tension. Use of thin ribbon gives a sizeable margin of permissible radial displacement before any slack develops. Figure 4.3-3 indicates the amount of radial elastic displacement occurring as a function of cable size and spin rate. It is apparent that a relatively flexible structure is desirable in order that it remain in a continuous state of tension, thereby avoiding the complicated non-linear effects caused by slacking of the cables.

4.3.3 Determination of Sag of an Elastic Cable Subject to Constant Radial Loading

The peripheral cables of the rotating satellite will be

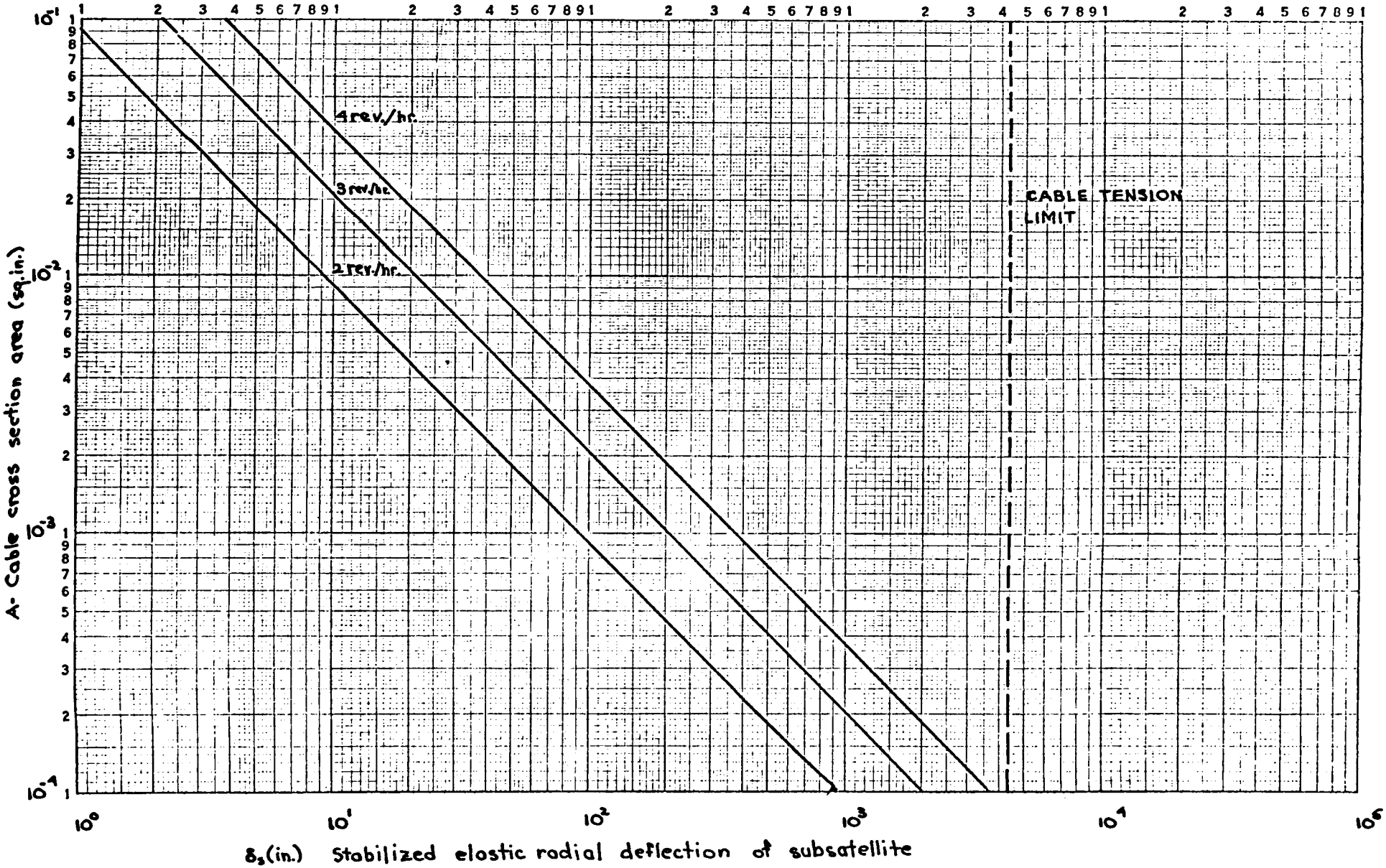

Figure 4.3-3 Elastic displacement as a function of cable size and spin rate.

subject to centrifugal forces creating cable sag. Since the centrifugal force is proportional to the radial distance of a cable element from the spin axis it follows that for the square configuration being considered here, the radial centrifugal loading will be greatest at the cables extremities. See Figure 4.3-4.

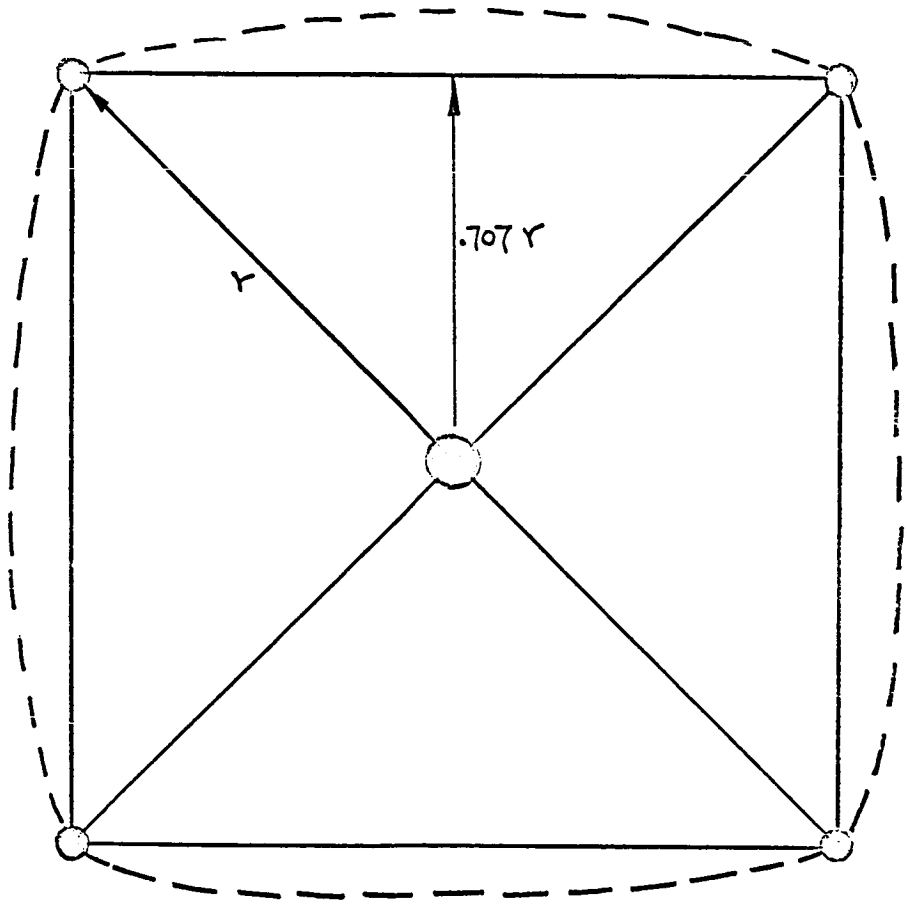

Figure 4.3-4 Illustration of Effect of Cable Sag on Shape of Peripheral Cables.

In the following analysis it will be assumed that the radial loading on a cable is constant. This assumption would not be valid for a peripheral cable joining two subsatellites but since intermediate supports will be provided then it may be assumed that each section of the peripheral cable between radial supports is sufficiently short that a constant radial loading condition exists.

In the model the elastic cable has been connected between two fixed points, and the cable has negligible bending stiffness, yielding the basic equation of the form

$$T \frac{dx}{dS} = H \qquad (4.3\text{-}13)$$

$$\frac{\partial}{dS}\left(T \frac{dy}{dS}\right) = w^2 Rm \qquad (4.3\text{-}14)$$

where

H = constant, horizontal component of tension

W = loading per unit length

m = mass/unit length

R = average radial distance of peripheral cable from the spin axis

The solution of the above equations 4.3-13 and 4.3-14 lead to the expression for the maximum sag in the cable as:

$$y = c\left(\cosh \frac{x}{c} - 1\right) \qquad (4.3\text{-}15)$$

Using the above relation 4.3-15 it is possible to determine the initial length of straight cable to the final extended length as

$$\ell = c \sinh \frac{a}{c} \tag{4.3-16}$$

For KWOT considerations the extension in the cable length will be due to elastic deformation. If T_o is the initial cable tension in the undeformed case and T_δ is the additional tension due to "spin sag" then the tension is

$$T = T_o + T_\delta \tag{4.3-17}$$

the extended length in terms of cable parameters is approximately

$$\ell = a + \int_o^a \frac{T}{AE}\, dx \tag{4.3-18}$$

assuming initial strain due to T_o is negligible, or

$$\ell = a + \frac{HC}{AE} \sinh \frac{a}{C} - \frac{T_o a}{AE} \tag{4.3-19}$$

Equating equations 4.3-16 and 4.3-19 yields an expression

$$\sinh\left(\frac{a}{c}\right)\left[cAE - wc^2\right] = a\left[AE - T_o\right] \tag{4.3-20}$$

which may be solved for "c" by using numerical techniques and the following values for the other parameters:

T_o = 0.258# (spin rate 2 revs/hr.)

a = 11600 ft. (peripheral cable)

$$W = \omega^2 R \frac{m}{32.2}$$

$$= .46 \times 10^{-4} \text{ lb/ft.}$$

$$E = .5 \times 10^{6} \text{ lb/sq.in.}$$

$$A = 1.45 \times 10^{-2}$$

$$AE = .725 \times 10^{4}$$

where:

$\omega = 349 \times 10^{-5}$ (2 revs/hr.)

R = .85 x 16400 (average radial distance of cable from spin axis).

m = .0087 lb/ft. (thick mylar)

It will be noted that we are assuming a cable having the length of a peripheral member connected between two subsatellites. There is no doubt that the peripheral member will have intermediate ties to prevent sag but this calculation was performed to determine a worst case of sag assuming constant radial loading and no intermediate connecting members.

Table 4.3-1 compares the values resulting from a solution of equation 4.3-20 and 4.3-15.

TABLE 4.3-1

	C(x 10^5)	Sag (ft.)
Thick Mylar	1.5	605
Thin Mylar	5.65	130

It is apparent from the above table that the maximum sag of an unsupported peripheral cable is not significant if it is assumed to be connected between two fixed points.

The calculated tension in an unsagged peripheral cable was found to be 0.258 lb. Introduction of sag modifies this tension load and the component of tension along a straight line between the two fixed points to which the cable is attached is given by

$$H = wc \tag{4.3-21}$$

For thick Mylar $H = 5.06$ lb. (4.3-22)

For thin Mylar $H = 0.260$ lb. (4.3-23)

Since, in both cases, this component of tension is greater than the unsagged value, it follows that there will be a tendency for the subsatellites to move towards each other. It is obviously possible, by an iteration process, to determine the final equilibrium position of the subsatellites with sagging interconnecting cables. It should be noted that use of a thick unsupported peripheral mylar cable would result in an unacceptable amount of sag due to the additional tension loads induced in the spinning configuration.

4.3.4 Determination of the Frequencies of the Normal Modes of Lateral Vibration of the Connecting Cables

The present analysis will be restricted to a consideration of the natural frequency of vibration of the connecting cables as a consequence of their tension. It will be assumed that the cables are initially straight. This is obviously a valid assumption for radial members and it has been shown in the previous section that the sag of a thin mylar peripheral member will be of the order of 1/2% of its total length, a negligible amount.

The assumption made in the analysis of a vibrating cable is that the amplitudes of vibration are so small that the elastic extension of the cable is negligible. Under these circumstances the tension in the cable remains constant. This is the assumption made in the classical analysis of a vibrating string and the expression for the frequency of vibration is

$$\omega_n = \frac{n\pi}{L}\sqrt{\frac{T}{m}} \qquad (4.3\text{-}24)$$

where T is the cable tension
m is mass/unit length
L is length of cable
n is number of mode.

For an unsupported thin mylar radial member

$L = 16400$ ft.

$T = .258$ lb. (2 revs/hr. spin rate)

$m = .87 \times 10^{-4}$ lb/ft.

$\omega_1 = .0592$ rad/sec (1 cycle per 1.76 minutes)

For an unsupported thin mylar peripheral member

$$\omega_1 = .0418 \text{ rad/sec.} \quad (1 \text{ cycle per } 2.49 \text{ minutes})$$

The above values give the frequencies of the first mode of lateral vibration of unsupported peripheral and radial members of the KWOT structure. Inclusion of intermediate supports for the cables will increase the values of these calculated frequencies.

It should be noted that if the above frequencies are considerably higher than the frequencies of the free modes of the complete KWOT structure (in which the cables are assumed straight) then the assumption of straight cables (Section 2.4) will be validated. The argument is based on the separation of the frequencies of the component modes of the total system.

4.3.5 Procedure for Determination of Frequencies of Normal Modes of KWOT Planar Model

The following analysis indicates the specific procedure used to determine the natural frequencies of free vibration of the KWOT satellite for planar motion in the Y-Z plane.

This procedure differs from the type of modes used in the analysis of section 2.4 in that the elements of the structure are free to vibrate in both the Y and Z directions simultaneously. The purpose of this calculation is to determine the frequencies of free Y-Z planar modes of the KWOT structural system so that they may be compared with calculated frequencies of the lateral modes of vibration of the connecting cables determined above.

It is obvious that the out of plane modes (which are neglected) are decoupled from the planar modes being considered due to symmetry.

The general equation of vibration in the Y-Z plane may be written as (refer to figure 4.3-5)

$$-\omega^2\begin{bmatrix} M & 0 & 0 \\ 0 & M & 0 \\ 0 & 0 & I \end{bmatrix}\begin{bmatrix} Y_o \\ Z_o \\ \phi_o \end{bmatrix} - \omega^2\begin{bmatrix} m_r & 0 \\ 0 & m_r \\ (-Z_m)_r & (Y_m)_r \end{bmatrix}\begin{bmatrix} Y \\ Z \end{bmatrix} = 0 \qquad (4.3\text{-}25)$$

$$\begin{bmatrix} Y_o \\ Z_o \\ \phi_o \end{bmatrix} = -\begin{bmatrix} M & 0 & 0 \\ 0 & M & 0 \\ 0 & 0 & I \end{bmatrix}^{-1}\begin{bmatrix} m_r & 0 \\ 0 & m_r \\ (-Z_m)_r & (Y_m)_r \end{bmatrix}\begin{bmatrix} Y \\ Z \end{bmatrix} \qquad (4.3\text{-}26)$$

where

I is total inertia of satellite system about its spin axis.

M is total mass of satellite system

m is a diagonal matrix of satellite masses

mr, mc - row and column representations of matrix m

$(-Zm)_r$ - row matrix, each element consisting of the product of a mass and its body axis -z coordinate.

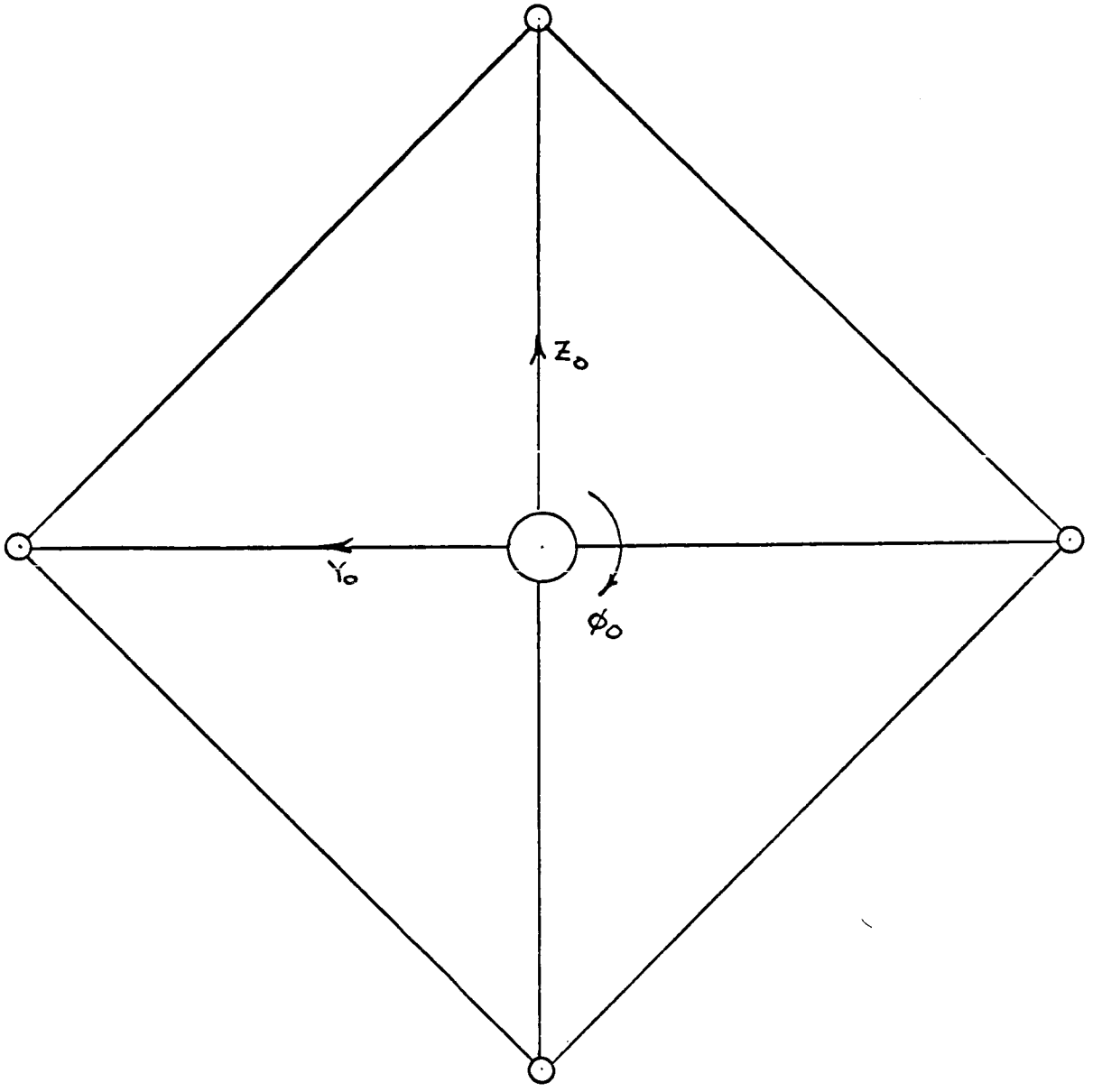

Figure 4.3-5 Coordinates for Planar KWOT Vibration Model

$(Ym)_r$ - row matrix, each element consisting of the product of a mass and its body axis Y coordinate.

Y_o, Z_o - translations of total system.

o - rotation of total system.

X, Z - column vectors of the displacements of the structural elements with respect to the center body.

E_{yy}, E_{zz}, etc. - stiffness matrix of structural elements with respect to the center body.

The above equation is in a convenient form for iteration of the normal modes of free planar vibration. The rigid body eigenvectors may then be determined from equation (4.3-26)

It will be noted that the KWOT structure given in Figure 2.5-1 contains approximately 226,240 feet of mylar cable. If the cable has a cross-sectional area of 1.45×10^{-4} (thin mylar) having a mass per unit length of $.87 \times 10^{-4}$ lb/ft. then the total mass of the complete cable structure is only 19.7 lbs. It would therefore seem unlikely that the cables would have significant inertial contributions to the dynamic modes of the complete structure since the mass of each subsatellite is 100 lb. (approximately) and the centerbody mass is 20000 lbs.

4.3.6 Traveling Waves in Support Cables

Any motion disturbance generated at a point on a cable in tension will result in traveling waves propagated along the cable at a velocity C where

$$C = \sqrt{\frac{T}{m}} \qquad (4.3\text{-}27)$$

where

T is the cable tension

M is the cable mass per unit length.

For thin mylar

C = 309 ft/sec. for an assumed 2 rev/hr spin rate. It should be noted that a damping force assumed proportional to the velocity of the deflections results in a wave propagation velocity less than the above value. There is little doubt that dissipative forces will be present in the wave propagation mechanism in the mylar cable although the exact magnitude and mechanism of the dissipative forces is not known. It seems apparent, however, that the low tension forces which exist in the mylar cables will result in significant dissipation of wave disturbance. Neglecting any dissipation energy it is apparent that a wave would take 1.25 minutes to travel the complete length of an unsupported peripheral cable. Further examination of the wave propagation equation (Equation

for an infinitely long cable (neglecting energy dissipation) indicates

$$Y = A\cos(pt - p\frac{x}{c}) \qquad (4.3\text{-}28)$$

where A is the wave amplitude and x is the distance along the cable, p is the angular frequency of a disturbance input and y is the cable lateral deflection.

that the total cable would respond instantaneously to a disturbance input if the velocity of wave propagation is infinite or if the frequency of motion excitation is effectively zero. It would appear that the velocity of wave propagation is fairly low in comparison with the lengths of cable being considered and it follows that the motion of a cable due to some disturbance such as subsatellite disturbance will result in a traveling wave form down the cable unless the subsatellite response is very slow. If the response of the subsatellite is very slow then the cables interconnecting the disturbed and undisturbed subsatellite will remain straight.

4.3.7 Summary

A number of aspects of the dynamic behavior of the KWOT satellite mylar cables have been investigated. A digital computer will be necessary to determine the frequencies of the planar KWOT model formulated in section 4.3.5 and it is therefore difficult, in this present study, to draw any conclusions on the necessity for considering the dynamic behavior of the mylar cables in future analysis.

A number of conclusions may be drawn on the basis of the present results.

It is apparent that the use of the thinnest mylar cable compatible with strength requirements will result in the following desirable properties.

(1) Large elastic deflections due to spin thereby ensuring that no slackening of cables is likely to occur.

(2) Low spin sag reducing the necessity for extra radial restraints of the perpheral cable.

(3) High cable vibration mode frequencies thereby leading to improved cable response to relative motions of the subsatellites.

(4) Low structural weight.

The thinnest mylar cable considered in the above work has a cross section area of 1.452×10^{-4} in.^{2} and numerical

computations indicate that this particular cable has desirable properties in the areas that have been investigated. The loading requirements for the mylar structure are yet to be investigated and will largely depend on the ability of the control system to maintain subsatellite relative position control within specified tolerances.

The effect of gravity gradient on the cable shape is not considered to be an important factor by virtue of the orbital orientations developed in this study.

SECTION V

LINEARIZED DEPLOYMENT CONSIDERATIONS

5.1 GENERAL

During the course of this study it has become apparent from several considerations (viz. esp. Sect. 3) that the desirable sequence of KWOT operations after orbit injection is a) stabilization of the hub with the cylinder axis directed toward the center of the earth b) deployment of the subsatellite and antenna structure c) spin-up to the desired rate. Given that the desired terminal position of the cylinder axis is along an earth radial, deployment in any other orientation would require subsequent ferrying operations of the entire structure. It will also be seen below that condition a) above is the most desirable orientation for deployment.

A common deployment procedure is to spin stabilize the satellite in orbit, at which time the satellite appendages are released and allowed to extend and lock at their respective fully deployed conditions. The deployment energy is derived from the despinning of the entire satellite system. However, the tenuous nature of KWOT and the large extensions encountered, complicate the "spinning" type deployment maneuver. In this section, a method of deployment is considered that can be implemented with state of the art components and techniques, using the subsatellites to ferry themselves and the support structure

out to the deployed condition. During the deployment maneuver, entanglement of the structure is prevented by judicious packaging and maintaining tension on the structure. A comparative investigation of the constraints on deployment velocity is given in section 4.3.1.

5.2 DEPLOYMENT CONCEPTS

As noted in section 4.2, the gravity-gradient moments on the KWOT hub are zero when the cylinder (spin) axis lies on an earth radial or is perpendicular to it. It is further indicated in section III that the desirable mode of precession of the deployed structure is that the spin axis lie on an earth radial at all times. It is easily seen that from a deployment standpoint, this mode is also the most desirable one.

The prime criterion for selecting a deployment scheme is simplicity of implementation, in that the probability of success is necessarily less for a complex scheme requiring more complicated mechanisms. The first task of the KWOT, after orbit injection and stabilization of the central package has been accomplished, is the deployment of the four subsatellites and the antenna and supporting structure. It is assumed that deployment is accomplished prior to spin-up, in order to reduce the liklihood of cable fouling or distortion of the structure. Three possible orientations of the structure during deployment are shown in Figure 5.2-1.

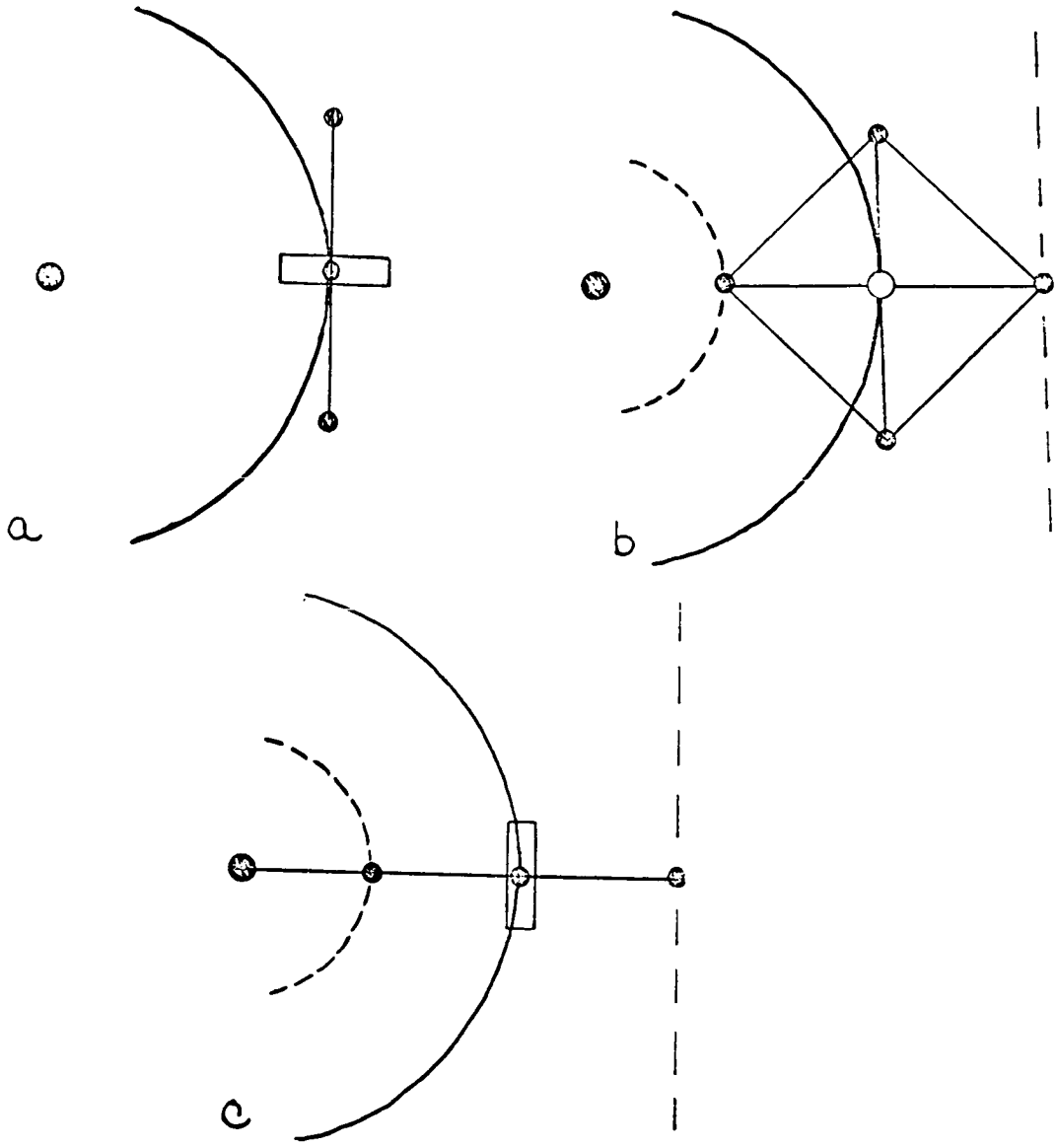

Figure 5.2-1

It is obvious that in configuration b) or c), small velocity differences will exist between the inner and outer subsatellites and the hub due to the difference in final orbital altitude. The differences, while small, (about 1 part in 10,000) nevertheless constitute an orbital transfer problem which is an unnecessary complication to the deployment scheme; especially in view of the desired final orientation of the cylinder axis.

For ease of analysis, an exponential type of subsatellite guidance is assumed, resulting in a linearized first order requirement for the control system. The central hub is assumed to contain equipment that monitors the location of the subsatellite and provides deployment guidance information. The control information consists of 1) separation distance, 2) its time rate of change, and 3) angular velocity of the line of sight with respect to inertial space. As a suggestion, radar or laser beam systems may be used to provide the distance and the rate of separation; the rate of rotation of the line of sight and satellite orientation may be referenced from a gyro, the earth or the starts. Deployment guidance computation may be performed on KWOT, or the earth.

For analysis purposes the deployment guidance model considered is equivalent to a one-dimensional exponential guidance in each of the two directions of the relative cartesian coordinate system shown in Figure 5.2-2.

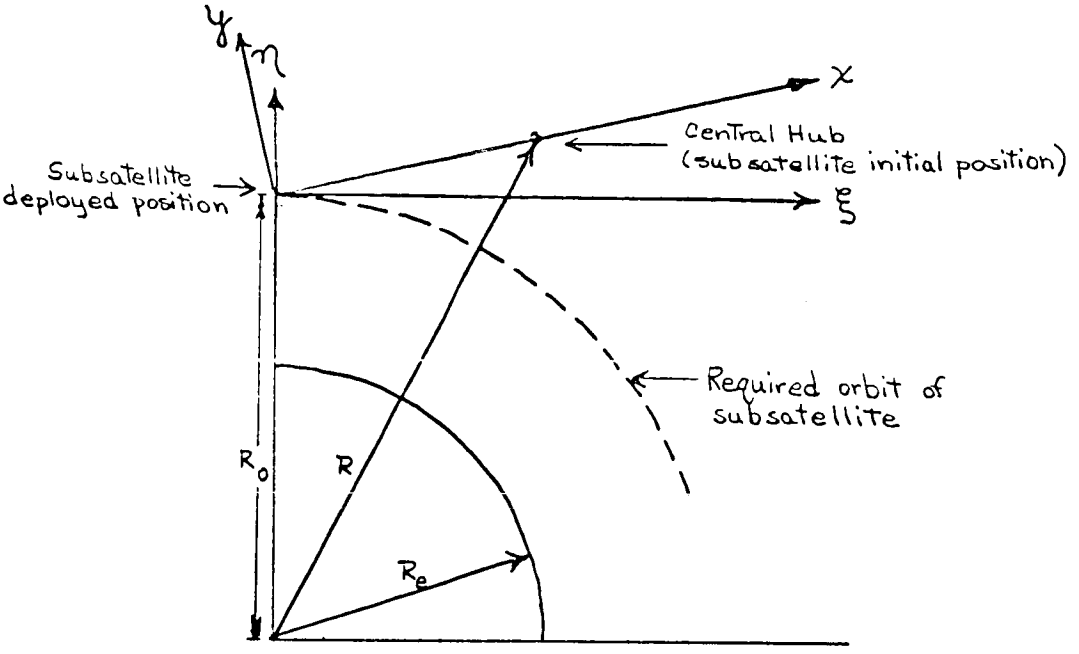

Figure 5.2-2 Deployment Model

The deployment guidance equations are:

$$F_x = m(\alpha \dot{x} + \beta x) \tag{5.2-1}$$

$$F_y = m(\alpha \dot{y} + \beta y) \tag{5.2-2}$$

The equations of motion are:

$$F_x = -m\ddot{x} = m(\alpha \dot{x} + \beta x) \tag{5.2-3}$$

or

$$\ddot{x} + \alpha\dot{x} + \beta x = 0 \qquad (5.2\text{-}4)$$

similarly

$$\ddot{y} + \alpha\dot{y} + \beta y = 0 \qquad (5.2\text{-}5)$$

The solutions of Equations 5.2-4 and 5.2-5 with the initial conditions

$$\begin{aligned} x &= x_0 & \dot{x} &= u_0 = V\cos\theta \\ y &= 0 & \dot{y} &= v_0 = V\sin\theta \end{aligned} \qquad (5.2\text{-}6)$$

and at critical damping are:

$$\begin{aligned} X &= x_0 \epsilon^{-at}\left[1 + \left(1 + \frac{V}{a x_0}\cos\theta\right) at\right] \\ Y &= x_0 \epsilon^{-at}\left[\left(\frac{V}{a x_0}\sin\theta\right) at\right] \end{aligned} \qquad (5.2\text{-}7)$$

where

α, b = guidance coefficients

$a = \frac{\alpha}{2}$

$\beta = \sqrt{\left(\frac{\alpha}{2}\right)^2 - \beta} = 0$

θ = firing angle measured from positive X axis

V = initial velocity.

The paths of the subsatellite for various firing angles and the parameter $\frac{V}{a x_o}$ are plotted in Figures 5.2-3, 5.2-4, and 5.2-5. As the value of $\frac{V}{a x_o}$ is increased, the subsatellite takes a less direct path and tends to wander further out from the radial increasing the possibility of entanglement of the structure.

To determine the chemical propellant consumed during deployment by one subsatellite, the specific impulse equation

$$I_{sp} = \frac{1}{W_p} \int_o^t T \, dt \qquad (5.2\text{-}9)$$

must be written in the form:

$$W_p = \frac{1}{I_{sp}} \int_o^t T \, dt \qquad (5.2\text{-}10)$$

or

$$W_p = \frac{m_s}{I_{sp}} \int_o^t a \, dt \qquad (5.2\text{-}11)$$

considering only the radial case, i.e., $\Theta = 180^\circ$, Equation 5.2-11 can easily be integrated, yielding

$$W_p = \frac{m_s}{I_{sp}} V \qquad (5.2\text{-}12)$$

Figure 5.2-6 shows one radial subsatellite propellant consumption as a function of initial velocity. For the velocities considered the maximum propellant consumption is approximately 3% of the subsatellite weight.

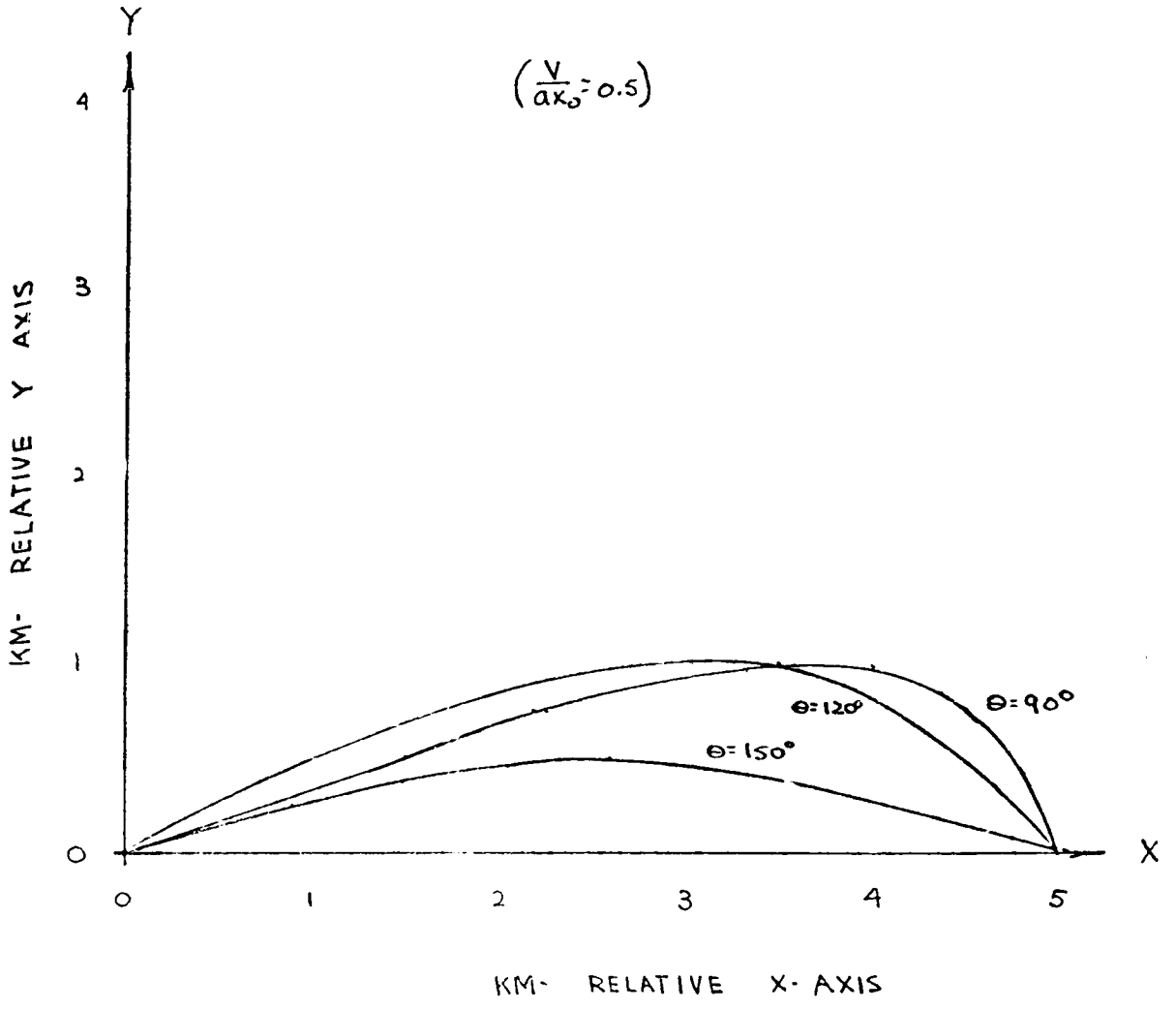

FIGURE 5.2-3 Relative paths for various firing angles $\left(\frac{V}{ax_0}=0.5\right)$

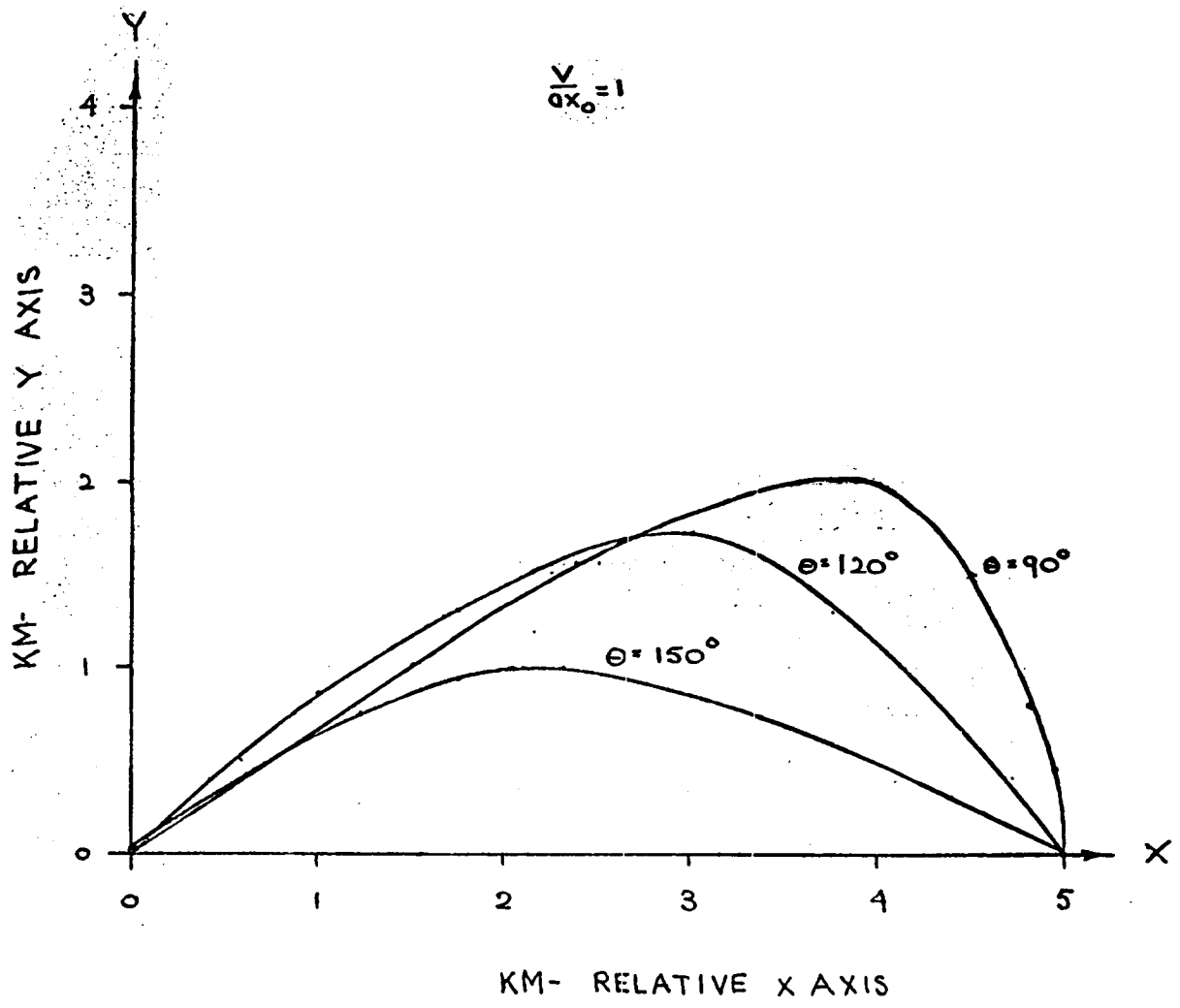

FIGURE 5.2-4 Relative paths for various firing angles. $\left(\frac{V}{ax_0}=1\right)$

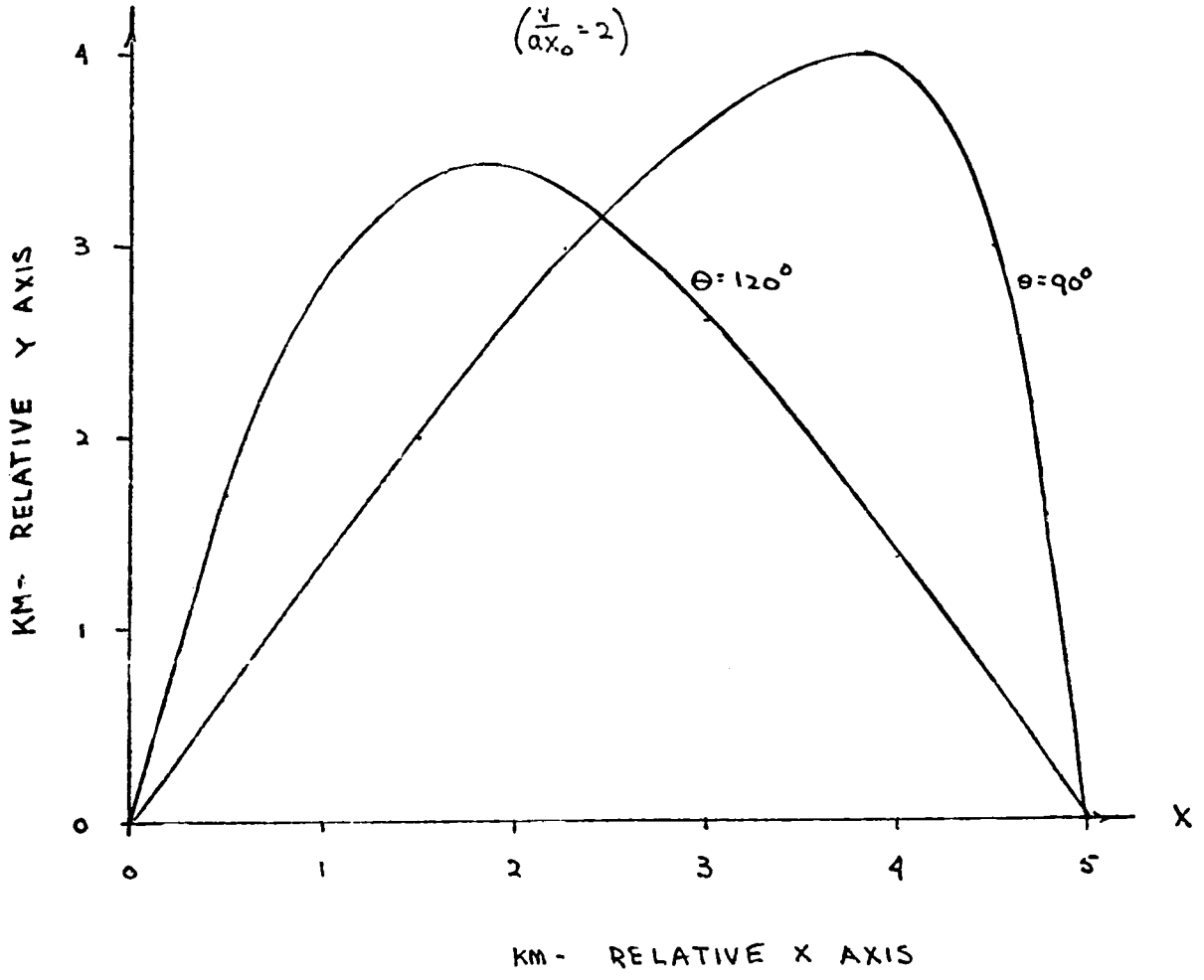

FIGURE 5.2-5 Relative paths for various firing angles $\left(\frac{V}{aX_0}=2\right)$

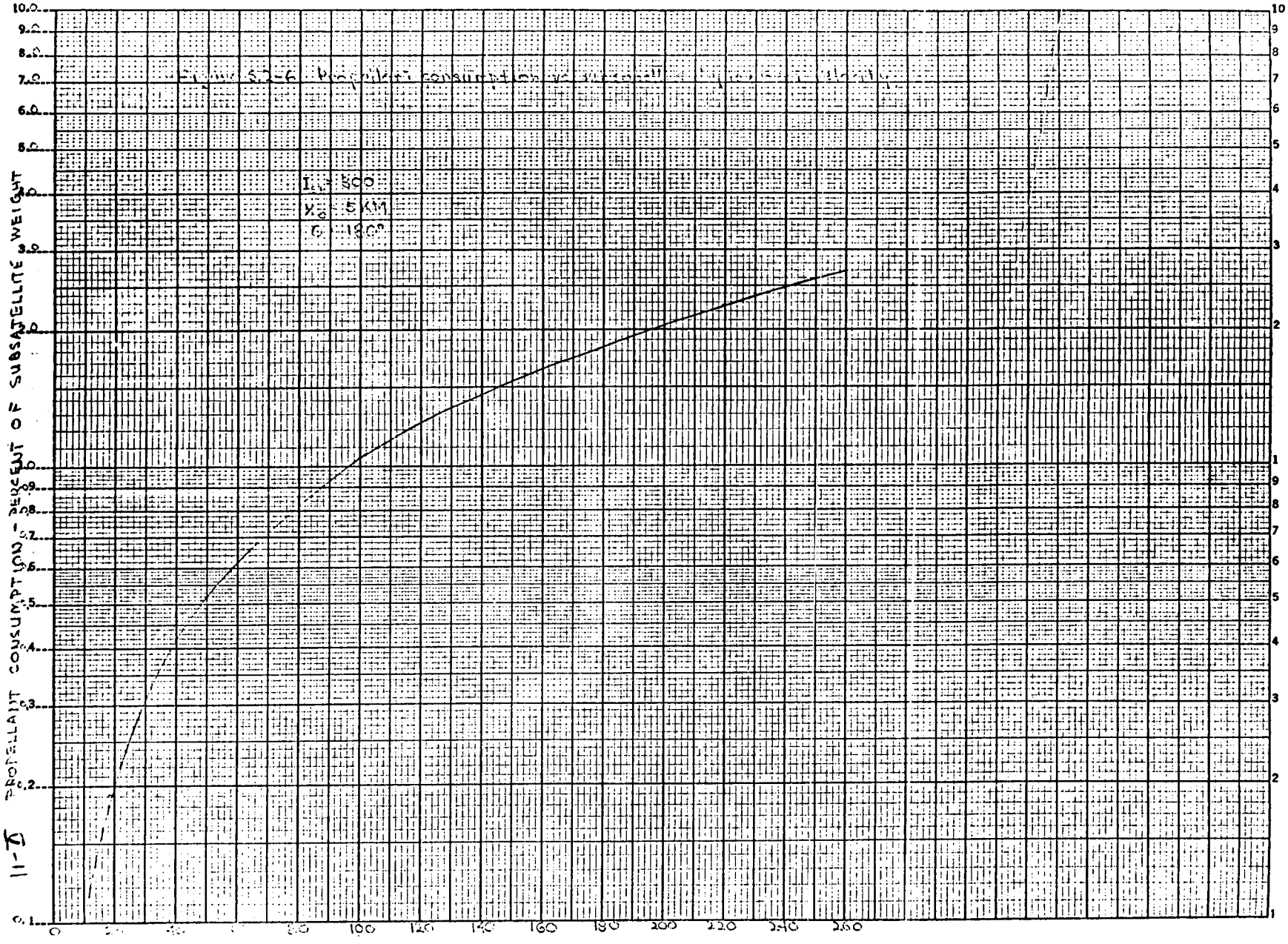
PROPELLANT CONSUMPTION - PERCENT OF SUBSATELLITE WEIGHT
I_{sp} = 500
X_0 = 5 KM
θ = 190°
10.0
9.0
8.0
7.0
6.0
5.0
4.0
3.0
2.0
1.0
0.9
0.8
0.7
0.6
0.5
0.4
0.3
0.2
0.1
0
20
40
60
80
100
120
140
160
180
200
220
240
260
10
9
8
7
6
5
4
3
2
1
9
8
7
6
5
4
3
2
1

11-7

SECTION VI

CONCLUSIONS AND RECOMMENDATIONS

This study established the feasibility of a KWOT vehicle in achieving its maneuvering requirements. The generalized dynamic equations of motion that are necessary for a non-linear analysis have been defined. These equations have been simplified and linearized to enable their use in this feasibility study with the following results:

1. Established an orbital maneuver (spin and precession rates) that provides observation of the complete celestial sphere. Determined a control system that will accomplish these orbital maneuvers. Based on the analysis it is recommended that the hub spin axis point continuously at the earth and that for stability the maximum moment of inertia be about the spin axis. The latter design goal should be accomplished by minimizing the moments about the other two axes, rather than by enhancing the moment about the spin axis.

2. Considered various deployment concepts and recommended an inertial orientation and a non-spinning type deployment mode. Calculated permissible deployment velocities (22 fps max.), based upon cable properties

and structural dynamics. Calculated propellant requirements necessary to accomplish deployment and determined to be approximately 3% of subsatellies gross weight.

4. Based upon structural dynamics considerations the use of the 1.452×10^{-4} $in.^2$ cross-sectional area mylar cable will result in the following desirable behavior:
   a. The region of elastic deflection (linear motion) due to spin, is large enough to fall within the control system capability.
   b. Reduced radial sag due to centrifugal forces, thus reducing requirements for peripheral restraints.
   c. High cable vibration mode frequencies thereby preventing energy interchange with lower frequency subsatellite motions.
   d. Low structural weight.
   e. Sufficient strength to arrest satellites being deployed at a reasonable velocity.
5. Equations have been established for both 2- and 3-dimensional structural stiffness matrices that can be used in defining design criteria for future structural consideration.

APPENDIX A

NORMAL STIFFENING CONSIDERATION

Stiffening the structure in the direction normal to the plane of the antenna was also considered. This may be accomplished by the basic pyramidal configuration, symmetric about the antenna plane, shown in Figure A-1. Three schemes have been considered for the erection and maintenance of the central stiffener at the hub, in the direction of the hub axis. These are:

(1) Deployment of large masses in the axial direction. This may be accomplished by the ejection of a considerable but otherwise unusable portion of the hub structure in opposite hub axis directions. These masses will be attached by the pyramidal configuration of ribbon members to the KWOT plane. Centrifugal force, due to the precession of the structure would keep the configuration stable. This is shown in Figure A-1a.

Assume the masses are approximately 1/4 of the hub structure, of earth weight about 5,000 lbs., and the precession rate is one degree per hour. Let the distance to the hub be 10,000 ft. The centrifugal force generated in the hub axis

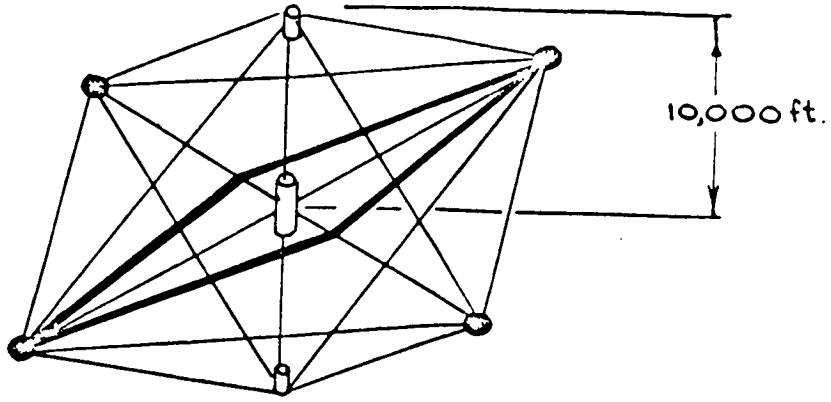

Figure A-1a. Pyramidal Configuration for KWOT. (Intermediate Ribbons From Apex to Antenna and Other Members Not Shown.)

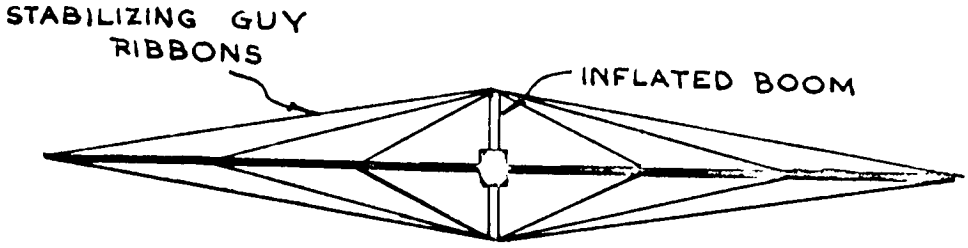

Scale: Approximate

Figure A-1b. Inflatable Boom Stabilized KWOT (Side View)

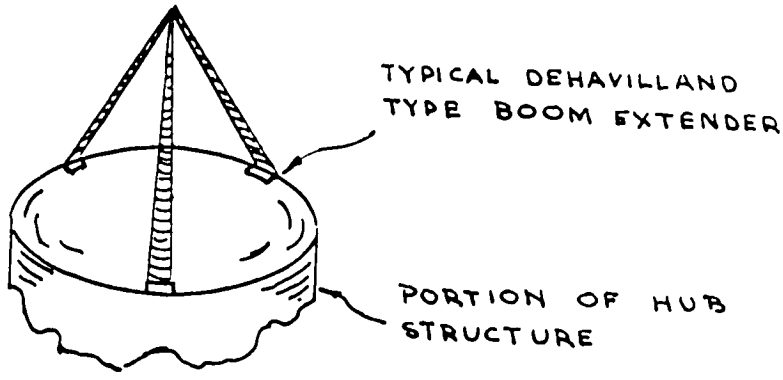

Figure A-1c. DeHavilland Type Boom Tripod Partially Deployed

direction would then be

$$F = m\omega^2 r \qquad \text{(A-1)}$$

where $m = \frac{5000}{32.2} \ \frac{\text{lb.}}{\text{ft.}} \cdot \text{sec.}^2$

$\omega = \frac{2\pi}{3600} = \frac{1}{360} \left(\frac{1}{\text{sec.}}\right)$

$r = 10000$ ft.

resulting in

$$F = 0.37 \cdot 10^{-4} \text{ lb.} \qquad \text{(A-2)}$$

This is too small a force, a situation which could be remedied only by increasing the precession rate (which by definition is not feasible) to, say, 100° per hour, in which case the force would be

F = 0.37 lb. at precession = 100° per hour.

(2) Erection of an Inflatable Boom

The use of inflatable structures for space application has been studied for several years. In space there are several advantages, since the stability required is very low, and because the pressurization required for this stabilization is very low, and relatively easy to maintain through the sublimiation of certain crystalline chemicals. Suppose then that a boom of the order of 1,000 ft. be

erected from the hub as illustrated in Figure A1-b. The Euler buckling load for such a simple boom is

$$P = \frac{\pi^2 E I}{4 \ell^2} \tag{A-3}$$

The required moment of inertia is

$$I = \frac{4 P \ell^2}{\pi^2 E} \tag{A-4}$$

Considering $P = 1$ lb.

$\ell = 1{,}000$ ft.

$E = .5 \times 10^6$ ("Mylar" plastic)[2]

$$I = 116.5 \text{ in}^4 \tag{A-5}$$

For a circular cross section,

$$I = \pi r^3 t \tag{A-6}$$

A minimum wall thickness would be 0.0005 in. Then

$$r = \sqrt[3]{\frac{I}{\pi t}} = 42 \text{ in} \tag{A-7}$$

The weight would be

$$w = 2\pi r t \ell \delta \tag{A-8}$$

Where σ = density

For Mylar, $\sigma = .05 \frac{\text{lb.}}{\text{in.}^3}$

Then

$$W = 79 \text{ lbs.} \qquad \text{(A-9)}$$

For this configuration, the local buckling stress should not exceed the pretension due to the pressurization. Conservatively assume local buckling at zero stress. The pressurization must therefore yield a total tensile load equal to the design compressive force of 1 lb. The pressurization requirement is therefore such that

$$\text{(end load)}\ \mathbb{P} = \pi r^2 p \qquad \text{(A-10)}$$

where p = pressure

resulting in

$$p = \frac{\mathbb{P}}{\pi r^2} = 1.8 \times 10^{-4} \text{ psi} \qquad \text{(A-11)}$$

Thus the weight, geometry, and pressurization required all appear very reasonable. One of the major problems would be the thermally induced bending from solar radiation.

Assuming that the temperature varies linearly across the diameter of the tube, and that the temperature

difference, ΔT, is maintained at 20° Farenheit. The thermal rotational strain in the boom is $\frac{\alpha \Delta T}{2r}$ where α is the thermal coefficient of expansion. Then the lateral deflection, Δ, at the tip would be a maximum, if the end were unrestrained:

$$\Delta = \int_0^{\ell}\int_0^{x} \frac{\alpha \Delta T}{2r}\, dx\, dx \qquad \text{(A-12)}$$

resulting in

$$\Delta = 26.8 \text{ ft.} \qquad \text{(A-13)}$$

where:

$$\alpha = 0.94 \times 10^{-5} \ \frac{\text{in}}{\text{in}^{\circ}\text{F}}$$

and

$$\ell = 12000 \text{ in}$$

This is not an unreasonable deflection, although it would affect the stability of the column. Suitable coatings may bring this deflection down by a factor of 3.

The maximum compressive stress must then be negated by pressurization for local stability.

$$\text{Moment} = P\Delta = 26.8 \times 12 \text{ in.-lb.} \qquad \text{(A-14)}$$

$$\text{stress} = -\frac{Mr}{I} = -116 \text{ psi} \qquad \text{(A-15)}$$

Let $\frac{F}{A}$ be the pressurization stress. To make the compressive stress zero,

$$\frac{F}{A} - \frac{Mr}{I} = 0 \qquad \text{(A-16)}$$

Pressurization stress is therefore:

$$\frac{F}{A} = \frac{pr}{2t} = 116 \text{ psi} \qquad \text{(A-17)}$$

Then

$$p = \frac{2t \cdot 116}{r} = 0.276 \times 10^{-3} \text{ psi} \qquad \text{(A-18)}$$

This is therefore the critical pressurization requirement. Thus for the pressurized boom consideration the parameters are:

Length = 1,000 ft.

Diameter = 2r = 84 in.

Material = Mylar

Thickness = 0.0005 in.

Pressurization = 0.28×10^{-3} psi

Critical Load = 1 lb.

Maximum Δ T = 20°F.

(3) DeHavilland Type Boom Tripod

This configuration is shown in Figure A-1c. Three

boom generators are placed circumferentially equidistant on the hub ends. The boom ribbons are joined at the hub axis. When extended, the booms would deploy, with the common central joint as the vertex of a tripod with a 20 ft. diameter base. A reasonable extension length might be on the order of 225 ft. The critical compressive strength required is given by the Euler load of one member of the tripod. This must equal approximately 1/3 lb., the compressive design load. The required moment of inertia may be obtained as before:

$$I = \frac{4P\ell^2}{\pi^2 E} \qquad \text{(A-19)}$$

If steel is used, ($E = 30 \times 10^6$)

$$I = 0.03218\ in^4 \qquad \text{(A-20)}$$

Assuming r = 1 in.

$$t_{reqd} = \frac{I}{\pi r^3} = 0.0104\ in. \qquad \text{(A-21)}$$

Due to thermal bending, the lateral displacement is approximately given by:

$$\Delta = \frac{\alpha \Delta T}{2r} \cdot \frac{\ell^2}{2} \qquad \text{(A-22)}$$

Assuming $\Delta T = 3^{\circ}F$

$$\alpha \approx 0.000006$$

$$\Delta = 32.8 \text{ in.} \qquad \text{(A-23)}$$

The maximum compressive stress due to the compressive force acting on the bent boom is

$$\sigma = \frac{Mc}{I} = -112 \text{ psi} \qquad \text{(A-24)}$$

The buckling stress is

$$\sigma_{bu} = CE\frac{t}{r} = 172000 \text{ psi} \quad (\text{with } C = 0.55) \qquad \text{(A-25)}$$

Therefore the boom will not buckle locally.
In order to assure that the critical load is not exceeded by the design load of 1/3 lb. in each boom, the foil thickness should be increased to t = 0.012 in. Then P_{cr} is increased to

$$P_{cr} = 0.3831\text{b.} \qquad \text{(A-26)}$$

This is adequate to overcome the additional load increment caused by the basic slope of the tripod and the thermal displacements.

The last two designs appear most reasonable. The inflatable design has the advantage of a higher pyramid apex, but a possible pressurization reliability problem. The De Havilland type boom design, however, may still encounter deployment reliability problems, and offers a much lower apex. Also, the metallic foil used therein may affect the antenna radiation patterns.

APPENDIX B

STABILITY OF CANTILEVERED RIGIDIZED MEMBRANE CYLINDERS

It has recently been shown by Jahsman[1] that pressurized circular cylindrical membrane columns possess stability well beyond the initial wrinkling stage when subjected to compression and bending. It was also shown therein that linear behavior is expected up to the point of wrinkling, conservatively assumed to be reached when the combined bending, axial compression and pressurization stress is zero. The use of such a column as a central boom was proposed for out-of-plane stabilization of the KWOT in the Interim Progress Report. The configuration parameters are repeated here in Table B-1. However, because of the problem of the continuous pressurization requirements of the boom, considering that it might become punctured by space debris, it was deemed necessary to investigate the possibilities of using an inflatable column, rigidized by foamed in-place walls. The physical parameters of Mylar and foam materials may be obtained from the Expandable Structures Design Handbook[2].

Without the continuing aid of pressurization, the stability of the column is dependent upon the classical buckling stress[3].

$$\sigma_{bu} = .605\, E\left(\frac{t}{R}\right) \qquad \text{(B-1)}$$

To find the foam thickness required in the case of a composite mylar-foam-mylar sandwich membrane, let us assume that an optimum condition is reached when the buckling stress is the same for all elements of the cross-section shown in Figure B-1.

Symbols

r = radius of cross-section

I = area moment of inertia

A = cross-sectional area

E = Young's Modulus

t = thickness

σ = stress

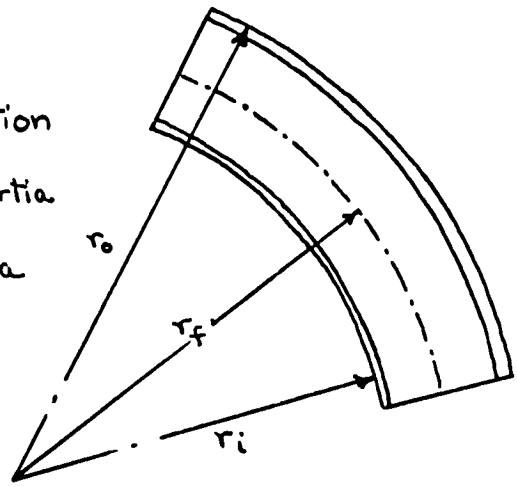

Figure B.1 Foamed Wall Erectable Cylinder - Section Geometry

Assuming furthermore that the overall thickness $(r_o+\frac{t_o}{2}) - (r_i-\frac{t_i}{2})$ is small compared to r_f, the buckling formula applies. Then from (B-1)

$$\sigma_{bu} = .605\left(\frac{t_o}{r_o}\right)E_{(mylar)} = .605\left(\frac{t_i}{r_i}\right)E_{(mylar)} \qquad (B-2)$$

$$= .605\left(\frac{t_f}{r_f}\right)E_{(foam)} \qquad (B-3)$$

Since the outer membrane may be chosen as a design parameter,

$$t_f = r_f \left(\frac{t_o}{r_o}\right) \frac{E\,(mylar)}{E\,(foam)} \tag{B-4}$$

From this one can also determine

$$\begin{aligned} t_i &= r_i \left(\frac{t_o}{r_o}\right) \\ &= \left\{\left(r_o - \frac{t_o}{2}\right) - t_f\right\} \left(\frac{t_o}{r_o}\right) \\ &\cong (r_o - t_f)\left(\frac{t_o}{r_o}\right) \end{aligned} \tag{B-5}$$

Then due to combined bending from thermal gradients, there appears a moment

$$M_T = P\Delta_t \tag{B-6}$$

where Δ_t = free thermal end displacement

P = axial compressive force

Hence the buckling stress must not exceed

$$\sigma_{bu_{max}} = \frac{M_T r_o}{I} + \frac{P}{A} \,. \tag{B-7}$$

The share of the moment in the foamed material is given by

$$\frac{M_f}{M_{Total}} = \frac{E_f I_f}{E_f I_f + E_m I_m} \tag{B-8}$$

$$M_{Total} = P\Delta T$$

$$\Delta T \cong \frac{\alpha(\Delta T)}{2r_o} L^2$$

Similarly, the share of the axial load for the foam is

$$P_f = P_{Total} \frac{E_f A_f}{E_f A_f + E_M A_M} \qquad \text{(B-9)}$$

where the subscript $_M$ designates Mylar and $_f$ designates the foam.

Therefore, from (B-3)

$$\sigma_{bu(max)} = .605 \left(\frac{t_f}{r_f}\right) E_f = \left[\frac{\alpha \Delta T L^2}{2\left(I_f + \frac{E_m}{E_f} I_m\right)} + \frac{1}{\left(A_f + \frac{E_m}{E_f} A_m\right)}\right] \qquad \text{(B-10)}$$

Now from Euler's critical load one obtains

$$P_{cr} = \frac{\pi^2 EI}{4L^2} \qquad \text{(B-11)}$$

The required EI is then

$$EI_{Total(Req'd)} = \frac{4 P_{cr} L^2}{\pi^2} \qquad \text{(B-12)}$$

But

$$EI_{Total} = (EI)_{mylar} + (EI)_{foam} \qquad \text{(B-13)}$$

the solution of which becomes an iterative procedure. Choosing some ratio of $\frac{(EI)_{foam}}{(EI)_{Mylar}}$, one may determine A_f, A_m, assume a ΔT, and thus calculate $(\sigma_{bu})_{max}$. If this is not equal to the buckling stress

$$\sigma = .605 \left[E\left(\frac{t}{r}\right)\right]_{(mylar)} \qquad \text{(B-14)}$$

the process must be repeated for a new ratio of $\frac{(EI)_{foam}}{(EI)_{Mylar}}$, until the desired equality of buckling stress and combined axial and bending stress has been achieved. Numerical values of the solution have not been determined at this time.

References

1. Jahsman, W. E., "Combined Bending and Compression of a Pressurized Circular Cylindrical Column," J. of Engineering for Industry, (in Transactions of the ASME), August 1965.
2. Expandable Structures Design Handbook, ASD, TDR 63-4275, June 1965, Air Force Materials Laboratory, Research & Technology Division, Air Force Systems Command, WPAFB, Ohio.
3. Timoshenko, S., "Theory of Elastic Stability," 1936.

APPENDIX C

EFFECT OF INTIAL TENSION ON THE STIFFNESS OF THE KWOT

The centrifugal forces on the KWOT peripheral satellites produce initial stresses in the KWOT structural members. It is shown in the following discussion that in the case of assumed geometric linearity of behavior, the stiffness coefficients of the KWOT are not affected by this initial stress condition.

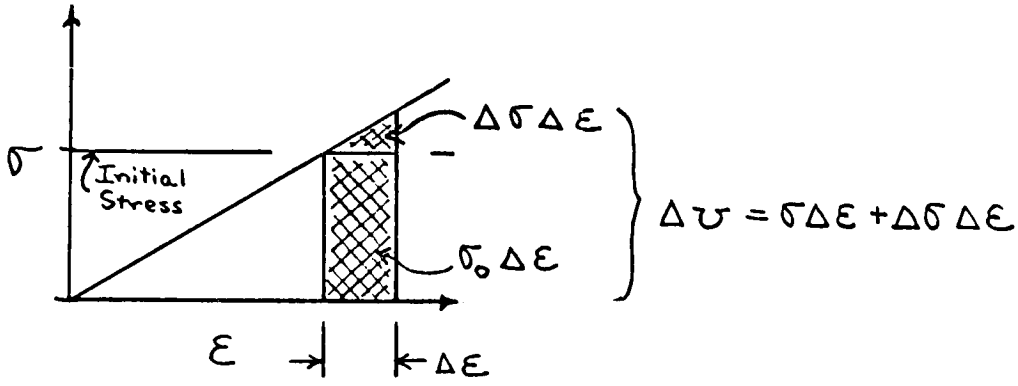

Figure C-1 Stress-Strain Diagram of Member.

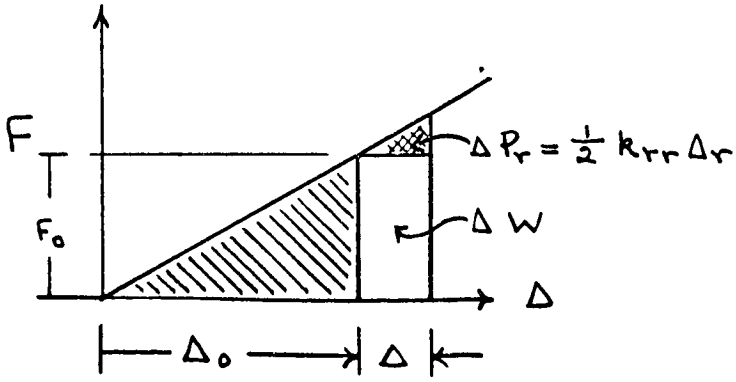

Figure C-2 Force-Displacement Diagram of a Typical Point.

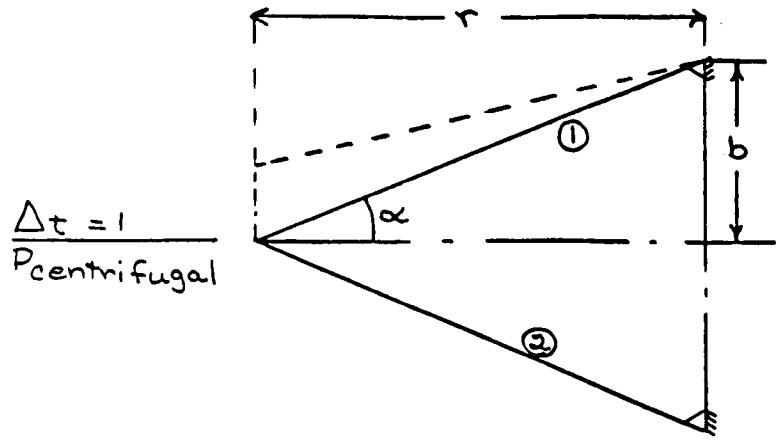

Figure C-3 Tangential Displacemnt of a KWOT Satellite

Let:

ΔW = Change in work due to Δt

ΔU = Change in strain energy due to Δt

k = Stiffness

Δ = Displacement or increment

σ = Stress

ε = Strain

δ = Member extension

L = Length of member

v = Volume per unit length of member

$$\Delta W = \tfrac{1}{2}\left(k_{t,t} \times \Delta_t\right) \times \left(\Delta_t\right) \qquad \text{(C-1)}$$

$$\Delta U = \int \sigma_o \, \Delta\varepsilon \, dv + \int \frac{\Delta\sigma \, \Delta\varepsilon}{2} \, dv \qquad \text{(C-2)}$$

but

$$\Delta\varepsilon = \frac{\delta}{L} \tag{C-3}$$

and

$$\delta_I = -\Delta_t \sin\alpha \tag{C-4}$$

$$\delta_{II} = \Delta t \sin\alpha \tag{C-5}$$

$$\Delta\sigma = E\,\Delta\varepsilon \tag{C-6}$$

Then from (C-6)

$$\frac{\Delta\sigma\,\Delta\varepsilon}{2} = \frac{E(\Delta\varepsilon)^2}{2} = \frac{E}{2}\,\frac{\Delta t^2 \sin^2\alpha}{L^2} \tag{C-7}$$

Substituting (C-7 in (C-2)

$$\Delta U = \sigma_0 \underbrace{\left(\int \frac{\delta_1}{L_1}\, dv_1 + \int \frac{\delta_2}{L_2}\, dv_2\right)}_{=0} + \tag{C-8}$$

$$+ 2\int \frac{E}{2}(\Delta t)^2 \frac{\sin^2\alpha}{L_2}\, A\, dl$$

Solving the integral

$$\Delta U = \frac{EAb}{L^2} \sin\alpha\, \Delta t^2 \tag{C-9}$$

but

$$\Delta U = \Delta W \tag{C-10}$$

$$\therefore k_{tt} = \frac{2AE\,b\sin\alpha}{L^2} \tag{C-11}$$

Which is identical with the usual result, in the case of no initial stress. A similar result obtains in the radial extension case, $\Delta_r = 1$.

In that case,

$$\Delta W = \left(P_r + \tfrac{1}{2} k_{rr} \Delta r \right) \Delta r \qquad \text{(C-12)}$$

$$\Delta U = 2 \sigma_o A \cos\alpha \, \Delta r + \frac{EA}{L} \cos^2\alpha \, (\Delta r)^2 \qquad \text{(C-13)}$$

but

$$\Delta U = \Delta W \qquad \text{(C-10)}$$

$$\therefore P_r + \tfrac{1}{2} k_{rr} \Delta r = 2 \sigma_o A \cos\alpha + \frac{EA}{L} \cos^2\alpha \, \Delta r \qquad \text{(C-14)}$$

but

$$2 \sigma_o A \cos\alpha = 2 \left(\frac{P_r}{2A \cos\alpha} \right) A \cos\alpha = P_r \qquad \text{(C-15)}$$

Therefore

$$k_{rr} = 2 \frac{EA}{L} \cos^2\alpha \qquad \text{(C-16)}$$

Which again is identical with the usual result of no initial stress.

APPENDIX D

KWOT OCTANT STIFFNESS MATRIX

The structural and dynamic analyses of a three dimensional KWOT configuration, stiffened by a central boom against out-of-line deflection, would be based upon the stiffness matrix presented in the following discussion. In order to minimize the computational labor, the analysis takes advantage of the assumed symmetry in the three planes x-y, y-z, and x-z, by analyzing only one octant of KWOT, whose geometry is given in Figure D-1, for appropriate combinations of symmetry and antisymmetry of the boundary conditions on the plane of symmetry. Figure D-2 illustrates the degrees of freedom of the simplified KWOT octant.

The numerical values of the octant stiffness matrix are given in Figure D-3 and the designation of the non-restrained degrees of freedom are given in Figures D-4 through D-11. The stiffness matrix was computed for the whole octant. By applying the illustrated boundary conditions, the stiffness matrices of each case were extracted, and are given in Figures D-12 through D-19.

The element stiffnesses are obtained by assuming a guy wire area as used for the stiffness matrix of the planar KWOT given in the Interim Progress Report. The material is Mylar.

The boom was also assumed to have the same configuration as previously calculated in the Interim Progress Report.

The stiffnesses were apportioned to the octant according to the share of the element's stiffness contributed to it. There results:

$$k_{①} = \left(\frac{1}{2}\right)\frac{EA_{①}}{L_{①}} = .014326$$

$$k_{②} = \left(\frac{1}{2}\right)\frac{EA_{②}}{L_{②}} = .019655$$

$$k_{③} = \left(\frac{1}{4}\right)\frac{EA_{③}}{L_{③}} = .041866$$

$$k_{④} = \left(\frac{1}{4}\right)\frac{EA_{④}}{L_{④}} = .010128$$

$$k_{⑤} = \left(\frac{1}{4}\right)\frac{EA_{⑤}}{L_{⑤}} = .013360$$

$$k_{⑥} = \left(\frac{1}{2}\right)\frac{EA_{⑥}}{L_{⑥}} = .020219$$

$$k_{⑦} = \left(\frac{1}{2}\right)\frac{EA_{⑦}}{L_{⑦}} = .020219$$

$$k_{⑧} = \left(\frac{1}{2}\right)\frac{EA_{⑧}}{L_{⑧}} = .081194$$

$[k]_{boom}$ =

$k_{9,9} = .00011112$
$k_{12,9} = -.00011112$
$k_{16,9} = 1.33349$
$k_{10,10} = .00011112$
$k_{13,10} = -.00011112$
$k_{15,10} = -1.33349$
$k_{11,11} = 6.0475$
$k_{14,11} = -6.0475$
$k_{12,12} = .00011112$
$k_{16,12} = -1.33349$
$k_{13,13} = .00011112$
$k_{15,13} = 1.33349$
$k_{14,14} = 6.0475$
$k_{15,15} = 16001.$
$k_{16,16} = 16001.$

All matrices are symmetric.

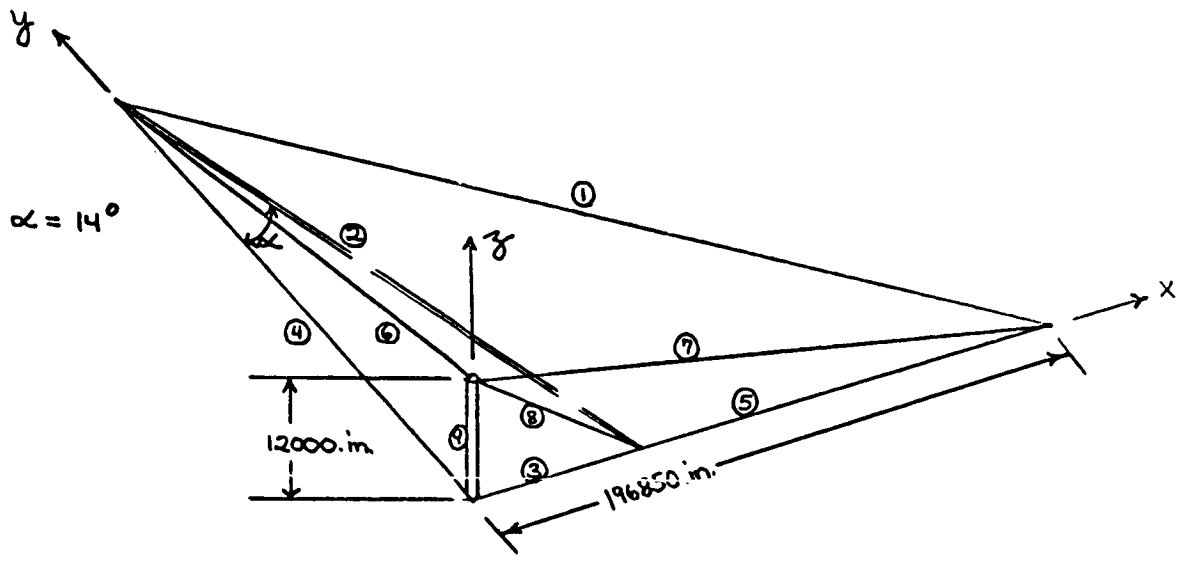

Figure D-1 Octant Geometry.

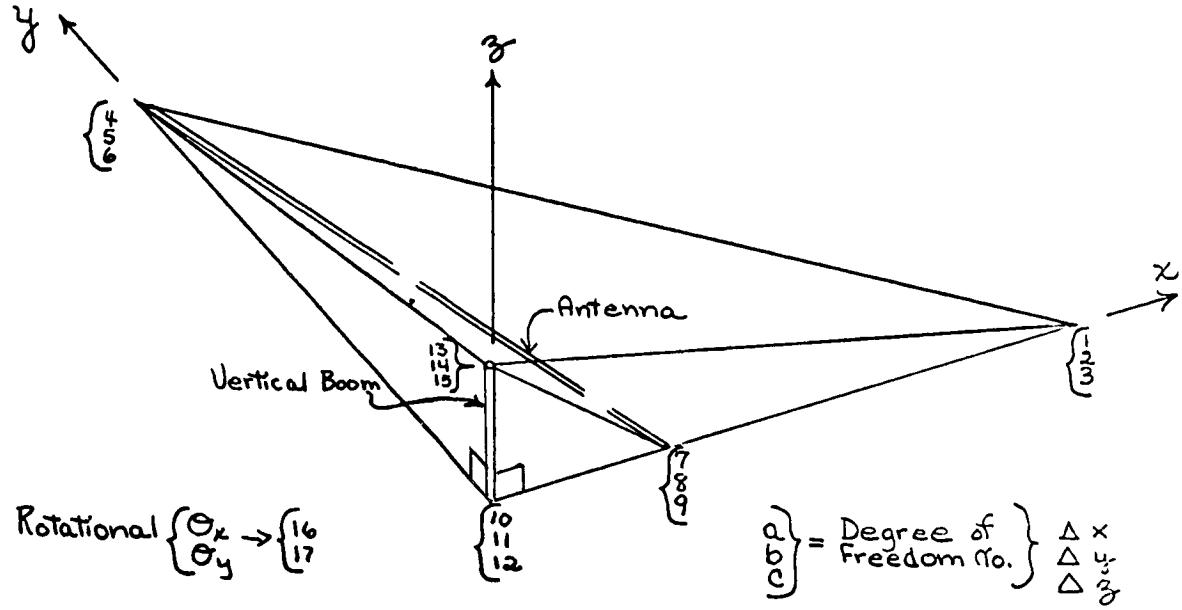

Figure D-2 Simplified KWOT Octant Degrees of Freedom

	1	2	3	4	5	6	7	8	9	10	11	12	13	14	15	16	17
1	4.066411×10^{-3}	$-.716151 \times 10^{-2}$	-7.3319×10^{-2}	$-.716151 \times 10^{-2}$	$-.716151 \times 10^{-2}$	0	$-.01336$	0					$-.0201426$		.00133186		
2		$.716151 \times 10^{-2}$		$.716151 \times 10^{-2}$	$-.716151 \times 10^{-2}$												
3			8.13984×10^{-5}										1.23104×10^{-3}		-8.13984×10^{-5}		
4				8.31182×10^{-3}	-7.1775×10^{-2}		-1.15031×10^{-3}	4.61390×10^{-3}									
5					5.60897×10^{-2}	-1.33186×10^{-3}	4.61368×10^{-3}	-1.85056×10^{-2}			-1.0128×10^{-2}			-2.01426×10^{-2}	1.33186×10^{-3}		
6						8.13984×10^{-5}								1.23104×10^{-3}	-8.13984×10^{-5}		
7							1.32740×10^{-1}	-4.6139×10^{-3}	-1.92913×10^{-2}	-4.1866×10^{2}			-7.63640×10^{-2}		1.92913×10^{-2}		
8								1.85056×10^{2}									
9									4.87354×10^{-3}				1.92918×10^{-2}		-4.87354×10^{-3}		
10										4.1977×10^{-2}			$-.11112 \times 10^{-3}$				-1.33349
11											1.0239×10^{-2}			$-.11112 \times 10^{-3}$		1.33349	
12												6.0475			-6.0475		
13													9.66177×10^{-2}		-2.06231×10^{-2}		1.33349
14														2.02537×10^{-2}	-1.33186×10^{-3}	-1.33349	
15															6.05254		
16																16001.	
17																	16001.

Figure D-3 $[bmh]^T \times [K] \times [bmh]$

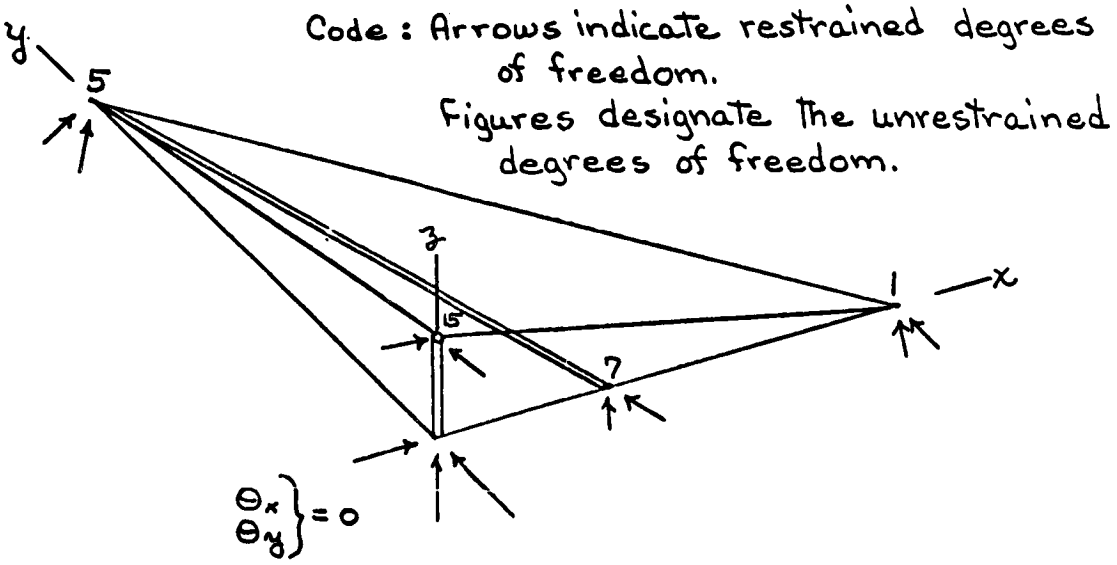

Configuration (a)

Figure D-4 Symmetric About Planes { x-y, y-z, z-x }

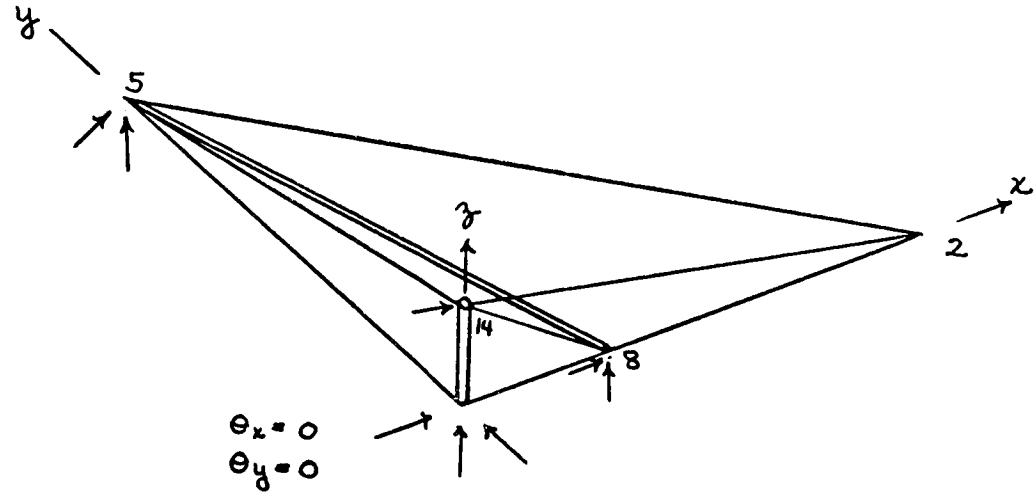

Configuration (b)

Figure D-5 Symmetric About Plane { x-y, y-z }

Antisymmetric About Plane z-x

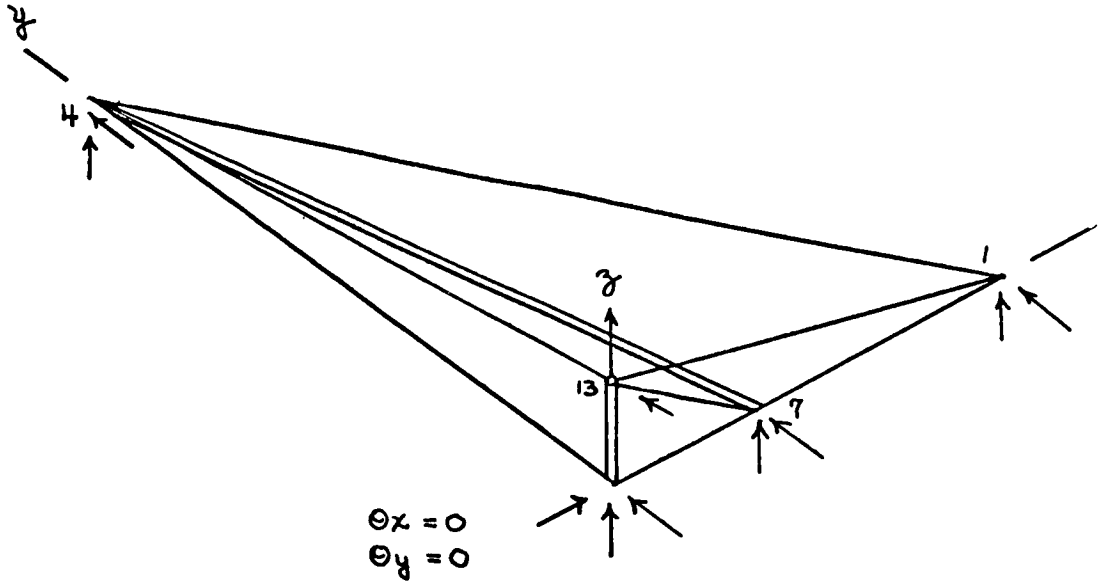

Configuration (c)
Figure D-6 Symmetric About Planes {x-y, z-x}
Antisymmetric About Plane y-z

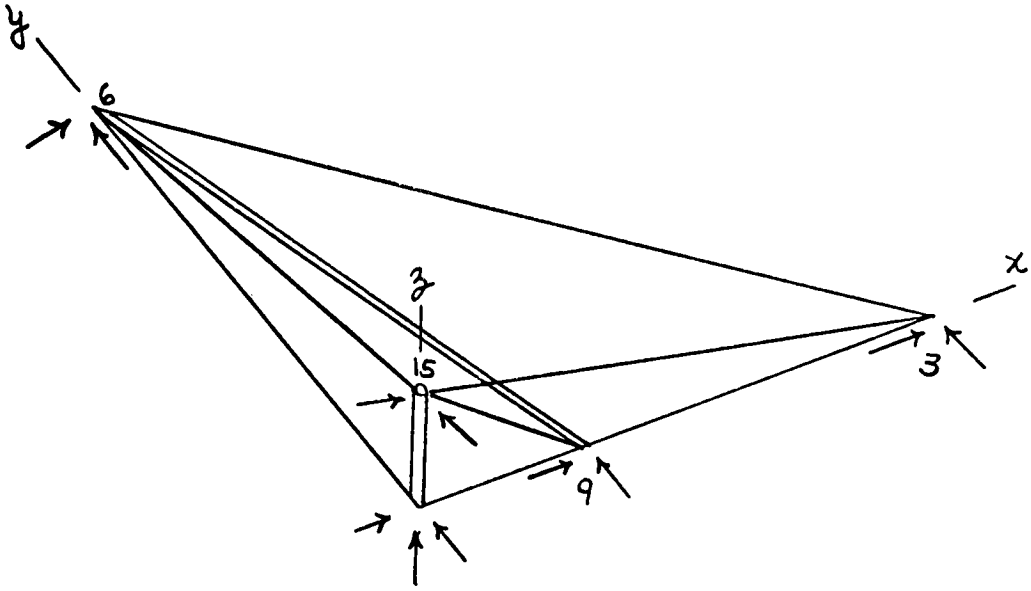

Configuration (d)
Figure D-7 Antisymmetric About Plane x-6
Symmetric About Planes {y-z, z-x}

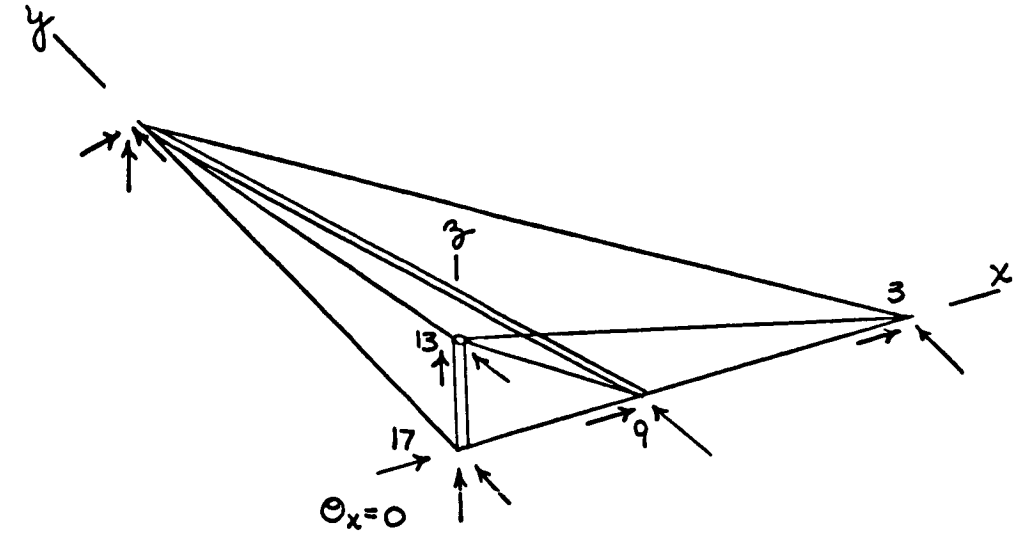

Configuration (e)
Figure D-8 Antisymmetric About Planes {x-y, z-z}
Symmetric About Plane x-z

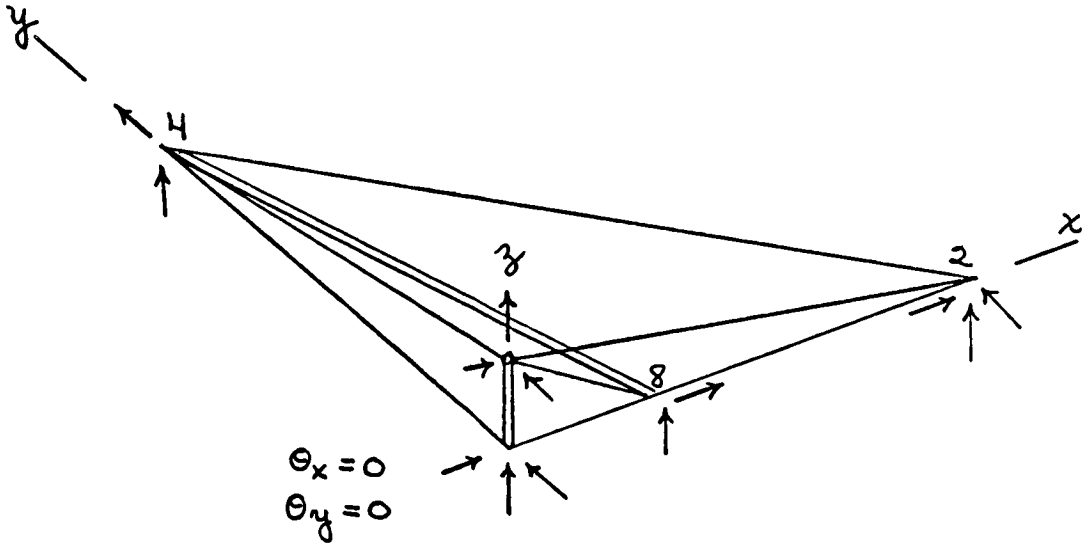

Configuration (f)
Figure D-9 Antisymmetric About Planes {y-z, z-x}
Symmetric About Plane x-y

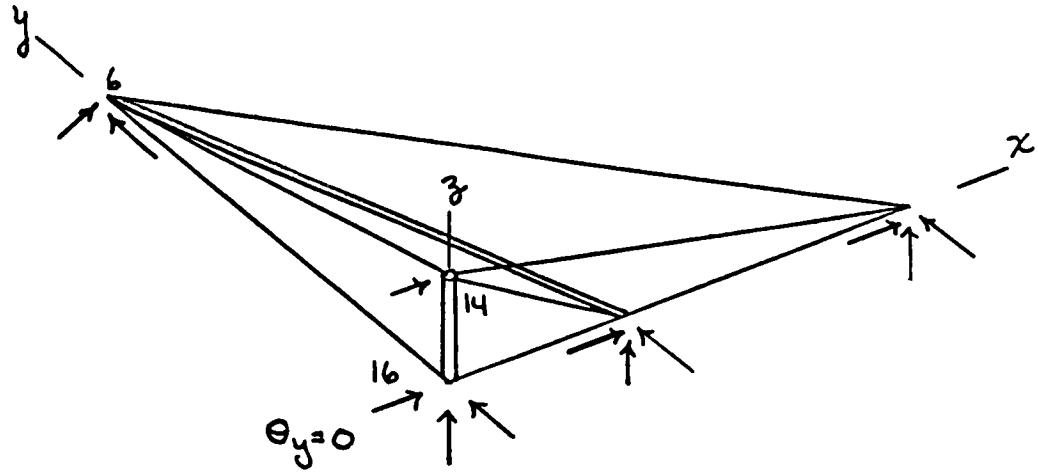

Configuration (g)
Figure D-10 Antisymmetric About Planes {x-y, z-x}
Symmetric About Plane y-z

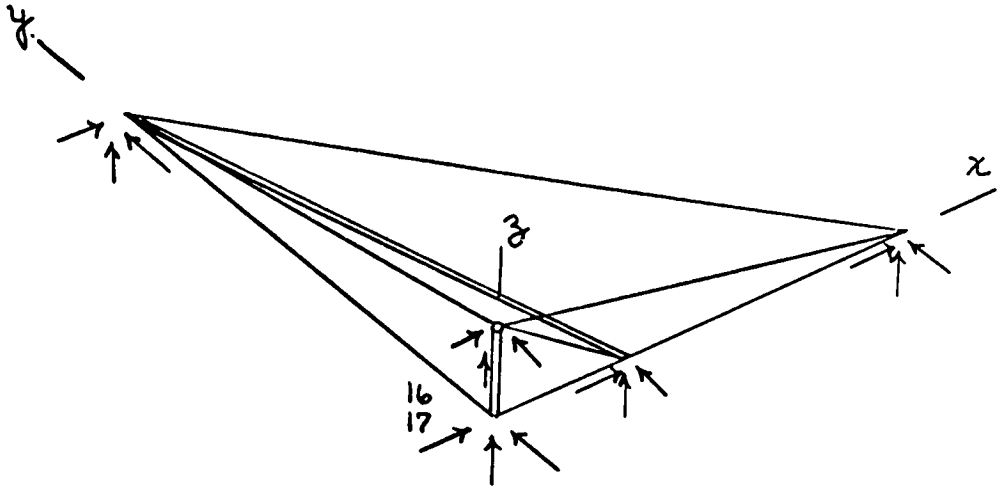

Configuration (h)
Figure D-11 Antisymmetric About Planes {x-y, y-z, z-x}

	1	5	7	15
1	4.066411 ×10-2	7.16151 ×10-3	-1.336 ×10-2	1.33186 ×10-3
5		5.60897 ×10-2	4.61368 ×10-3	1.33186 ×10-3
7			1.32740 ×10-1	1.92913 ×10-2
15				6.05254

Figure D-12 K Matrix of Configuration (a)

	2	5	8	14
2	7.16151 ×10-3	-7.16151 ×10-3	0	0
5		5.60897 ×10-2	-1.85056 X 10-2	-2.01426 ×10-2
8			-1.85056 X 10-2	0
14				2.02537 ×10-2

Figure D-13 K Matrix of Configuration (b)

	1	4	7	13
1	4.066411 ×10-2	-7.16151 ×10-3	-1.336 ×10-2	-2.01426 ×10-2
4		8.31182 ×10-3	-1.15031 ×10-3	0
7			1.32740 ×10-1	-7.63640 ×10-2
13				9.66177 ×10-2

Figure D-14 K Matrix of Configuration (c)

	3	6	9	15
3	8.13984 .10-5	0	0	-8.13984 .10-5
6		8.13984 .10-5	0	-8.13984 .10-5
9			4.87354 .10-3	-4.87354 .10-3
15				6.05254

Figure D-15 K Matrix of Configuration (d)

	3	9	13	17
3	8.13984 .10-5	0	1.23104 .10-3	0
9		4.87354 .10-3	1.92918 .10-2	0
13			9.66177 .10-2	1.33349
17				16001.0

Figure D-16 K Matrix of Configuration (e)

	2	4	8
2	7.16151 .10-3	7.16151 .10-3	0
4		8.31182 .10-3	4.61390 .10-3
8			0

Figure D-17 K Matrix of Configuration (f)

	6	14	16
6	$8.13984 \cdot 10^{-5}$	$1.23104 \cdot 10^{-3}$	0
14		$2.02537 \cdot 10^{-2}$	-1.33349
16			16001.0

Figure D-18 K Matrix of Configuration (g)

	16	17
16	16001.0	0
17		16001.0

Figure D-19 K Matrix of Configuration (h)

APPENDIX G

INCREMENTAL THRUST BURSTS FOR PRECESSING THE KWOT SCAN PLANE

When KWOT is operating in a spin-scanning mode, the spin plane can be changed either continuously, or in increments, in order to cover the entire sky. This paper discusses a method of accomplishing the change of plane incrementally, in steps of one or two degrees. It will be shown that the orientation of the plane can be changed by one increment in a time interval that is only slightly longer than one-quarter revolution.

An evaluation is made of the fuel required to scan the sky by incremental changes in plane, and it is shown that the expenditure of about 1.5 lbs. of fuel is typical for a 100 lb. sub-satellite.

Description of the Method

To change the plane of rotation by an angle $\Delta\phi$, it is necessary to change the direction of the velocity vector of each sub-satellite as it crosses the line of intersection of the old plane with the new plane. If the correct thrust burst is applied to a sub-satellite at this time, it will then be moving in the new plane, and should need no further correction. Since the four sub-satellites are spaced at 90° angles around the center, two of them will cross this line of intersection at the same time, and the other two will cross it one quarter revolution later.

This sequence of events is illustrated in Figure 1. Figure 1A shows the structure still rotating in its original plane, which is indicated by the broken line. Sub-satellites A and C are just crossing the line of intersection, and a burst of thrust is being applied to each to alter its direction. In Figure 1B, sub-satellites A and C have proceeded along the new path, indicated by the solid line. C and D are still on the old path. Note, however, that A, B, C, and D are still contained in a plane, and their relative positions are little disturbed, so the dimensions of the structure are preserved, and the beam should not seriously deteriorate. In Figure 4C, B and D have arrived at the line of intersection, and thrust is being applied to them to put them in the new plane. In Figure 4D, all four sub-satellites are now moving in the new plane.

Total Thrust Required for Scanning

The change of velocity, ΔV, required to change the motion of a sub-satellite from one plane to another which is inclined to the first by an angle $\Delta\phi$ is (for small $\Delta\phi$):

$$\Delta V = V \sin \Delta\phi,$$

where ΔV is the magnitude of the velocity change, V is the magnitude of the velocity, and $\Delta\phi$ is the dihedral angle between the old plane and the new plane. For a sub-satellite revolving at a radius of 5 km in a structure rotating at one revolution per hour, $V = 10\pi$ km/hr = 31.42 km/hr, = 0.873×10^3 cm/sec and

ΔV for a $\Delta\phi$ of 1° is

$$\Delta V\ (1°) = V \sin \Delta\phi = 1.52 \times 10 \text{ cm/sec.}$$

If 180 such changes in plane are executed, the KWOT beam will have scanned the entire sky with a maximum separation between adjacent scans of 1°. The total impulse required of each sub-satellite to make 180 incremental changes of plane of 1° each is

$$\Delta V = 180\ \Delta V\ (1°) = 2.74 \times 10^3 \text{ cm/sec.}$$

An approximate equation for the velocity change which can be accomplished by a given expenditure of fuel is:

$$\Delta V = gI_{sp} \ln \frac{m_i}{m_f} \quad ,$$

where ΔV is the total change of velocity, g is the acceleration of gravity at the surface of the earth, expressed in the same unit of length that is used to express ΔV, and the same unit of time as is used for ΔV and I_{sp}. The parameter I_{sp} is the "specific impulse" associated with the fuel system, expressed in time units, m_i is the initial mass of the vehicle, including fuel, and m_f is the final mass. It is assumed that $m_i - m_f$ is the mass of fuel expended. (gI_{sp} is approximately equal to the exhaust velocity.)

From this equation:

$$\ln \frac{m_i}{m_f} = \frac{\Delta V}{gI_{sp}} \quad .$$

If we use the figure derived above for ΔV, and assume I_{sp} is 200 sec., we have

$$\ln \frac{m_i}{m_f} = \frac{2.74 \times 10^3 \text{ cm/sec}}{980 \times 200} = 1.395 \times 10^{-2}$$

$$\frac{m_i}{m_f} = 1.014$$

If, therefore, the initial mass of the sub-satellite is 100 lbs., only about 1.5 lbs. of fuel need to be expended to incrementally precess the structure by 180°, and scan the entire sky.

FIGURE 1

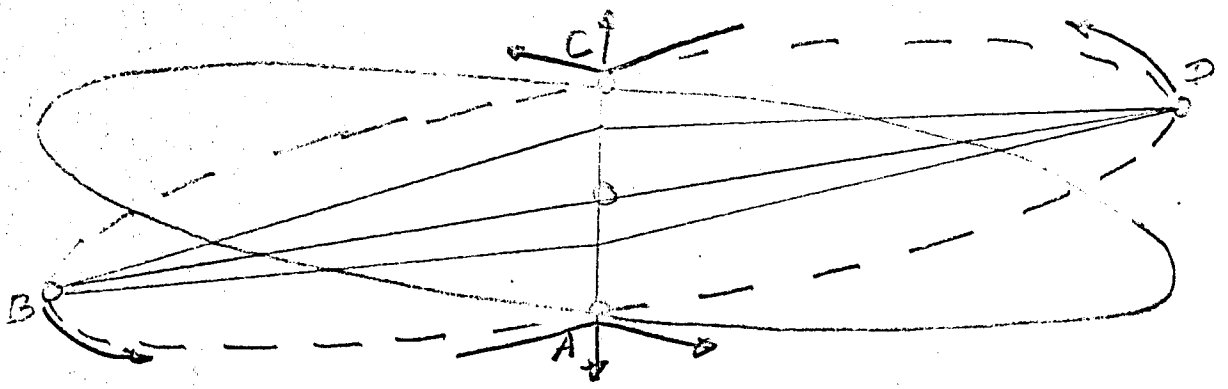

Figure 1A

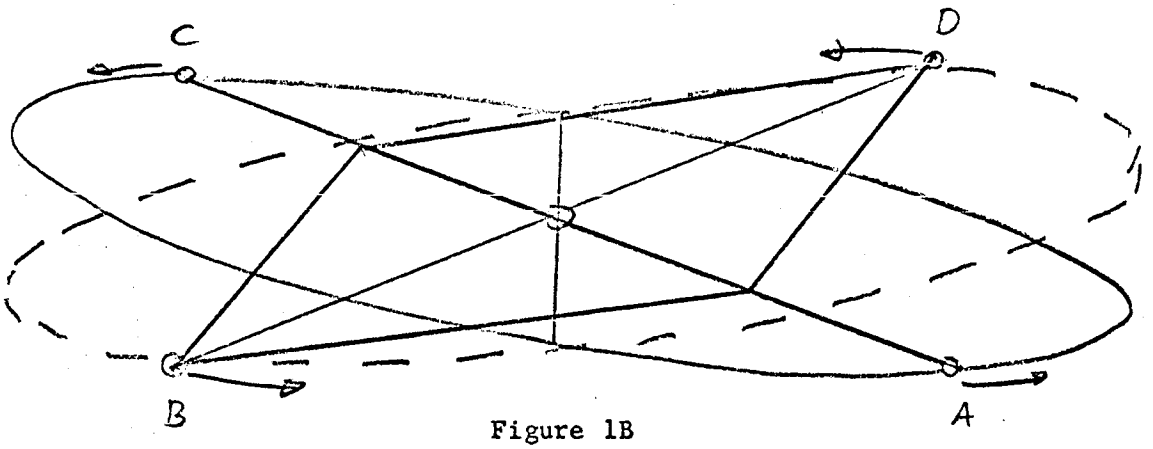

Figure 1B

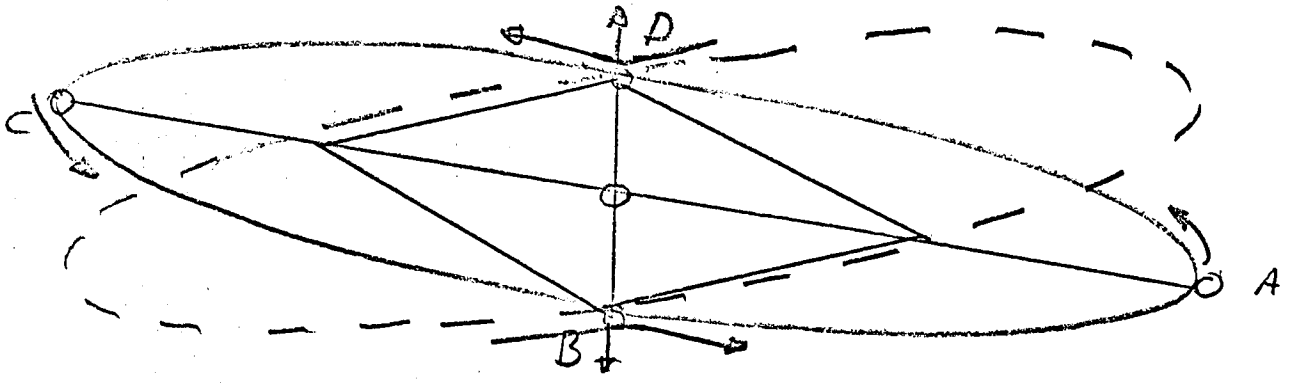

Figure 1C

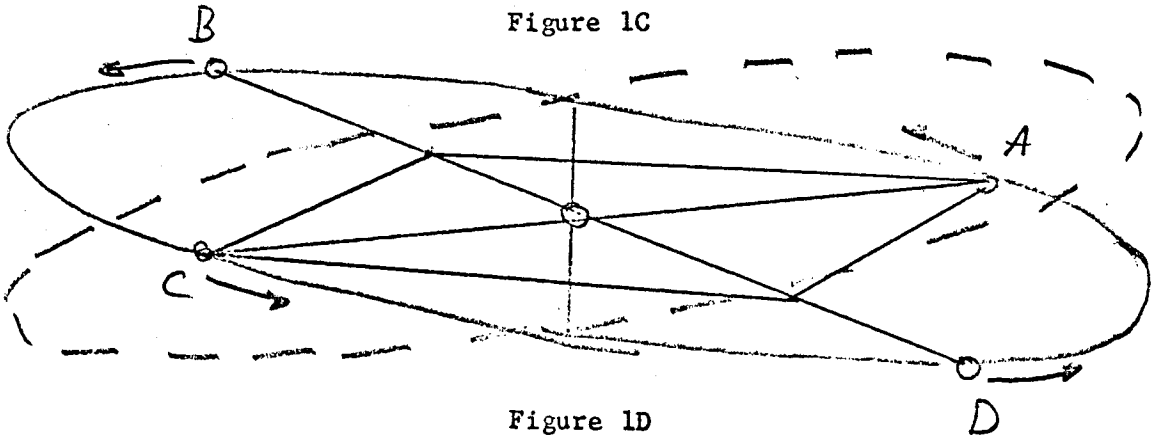

Figure 1D

APPENDIX H

OUT OF PLANE PERTURBATION OF RHOMBIC ANTENNA

Let us consider the perfectly conducting rhombic antenna subjected to an out of plane displacement. This perturbation is accomplished by displacing the vertex of legs 2 and 3 along a circular arc in the x-z plane, centered at the intersection of the minor and major axes of the rhombic. The degree of the perturbation is specified by the angle θ_o which the circular arc subtends. Legs 2 and 3 are then raised out of the x-y plane as if they were hinged along the minor axis, while legs 1 and 4 retain their original position. The resultant configuration is shown in Figure 1.

Since the final rhombic configration is relatively simple, it is not difficult to obtain the resultant far field pattern by a direct integration of the unperturbed current over the displaced structure. This approach implies that the current distribution is not greatly altered by the out of plane displacement. We may also obtain the pattern by using the perturbation procedure described elsewhere in this report, and if the same assumption concerning the alteration of the current distribution is made the results from this approach are in excellent agreement with those of the preceeding method for $\theta_o < 1$. Since, at this time, we do not have any numerical results pertaining to the equilibrium current distribution on the rhombic it was felt that the usual assumption of the current being comprised of uniform traveling waves would allow reasonable estimates of the resultant power pattern of the perturbed structure.

The computed results which follow were obtained from the direct calculation. They present suitable normalized radiation patterns plotted against the spherical coordinate angles θ and ϕ, for various values of θ_o. The antenna considered is comprised of 17 wavelength long legs with a half-vertex angle of 13.3°.

Figure 2 indicates the manner in which the E-plane radiation pattern of the rhombic is disturbed by the out of plane displacement. Calculations showed that for θ equal to 0.1° and 1°, the departure from the unperturbed

pattern was negligible. It is seen from Figure 2 that an out of plane perturbation of 5° which corresponds to the rhombic vertex being displaced 1.45 wavelengths above the x-y plane, leaves the beamwidth virtually unchanged at 6°, while the major sidelobe increases slightly from -8.94 db to -8.41 db, and the maximum value at $\phi = 0°$ decreases by slightly less than 10%.

Figure 3 displays the variation in the H-plane radiation pattern for out of plane displacements of $\theta = 1°$ and 5°. When $\theta_o = 0.1°$ the departure from the unperturbed pattern is negligible. We see that at $\theta = 1.0°$, the major sidelobes have decreased slightly, the beamwidth has remained unchanged at 15° and the maximum value of the radiation pattern has decreased by less than 1/2% and displays a negligible shift (possibly 1/2°). At $\theta_o = 5.0°$, the beamwidth has remained the same. There is a slight upward shift of 2.5° of the main beam and the sidelobe level has decreased to -15.6 db. These results are summarized below.

θ_o	Vertical Displacement of Vertex	Beamwidth	Max. Value	Maximum Sidelobe Level
0°	0	6°	1.000	-8.84 db
0.1°	.0289λ	6°	1.000	-8.84 db
1.0°	.2888λ	6°	1.000	-8.84 db
5.0°	1.447λ	6°	0.905	-8.41 db

Table I

E-Plane Radiation Pattern Variation

θ_o	Vertical Displacement of Vertex	Beamwidth	Max. Value	Beamshift	Maximum Sidelobe Level
0°	0	15°	1.000	0	-10 db
0.1	0.0289λ	15°	1.000	~ 0°	-10.0 db
1.0°	0.2888λ	15°	0.995	0°-0.5°	-10.4 db
5.0°	1.447λ	15°	0.955	2.5°	-15.6 db

Table II

H-Plane Radiation Pattern Variation

Conclusions:

The results of this study have shown that the out of plane displacement of the rhombic illustrated in Figure 1, produces no adverse changes in the E-plane and H-plane radiation patterns as far as beamwidth and sidelobe levels are concerned. In the case of the 5° perturbation there is a very slight loss of gain in the E-plane pattern. The H-plane pattern is affected only by a canting of the main lobe equal to about one-half the angular displacement. This is equivalent to introducing a deterministic phase error or a random phase error with non-zero mean in the case of the synthetic array. It was shown in this case, however, that the beamwidth was greatly increased and the gain was severely decreased by the introduction of a random phase error with a maximum variance of 180°.

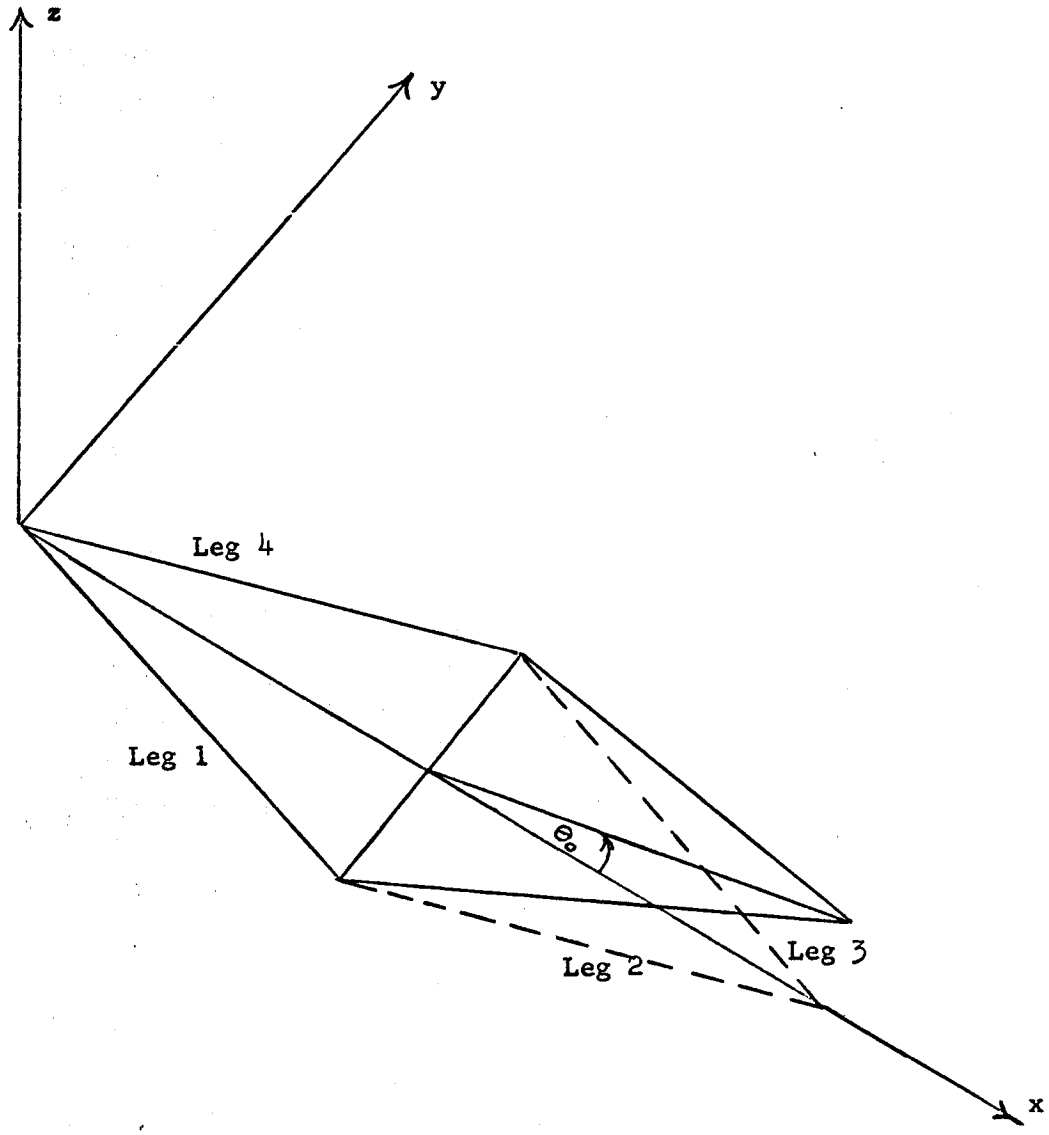

Figure 1. Rhombic Displaced Out of Plane

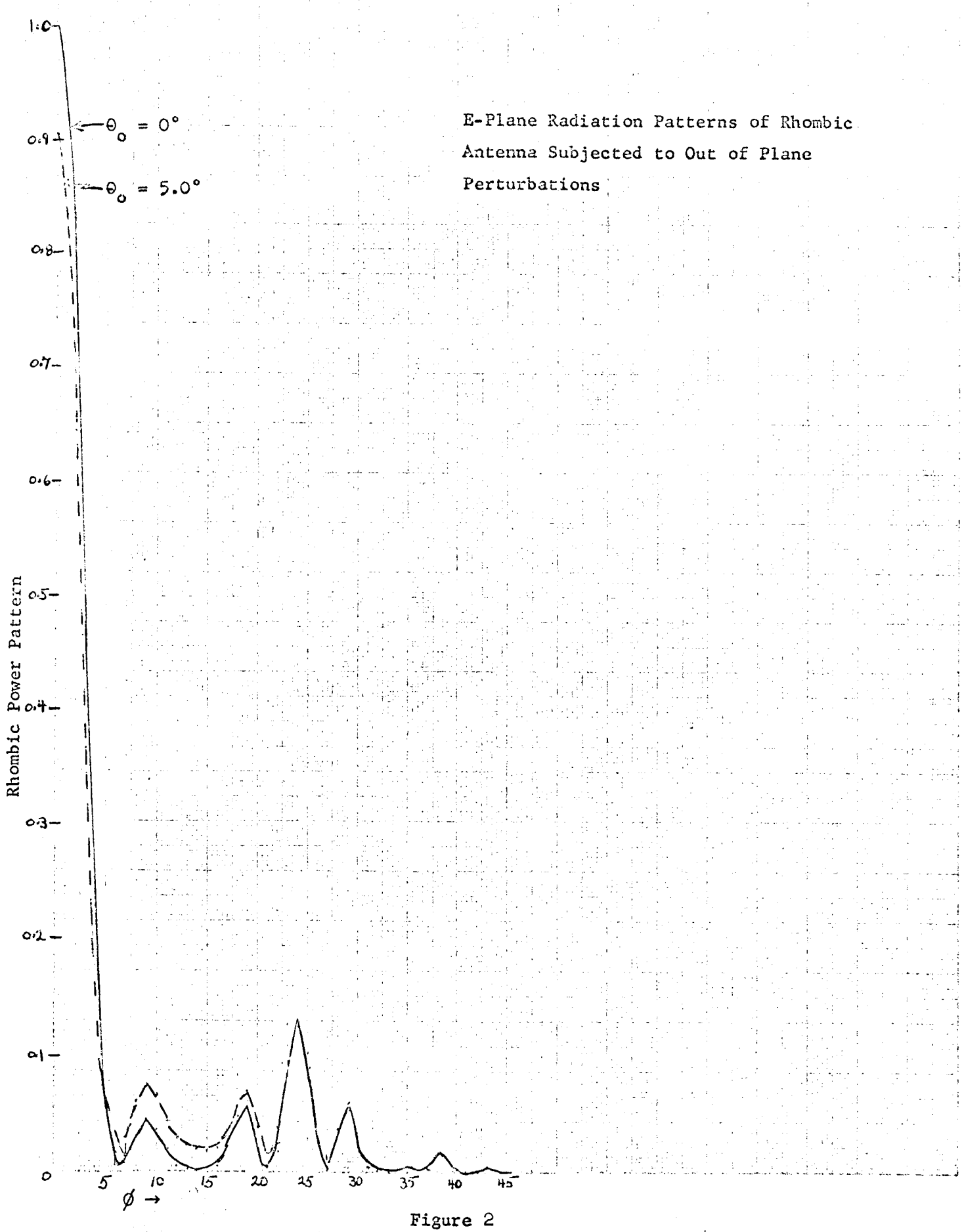
E-Plane Radiation Patterns of Rhombic Antenna Subjected to Out of Plane Perturbations
$\theta_o = 0°$
$\theta_o = 5.0°$
Rhombic Power Pattern
1.0
0.9
0.8
0.7
0.6
0.5
0.4
0.3
0.2
0.1
0
5
10
15
20
25
30
35
40
45
$\phi \rightarrow$

Figure 2

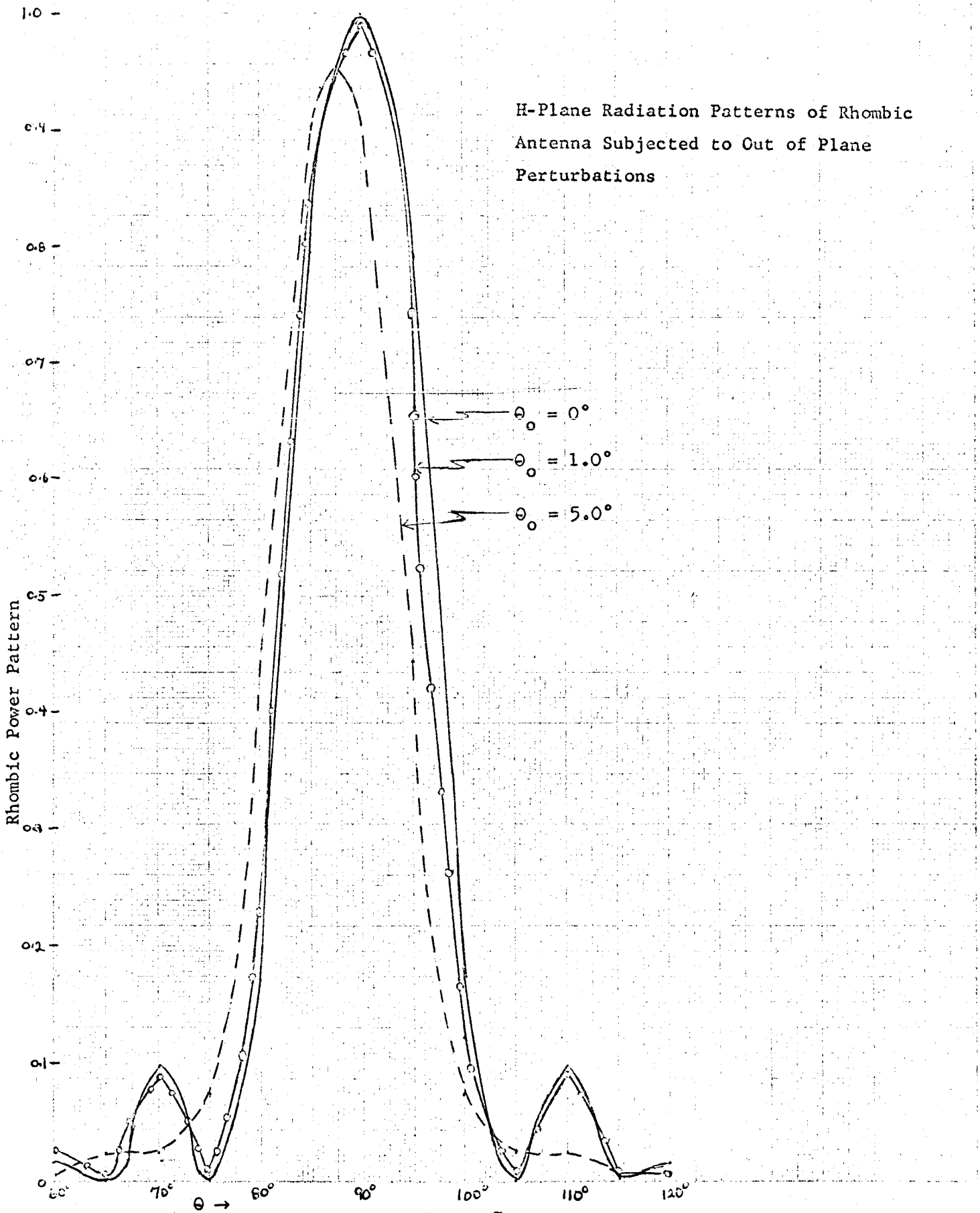
H-Plane Radiation Patterns of Rhombic Antenna Subjected to Out of Plane Perturbations
$\Theta_o = 0°$
$\Theta_o = 1.0°$
$\Theta_o = 5.0°$
Rhombic Power Pattern
1.0
0.9
0.8
0.7
0.6
0.5
0.4
0.3
0.2
0.1
0
70°
80°
90°
100°
110°
120°
Θ →

Figure 3

APPENDIX I

THE GENERAL RHOMBIC ANTENNA

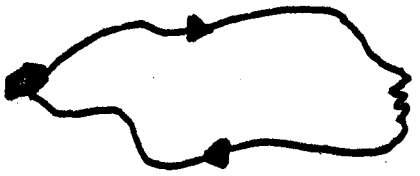

General rhombic
Figure 1

We wish to consider what can be called a general rhombic antenna, which consists of two wires connecting the transmitter or receiver and a terminating resistance which is chosen to eliminate a reflected current. We will think of it as a transmitting antenna since reciprocity enables us to obtain the performance of a receiving antenna. We will assume that the currents in the wires are travelling waves of constant amplitude, specifically that

$$\vec{J}_1 = \hat{s}e^{iks}$$

$$\vec{J}_2 = -\hat{s}e^{iks}$$

where s is the distance from the transmitter measured along the wire, $\hat{s}$ is the unit vector along the wire in the direction of increasing s, $k = \frac{2\pi}{\lambda}$, and λ is the wavelength.

The radiated field is proportional to $\vec{E}_1 - \vec{E}_2$ where

$$\vec{E}_n \equiv \int_{\text{wire } n}^{L} \left[\hat{s} - (\hat{s}\cdot\hat{r})\hat{r}\right] e^{ik\left(s - \int_0^s \hat{s}\cdot\hat{r}\, dt\right)} ds$$

Here L is the length of each of the wires and $\hat{r}$ is the unit vector pointing towards the field point. Assuming that the terminating resistance lies a distance D in the direction given by the unit vector $\hat{r}_0$ from the transmitter, we have that

$$\int_0^L \hat{s}\, ds = D\hat{r}_0$$

for both of the wires.

In order to see the nature of the integrals for the field it is usual to introduce the integral

$$\vec{E}(z) = \int_0^z \left[\hat{s}-(\hat{s}\cdot\hat{r})\hat{r}\right] e^{ik\left(s-\int_0^s \hat{s}\cdot\hat{r}\, dt\right)} ds$$

and study what happens as z increases from 0 to L.

Now we would like to have the main beam along the axis, that is in the direction $\hat{r}_o$. In figures 2-8 we show E(z) for an ordinary rhombic for $L=30\lambda$ and for various values of L-D for the direction $\hat{r} = \hat{r}_o$ (for $\hat{r} = \hat{r}_o$, $\vec{E}(z)$ is in the direction in the plane of the rhombic perpendicular to $\hat{r}_o$ so that we can forget about its vector character for these figures, and $\vec{E}_1 = -\vec{E}_2$ so that we need consider only one integral). The figures show the shape of the rhombic, and then a trace of E(z) is the complex plane as z goes from 0 to L.

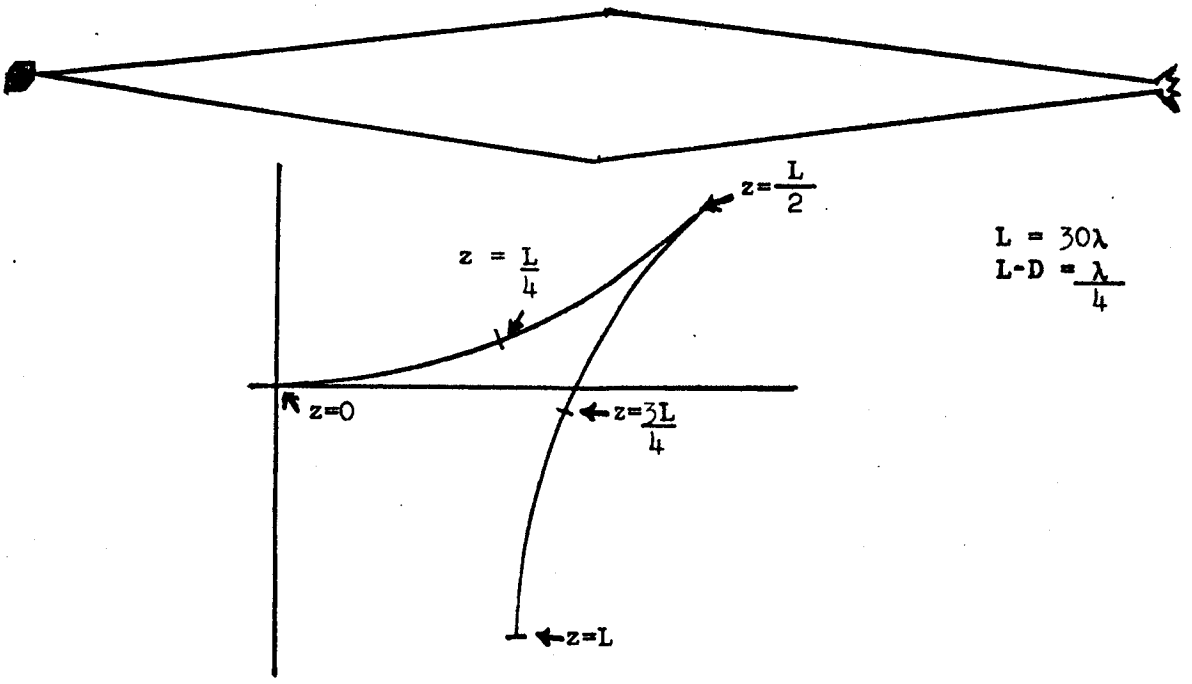

Figure 2

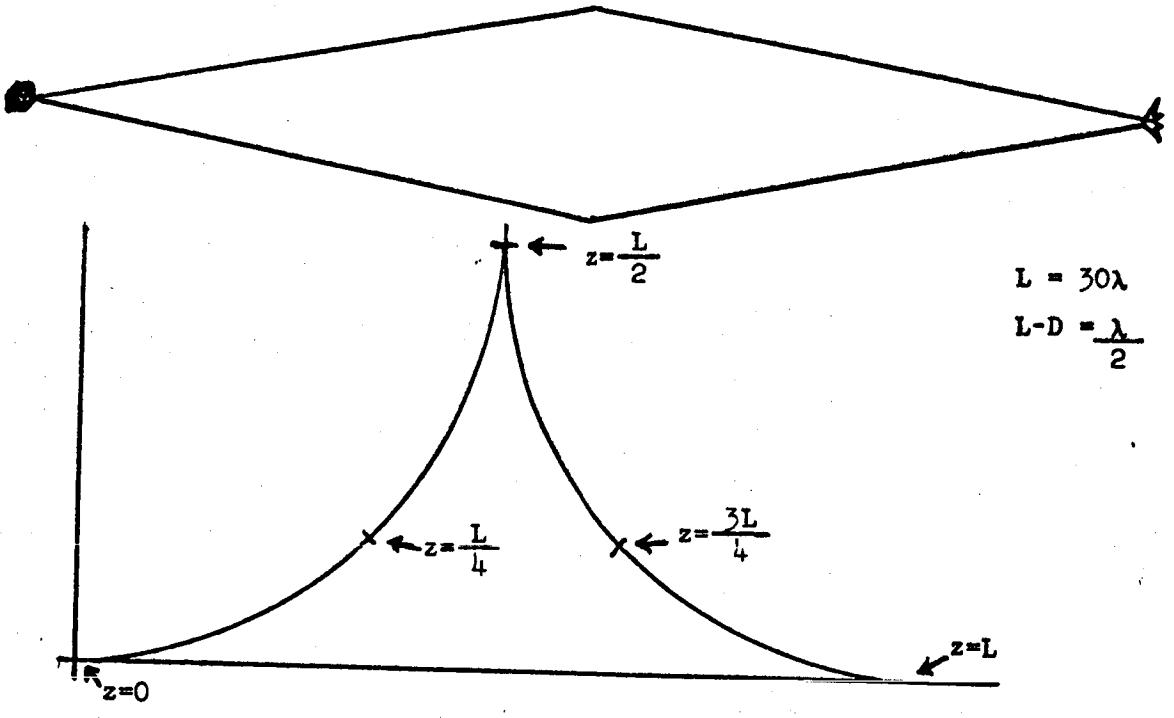

Figure 3

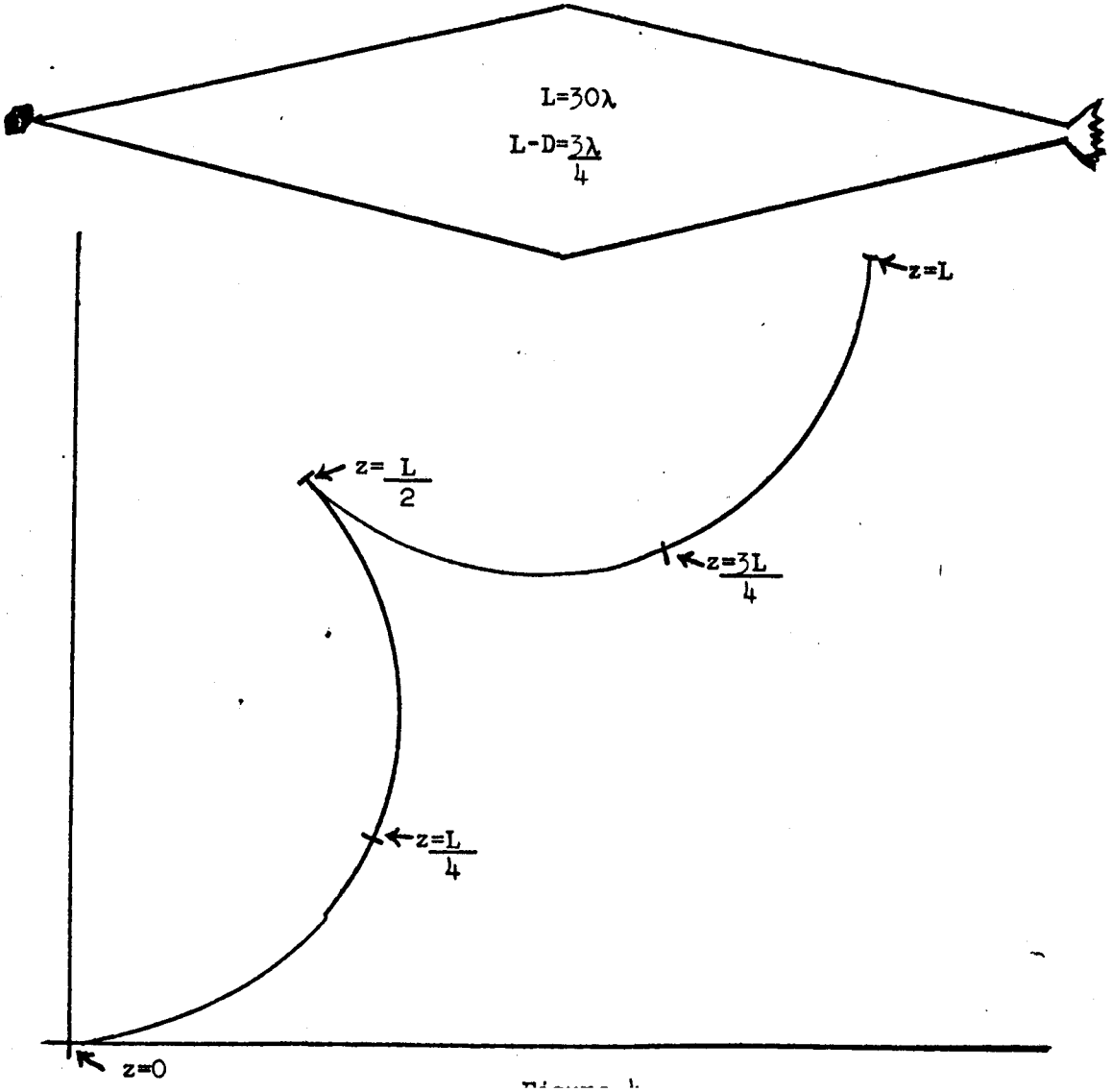

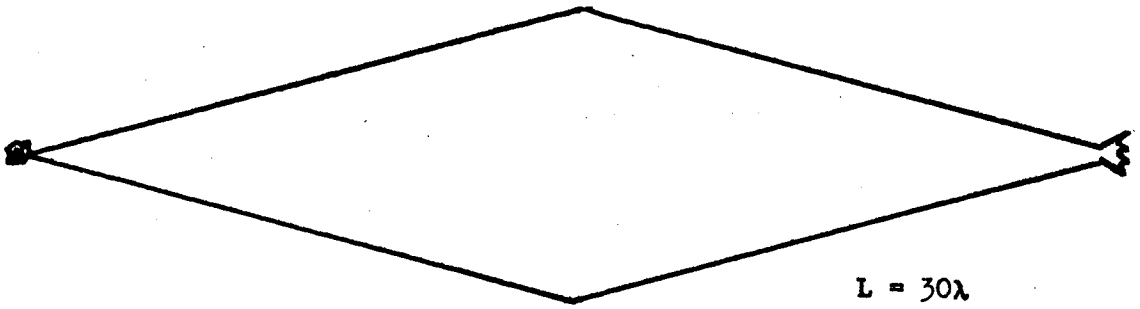

$L = 30\lambda$

$L\text{-}D = \lambda$

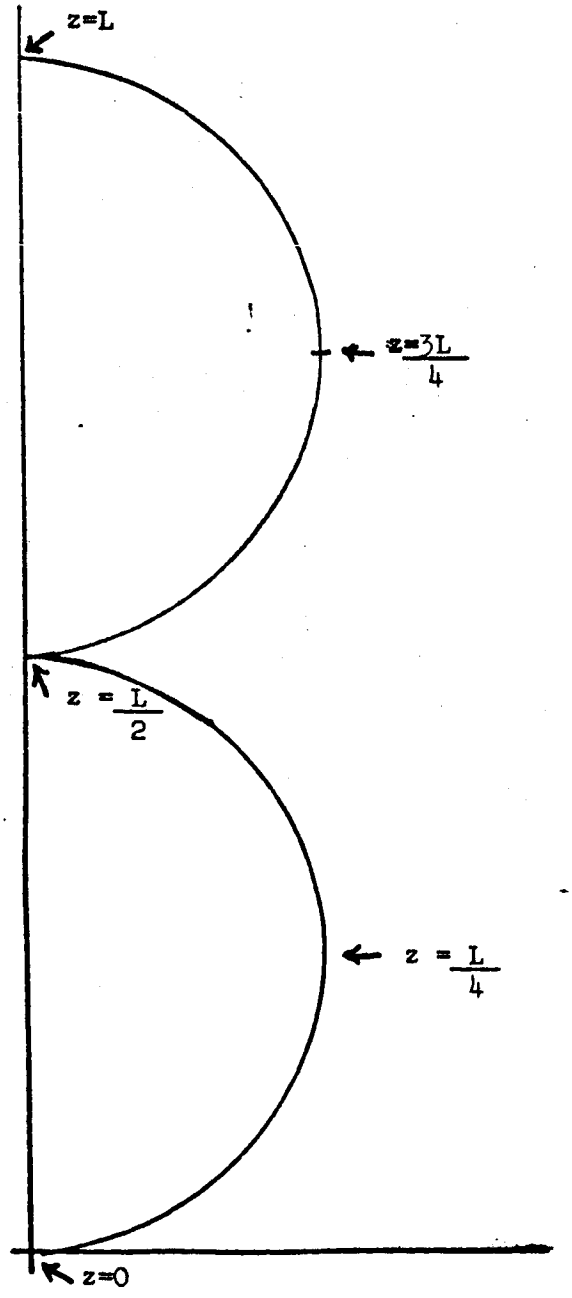

Figure 5

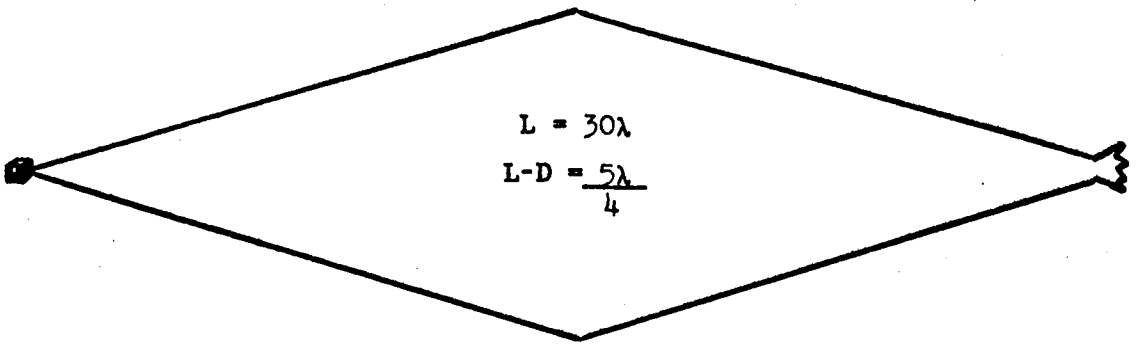

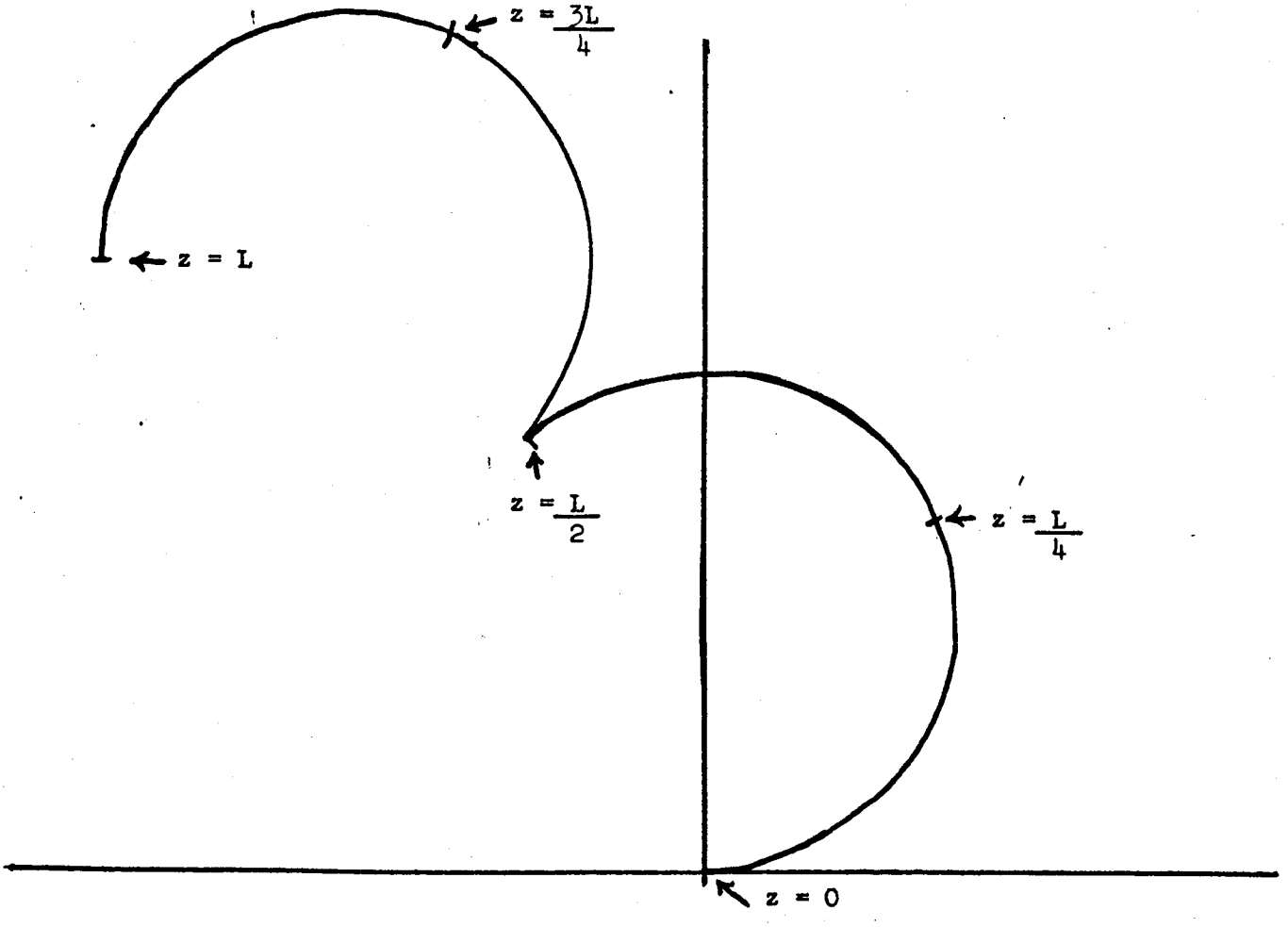

Figure 6

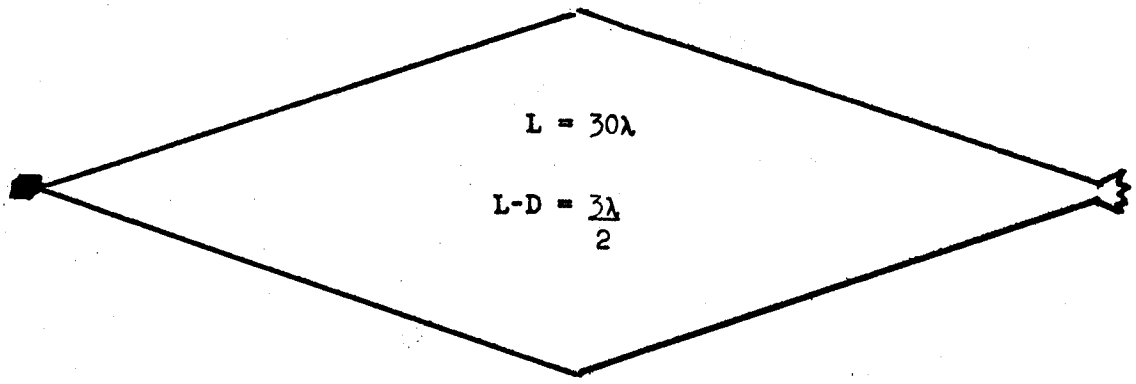

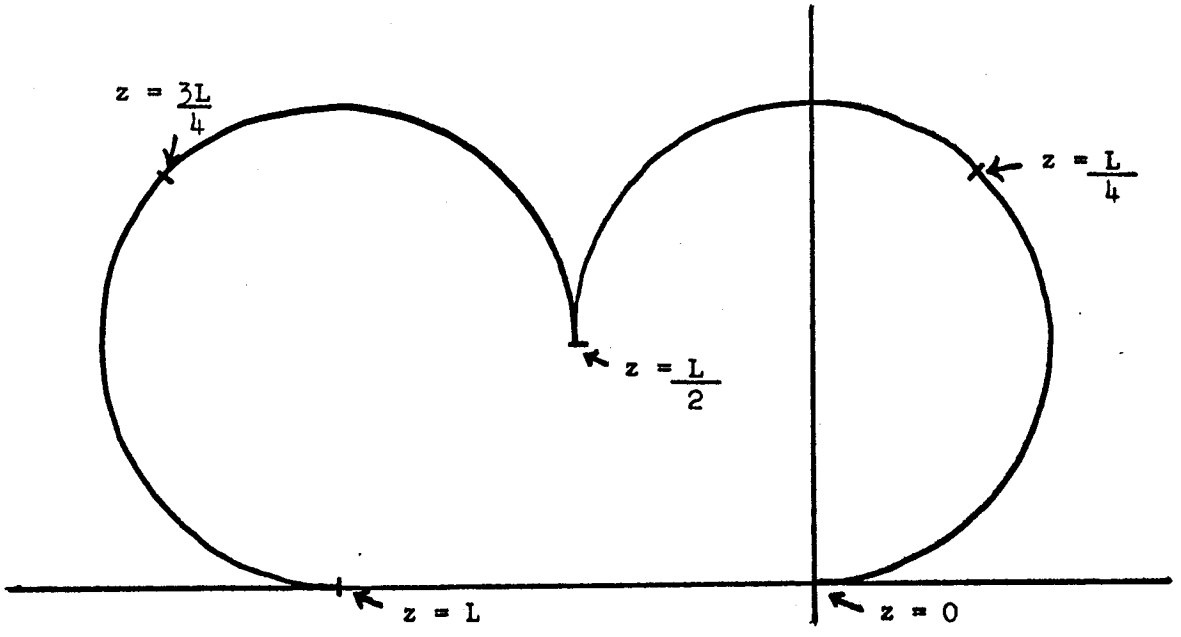

Figure 7

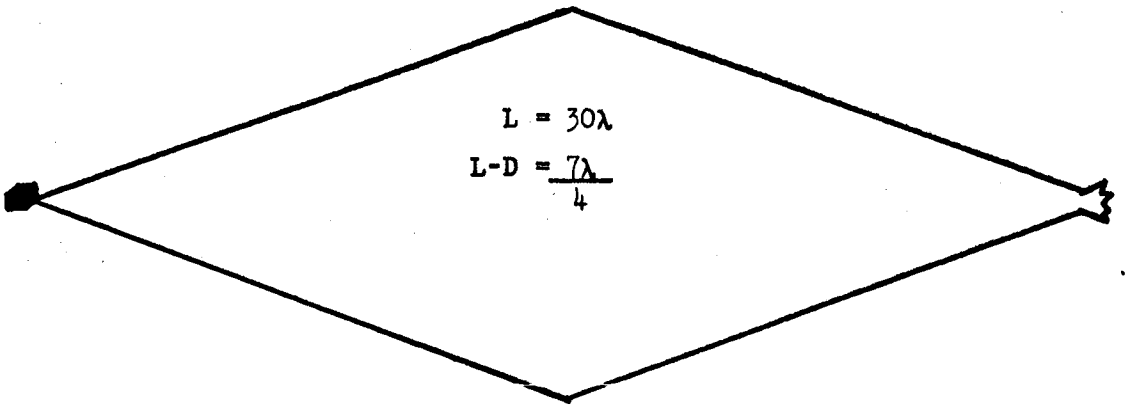

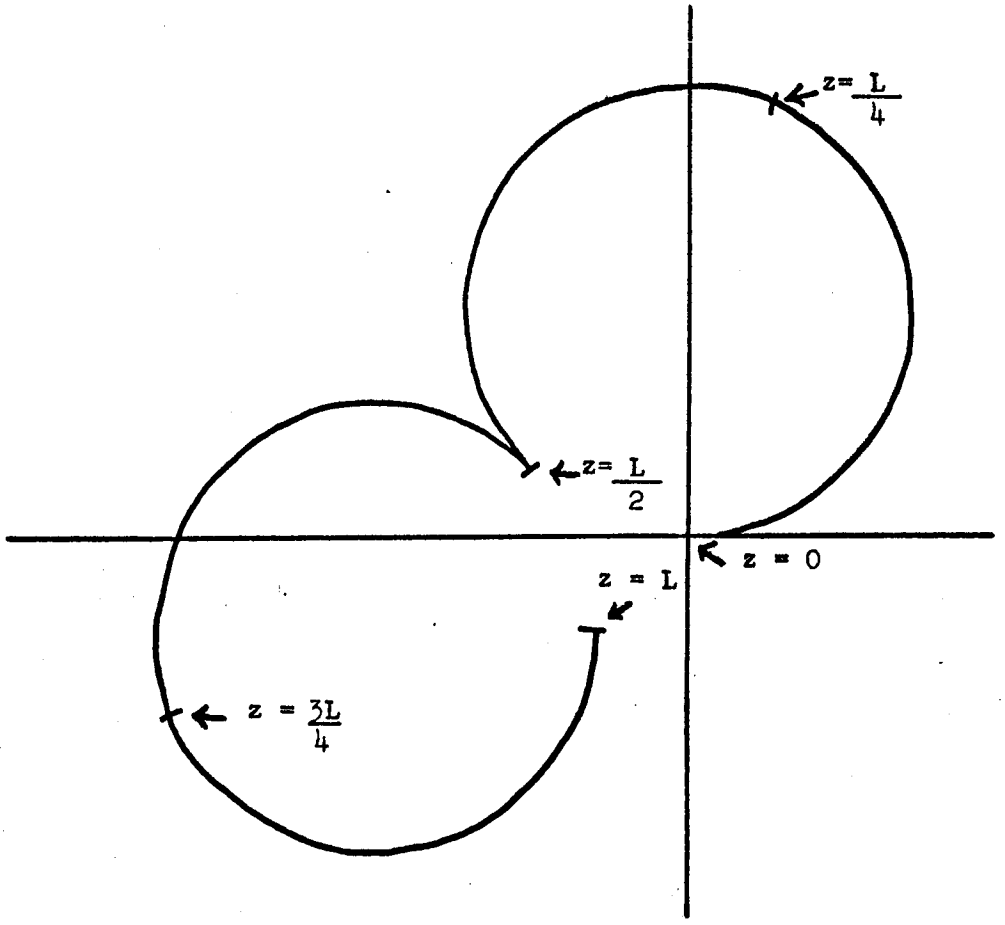

Figure 8

In figure 9 we show the variation of $|E(L)|$ with L-D for the cases plotted above.

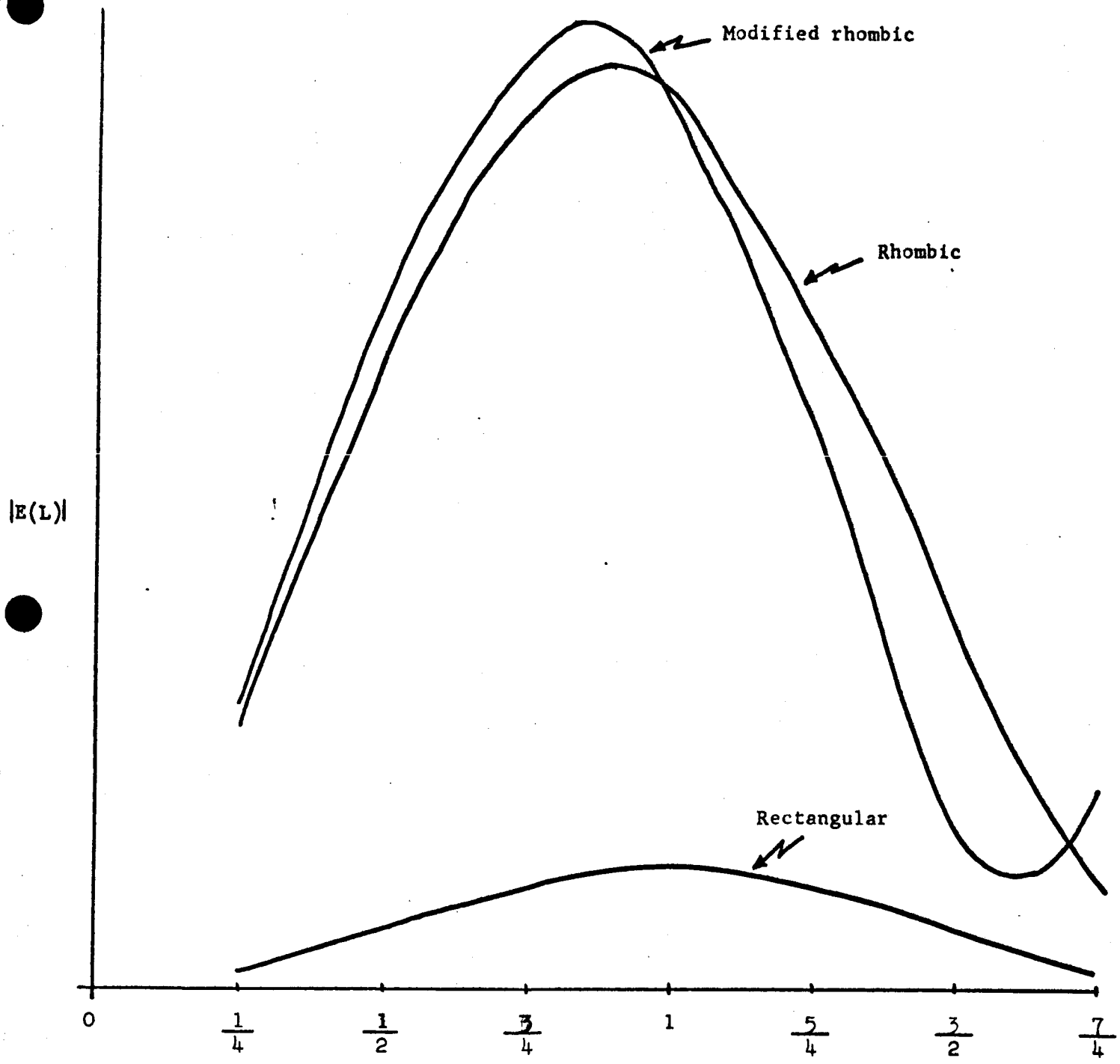
Modified rhombic
Rhombic
Rectangular
|E(L)|
0
1/4
1/2
3/4
1
5/4
3/2
7/4
L-D/λ

Figure 9

Figures 10-16 correspond to figures 2-8 except that the rhombic has been distorted to a rectangular shape.

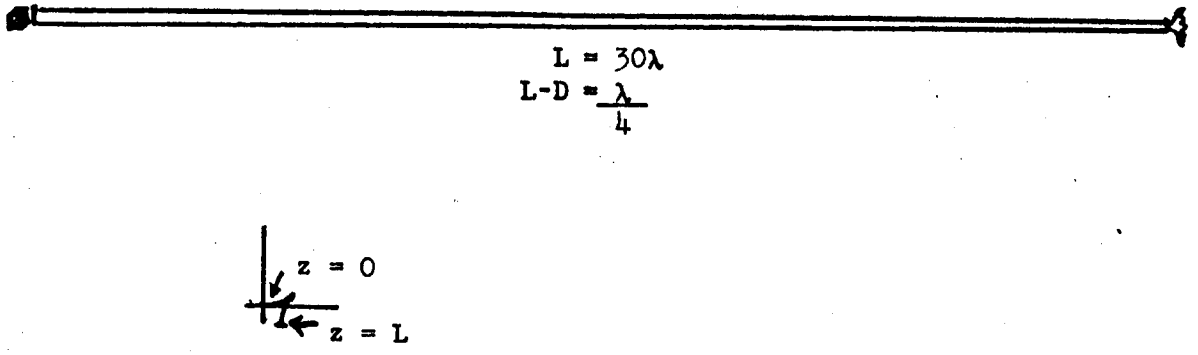

Figure 10

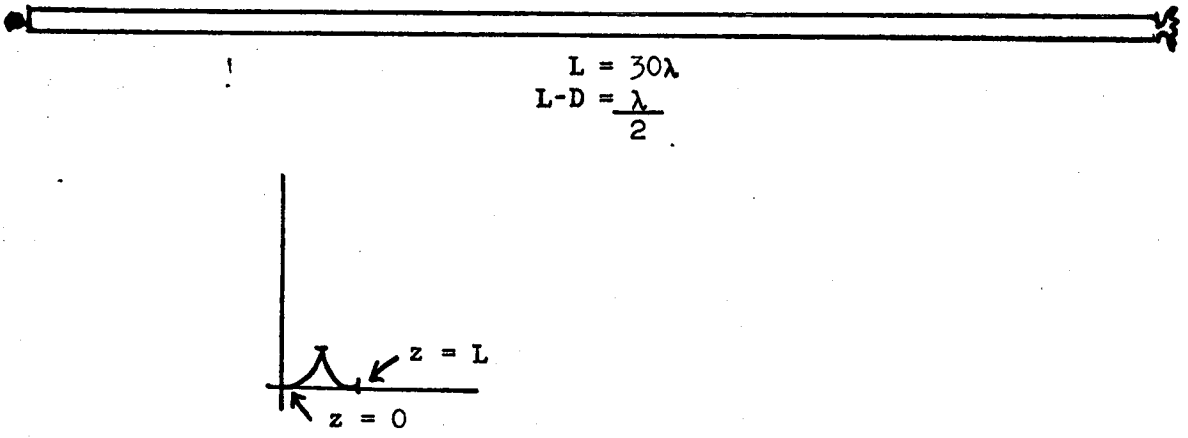

Figure 11

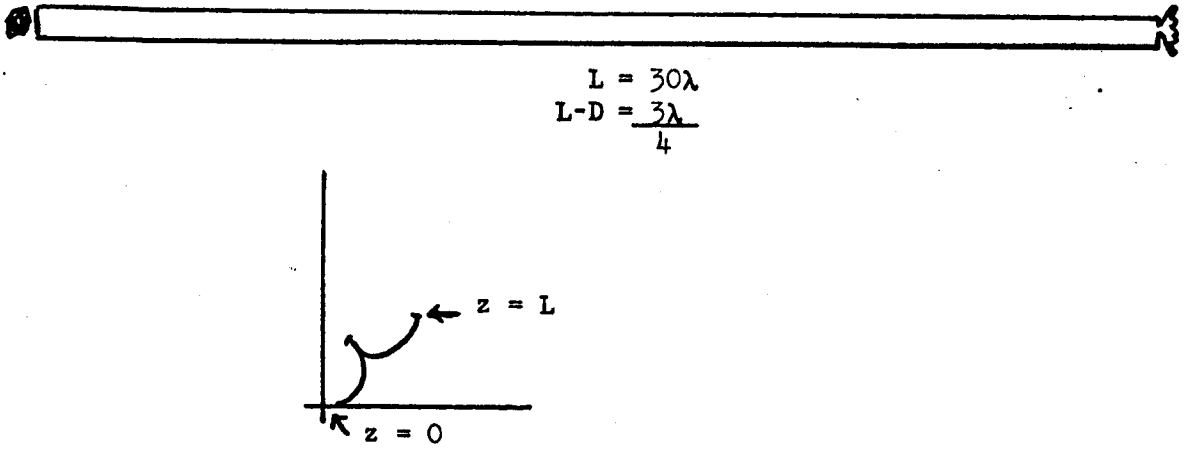

Figure 12

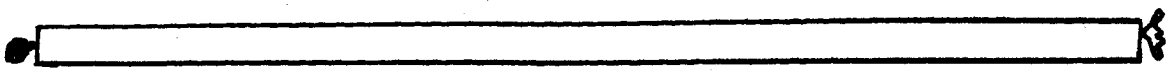

$L = 30\lambda$
$L\text{-}D = \lambda$

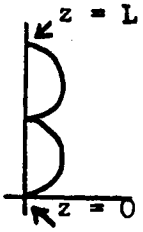

Figure 13

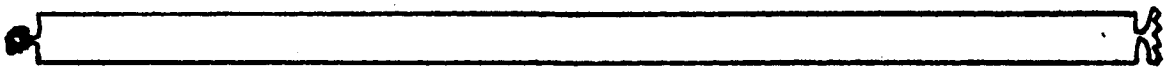

$L = 30\lambda$
$L\text{-}D = \frac{5}{4}\lambda$

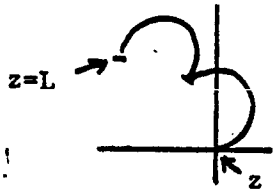

Figure 14

$L = 30\lambda$
$L\text{-}D = \frac{3\lambda}{2}$

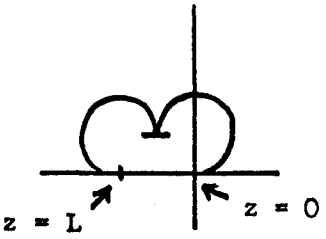

Figure 15

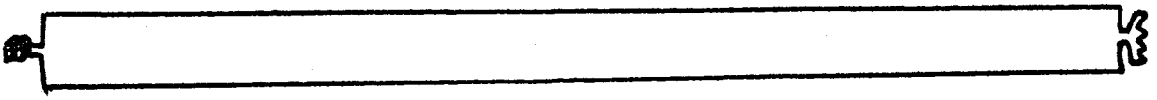

$L = 30\lambda$
$L\text{-}D = \frac{7\lambda}{4}$

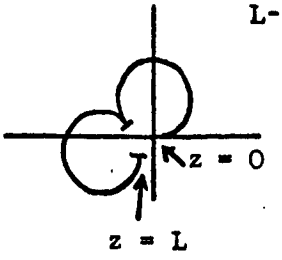

Figure 16

In figures 17-23 we have a modified rhombic.

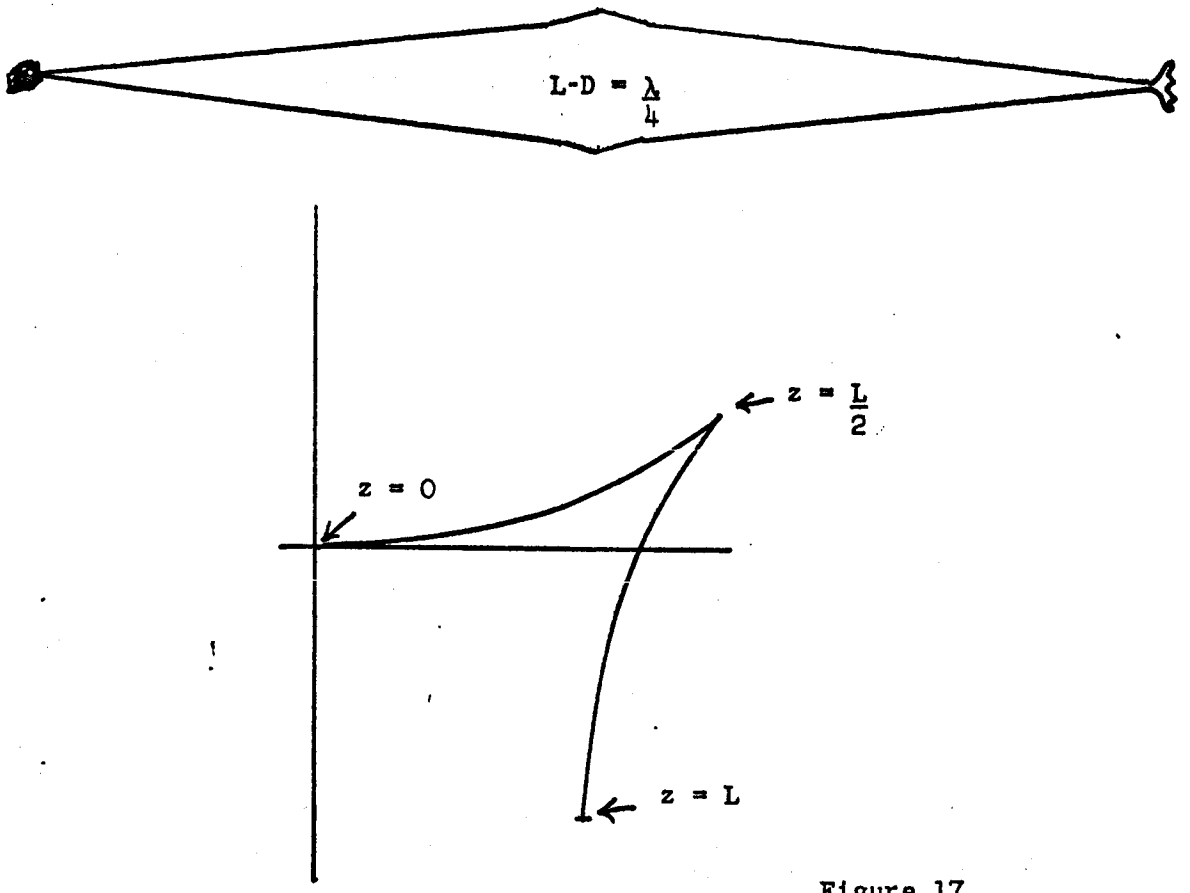

Figure 17

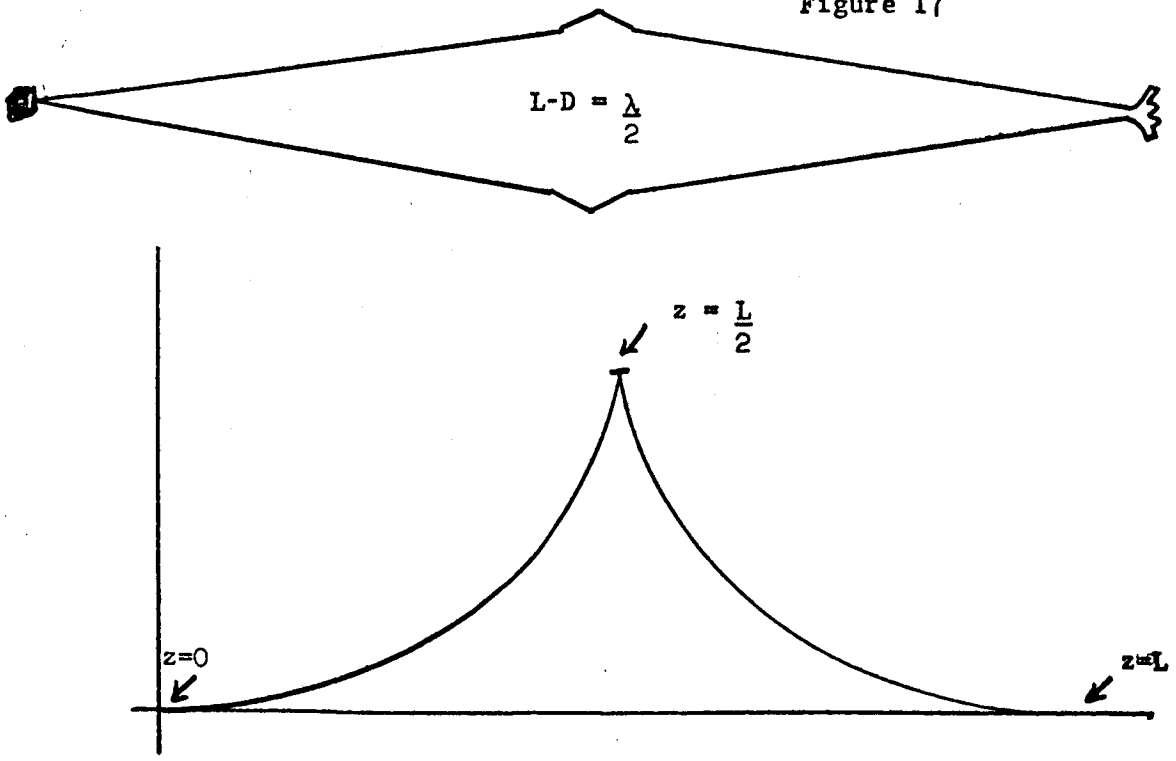

Figure 18

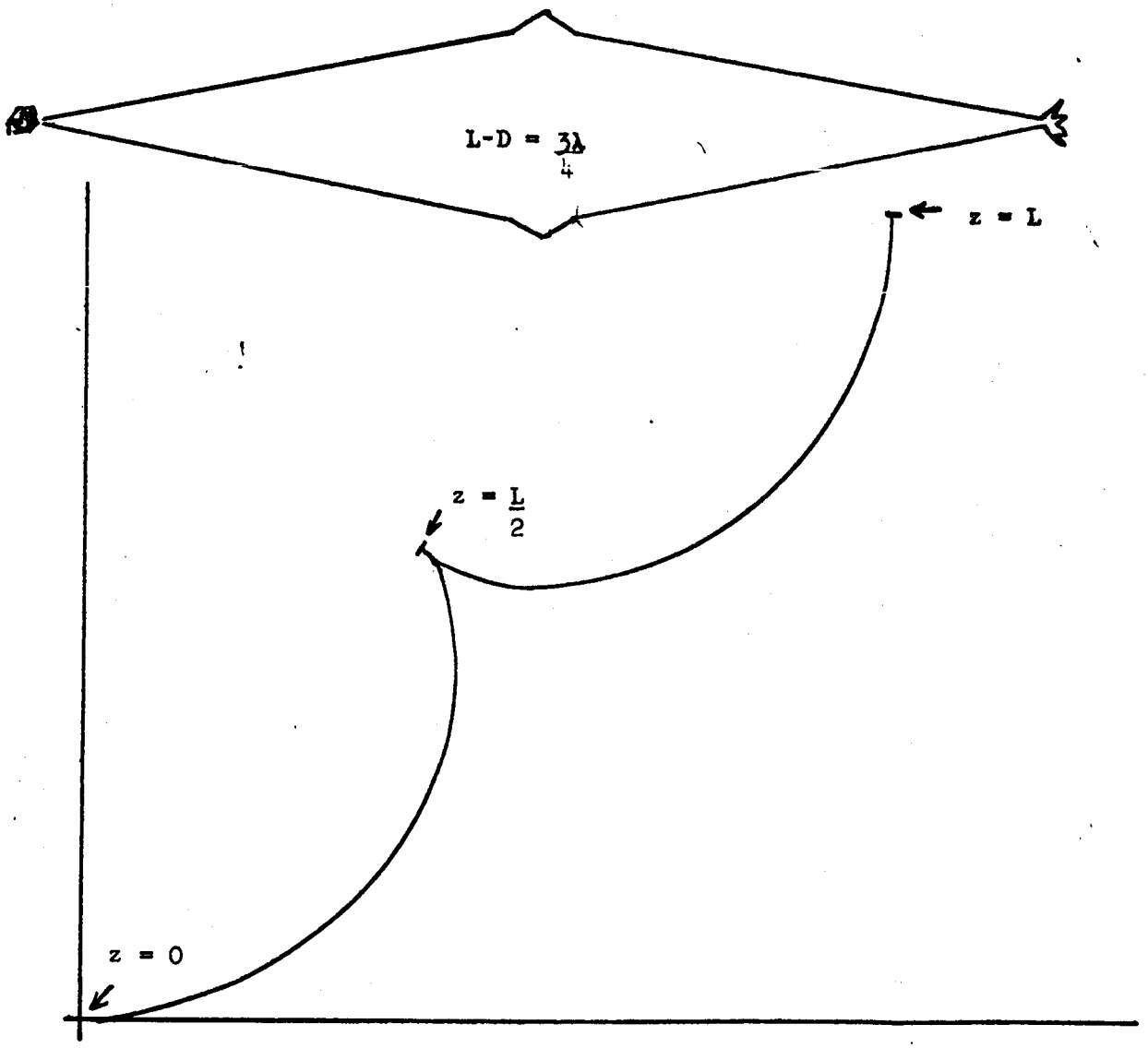

Figure 19

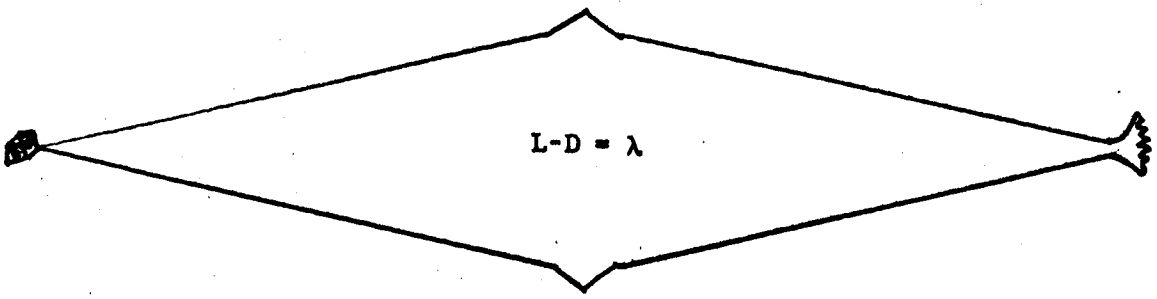

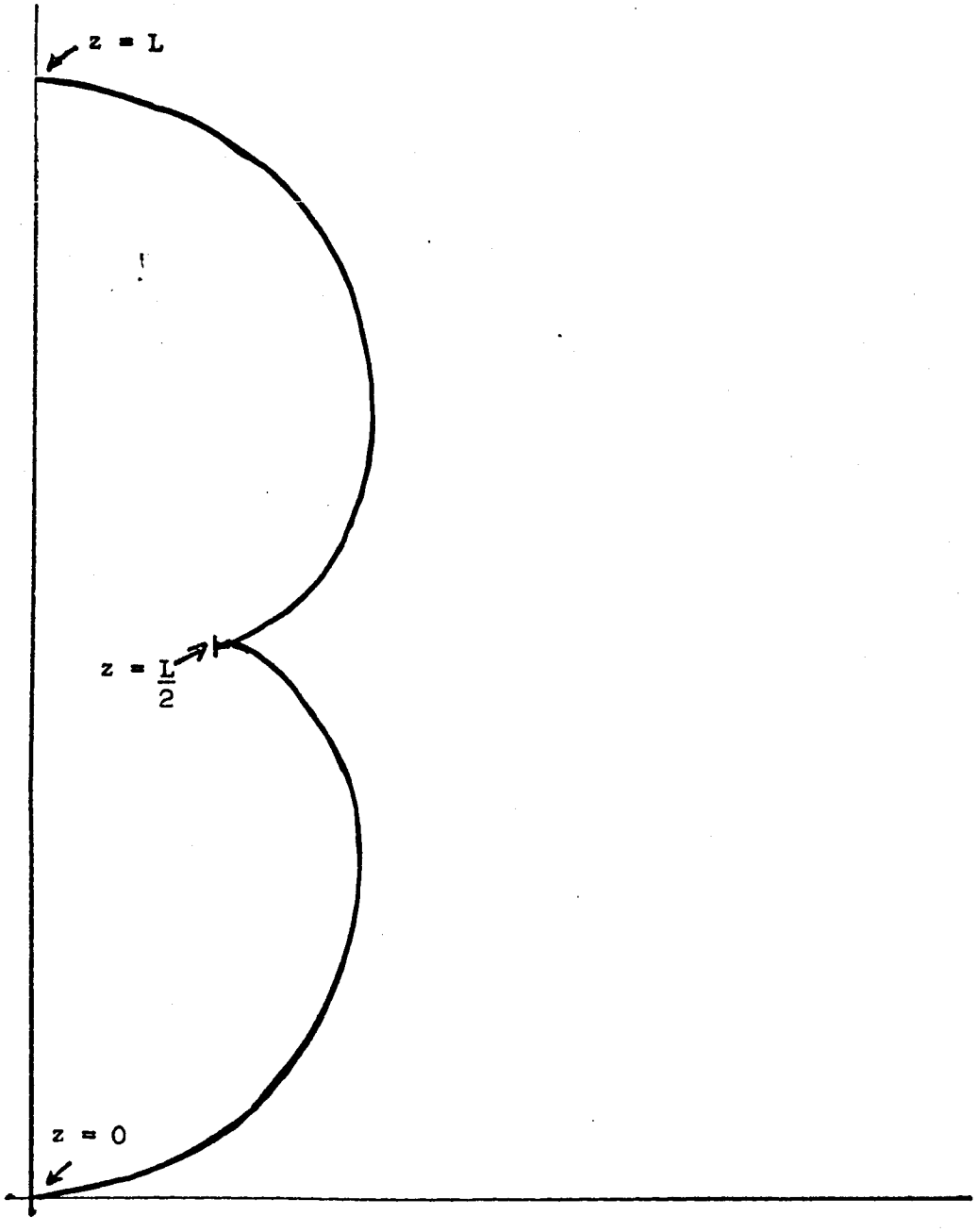

Figure 20

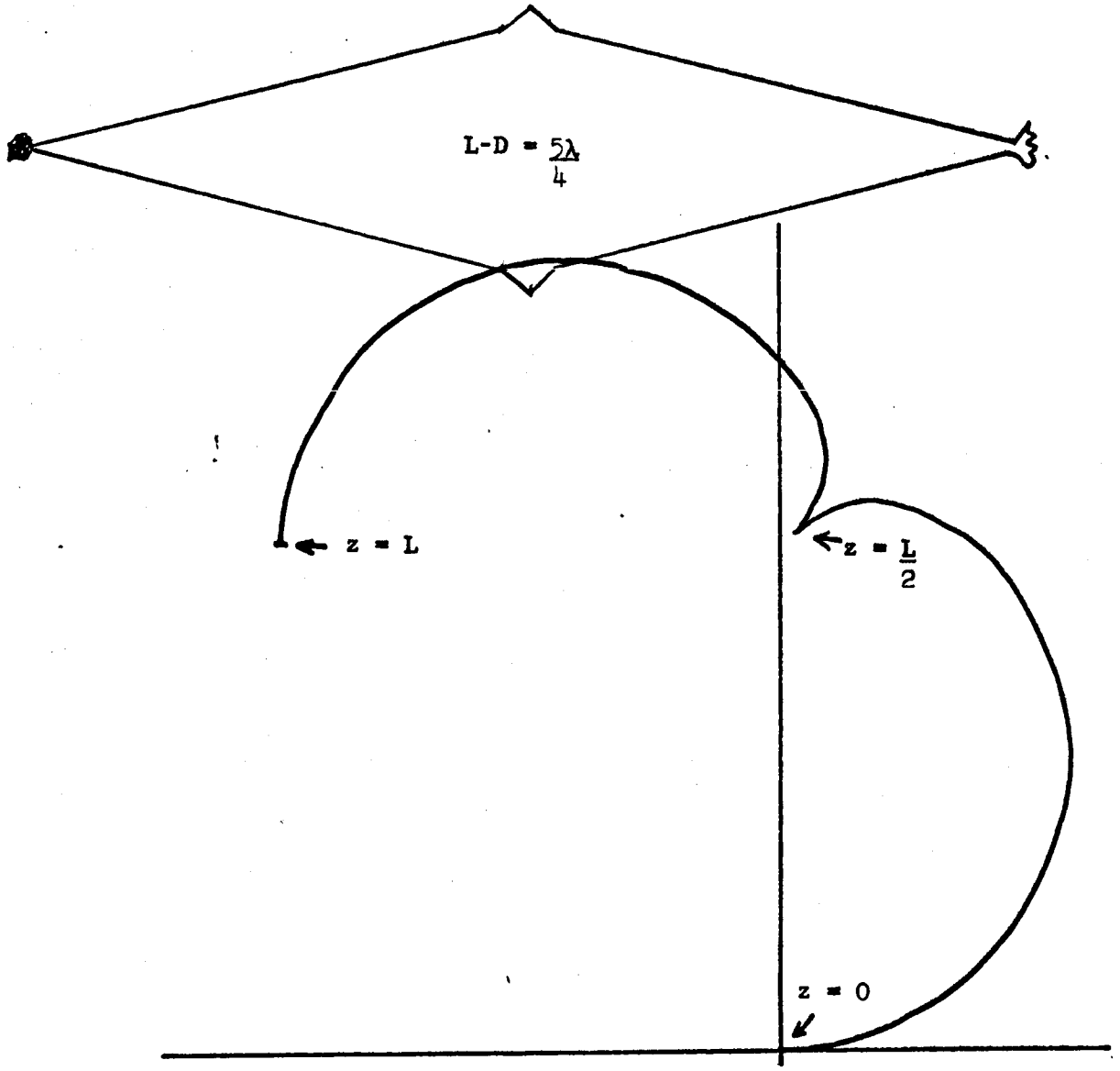

Figure 21

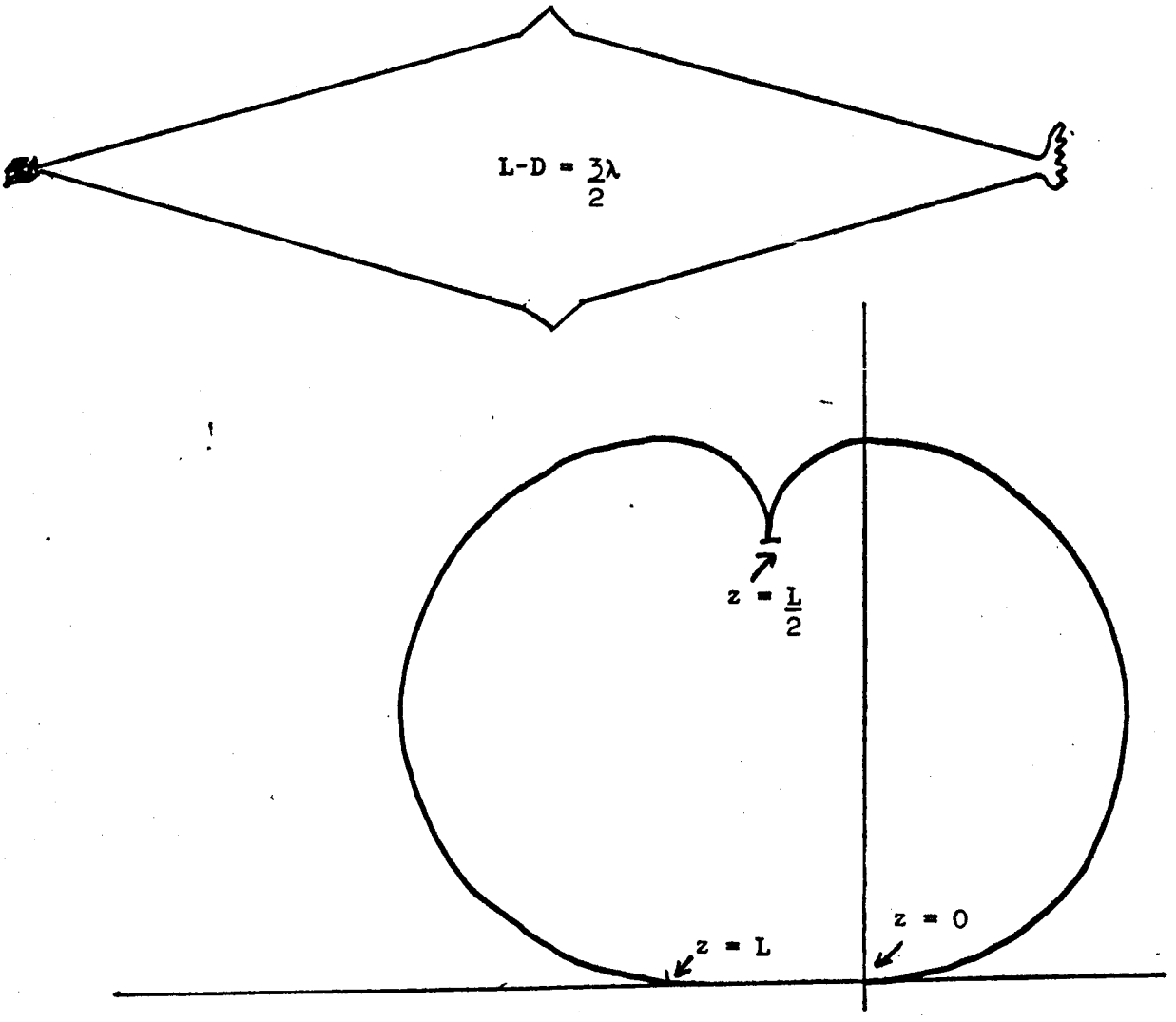

Figure 22

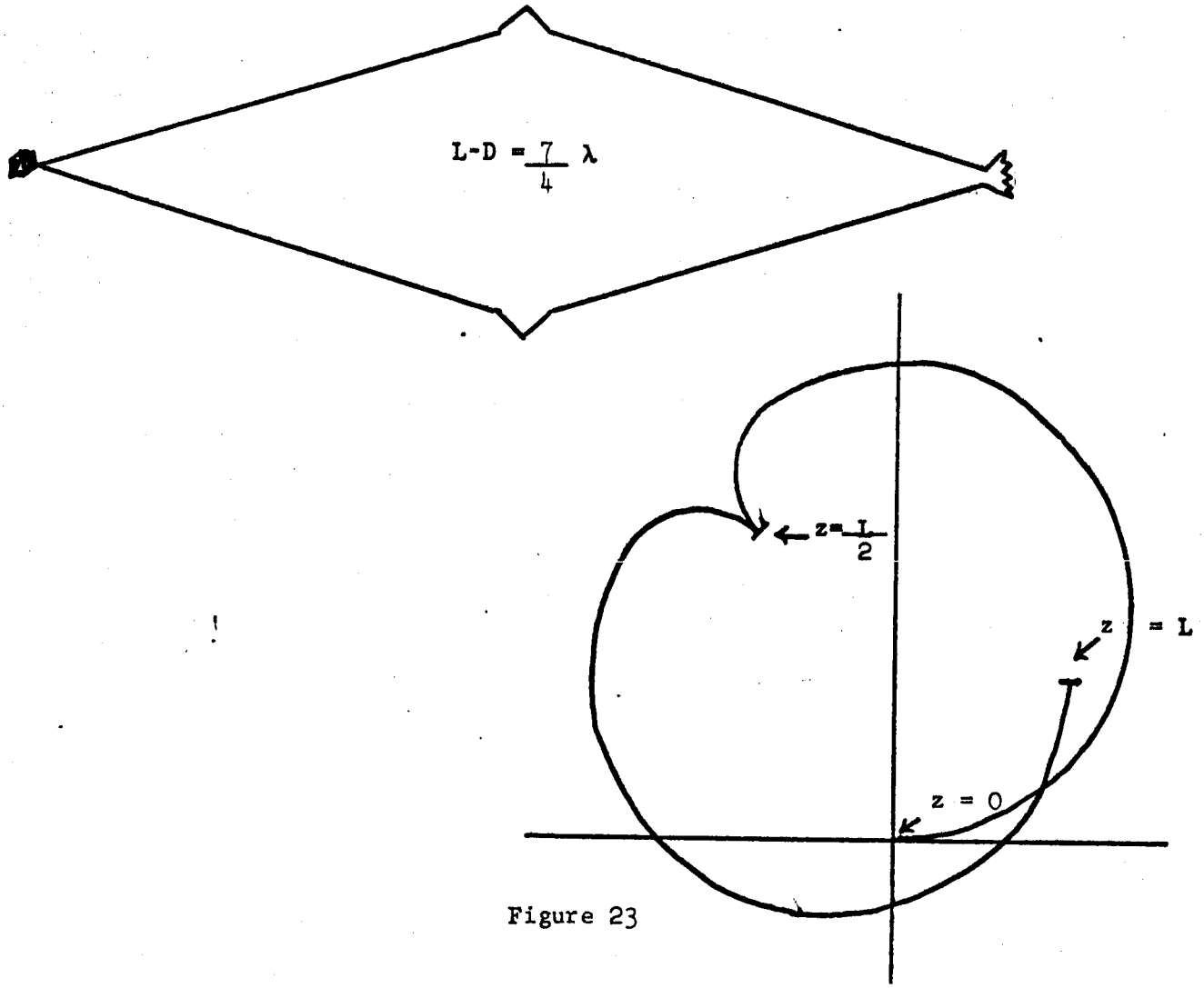

Figure 23

The variation of $|E(L)|$ with L-D is also shown on figure 9 for the modified rhombic.

For the three types of antenna considered we see from figure 9 that $|E(L)|$ reaches its peak value for L-D ~ λ with some variation depending on the antenna shape. We now want to consider the integral $\vec{E}(z)$ in more detail in order to show that we expect such a result to hold for a wide range of antenna shapes.

We want to consider $\vec{E}(z)$ when the field direction is along the axis, that is when $\hat{r} = \hat{r}_o$. For simplicity we will assume the antenna lies in a plane so that we can factor the vector direction out of the integral.

Then the amplitude factor $\hat{s} - (\hat{s}\cdot\hat{r})\hat{r}$ becomes $\sin\alpha$ and the phase factor $\phi = k(s-\int_0^s (\hat{s}\cdot\hat{r})dt)$ becomes $k\int_0^s(1-\cos\gamma)dt$ where γ is the angle between the wire and the direction to the field point. Now we have

$$E(z) = \int_0^z \sin\gamma\, e^{ik\int_0^s (1-\cos\gamma)dt}ds$$

Expressing this in terms of ϕ we have

$$kE(z) = \int_0^\theta \frac{\sin\gamma}{1-\cos\gamma} e^{i\phi}d\phi = \int_0^\theta \frac{e^{i\phi}}{\tan\frac{\gamma}{2}}\, d\phi = V(\theta)$$

where $\theta = k\int_0^z (1-\cos\gamma)ds$.

Now when $\hat{r} = \hat{r}_o$ we have $\int_0^L \cos\gamma\, ds = D$ so that, as z varies from 0 to L, θ varies from 0 to $k(L-D) = \Phi$. If α is given as a function of ϕ then the length of the wires is given by

$$L = \int_0^\Phi \frac{d\phi}{k(1-\cos\gamma)} = \int_0^\Phi \frac{d\phi}{2k\sin^2\frac{\gamma}{2}}$$

If we approximate the integral $V(\theta)$ by a sum

$$\int_0^\theta \frac{e^{i\phi}}{\tan\frac{\gamma}{2}}\, d\phi \sim \Sigma \frac{e^{i\phi}\Delta\phi}{\tan\frac{\gamma}{2}}$$

then we see that $V(\theta)$ is the sum of a number of vectors in the complex plane where the length of a vector is $\frac{\Delta\phi'}{\left|\tan\frac{\gamma}{2}\right|}$ and the direction of the vector is that of $e^{i\phi}$ if $\gamma>0$ (wire going away from axis) and is the opposite direction if $\gamma<0$ (wire going toward axis).

Now from the figures above we can see that the trace of $E(z)$ can be broken into two parts. In one part the wire is going away from the

axis ($z < \frac{L}{2}$ in the cases above) and in the other it is going toward the axis ($z > \frac{L}{2}$).

The reason that E(L) takes on its peak value for L-D ~ λ or $\Phi \sim 2\pi$ is that the two parts are in phase near this value. The exact value of Φ at which the two parts will be in phase will depend on the shape of the wire.

If the first half of the wire goes away from the axis, then for L-D = λ the first part of the trace must start out tangential to the real axis going in the positive direction and continuously bend around until it is headed parallel to the real axis in the negative direction as indicated in figure 24.

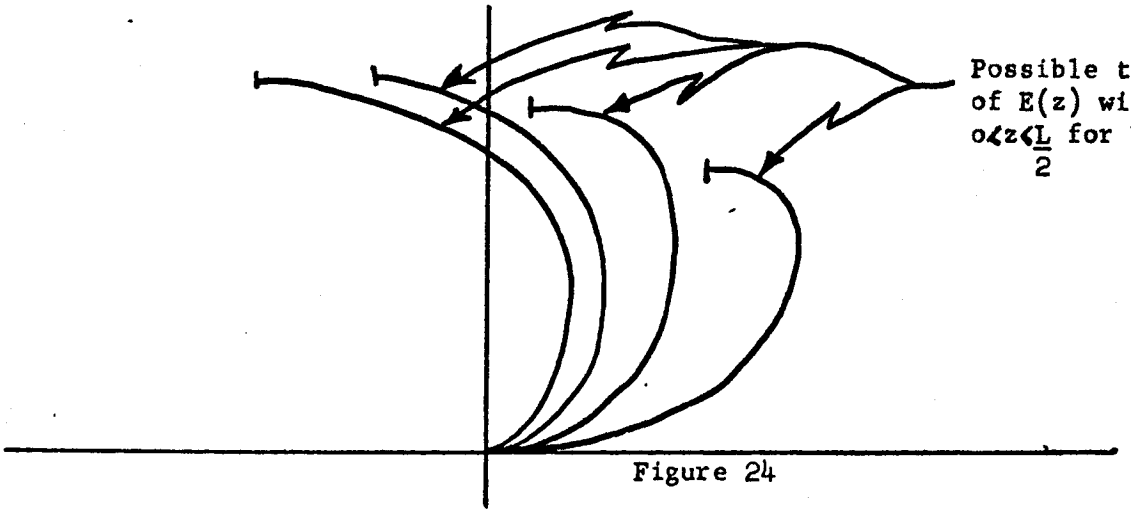

Figure 24

Thus the resultant will tend to lie near the imaginary axis. If the second half of the wire is going toward the axis then it will similarly have a resultant near the imaginary axis and the two will tend to add up leading to a peak near L-D ~ λ for a wide range of wire shapes.

If we consider how $V(\Phi)$ varies for a larger range of Φ we see that we should expect the two parts to add up for $\Phi \sim 2\pi$ giving a maximum, then to cancel for $\Phi \sim 4\pi$ giving a minimun, then to add up again

for $\Phi \sim 6\pi$ giving another maximum, etc. However, for large Φ we would expect each part to be wound up on itself so that the maximum for $\Phi \sim 2\pi$ would be the principal one, as indicated in figure 25.

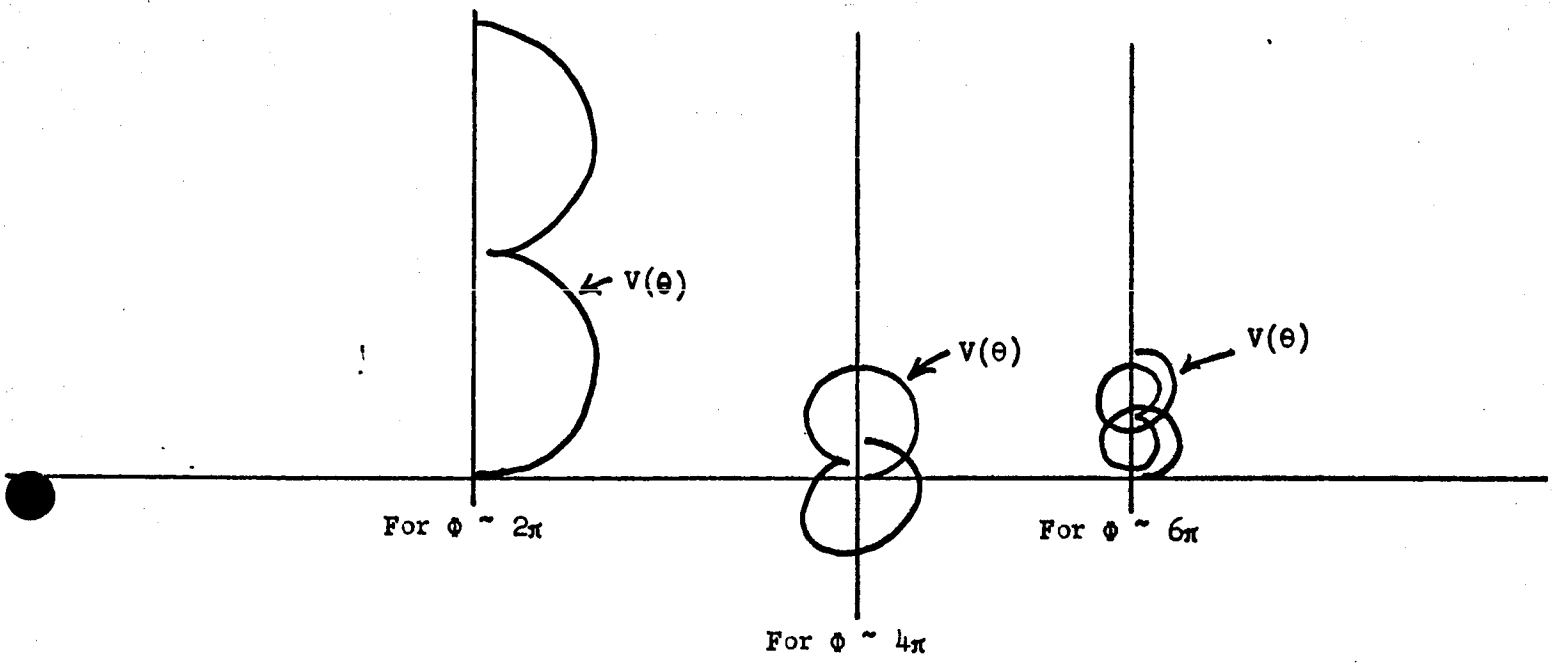

Figure 25

If we consider field points off the axis then we see that the length of the wire, L, remains unchanged but the overall length of the antenna, D, is multiplied by the cosine of the angle between the axis and the field point. Thus $\Phi = k(L-D)$ is increased and we see that the main beam is on the axis.

In the integral $\int_0^{\Phi} \frac{e^{i\phi}}{\tan\frac{\gamma}{2}}\, d\phi$ for the field, if we are not considering the main beam then the phase factor $e^{i\phi}$ is rapidly varying and we can approximate the integral by integration by parts and neglecting the integral

which remains. This means that the value of the integral is determined principally by the singularities. If we want small side-lobes then we must make the singularities small. We can eliminate singularities in the interior of the region of integration by making γ a smooth function of ϕ, but in order to eliminate the singularities at the ends of the region of integration we must make $\frac{1}{\tan \frac{\gamma}{2}}$ increase smoothly from very small values at the ends of the integration region. This corresponds to tapering the illumination of an antenna.

The purpose of the above has been to give a qualitative picture of the behavior of a general rhombic and to show that the precise shape of the antenna is not critical as long as we keep L-D ~ λ. Also we see how we can reduce the side-lobe levels of a rhombic by appropriate reshaping.

While the conclusions reached above should be reliable for an antenna which is meant to operate like an ordinary rhombic, we cannot expect them to hold for completely arbitrary antennas. Thus by using the qualitative approach outlined above we can arrive at the antenna shown in figures 26 and 27. Here although $\Phi = 6\pi$ we have the main beam on axis.

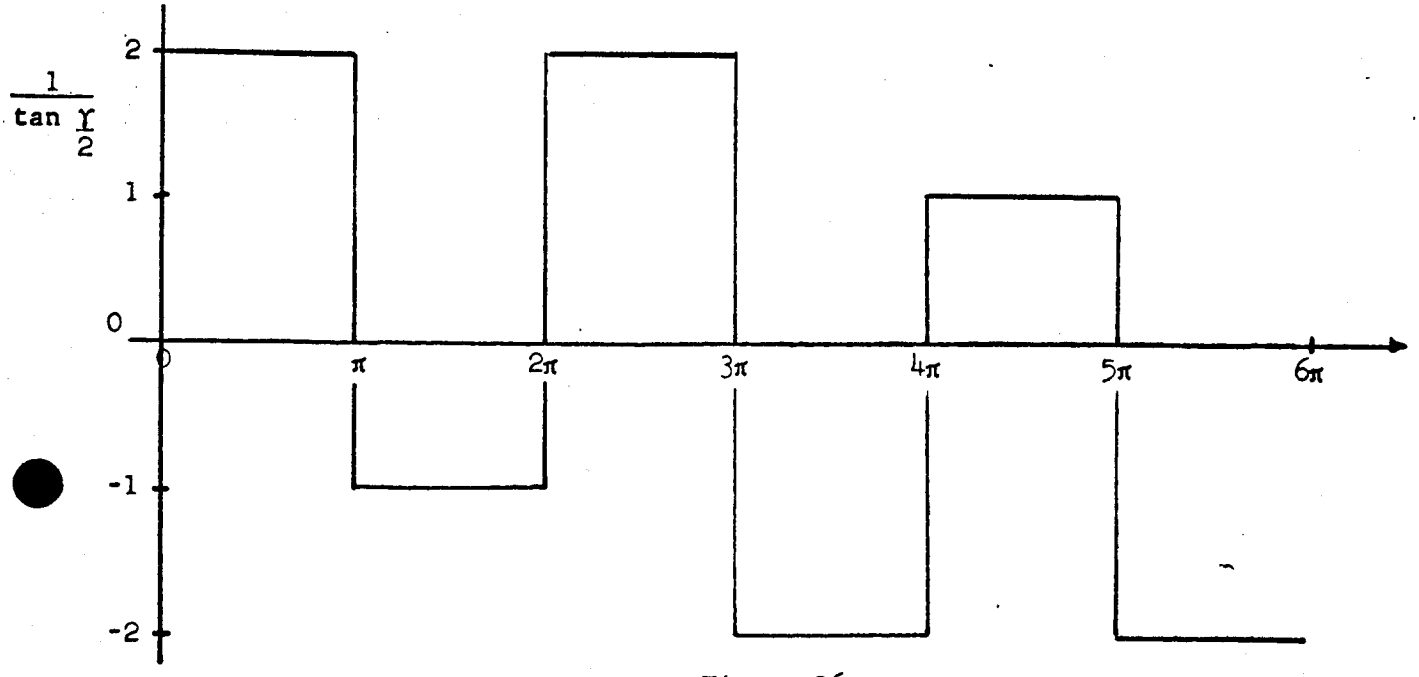

Figure 26

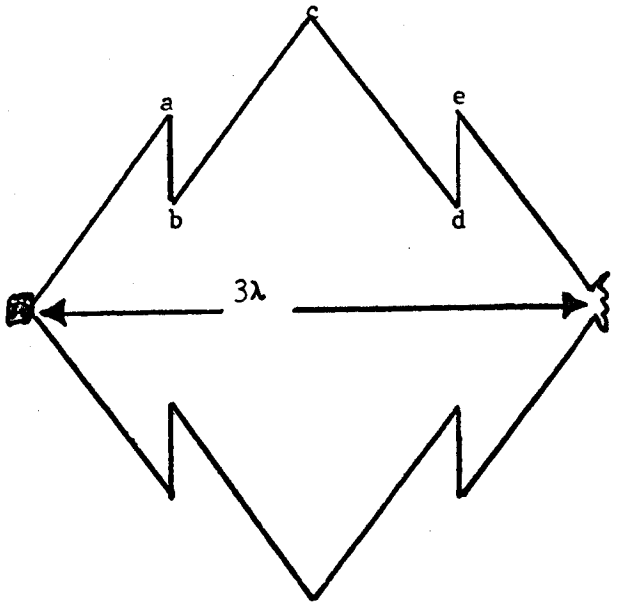

L = 6λ
L-D = 3λ

Figure 27

The plot of V(θ) is given in figure 28.

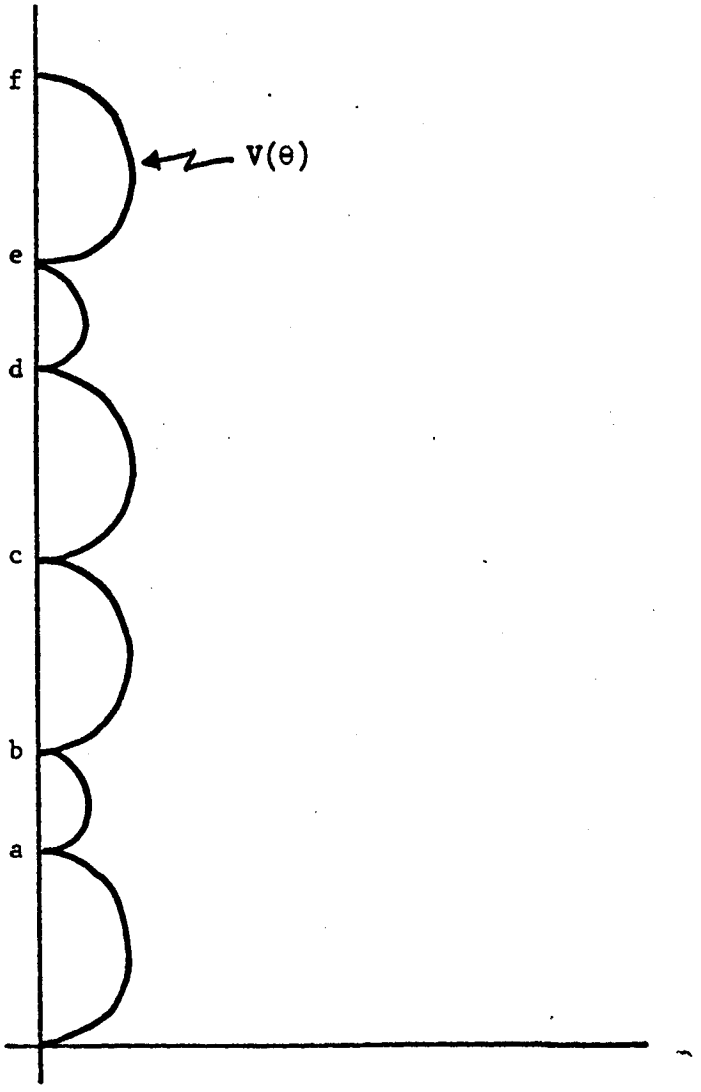

Figure 28

Here we have a cross between a rhombic and an array. In this way we may be able to obtain greater sensitivity and a sharper beam than a rhombic by sacrificing some of its broadbandedness.

One of the features of the generalized rhombic is that it might be feasible to change the shape in orbit thus changing either the operating frequency or the pattern. A possibility mentioned by Professor Haddock is changing the pattern and simply averaging the results in order to smooth out the side-lobes.

EXPRESSIONS FOR THE FIELD OF A GENERAL RHOMBIC

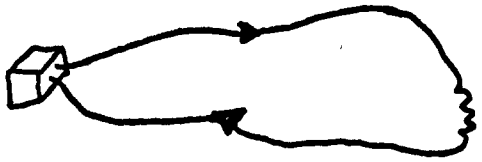

A general rhombic consists of two wires going from a transmitter or receiver to a terminating impedance which is chosen to eliminate reflected currents. The field due to this rhombic consists of two terms of the form

$$\vec{E} = \pm \int_0^L [\hat{s}-(\hat{s}\cdot\hat{r})\hat{r}]\ e^{ik\int_0^s [1-\hat{s}\cdot\hat{r}]\ dt}\,ds \qquad (1)$$

(one term has the + sign and the other term has the - sign due to the fact that the currents travel in opposite directions in the two wires). Here L is the length of the wire, $\hat{s}$ is a unit vector along the wire, $\hat{r}$ is a unit vector in the direction of the field point, $k = \frac{2\pi}{\lambda}$, λ is the wave length, s is distance along the wire. The assumption in equation (1) is that the current is constant in magnitude along the wire and has a phase characteristic of a wave travelling along the wire at the velocity of light.

We will consider first the case where the antenna lies in a plane and the field point is in this plane. Then $\hat{s}-(\hat{s}\cdot\hat{r})\hat{r}$ is a vector in this plane which is perpendicular to the direction to the field point and which has magnitude $\sin\alpha$ where α is the angle between the wire and the direction to the field point. Also $\hat{s}\cdot\hat{r} = \cos\alpha$ so that the integrals in (1) take the form

$$\vec{E} = \hat{x}\int_0^L \sin\alpha\, e^{ik\int_0^s (1-\cos\alpha)dt}\,ds \qquad (2)$$

The phase angle $k\int_0^s (1-\cos\alpha)dt$ varies from 0 to $k\int_0^L (1-\cos\alpha)dt = k(L-D)$ where L is the length of the wire and D is the length of the projection of the wire on the direction to the field point.

If we transform the integration variable from arc length, s, to phase angle $\phi = k\int_0^s (1-\cos\alpha)dt$ we find

$$d\phi = k(1-\cos\alpha)ds$$

$$k\vec{E} = \hat{x}\int_0^{\Phi} \frac{\sin\alpha}{1-\cos\alpha}\, e^{i\phi}d\phi = \hat{x}\int_0^{\Phi} \frac{e^{i\phi}}{\tan\frac{\alpha}{2}}\, d\phi \qquad (3)$$

where $\Phi = k(L-D)$. In terms of α and ϕ we can give the following expression for the length of the wire:

$$L = \int_0^L ds = \int_0^{\Phi} \frac{d\phi}{k(1-\cos\alpha)} = \frac{\lambda}{4\pi}\int_0^{\Phi} \frac{d\phi}{\sin^2\frac{\alpha}{2}} \qquad (4)$$

In the general case in which the antenna and the field point do not all lie in a single plane we must replace the $\hat{x}$ in (2) and (3) by $\hat{x}\cos\beta + \hat{y}\sin\beta$ and this expression must now go inside the integral. Here $\hat{x}$ and $\hat{y}$ are two fixed unit vectors perpendicular to $\hat{r}$ and $\hat{s} - (\hat{s}\cdot\hat{r})\hat{r} = \hat{x}\sin\alpha\cos\beta + \hat{y}\sin\alpha\sin\beta$.

If we are given α as a function of s and want to draw a picture of the antenna, we plot $\int_0^s \sin\alpha\, dt$ versus $\int_0^s \cos\alpha\, dt$. If we are given instead α as a function of ϕ then we plot $\int_0^{\phi} \frac{d\theta}{k\tan\frac{\alpha}{2}}$ versus $\int_0^{\phi} \frac{\cos\alpha\, d\theta}{k(1-\cos\alpha)}$.

APPENDIX J

THE CURRENT DISTRIBUTION ON A RESISTIVE CYLINDRICAL ANTENNA

I. Introduction

The purpose of this work is to study the current distribution on a thin, finite, cylindrical antenna when the antenna material is not a perfect conductor. Wu and King[1] have treated this problem for the case when the impedance per unit length is a particular function of the distance from the end of antenna. They have, however, only obtained a solution for the case of the current being represented by an outward traveling wave emanating from a source at the center of the wire. This result neglects the effect of waves reflected from the end of the antenna.

In the present case we consider a source located at an orbiting position on the structure and calculate the complete current distribution on the wire by utilizing a variational principle. We then show how this result may be used to obtain the current induced on the same antenna when it is illuminated by a plane wave.

II. The Equation for the Current on a Finite, Resistive Transmitting Antenna

We shall investigate the current on a thin, imperfectly conducting cylinder of length 2l, radius a and internal impedance per unit length Z_i. The cylinder extends from $z = -l$ to $z = +l$ and is excited by a voltage V_o applied at the point $z = z_o$. The total current I, is assumed to be axially directed and to possess aximuthal symmetry, following boundary conditions at the surface of the cylinder

$$E_z + E_z^e = I(z)\, Z_i; \quad r = a \quad \text{and} \quad -l \leqslant z \leqslant l, \tag{1}$$

where E_z is the electric field, (axially directed), induced by the current on the cylinder and E_z^e is given by

$$E_z^e = V_o\, \delta(z - z_o) \tag{2}$$

The induced field, E_z, is obtained by utilizing the vector potential A_z on the surface of the cylindrical structure,

$$A_z(z) = \frac{\mu_o}{4\pi} \int_{-\ell}^{+\ell} I(\zeta) \frac{e^{ik\sqrt{(z-\zeta)^2 + a^2}}}{\sqrt{(z-\zeta)^2 + a^2}} d\zeta \,. \tag{3}$$

Here, we have assumed an $e^{-i\omega t}$ time dependence and the wavenumber k is given by $\frac{\omega}{c}$. Equation (3) is the thin wire approximation for the exact vector potential which is widely used in the treatment of thin antennas when the end surfaces are of no particular concern[2,3]. We may now write the induced field E_z as

$$E_z = \frac{i\omega}{k^2}\left[\frac{d^2}{dz^2} + k^2\right] A_z. \tag{4}$$

If we assume the cylinder to be so thin that

$$a \ll 2\ell \qquad \text{and} \qquad ka \ll 1, \tag{5}$$

and take into account the fact that the current I(z) must go to zero at $z = \pm 1$, we may rewrite the integral in equation (3) as shown below[4]:

$$\int_{-\ell}^{+\ell} I(\zeta) \frac{e^{ik\sqrt{(z-\zeta)^2 + a^2}}}{\sqrt{(z-\zeta)^2 + a^2}} d\zeta = \int_{-\ell}^{+\ell} \ln \frac{2|z-\zeta|}{a} \operatorname{sgn}(z-\zeta) \cdot \frac{d}{d\zeta}\left[I(\zeta)e^{ik|z-\zeta|}\right] d\zeta \,, \tag{6}$$

Equation (4) therefore becomes

$$E_z = -\frac{1}{i\omega 4\pi\epsilon_o}\left[\frac{\partial^2}{\partial z^2} + k^2\right] L\left[I, z\right] , \tag{7}$$

where the functional L [I,z] is given by

$$L[I,z] = \int_{-\ell}^{+\ell} \ln \frac{2|z-\zeta|}{a} \operatorname{sgn}(z-\zeta) \frac{d}{d\zeta} \left[I(\zeta) e^{ik|z-\zeta|} \right] d\zeta \qquad (8)$$

We may now rewrite equation (1) in the form

$$GI + K = 0 \qquad (9)$$

where the operator G is defined by

$$GI = -\frac{1}{i\omega 4\pi\epsilon_o} \left[\frac{\partial^2}{\partial z^2} + k^2 \right] L[I,z] - Z_i I \qquad (10)$$

and the driving force K is given by

$$K = V_o \delta(z-z_o). \qquad (11)$$

Vainshtein[5] has formulated a variational principle for equation (9) which is briefly described below. We consider the two driving forces K_α and K_β given for the same antenna and their corresponding currents I_α and I_β which satisfy the equations

$$GI_\alpha + K_\alpha = 0.$$

$$GI_\beta + K_\beta = 0. \qquad (12)$$

The operator G, defined by equation (10) satisfies the symmetry conditions

$$\langle I_\alpha, GI_\beta \rangle = \langle I_\beta, GI_\alpha \rangle \qquad (13)$$

where for the present one dimensional problem, the inner product $\langle I_\beta, GI_\alpha \rangle$

is defined as

$$\left\langle I_\beta, GI_\alpha \right\rangle = \int_{-\ell}^{+\ell} I_\beta \, GI_\alpha \, dz \tag{14}$$

The function, S_{α_β} as shown below

$$S_{\alpha_\beta} = - \frac{\left\langle I_\alpha, GI_\beta \right\rangle}{\left\langle K_\alpha, I_\beta \right\rangle \left\langle K_\beta, I_\alpha \right\rangle} \tag{15}$$

is then stationary with respect to variations in I_α and I_β, when the unvaried functions I_α and I_β satisfy equation (12). If I_α and I_β are exact solutions of equation (12), then

$$\frac{1}{S_{\alpha\beta}} = \left\langle K_\alpha, I_\beta \right\rangle = \left\langle K_\beta \, I_\alpha \right\rangle \tag{16}$$

If the functions I_α and I_β are known only approximately then equation (15) gives a more precise calculation of the quantity $S_{\alpha\beta}$ than does equation (16). Since the precision in calculating S_{α_β} by equation (15) is higher than the precision of the initial trial functions, I_α and I_β, we can take (13) as the basis of a method of successive approximations when K_α and K_β are delta functions.

Vainshtein[5] has shown that, by choosing simple initial trial functions comprised of traveling waves which satisfy the proper end conditions, one obtains sufficient precision by simply substituting into the stationary expression one time. In particular he considers the case of an infinite, perfectly conducting cylinder and compares the solution obtained by the variational method with that obtained by a "direct" solution[4] of the integral equation. This comparison shows excellent correlation between the results of the two methods. Furthermore, the accuracy of the results obtained through the variational method increases as the quantity k^2a^2

decreases. Since the current on the finite, resistive wire is comprised of functions which are similar to those in the case dexcribed above, we may expect to obtain similar accuracy. Furthermore, Vainshtein shows that the results obtained from the variational approximation may be applied when ka is as large as 0.2, so that we can expect the results to be very precise for the particular case of interest.

III. The Current Distribution on the Transmitting Antenna

A current wave varying with z exponentially ($e^{iw_p z}$) can propagate along an impedance conductor. The wave number w_p of this wave is the solution of the equation[5,6]

$$\frac{2i}{4\pi\epsilon_o \omega} v_p^2 \ln \frac{2i}{\gamma v_p a} = Z_i \tag{17}$$

where

$$v_p = \sqrt{k^2 - w_p^2}, \quad \gamma = 1.781... \tag{18}$$

and $\mathrm{Im}\, w_p > 0$ when $\mathrm{Re} Z_i > 0$. It follows that w_p coincides with k when Z_i is zero.

Since we are interested in obtaining the current for an excitation by a concentrated voltage at the point $z = z_\alpha$ we consider the following two driving functions

$$K_\alpha = V_\alpha \delta(z - z_\alpha), \qquad K_\beta = V_\beta \delta(z - z_\beta) \tag{19}$$

We see, therefore, from (16) that

$$\frac{1}{S_{\alpha\beta}} = \langle K_\beta, I_\alpha \rangle = V_\beta I_\alpha(z_\beta) \tag{20}$$

We choose a trial function for the current made up of waves propagating from the point of excitation and traveling waves which constrain the current to be zero at $z = \pm 1$. The trial currents are therefore given by

$$I_\alpha(z) = CV_\alpha\left[e^{iw_p|z-z_\alpha|} + Ae^{iw_p(z-z_\alpha)} + Be^{-iw_p(z-z_\alpha)}\right]$$

$$I_\beta(z) = CV_\beta\left[e^{iw_p|z-z_\beta|} + A'e^{iw_p(z-z_\beta)} + B'e^{-iw_p(z-z_\beta)}\right], \qquad (21)$$

where C is an unknown constant and A, B, A', and B' are given by

$$A' = \frac{e^{2iw_p z_\alpha} - e^{2iw_p \ell}}{2\, i \sin 2w_p \ell} \qquad (22a)$$

$$B = \frac{e^{-2iw_p z_\alpha} - e^{2iw_p \ell}}{2\, i \sin 2w_p \ell} \qquad (22b)$$

$$A' = \frac{e^{2iw_p z_\beta} - e^{2iw_p \ell}}{2\, i \sin 2w_p \ell} \qquad (22c)$$

$$B' = \frac{e^{-2iw_p z_\beta} - e^{2iw_p \ell}}{2\, i \sin 2w_p \ell} \qquad (22d)$$

Substitutine these trial currents into the right hand side of the stationary expression (15) and utilizing equation (20) we obtain the following expression for the current I_α

$$I_\alpha(z) = -\frac{c^2}{V_\beta} \frac{\left[e^{iw_p|z_\alpha - z_\beta|} + \Delta_1 e^{iw_p z_\beta} + \Delta_2 e^{-iw_p z_\beta} \right]^2}{\langle I_\alpha, GI_\beta \rangle} \tag{23}$$

where

$$\Delta_1(z_\alpha) = \frac{e^{iw_p z_\alpha} - e^{2iw_p \ell} e^{-iw_p z_\alpha}}{2i \sin 2w_p \ell} \tag{24a}$$

and

$$\Delta_2(z_\alpha) = \frac{e^{-iw_p z_\alpha} - e^{2iw_p \ell} e^{iw_p z_\alpha}}{2i \sin 2w_p \ell} \tag{24b}$$

We must now calculate the quantity $\langle I_\alpha, GI_\beta \rangle$ in order to obtain the final expression for $I_\alpha(z_\beta)$. It follows from the symmetry property (13) and equations (10), (14) and (17) that

$$\langle I_\alpha, GI_\beta \rangle = -\frac{1}{4\pi\epsilon_o} \left[\frac{1}{i\omega} \int_{-\ell}^{+\ell} I_\beta(z) \left[\frac{\partial^2}{\partial z^2} + k^2 \right] L[I_\alpha, z]\, dz \right.$$

$$\left. + \frac{2i}{\omega} v_p^2 \ln \frac{2i}{\gamma v_p a} \int_{-\ell}^{+\ell} I_\alpha(z)\, I_\beta(z)\, dz \right] \tag{25}$$

the first integral in (25) may be written as shown

$$\int_{-\ell}^{+\ell} I_\beta(z) \left[\frac{\partial^2}{\partial z^2} + k^2 \right] L\,[I_\alpha, z]\, dz =$$

$$= \int_{-\ell}^{+\ell} \left[\frac{d^2}{dz^2} + k^2 \right] I_\beta(z) \cdot L[I_\alpha, z]\, dz - Q\,, \tag{26}$$

where

$$Q = L[I_\alpha\ z]\ \frac{dI_\beta}{dz}\bigg|_{z=\ell} - L[I_\alpha\ z]\ \frac{dI_\beta}{dz}\bigg|_{z=-\ell}$$

by substituting the currents shown in equation (21) into (25) and (26) we obtain the following expression for the desired inner product

$$\langle I_\alpha, GI_\beta \rangle = -\frac{1}{4\pi\epsilon_o}\left\{ \frac{i}{i\omega}\left[J_1 + J_2 - Q\right] + \frac{2i}{\omega}\, v_p^2 \ln\frac{2i}{\gamma v_p a}\, J_3 \right\} \tag{28}$$

where

$$J_1' = 2iw_p C V_\beta \int_{-\ell}^{+\ell} \delta(z-z_\beta)\ e^{iw_p|\ z-z_\beta|}\ L[I_\alpha, z]\ dz, \tag{29}$$

$$J_2 = v_p^2 \int_{-\ell}^{+\ell} I_\beta(z)\ L[I_\alpha, z]\ dz \tag{30}$$

and

$$J_3 = \int_{-\ell}^{+\ell} I_\alpha(z)\ I_\beta(z)\ dz. \tag{31}$$

The operator, L, is linear so that $L[I_\alpha, z]$ may be written as

$$L[I_\alpha, z] = CV_\alpha\left\{ L\left[\ e^{iw_p|\ z-z_\alpha|},\ z\right] + Ae^{-iw_p z}\, L\left[e^{iw_p z}, z\ \right] + Be^{iw_p z_\alpha}\, L\left[e^{-iw_p z},\ z\ \right] \right\} \tag{32}$$

Substituting the desired exponential quantity into equation (8) leads to the following results:

$$L\left[e^{iw_p z}, z\right] = [g_+(o) + g_-(o)]e^{iw_p z} - g_+(\ell - z)e^{i(k+w_p)\ell}e^{-ikz}$$

$$- g_-(\ell + z)e^{i(k-w_p)\ell}e^{ikz}, \tag{33a}$$

$$L\left[e^{-iw_p z}, z\right] = [g_+(o) + g_-(o)]e^{-iw_p z} - g_+(\ell + z)e^{i(k+w_p)\ell}e^{ikz}$$

$$- g_-(\ell - z)e^{i(k-w_p)\ell}e^{-ikz} \tag{33b}$$

and

$$L\left[e^{iw_p|z-z_\alpha|}, z\right] = [g_+(o) + g_-(o)]\, e^{iw_p|z-z_\alpha|} + [g_+(|z-z_\alpha|) - g_-(|z-z_\alpha|)]$$

$$\cdot e^{ik|z-z_\alpha|} - g_+(\ell + z)e^{i(k+w_p)\ell}e^{iw_p z_\alpha}\, e^{ikz}$$

$$- g_+(\ell - z)e^{i(k+w_p)\ell}\, e^{-iw_p z_\alpha}\, e^{-ikz} \tag{33c}$$

where

$$g_+(z) = \ln \frac{2z}{a} - e^{-i(k+w_p)z}\, \mathcal{E}i\,[i(k+w_p)z]$$

and (34)

$$g_-(z) = \ln \frac{2z}{a} - e^{-i(k-w_p)z}\, \mathcal{E}i\,[i(k-w_p)z]$$

The exponential integral $\mathcal{E}i(i\alpha z)$ is defined as

$$\mathcal{E}i(i\alpha z) = -\int_{\alpha z}^{\infty} \frac{e^{it}}{t}\, dt \tag{35}$$

and the sum $[g_+(o) + g_-(o)]$ is given by

$$[g_+(o) + g_-(o)] = 2 \ln \frac{2i}{\gamma v_p a} \tag{36}$$

By substituting equations (33a-c) into equations (28) - (31) we obtain, after considerable algebra, the following expression for $\left\langle I_\alpha, GI_\beta \right\rangle$:

$$\left\langle I_\alpha, GI_\beta \right\rangle = - \frac{c^2 V_\alpha V_\beta}{4\pi\epsilon_o} \left[\delta_1 e^{ikz_\beta} + \delta_2 e^{-ikz_\beta} + \delta_3 e^{iw_p z_\beta} \right.$$

$$\left. + \delta_4 e^{-iw_p z_\beta} + \delta_5 e^{iw_p |z_\alpha - z_\beta|} + \delta_6 e^{ik|z_\alpha - z_\beta|} \right] \tag{37}$$

where the coefficients, $\delta_1 \ldots, \delta_6$ are expressed as shown below:

$$\delta_1(z_\alpha z_\beta) = \frac{v_p^2}{i\omega} \left\{ \left[\frac{1}{i(k+w_p)} - (\ell + z_\beta)\Delta g_+ (\ell + z_\beta) \right.\right.$$

$$\left. + \frac{k + w_p}{2i(k-w_p)w_p} \left[g_+(\ell+z_\beta) - g_-(\ell+z_\beta) \right] \right] e^{i(k+w_p)\ell} \left[1+B\right] e^{iw_p z_\alpha}$$

$$- \left[\frac{1}{i(k-w_p)} + (\ell+z_\beta)\Delta g_-(\ell+z_\beta) + \frac{(k-w_p)}{2i(k+w_p)w_p} \left[g_+(\ell+z_\beta) - g_-(\ell+z_\beta) \right] \right]$$

$$\left. \cdot e^{i(k-w_p)\ell} A e^{-iw_p z_\alpha} \right\}, \tag{38}$$

$$\delta_2(z_\alpha, z_\beta) = \delta_1(-z_\alpha, z_\beta) \quad , \tag{39}$$

$$\delta_3(z_\alpha) = \frac{v_p^2}{i\omega}\left[T(z_\alpha) - T(-z_\alpha)e^{2iw_p\ell}\right] - \frac{w_p}{i\omega \sin 2w_p\ell}\left[g_+(\ell - z_\alpha) - g_-(\ell - z_\alpha)\right]$$

$$\cdot\left[e^{-ikz_\alpha} - e^{-2iw_p\ell}\, e^{ikz_\alpha}\right] e^{i(k+w_p)\ell} + \frac{2w_p A}{\omega}$$

$$\cdot\left[g_+(o) + g_-(o) - 1\right] e^{-iw_p z_\alpha} + \frac{k}{2iw \sin 2w_p\ell}\left[S(z_\alpha) + e^{2ik\ell}\, S(-z_\alpha)\right]$$

$$+ \frac{(k^2 + w_p^2)}{4i\omega w_p \sin 2w_p\ell}\left[\left(g_+(o) - g_-(o)\right)S(z_\alpha) + e^{2ik\ell}\left(g_+(2\ell) - g_-(2\ell)\right)S(-z_\alpha)\right]$$

$$+ \frac{\ell v_p^2\, e^{2i(k+w_p)\ell}}{\omega \sin 2w_p\ell}\left[\Delta g_-(2\ell) + \Delta g_+(2\ell)e^{2iw_p\ell}\right] U(z_\alpha)$$

$$+ \frac{2\ell v_p^2}{i\omega}\, \Delta g_+(2\ell) e^{2i(k+w_p)\ell}\, e^{-iw_p z_\alpha} \quad , \tag{40}$$

$$\delta_4(z_\alpha) = \delta_3(-z_\alpha) \tag{41}$$

$$\delta_5 = \frac{2w_p}{\omega}\left[g_+(o) + g_-(o) - 1\right] \tag{42}$$

and

$$\delta_6(z_\alpha, z_\beta) = \frac{k^2 + w_p^2}{\omega w_p}\left[g_+(|z_\alpha - z_\beta|) - g_-(|z_\alpha - z_\beta|)\right]$$

$$+ \frac{2k}{\omega} - \frac{v_p^2}{i\omega}\,|z_\alpha - z_\beta|\left[\Delta g_+(|z_\alpha - z_\beta|) + \Delta g_-(|z_\alpha - z_\beta|)\right] \tag{43}$$

The functions $\Delta g_{\pm}$, S, T, and U are written as

$$\Delta g_{\pm}(z) = -e^{-i(k\pm w_p)z}\, Ei[i(k \pm w_p)z], \tag{44}$$

$$S(z_\alpha) = \frac{2}{i \sin 2w_p \ell}\left[\cos 2w_p \ell\, e^{iw_p z_\alpha} - e^{-iw_p z_\alpha}\right], \tag{45}$$

$$T(z_\alpha) = \frac{[g_+(\ell+z_\alpha) - g_-(\ell+z_\alpha)]\, e^{i(k-w_p)\ell}\, e^{ikz_\alpha}}{2w_p \sin 2w_p \ell} + \frac{k e^{i(k-w_p)\ell}}{v_p^2 \sin 2w_p \ell}\, e^{ikz_\alpha}$$

$$- \frac{(\ell+z_\alpha)e^{i(k-w_p)\ell}}{2i \sin 2w_p \ell}\, [\Delta g_+(\ell+z_\alpha) + \Delta g_-(\ell+z_\alpha)]\, e^{ikz_\alpha} \tag{46}$$

and

$$U(z_\alpha) = Be^{-2iw_p\ell}\, e^{iw_p z_\alpha} - Ae^{-iw_p z_\alpha}. \tag{47}$$

We see therefore, that the current distribution, $I(z)$, on a thin, imperfectly conducting wire, extending from $z = -\ell$ to $z = +\ell$, excited by a voltage generator of strength V located at the point $z = z_0$ may be written as

$$I(z) = \frac{4\pi\epsilon_o V\left[e^{iw_p|z_0-z|} + \Delta_1(z_0)e^{iw_p z} + \Delta_2(z_0)\, e^{-iw_p z}\right]^2}{D}, \tag{48a}$$

where

$$D = \delta_1(z_0,z)e^{ikz} + \delta_2(z_0,z)e^{-ikz} + \delta_3(z_0)e^{iw_p z} + \delta_4(z_0)e^{-iw_p z}$$

$$+ \delta_5 e^{iw_p|z_0-z|} + \delta_6(z_0,z)e^{ik|z_0-z|}, \tag{48b}$$

Δ_1 and Δ_2 are given by equation (24) and δ_1 through δ_6 are given by equations (38) - (43).

We can easily show that as ℓ approaches infinity equation (48) reduces to the expression for the current distribution obtained for the infinite wire in reference 5.

IV. The Current on a Thin, Finite, Resistive Cylinder Illuminated by a Plane Wire

Stevenson[7] has shown that the current induced on an antenna by a plane wave excitation may be obtained from the solution of the transmission problem. This theory is only approximately valid, as it is contingent upon the vanishing of the tangential electric field around the gap and over the ends of the gap on the transmitting antenna. Since we are dealing with a thin wire antenna, it is reasonable to adopt these assumptions and thus obtain the current for the case of a parasitic and a receiving antenna.

It follows then, from reference[6], that the current induced at the gap (i.e., at the point $z = z_0$) on the parasitic antenna (i.e., zero load) is given by

$$I(z_0) = \frac{E_{inc} f(\theta,\varphi,\psi)}{k\, z_t} \tag{49}$$

where E_{inc} is the amplitude of the incident plane wave and z_t is the "transmitting impedance." This impedance is defined, for the present problem, as

$$z_t = \frac{V}{I(z_0)} \cdot \tag{50}$$

In order to define the function $f(\theta,\varphi,\psi)$ we consider the plane wave to be replaced by the field of an equivalent Hertzian dipole at a very large distance from the antenna. The function, $f(\theta,\varphi,\psi)$, is then proportional to the component along the axis of the equivalent dipole of the electric field, which is generated when the antenna is transmitting with unit current in the gap. Since we are interested in the far field of the straight wire

antenna we write $f(\theta,\varphi,\psi)$ as

$$f(\theta,\varphi,\psi) = \sin\theta\, g(\theta) \cos\psi, \tag{51}$$

where

$$g(\theta) = \frac{k}{I(z_0)} \int_{-\ell}^{+\ell} I(z')e^{-ikz'\cos\theta}\, dz' \quad . \tag{52}$$

We take θ to be the angel which the direction of the incident wave makes with the antenna and ψ is the angle between the electric field of the incident wave and the plane containing the antenna and the direction of the incident wave, (see Figure 1).

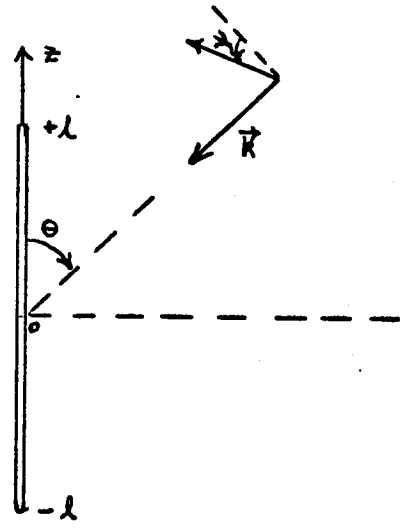

Figure 1

Since equation (48) describes the current distribution on the transmitting antenna for a generator located at any point $z = z_0$, we may now obtain the current distribution induced on this antenna by a plane wave by utilizing equations (49) - (52).

References

1. T. T. Wu and R. W. P. King, I.E.E.E. Trans. on Antennas and Propagation, AP-13, 369, (1965).
2. E. Hallen, Electromagnetic Theory, Wiley, 1962.
3. E. Hallen, I.R.E. Trans. on Antennas and Propagation, AP-4, 479, (1956).
4. L. A. Vainshtein, Soviet Phys. Tech. Phys., 4, 601, (1959).
5. L. A. Vainshtein, Soviet Phys. Tech. Phys., 6, 19, (1961).
6. L. A. Vainshtein, Soviet Phys. Tech. Phys., 4, 617, (1959).
7. A. F. Stevenson, Quart. Appl. Math., 5, 369, (1948).

APPENDIX K

THE CURRENT DISTRIBUTION ON THE VEE ANTENNA

I. Equations for the Current on a Vee Antenna

We shall investigate the current excited on the Vee antenna of Figure 1, by a voltage source of magnitude $\mathcal{E}$ applied at any point on the structure. Each leg of the antenna has a length ℓ, radius a, and internal impedance per unit length Z. The quantities ℓ and a satisfy the conditions

$$k\ell > 1 \quad \text{and} \quad ka \ll 1, \tag{1}$$

where k is the wave number $\frac{\omega}{c}$ and the time dependence of all quantities is taken as $e^{-i\omega t}$ throughout. The result of this work will be to present a prescription for obtaining the current distribution on the antenna, utilizing a variational principle and a successive approximation scheme.

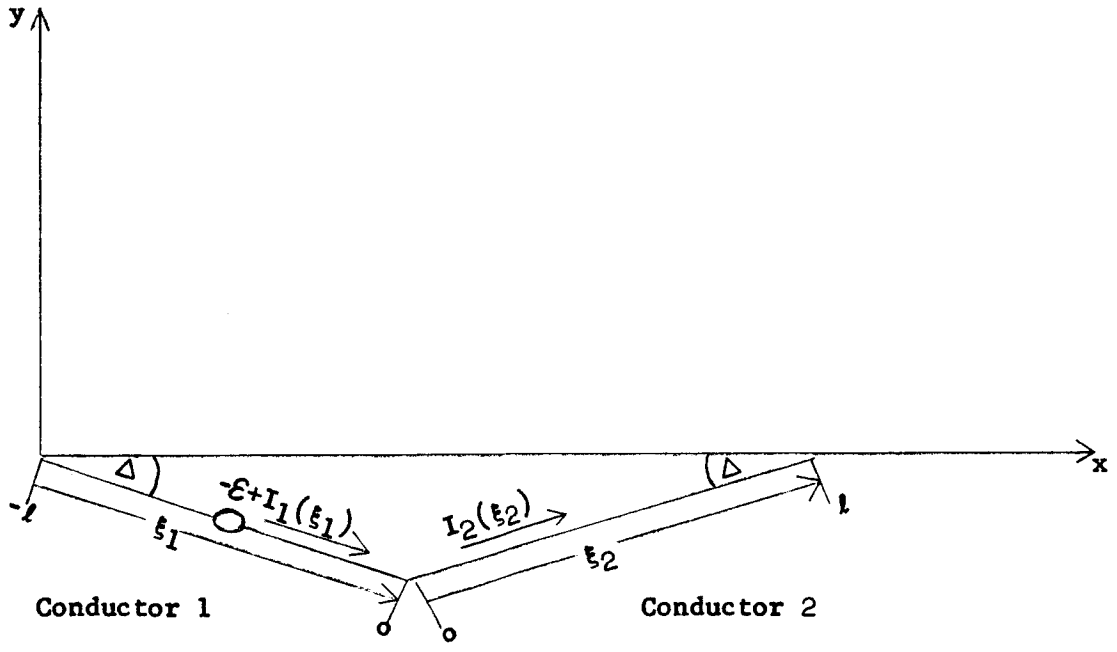

Figure 1.

We define the ξ_1 and ξ_2 coordinate axes as those which lie parallel to wires 1 and 2 respectively. The conductors are joined at the point $\xi_1=\xi_2=o$ and the free end of each wire is located at $\xi_1=-\ell$ and $\xi_2=+\ell$, respectively.

The currents and induced tangential surface fields on each wire are denoted by $I_1(\xi_1)$, $I_2(\xi_2)$, E_{ξ_1} and E_{ξ_2}. Let the structure be excited by two generators of magnitude $\mathcal{E}_1$ and $\mathcal{E}_2$, located at the points $\xi_1 = - \xi_\alpha$ and $\xi_2 = + \xi_\alpha$ respectively and directed as shown in Figure 2.

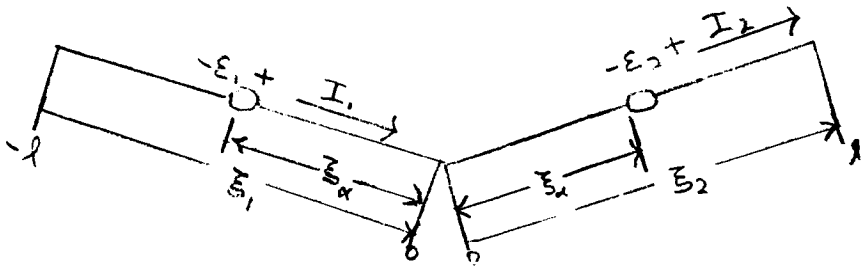

Figure 2

This arrangement, of a generator symmetrically placed on each wire, will allow us to divide the current into its symmetric and antisymmetric components for an arbitrary generator location. We must now satisfy the following boundary conditions on the conductor surfaces

$$E_{\xi_1} + \mathcal{E}_1 \delta(\xi_1 + \xi_\alpha) = I_1(\xi_1)\, Z. \tag{2}$$

and

$$E_{\xi_2} + \mathcal{E}_2 \delta(\xi_2 - \xi_\alpha) = I_2(\xi_2)\, Z. \tag{3}$$

In addition, the current I_1 and I_2 are subject to the following end constraints:

$$I_1(-\ell) = I_2(\ell) = o \quad , \tag{4}$$

$$I_1(o) = I_2(o) \tag{5}$$

and

$$\frac{dI_1}{d\xi_1}\bigg|_{\xi_1=o} = \frac{dI_2}{d\xi_2}\bigg|_{\xi_2=o} \tag{6}$$

Equations (5) and (6) are the current and charge continuity conditions at the bend.

In order to obtain the induced fields on each conductor we define the following four quantities:

$$\vec{A}_{11}(\xi_1) = \frac{\mu_o}{4\pi}\int_{-\ell}^{o} \vec{I}_1(\zeta)\,\frac{e^{ikR_{11}}}{R_{11}}\,d\zeta \quad , \tag{7a}$$

$$\vec{A}_{12}(\xi_1) = \frac{\mu_o}{4\pi}\int_{o}^{\ell} \vec{I}_2(\zeta)\,\frac{e^{ikR_{12}}}{R_{12}}\,d\zeta \quad , \tag{7b}$$

$$\vec{A}_{21}(\xi_2) = \frac{\mu_o}{4\pi}\int_{-\ell}^{o} \vec{I}_1(\zeta)\,\frac{e^{ikR_{21}}}{R_{21}}\,d\zeta \quad , \tag{7c}$$

and

$$\vec{A}_{22}(\xi_2) = \frac{\mu_o}{4\pi}\int_{o}^{\ell} \vec{I}_2(\zeta)\,\frac{e^{ikR_{22}}}{R_{22}}\,d\zeta \quad , \tag{7d}$$

where

$$R_{11} = \sqrt{(\xi_1-\zeta)^2+a^2} \quad ; \quad R_{21} = \sqrt{\xi_2^2+\zeta^2-2\zeta\xi_2\cos 2\Delta+a^2}$$

$$R_{12} = \sqrt{\xi_1^2+\zeta^2-2\zeta\xi_1\cos 2\Delta+a^2} \quad , \quad R_{22} = \sqrt{(\xi_2-\zeta)^2+a^2} \tag{8}$$

The vectors $\vec{A}_{mn}$ describe the potential measured on the surface of wire m due to a current in conductor n, the expressions shown above for these quantities are valid when $ka \ll |< k\ell$.

In order to determine the tangential component of the induced electric field at the surface of wire 1 we must consider the variation of the quantity $\vec{A}_{12}$ with respect to a displacement normal to wire 1 and in the plane of the antenna the coordinate defining this normal displacement is denoted as ξ_3, and is directed so that $\hat{\xi}_1 \times \hat{\xi}_3 = \hat{z}$. It follows then, that E_{ξ_1} is given by

$$E_{\xi_1} = \frac{i\omega}{k^2}\left[\frac{\partial^2}{\partial\xi_1^2} + k^2\right] A_{11} + \frac{i\omega}{k^2}\cos 2\Delta \left[\frac{\partial^2}{\partial\xi_1^2} + k^2\right]$$

$$A_{12} + \frac{i\omega}{k^2}\sin 2\Delta \frac{\partial^2 A_{12}}{\partial\xi_1\partial\xi_3}\Bigg|_{\xi_3=o} \qquad (9)$$

Here, the scalar quantities, A_{11} and A_{12} are simply the magnitude of the vectors $\vec{A}_{11}$ and $\vec{A}_{12}$. The induced tangential field at the surface of wire 2 is written in a similar fashion as

$$E_{\xi_2} = \frac{i\omega}{k^2}\left[\frac{\partial^2}{\partial\xi_2^2} + k^2\right] A_{22} + \frac{i\omega}{k^2}\cos 2\Delta \left[\frac{\partial^2}{\partial\xi_2^2} + k^2\right]$$

$$A_{21} - \frac{i\omega}{k^2}\sin 2\Delta \frac{\partial^2 A_{21}}{\partial\xi_2\partial\xi_4}\Bigg|_{\xi_4=o} \quad ; \qquad (10)$$

where ξ_4 is the coordinate measured from the surface of wire 2, normal to ξ_2; and in the plane of the structure. It is directed so that $\hat{\xi}_2 \times \hat{\xi}_4 = \hat{z}$.

The normal derivatives of A_{12} and A_{21} are obtained by rewriting the quantities R_{12} and R_{21} for observation points at a distance ξ_3 and ξ_4 above the surface of conductors 1 and 2 respectively. The derivatives are then taken with respect to these distances and ξ_3 and ξ_4 are then set equal to zero in the resultant expressions. The results of this operation are shown below:

$$\frac{\partial A_{12}}{\partial \xi_3}\Bigg|_{\xi_{3=o}} = -\frac{\mu_o}{4\pi}\sin 2\Delta \int_o^{\ell} I_2(\zeta)\frac{e^{ikR_{12}}}{R_{12}^3}\left[ikR_{12}-1\right]\zeta d\zeta \qquad (11)$$

and

$$\frac{\partial A_{21}}{\partial \xi_4}\Bigg|_{\xi_4=o} = \frac{\mu_o \sin 2\Delta}{4\pi}\int_{\ell}^{o} I_1(\zeta)\frac{e^{ikR_{21}}}{R_{21}^3}\left[ikR_{21}-1\right]\zeta d\zeta \quad . \qquad (12)$$

By substituing equations (9), (10), (11) and (12) into (2) and (3) we obtain the following set of simultaneous equations for the current I_1 and I_2

$$G_1(\xi_1)I_1 + G_2(\xi_2)I_2 + \mathcal{E}_1\delta(\xi_1+\xi_\alpha) = I_1(\xi_1)\, Z \tag{13}$$

and

$$G_3(\xi_2)I_1 + G_4(\xi_2)I_2 + \mathcal{E}_2\delta(\xi_2-\xi_\alpha) = I_2(\xi_2)\, Z \quad , \tag{14}$$

where

$$G_1(\xi_1)I_1 = \frac{i\omega\mu_o}{4\pi k^2}\left[\frac{d^2}{d\xi_1^2} + k^2\right]\int_{-\ell}^{o} I_1(\zeta)\,\frac{e^{ikR_{11}}}{R_{11}}\,d\zeta \quad , \tag{15a}$$

$$G_2(\xi_1)I_2 = \frac{i\omega\mu_o}{r\pi k^2}\left\{\cos 2\Delta\left[\frac{d^2}{d\xi_1^2} + k^2\right]\int_{o}^{\ell} I_2(\zeta)\,\frac{e^{ikR_{12}}}{R_{12}}\,d\zeta\right.$$

$$\left. -\sin^2 2\Delta\,\frac{d}{d\xi_1}\int_{o}^{\ell} I_2(\zeta)\,\frac{e^{ikR_{12}}}{R_{12}^3}\,[ikR_{12} - 1]\,\zeta d\zeta\right\} \quad , \tag{15b}$$

$$G_3(\xi_2)I_1 = \frac{i\omega\mu_o}{4\pi k^2}\left\{\cos 2\Delta\left[\frac{d^2}{d\xi_2^2} + k^2\right]\int_{-\ell}^{o} I_1(\zeta)\,\frac{e^{ikR_{21}}}{R_{21}}\,d\zeta\right.$$

$$\left. -\sin^2 2\Delta\,\frac{d}{d\xi_2}\int_{-\ell}^{o} I_1(\zeta)\,\frac{e^{ikR_{21}}}{R_{21}^3}\,[ikR_{21} - 1]\,\zeta d\zeta\right\} \tag{15c}$$

and

$$G_4(\xi_2)\, I_2 = \frac{i\omega\mu_o}{4\pi k^2}\left[\frac{d^2}{d\xi_2^2} + k^2\right]\int_{o}^{\ell} I_2(\zeta)\,\frac{e^{ikR_{22}}}{R_{22}}\,d\zeta \quad . \tag{15d}$$

The simultaneous solution of equations (13) and (14) is facilitated by dividing the currents $I_1(\xi_1)$ and $I_2(\xi_2)$ into their symmetrical and antisymmetrical

components. This procedure allows us to uncouple the two equations, thereby replacing the solution of (13) and (14) by the solution of two independent equations. The current distribution on the structure for a single generator at an arbitrary location is then obtained by the construction of a linear combination of the symmetrical and antisymmetrical components of the currents.

In order to obtain the symmetrical component of the current we set $\mathcal{E}_1 = \mathcal{E}_2$ in equations (13) and (14). Under this condition we have that

$$I_1(\xi_1) = I_2(\xi_2) \quad ; \quad \text{when } \xi_1 = -\xi_2 \quad . \tag{16}$$

Utilizing these simplifications we may now obtain the following equation for the current $I_2(\xi_2)$ from equations (13) or (14)

$$S(\xi_2)\, I_2 + \mathcal{E}_2\, \delta(\xi_2 - \xi_\alpha) = 0 \quad , \tag{17}$$

where the operator $S(\xi_2)$ is defined below

$$S(\xi_2)I_2 = \frac{i\omega\mu_o}{4\pi k^2} \left\{ \left[\frac{\partial^2}{\partial\xi_2^2} + k^2\right] L_1\,[I_2, \xi_2] + \cos 2\Delta \left[\frac{\partial^2}{\partial\xi_2^2} + k^2\right] \right.$$

$$\left. L_2\,[I_2,\xi_2] + \sin^2 2\Delta \frac{\partial}{\partial\xi_2} L_3\,[I_2,\xi_2] - I_2(\xi_2)\, z \right\} \quad . \tag{18}$$

The functionals, L_1, L_2, and L_3 are written as

$$L_1\,[I_2,\xi_2] = \int_o^\ell I_2(\zeta)\, \frac{e^{ikR_{22}}}{R_{22}}\, d\zeta \quad , \tag{19a}$$

$$L_2\,[I_2,\xi_2] = \int_o^\ell I_2(\zeta)\, \frac{e^{ikR}}{R}\, d\zeta \tag{19b}$$

and

$$L_3\,[I_2,\zeta] = \int_o^\ell I_2(\zeta)\, \frac{e^{ikR}}{R^3}\, [ikR-1]\, \zeta d\zeta \quad , \tag{19c}$$

where

$$R = \sqrt{\xi_2^2 + \zeta^2 + 2\xi_2\zeta\cos 2\Delta + a^2} \qquad (20.)$$

We see that the symmetrically driven structure automatically satisfies the continuity of current constraint at the corner and from equation (16) it follows that

$$\left.\frac{dI_2(\xi_2)}{d\xi_2}\right|_{\xi_2} = 0 \qquad (21)$$

in order to satisfy the conservation of charge at the corner. We denote the fact that the solution of equation (17) is the symmetrical component of the current $I_2(\xi_2)$ on the structure by placing a superscript s on the current.

We may therefore write that $I_2^s(\xi_2)$ is a solution of

$$S(\xi_2)\, I_2^s + \mathcal{E}_2\delta(\xi_2 - \xi_\alpha) = 0 \qquad (22)$$

Subject to the conditions

$$I_2^s(\ell) = 0 \quad \text{and} \quad \left.\frac{dI_2^s(\xi_2)}{d\xi_2}\right|_{\xi_2 = 0} = 0 \,. \qquad (23)$$

The symmetric component of the current on leg No. 1, $I_1^s(\xi_1)$ is given by

$$I_1^s(\xi_1) = I_2^s(\xi_2) \;;\; \text{when } \xi_1 = -\xi_2 \qquad (24)$$

The antisymmetrical component of the current is obtained by setting $\mathcal{E}_1 = -\mathcal{E}_2$ (i.e., reversing the direction of the generator on leg 1) in equations (13) and (14). It follows then that I_1 and I_2 obey the following relationship

$$I_1(\xi_1) = -I_2(\xi_2) \;, \text{ when } \xi_1 = -\xi_2 \;, \qquad (25)$$

and the current $I_2(\xi_2)$ is a solution of

$$A(\xi_2)\, I_2 + \mathcal{E}_2\delta(\xi_2 - \xi_\alpha) = 0 \,. \qquad (26)$$

The operator $A(\xi_2)$ is given by

$$A(\xi_2)I_2 = \frac{I\omega\mu_o}{4\pi k^2}\left\{ \left[\frac{\partial^2}{\partial\xi_2^2} + k^2\right] M_1[I_2,\xi_2] - \cos 2\Delta \left[\frac{\partial^2}{\partial\xi_2^2} + k^2\right] \right.$$

$$\left. M_2[I_2,\xi_2] - \sin^2 2\Delta \frac{\partial}{\partial\xi_2} M_3[I_2,\xi_2] - I_2(\xi_2)\, Z \right\} \tag{27}$$

where the functionals M_1, M_2, and M_3 are written as

$$M_1[I_2,\xi_2] = \int_o^\ell I_2(\zeta)\, \frac{e^{ikR_{22}}}{R_{22}} d\zeta \quad , \tag{28a}$$

$$M_2[I_2,\xi_2] = \int_o^\ell I_2(\zeta)\, \frac{e^{ikR}}{R}\, d\zeta \quad , \tag{28b}$$

and

$$M_3[I_2,\xi_2] = \int_o^\ell I_2(\zeta)\, \frac{e^{ikR}}{R^3}\, [ikR - 1]\, \zeta d\zeta \quad . \tag{28c}$$

We see from equation (25) that the currents on the antisymmetrically driven antenna satisfy the charge conservation condition at the corner and in order to satisfy current continuity at this point we must have

$$I_2(o) = 0 \quad . \tag{29}$$

We denote the fact that the solution of equation (26) is the antisymmetrical component of the current $I_2(\xi_2)$ on the structure by placing a superscript a on the current. It follows then that $I_2^a(\xi_2)$ is a solution of

$$A(\xi_2)I_2^a(\xi_2) + \epsilon_2\delta(\xi_2-\xi_\alpha) = o \tag{30}$$

subject to the conditions

$$I_2^a(\ell) = o \quad ,$$

$$I_2^a(o) = o \quad , \tag{31}$$

and that the antisymmetric component of the current on leg No. 1, $I_1^a(\xi_1)$ is given by

$$I_1^a(\xi_1 0 = -I_2^a(\xi_2) \text{ , when } \xi_1 = -\xi_2 \quad . \tag{32}$$

Figure 3 shows the direction of the generators for the symmetrical and antisymmetrical cases discussed above.

Symmetric Excitation

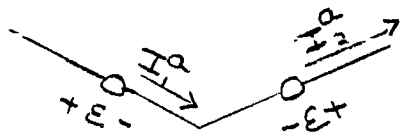

Antisymmetric Excitation

Figure 3

When the antenna is excited by a generator of $+\mathcal{E}$ volts, located on leg 1, the current is given by

$$I_{1\,2} = \frac{1}{2}\left[I_{1\,2}^s - I_{1\,2}^a \right] \tag{33}$$

and when the generator is on leg 2 as

$$I_{1\,2} = \frac{1}{2}\left[I_{1\,2}^s + I_{1\,2}^a \right] \quad . \tag{34}$$

When the generator is located at the corner, the antenna is driven symmetrically and the current on each leg is given by

$$I_{1\,2} = \frac{1}{2} I_{1\,2}^s \tag{35}$$

II. Variational Method for Determining the Current

In Appendix J a variational principle that leads to a solution of equations similar to (22) and (26) by a method of successive approximations was described.

In order to be able to apply this method to the present problem, the operators S and A must display the following symmetry property

$$\left\langle I_\alpha,\ SI_\beta \right\rangle = \left\langle I_\beta\ SI_\alpha \right\rangle$$

and

$$\left\langle I_\alpha,\ AI_\beta \right\rangle = \left\langle I_\beta,\ AI_\alpha \right\rangle \tag{36a.}$$

for any two functions I_α and I_β from their field of definition. Here, the brackets indicate the inner product, defined as

$$\left\langle I_\alpha,\ SI_\beta \right\rangle = \int_0^\ell I_\alpha \cdot SI_\beta \, d\xi_2 \quad . \tag{36 b.}$$

It is shown in Appendix K-I, that equation (36) is indeed satisfied, thereby allowing us to apply the previously mentioned variational principle.

In the work that follows we shall obtain expressions solely for the current on leg 2 of the antenna and therefore we drop the subscript 2 on our current notation. The current on leg 1 is easily obtained from these expressions by utilizing equations (24) and (32).

We first examine the symmetrical component of the current on leg 2, I^s. This quantity is a solution of the equation

$$SI^s + K = 0 \tag{37}$$

where K represents the driving function $\varepsilon\delta(\xi_2 - \xi_\alpha)$. The current is furthermore subject to the following end conditions

$$I^s(\ell) = 0$$

$$\left.\frac{dI^s}{d\xi_2}\right|_{\xi_2 = 0} = 0 \tag{38}$$

Let us consider the driving functions K_α and K_β and their corresponding currents I^s_α and I^s_β on leg 2. These quantities satisfy the equations

$$SI_\alpha^s + K_\alpha = 0 \quad ,$$

$$SI_\beta^s + K_\beta = 0 \tag{39}$$

and the current, I_α^s and I_β^s satisfy the end conditions (38). The function

$$z_{\alpha\beta} = \frac{-\left\langle I_\alpha^s,\ SI_\beta^s \right\rangle}{\left\langle K_\alpha,\ I_\beta^s \right\rangle \left\langle K_\beta,\ I_\alpha^s \right\rangle} \quad , \tag{40}$$

is then stationary with respect to variations in I_α^s and I_β^s, when the unvaried functions I_α^s and I_β^s satisfy (39). If I_α^s and I_β^s are exact solutions of (39) then

$$\frac{1}{z_{\alpha\beta}} = \left\langle \bar{K}_\alpha,\ \bar{I}_\beta^s \right\rangle = \left\langle \bar{K}_\beta,\ \bar{I}_\alpha^s \right\rangle \tag{41}$$

As was described in Appendix J, the precision in calculating $z_{\alpha\beta}$ by means of (40) is greater than the precision of the initial trial functions I_α^s and I_β^s, so that (40) may be taken as a basis of a method of successive approximations when K_α and K_β are delta functions.

Thus, if we choose

$$K_\alpha = \mathcal{E}\delta(\xi_2 - \xi_\alpha) \tag{42}$$

and

$$K_\beta = \mathcal{E}_\beta\delta(\xi_2 - \xi_\beta) \tag{43}$$

we have that

$$\frac{1}{z_{\alpha\beta}} = \left\langle K_\beta,\ I_\alpha^s \right\rangle = \mathcal{E}_\beta\ I_\alpha^s(\xi_\beta) \tag{44}$$

Substituting (44) into the left hand side of (40) we obtain

$$I_\alpha^s(\xi_\beta) = \frac{-\left\langle K_\alpha,\ I_\beta^s \right\rangle \left\langle K_\beta,\ I_\alpha^s \right\rangle}{\mathcal{E}_\beta \left\langle I_\alpha^s,\ SI_\beta^s \right\rangle} \quad . \tag{45}$$

Equation (45) is our variational principle for the current I^s_α. By substituting a set of trial functions for I^s_α and I^s_β, which satisfy the boundary bonditions, (38), into the right hand side of (45), we will obtain a more precise expression for I^s_α if the initial trial functions are reasonably close to the exact solution. Greater accuracy may be obtained by repeating the calculation a second time utilizing the resultant current from the first calculation. Repetition of this procedure obviously leads to a successive approximation method. Vainshtein[1] has shown that on a straight wire a trial function composed of a sum of traveling waves satisfying the proper end conditions leads to an extremely accurate expression for the current on the first calculation. It is for this reason that we will choose the same type of expression for our first trial function; see Appendix K-II.

It is convenient at this point to consider the inner product $\left\langle I^s_\alpha, SI^s_\beta \right\rangle$. We see from (18) that it may be written in the following manner:

$$\left\langle I^s_\alpha, SI^s_\beta \right\rangle = \int_0^\ell I^s_\alpha(\xi_2)\, SI^s_\beta \, d\xi_2 =$$

$$\frac{i\omega\mu_0}{4\pi k^2} \left[J_1 + \cos 2\Delta\, J_2 + \sin^2 2\Delta J_3 - ZJ_4 \right] , \tag{46}$$

where

$$J_1 = \int_0^\ell I^s_\alpha(\xi_2) \left[\frac{\partial^2}{\partial \xi_2^2} + k^2 \right] L_1[I^s_\beta\ \xi_2] d\xi_2 , \tag{47}$$

$$J_2 = \int_0^\ell I^s_\alpha(\xi_2) \left[\frac{\partial^2}{\partial \xi_2^2} + k^2 \right] L_2[I^s_\beta\ \xi_2]\, d\xi_2 , \tag{48}$$

$$J_3 = \int_0^\ell I^s_\alpha(\xi_2)\ \frac{\partial}{\partial \xi_2} L_3\ [I^s_\beta\ \xi_2]\, d\xi_2 \tag{49}$$

and

$$J_4 = \int_0^{\ell} I_\alpha^s(\xi_2)\, I_\beta^s(\xi_2)\, d\xi_2 \tag{50}$$

Utilizing equation (38) J_1, J_2 and J_3 may be written in a more convenient manner:

$$J_1 = \int_0^{\ell} \left[\frac{d^2}{d\xi_2^2} + k^2\right] I_\alpha^s(\xi_2) \cdot L_1[I_\beta^s, \xi_2]\, d\xi_2 - I_\alpha^s(o) \left.\frac{\partial L_1[I_\beta^s, \xi_2]}{\partial \xi_2}\right|_{\xi_2=o}$$

$$\left. - \frac{dI_\alpha^s(\xi_2)}{d\xi_2} \cdot L_1\,[I_\beta^s, \xi_2]\right|_{\xi_2=\ell}, \tag{51}$$

$$J_2 = \int_0^{\ell} \left[\frac{d^2}{d\xi_2^2} + k^2\right] I_\alpha^s(\xi_2) \cdot L_2[I_\beta^s, \xi_2]\, d\xi_2 - I_\alpha^s(o) \left.\frac{\partial L_2[I_\beta^s, \xi_2]}{\partial \xi_2}\right|_{\xi_2=o}$$

$$\left. - \frac{dI_\alpha^s}{d\xi_2} \cdot L_2\,[I_\beta^s,\, \xi_2]\right|_{\xi_2=\ell} \tag{52}$$

and

$$J_3 = -\int_0^{\ell} \frac{dI_\alpha^s(\xi_2)}{d\xi_2}\, L_3\,[I_\beta^s,\, \xi_2]\, d\xi_2 - I_\alpha^s(o)\, L_3\,[I_\beta^s,\, \xi_2] \Big|_{\xi_2=0} \tag{53}$$

Thus, equation (45) along with (46) and (50) - (53) enable us to prescribe the symmetrical component of the current on a Vee antenna, when the trial functions are chosen to satisfy (38).

A similar prescription for the antisymmetric component of the current on leg 2 may be obtained by using the same procedure outlined above. In this case, the currents I^a_α and I^a_β and their corresponding driving functions K_α and K_β satisfy

$$\begin{aligned} AI^a_\alpha + K_\alpha &= o \\ AI^a_\beta + K_\beta &= o \end{aligned} \tag{54}$$

and the end conditions on the current are

$$I^a_{\substack{\alpha \\ \beta}}(o) = I^a_{\substack{\alpha \\ \beta}}(\ell) = o. \tag{55}$$

We again select a delta function excitation so that

$$K_\alpha = \mathcal{E}\,\delta(\xi_2 - \xi_\alpha)$$

and (56)

$$K_\beta = \mathcal{E}_\beta \delta(\xi_2 - \xi_\beta) \quad ,$$

thereby permitting us to write the following stationary expression for the antisymmetric component of current on leg 2:

$$I^a_\alpha(\xi_\beta) = \frac{-\langle K_\alpha, I^a_\beta\rangle \langle K_\beta, I^a_\alpha\rangle}{\mathcal{E}_\beta \langle I^a_\alpha, AI^a_\beta\rangle} \quad . \tag{57}$$

Here, the first trial function to be substituted into the right hand side of (57) is composed of a sum of traveling waves satisfying (55); see Appendix K-II.

We see from equation (27) that the inner product, $\langle I^a_\alpha, AI^a_\beta\rangle$, may be written as

$$\langle I^a_\alpha, AI^a_\beta\rangle = \int_o^\ell I^a_\alpha(\xi_2)\, AI^a_\beta \, d\xi_2 = \frac{i\omega\mu_o}{4\pi k^2}\left[N_1 - \mathrm{Cos}2\Delta N_2 - \mathrm{Sin}^2\Delta N_3 - ZN_4\right], \tag{58}$$

where

$$N_1 = \int_o^{\ell} I_\alpha^a(\xi_2)\left[\frac{\partial^2}{\partial \xi_2^2} + k^2\right] M_1[I_\beta^a \quad \xi_2]\, d\xi_2 \quad , \tag{59}$$

$$N_2 = \int_o^{\ell} I_\alpha^a(\xi_2)\left[\frac{\partial^2}{\partial \xi_2^2} + k^2\right] M_2[I_\beta^a \, , \, \xi_2]\, d\xi_2 \quad , \tag{60}$$

$$N_3 = \int_o^{\ell} I_\alpha^a(\xi_2) \frac{\partial}{\partial \xi_2} M_3\, [I_\beta^a \quad \xi_2]\, d\xi_2 \tag{61}$$

and

$$N_4 = \int_o^{\ell} I_\alpha^a(\xi_2)\; I_\beta^a\,(\xi_2)\, d\xi_2 \quad . \tag{62}$$

Utilizing equation (55) we rewrite N_1, N_2 and N_3 as

$$N_1 = \int_o^{\ell} \frac{d^2}{d\xi_2^2} + k^2 \quad I_\alpha^a(\xi_2) \cdot M_1\, [I_\beta^a, \, \xi_2]\, d\xi_2 - \frac{dI_\alpha^a}{d\xi_2} M_1\, [I_\beta^a, \, \xi_2] \Bigg|_o^{\ell} \quad , \tag{63}$$

$$N_2 = \int_o^{\ell} \left[\frac{d^2}{d\xi_2^2} + k^2\right] I_\alpha^a\,(\xi_2) \cdot M_2\, [I_\beta^a, \, \xi_2]\, d\xi_2 \tag{64}$$

and

$$N_3 = -\int_0^{\ell} \frac{dI_\alpha^a}{d\xi_2} \, M_3 \left[I_\beta^a, \xi_2 \right] d\xi_2 \quad . \tag{65}$$

Thus, equation (57) along with (58) and (62) - (65) enable us to prescribe the antisymmetrical component of the current on a Vee antenna, when the trial functions are chosen to satisfy (55).

It is now possible to determine the current distribution at any point on the antenna for a generator at an arbitrary location, by using the above results in conjunction with equations (24), (32), (33) and (34).

III. The Current Distribution on a Vee Antenna Illuminated by a Plane Wave

Stevenson[2] has shown that the current induced on an antenna by a plane wave may be obtained from the solution of the transmission problem. In particular, this method allows us to determine the induced current on the parasitic antenna at the position of the generator on the corresponding transmitting antenna. Since we have been able to prescribe a solution for the current distribution in the transmission case for an arbitrary generator location, we may therefore determine the induced current in the parasitic case at any point on the antenna. The current induced at the position of the gap on the passive antenna is given by

$$I(\xi_\alpha) = \frac{E_{inc} f(\theta,\phi,\psi)}{kZ_t} \tag{66}$$

where ξ_α denotes the gap location, E_{inc} is the amplitude of the incident plane wave and Z_t is the transmitting impedance. This impedance is defined from the transmission problem as

$$Z_t = \frac{\mathcal{E}}{I(\xi_\alpha)} \tag{67}$$

The function $f(\theta, \phi, \psi)$ is proportional to the component of the far field, obtained when the antenna is transmitting with unit current in the gap, along the direction of the incident electric field. The angle ψ defines the polarization angle of the incident plane wave and the angles θ and ϕ are the elevation and azimuthal angles respectively which define the direction of incidence of the plane wave.

If we consider the Vee transmitting antenna and the geometry displayed in figure 4, it is not difficult to show that for a current I_1 on leg 1 and a current I_2 on leg 2, the radiated far field, $\vec{E}$, at an observation point (r, θ, ϕ) is given by

$$\vec{E} = \frac{i}{4\pi\epsilon_o} \frac{e^{ikr}}{cr} \left\{ k \left[\hat{\theta} F_\theta + \hat{\phi} F_\phi \right] \right\} \tag{68}$$

where

$$F_\theta = F_1 \cos\theta \cos(\phi + \Delta) + F_2 \cos\theta \cos(\phi - \Delta) ,$$

$$F_\phi = -F_1 \sin(\phi + \Delta) - F_2 \sin(\phi - \Delta) \tag{69}$$

and

$$F_1 = \int_{-\ell}^{0} I_1(\zeta)\, e^{-ik \sin\theta \cos(\phi+\Delta)\cdot\zeta}\, d\zeta ,$$

$$F_2 = \int_{0}^{\ell} I_2(\zeta)\, e^{-ik \sin\theta \cos(\phi-\Delta)\zeta}\, e^{-ik\ell \sin\theta \cos(\phi+\Delta)}\, d\zeta . \tag{70}$$

The polarization of the incident electric field may in general be written as

$$\hat{e}_{inc} = -\hat{\theta} \cos\psi - \hat{\phi} \sin\psi , \tag{71}$$

where ψ the polarization angle, shown in figure (4), is the angle between the incident electric field and the plane containing the Z axis and the direction of the incident wave. The function $f(\theta, \phi, \psi)$ is then given by

$$f(\theta,\phi,\psi) = -k[\bar{F}_\theta \cos\psi + \bar{F}_\phi \sin\psi] \tag{72}$$

where the bar indicates that the currents I_1 and I_2 have been normalized so that a unit current flows at the generator terminals.

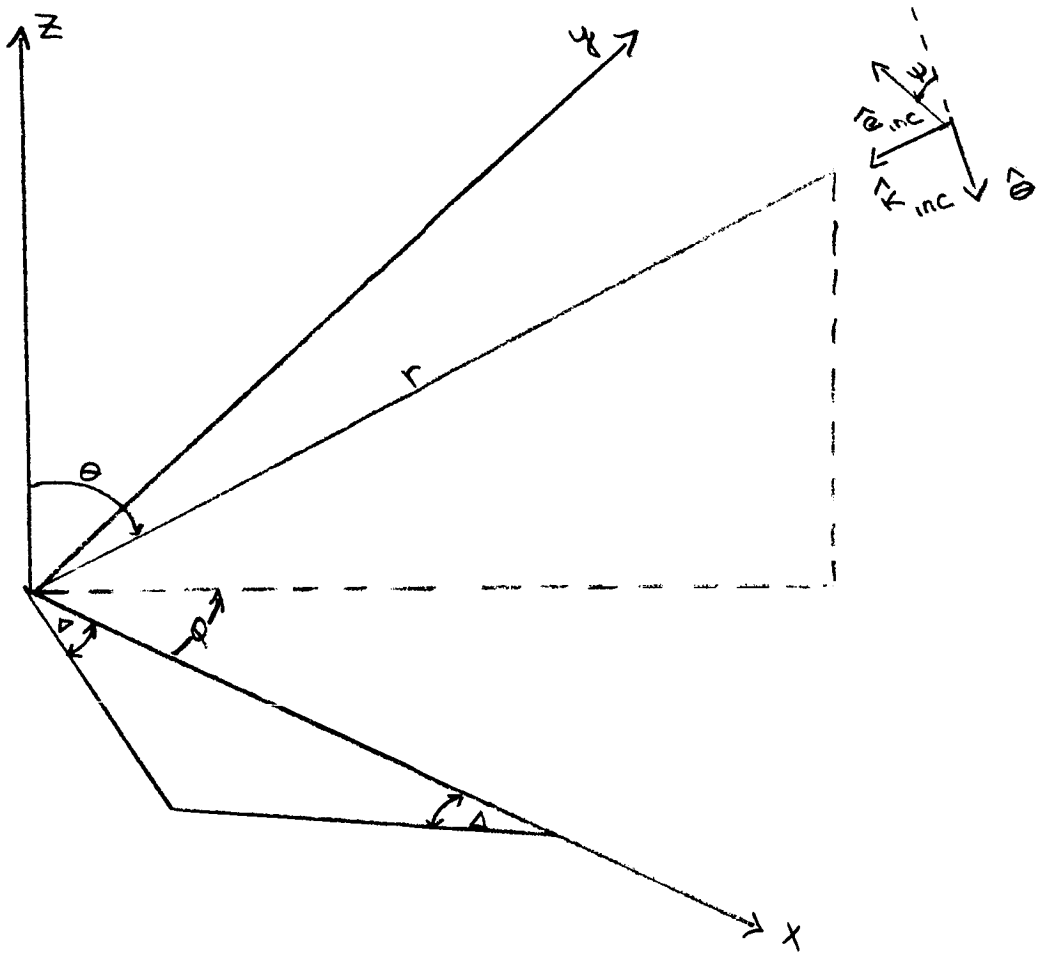

Figure 4

As an example of the procedure involved in calculating the induced current on the antenna, we consider the problem of determining the current distribution on leg 2 when the structure is illuminated by a plane wave. We therefore consider the transmitting antenna to be excited by a generator of $\mathcal{E}$ volts located on leg 2 at the point $\xi_2 = \xi_\alpha$. We then have from (34) that the currents on legs 1 and 2 are given by

$$I_{\frac{1}{2}} = \frac{1}{2}[I_{\frac{1}{2}}^{s} + I_{\frac{1}{2}}^{a}] \tag{73}$$

The symmetric component of the current on leg 2 is determined from (45). In general this current will be a function of the generator position ξ_α and the coordinate ξ_2. The variable ξ_β is replaced on both sides

of (45) by ξ_2. In a like manner, the antisymmetrical component of the current is obtained from (57) as a function of ξ_2 and ξ_α. We then have that

$$I_1^{s}(\xi_1,\xi_\alpha) = I_2^{s}(\xi_2,\xi_\alpha), \quad \text{when } \xi_1 = -\xi_2$$

and

$$I_1^{a}(\xi_1,\xi_\alpha) = -I_2^{a}(\xi_2,\xi_\alpha), \quad \text{when } \xi_1 = -\xi_2.$$

We obtain the total current distribution on each wire [i.e. $I_1(\xi_1,\xi_2)$ and $I_2(\xi_2,\xi_\alpha)$] from equation (73). The transmitting impedance Z_t is then given by

$$Z_t = \frac{\mathcal{E}}{I_2(\xi_\alpha^{\circ}, \xi_\alpha)} \tag{75}$$

and the functions F_Θ and F_ϕ, necessary for the calculation of $f(\Theta,\phi,\psi)$, are obtained from the following normalized values of F_1 and F_2

$$\bar{F}_1 = \frac{1}{I_2(\xi_\alpha,\xi_\alpha)} \int_{-\ell}^{o} I_1(\zeta,\xi_\alpha)\, e^{-ik \sin\Theta \cos(\phi+\Delta)\zeta}\, d\zeta \quad ,$$

$$\bar{F}_2 = \frac{1}{I_2(\xi_\alpha,\xi_\alpha)} \int_{o}^{\ell} I_2(\zeta,\xi_\alpha)\, e^{-ik \sin\Theta \cos(\phi-\Delta)\zeta} e^{-ik\ell \sin\Theta\cos(\phi+\Delta)}\, d\zeta \quad . \tag{76}$$

We calculate $f(\Theta,\phi,\psi)$ from (69) and (72), and substitute these results back into (66), giving us an expression for the induced current on wire 2 as a function of the variable ξ_α and the angles Θ,ϕ,ψ. The current distribution of the entire wire is then obtained by varying ξ_α from o to ℓ.

The procedure utilized to obtain the induced current on wire 1 follows directly from the above discussion.

APPENDIX K-I

In order to prove the symmetry condition for the operators S and A we will show that both operators may be divided into components S_n and A_n such that, the inner product for each component may be written in the form

$$\left\langle I_\alpha S_n I_\beta \right\rangle = \int_0^\ell \int_0^\ell I_\alpha(\xi_2)\, I_\beta(\zeta)\, h_n(\xi_2,\zeta)\, d\zeta d\xi_2 \,, \tag{1}$$

where

$$h_n(\xi_2,\zeta) = h_n(\zeta,\xi_2) \tag{2}$$

It can then be seen through an interchange of integration variables in (1) and application of (2) that

$$\left\langle I_\alpha, S_n I_\beta \right\rangle = \left\langle I_\beta, S_n I_\alpha \right\rangle \quad , \tag{3}$$

and thus since the sum of symmetric operators is also a symmetric operator, our proof will be complete. We write the quantity SI_β as

$$SI_\beta = \sum_{n=1}^{s} S_n I_\beta \tag{4}$$

where

$$S_1 I_\beta = k^2 L_1 [I_\beta \xi_2] \,, \tag{5}$$

$$S_2 I_\beta = \frac{\partial^2}{\partial \xi_2^2} L_1[I_\beta \xi_2] \tag{6}$$

$$S_3 I_\beta = k^2 \cos 2\Delta L_2[I_\beta \xi_2] \tag{7}$$

$$S_4 I_\beta = Z I_\beta(\xi_2) \tag{8}$$

and

$$S_5 I_\beta = \text{Cos } 2\Delta \frac{\partial^2}{\partial \xi_2^2} L_2[I_\beta \xi_2] + \sin^2 2\Delta \frac{\partial}{\partial \xi_2} L_3[I_\beta, \xi_2] \tag{9}$$

We see from equation (19a) that $h_1(\xi_2, \zeta)$ is given by

$$h_1(\xi_2, \zeta) = \frac{e^{ik\sqrt{(\xi_2-\zeta)^2 + a^2}}}{\sqrt{(\xi_2-\zeta)^2 + a^2}} \tag{10}$$

which obviously satisfies (2), thereby proving S_1 to be symmetric. The function $h_2(\xi_2, \zeta)$ is given by

$$h_2(\xi_2, \zeta) = \frac{\partial^2}{\partial \xi_2^2} h_1(\xi_2, \zeta) = 2 \frac{\partial h_1}{\partial r} + 4(\xi_2-\zeta)^2 \frac{\partial^2 h_1}{\partial r^2} \tag{11}$$

where

$$r = (\xi_2 - \zeta)^2 \tag{12}$$

Thus, $h_2(\xi_2, \zeta)$ obviously satisfies the condition of (2), thereby proving S_2 to be symmetric. The function $h_3(\xi_2, \zeta)$ is obtained from (19b) and is given by

$$h_3(\xi_2,\zeta) = \frac{e^{ikR}}{R} \tag{13}$$

where

$$R = \sqrt{\xi_2^2 + \zeta^2 + 2\zeta\xi_2 \cos 2\Delta + a^2} \tag{14}$$

It is obvious that h_3 satisfies (2). The function h_4 is a constant so that (2) is automatically satisfied, and we are left with showing that h_5 satisfies equation (2).

The function $h_5(\xi_2,\zeta)$ is obtained from (19b) and (19c) and is given by

$$h_5(\xi_2,\zeta) = \cos 2\Delta \frac{\partial^2}{\partial\xi_2^2} \frac{e^{ikR}}{R} + \xi \sin^2 2\Delta \frac{\partial}{\partial\xi_2}\left[\frac{e^{ikR}}{R^3}(ikR - 1)\right] \tag{15}$$

Performing these indicated operations we obtain

$$h_5(\xi_2,\zeta) = \cos 2\Delta \frac{e^{ikR}}{R^3}[ikR - 1] + \frac{(\zeta + \xi_2 \cos 2\Delta)(\xi_2 + \zeta \cos 2\Delta)}{R} \frac{d}{dR}\left[\frac{e^{ikR}}{R^3}(ikR-1)\right] \tag{16}$$

Since the function $R(\xi_2,\zeta)$ satisfies equation (2) we see that $h_5(\xi_2,\zeta)$ must also satisfy (2), thereby completing the proof. The proof of the symmetry for the operator A, follows directly from that given above since the A_n may be constructed so that they have the same form as the S_n terms.

APPENDIX K-II

As an example of the first order trial functions that may be substituted into equations (45) and (57), we consider currents made up of traveling waves which satisfy the appropriate boundary conditions. Thus, in the case of (45), the symmetrical component of the current on wire 2 may be approximated by

$$I^s_\alpha(\xi_2) = e^{iw_p|\xi_2-\xi_\alpha|} + c_1 e^{iw_p(\xi_2-\xi_\alpha)} + c_2 e^{-iw_p(\xi_2-\xi_\alpha)}, \tag{1}$$

where w_p is an appropriate wavenumber for the lossy conductor. The first term in (1) represents a current wave diverging from the source, while the second and third terms represent contributions due to reflections from the ends. In order to satisfy the end conditions, (38), the constants c_1 and c_2 are given by

$$c_1 = \frac{e^{2iw_p\xi_\alpha} e^{-iw_p\ell} - e^{iw_p\ell}}{2\cos w_p\ell} \tag{2}$$

$$c_2 = \frac{-e^{iw_p\ell}\left[1 + e^{-2iw_p\xi_\alpha}\right]}{2\cos w_p\ell} \tag{2}$$

The trial function $I^s_\beta(\xi_2)$ is given by a similar expression with ξ_α replaced by ξ_β.

The first trial function for the antisymmetrical current component to be substituted into (57) is given by

$$I^s_\alpha(\xi_2) = e^{iw_p|\xi_2-\xi_\alpha|} + c_3 e^{iw_p(\xi_2-\xi_\alpha)} + c_4 e^{-iw_p(\xi_2-\xi_\alpha)} \tag{3}$$

where

$$c_3 = \frac{e^{2iw_p\xi_\alpha} e^{-iw_p\ell} - e^{iw_p\ell}}{2i \sin w_p\ell} \tag{4}$$

and

$$c_4 = \frac{e^{iw_p\ell}\left[e^{-2iw_p\xi_\alpha}-1\right]}{2i \sin w_p\ell} \tag{5}$$

The trial function $I_\beta^{\bar{a}}(\xi_2)$ is obtained by replacing ξ_α with ξ_β in equations (3) through (5).

REFERENCES

1. L. A. Vainshtein, Soviet Phys. Tech. Phys., 6, 19, (1961).
2. A. F. Stevenson, Quart. Appl. Math., 5, 369, (1948).

APPENDIX L

THE EFFECTS OF CONFIGURATION AND MATERIAL VARIATIONS ON ANTENNA PERFORMANCE

I. Introduction

We wish to investigate the manner in which variations in geometry and/or material affect the performance of an antenna. In order to accomplish this goal, we first consider a general perturbation method which permits us to determine the change in the current distribution on the structure. This procedure is then applied to an arbitrary thin wire antenna, and the appropriate equations for the current variation on such a structure are obtained. These results are used to aid in determining the variation in the far field pattern, power dissipated and efficiency of the thin wire antenna.

2. General Consideration of Current Perturbations

In this section, we consider a perturbation technique similar to that used by Karal and Keller[1] in a study of wave propagation in a random, sourceless medium. The axial current distribution $I_o(s)$, on an arbitrary thin wire antenna excited by an applied electric field is a solution of

$$GI_o + K = 0 , \tag{1}$$

where K is the component of the applied field that is tangent to the axis of the wire, and s is the arc length along the axis of the wire. In addition, this current distribution is subject to the two end conditions

$$I_o(s_1) = F_1(s_1) \quad \text{and} \quad I_o(s_2) = F_2(s_2) , \tag{2}$$

where F_1 and F_2 are functions of the end terminations. The operator G is a function of the antenna geometry and material and we constrain the antenna terminations to retain their original electrical properties after the structure is perturbed. That is, if the antenna originally has open circuited terminations, the perturbed antenna will have the same terminations although the end surfaces of the antenna may be displaced in space.

Let us vary the antenna geometry and/or material, so that this perturbed structure is characterized by the operator G^*

$$G^* = G + \epsilon G_1 + \epsilon^2 G_2 + \mathcal{O}(\epsilon^3) . \tag{3}$$

Here, ϵ is a measure of the variation of the antenna from the original geometrical and material configuration, and the perturbing operators G_1 and G_2 represent the effects of the departure from the original state.

A variation of the antenna geometry will affect the tangential component of the applied field thereby subjecting the antenna to a different excitation force K^* given by

$$K^* = K + \epsilon K_1 + \epsilon^2 K_2 + \mathcal{O}(\epsilon^3) . \tag{4}$$

It follows then, that the current distribution $I^*(s^*)$ on the perturbed antenna is a solution of the equation

$$[G + \epsilon G_1 + \epsilon^2 G_2 + \mathcal{O}(\epsilon^3)]I^* + K + \epsilon K_1 + \epsilon^2 K_2 + \mathcal{O}(\epsilon^3) = 0 . \tag{5}$$

Here, s^* represents the arc length along the axis of the perturbed antenna. We may rewrite equation (5) by premultiplying it by the inverse operator G^{-1} and utilizing equation (1), thereby obtaining

$$I^* = I_o - \epsilon[G^{-1} G_1 I^* + G^{-1} K_1] - \epsilon^2[G^{-1} G_2 I^* + G^{-1} K_2] + \mathcal{O}(\epsilon^3) . \tag{6}$$

Successive iterations of equation (6) allow us to write the following equation for the current distribution $I^*(s^*)$ in terms of the original current $I_o(s)$:

$$I^*(s^*) = I_o(s) - \epsilon[G^{-1} G_1 I_o + G^{-1} K_1]$$
$$+ \epsilon^2[G^{-1} G_1 G^{-1} G_1 I_o - G^{-1} G_2 I_o + G^{-1} G_1 G^{-1} K_1 - G^{-1} K_2]$$
$$+ \mathcal{O}(\epsilon^3) . \qquad (7)$$

By setting K_1 and K_2 equal to zero in the above equation one obtains the results referred to in reference [1]. The variation in current distribution, ΔI, due to the perturbation of the antenna may now be expressed as

$$\Delta I = I^*(s^*) - I_o(s) = \epsilon\, i_1(s) + \epsilon^2\, i_2(s) + \mathcal{O}(\epsilon^3) , \qquad (8)$$

where

$$i_1(s) = - [G^{-1} G_1 I_o + G^{-1} K_1] \qquad (9)$$

and

$$i_2(s) = [G^{-1} G_1 G^{-1} G_1 I_o - G^{-1} G_2 I_o + G^{-1} G_1 G^{-1} K_1 - G^{-1} K_2] .$$

Equations (8) and (9) present a general expression for the current variation in terms of the original current. It is now necessary to consider the determination of the inverse operator G^{-1} and the perturbing operators, G_1 and G_2.

The Greens function of the operator G, denoted by $g(s,s')$, is defined by the equation

$$G\, g(s,s') = \delta(s-s') \qquad (10)$$

where $\delta(s-s')$ is the Dirac delta function and g is subject to the boundary conditions given by equation (2). The inverse operator G^{-1}, may then be written in terms of g, as shown

$$G^{-1} f = \int_{s'} g(s,s')f(s')ds' \qquad (11)$$

where the integration is carried out along the axis of the antenna structure. It is easily seen that if the original antenna is excited by a delta function generator of $\mathcal{E}$ volts at the point $s = s'$, then

$$K = \mathcal{E}\, \delta(s-s') \qquad (12)$$

and therefore

$$G^{-1} f = - \frac{1}{\mathcal{E}} \int_{s'} I_o(s,s')f(s')ds' , \qquad (13)$$

where $I_o(s,s')$ is the current at the point s due to a generator located at the point s'. When the antenna is located in an isotropic medium, we may utilize the reciprocity theorem and rewrite (13) in terms of the current at the point s' due to a source located at s,

$$G^{-1} f = -\frac{1}{\epsilon} \int_{s'} I_o(s',s) f(s') ds' . \qquad (14)$$

Utilizing equations (8), (9) and (13) or (14) we may now determine the variation in the current distribution on the perturbed antenna, in terms of the original current distribution.

The operators G_1 and G_2 and the functions K_1 and K_2 will be calculated for the case of an arbitrary thin wire antenna in the next section.

3. Current Variation in an Arbitrary Thin Wire Antenna

We consider a curved cylindrical coordinate in which s is the arc length along the axis of the antenna and $\hat{s}$ is the unit tangent vector at the point s. If the radius a of the wire is sufficiently small so that the current density may be considered uniform around the periphery of the wire, the induced tangential electric field at the surface of the wire is given by(2)

$$(E_{tan})_{induced} = \frac{1}{i\omega\, 4\pi\, \epsilon_m} \int_{s'} I_o(s') \left[\frac{\partial^2}{\partial s \partial s'} G_a(s,s') - k^2(\hat{s}\cdot\hat{s}')G_a(s,s')\right] ds' \quad (15)$$

where $I_o(s')$ is the current at s' in the direction parallel to the axial tangent $\hat{s}'$, and the integration is carried out along the axis of the wire. An $e^{-i\omega t}$ time dependence has been assumed and the quantity ϵ_m is the permitivity of the medium in which the antenna is immersed. The function $G_a(s,s')$ is given by

$$\frac{e^{ikr(s,s',a)}}{r(s,s',a)} \quad (16)$$

where

$$r = \sqrt{r_o^2 + a^2} \quad (17)$$

and r_o is the linear distance between the points p(o,o,s) and p'(o,o,s'). For a δ-function excitation of the antenna at the point $p_o(o,o,s_o)$ we express the applied tangential electric field as

$$K = \mathcal{E}\, \delta(s-s_o) \,. \quad (18)$$

The internal impedance of the wire per unit length is denoted as $Z_i(s)$ so that the boundary value problem of the wire antenna may finally be formulated as

$$\frac{1}{i\omega\, 4\pi\, \epsilon_m} HI_o - I_o Z_i + K = 0 \,, \quad (19)$$

where

$$HI_o = \int_{s'} I_o(s') \left[\frac{\partial^2}{\partial s \partial s'} G_a(s,s') - k^2(\hat{s}\cdot\hat{s}')G_a(s,s')\right] ds' \quad (20)$$

and K is given by (18). We now see by comparison with equation (1) that the operator G is defined by

$$GI_o = \left[\frac{1}{i\omega\, 4\pi\, \epsilon_m} H - Z_i\right] I_o \,. \quad (21)$$

The variation in G may be determined by calculating the variation in H

and the variation in Z_i independently, thereby allowing us to separate to some extent† the material and geometrical variations. We first consider the variation in H and rewrite equation (20) as follows

$$HI_o = \int_{s'} I_o(s')F\, ds' , \tag{22}$$

where

$$F = \frac{\partial^2}{\partial s \partial s'} G_a(s,s') - k^2(\hat{s}\cdot\hat{s}')\, G_a(s,s') . \tag{23}$$

Performing the indicated operations on the function G_a we may express F as

$$F = r_{s'}\, r_s\, g_2(r) + r_{ss'}\, g_1(r) - k^2\, \tau\, G_a(r) = F(r, r_{s'}, r_s, r_{ss'}, \tau) , \tag{24}$$

where

$$G_a(r) = \frac{e^{ikr}}{r} , \tag{25a}$$

$$g_1(r) = \frac{d\, G_a(r)}{dr} = \frac{[ikr - 1]}{r^2} e^{ikr} , \tag{25b}$$

$$g_2(r) = \frac{d^2\, G_a(r)}{dr^2} = -\frac{[k^2 r^2 + 2ikr - 2]}{r^2} e^{ikr} , \tag{25c}$$

$$\tau(s,s') = \hat{s}\cdot\hat{s}' , \tag{25d}$$

$$r_s(s,s') = \frac{\partial r}{\partial s} , \tag{25e}$$

$$r_{s'}(s,s') = \frac{\partial r}{\partial s'} , \tag{25f}$$

and

$$r_{ss'} = \frac{\partial^2 r}{\partial s \partial s'} . \tag{25g}$$

We now permit the geometrical configuration of the antenna to be varied so that the arc length s' is carried into another arc length s'* given by

$$s'^* = s' + \epsilon\, \phi_1(s') + \epsilon^2\, \phi_2(s') + \mathcal{O}(\epsilon^3) . \tag{26}$$

†The variation in $Z_i(s)$ will be dependent on the geometrical perturbation.

This equation represents the known variation of the antenna geometrical configuration and the transformation of the remainder of the variables of F may be determined in terms of it. Denoting the transformed functions and variables by a star we have

$$s^* = s + \epsilon\,\phi_1(s) + \epsilon^2\,\phi_2(s) + \mathcal{O}(\epsilon^3)\ , \tag{27a}$$

$$r^*(s^*,s'^*) = r(s,s') + \epsilon\,\psi_1(s,s') + \epsilon^2\,\psi_2(s,s') + \mathcal{O}(\epsilon^3)\ , \tag{27b}$$

$$r^*_s(s^*,s'^*) = r_s(s,s') + \epsilon\,\nu_1(s,s') + \epsilon^2\,\nu_2(s,s') + \mathcal{O}(\epsilon^3)\ , \tag{27c}$$

$$r^*_{s'}(s^*,s'^*) = r_{s'}(s,s') + \epsilon\,\mu_1(s,s') + \epsilon^2\,\mu_2(s,s') + \mathcal{O}(\epsilon^3)\ , \tag{27d}$$

$$r^*_{ss'}(s^*,s'^*) = r_{ss'}(s,s') + \epsilon\,\lambda_1(s,s') + \epsilon^2\,\lambda_2(s,s') + \mathcal{O}(\epsilon^3)\ , \tag{27e}$$

and

$$\tau^*(s^*,s'^*) = \tau(s,s') + \epsilon\,\alpha_1(s,s') + \epsilon^2\,\alpha_2(s,s') + \mathcal{O}(\epsilon^3)\ . \tag{27f}$$

In order to calculate the variation of H, denoted by ΔH, we let q^* represent the collection of the transformed arguments of F, q the original arguments and we write

$$(\Delta H)I_o = \Delta(HI_o)\big|_{\Delta I_o = 0} = \int_{s'^*} I_o(s')F(q^*)ds'^* - \int_{s'} I_o(s')F(q)ds'$$

$$= \int_{s'} I_o(s')\left[F(q^*)\,\frac{\partial s'^*}{\partial s'} - F(q)\right]ds'\ . \tag{28}$$

It follows then from (26) that

$$(\Delta H)I_o = \int_{s'} I_o(s')\{[F(q^*) - F(q)] + \epsilon\,F(q^*)\phi_1(s') + \epsilon^2\,F(q^*)\phi_2(s')\}ds'. \tag{29}$$

We now expand $F(q^*)$, about the point $q^* = q$, in a Taylor series and obtain

$$F(q^*) = F(q) + \epsilon\,M_1\,F(q) + \epsilon^2\,M_2\,F(q) + \mathcal{O}(\epsilon^3)\ , \tag{30}$$

where the operators M_1 and M_2 are given by

$$M_1 = \alpha_1(s,s')\,\frac{\partial}{\partial\tau} + \psi_1(s,s')\,\frac{\partial}{\partial r} + \mu_1(s,s')\,\frac{\partial}{\partial r_{s'}} + \nu_1(s,s')\,\frac{\partial}{\partial r_s} + \lambda_1(s,s')\,\frac{\partial}{\partial r_{ss'}} \tag{31}$$

and

$$M_2 = \alpha_2(s,s')\,\frac{\partial}{\partial\tau} + \psi_2(s,s')\,\frac{\partial}{\partial r} + \mu_2(s,s')\,\frac{\partial}{\partial r_{s'}}$$

$$+ \nu_2(s,s')\,\frac{\partial}{\partial r_s} + \lambda_2(s,s')\,\frac{\partial}{\partial r_{ss'}} + \frac{1}{2}\,L_2\ . \tag{32}$$

The operator L_2 is shown below

$$L_2 = \left[\alpha_1(s,s') \frac{\partial}{\partial \tau} + \psi_1(s,s') \frac{\partial}{\partial r} + \mu_1(s,s') \frac{\partial}{\partial r_{s'}} + \nu_1(s,s') \frac{\partial}{\partial r_s} + \lambda_1(s,s') \frac{\partial}{\partial r_{ss}}\right]^2 . \tag{33}$$

By substituting equation (30) into (29) we may write the variation of H in the form of a power series in ϵ

$$(\Delta H) I_o = \epsilon\, h_1\, I_o + \epsilon^2\, h_2\, I_o + \mathcal{O}(\epsilon^3) , \tag{34}$$

where

$$h_1\, I_o = \int_{s'} I_o(s') \left[M_1 + \frac{d\phi_1(s')}{ds'}\right] F(q)\, ds' , \tag{35}$$

$$h_2\, I_o = \int_{s'} I_o(s') \left[M_2 + \frac{d\phi_1(s')}{ds'} M_1 + \frac{d\phi_2(s')}{ds'}\right] F(q)\, ds' \tag{36}$$

and the function $F(q)$ is given by (24).

In order to complete the calculation of the variation of H we must obtain explicit expressions for the variations of the functions which constitute the collection q. The variation of the function $r(s,s')$, given by

$$\Delta r = r^*(s^*,s'^*) - r(s,s') = \epsilon\, \psi_1(s,s') + \epsilon^2\, \psi_2(s,s') + \mathcal{O}(\epsilon^3) \tag{37}$$

defines the change in the r coordinate as we go from the point $(s,s', r(s,s'))$ on the surface σ, defined by $r = r(s,s')$, to its image $(s^*,s'^*, r^*(s^*,s'))$ under the transformation of (26), (27a) and (27b). In order to obtain Δr we also consider the increment

$$\bar{\Delta r} = r^*(s,s') - r(s,s') = \epsilon\, t_1(s,s') + \epsilon^2\, t_2(s,s') + \mathcal{O}(\epsilon^3) , \tag{38}$$

which expresses the change in r as we move from the surface σ to a point on the surface σ^* [the image of σ under the transformations (26), (27a) and (27b)], with the same coordinates (s,s'). The quantity Δr may now be written as

$$\Delta r = r^*(s^*,s'^*) - r^*(s,s') + \bar{\Delta r} , \tag{39}$$

the function $r^*(s^*,s'^*)$ may be expanded about the point (s,s') in a Taylor series leading to

$$r^*(s^*,s'^*) - r^*(s,s') = \frac{\partial r^*(s,s')}{\partial s}\,\Delta s + \frac{\partial r^*(s,s')}{\partial s'}\,\Delta s'$$

$$+ \frac{1}{2}\left[\Delta s\,\frac{\partial}{\partial s} + \Delta s'\,\frac{\partial}{\partial s'}\right]^2 r^*(s,s') + \ldots \quad (40)$$

Substituting this equation along with (38) and the expressions for Δs and $\Delta s'$ given in (26) and (27a), back into (39) results in the following expression for ψ_1 and ψ_2:

$$\psi_1(s,s') = t_1(s,s') + \left[\phi_1(s')\,\frac{\partial}{\partial s'} + \phi_1(s)\,\frac{\partial}{\partial s}\right] r(s,s') \quad (41)$$

and

$$\psi_2(s,s') = t_2(s,s') + \left[\phi_2(s')\,\frac{\partial}{\partial s'} + \phi_2(s)\,\frac{\partial}{\partial s}\right] r(s,s')$$

$$+ \left[\phi_1(s')\,\frac{\partial}{\partial s'} + \phi_1(s)\,\frac{\partial}{\partial s}\right] t_1(s,s') + \frac{1}{2}\left[\phi_1(s)\,\frac{\partial}{\partial s} + \phi_1(s')\,\frac{\partial}{\partial s'}\right]^2 r(s,s'). \quad (42)$$

In order to obtain expressions for Δr_s and $\Delta r_{s'}$, we utilize the chain rule of differentiation to show that

$$\frac{\partial}{\partial s} - \frac{\partial}{\partial s^*} = \epsilon\,\frac{d\phi_1(s)}{ds}\,\frac{\partial}{\partial s} + \epsilon^2\left[\frac{d\phi_2(s)}{ds}\,\frac{\partial}{\partial s} - \left(\frac{d\phi_1(s)}{ds}\right)^2\frac{\partial}{\partial s}\right] . \quad (43)$$

The quantity Δr_s is then written in the following manner

$$\Delta r_s = \frac{\partial r^*(s^*,s'^*)}{\partial s^*} - \frac{\partial r(s,s')}{\partial s} = \frac{\partial}{\partial s^*}\left[r^*(s^*,s'^*) - r(s^*,s'^*)\right]$$

$$+ \frac{\partial}{\partial s}\left[r(s^*,s'^*) - r(s,s')\right] + \left[\frac{\partial}{\partial s^*} - \frac{\partial}{\partial s}\right] r(s^*,s'^*) . \quad (44)$$

It is seen from (38) that

$$r^*(s^*,s'^*) - r(s^*,s'^*) = \epsilon\,t_1(s^*,s'^*) + \epsilon^2\,t_2(s^*,s'^*) + \mathcal{O}(\epsilon^3) . \quad (45)$$

Expanding $t_1(s^*,s'^*)$ and $t_2(s^*,s'^*)$ in a Taylor series about the point $(s^*,s'^*) = (s,s')$ and then utilizing equation (43) one may obtain a power series expansion in ϵ for the first term on the right hand side of (44). The second term on the right hand side is expanded by writing $r(s^*,s'^*)$ in

a Taylor series about (s,s') and the third term is calculated by using this same Taylor series in conjunction with (43). The resultant expressions for ν_1 and ν_2, the first and second order variations in Δr_s may now be written as

$$\nu_1(s,s') = \frac{\partial t_1}{\partial s} + \left[\phi_1(s') \frac{\partial^2}{\partial s \partial s'} + \phi_1(s) \frac{\partial^2}{\partial s^2}\right] r(s,s') \quad , \tag{46}$$

$$\begin{aligned} \nu_2(s,s') = {} & \frac{\partial t_2}{\partial s} + \left[\phi_1(s') \frac{\partial^2}{\partial s \partial s'} + \phi_1(s) \frac{\partial^2}{\partial s^2}\right] t_1(s,s') \\ & + \left[\phi_2(s') \frac{\partial^2}{\partial s \partial s'} + \phi_2(s) \frac{\partial^2}{\partial s^2}\right] r(s,s') \\ & + \frac{1}{2} \frac{\partial}{\partial s} \left[\phi_1(s) \frac{\partial}{\partial s} + \phi_1(s') \frac{\partial}{\partial s'}\right]^2 r(s,s') \\ & - \frac{d\phi_1(s)}{ds} \left[\phi_1(s') \frac{\partial^2}{\partial s \partial s'} + \phi_1(s) \frac{\partial^2}{\partial s^2}\right] r(s,s') \quad . \end{aligned} \tag{47}$$

The expansion for $\Delta r_{s'}$ is similarly obtained, resulting in the following expressions for μ_1 and μ_2,

$$\mu_1(s,s') = \frac{\partial t_1}{\partial s'} + \left[\phi_1(s) \frac{\partial^2}{\partial s \partial s'} + \phi_1(s') \frac{\partial^2}{\partial s'^2}\right] r(s,s') \quad , \tag{48}$$

and

$$\begin{aligned} \mu_2(s,s') = {} & \frac{\partial t_2}{\partial s'} + \left[\phi_1(s) \frac{\partial^2}{\partial s \partial s'} + \phi_1(s') \frac{\partial^2}{\partial s'^2}\right] t_1(s,s') \\ & + \left[\phi_2(s) \frac{\partial^2}{\partial s \partial s'} + \phi_2(s') \frac{\partial^2}{\partial s'^2}\right] r(s,s') \\ & + \frac{1}{2} \frac{\partial}{\partial s'} \left[\phi_1(s) \frac{\partial}{\partial s} + \phi_1(s') \frac{\partial}{\partial s'}\right]^2 r(s,s') \\ & - \frac{d\phi_1(s')}{ds'} \left[\phi_1(s) \frac{\partial^2}{\partial s \partial s'} + \phi_1(s') \frac{\partial^2}{\partial s'^2}\right] r(s,s') \quad . \end{aligned} \tag{49}$$

The expansion of the quantity $\Delta r_{ss'}$ is obtained in an analogous manner. The variation in the differentiation operation corresponding to equation (43) is given by

$$\frac{\partial^2}{\partial s \partial s'} - \frac{\partial^2}{\partial s^* \partial s'^*} = \epsilon N_1 - \epsilon^2 N_2 \quad , \tag{50}$$

where

$$N_1 = \left[\frac{d\phi_1(s')}{ds'} + \frac{d\phi_1(s)}{ds}\right] \frac{\partial^2}{\partial s \partial s'} \quad , \tag{51}$$

and

$$N_2 = \left\{ \left[\frac{d\phi_1(s')}{ds'}\right]^2 + \left[\frac{d\phi_1(s)}{ds}\right]^2 + \frac{d\phi_1(s')}{ds'} \frac{d\phi_1(s)}{ds} - \frac{d\phi_2(s')}{ds'} - \frac{d\phi_2(s)}{ds} \right\} \frac{\partial^2}{\partial s \partial s'} \quad . \tag{52}$$

By utilizing equation (50) and a separation similar to equation (44) we obtain the following expressions for λ_1 and λ_2:

$$\lambda_1(s,s') = \frac{\partial^2 t_1}{\partial s \partial s'} + \frac{\partial^2}{\partial s \partial s'} \left[\phi_1(s') \frac{\partial}{\partial s'} + \phi_1(s) \frac{\partial}{\partial s}\right] r(s,s') - N_1 r(s,s') \quad , \tag{53}$$

$$\begin{aligned} \lambda_2(s,s') = {} & \frac{\partial^2 t_2}{\partial s \partial s'} + \frac{\partial^2}{\partial s \partial s'} \left[\phi_1(s') \frac{\partial}{\partial s'} + \phi_1(s) \frac{\partial}{\partial s}\right] t_1(s,s') - N_1 t_1(s,s') \\ & + \frac{\partial^2}{\partial s \partial s'} \left[\phi_2(s') \frac{\partial}{\partial s'} + \phi_2(s) \frac{\partial}{\partial s}\right] r(s,s') \\ & + \frac{1}{2} \frac{\partial^2}{\partial s \partial s'} \left[\phi_1(s') \frac{\partial}{\partial s'} + \phi_1(s) \frac{\partial}{\partial s}\right]^2 r(s,s') \\ & - N_1 \left[\phi_1(s) \frac{\partial}{\partial s} + \phi_1(s') \frac{\partial}{\partial s'}\right] r(s,s') + N_2 r(s,s') \quad . \end{aligned} \tag{54}$$

It now remains to calculate the variation of $\tau = \hat{s} \cdot \hat{s}'$. This quantity is obtained by a calculation which parallels that used in obtaining Δr. We define $\Delta\overline{\tau}$ as

$$\Delta\overline{\tau} = \tau^*(s,s') - \tau(s,s') = \epsilon \beta_1(s,s') + \epsilon^2 \beta_2(s,s') + \mathcal{O}(\epsilon^3) \tag{55}$$

and then obtain the following expressions for α_1 and α_2, the first and second order variations in τ,

$$\alpha_1(s,s') = \beta_1(s,s') + \left[\phi_1(s') \frac{\partial}{\partial s'} + \phi_1(s) \frac{\partial}{\partial s}\right] \tau(s,s') \quad , \tag{56}$$

and

$$\alpha_2(s,s') = \beta_2(s,s') + \left[\phi_2(s')\frac{\partial}{\partial s'} + \phi_2(s)\frac{\partial}{\partial s}\right]\tau(s,s')$$

$$+ \left[\phi_1(s')\frac{\partial}{\partial s'} + \phi_1(s)\frac{\partial}{\partial s}\right]\beta_1(s,s')$$

$$+ \frac{1}{2}\left[\phi_1(s')\frac{\partial}{\partial s'} + \phi_1(s)\frac{\partial}{\partial s}\right]^2 \tau(s,s') \quad . \qquad (57)$$

We are now able to calculate the variation of the operator H, since the increments in all the required quantities have been obtained.

In order to complete the expression for the variation of the operator G, defined by equation (21), the increment of the internal impedance per unit length Z_i, must be obtained. This quantity ΔZ_i, is obtained in the same manner at $\Delta\tau$ or Δr and may be written as

$$\Delta Z_i' = Z_i^*(s^*) - Z_i(s) = \epsilon\, z_1(s) + \epsilon^2\, z_2(s) + \mathcal{O}(\epsilon^3) \qquad (58)$$

where

$$z_1(s) = X_1(s) + \phi_1(s)\frac{dZ_i(s)}{ds} \quad , \qquad (59)$$

$$z_2(s) = X_2(s) + \phi_1(s)\frac{dX_1(s)}{ds} + \phi_2(s)\frac{dZ_i(s)}{ds} + \frac{1}{2}\phi_1^2(s)\frac{d^2Z_i(s)}{ds^2} \qquad (60)$$

and

$$\Delta\bar{Z}_i = Z_i^*(s) - Z_i(s) = \epsilon\, X_1(s) + \epsilon^2\, X_2(s) \quad . \qquad (61)$$

It follows then, from (21) that the perturbation operators G_1 and G_2 are defined by

$$G_1\, I_o = \left[\frac{1}{i\omega\, 4\pi\, \epsilon_m} h_1 - z_1\right] I_o \qquad (62)$$

and

$$G_2\, I_o = \left[\frac{1}{i\omega\, 4\pi\, \epsilon_m} h_2 - z_2\right] I_o \qquad (63)$$

where h_1 and h_2 are given by (35) and (36) and z_1 and z_2 by equations (59) and (60).

The calculation of the variation of the current on the perturbed antenna is concluded by obtaining expressions for K_1, K_2 and the quantities $G^{-1} K_1$ and $G^{-1} K_2$. Since we have assumed a delta function generator on the unperturbed antenna (i.e. $K = \mathcal{E}\,\delta(s-s_o)$), the perturbed antenna will also be excited by a delta function generator so that

$$\Delta\bar{K} = K^*(s,s_o) - K(s,s_o) = 0 \quad , \tag{64}$$

leading to

$$K_1(s,s_o) = \mathcal{E}\left[\phi_1(s)\,\frac{\partial}{\partial s} + \phi_1(s_o)\,\frac{\partial}{\partial s_o}\right]\delta(s-s_o) \tag{65}$$

and

$$K_2(s,s_o) = \mathcal{E}\left[\phi_2(s)\,\frac{\partial}{\partial s} + \phi_2(s_o)\,\frac{\partial}{\partial s_o} + \frac{1}{2}\,\phi_1^2(s)\,\frac{\partial^2}{\partial s^2} + \phi_1(s)\phi_1(s_o)\,\frac{\partial^2}{\partial s \partial s_o}\right.$$

$$\left. + \frac{1}{2}\,\phi_1^2(s_o)\,\frac{\partial^2}{\partial s_o^2}\right]\delta(s-s_o) \quad . \tag{66}$$

It is seen from (13) that for the thin wire antenna we may write

$$G^{-1} K_{\frac{1}{2}} = -\frac{1}{\mathcal{E}}\int_{s_1}^{s_2} I_o(s,s')K_{\frac{1}{2}}(s',s_o)ds' \tag{67}$$

where $I_o(s,s')$ is the current at the point s due to a source located at s', and s_1 and s_2 denote the endpoints of the antenna. Under the condition

$$s_1 < s_o < s_2 \quad , \tag{68}$$

it may be shown, through partial integrations, that

$$G^{-1} K_1 = I_o(s_o,s_o)\,\frac{d\phi_1(s)}{ds}\bigg|_{s = s_o} \quad , \tag{69}$$

and

$$G^{-1} K_2 = I_o(s_o,s_o)\left[\frac{d\phi_2(s)}{ds} - \left(\frac{d\phi_1(s)}{ds}\right)^2\right]_{s = s_o} \quad . \tag{70}$$

The variation in the current distribution on a thin wire antenna subject to a displacement from the original configuration may now be determined from equation (8) and (9) as all the quantities appearing in these expressions have been determined.

4. Variation of the Far Field and the Time Average Input Power and Dissipated Power

The far field of a thin wire antenna is given by

$$\vec{E} = \frac{i\omega}{k^2} [\nabla(\nabla\cdot A) + k^2 \vec{A}] \quad , \tag{71}$$

where the vector potential in this region may be written as

$$\vec{A} = \frac{\mu_o}{4\pi} \frac{e^{ikr}}{r} \int_{s'} \hat{s}' \, I_o(s') \, e^{-ik\hat{r}\cdot\vec{r}'} ds' \quad . \tag{72}$$

Here, $\vec{r}$ is a vector from the origin to the point of observation, $\vec{r}'$ is a vector from the origin to the source point s' on the antenna and r is the magnitude of the vector $\vec{r}$. The quantity $\hat{r}\cdot\vec{r}'$ will be a function of the observer coordinates and s' and is denoted by $\psi(s')$. Since the observer coordinates do not change, the variation in the far field is given by

$$\Delta\vec{E} = \frac{i\omega}{k^2} [\nabla(\nabla\cdot\Delta\vec{A}) + k^2 \Delta\vec{A}] \, , \tag{73}$$

where

$$\Delta\vec{A} = \frac{\mu_o e^{ikr}}{4\pi r} \left\{ \int_{s'^*} \hat{s}'^* \, I^*(s'^*) e^{-ik\psi^*(s'^*)} ds'^* - \int_{s'} \hat{s}' \, I(s') e^{-ik\psi(s')} ds' \right\} \tag{74}$$

We define the function $T(I,\psi)$ in the following manner

$$T(I,\psi) = I_o(s') e^{-ik\psi(s')} \tag{75}$$

and then rewrite (74) as

$$\Delta\vec{A} = \frac{\mu_o e^{ikr}}{4\pi r} \int_{s'} \left[\hat{s}'^* \, T(I^*,\psi^*) \frac{ds'^*}{ds'} - \hat{s}' \, T(I,\phi) \right] ds' \quad . \tag{76}$$

Denoting the variation in the unit vector $\hat{s}'$ and the function $\psi(s')$ as shown below

$$\Delta\hat{s}' = \hat{s}'^*(s'^*) - \hat{s}'(s') = \epsilon \, \vec{\xi}_1(s') + \epsilon^2 \, \vec{\xi}_2(s') + \mathcal{O}(\epsilon^3) \quad , \tag{77}$$

$$\Delta\psi = \psi^*(s'^*) - \psi(s') = \epsilon \, \theta_1(s') + \epsilon^2 \, \theta_2(s') + \mathcal{O}(\epsilon^3) \quad , \tag{78}$$

we may expand the integrand of (76) in a Taylor series about the point $(\hat{s}', I, \psi)$. This operation leads to the following expression for the variation of A:

$$\vec{\Delta A} = \frac{\mu_0 e^{ikr}}{4\pi r} [\epsilon \vec{a}_1 + \epsilon^2 \vec{a}_2 + \mathcal{O}(\epsilon^3)] \quad , \tag{79}$$

where

$$\vec{a}_1 = \int_{s'} \left[\hat{s}' J_1 T(I,\psi) + \hat{s}' T(I,\psi) \frac{d\phi_1(s')}{ds'} + \vec{\xi}_1(s') T(I,\psi)\right] ds' \quad , \tag{80}$$

and

$$\vec{a}_2 = \int_{s'} \left[\hat{s}' J_2 T(I,\psi) + \hat{s}' \frac{d\phi_1(s')}{ds'} J_1 T(I,\psi) + \hat{s}' T(I,\psi) \frac{d\phi_2(s')}{ds'}\right.$$

$$\left. + \vec{\xi}_1(s') J_1 T(I,\psi) + \vec{\xi}_1(s') T(I,\psi) \frac{d\phi_1(s')}{ds'} + \vec{\xi}_2(s') T(I,\psi)\right] ds' \quad . \tag{81}$$

The terms $J_1 T$ and $J_2 T$ are given by

$$J_1 T(I,\psi) = i_1(s') e^{-ik\psi} - ik\, \theta_1(s') I_0(s') e^{-ik\psi} \quad , \tag{82}$$

and

$$J_2 T(I,\psi) = i_2(s') e^{-ik\psi} - ik\, \theta_2(s') I_0(s') e^{-ik\psi} - ik\, i_1(s') \theta_1(s') e^{-ik\psi}$$

$$- \frac{1}{2} k^2 \theta_1^2(s') I_0(s') e^{-ik\psi} \quad . \tag{83}$$

The variation of the function $\psi(s')$ is calculated in a similar fashion to the calculation of $\Delta r(s,s')$ in the previous section. We have that

$$\Delta\psi = \hat{r} \cdot [\vec{r}'^*(s'^*) - \vec{r}'(s')] \tag{84}$$

and defining $\Delta\vec{r}'$ as shown

$$\Delta\vec{r}' = \vec{r}'^*(s') - \vec{r}'(s') = \epsilon\vec{\gamma}_1(s') + \epsilon^2 \vec{\gamma}_2(s') + \mathcal{O}(\epsilon^3) \quad , \tag{85}$$

we obtain for the first and second order variations of ψ,

$$\theta_1(s') = \hat{r} \cdot \left[\vec{\gamma}_1(s') + \phi_1(s') \frac{d\vec{r}'(s')}{ds'}\right] \tag{86}$$

and

$$\theta_2(s') = \hat{r} \cdot \left[\vec{\gamma}_2(s') + \phi_2(s') \frac{d\vec{r}'(s')}{ds'} + \frac{1}{2} \phi_1^2(s') \frac{d^2\vec{r}(s')}{ds'^2} + \phi_1(s') \frac{d\vec{\gamma}_1(s')}{ds'}\right] . \tag{87}$$

Now the quantity $d\vec{r}'(s')/ds'$ is simply the unit tangent vector $\hat{s}'(s')$ and the second derivative of $\vec{r}'(s')$ is given by

$$\frac{d^2\vec{r}'(s')}{ds'^2} = \frac{1}{\rho(s')}\hat{n}'(s') \quad , \tag{88}$$

where $\rho(s')$ is the radius of curvature of the unperturbed antenna and $\hat{n}'$ is the principal normal to this structure. We may therefore rewrite the expressions for θ_1 and θ_2 as

$$\theta_1(s') = \hat{r}\cdot[\vec{\gamma}_1(s') + \hat{s}'\,\phi_1(s')] \tag{89}$$

and

$$\theta_2(s') = \hat{r}\cdot\left[\vec{\gamma}_2(s') + \phi_1(s')\frac{d\gamma_1(s')}{ds'} + \hat{s}'\,\phi_2(s') + \hat{n}'\frac{\phi_2(s')}{2\rho(s')}\right] . \tag{90}$$

The expression for the variation of $\hat{s}'$ is obtained in a similar manner and results in the following expressions for $\vec{\xi}_1(s')$ and $\vec{\xi}_2(s')$:

$$\vec{\xi}_1(s') = \vec{\sigma}_1(s') + \phi_1(s')\frac{d\hat{s}'(s')}{ds'} \tag{91}$$

and

$$\vec{\xi}_2(s') = \vec{\sigma}_2(s') + \phi_1(s')\frac{d\vec{\sigma}_1(s')}{ds'} + \phi_2(s')\frac{d\hat{s}'(s')}{ds'} + \frac{1}{2}\phi_1^2(s')\frac{d^2\hat{s}'(s')}{ds'} , \tag{92}$$

where

$$\overline{\Delta\hat{s}'} = \hat{s}'^*(s') - \hat{s}'(s') = \epsilon\vec{\sigma}_1(s') + \epsilon^2\vec{\sigma}_2(s') + \mathcal{O}(\epsilon^3) \tag{93}$$

The expressions for $\vec{\xi}_1$ and $\vec{\xi}_2$ may be rewritten using equation (88) and the following

$$\frac{d^2\hat{s}'(s')}{ds'^2} = -\hat{n}'(s')\frac{1}{\rho^2(s')}\frac{d\rho(s')}{ds'} + \hat{b}'(s')\frac{1}{\rho(s')\tau(s')} - \hat{s}'(s')\frac{1}{\rho^2(s')} . \tag{94}$$

The vector $\hat{b}'$ is the binormal of the unperturbed antenna defined by the cross product

$$\hat{b}' = \hat{s}' \times \hat{n}' \quad , \tag{95}$$

and $1/\tau$ is the torsion of the antenna, given by

$$\frac{1}{\tau} = -\hat{n}'\cdot\frac{d\hat{b}'(s')}{ds'} . \tag{96}$$

When the antenna is planar, the torsion is zero. Equations (91) and (92) may now be expressed as follows:

$$\vec{\xi}_1(s') = \vec{\sigma}_1(s') + \frac{\phi_1(s')}{\rho(s')}\hat{n}'(s') \tag{97}$$

and

$$\vec{\xi}_2(s') = \vec{\sigma}_2(s') + \frac{d\sigma_1(s')}{ds'}\phi_1(s') + \hat{n}'(s')\left[\frac{\phi_2(s')}{\rho(s')} - \frac{\phi_1^2(s')}{2\rho^2(s')}\frac{d\rho(s')}{ds'}\right]$$

$$+ \hat{b}'(s')\frac{\phi_1^2(s')}{2\rho(s')\tau(s')} - \hat{s}'(s')\frac{\phi_1^2(s')}{2\rho^2(s')} \quad . \tag{98}$$

The quantities which are necessary for the calculation of $\Delta\vec{A}$ from equations (79), (80) and (81) have now been obtained, and utilization of equation (73) then results in an expression for the variation of the far field.

The time averaged power dissipated on the antenna, P_D, is given by

$$P_D = \frac{1}{2}\int_{s'} I_o(s')\bar{I}_o(s')\cdot \text{Real}\{Z_1(s')\}\cdot ds' \quad , \tag{99}$$

where the bar indicates complex conjugate. Using the same procedure described in the calculation of the variation of $\vec{A}$ we obtain

$$\Delta P_D = \epsilon\, p_{d_1} + \epsilon^2 p_{d_2} + \mathcal{O}(\epsilon^3) \quad , \tag{100}$$

where

$$p_{d_1} = \frac{1}{2}\int_{s'}\left[f_1(s') + I_o(s')\bar{I}_o(s')R(s')\frac{d\phi_1(s')}{ds'}\right]ds' \tag{101}$$

and

$$P_{d_2} = \frac{1}{2}\int_{s'}\left[f_2(s') + f_1(s')\frac{d\phi_1(s')}{ds'} + I_o(s')\bar{I}_o(s')R(s')\frac{d\phi_2(s')}{ds'}\right]ds' \quad . \tag{102}$$

The quantities f_1, f_2 and R are given by

$$R(s') = \text{Real}\{Z_2(s')\} \quad , \tag{103}$$

$$f_1(s') = 2\,\text{Real}\{i_1(s')\bar{I}_o(s')R(s')\} + v_1(s')I_o(s')\bar{I}_o(s') \tag{104}$$

and

$$f_2(s') = 2\,\text{Real}\,\{i_2(s')\bar{I}_o(s')R(s')\} + v_2(s')I_o(s')\bar{I}_o(s')$$

$$+ 2\,i_1(s')\bar{I}_1(s')R(s') + 4\,\text{Real}\,\{i_1(s')v_1(s')\bar{I}_o(s')\}, \quad (105)$$

where

$$v_1(s') = \text{Real}\,\{z_1(s')\} \quad (106)$$

and

$$v_2(s') = \text{Real}\,\{z_2(s')\} \quad . \quad (107)$$

The quantities z_1 and z_2 were given in equations (59) and (60).

The time averaged input power, P_{in}, for the antenna for a source of $\mathcal{E}$ volts located at $s = s_o$ is given by

$$P_{in} = \frac{1}{2}\mathcal{E}\,\text{Real}\,\{\bar{I}(s_o)\} \quad , \quad (108)$$

so that the variation of this quantity is easily seen to be

$$\Delta P_{in} = \frac{1}{2}\mathcal{E}[\epsilon\,\text{Real}\{i_1(s_o)\} + \epsilon^2\,\text{Real}\,\{i_2(s_o)\}] \quad . \quad (109)$$

We have now obtained general expressions for the variation in the current, far field, time averaged power dissipated and time averaged input power of an arbitrary thin wire antenna subjected to disturbances in its material and/or geometrical configuration.

References

1. F.C. Karal and J.B. Keller, J. Math. Phys., 5, 537, (1964).

2. C.H. Tang, IEEE Trans. on Antennas and Propagation, AP-12, 2, (1964).

APPENDIX M

INVESTIGATION OF A SYNTHETIC ANTENNA SYSTEM

1. The Pattern

The purpose of this work is to investigate the operation of a rotating array of two elements whose spacing is varied in a prescribed manner, so as to permit the construction of a highly directive antenna pattern. We will obtain the far field power pattern of this system under ideal conditions such as the neglect of mutual coupling between elements, and then determine the effect of the presence of random phase errors and temporal variations of the background on this idealized power pattern.

Let us consider two elements situated in the x-y plane, separated by a distance r and symmetrically displaced with respect to the origin, as shown in Figure 1. These elements rotate about the z axis, so that their instantaneous position may be defined by the distance r and the angle β between the negative y axis and the straight line drawn through the origin connecting the two elements. The radiation pattern is constructed by increasing the element spacing from zero to a maximum length D and summing the individual returns at each spacing over a complete rotation. Throughout this analysis the effect of the mutual interaction between the two elements is neglected, although this coupling is certainly not negligible at the smaller spacings and will lead to some deterioration in the resultant power pattern.

The beam of this array may be pointed in any desired direction by inserting the appropriate phase shift between the two elements. We will denote the observation or field point by the usual spherical coordinate angles $(\theta.\phi)$, while the desired beam direction is specified by the polar angle γ measured from the z axis and azimuthal angle α, measured from the x axis.

When the two elements are operated without any external phase shift introduced, the space factor S at any given instant of time is

$$S = e^{ik\frac{r}{2}\sin\theta\cos(\beta-\phi)} + e^{-ik\frac{r}{2}\sin\theta\cos(\beta-\phi)} \tag{1}$$

The prescribed motion of the elements, in the case of isotropic radiators, would then result in two broadside beams of circular cross section directed along the positive and negative z axes. In order to shift the beam to any arbitrary direction, (γ,α), it is necessary to introduce a continuously varying phase factor $\frac{kr}{2}\sin\gamma\cos(\beta-\alpha)$ on each element, which leads to the following instantaneous space factor

$$S = e^{i\frac{kr}{2}\tau} + e^{-i\frac{kr}{2}\tau} \tag{2}$$

where

$$\tau = \sin\theta\cos(\beta-\phi) - \sin\gamma\cos(\beta-\alpha). \tag{3}$$

The instantaneous power pattern of this two element array, Φ_i, is given by

$$\Phi_i = F^2 |S|^2 ,$$

where F^2 is the radiation pattern of a single element and S is given by (2). We will concern ourselves at present with the case of isotropic radiators, since the results which will be presented may be modified to account for directional elements by the insertion of an appropriate multiplicative factor.

The introduction of phase switching into the system allows us to write $|S|^2$ as

$$|S|^2 = \cos kr\tau. \tag{4}$$

The pattern which results when the two elements are rotated about the z axis and the instantaneous signals received at each angle β are summed may be obtained by integrating (4) over β. This manipulation assumes that the patterns may be combined continuously, and thus represents another idealization of the actual system. In this case, the pattern for the rotating isotropic radiators, Φ_s, is given by

$$\Phi_s = \frac{1}{2\pi}\int_0^{2\pi} |S|^2 \, d\beta = J_o(kr\psi), \tag{5}$$

where J_o is the zeroth order Bessel function of the first kind and

$$\psi = \sqrt{\sin^2\theta + \sin^2\gamma - 2\sin\gamma \sin\theta \cos(\alpha-\phi)}. \tag{6}$$

The variation of the interelement spacing from 0 to D leads to the following expression for the resultant power pattern Φ,

$$\Phi = \frac{1}{T} \int_0^T J_o(t)dt, \tag{7}$$

where

$$T = kD\psi \tag{8}$$

The radiation pattern ϕ achieves a maximum value of unity when $\psi = 0$, which occurs when θ and ϕ satisfy one of the following two relationships

$$\theta = \gamma, \qquad \phi = \alpha \tag{9}$$

and

$$\theta = \pi - \gamma, \quad \phi = \alpha \tag{10}$$

We see therefore that, except for the case $\gamma = \frac{\pi}{2}$, there will always be two main beams directed in the same aximuthal direction and symmetrically displaced with respect to the polar angle about the x-y plane. When $\gamma = \frac{\pi}{2}$, the system is operating as an endfire array and the single beam is symmetrical about the x-y plane.

A plot of the function ϕ (T), defined by equation (7), is shown in Figure 2. It is seen that the maximum sidelobe occurs at T = 8 and is down 8.2 db from the main beam and that the half power point in the main beam occurs at T = 2.85. When the system is operated as a broadside array (i.e., $\gamma = 0$), we have $\psi = \sin\theta$ and the beam cross section is circular. By varying the value of γ we not only change the direction of the main beam, but also change the shape of the beam cross section.

In order to present some numerical calculations of beamwidths we will consider a maximum interelement spacing of 30 wavelengths, (i.e., $D = 30\lambda$). When the system is operated as a broadside array, the width of the main beam (angular distance between half-power points) is 1.73° and the maximum sidelobes are displaced 2.43° from the center of the main beam. Although this mode of operation permits very high resolution, it has the major disadvantage of allowing an ambiguity to exist due to the presence of a main beam along the positive and the negative z axis. We therefore turn our attention to the endfire mode of operation in which this ambiguity is no longer present. In this case the beam cross section loses its circular symmetry, and the E-plane beamwidth is 1.73°, while the H-plane beamwidth is 19.93°, thereby resulting in a beam area of 34.38 square degrees. The results of these two calculations are shown below:

Operative Mode	Beamwidth	Beam Area	Sidelobe Level
Broadside	1.73° (circularly symmetric beam)	2.36 sq. degrees	-8.2 db
Endfire	1.73° (E-plane);19.93° (H-plane)	34.38 sq. degrees	-8.2 db

System Performance for $D - 30\lambda$

Table I

2. The Effect of Random Phase Errors on System Performance

In the practical formation of synthetic array patterns, the individual terms which are integrated to form the resultant pattern will be subjected to random phase shifts. These errors may be produced by agencies such as the random motion of the elements around their "equilibrium" positions. This section will therefore be devoted to the determination of statistical measures of the effects of these phase shifts.

We first assume that the random phase errors introduced into the system vary solely with the spacing r and not with the rotation angle β. Then denoting this spurious phase shift by $\delta(r)$ we may write the instantaneous

space factor, prior to introducing phase shifting, as

$$S = e^{i[\frac{kr}{2}\tau + \delta(r)]} + e^{-i[\frac{kr}{2}\tau + \delta(r)]} . \qquad (11)$$

Repetition of the same calculations performed in the preceeding section leads to the following expression for the resultant power pattern Φ,

$$\Phi = \frac{1}{D}\int_0^D \cos 2\delta(r) J_o(kr\psi)dr. \qquad (12)$$

Since the phase error $\delta(r)$ is a random quantity we will direct our attention to obtaining the expected value of Φ, which will be denoted as $< \Phi >$,

$$< \Phi > = \frac{1}{D} \int_0^D < \cos 2\delta(r)> J_o (kr\psi)dr. \qquad (13)$$

We now choose $\delta(r)$ to be a non-stationary random process varying linearly with r,

$$\delta(r) = \frac{1}{2} \eta r, \qquad (14)$$

where η is a random variable with the Gaussian distribution shown below:

$$p(\eta) = \frac{1}{\sqrt{2\pi}\ \sigma} e^{-\frac{\eta^2}{2\sigma^2}} \qquad (15)$$

Thus, equation (13) may be rewritten as

$$<\Phi> = \frac{1}{\sqrt{2\pi}\ \sigma} \int_{-\infty}^{+\infty} \int_0^D \cos\eta r J_o(kr\psi)\ e^{-\frac{\eta^2}{2\sigma^2}} drd\eta \qquad (16)$$

and integration with respect to η results in

$$\langle \Phi \rangle = \frac{1}{D} \int_0^D J_o(kr\psi) e^{-\frac{\sigma^2 r^2}{2}} dr. \tag{17}$$

We would expect the maximum variance of $\delta(r)$ to be at least 90° so that $Z = \sigma D > 1$, and the integral in (17) may be evaluated by asymptotic methods.

The resultant expression for $\langle \Phi \rangle$ when $T = kD\psi$ is not zero, can then be shown to be

$$\langle \Phi \rangle = \sqrt{\frac{\pi}{2}} \frac{e^{\frac{T^2}{4Z^2}}}{Z} I_o \frac{T^2}{4Z^2}$$

$$= \frac{2e^{-\frac{T^2}{4Z^2}}}{\pi Z} \text{Real} \left\{ \sum_{n=0}^{n-1} \frac{(-1)^n \Gamma(n+1/2)}{n!\, Z^n T^{1/2}} \cdot \right.$$

$$\left. \cdot \sum_{m=0}^{\infty} \frac{(-n)^m (2m+n)!\, e^{-\frac{\pi i}{4}} e^{iT}}{m!\, 2^m \left[Z - \frac{iT}{Z}\right]^{2m+n+1}} \right\} \tag{18}$$

When T is equal to zero direct evaluation of (17) leads to

$$\Phi = \sqrt{\frac{\pi}{2}} \frac{1}{Z} \operatorname{erf} \frac{Z}{\sqrt{2}} \tag{19}$$

The function I_o, is the modified Bessel function of zeroth order.

When the maximum variance of the phase error is greater or equal to 90° (k.e., $Z = \sigma D \geq \pi$), it can easily be shown that the first term of equation (18) provides an adequate representation of the expected value of Φ,

$$\langle \Phi \rangle \approx \sqrt{\frac{\pi}{2}} \; \frac{e^{-\frac{T^2}{4Z^2}}}{Z} \; I_o\left(\frac{T^2}{4Z^2}\right) \qquad (20)$$

Figure 3 displays a graph of $\langle \Phi \rangle$ for the case $Z = \pi$, superimposed on the graph of Φ obtained previously. We note that the maximum value of $\langle \Phi \rangle$ is slightly less than 0.4, as compared to a maximum value of unity for the case of no phase error. Thus a marked decrease in gain is seen to be one immediate consequence of the random phase error. We note also that the beamwidth of the system reflects a large increase, since the half-power point now occurs at $T = 5.85$. In particular, it is seen that for endfire operation, the expected value of the E-plane beamwidth is now 3.53°, while the expected value of the H-plane beamwidth is 28.37°, resulting in an expected beam area of 99.77 square degrees. The expected beam area has therefore increased by almost a factor of 3 due to the introduction of a linear, non-stationary random phase error with zero mean and maximum variance of 90°. If the mean value of the random phase were not zero, the expected beam direction would be shifted, in addition to the occurrence of beam broadening.

3. The Effect of Source Variations on the Observed Distribution

The non-stationary behavior of the observed source during the formation of a synthetic array pattern is another cause of noise in the system, which leads to an effective deterioration of the antenna pattern and thus to errors in interpreting the observed brightness distribution. We turn our attention in this section to the problem of determining the effective change in antenna pattern, or in the observed brightness distribution, due to this temporal variation during the pattern construction period.

We will consider the rotation time of the elements to be very small compared to the time scale of the background variations, so that the background remains stationary throughout a rotation at a given inter-element spacing. The source brightness distribution is denoted as $F(\theta,\phi,\tau)$, where τ is the time interval necessary for the construction of the antenna pattern. By assuming that the change in interelement spacing occurs at a constant velocity, v, equation (8) for the array radiation pattern may be rewritten as

$$\Phi\ (\theta,\phi,\tau) = \frac{1}{\tau} \int_0^{\tau} A(\theta,\phi,t)dt, \tag{21}$$

where

$$A(\theta\cdot\phi,t) = J_o\ \ [kvt\psi(\theta,\phi)]\ . \tag{22}$$

The observed brightness distribution, $W(\theta,\phi,\tau)$, may then be calculated by constructing a spatial convolution at each instant of time of the function A with the source distribution F and then summing these individual terms over the duration of the pattern construction period. This summing operation is again approximated by an integration so that the resultant expression for $W(\theta,\phi,\tau)$ may be written as

$$W(\theta,\phi,\tau) = \frac{1}{\tau} \int_0^{\tau} \int_0^{2\pi} \int_0^{\pi} A(\theta - \theta',\ \phi - \phi';\ t)F(\theta',\phi',t)\sin\theta'd\theta'd\phi'dt. \tag{23}$$

If the source distribution is a point source which remains constant in time

$$F(\theta,\phi,t) = \frac{\delta(\theta)\delta(\phi)}{\sin\theta} = \delta(\Omega), \tag{24}$$

the observed brightness distribution is a reconstruction of the exact antenna pattern. We may therefore determine how this observed distribution will vary due to a temporal disturbance by considering a time

variation in F, superimposed on the constant point source. This is equivalent to obtaining an effective change in the antenna pattern due to a prescribed source variation. By constructing the following source brightness distribution,

$$F(\theta,\phi,t) = \delta(\Omega) + \delta(\Omega)f(t) \tag{25}$$

where f(t) represents the spurious time variation in the source distribution, and substituting this expression into equation (23) we obtain

$$W(\theta,\phi,\Omega) = \Phi(\theta,\phi,\tau) + \Delta\,\Phi(\theta,\phi,\tau), \tag{26}$$

Here, $\Phi(\theta,\phi,\tau)$ is the unperturbed antenna pattern defined by equation (8), (i.e., the observed source distribution in the absence of temporal variations) and $\Delta\,\Phi\,(\theta,\phi,\tau)$ is the effective change in the antenna pattern or the change in the observed distribution due to the temporal variation occurring over the beam construction period. The quantity $\Delta\Phi(\theta,\phi,\tau)$ is given by

$$\Delta\,\Phi\,(\theta,\phi,\tau) = \frac{1}{\tau}\int_0^{\tau} J_o\,[kvt\psi(\theta,\phi)]\,f(t)dt. \tag{27}$$

If we assume the source variation to be a burst of constant amplitude, N, over a portion of the pattern construction period, equation (27) becomes

$$\Delta\Phi(\theta,\phi,\tau) = \frac{N}{T}\int_{T_1}^{T_2} J_o(u)du \tag{28}$$

where T is defined by equation (8) and T_1 and T_2 are given by

$$T_1 = \frac{d_1}{D}\,T, \qquad T_2 = \frac{d_2}{D}\,T \tag{29}$$

The spacing of the elements at the inception and cessation of the noise burst are denoted by d_1 and d_2, respectively.

Figures 4 and 5 display the observed distribution or perturbed antenna pattern, $W(\theta,\phi,\tau)$, along with the unperturbed pattern $\Phi(0,\phi,\tau)$, for the case N = 1, and for various burst durations. The two cases shown in Figure 4 depict a disturbance which extends over 30% of the entire pattern construction time. It is seen that the disturbance which occurs during the first half of the interval ($d_1 = 0.20$, $d_2 = 0.50$) results in an increase in beamwidth, or a decrease in resolution capability on the order of 10%, while the burst which occurs during the latter half of the construction interval results in an increased sidelobe level. The results for the case of the shorter duration pulse depicted in Figure 5 follow the same trend with slightly larger increases in sidelobe levels.

4. Conclusions

We have investigated the properties of a two element synthetic aperture system neglecting the effects of mutual coupling between elements. After obtaining the radiation pattern of this system for the case of isotropic radiators, we have shown how the pattern is distorted by the introduction of moderate random phase errors and temporal variations in the source brightness distribution.

It can be shown that the analyses performed in this work will not be greatly affected by the introduction of directional elements into the array. If we consider the elements to be short dipoles of length ℓ lying in the x-y plane and directed radially, the resultant antenna pattern can easily be shown to be

$$\Phi = \frac{I^2\ell^2(1-1/2\ \sin^2\theta)}{T} \int_0^T J_o\ (t)dt. \qquad (30)$$

It follows then that the resultant expressions for $<\Phi>$ and $W(\theta,\phi,\tau)$ will also be multiplied by the same factor, $(1-1/2\ \sin^2\theta)$. This system will have greater resolution capabilities than the array of isotropic radiators, but the increase in beamwidth and sidelobe levels due to the random phase

errors and temporal source variations will remain the same. In addition one would expect a larger variance in the phase error due to the random motion of these elements than in the case of the isotropic radiators, and therefore the magnitude of the deterioration of the antenna pattern for this type of disturbance would increase.

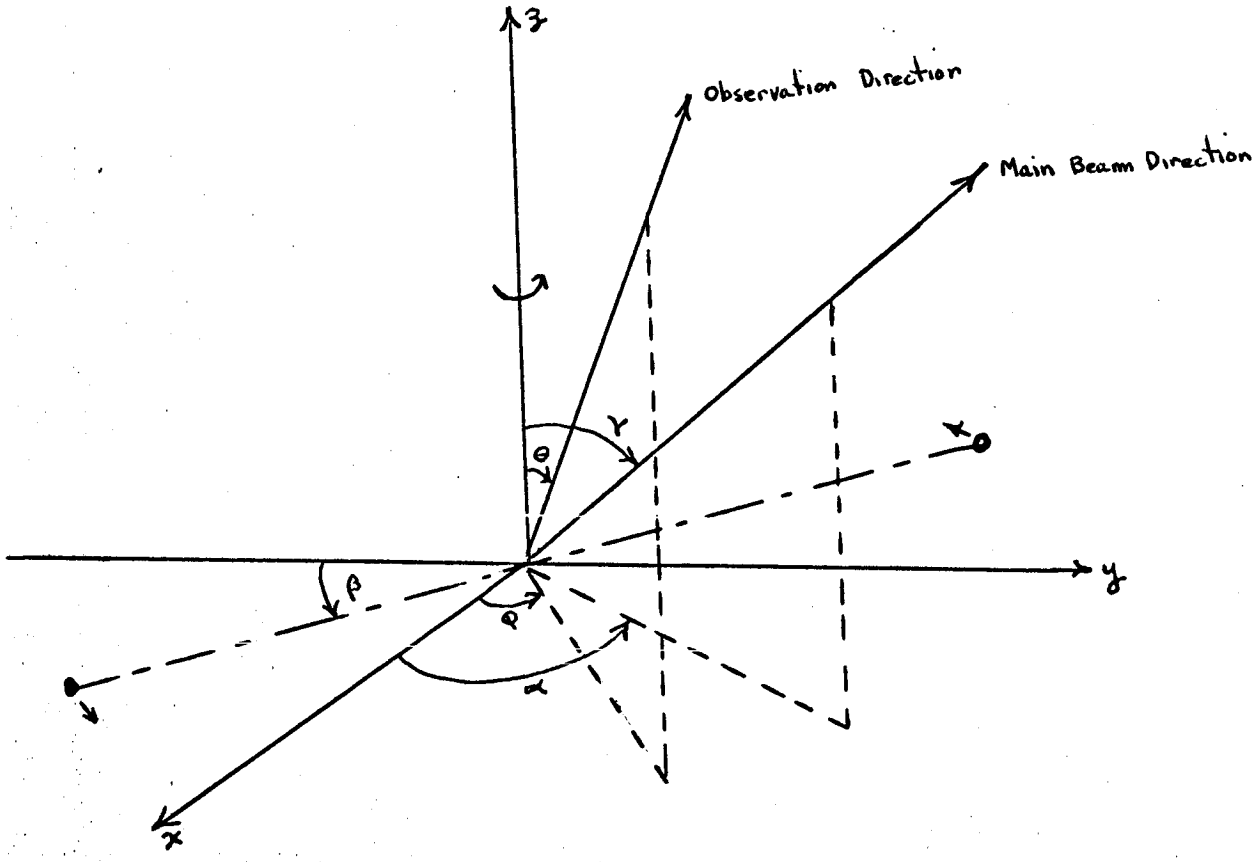

Synthetic Array

Figure 1

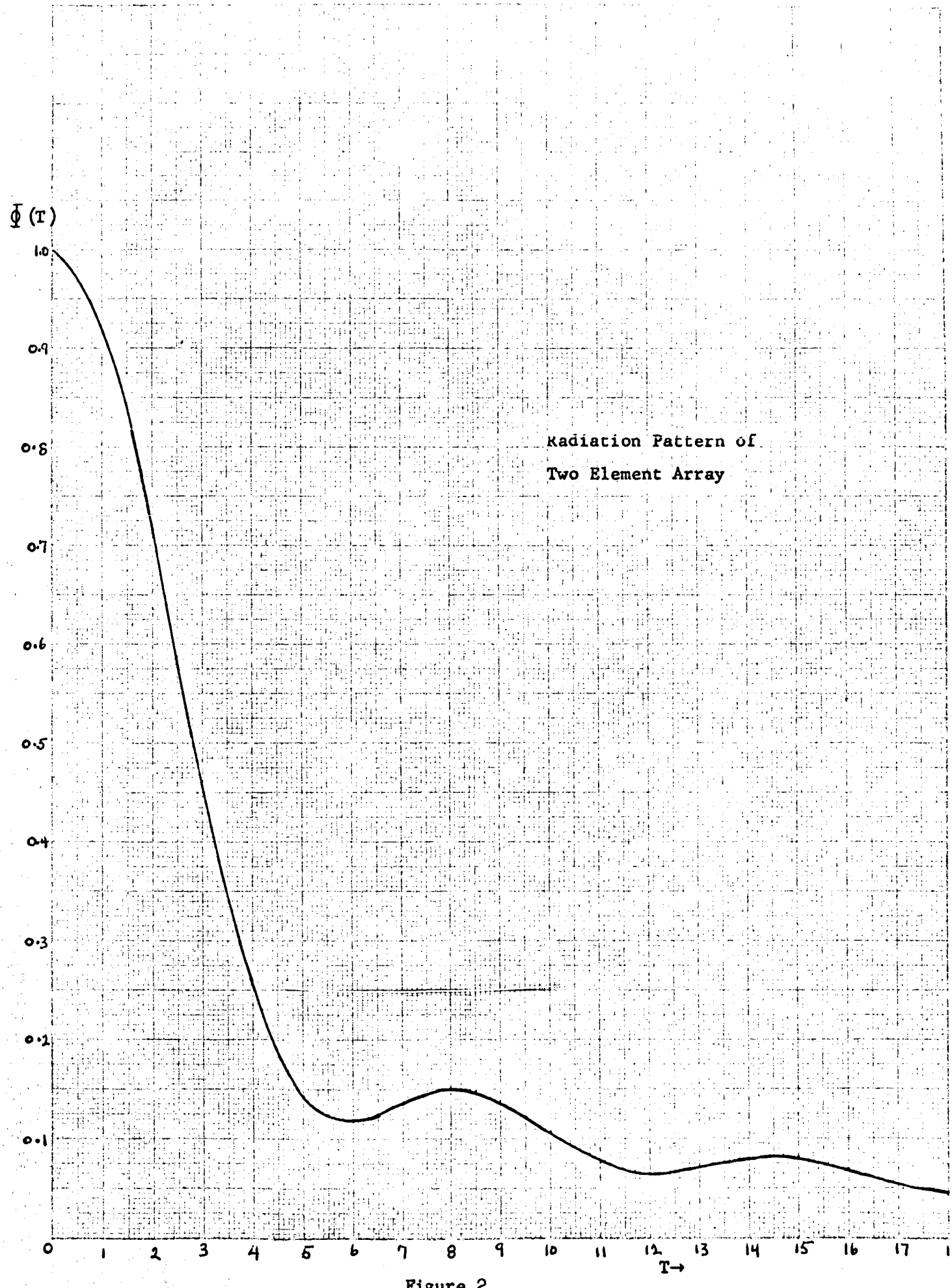
Φ (T)
1.0
0.9
0.8
0.7
0.6
0.5
0.4
0.3
0.2
0.1
0
1
2
3
4
5
6
7
8
9
10
11
12
13
14
15
16
17
18
T→
Radiation Pattern of
Two Element Array

Figure 2

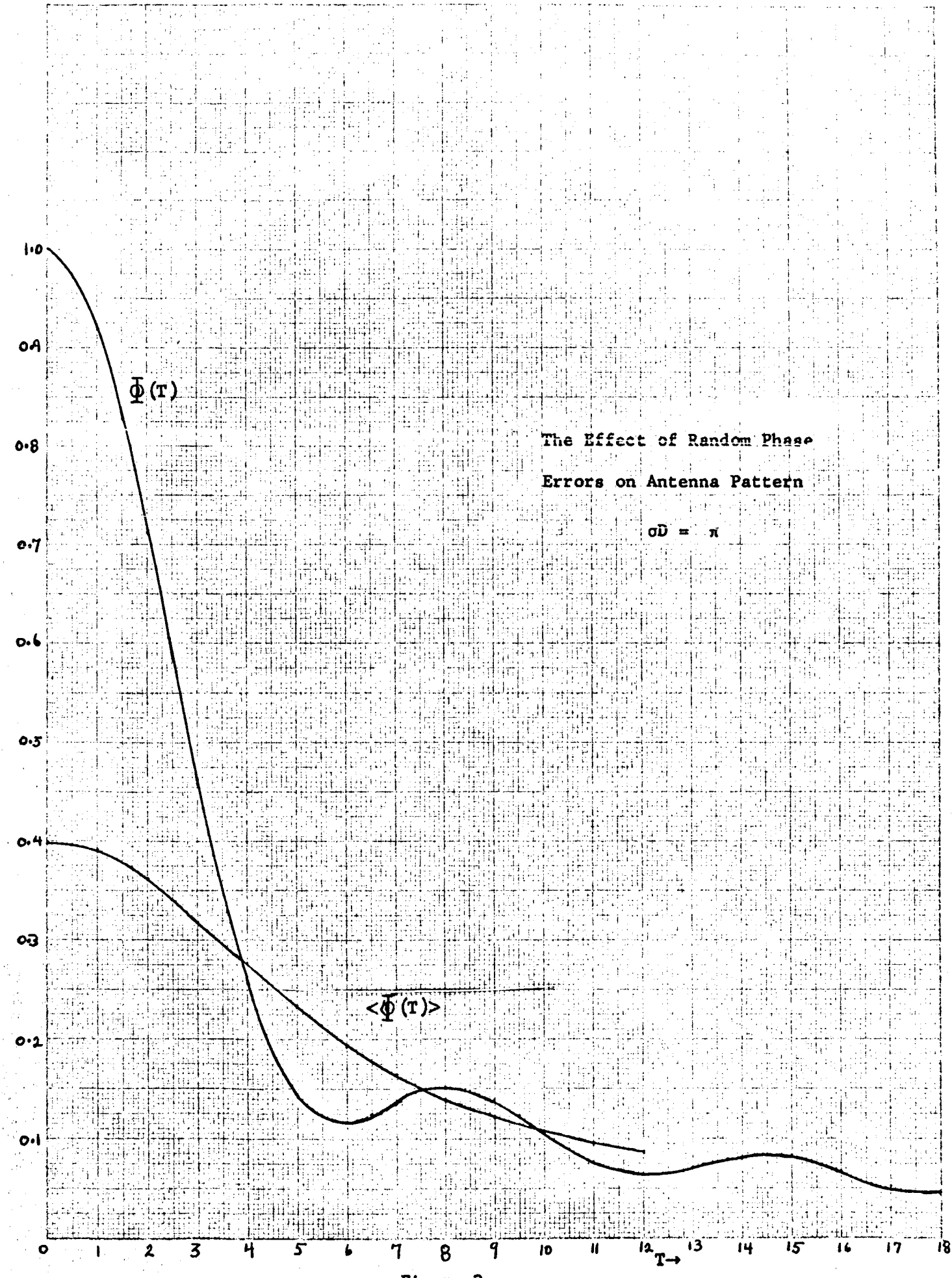
1.0
0.9
0.8
0.7
0.6
0.5
0.4
0.3
0.2
0.1
Φ(T)
The Effect of Random Phase
Errors on Antenna Pattern
σD = π
<Φ(T)>
0 1 2 3 4 5 6 7 8 9 10 11 12 13 14 15 16 17 18
T→

Figure 3

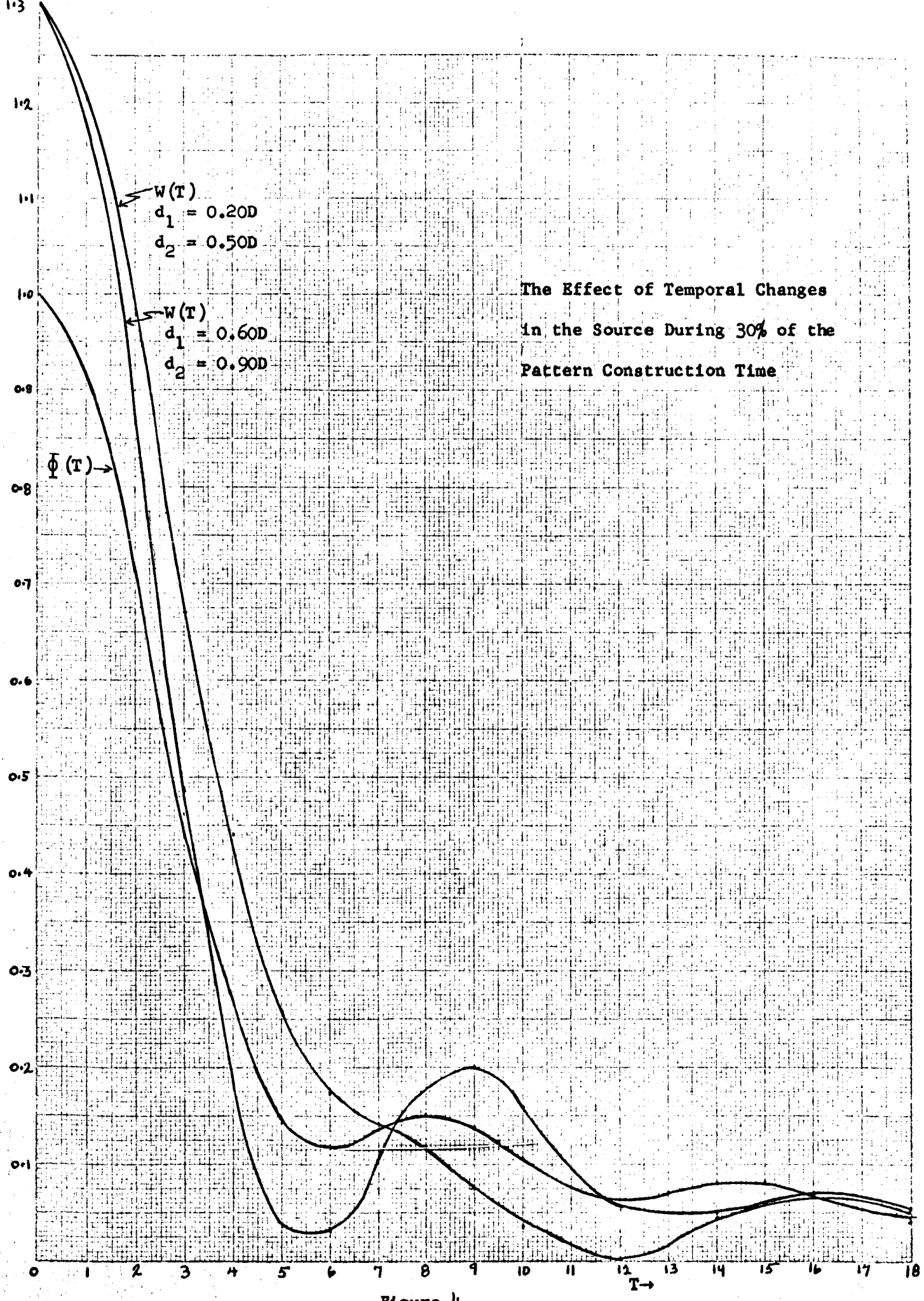
W(T)
d_1 = 0.20D
d_2 = 0.50D
W(T)
d_1 = 0.60D
d_2 = 0.90D
Φ(T)
The Effect of Temporal Changes in the Source During 30% of the Pattern Construction Time
T→

Figure 4